Metabolic signatures of sepsis in critical care: an individualised approach to diagnosis and management

A thesis submitted by
Natalie McLymont

for the degree of Doctor of Philosophy of Imperial College London

Department of Surgery and Cancer
Faculty of Medicine
Imperial College London

2017

Abstract

Sepsis is a clinical syndrome of great importance associated with a high rate of multiple organ failure and death and currently no accurate means of predicting those at particular risk of such outcomes. Energy metabolism involves many interdependent processes performed by the liver and kidneys and adequate function is essential to survival; conversely detrimental changes are associated with adverse outcomes. Thus, changes in energy metabolism in sepsis have the potential to be utilised in the early diagnosis of sepsis-related liver and kidney injury and general risk stratification.

This thesis describes the metabolic response of a cohort of critically ill patients (n=50) with severe sepsis, specifically sepsis-related organ dysfunction and survival using metabolic profiling techniques based on ^{1}H-Nuclear Magnetic Resonance (NMR) spectroscopy and Ultra-Performance Liquid Chromatography-Mass Spectrometry (UPLC-MS) and multivariate statistical analyses. This consisted of three parts: (1) demonstration of the feasibility of ^{1}H-NMR analyses of urine as a method of global metabolic profiling in a cohort of critically ill patients including the development of a ^{1}H-NMR spectroscopy drug standards database to aid drug metabolite identification. (2) Characterisation of metabolic changes associated with sepsis-related liver injury (SRLI) using ^{1}H-NMR of urine and serum samples from the sepsis cohort. (3) Characterisation of lipid changes associated with SRLI using lipid profiling based on UPLC-MS analyses of plasma from the sepsis cohort.

The feasibility of metabolic profiling based on ^{1}H-NMR analyses of urine was demonstrated in the critically ill cohort. Together, ^{1}H-NMR analyses of serum and lipid profiling of plasma demonstrated changes in lysine and methionine and 18 plasma lipids associated with liver dysfunction in severe sepsis that were in keeping with our current understanding, and provided further insights into the pathophysiology of SRLI. These findings could also be used in the early diagnosis of SRLI and improve its prognosis and warrants further investigation.

Tables of contents

Abstract **1**
Tables of contents **2**
Acknowledgements **9**
Declaration of originality **10**
Copyright declaration **11**
List of figures **12**
List of tables **20**
List of abbreviations **25**
List of symbols **29**
Chapter 1: Introduction **30**
1.1 Aims and objectives 30
1.2 Introduction to metabonomics 30
1.3 Sepsis 31
1.3.1 Importance 31
1.3.2 Clinical challenges 33
1.3.2.1 Early diagnosis of sepsis-induced organ dysfunction 33
1.3.3 Metabolic changes in sepsis 37
1.3.3.1 Lipoproteins and sepsis 41
1.3.3.2 Amino acids in sepsis 43
1.3.4 Metabolic profiling studies in critical illness and sepsis 45
1.3.4.1 Animal studies 45
1.3.4.2 Clinical Studies 56
1.3.4.2.1 Critically ill patients with SIRS versus healthy controls 56
1.3.4.2.2 Critically ill patients with sepsis versus healthy controls 62
1.3.4.2.3 Critically ill patients with sepsis versus non-infected SIRS 63
1.4 Nuclear magnetic resonance spectroscopy 68
1.4.1 Two-dimensional Nuclear magnetic resonance spectroscopy 76
1.5 Mass Spectroscopy 79
1.5.1 LCMS 80
1.5.1.1 Ultra-Performance LCMS 80
1.6 Multivariate statistical data analysis 81
1.6.1 Data reduction and pre-processing of the spectral data prior to statistical analysis 81
1.6.2 Principal Component analysis 82
1.6.3 PLS, OPLS and OPLS-DA 85

1.6.4 Metabolite identification: STOCSY, databases; literatures 88
1.7 Aims and objectives 89
Chapter 2: Methodology 91
2.1 Materials 91
2.1.1 NMR 91
2.1.1.1 Chemicals 91
2.1.1.2 Equipment 91
2.1.2 UPLC-MS 92
2.1.2.1 Chemicals 92
2.1.2.2 Equipment 92
2.2 Validation cohort: unselected critically ill patients 92
2.2.1 Study patients 92
2.2.2 Sample collection 92
2.2.3 Clinical data collection 92
2.2.4 Sample preparation for NMR analysis 92
2.2.5 ^{1}H NMR spectroscopic analysis of filtered and non-filtered urine 93
2.2.6 Pre-processing of the spectral data 94
2.3 ^{1}H NMR Drug standards database 94
2.3.1 List of drugs 94
2.3.2 Sample preparation 94
2.3.3 NMR analysis of drug standards 95
2.4 Sepsis cohort of critically ill patients 95
2.4.1 Study patients 95
2.4.2 Sample collection 95
2.4.3 Clinical data collection 95
2.4.4 Sample preparation for NMR analysis 96
2.4.4.1 Urine 96
2.4.4.2 Serum 96
2.4.5 NMR analysis of urine and serum 96
2.5 Pre-processing, data reduction and multivariate statistical data analyses of each NMR dataset 97
2.6 Metabolite identification 99
2.6.1 STOCSY, databases and the literature 99
2.6.2 NMR data: 2D-NMR 100
2.7 UPLC-MS analyses 100

Chapter 3: Validation of ^{1}H NMR spectroscopic analysis of urine as a global metabolic profiling method in critically ill patients **101**
3.1 Introduction 101
3.1.1 Critical illness and sepsis 101
3.1.2 Complexity of the metabolome of patients with critical illness 101
3.2 Aim 102
3.3 Materials and methods 103
3.3.1 Study patients 103
3.3.2 Sample collection 103
3.3.3 Clinical data collection 104
3.3.4 Sample preparation for NMR analysis 107
3.3.5 ^{1}H NMR spectroscopic analyses of filtered and non-filtered urine and multivariate data analyses 107
3.4 Results 107
3.4.1 Patient Meta data - demographics and clinical data of the validation cohort 107
3.4.2 ^{1}H NMR spectroscopy of urine from critically ill patients 109
3.4.3 Methods used to identify metabolites in urinary spectra: non-drugs & drugs 118
3.4.3.1 ^{1}H NMR spectroscopy of drugs commonly used in ICU 118
3.4.3.1.1 Identification of ^{1}H NMR signals of parent drugs using drug standards 118
3.4.3.1.2 Identification of drug metabolites using statistical total correlation spectroscopy (STOCSY) 121
3.4.4 Multivariate statistical analyses of ^{1}H NMR spectra of unfiltered validation cohort urine – organ dysfunction and ICU Survival 127
3.4.5 Multivariate statistical analyses of ^{1}H NMR spectra of unfiltered validation cohort urine - Hydroxyethyl starch classes 133
3.4.6 ^{1}H NMR spectroscopy of filtered urine from critically ill patients 137
3.4.7 Multivariate statistical analyses of ^{1}H NMR spectra of filtered validation cohort urine – organ dysfunction and ICU survival 140
3.5 Discussion 146
3.5.1 ^{1}H NMR spectroscopy as a feasible method of global metabolic profiling of urine from critically ill patients 146
3.5.2 The clinical utility of metabolic profiling based on ^{1}H NMR spectroscopy of urine in predicting outcomes of critically ill patients 150
3.6 Summary 153
Chapter 4: Global metabolic responses in patients with severe sepsis and sepsis-induced organ dysfunction **154**
4.1 Introduction 154
4.2 Aim 154

4.3 Materials and methods 155
4.3.1 Study patients 155
4.3.2 Sample collection 156
4.3.3 Clinical data collection 157
4.3.4 Sample preparation, ^{1}H NMR spectroscopy and pre-processing of the spectral data 159
4.3.5 Multivariate statistical analyses and metabolite identification 159
4.4 Results 160
4.4.1 Patient Meta data - demographics and clinical data of the sepsis cohort 160
4.4.2 ^{1}H NMR spectroscopy-based metabolic profiling of urinary samples 162
4.4.2.1 ^{1}H NMR spectroscopy of urine in severe sepsis 162
4.4.2.2 Multivariate analyses of ^{1}H NMR spectra of urine from patients with severe sepsis: identification of metabolites characterising the clinical classes 168
4.4.3 ^{1}H NMR spectroscopy-based metabolic profiling of serum 173
4.4.3.1 ^{1}H NMR spectroscopy of serum in severe sepsis 173
4.4.3.2 Multivariate analyses of ^{1}H NMR spectroscopy of serum from patients with severe sepsis 180
4.4.3.2.1 Multivariate analyses of 1-D standard ^{1}H NMR spectroscopy of serum from patients with severe sepsis 180
4.4.3.2.2 Multivariate analyses of ^{1}H CPMG NMR spectroscopy of serum from patients with severe sepsis 185
4.5 Discussion 194
4.5.1 Amino acids in sepsis related liver injury 194
4.5.1.1 Increases in serum levels of lysine and methionine 194
4.5.5 Lipoproteins and lipids in sepsis related liver injury 200
4.5.5.1 Decreases in serum levels of VLDL and LDL 200
4.5.5.2 Decreases in serum levels of lipids 203
4.5.6 Placebo versus steroid treatment groups 204
4.5.7 Acute Kidney Injury 206
4.6 Summary 208
Chapter Five: Lipid responses to severe sepsis and sepsis-induced organ dysfunction 209
5.1 Introduction 209
5.2 Aim 210
5.3 Materials and methods 210
5.3.1 Study patients 210
5.3.2 Sample collection 210
5.3.3 Clinical data collection 210

5.3.4 Sample preparation and lipid profiling using ultra-performance liquid chromatography coupled with mass spectroscopy analyses of plasma 211
5.3.4.1 Plasma sample preparation 211
5.3.4.2 UPLC-MS lipid profiling 211
5.3.5 Processing of MS data, multivariate statistical analyses, and metabolite identification 212
5.3.5.1 Selection of statistically significant features (metabolite signals) 213
5.3.5.2 Metabolite identification: MS-MS; MS ^{E} 216
5.4 Results 217
5.4.1 Demographics and clinical data of the sepsis cohort 217
5.4.2 Ultra-Performance Liquid Chromatography-Mass Spectroscopy-based lipid profiling of plasma 218
5.4.2.1 Multivariate analyses of lipid profiling using UPLC-mass spectroscopy: investigation of the lipid metabolites characterising the clinical classes 218
5.4.2.2 Structural assignment of the lipid metabolites characterising the liver dysfunction classes 241
5.4.2.3 Structural assignment of the lipid metabolites characterising haematological dysfunction classes 247
5.5 Discussion 256
5.5.1 Liver dysfunction 256
5.5.2 Haematological dysfunction 269
5.5.3 Placebo versus steroids treatment groups 271
5.6 Summary 272
Chapter 6: Conclusion 274
6.1 Integration of the hypotheses and the empirical findings of the study 274
6.1.1 Validation of metabonomics based on ^{1}H NMR spectroscopic analysis of urine as a global metabolic profiling method in critically ill patients 274
6.1.2 The clinical utility of metabonomics based on 1-D ^{1}H standard NMR analyses of urine and serum in the sepsis cohort 275
6.1.3 Metabolic signatures of acute liver dysfunction in the sepsis cohort demonstrated by ^{1}H CPMG NMR analyses of serum and UPLC-MS analyses of plasma 276
6.2 Unanswered questions 278
6.3 Theoretical and practical implications of the study's findings 281
6.4 Limitations of the study 282
6.5 Future directions 287
References 288
1 Hydroxyethyl Starch Removal Experiments 299
1.1 Introduction: Hydroxyethyl Starch 299

1.2 The removal of Hydroxyethyl Starch 299
1.3 Hypotheses 300
1.4 Aims and objectives 301
1.5 Methodology 301
1.5.1 Materials 301
1.5.2 Precipitation method 1: Iodine and electrolytes 302
1.5.3 Precipitation method 2: Colloidal Iron and electrolytes 302
1.5.3.1 Preparation for NMR analysis 303
1.5.4 Ultrafiltration method 304
1.5.4.1 Preparation for NMR analysis 305
1.5.4.2 NMR analysis of the filtration experiment samples 305
1.5.4.3 Comparison of filtered and unfiltered samples 305
1.6 Results 306
1.6.1 Precipitation method 1: Iodine and electrolytes 306
1.6.2 Precipitation method 2: Colloidal iron and electrolytes 306
1.6.3 Ultrafiltration experiments 308
1.6.4 Hydroxyethyl starch removal 312
1.6.4.1 Centriprep device 312
1.6.4.2 Nasosep device 312
1.6.4.3 Amicon 313
1.6.5 Pre-rinsing of the filters 313
1.7 References 314
Appendix II 315
Appendix III 324

This thesis is dedicated to my family, especially my Dad, Danielle, and Derek.

Acknowledgements

I would like to acknowledge my supervisors Prof Anthony Gordon, Prof Stephen Brett, Dr Jia Li, Prof Elaine Holmes and Dr Panagiotis Vorkas for all their continuous support and help. I am also very grateful for all the help and work from the research team at Imperial NHS Healthcare trust.

I would also like to thank Prof Masao Takata, James Kinross, Mathieu Gaudi, Kirill Veselkov, David Antcliffe, and Prof Jeremy Nicholson.

Declaration of originality

I certify that this thesis (except for the collection of the biofluid samples), and the research to which it refers, are the product of my own work, and that any ideas or quotations from the work of other people, published or otherwise, are fully acknowledged in accordance with the standard referencing practices of the discipline.

Copyright declaration

The copyright of this thesis rests with the author and is made available under a Creative Commons Attribution Non-Commercial No Derivatives licence. Researchers are free to copy, distribute or transmit the thesis on the condition that they attribute it, that they do not use it for commercial purposes and that they do not alter, transform or build upon it. For any reuse or redistribution, researchers must make clear to others the licence terms of this work.

List of figures

Figure 1.1 Illustration of the conversion of longitudinal magnetization (Mz) to transverse (Mxy) magnetization (signal) with the application of a 90° RF pulse. KEY: RF: radiofrequency ……..70

Figure 1. 2 Illustration of the process of Fourier transformation used to convert the NMR time domain signals into a frequency domain spectrum ……72

Figure 1.3 Illustration of 1H NMR spectrum of ethanol demonstrating the singlet, quartet, and triplet of its hydroxy (OH), methylene (CH2) and methyl (CH3) groups, respectively ……73

Figure 1.4 Illustration of the possible spin orientations of methylene (CH2) and methyl (CH3) groups……..73

Figure 1.5 Illustration of the effect of magnet inhomogeneity using a vector model in which two vectors rotating in the transverse plane are used to represent two nuclei magnetisations rotating at different frequencies and the effect of a 180-degree RF pulse. KEY: RF: radiofrequency pulse.
A. Vector b is rotating at a lower frequency due to exposure to lower field strength; whereas vector a is rotating with a higher frequency due to exposure to a higher field strength.
B. Following the application of a 180-degree RF pulse the vectors are rotated around the x axis by 180 degrees resulting in vector b being ahead of vector a.
C. The frequencies of the two vectors remains unchanged with vector b rotating at a slower frequency than vector a. Eventually vector a catches up with vector b and they are then described as being re-focussed……..76

Figure 1.6. A schematic illustration of a topographical map representing a 2-D 1H-1H (homonuclear) NMR COSY spectrum of glutamic acid (From: Anthony Crasto 2-D COSY NMR spectroscopy lecture, online) are shown on left and top, and their corresponding frequency axes are on the right and bottom, respectively. This topographical map demonstrates connectivity of adjacent nuclei by the lack of the same precession frequency in the 2 NMR spectra (2 and 3 and 3 and 4) resulting in cross peaks (in red) that are off the diagonal. Conversely, a lack of connectivity between adjacent nuclei is demonstrated by retention of the same precession frequency in the 2 NMR spectra (2 and 4) resulting in diagonal peaks (in blue)…….78

Figure 1.7 Illustration of different types of PCA outliers. The two-dimensional PCA plane is highlighted in grey. The unnumbered black observations fit the PCA model that is representative of the majority of the dataset and they therefore lie within the Hotelling's perimeter of the scores plot (black ellipse). The green observations are called score outliers. They follow the PCA model and therefore lie within the two-dimensional plane of the scores plot but have extreme score values causing them to lie outside of the Hotelling's perimeter. The blue and red observations are not well represented by the PCA model. They contain variables that are not shared by the majority of the dataset. This causes them to lie outside of two-dimensional plane of the scores plot at perpendicular distance called the orthogonal distance and are called orthogonal outliers. The blue observations have small values for the variables of importance to the two PCs of the PCA and so lie in close proximity to the black observations whereas the red observations have large scores for these variables are therefore both score and orthogonal outliers……84

Figure 3.1 A typical 600MHz 1D 1H NMR spectrum of regions 9.7-4.8 ppm (A) and 4.6-0.8 ppm (B) from a urine sample from a healthy control illustrating the urinary metabolites usually detected by this method of metabolic profiling……..111

Figure 3.2 A 600MHz 1-D 1H NMR spectrum of regions 9.7-4.8 ppm (A) and 4.6-0.8 ppm (B) of urine from an individual from the validation cohort not given the hydroxyethyl starch based fluid Volulyte or any antibiotics, illustrating the metabolites detected by this method in urine from this cohort……112

Figure 3.3 A 600MHz 1-D 1H NMR spectrum of regions 9.7-4.8 ppm (A) and 4.6-0.8 ppm (B) of unfiltered urine from a hydroxyethyl starch (Volulyte) recipient from the validation cohort demonstrating a combination of urinary metabolites typical detected by this method in addition to signals of the hydroxyethyl starch. Key: All the signals marked Co-amoxiclav are signals of the parent drug of Co-amoxiclav unless otherwise indicated; KEY: *: signal present in both Tazocin and Co-amoxiclav drug standard……113

Figure 3.4 A composite of two 600MHz 1-D 1H NMR spectra of regions 9.7-4.8 ppm (A) and 4.6-0.8 ppm (B) of unfiltered urine from individuals from validation cohort, illustrating the differences between spectra from a recipient (red) and non-recipient (blue) of hydroxyethyl starch. ……114

Figure 3.5. A 600MHz 1D ^{1}H NMR spectrum of urine from a recipient of the drug Tazocin as the only antibiotic, or structurally similar drug administered, regions 9.7-4.8 ppm (A) and 4.6-0.8 ppm (B) illustrating the detection of usual urinary metabolites in addition to signals of Tazocin. KEY: *: signal present in both the Tazocin and Co-amoxiclav drug standards……116

Figure 3.6. A 600MHz 1D 1H NMR spectrum of urine from a recipient of the drug of Co-amoxiclav as the only antibiotic, or structurally similar drug administered, divided into 9.7-4.8 ppm (A) and 4.6-0.8 ppm (B) illustrating of the detection of usual urinary metabolites in addition to signals of Co-amoxiclav. KEY: *: signal present in both the Tazocin and Co-amoxiclav drug standards……117

Figure 3.7 A composite of 600MHz 1-D 1H NMR spectra regions 9.7-4.8 ppm (A) and 4.6-0.8 ppm (B) of the Tazocin (red) and Co-amoxiclav (blue) drug standards illustrating signals of these two antibiotics and highlighting their differences……120

Figure 3.8 A 600MHz 1D ^{1}H NMR spectra of the drug standard of Tazocin: δ^{1}H 10-0.5 ppm and inserts of the structure of two components of Tazocin: Piperacillin (top) and Tazobactam (bottom)……124

Figure 3.9. Illustration of the use of 1-D STOSCY of 600MHz 1-D ^{1}H NMR spectra of unfiltered urine from the validation cohort utilising the signal at δ^{1}H 7.48, as the 'driver' peak, to identify parent drug (labelled) and metabolites of the drug Tazocin. Signals from the parent drug are labelled and those with a low correlation with the driver peak are also starred (*)……124

Figure 3.10 600MHz 1D ^{1}H NMR spectra of the drug standard of Co-amoxiclav: δ^{1}H 10 - 0.5 ppm and inserts of the structure of two components of Co-amoxiclav: Amoxicillin (top) and Clavulanic acid (bottom)……125

Figure 3.11 Illustration of the use of 1-D STOSCY of 600MHz 1D 1H NMR spectra of unfiltered urine from the validation cohort utilising the signal at δ1H 7.31ppm as the 'driver' peak, to identify signals of the parent drug (labelled) and metabolites of Co-amoxiclav δ1H 10-0.5ppm. The signal that is both labelled and starred is an example of a signal with a high correlation with the driver peak that is not present in the drug standard of Co-amoxiclav; and may or may not a metabolite of Co-amoxiclav....125

Figure 3.12 A δ^{1}H 9.8 - 0.8 ^{1}H NMR spectra of the hydroxyethyl starch Volulyte drug standard and an insert of the structure the hydroxyethyl starch……126

Figure 3.13 Illustration of the use of 1-D STOSCY of 600MHz 1D 1H NMR spectra of unfiltered urine from the validation cohort utilising the signal at δ1H 3.79ppm as the 'driver' peak, to identify signals of the parent drug (labelled) and metabolites of the hydroxyethyl starch Volulyte……..126

Figure 3.14 PCA scores plot derived from 1H NMR spectra of unfiltered urine from the validation cohort (47 samples) illustrating the metabolic variation of the data set as a whole and three outliers: one extreme (circled in red) and two intermediate outliers (circled in blue) of the perimeter of the Hotelling's T2 95% confidence ellipse……..128

Figure 3.15 PCA scores plot derived from 1H NMR spectra of unfiltered urine from the validation cohort (46 samples) following the exclusion of one extreme outlier illustrating the metabolic variation of this data set as a whole……128

Figure 3.16 PCA scores plot based on 1H NMR spectra of unfiltered urine from the validation cohort taken at time point zero (22 samples) illustrating no separation of samples according to presence (1) or absence (0) of renal dysfunction……129

Figure 3.17 PCA scores plot based on 1H NMR spectra of unfiltered urine from the validation cohort taken at time point one (24 samples) illustrating no separation of samples according to presence (1) or absence (0) of renal dysfunction……..130

Figure 3.18 Scores (A) and loadings (B) plots of a PCA based on 1H NMR spectral data of unfiltered urine from the validation cohort with samples colour coded according to receipt (1) and non-receipt (0) of the hydroxyethyl starch Volulyte. A. PCA scores plot illustrating evidence of separation of the samples based on the receipt of the hydroxyethyl starch. B. PCA Loading Column plot of the first PC demonstrating the contribution of the urinary metabolite signals detected by 1H NMR responsible for the partial separation of the samples based on the receipt of the hydroxyethyl starch by the first PC. This illustrates metabolite signals with the highest positive loadings of the first PC (associated with receipt of HES) between δ1H 6.21-5.53; δ1H 5.49-5.30; δ1H 5.01–4.99; δ1H 4.01-3.71 and δ1H 3.29-3.28ppm. KEY: Colour scale of the loadings ranges from the highest positive and negative loadings in red and blue, respectively. KEY: HES: hydroxyethyl starch.……135

Figure 3.19 O-PLS-DA scores (A) and cross-validated scores (B) plots derived from 1H NMR spectral data of unfiltered urine samples from the validation cohort illustrating separation of samples according to the non-receipt (0) and receipt (1) of the hydroxyethyl starch based fluid Volulyte (R2X=0.237, R2Y =0.695; Q2Y=0.354). The cross-validated scores plot illustrates the significance of the observed group separation measured using a method of CV-ANOVA (p=0.002). The corresponding O-PLS-DA loadings plot (C) illustrating the covariance and correlation coefficients of the metabolite signals of the predictive component of the model responsible for the separation of the two hydroxyethyl starch groups. KEY: CV-ANOVA: cross-validated analysis of variance, HES: hydroxyethyl starch.……136

Figure 3.20 A composite of two 600MHz 1D 1H NMR spectra of urine aliquots taken at the same time point from an individual from the validation cohort given hydroxyethyl starch, one unfiltered (blue) and one filtered (red), prior to NMR analysis. Regions δ1H 9.7-0.5, 9.7-4.8 and 4.6-0.8 ppm of the 1H NMR spectra are shown in Figures (A), (B) and (C), respectively. An illustration of broad signals of HES at δ1H 5.69 (δ1H 5.72-5.59), δ1H 5.55 δ1H (5.60-5.50) and δ1H 5.42 (δ1H 5.46-5.36), a multiplet at δ1H 3.78 (4.09-3.43); a singlet at δ1H 1.92 (acetate); and the greater resolution of the non-HES signals present in the same region following the removal of the starch via filtration……138

Figure 3.21. A composite of two 600MHz 1D 1H NMR spectra of urine aliquots taken at the same time point from an individual from the validation cohort not given hydroxyethyl starch, one unfiltered (blue) and one filtered (red), prior to NMR analysis illustrating of no apparent loss of metabolites associated with use of filtration. Regions δ1H 9.7-0.5, 9.7-4.8 and 4.6-0.8 ppm of the 1H NMR spectra are shown in Figures (A), (B) and (C), respectively……139

Figure 3.22 A PCA scores plot based on 1-D 1H NMR spectral data of all the filtered urine samples from the validation cohort illustrating the metabolic variation of the data set as a whole (60 samples) and three extreme outliers (circled in red)……141

Figure 3.23 A PCA scores plot derived from 1D ^{1}H NMR spectral data of all the filtered urine samples from the validation cohort, following the exclusion of the three extreme outliers, illustrating the metabolic variation of the remaining 57 samples……141

Figure 3.24 A PCA scores plot based on 1-D 1H NMR spectra of filtered urine from the validation cohort taken at time point zero (28 samples) illustrating a lack of separation of samples according to presence (1) or absence (0) of renal dysfunction……..142

Figure 3.25 A PCA scores plot of 1-D ^{1}H NMR spectra of filtered urine from the validation cohort taken at time point one (29 samples) illustrating no clear separation of samples according to presence (1) or absence (0) of renal dysfunction……..143

Figure 4.1. A typical 600MHz 1-D 1H NMR spectrum of regions 9.7-4.8 ppm (A) and 4.6-0.8 ppm (B) from a urine sample from a healthy control illustrating the urinary metabolites usually detected by this method of metabolic profiling……...164

Figure 4.2. A 600MHz 1-D 1H NMR spectrum of urine from a recipient of the drug of Co-amoxiclav as the only antibiotic, or structurally similar drug administered, divided into 9.7-4.8 ppm (A) and 4.6-0.8 ppm (B) illustrating of the detection of usual urinary metabolites in addition to signals of Co-amoxiclav……165

Figure 4.3. A 600MHz 1-D 1H NMR spectrum of urine from a recipient of the drug Tazocin as the only antibiotic, or structurally similar drug administered, regions 9.7-4.8 ppm (A) and 4.6-0.8 ppm (B) illustrating the detection of usual urinary metabolites in addition to signals of tazocin. KEY: *: signal present in both the Tazocin and Co-amoxiclav drug standards……..166

Figure 4.4 A composite of 600MHz 1-D 1H NMR spectra of the Co-amoxiclav (blue) and Tazocin (red) drug standards regions 9.7-4.8 ppm (A) and 4.6-0.8 ppm (B) illustrating signals of these two antibiotics and highlighting their differences……..167

Figure 4.5. A PCA scores plot based on 1-D 1H NMR spectra of all the 125 urinary samples from the sepsis cohort illustrating the metabolic variation of the data set as a whole and one extreme outlying sample (circled in red). Samples from time points 0, 1, 2 and 3 are colour coded in green, blue, red, and yellow, respectively……171

Figure 4.6 PCA scores plot derived from 1-D 1H NMR spectra of 124 of the urinary samples from the sepsis cohort illustrating the metabolic variation of the data set as a whole following the exclusion of the extreme outlier shown in figure 4.5. Samples from time points 0, 1, 2 and 3 are colour coded in green, blue, red, and yellow, respectively……171

Figure 4.7. Typical 600MHz standard 1-D 1H NMR spectrum of regions 9.7-4.8 ppm (A) and 4.6-0.8 ppm (B) from a serum sample from a healthy control illustrating the serum metabolites usually detected by this method of metabolic profiling. KEY: GPC: glycerophosphorylcholine……175

Figure 4.8. Typical 600MHz 1-D CPMG 1H NMR spectrum of regions 9.7-4.8 ppm (A) and 4.6-0.8 ppm (B) from a serum sample from a healthy control illustrating the serum metabolites usually detected by this method of metabolic profiling. KEY: GPC: glycerophosphorylcholine……176

Figure 4.9 A 600MHz standard 1-D 1H NMR spectra of serum from a recipient Co-amoxiclav as the only antibiotic, or structurally similar drug administered from the sepsis cohort, divided into 9.7-4.8 ppm (A) and 4.6-0.8 ppm (B) illustrating of the detection of serum metabolites in addition to signals of Co-amoxiclav. KEY: GPC: glycerophosphorylcholine……..177

Figure 4.10 A 600MHz CPMG 1H NMR spectra of serum from a recipient Co-amoxiclav as the only antibiotic, or structurally similar drug administered from the sepsis cohort, divided into 9.7-4.8 ppm (A) and 4.6-0.8 ppm (B) illustrating of the detection of serum metabolites in addition to signals of Co-amoxiclav. KEY: GPC: glycerophosphorylcholine……178

Figure 4.11 A PCA scores plot based on 1-D standard 1H NMR spectra of all 100 serum samples from the sepsis cohort illustrating the metabolic variation of the data set as a whole and seven outlying samples: two extreme (circled in red) and five in close proximity to other samples (circled in blue). Samples from time points 0, 1, 2 and 3 are colour coded in green, blue, red, and yellow, respectively……182

Figure 4.12. A PCA scores plot derived from 1-D standard 1H NMR spectra of 98 serum samples from the sepsis cohort illustrating the metabolic variation of the data set as a whole following the exclusion of two extreme outlying samples shown in Figure 4.11. Samples from time points 0, 1, 2 and 3 are colour coded in green, blue, red, and yellow, respectively……182

Figure 4.13. A PCA scores plot based on 1-D CPMG 1H NMR spectra of all the 100 serum samples from the sepsis cohort illustrating the metabolic variation of the data set as a whole and two extreme outliers (circled in red). Samples from time points 0, 1, 2 and 3 are colour coded in green, blue, red, and yellow, respectively)……186

Figure 4.14. A PCA scores plot of 1-D CPMG 1H NMR spectra of 98 serum samples from the sepsis cohort illustrating the metabolic variation of the data set as a whole following the exclusion of two extreme outlying samples shown in Figure 4.13. Samples from time points 0, 1, 2 and 3 are colour coded in green, blue, red, and yellow, respectively……..186

Figure 4.15. A PCA scores plot derived from 1-D CPMG 1H NMR spectra of serum samples from the sepsis cohort from time point three (day seven) illustrating a degree of separation according to their acute liver dysfunction classes. KEY: Group 0: no acute liver dysfunction (green); Group 1: acute liver dysfunction (blue)……187

Figure 4.16. O-PLS-DA scores (A) and cross validated scores (B) plots derived from 1-D CPMG 1H NMR spectra of serum from the sepsis cohort taken at time point three (day seven) illustrating separation of samples according to the presence or absence of acute liver dysfunction (R2X=0.175, R2Y=0.639; Q2Y=0.340). The cross-validated scores plot illustrates the significance of the observed group separation measured using a method of CV-ANOVA (p=0.029). The corresponding O-PLS-DA loadings plot (C) illustrating the covariance and correlation coefficients of the metabolite signals of the

predictive component of the model responsible for the separation of the acute liver injury groups. KEY: CV-ANOVA: cross-validated analysis of variance, UNK: unknown.....191

Figure 5.1 Metabolite feature selection initial screening process. KEY: P(corr): correlation coefficient, P [1]: covariance; reject R.....215

Figure 5.2. PCA scores plots of lipid profiles based on positive mode UPLC-MS of the plasma samples from the sepsis cohort from all four time points (n=154) labelled according to their liver injury groups: no injury in green (group 0) and liver injury in blue (group 1). This demonstrates a degree of separation of the samples according to their liver injury classes along the second principal component. KEY: PC: principal component.....220

Figure 5.3. PCA scores plots of lipid profiles based on negative mode UPLC-MS of the plasma samples from the sepsis cohort from all four time points (n=154) labelled according to their liver injury groups: no injury in green (group 0) and liver injury in blue (group 1). This illustrates partial separation along the first PC that appears in part to be related to metabolic changes of liver injury. KEY: PC: principal component.....220

Figure 5.4. OPLS-DA scores plot (A) and cross-validated scores plot (B) based on positive mode (ESI) lipid profiling using UPLC-MS of plasma samples from the sepsis cohort taken at time point zero. This demonstrates evidence of separation between acute liver dysfunction (blue) and no liver dysfunction (R2X=0.118, R2Y=0.618; Q2Y=0.243). Both models misclassified two samples from each group (four and six from the group without dysfunction and five and 11 from group with dysfunction). The cross-validated model (p=0.047) misclassified three additional samples from the group without dysfunction (10, 14 and 24). KEY: ESI: electron spray ionisation.....226

Figure 5.5. OPLS-DA scores plot (A) and cross-validated scores plot (B) derived from positive mode (ESI) lipid profiling using UPLC-MS spectroscopy spectra of plasma samples from the sepsis cohort taken at time point one. This demonstrates evidence of separation of the samples according to metabolic changes associated with acute liver dysfunction (blue) from those without acute liver dysfunction (green) (R2X=0.105, R2Y=0.490; Q2Y=0.208). Six of the 30 no dysfunction samples (eight, 11, 16, 39, 42 and 44) and four of the 20 dysfunction samples (four, nine 17 and 31) were misclassified by both models. The cross-validated model (p=0.004) misclassified five additional samples: three from the no dysfunction group (one, 47 and 49) and two from the dysfunction group (28 and 32).....227

Figure 5.6. OPLS-DA scores plot (A) and cross-validated scores plot (B) derived from positive mode (ESI) lipid profiling using UPLC-MS spectroscopy spectra of plasma samples from the sepsis cohort taken at time point two. This demonstrates evidence of separation of the samples according to metabolic changes associated with acute liver dysfunction (blue) from those without acute liver dysfunction (green) (R2X=0.140, R2Y=0.864; Q2Y=0.401). The un-cross validated model demonstrated no misclassified samples. The cross-validated model (p=1.60E-04) demonstrated seven misclassified samples: four samples from the group without dysfunction and three from the group with dysfunction.....228

Figure 5.7. OPLS-DA scores plot (A) and cross-validated scores plot (B) derived from positive mode (ESI) lipid profiling using UPLC-MS spectroscopy spectra of plasma samples from the sepsis cohort taken at time point three. This demonstrates evidence of separation of the samples according to metabolic changes associated with acute liver dysfunction (blue) from those without acute liver dysfunction (green) (R2X=0.352, R2Y=0.938; Q2Y=0.5). The un-cross validated model demonstrated no misclassified samples. The cross-validated model (p=0.006) demonstrated seven misclassified samples: five samples from the group without dysfunction and two from the group with dysfunction.....229

Figure 5.8. OPLS-DA scores plot (A) and cross-validated scores plot (B) derived from negative mode (ESI) lipid profiling using UPLC-MS spectroscopy spectra of plasma samples from the sepsis cohort taken at time point zero. This demonstrates evidence of separation of the samples according to metabolic changes associated with acute liver dysfunction (blue) from those without acute liver dysfunction (green) (R2X=0.095, R2Y=0.722; Q2Y=0.281). Both models demonstrated the misclassification of one no dysfunction group sample (10). The cross-validated model (p=0.026) misclassified six additional samples: three from group without dysfunction (four, 11 and 24) and three from group with dysfunction (five, eight and 20)…….....230

Figure 5.9. OPLS-DA scores plot (A) and cross-validated scores plot (B) derived from negative mode (ESI) lipid profiling using UPLC-MS spectroscopy spectra of plasma samples from the sepsis cohort taken at time point one. This demonstrates evidence of separation of the samples according to metabolic changes associated with acute liver dysfunction (blue) from those without acute liver dysfunction (green) (R2X=0.105, R2Y=0.591; Q2Y=0.383). Both models demonstrated the misclassification of eight samples: four from the group without dysfunction (eight, 16, 42 and 44) and four from the group with dysfunction (four, nine, 31 and 32). The cross-validated model (p=1.19E-05) misclassified additional samples: two from the group without dysfunction (14, 16, 21and 46) and three from the group with dysfunction (14, 34 and 45)…….231

Figure 5.10. OPLS-DA scores plot (A) and cross-validated scores plot (B) derived from negative mode (ESI) lipid profiling using UPLC-MS spectroscopy spectra of plasma samples from the sepsis cohort taken at time point two. This demonstrates evidence of separation of the samples according to metabolic changes associated with acute liver dysfunction (blue) from those without acute liver dysfunction (green) (R2X=0.103, R2Y=0.643; Q2Y=0.438). Both models demonstrated the misclassification of six samples: three from group without the dysfunction (eight, 10 and 44) and three from the group with dysfunction (four, 31 and 43). The cross-validated plot (p=2.36E-06) misclassified three additional samples: one by the group without dysfunction (25) and two by the group with dysfunction (six and 17)…….232

Figure 5.11. OPLS-DA scores plot (A) and cross-validated scores plot (B) derived from negative mode (ESI) lipid profiling using UPLC-MS spectroscopy spectra of plasma samples from the sepsis cohort taken at time point three. This demonstrates evidence of separation of the samples according to metabolic changes associated with acute liver dysfunction (blue) from those without acute liver dysfunction (green) (R2X=0.182, R2Y=0.525; Q2Y=0.315). Both models demonstrated the misclassification of five samples: three from group without the dysfunction (six, 24 and 31) and two from the group with dysfunction (21 and 27). The cross-validated plot (p=0.005) misclassified one additional sample from each group, (seven and 25, for group without and with dysfunction, respectively).....233

Figure 5.12. OPLS-DA scores plot (A) and cross-validated scores plot (B) derived from positive mode (ESI) lipid profiling using UPLC-MS spectroscopy spectra of plasma samples from the sepsis cohort taken at time point two. This demonstrates evidence of separation of the samples according to metabolic changes associated with acute haematological dysfunction (blue) from those without acute haematological dysfunction (green) (R^2X=0.165, R^2Y=0.778; Q^2Y=0.299). One samples from each group was misclassified by the un-crossed validated model (A). The cross-validated model (p=0.004) demonstrated 14 samples that were misclassified: seven from each group. ……..236

Figure 5.13. OPLS-DA scores plot (A) and cross-validated scores plot (B) derived from positive mode (ESI) lipid profiling using UPLC-MS spectroscopy spectra of plasma samples from the sepsis cohort taken at time point three. This demonstrates evidence of separation of the samples according to metabolic changes associated with acute haematological dysfunction (blue) from those without acute

haematological dysfunction (green) (R^2X=0.167, R^2Y=0.538; Q^2Y=0.322). One sample from the group without dysfunction (23) and three from the group with dysfunction (four, nine and 26) were misclassified by both model. The cross-validated model (p=0.004) misclassified four additional samples: one from group without dysfunction (seven) and three from the group with dysfunction (10, 12 and 31)……237

Figure 5.14. OPLS-DA scores plot (A) and cross-validated scores plot (B) derived from negative mode (ESI) lipid profiling using UPLC-MS spectroscopy spectra of plasma samples from the sepsis cohort taken at time point three. This demonstrates evidence of separation of the samples according to metabolic changes associated with acute haematological dysfunction (blue) from those without acute haematological dysfunction (green) (R^2X=0.187, R^2Y=0.505; Q^2Y=0.281). Both models misclassified six samples: one from the group without dysfunction (23) and five from the group with dysfunction (four, nine, 12, 22 and 26). The cross-validated model (p=0.01) misclassified two additional samples from the group with dysfunction (27 and 31)……238

List of tables

Table 1.1 Animal metabolic profiling studies of sepsis. KEY: ANOVA: analysis of variance, BCAA: branched-chain amino acid, CLP: caecal ligation and puncture, FA: fatty acids, FDR: false discovery rate, GPC: glycerophosphocholine, lysoPC: lysophosphatidylcholine, O-PLS: orthogonal-PLS, PC: phosphatidylcholine, PLS: projection to latent structures, PLS-DA: PLS-discriminative analysis, PCA: principal component analysis; TAG: triacylglycerides.....47

Table 1.2 Clinical metabolic profiling studies of critically ill patients with non-infected SIRS and sepsis. KEY: 11-HETE: 11-hydroxyeicosatetraenoic acid, ANOVA: analysis of variance, AA: arachidonic acid, BCAA: branched-chain amino acid, COX: cyclooxygenase, FDR: false discovery rate, FA: fatty acid, GPC: glycerophosphocholine, HC: healthy control, lysoPC: lysophosphatidylcholine, MODS: multi-organ dysfunction syndrome, O-PLS: orthogonal-PLS, PC: phosphatidylcholine; PLS: projection to latent structures, PLS-DA: PLS-discriminative analysis, PCA: principal component analysis, PGE2: prostaglandin E2, SIRS: systemic inflammatory response syndrome, TAG: triacylglyceride, TCA: tricarboxylic acid; TXB2: thromboxane B2.....58

Table 3.1 Acute Physiology and Chronic Health Evaluation II scoring system. APACHE II score is the sum of the Acute Physiology Score (A), age points (B) and the chronic health status points (C). Key: A-a DO2: alveolar to arterial oxygen gradient; FiO2: fractional inspired O2, K: potassium, Na: sodium.....105

Table 3.2 Sequential Organ Failure Assessment (SOFA) scoring system. Key: *: with respiratory support; ~: adrenergic agents administered for at least 1 hour; doses in µg/kg per minute.....106

Table 3.3 Acute Kidney Injury Network (AKIN) scoring system. Key SCr: serum creatinine.....106

Table 3.4 Characteristics of the validation cohort: demographics and baseline clinical variables (A) including the baseline Acute Kidney Injury Network (AKIN) and Sequential Organ Failure Assessment (SOFA) scores in more detail (B). Key: APACHE II: Acute Physiology and Chronic Health Evaluation II, COPD: Chronic Obstructive Pulmonary Disease, ICU: Intensive Care Unit, IHD: Ischaemic Heart Disease, IQR: interquartile range, NYHA: New York Heart Association functional classification, *: SOFA scores with the exception of renal, which is AKIN score.....108

Table 3.5 Non-drug metabolites identified in the 600MHz 1-D 1H NMR spectra of urine from (i) the validation cohort and (ii) the healthy control shown in Figure 3.1 and their chemical shifts and signal multiplicities. Key: s: singlet; d: doublet; t: triplet; q: quartet; o: octet; m: multiplet; bs: broad signal; dd: doublet of doublets.....115

Table 3.6. Results of the evaluation parameters of PCAs of 1-D 1H NMR spectra of unfiltered urine from the validation cohort taken at time points zero and one: the percentage of the variation explained (R2X) and predicted (Q2X) by the model. KEY: PC: principal component.....130

Table 3.7 Results of the evaluation parameters of O-PLS-DA models based on 1-D 1H NMR spectra of unfiltered urine from the validation cohort taken at time points zero and one. Illustration of the percentage of the variation explained by the X (R2X) and Y matrices (R2Y) and predicted by the Y matrix* (Q2Y) of the models evaluating samples based on their renal, liver and ICU survival classes. Key: CV-ANOVA: cross-validated analysis of variance, *: Y matrix contains the class information.....132

Table 3.8 Results of the evaluation parameters of O-PLS-DA models based on 1-D 1H NMR spectra of unfiltered urine from the validation cohort at time points zero and one. Illustration of the percentage of the variation explained by the X (R2X) and Y matrices (R2Y) and predicted by the Y matrix* (Q2Y) of the models evaluating samples based on their respiratory, cardiovascular, haematological, and central

nervous system classes with the samples divided into two (A) and five groups (B). Key: CV-ANOVA: cross-validated analysis of variance; SOFA: Sequential Organ Failure Assessment, *: Y matrix contains the class information……..132

Table 3.9 Results of the evaluation parameters of PCAs of 1-D 1H NMR spectra of filtered urine from the validation cohort taken at time points one and two: the percentage of the variation explained (R2X) and predicted (Q2X) by the model. KEY: PC: principal component. ……142

Table 3.10 Results of the evaluation parameters of O-PLS-DA models based on 1-D 1H NMR spectra of filtered urine from the validation cohort taken at TP0 and TP1. Illustration of the percentage of the variation explained by the X (R2X) and Y matrices (R2Y) and predicted by the Y matrix* (Q2Y) of the models evaluating samples based on their renal, liver and ICU survival classes. Key: CV-ANOVA: cross-validated analysis of variance, *: Y matrix contains the class information……144

Table 3.11 Results of the evaluation parameters of O-PLS-DA models based on 1-D 1H NMR spectra of filtered urine from the validation cohort taken at TP0 and TP.1 Illustration of the percentage of the variation explained by the X (R2X) and Y matrices (R2Y) and predicted by the Y matrix* (Q2Y) of the models evaluating samples based on their respiratory, cardiovascular, haematological, and central nervous system classes with the samples divided into two (A) and five groups (B). Key: CV-ANOVA: cross-validated analysis of variance, SOFA: Sequential Organ Failure Assessment, *: Y matrix contains the class information……..145

Table 4.1 Characteristics of the sepsis cohort: demographics and baseline clinical variables (A) including the baseline Acute Kidney Injury Network (AKIN) and Sequential Organ Failure Assessment (SOFA) scores in more detail (B and C: for all patients with urine and serum samples available, respectively). Key: APACHE II: Acute Physiology and Chronic Health Evaluation II, COPD: Chronic Obstructive Pulmonary Disease, ICU: Intensive Care Unit, IHD: Ischaemic Heart Disease, IQR: interquartile range, NYHA: New York Heart Association functional classification, *: SOFA scores except for renal, which are AKIN scores……161

Table 4.2 Results of the evaluation parameters of PCAs based on 1-D 1H NMR spectra of urine from the sepsis cohort. Key: PC: principal component; R2X and Q2X: variation explained and predicted by the model, respectively. ……172

Table 4.3. Results of the evaluation parameters of O-PLS-DA models of 1-D 1H NMR spectra of urine from the sepsis cohort. Illustration of the percentage of the variation explained by the X (R2X) and Y matrices (R2Y) and predicted by the Y matrix (Q2Y) of the models evaluating samples based on five clinical classes: the development of AKI after TP0, acute kidney injury*, acute liver injury*, 28-day survival and treatment group. KEY: CV-ANOVA: cross-validated analysis of variance, Group 0: good outcome (no injury or survival) or placebo treatment group, Group 1: poor outcome (injury or non-survival) or hydrocortisone treatment group, TP: time point; *: at that time point……..172

Table 4.4 Results of the evaluation parameters of O-PLS-DA models of 1-D 1H NMR spectra of urine from the sepsis cohort. Illustration of the percentage of the variation explained by the X (R2X) and Y matrices (R2Y) and predicted by the Y matrix (Q2Y) of the models evaluating samples based on their respiratory, cardiovascular, and haematological clinical classes with the samples divided into two (A) and five groups (B). KEY: CV-ANOVA: cross-validated analysis of variance, SOFA: Sequential Organ Failure Assessment, TP: time point……173

Table 4.5 Non-drug metabolites identified in 600MHz standard 1-D 1H NMR spectra of urine, and 1-D standard and CPMG 1H NMR spectra of serum from: (i) the sepsis cohort and (ii) the healthy control (shown above) and their chemical shifts and signal multiplicities. Key: s: singlet; d: doublet; t: triplet; q: quartet; o: octet; m: multiplet; bs: broad signal; dd: doublet of doublets……179

Table 4.6. Results of the evaluation parameters of PCAs based on 1-D standard 1H NMR spectra of serum from the sepsis cohort. Key: PC: principal component; R2X and Q2X: variation explained and predicted by the model, respectively……..183

Table 4.7 Results of the evaluation parameters of O-PLS-DA models of 1-D standard 1H NMR spectra of serum from the cohort. Illustration of the percentage of the variation explained by the X (R2X) and Y matrices (R2Y) and predicted by the Y matrix (Q2Y) of the models evaluating samples based on five clinical classes: the development of AKI after TP0, acute kidney injury*, acute liver injury*, 28-day survival and treatment group. KEY: CV-ANOVA: cross-validated analysis of variance, Group 0: good outcome (no injury or survival) or placebo treatment group, Group 1: poor outcome (injury or non-survival) or hydrocortisone treatment group, TP: time point; *: at that time point……183

Table 4.8 Results of the evaluation parameters of O-PLS-DA models of 1-D standard 1H NMR spectra of serum from the cohort. Illustration of the percentage of the variation explained by the X (R2X) and Y matrices (R2Y) and predicted by the Y matrix (Q2Y) of the models evaluating samples based on their respiratory, cardiovascular, and haematological clinical classes with the samples divided into two (A) and five groups (B). KEY: CV-ANOVA: cross-validated analysis of variance, SOFA: Sequential Organ Failure Assessment, TP: time point……184

Table 4.9 Results of the evaluation parameters of PCAs based on 1-D CPMG 1H NMR spectra of serum from the sepsis cohort. Key: R2X and Q2X: variation explained and predicted by the model, respectively ……..189

Table 4.10. Composition and evaluation parameters of O-PLS-DA models of 1-D CPMG 1H NMR spectra of serum from the sepsis cohort. Illustration of the percentage of the variation explained by the X (R2X) and Y matrices (R2Y) and predicted by the Y matrix (Q2Y) of the models evaluating samples based on five clinical classes: the development of AKI after TP0, acute kidney injury*, acute liver injury*, 28-day survival and treatment group. KEY: CV-ANOVA: cross-validated analysis of variance, Group 0: good outcome (no injury or survival) or placebo treatment group, Group 1: poor outcome (injury or non-survival) or hydrocortisone treatment group, TP: time point; *: at that time point……189

Table 4.11 Results of the evaluation parameters of O-PLS-DA models of 1-D CPMG 1H NMR spectra of serum from the cohort. Illustration of the percentage of the variation explained by the X (R2X) and Y matrices (R2Y) and predicted by the Y matrix (Q2Y) of the models evaluating samples based on their respiratory, cardiovascular, and haematological clinical classes with the samples divided into two (A) and five groups (B). KEY: CV-ANOVA: cross-validated analysis of variance, SOFA: Sequential Organ Failure Assessment, TP: time point……190

Table 4.12. Metabolic differences identified by O-PLS-DA models of acute liver injury based on 1H NMR CPMG spectra of serum taken at time point three (day seven) from the sepsis cohort, constructed with one predictive and no orthogonal components. The percentage of the variation explained by the X (R2X) and Y matrices (R2Y), and predicted by the Y matrix (Q2Y) of this model was 0.175, 0.639 and 0.340, respectively, and the p value of the CV-ANOVA was 0.029. Key: CV-ANOVA: cross-validated analysis of variance, s: singlet; d: doublet; t: triplet; q: quartet; m: multiplet; bs: broad signal; ↑ and ↓: increased and decreased levels of metabolites in acute liver injury compared with patients without liver injury, respectively……193

Table 5.1 Characteristics of the sepsis cohort: demographics and baseline clinical variables (A) including the baseline Acute Kidney Injury Network (AKIN) and Sequential Organ Failure Assessment (SOFA) scores in more detail (B) for all patients with plasma samples available. Key: APACHE II: Acute Physiology and Chronic Health Evaluation II, COPD: Chronic Obstructive Pulmonary Disease, ICU: Intensive Care Unit, IHD: Ischaemic Heart Disease, IQR: interquartile range, NYHA: New York Heart Association functional classification, *: SOFA scores except for renal, which are AKIN scores……217

Table 5.2 Summary of the principal component analysis models of lipid profiling based on positive (A) and negative (B) mode UPLC-MS analyses of the plasma samples from the sepsis cohort. Key: PC: principal component; R2X and Q2X: variation explained and predicted by the model, respectively……221

Table 5.3. Results of the evaluation parameters of OPLS-DA models derived from a lipid profiling method based on positive (A) and negative mode (B) UPLC-MS analyses of the plasma samples from the sepsis cohort. Illustration of the percentage of the variation explained by the X (R2X) and Y matrices (R2Y) and predicted by the Y matrix (Q2Y) of the models evaluating samples based on five clinical classes: the development of AKI after TP0, acute kidney injury*, acute liver injury*, 28-day survival and treatment group. KEY: CV-ANOVA: cross-validated analysis of variance, Group 0: good outcome (no injury or survival) or placebo treatment group, Group 1: poor outcome (injury or non-survival) or hydrocortisone treatment group, TP: time point; *: at that time point……224

Table 5.4 Results of the evaluation parameters of OPLS-DA models derived from a lipid profiling method based on positive (A) and negative mode (B) UPLC-MS analyses of the plasma samples from the sepsis cohort. Illustration of the percentage of the variation explained by the X (R2X) and Y matrices (R2Y) and predicted by the Y matrix (Q2Y) of the models evaluating samples based on their respiratory, cardiovascular, and haematological clinical classes with the samples divided into two groups. KEY: CV-ANOVA: cross-validated analysis of variance, TP: time point……235

Table 5.5 Results of the evaluation parameters of OPLS-DA models derived from a lipid profiling method based on positive (A) and negative mode (B) UPLC-MS analyses of the plasma samples from the sepsis cohort. Illustration of the percentage of the variation explained by the X (R2X) and Y matrices (R2Y) and predicted by the Y matrix (Q2Y) of the models evaluating samples based on their respiratory, cardiovascular, and haematological clinical classes with the samples divided into five groups. KEY: CV-ANOVA: cross-validated analysis of variance, SOFA: Sequential organ failure assessment, TP: time point……..240

Table 5.6 List of the statistically significant features of the OPLS-DA models of liver dysfunction derived from positive (A) and negative (B) ESI modes of lipid profiling using UPLC-MS of plasma samples from the sepsis cohort taken at enrolment to the study (TP0) and days one (TP1), two (TP2), and seven (TP3), after enrolment.

KEY: ESI: electrospray ionization; m/z: mass-to-charge ratio; ΔDa (found - theoretical m/z): difference between the identified metabolite and the theoretical m/z in Daltons; p(1) and p(corr): covariance and correlation coefficient of the metabolite to the clinical class of the OPLS-DA model, where a positive correlation means higher concentrations of the metabolites in the liver dysfunction group compared to the non-dysfunction group; QC CV: cross variance of the metabolite concentration in the quality control samples; MS/MS: tandem MS; MSE: an iterative process of MS leading to the generation of non-selective metabolite fragments; TP: time point; values highlighted in red: a p value of >0.05 (non-statistically significant) on univariate t-testing comparing the liver dysfunction and non-liver dysfunction groups; values highlighted in blue: low p (corr) i.e. between > -0.4 and < 0.4; values highlighted in bold: QC CV >30%.

For all the phospholipids, the abbreviations refer to the head group (fatty acid at sn-1: sn-2 positions) PC: phosphatidylcholine; PC (0-): phosphatidylcholine ether; lysoPC: lysophosphatidylcholine; PI: phosphatidylinositol; SM: sphingomyelin; UKN: unknown i.e. unidentified……243

Table 5.7 List of the structurally assigned statistically significant features of the OPLS-DA models of haematological dysfunction derived from positive ESI modes of lipid profiling using UPLC-MS of plasma samples from the sepsis cohort taken on days two (TP2), and seven (TP3), after enrolment.

KEY: ESI: electrospray ionization; m/z: mass-to-charge ratio; ΔDa (found - theoretical m/z): difference between the identified metabolite and the theoretical m/z in Daltons; p(1) and p(corr): covariance and correlation coefficient of the metabolite to the clinical class of the OPLS-DA model, where a negative correlation means higher concentrations of the metabolites in the haematological dysfunction group compared to the non-dysfunction group; QC CV: cross variance of the metabolite concentration in the quality control samples; MS/MS: tandem MS, MSE: an iterative process of MS leading to the generation of non-selective metabolite fragments; TP: time point; values highlighted in red: a p value of >0.05 (non-statistically significant) on univariate t-testing comparing the liver dysfunction and non-liver dysfunction groups; values highlighted in bold: QC CV >30%.

For all the phospholipids, the abbreviations refer to the head group (FA at sn-1: sn-2 positions) PC: phosphatidylcholine; PC (0-): phosphatidylcholine ether; lysoPC: lysophosphatidylcholine; SM: sphingomyelin……..249

Table 5.8 List of the unidentified statistically significant features of the OPLS-DA models of haematological dysfunction derived from positive ESI modes of lipid profiling using UPLC-MS of plasma samples from the sepsis cohort taken on days one (TP1), two (TP2), and seven (TP3), after enrolment; only features that were present in two or more of the models are shown here.

KEY: ESI: electrospray ionization; m/z: mass-to-charge ratio; p(1) and p(corr): covariance and correlation coefficient of the metabolite to the clinical class of the OPLS-DA model, where a negative correlation means higher concentrations of the metabolites in the haematological dysfunction group compared to the non-dysfunction group; QC CV: cross variance of the metabolite concentration in the quality control samples; TP: time point……..251

Table 5.9 List of the structurally assigned statistically significant features of the OPLS-DA models of haematological dysfunction derived from negative ESI modes of lipid profiling using UPLC-MS of plasma samples from the sepsis cohort taken on day seven (TP3), after enrolment.

KEY: ESI: electrospray ionization; m/z: mass-to-charge ratio; ΔDa (found - theoretical m/z): difference between the identified metabolite and the theoretical m/z in Daltons; TP: time point; p(1) and p(corr): covariance and correlation coefficient of the metabolite to the clinical class of the OPLS-DA model, where a negative correlation means higher concentrations of the metabolites in the haematological dysfunction group compared to the non-dysfunction group; QC CV: cross variance of the metabolite concentration in the quality control samples; MS/MS: tandem MS, MSE: an iterative process of MS leading to the generation of non-selective metabolite fragments.

For all the phospholipids, the abbreviations refer to the head group (fatty acid at sn-1: sn-2 positions) PC: phosphatidylcholine; PC (0-): phosphatidylcholine ether; lysoPCs: lysophosphatidylcholine; SM: sphingomyelin……..253

Table 5.10 List of the unidentified statistically significant features of the OPLS-DA models of haematological dysfunction derived from negative ESI modes of lipid profiling using UPLC-MS of plasma samples from the sepsis cohort taken on day seven (TP3), after enrolment.

KEY: ESI: electrospray ionization; m/z: mass-to-charge ratio; p(1) and p(corr): covariance and correlation coefficient of the metabolite to the clinical class of the OPLS-DA model, where a negative correlation means higher concentrations of the metabolites in the haematological dysfunction group compared to the non-dysfunction group; QC CV: cross variance of the metabolite concentration in the quality control samples; TP: time point……..254

List of abbreviations

1-D, 2-D; 3-D	1-dimensional, 2-dimensional; 3-dimensional
11-HETE	11-hydroxyeicosatetraenoic acid
α-GST	alpha-glutathione S-transferase
A-a DO_2	alveolar–arterial oxygen
AKI	acute kidney injury
AKIN	acute kidney injury network
ALI	acute lung injury
ANOVA	analysis of variance
APACHE II	Acute Physiology and Chronic Health Evaluation II
Apo	apoprotein
ATP	adenosine triphosphate
AUROC	area under the receiver operating characteristic
BCAA	branched chain amino acids
C*n1:n2*	carbon chain with *n1* number of carbon atoms and *n2* number of double bonds
CAPSOD	Community Acquired Pneumonia & Sepsis Outcome Diagnostics
CE	esterified cholesterol
CLP	caecal ligation and puncture
CoA	coenzyme A
COPD	Chronic Obstructive Pulmonary Disease
CPMG	Carr-Purcell-Meiboom-Gill
CysC	cystatin C
DHAP	Dihydroxyacetone phosphate
DMA	dimethylamine
DNA	deoxyribonucleic acid
ED	emergency department
EGDT	early goal directed therapy
FA	fatty acids
FC	free cholesterol
FDR	false discovery rate

FID	free induction decay
FiO_2	fractional inspired O_2
FT	Fourier transformation
G-3-P	glycerol-3-phosphate
GFR	glomerular filtration rate
GPC	glycerophosphorylcholine
GS	gas chromatography
HC	healthy control
HES	hydroxyethyl starch
HDL	high density lipoprotein
HPLC	high performance liquid chromatography
Hz	Hertz
ICG-PDR	indocyanine green plasma disappearance rates
ICNARC	Intensive Care National Audit & Research Centre
ICU	Intensive care unit
IgA	immunoglobulin A
IHD	ischaemic Heart Disease
IL-1β	interleukin-1 beta
IL-6	interleukin-6
IV	intravenous
LC	liquid chromatography
LP	lipoprotein
LPCAT2	lysophosphatidylcholine acyltransferase 2
LPS	lipopolysaccharide
Lyso-PC	lysophosphatidylcholine
MODS	multi-organ dysfunction syndrome
mPGES-1	microsomal prostaglandin E synthase-1
MS	mass spectrometry
MVA	multivariate statistical analyses
m/z	mass to charge ratio
NGAL	neutrophil gelatinase-associated lipocalin

NMR	nuclear magnetic resonance
NYHA	New York Heart Association functional classification
O-PLS-DA	orthogonal signal correction-projection to latent structures-discriminant analysis
OSC	orthogonal signal correction
PAF	platelet activating factor
PC	phosphorylcholine
PCaa	diacyl-glycerophosphatidylcholine
PCA	principal component analysis
pCysC	plasma cystatin C
PEA	phosphorylethanolamine
PGE_2	prostaglandin E_2
PI	phosphatidylinositol
PI3Kγ	phosphoinositide 3 kinase-gamma
PL	phospholipid
PLA_2	Phospholipase A_2
PLS	projection to latent structures
PLS-DA	projection to latent structures-discriminant analysis
PPV	positive predictive value
pre-β-HDL	pre-beta-high density lipoprotein
PROWESS	protein C worldwide evaluation in severe sepsis
PUFA	polyunsaturated fatty acid
Q-TOF	quadrupole time-of-flight
R^2	percentage of the variation explained by
RCT	randomised controlled trial
RD	recycle delay
RF	radio frequency
RIFLE	risk, injury, failure, loss, and end-stage kidney injury
RoCI	registry of critical illness
RNA	ribonucleic acid
RRT	renal replacement therapy
SIRS	systemic inflammatory response syndrome

SM	sphingomyelin
SOFA	sequential organ failure assessment
SR-AKI	sepsis-related acute kidney injury
SRLI	sepsis-related liver injury
STOCSY	statistical total correlation spectroscopy
sTNF-α RI	serum tumour necrosis factor-alpha receptor type one
TAG	triacylglycerol
TCA	tricarboxylic acid
TMA	trimethylamine
TMAO	trimethylamine-*N*-oxide
TNF-α	tumour necrosis factor-a
TMSP-d_4	3-(trimethylsilyl)-propionate-2,2,3,3-d_4
TOF	time-of-flight
TP	time point
TXB_2	thromboxane B_2
uCysC	urinary cystatin C
UPLC-MS	ultra-performance liquid chromatography-mass spectrometry
UKN	unknown

List of symbols

δ	chemical shift
B_o	external magnetic field
ΔE	energy difference between two states
F1, F2	frequency axes in a 2-D NMR spectrum
h	Planck's constant (6.626 x 1034 J-S)
I	nuclear spin quantum number
J	coupling constant
M_{xy}	transverse magnetisation
M_z	longitudinal magnetisation
γ	magnetogyric ratio
t_1	NMR experiment variable time
t_2	NMR experiment acquisition time
t_m	NMR experiment mixing time
v_0	frequency
ω_0	Larmor frequency
X, Y	represent a number of data matrices

Chapter 1: Introduction

1.1 Aims and objectives

The aim of the work described in this Thesis was to characterise the metabolic response of patients with severe sepsis and determine metabolic signatures associated with their clinical outcomes using methods of metabolic profiling based on both ^{1}H-Nuclear magnetic resonance (NMR) and mass spectroscopy (MS). This is divided into three parts. The first part was an exploration of the feasibility of ^{1}H-Nuclear magnetic resonance spectroscopy as a method of global metabolic profiling in patients with critical illness, of which severe sepsis is a leading cause. This included the development of a ^{1}H-nuclear magnetic resonance database of drug standards as a reference to aid the identification of drug metabolites and metabolic changes as a consequence of pharmaceutical drugs. The global metabolic consequences of severe sepsis were then examined in a cohort of patients using a method of metabolic profiling based on the ^{1}H-nuclear magnetic resonance spectroscopy of both urine and serum samples. This was followed by the characterisation of the changes in the lipid profiles of the patients from the sepsis cohort as a consequence of sepsis related liver injury using a technique optimised for the detection of lipid subspecies based on ultra-performance liquid chromatography coupled with mass spectroscopy (UPLC-MS) analyses of plasma samples.

1.2 Introduction to metabonomics

“Metabonomics” is a holistic approach to the study of changes in the metabolites within a biological system in response to a physiological processes such as sepsis (Nicholson & Lindon, 2008). It is a form of global metabolic profiling acquired using analytical platforms such as NMR and MS and analysed using multivariate statistical analyses. Metabolites are “downstream” from the system that includes the genome, transcriptome and proteome; if identifiable, they therefore potentially reflect all the changes that have occurred at all the other levels- as well as providing a dynamic response to pathophysiological stimuli (Nicholson & Lindon, 2008).

1.3 Sepsis

1.3.1 Importance

Sepsis is a syndrome of systemic inflammation caused by infection and is associated with a spectrum of complications ranging from hypotension to shock, organ failures and death (Bone, Balk, Cerra, *et al.*, 1992). It is responsible for about a half of all intensive care unit (ICU) admissions and more than a third of all hospital admissions (Blanco, Muriel-Bombin, Sagredo, *et al.*, 2008). This results in a large economic strain on healthcare funds, and this is likely to increase with evidence supporting a continued increase in the incidence of sepsis (Blanco, Muriel-Bombin, Sagredo, *et al.*, 2008). Such evidence includes reports from the Intensive Care National Audit & Research Centre (ICNARC) UK database demonstrating an increase in the incidence of treated severe sepsis from 46 to 66 per 100,000 population between 1996 and 2003 (Harrison, Welch & Eddleston, 2006). It is also associated with continued increases in two major risk factors for sepsis: the size of the elderly population and the use of immunosuppressive agents for an increasing number of illnesses (Blanco, Muriel-Bombin, Sagredo, *et al.*, 2008).

Mortality rates in sepsis are high (28-40%) and progressively increase with increasing number of organ failures (Blanco, Muriel-Bombin, Sagredo, *et al.*, 2008). It is the leading cause of death in the ICU and epidemiological studies of patients admitted to ICUs with sepsis have shown that approximately 30% of non-survivors will die within the first 48 hours. Moreover, this early mortality is associated with a worse degree of organ dysfunction on admission to the ICU (Blanco, Muriel-Bombin, Sagredo, *et al.*, 2008). This might support the notion that the early recognition and treatment of infection and hypotension in sepsis are crucial to the overall outcome (Rivers, Nguyen, Havstad, *et al.*, 2001; Kumar, Roberts, Wood, *et al.*, 2006; Dellinger, Carlet, Masur, *et al.*, 2004). This hypothesis was ignited in 2001, by Rivers *et al* following the publication of a study supporting the key factors determining the outcome in sepsis are early interventions to treat the infection and the prevention of hypotension and

associated organ failures (Rivers, Nguyen, Havstad, *et al.*, 2001; Kumar, Roberts, Wood, *et al.*, 2006; Dellinger, Carlet, Masur, *et al.*, 2004). In this landmark study by Rivers *et al*, early goal directed therapy involving the use of fluid resuscitation, inotropes, antibiotics and other adjuncts directed at specific targets in sepsis were associated with a reduction in 28-day mortality rates (Rivers, Nguyen, Havstad, *et al.*, 2001).

The principle of the early goal directed therapy (EGDT) advocated by this study was the optimisation of tissue oxygen delivery using a set of specific physiological targets with the aim of reversing cellular hypoxia. However, increasing evidence that bio-energetic failure and cellular hypoxia is usually confined to patients with in the late stages of septic shock has resulted in increasing scepticism of this theory and the results of this study. This growing scepticism has led to over thirty unsuccessful attempts to replicate the mortality benefit of this study, prompting the recent trilogy of randomised controlled trials (RCTs) that have also been unsuccessful. However, this is not surprising given the revolutionising effect the Rivers study has had on the management of sepsis. Since its publication in 2001, the definition of usual care to which such EDGT was compared, has been updated including sepsis bundles with attention to early recognition and treatment of sepsis with antibiotics, fluids escalation to a critical care environment for further management. Thus, although a prescriptive sets of physiological parameters (goals) are not aggressively targeted, early recognition, interventions and monitoring are now the foundations of what is deemed usual care; with great emphasis on the importance of acting quickly. The duration of hypotension prior to the administration of appropriate antibiotics was also shown to be one of the factors determining the outcome of sepsis in a subsequent study by Kumar *et al* (Kumar, Roberts, Wood, *et al.*, 2006). Thus, the prevention of sepsis associated organ failures relies on the early detection of organ dysfunctions when still at a reversible stage. This attractive approach is currently inhibited by the lack of accurate methods of detecting very early organ dysfunction secondary to sepsis, or indeed, organ dysfunction in general.

1.3.2 Clinical challenges

1.3.2.1 Early diagnosis of sepsis-induced organ dysfunction

There are over 150 studies on biomarkers of acute kidney injury (AKI). In spite of this, there are only nine studies of patients with sepsis-related acute kidney injury (SR-AKI) of reasonable methodological quality. Collectively, these have examined the diagnostic and predictive value of seven biomarkers: cystatin C (CysC), neutrophil gelatinase-associated lipocalin (NGAL), urinary alpha-glutathione S-transferase (α-GST), tumour necrosis factor-alpha (TNF-α); and serum TNF-α receptors type one and two (sTNF-α- RI and II). Although this list includes the most extensively studied biomarkers of AKI, this subset, and indeed, the majority of these studies of these AKI biomarkers have many problems preventing valid comparisons of these biomarkers. The main problem is their lack of consistency in both the definitions of AKI and in the reporting of the evaluation parameters of the diagnostic and predictive abilities of these biomarkers. Moreover, the validity of the use of positive predictive values (PPV) in many of studies is compromised by the low number of events- especially with regards to the need for renal replacement therapy (RRT).

Neutrophil gelatinase-associated lipocalin was the subject of investigation, in four of the nine aforementioned studies of SR-AKI. The best results were demonstrated by a study by Märtensson *et al*, exploring the predictive ability of both urinary and plasma NGAL in critically ill patients with sepsis (Martensson, Bell, Oldner, *et al.*, 2010). In this study, AKI was defined using the acute kidney injury network (AKIN) or Risk, Injury, Failure, Loss, and End-stage Kidney (RIFLE) criteria, and urinary and plasma NGAL were assessed in the cohort as a whole, in addition to an analysis of urinary NGAL in a subgroup with septic shock. In both groups, urinary NGAL was associated with an area under the receiver operating characteristic (AUROC) curve of 0.86 and a negative predictive value (NPV) of 100% for the prediction of AKI in sepsis. Where the AUROC curve gives the probability that a subject randomly selected from the AKI group will have a positive test result compared to a subject randomly

selected from the non-AKI group. However, the positive predictive value of urinary NGAL in the subgroup with septic shock (58%) was significantly lower than the group as a whole (84%). The whole group analysis of plasma NGAL, produced similar results to the whole group analysis of urinary NGAL, with an AUROC, NPV and PPV of 0.86, 79% and 88%, respectively.

The second study of the use of NGAL in SR-AKI involved a comparison of two subgroups of a cohort of critically ill patients: one with sepsis and the other with non-infected systemic inflammatory response syndrome (SIRS) (Bagshaw, Bennett, Haase, *et al.*, 2010). In this comparison, the ability of NGAL to predict worsening renal function, (defined using RIFLE criteria) and the need for renal replacement therapy (RRT) was assessed using plasma and urinary NGAL, respectively. This delineation of these two biomarkers is in keeping with the hypothesis that blood and urine markers are more likely to represent renal clearance and histological damage, respectively. The ability of plasma NGAL to detect progression of worsening AKI was associated with an AUROC curve of 0.71 and 0.78, for the cohort as a whole (both non-infected SIRS and sepsis) and the subgroup with sepsis, respectively. Whereas, the ability of urinary NGAL to predict the need for RRT was associated with an AUROC curve of 0.70 for both of the whole cohort and the subgroup with sepsis. Interestingly, the sepsis group was associated with significantly higher levels of NGAL in both plasma and urine at enrolment, compared to the group with non-infectious SIRS and this difference in the levels of urinary NGAL in these two groups persisted for up to 24 hours.

The other two studies evaluating the use of NGAL in the prediction of sepsis-related AKI, both involved blood samples: one investigated the use of serum NGAL in children with septic shock (Wheeler, Devarajan, Ma, *et al.*, 2008) and the other assessed the use of plasma NGAL in emergency department (ED) patients with suspected sepsis (Shapiro, Trzeciak, Hollander, *et al.*, 2010).

In both studies, the use of NGAL in prediction of SR-AKI was associated with variable results. In the ED study, the ability of NGAL to predict the onset of SR-AKI was associated with an AUROC curve and negative predictive value that were both good at 0.82 and 94%, respectively but a low positive predictive value (Shapiro, Trzeciak, Hollander, *et al.*, 2010). Whereas in the paediatric study, although the negative predictive value was good at 94%, the AUROC curve was low at 0.68 and the positive predictive value was very low at 39% (Wheeler, Devarajan, Ma, *et al.*, 2008).

Two the nine aforementioned studies of biomarkers of SR-AKI examined the utility of Cystatin C. Of these, the most recent study was also the most comprehensive (Nejat, Pickering, Walker, *et al.*, 2010). This examined the diagnostic and predictive utility of both urinary and plasma levels in critically ill patients with and without sepsis. In the sepsis cohort, plasma cystatin C (pCysC) was shown to be diagnostic of AKI with an AUC of 0.75; (CI, 0.63 to 0.86; $P < 0.0001$); whereas urinary cystatin C (uCysC), was shown to be predictive of the development of AKI (within 48 hours of the onset of sepsis) with an AUC curve of 0.71 (CI, 0.55 to 0.86). However, uCysC was non-diagnostic of the presence of AKI at the onset of sepsis and pCysC was not accurate at predicting the development of AKI.

Plasma Cystatin C was also shown to be a poor predictor of the development of AKI in sepsis by an earlier study by Mazul-Sunko *et al*, (Mazul-Sunko, Zarkovic, Vrkic, *et al.*, 2004) in which, the diagnostic accuracy of pCysC to predict AKI in sepsis was associated with both a sensitivity and a specificity of 0.50. This earlier study did however suffer from poor methodological quality including the use of an unfamiliar definition of AKI: an increase in serum creatinine of greater than 267 μmol/L or a diuresis of less than 30mL/h in absence of CKD.

The diagnostic ability of IL-6 in SR-AKI had been assessed by two of the studies (Iglesias, Marik & Levine, 2003)(Chawla, Seneff, Nelson, *et al.*, 2007). In the first study, three other biomarkers were also

investigated: TNF-α and- soluble TNF-α receptor I and II (Iglesias, Marik & Levine, 2003). Of these four biomarkers, only the sTNF-α RI and RII were shown to be predictive for the development of AKI in patients with septic shock: s-TNF-RI, 25 (+/- 16) versus 18 (+/- 13) ng/mL; P = 0.00006; S-TNF-RII, 25 (+/- 21) versus 18 (+/- 17) ng/mL; P = 0.0007). In the other IL-6 study, logarithmic IL-6 levels were shown in a multivariable Cox regression analysis (associated with P < 0.0001) to be predictive of the onset of AKI of a cohort of patients with severe sepsis taken from the Protein C Worldwide Evaluation in Severe Sepsis (PROWESS) Study (Chawla, Seneff, Nelson, *et al.*, 2007).

In the ninth study from this group of studies of biomarkers of SR-AKI, α-GST was shown to be incapable of predicting the development of AKI (Walshe, Odejayi, Ng, *et al.*, 2009).

There are currently no biomarkers capable of detecting sepsis-related liver injury early. There is however evidence supporting the use of ^{13}C labelled methacetin, a selective metabolite of the liver specific enzyme cytochrome P450 1A2, to measure maximal liver function capacity in this context, following demonstrations of its utility in the detection of early evidence of liver injury post-liver resection. This enzymatic liver function test is also known as the LiMAx test and is measured using a bedside test called the FLIP™ analyser (Humedics GmbH, Berlin, Germany).

Such evidence includes a recent study by Kaffarnik *et al* (Kaffarnik, Lock, Vetter, *et al.*, 2013) comparing the diagnostic and prognostic use of the LiMAx test to the use of indocyanine green plasma disappearance rates (ICG-PDR) test, as a measure of hepatic clearance and standard biochemical liver function tests. This study provided evidence that both that ICG-PDR and LiMAx can detect liver injury earlier than conventional markers such as bilirubin. Moreover, it revealed that changes in the levels of LiMAx, not only occurred earlier than the changes in ICG-PDR but that LiMAx was also superior to

ICG-PDR at predicting mortality. Evidence supporting the latter conclusion included the results of the AUROC of these tests for the prediction of death which demonstrated sensitivity and specificity of 100% and 77%, and 70% and 80%, for a LiMAx level <100μg/kg/hr and a ICG-PDR ≤10.3units, respectively. Other important findings of this study included demonstration of a close correlation between the patient's prognosis and hepatic impairment and impairments in LiMAx levels within two days of the onset of sepsis in the vast majority of the patients. These results therefore also support the increasing evidence that liver injury in sepsis usually occurs very early, including reports of liver injury within 15 hours in animal model of sepsis (Recknagel, Gonnert, Westermann, *et al.*, 2012).

1.3.3 Metabolic changes in sepsis

The provision of energy is at the centre of human metabolism. This involves many interdependent processes involving both the liver and kidneys, both commonly affected by sepsis (Carré & Singer, 2008). Changes in these metabolic processes therefore have the potential to be utilised in the early diagnosis of sepsis and sepsis related liver and kidney dysfunction. Energetic metabolism has been shown to vary between fasted and fed states (Wolfe & Martini, 2000). In both states, there is a reciprocal relationship between the importance of free fatty acids (FFAs) and glucose as the primary energy source. Fatty acids (FA) are of greater importance than glucose in the fasted state and vice versa in the fed state. Differences between these two states, in health and in sepsis in terms of the relationship of FA and glucose and its effect on other sources of energy such as proteins, will be discussed in turn, followed by a discussion of changes in lipoproteins and amino acids in sepsis.

In the fasted state, fatty acid stores are drawn upon first; this is promoted by the release of hormones such as glucagon, in response to a reduction in plasma glucose levels. This starts with the increased utilisation of fatty acids by tissues; both from their triacylglycerol (TAG) stores and circulating FFAs

released from the lipolysis of adipose tissue. Although, this energy source is not usually limited by substrate availability, it can be limited by the enzymes necessary for its metabolism (Wolfe & Martini, 2000). When this occurs, glucose derived from non-FA sources is used to supplement the energy derived from FAs. This includes the catabolism of glycogen stores, (predominantly in the liver and muscles), the recycling of carbon from non-glucose sources including metabolites of anaerobic metabolism such as lactate in the liver, in addition to protein catabolism (Wolfe & Martini, 2000). The liver plays a pivotal role in many of these processes and is therefore essential to the provision of a constant supply of energy to all the tissues of the body, including glucose for glucose-dependent tissues, in the fasted state. This is supported by gluconeogenesis in the kidneys which is responsible for 25% of the glucose produced in the fasted state. The liver is also responsible for the synthesis of macromolecules necessary to the transport lipids in plasma, namely, albumin for FFA and lipoproteins for cholesterol and TAGs (Murray & Davis, 2003).

In the fed state, the successful digestion of carbohydrates, protein and fats leads to increases in the plasma levels of glucose, amino acids and triacylglycerols (TAGs) transported by the lipoprotein chylomicrons (Wolfe & Martini, 2000). Under these conditions, glucose becomes the primary energy source for tissues throughout the body. Following its cellular uptake, glucose can either be metabolised aerobically via the tricarboxylic acid (TCA) pathway, anaerobically to form pyruvate, lactate, or alanine, or converted into an energy source that can be stored. In the liver and muscle tissues, glucose is stored as glycogen, whereas, in adipose tissue, it is converted to glycerol and used to synthesis TAGs. In the liver, glucose can also be utilised in the *de novo* synthesis of FAs, following its catabolism to acetyl coenzyme A (acetyl-CoA). Carbon atoms derived from products of anaerobic metabolism can also be recycled to produce glucose or metabolites of the TCA cycle, (this predominantly occurs in muscles) (Murray & Davis, 2003).

In contrast to the fasted state, in which catabolism predominates, the fed state is characterised by an initial surge in the levels of glucose which results in the uptake and anabolic metabolism of glucose to replenish energy stores, in addition to the use of glucose as the primary energy source (Wolfe & Martini, 2000). The release of hormones promotes this process such as insulin that stimulates glucose uptake and attenuates the catabolism of non-glucose sources such as lipids and proteins. The kidneys are responsible for 20% of the glucose uptake from the circulation, with the majority of the remaining glucose load being taken up by the peripheral tissues especially the muscles. The skeletal muscles and kidneys are also responsible for the clearance of insulin from the circulation. Such efficient uptake and conversion of glucose to glycogen and other storage molecules following a meal, usually causes problems with glucose (substrate) availability, one or two hours later. This leads to the use of energy stores such as TAGs and glycogen (secondary energy sources in the fed state). After ingestion, dietary TAGs are transported from the intestines to the portal circulation via the lymphatic system, by chylomicron lipoproteins. Following their release into the systemic circulation, chylomicrons must acquire apoproteins to enable their uptake and metabolism by both the liver and extra-hepatic tissues (Murray & Davis, 2003). This results in the liberation of FFAs, the majority of which are taken up by the peripheral tissues, and the rest are released into the circulation and eventually taken up by the liver and other tissues. In the fed state, the main fate of FAs in the liver is the synthesis of the TAGs which are packaged within very low density lipoproteins (VLDL), to enable their transport to peripheral tissues (Wolfe & Martini, 2000). However, when the supply of glucose is low, TAGs in adipose tissue are converted into FAs. In both the fasted and the fed state, the breakdown (lipolysis) of adipose tissue into FAs is usually in excess of the body's requirements. This is then followed by their re-esterification and combination with glycerol-3-phosphate (derived from glucose) to produce TAGS.

In sepsis, the reciprocal relationship between FAs and glucose is lost and there are accelerated rates of protein and lipid catabolism compared to normal, during both fasted and fed conditions (Günther

& Redl, 2012; Khovidhunkit, 2004). The fasted state is (still) characterised by increased catabolism of TAG stores in peripheral tissues such as muscle and adipose tissue. The FFAs from adipose tissue are mainly exported, whereas, other tissues retain the majority of the FAs produced from the catabolism of their TAG stores and use them as an energy source (Khovidhunkit, 2004). This results in increased levels of circulating FFAs leading to increased levels of FFA uptake by many tissues, especially the liver and adipose tissue. Increases in FA delivery to liver would ordinarily lead to the synthesis of ketone bodies (ketogenesis) and increased utilisation of FAs as a fuel source via beta-oxidation. In sepsis, however, ketogenesis and FA beta oxidation are both inhibited and much of the surplus of circulating FAs taken up by the liver are used to synthesize TAGs and are secreted as VLDLs (VLDL-TAGs) (Khovidhunkit, 2004). The combination of increases in the catabolism of TAGs into FAs and the inhibition of FA oxidation, in the fasted state in sepsis results in an increase in the proportion of FAs exported from adipose tissue that are re-esterified, converted back into TAGs and returned to the adipose tissue. Whereas, the reduction in ketogenesis in sepsis may contribute to the dependence of peripheral tissues on alternative sources of fuel such as proteolysis followed by gluconeogenesis in the fasted state (Khovidhunkit, 2004). These changes result in increased levels of the anaerobic metabolism of glucose and its metabolites, necessitating greater rates of carbon recycling by the liver; in addition to the by-products of increases in ureagenesis and gluconeogenesis. The liver and kidneys play important roles in these metabolic changes that could be exploited to provide potential markers of normal and abnormal liver and kidney function in sepsis.

Under normal conditions, glucose is the main fuel source in the fed state and lipids are a secondary source (Günther & Redl, 2012). In sepsis, however, a reduction in glucose uptake by insulin dependent uptake carriers (extra-hepatic tissues) and increases in the catabolism of both adipose tissue and muscle protein despite the provision of food, results in abnormally high levels of glucose, amino acids and circulating FFAs (Michie, 1996). Both changes can in part be explained by the relative insulin

insensitivity that occurs, resulting in a reduction in both glucose uptake and the inhibition of insulin on protein and lipid catabolism by the liver. The increased levels of circulating FFAs and glucose leads to accelerated rates of VLDL-TAG production and export by the liver, in addition to much greater levels of FA uptake and storage as TAGs by adipose tissue. This cycle of the catabolism and reforming of lipids also occurs in health as an overzealous response to an unmet energy requirement, whereas in sepsis in occurs in an uncontrolled manner.

Overall, the differentiation between the fed and the fasted state is less defined in sepsis, with many of the metabolic changes of energy sources occurring in both states. The integral role of liver in many of the changes involving lipids suggests these changes may be particularly useful in the detection of liver injury in sepsis.

1.3.3.1 Lipoproteins and sepsis.

Very low-density Lipoproteins and chylomicrons are two of the five lipoproteins (LPs) involved in lipid transport in humans. The other three are high density lipoproteins (HDL) and two remnants of VLDL: intermediary density lipoprotein (IDL) and low-density lipoprotein (LDL).

All five LPs contain a mixture of proteins and lipids including TAGS, free cholesterol (FC), esterified cholesterol (CE) and phospholipids (PLs), each with different ratios. Whereas, TAGS are the predominant lipid species in VLDL and chylomicrons, cholesterol predominates in HDL. Intermediary density lipoprotein contains similar amounts of TAGs, CEs and PLs; and LDL is 50% CE, 28% PL and 13% TAGs (Murray & Davis, 2003). In all five lipoproteins, free cholesterol constitutes roughly 10% of the total lipid content. All of the LPs have type specific apoproteins that are integral to both their functional roles and metabolism, including their cellular uptake and degradation (Murch, Collin, Hinds, *et al.*, 2007). Apolipoprotein E plays a central role in the transport of lipids between cells and

compartments of the body. It also regulates plasma and tissue lipid levels by facilitating the bind of lipoproteins and lipid complexes in plasma and other biofluids to specific receptors on the surface of cells resulting in the internalisation of the lipoproteins containing Apo-E, followed by the reorganisation of the lipids within the tissues.

Chylomicrons are synthesised by intestinal cells and transport dietary TAGs through the lymphatic system to liver. In the liver, TAGs are incorporated into VLDL and exported as VLDL-TAGs for delivery to peripheral tissues. In the circulation, nascent VLDL from the liver acquires apoprotein CII (Apo-C) and additional apoprotein E (Apo-E) from circulating HDL that enables it to interact with lipoprotein lipase on endothelial cells (Murray & Davis, 2003). This is followed by the exchange of TAGs, PLs and Apo-C from VLDL to HDL and the uptake of CE from HDL to HDL. This exchange ultimately results in the conversion VLDL to IDL, which then has three fates: uptake by either the liver or extra-hepatic tissues mediated by Apo-E receptors or remain in the circulation as LDL following its conversion by hepatic lipase which includes the loss of Apo-E (Murray & Davis, 2003).

High Density Lipoprotein, on the other hand is responsible for reverse cholesterol transport: the transport of cholesterol from circulation to the liver (Murch, Collin, Hinds, *et al.*, 2007). Unlike VLDL, HDL is constructed within the circulation from mainly PLs, enzymes and apoproteins from both peripheral and hepatic tissues, in addition to the aforementioned exchanges with LDL and VLDL. This interdependency between VLDL/LDL and HDL is responsible for the reciprocal relationship demonstrated by the circulating levels of VLDL and HDL (Murch, Collin, Hinds, *et al.*, 2007). This reciprocal relationship is maintained in sepsis: with the increases in VLDL-TAGs being accompanied by a reduction in HDL-cholesterol (Murch, Collin, Hinds, *et al.*, 2007) Moreover, there is increasing evidence of modifications of HDL that occur in sepsis, in addition to a protective role of HDL in sepsis. This includes the ability of HDL-associated proteins to neutralise lipopolysaccharide (LPS) and other

bacterial wall components by facilitating their transfer to lipoproteins that are capable of the attenuating LPS-mediated cytokine release in addition to HDL acting as a direct immune-modulator (Murch, Collin, Hinds, *et al.*, 2007).

1.3.3.2 Amino acids in sepsis

Amino acids can be divided into the following five groups based on their side chains: aromatic, aliphatic (branched chain), acidic, neutral and sulphur containing amino acids. Although there are over three hundred different amino acids only 20 are present in the peptides and proteins of humans. The amino acid changes in sepsis are the end result of increases in their utilisation, both as a fuel source and in protein synthesis, increases in protein catabolism and any factor affecting their metabolism (Günther & Redl, 2012). The catabolism of most amino acids starts with the removal of nitrogen via trans-amination, deamination, and the formation of urea in the liver, which is excreted by kidneys. The carbon backbone of an amino acid is usually preserved in the form of a carbohydrate (glucogenic) or fatty acids (ketogenic) precursors which can either be oxidised to provide energy or used to form glucose and fatty acids, respectively. Most amino acids are solely glucogenic; a small minority are both glucogenic and ketogenic, whereas lysine and leucine are the only amino acids that are solely ketogenic and can only give rise to fatty acid precursors that are either converted FAs, ketone bodies or are oxidised to CO_2 and H_2O (Murray & Davis, 2003).

Changes in sepsis that may affect the metabolism of ketogenic amino acids includes the inhibition of both ketogenesis and the oxidation of fatty acids (Michie, 1996). Whereas, sepsis induced liver injury is likely to cause an increase in the amino acids that are either totally dependent (such as the aromatic and sulphur containing amino acids) or partially dependent on the liver for the first stages in their catabolism, which includes all 20 of the amino acids found in humans (Nesseler, Launey, Aninat, *et al.*, 2012). This is with the exception of the aliphatic or branched-chain amino acids (BCAA) which are

unique in that their initial steps of catabolism takes place in skeletal muscle and therefore, all stages of their catabolism can occur independently of the liver (Dejong, van de Poll, Soeters, *et al.*, 2007). Sepsis induced liver injury is therefore not expected to cause an increase in BCAA. Various amino acids are either produced or transformed in the kidney; this includes some of the non-essential amino acids that are dependent on the kidneys for their synthesis such as arginine, cysteine, and tyrosine. Acute kidney injury in sepsis could therefore cause some of these non-essential amino acids to become essential dietary amino acids.

In summary, sepsis is associated with many changes in metabolism of glucose, proteins, amino acids, lipids, and lipoproteins (responsible for the transport of lipids). Dysfunction of organs integral to these metabolic changes such as the liver and the kidneys are likely to results in metabolic signature that could be used to differentiate between patients with and without such sepsis-related organ dysfunctions.

Critically ill patients with sepsis are given antibiotics in addition to a variable number of other pharmaceutical drugs depending on the severity of their sepsis and their other co-morbidities. The majority of these drugs depend on the liver and kidneys for their metabolism. Changes in the metabolism of these drugs occurs in liver and kidney dysfunction (Brunton, Parker, Blumenthal, *et al.*, 2008); these changes may therefore be potentially useful in the differentiation of patients with and without these organ dysfunctions. However, many of the changes in drug metabolism that can occur in sepsis secondary to liver and kidney dysfunction can become very complicated in view of the interdependence of the liver and kidney in the metabolism of many of these drugs (De Paepe, Belpaire & Buylaert, 2002).

1.3.4 Metabolic profiling studies in critical illness and sepsis

All forms of metabolic profiling consist of a combination of the acquisition of a metabolic profile of a biological system such as a biofluid coupled with statistical analyses to demonstrate associations between a metabolic response and a stimuli or biological process. The main division in metabolic profiling is the analytical approach used to demonstrate this association between metabolic changes and biological process being under investigation. Metabonomics involves a holistic approach that recognises the importance of the complex interactions between the metabolic changes that occur and utilises multivariate statistical analyses to demonstrate metabolic signatures of biological changes. Metabolomics, in contrast, focuses on analyses that quantify the changes of individual metabolites in response to biological changes using univariate analyses after the identification of differentiating metabolites using multivariate statistical analyses.

1.3.4.1 Animal studies

At the start of this project there were very few metabolic profiling studies of sepsis. In fact there was only one clinical study (Stringer, Serkova, Karnovsky, *et al.*, 2011); with all the other studies of metabolic profiling being carried out in animal models of sepsis (see Table 1.1). This included four studies in rats, three using sepsis induced using the caecal ligation and puncture (CLP) technique (Lin, Xu, Yan, *et al.*, 2009; Izquierdo-Garcia, Nin, Ruiz-Cabello, *et al.*, 2011; Liu, Zheng, Ji, *et al.*, 2010) and one involving lipopolysaccharide (LPS) induced endotoxaemia (Laiakis, Hyduke & Fornance Jr, 2012). In two of these studies, CLP-induced sepsis was compared with sham surgery controls and were based on NMR analyses of plasma (Lin, Xu, Yan, *et al.*, 2009; Izquierdo-Garcia, Nin, Ruiz-Cabello, *et al.*, 2011). In both studies, the metabolic differences between the sepsis and the control groups included increases in the sepsis group in alanine (a pyruvate metabolite), formate and the ketone body acetoacetate. Other metabolic differences between the sepsis and control groups of these two studies

included increases in the sepsis group of lipid metabolites (phosphoethanolamine and myoinositol) in one of the studies (Izquierdo-Garcia, Nin, Ruiz-Cabello, *et al.*, 2011) and increases in lactate and both ketones bodies and their metabolites (acetoacetate and hydroxybutyrate and acetate, respectively), in the other study (Lin, Xu, Yan, *et al.*, 2009). In the latter study, a comparison of the control group and the sepsis group divided into survivors and non-survivors was also performed. This demonstrated that the metabolic differences between septic patients and control group were more pronounced between comparison of non-survivors and controls but these metabolic differences between the two septic subgroups were not capable of differentiating between them (Lin, Xu, Yan, *et al.*, 2009). The increases in lactate, acetate, alanine, and ketone bodies in the sepsis group are consistent with the increased pyruvate, anaerobic and fatty acid metabolism seen in sepsis. The increased synthesis of nucleic acids could explain the rise in formate and contribute to the increase in lactate often seen in sepsis.

Table 1.1 Animal metabolic profiling studies of sepsis. KEY: ANOVA: analysis of variance, BCAA: branched-chain amino acid, CLP: caecal ligation and puncture, FA: fatty acids, FDR: false discovery rate, GPC: glycerophosphocholine, lysoPC: lysophosphatidylcholine, O-PLS: orthogonal-PLS, PC: phosphatidylcholine, PLS: projection to latent structures, PLS-DA: PLS-discriminative analysis, PCA: principal component analysis; TAG: triacylglycerides.

Year	Author	Samples; platform	Subjects	Results: differentiating metabolites identified	Additional results	Statistical methods
			Sepsis or lipopolysaccharide-induced endotoxaemia in rodents versus sham surgical controls			
2009	Lin *et al*	Plasma ^{1}H-NMR	3 groups: (1) CLP induced sepsis survivors (n= 19) (2) CLP induced sepsis non-survivors (n= 21) (3) Sham surgical controls (n = 20)	**Sepsis versus sham surgical controls** ↑alanine (pyruvate metabolite), formate, lactate and the three ketones bodies: acetoacetate, D-β-hydroxybutyrate and acetate		PCA and O-PLS
2010	Lui *et al*	Plasma LC-MS/MS	4 groups: (1) Burns (thermal injury)/sham CLP-induced sepsis (burns group) (n =10) (2) CLP-induced sepsis/sham burns (sepsis group) (n =10) (3) CLP-induced sepsis and burns (dual pathology group) (n =10) (4) Sham of both CLP-induced sepsis and burns (dual control group) (n =10)	**Differentiating metabolites associated with the groups** **(1) Sepsis and burns single pathology groups:** ↓uric acid (renal excreted end product of purine metabolism; role unclear: can act as both an anti- and pro-oxidant) and trihydroxycholanoic acid (bile acid) **(2) Sepsis and dual pathology groups:** ↑Uracil (nucleobase in RNA; naturally occuring pyrimidine derivative; aids enzyme synthesis and essential to cell function) and nitrotyrosine (associated to nitro-oxidative stress) **(3) Exclusively in dual pathology group** (NB.↑ in dual burns and sepsis pathology but not the single pathology groups): ↑hypoxanthine (catabolite of adenosine triphosphate); increases suggests tissue hypoperfusion and O2 deficiency), indoxylsulphate (metabolite of protein and tryptophan (marker of renal function; associated with tissue damage and oxidative stress); ↑ in glucurnic acid and gluconic acid (products of glucose oxidation and associated with oxidative stress); and proline		One way ANOVA(p value set at <0.05)
2011	Izquierdo-Garcia *et al*	Plasma ^{1}H-NMR	2 groups: (1) CLP-induced sepsis (n= 14) (2) Sham surgical controls (n= 14)	**Sepsis versus non-infected sham controls:** ↑alanine (pyruvate metabolite), formate, acetoacetate (ketone body); creatine and two lipid metabolites: phosphoethanolamine and myoinositol		PCA and PLS-DA
2012	Laiakis *et al*	Urinary LC-MS/MS	5 groups: (1) Lipopolysaccharide-endotoxin model (n = 12) (2) Radiation with 3Gy of γ rays (n = 10) (3) Radiation with 8Gy of γ rays (n = 11) (4) Radiation with 15Gy of γ rays (n = 8) (5) Controls (n = 12)	**Differentiating metabolites associated with the groups** **(1) Lipopolysaccharide-endotoxin group:** ↑cytosine (base in DNA and RNA; pyrimidine derivative), adenosine and O-propanolylcarnitine **(2) Lipopolysaccharide-endotoxin and 15Gy radiation groups:** ↑ isethionic acid, 2-hydroxyethane-1-sulfonic acid; (a strong anion; metabolite of the taurine: its role may be related to its effect on the charge on cell membrane by converting the zwitterion taurine into strong anion , which could effect the binding of cations, e.g. K+)		One-way ANOVA combined with Dunnett's multiple correction test for comparisons within multiple groups (lipopolysaccharide-sepsis or irradiated); p value set at <0.05

Table 1.1 continued

Additional sepsis versus sham surgerical controls studies: published after the start of this project						
2012	Li *et al*	Lymph LC-MS/MS	2 groups: (1) CLP induced sepsis (n= 14) (2) Sham surgical controls (n= 14)	**Sepsis versus non-infected sham controls:** ↑palmitoyl-L-carnitine, creatinine, phenylalanine, isonicotinic acid (vitamin B3), ; choline 5-azacytidine (a DNA methyltransferase inhibitor) and ↓: 1-O-Hexadecyl-2-lyso-glycero-3-phosphorylcholine (a lysoPC), alanine, 4-amino-5-hydroxymethyl-2-methylpyrimidine; asymmetric dimethylarginine	↑ plasma and lymph levels of the pro-inflammatory cytokines TNF-α, interleukin 1β and interleukin in sepsis group compared to the control	PCA and O-PLS; t test and ANOVA (p value set at 0.05)
2013	Li *et al*	Plasma ^{1}H-NMR	4 groups: (1) CLP-induced sepsis model group (n= 20) (2) Sham surgical control group (n= 10) (3) CLP-induced sepsis model administered Chinese herbal medicine A (n= 20) (4) CLP-induced sepsis model administered Chinese herbal medicine B (n= 20)	**Sepsis versus non-infected surgical sham controls:** Differences in 18 metabolites consisting predominantly of metabolites concerned with energy metabolism (↑ isobutyrate, 3-hydroxylbutrate, alanine, acetate, lactate and glucose); lipid transport and mobilisation (↑ lipids: TAG and FAs), and amino acids (↓proline, taurine, valine, isoleucine, arginine, lysine and ↑threonine); in additon to ↓choline and trimethylamine N-oxide		PCA and PLS-DA
2014	Langley *et al*	Plasma LC-MS/MS	Part (1) Metabonomic changes associated with the inoculation of primates with the bacteria E.coli (1) Sepsis non-survivors (n=4) (2) Sepsis survivors (n = 12 low dose; 4 high dose) (3) Healthy controls (n = 2) Part (2) Transcriptome (1) Sepsis non-survivors (n=4) (2) Sepsis survivors (n = 8 low dose;4 high dose) (3) Healthy controls (n = 2) Part (3) Integration of lung transcriptome and plasma metabolome	**(1) Temporal changes sepsis non-survivors versus survivors and differentiation of sepsis versus healthy controls** Metabolomic temporal changes from pre-innoculation and day 1, 2 and 5 after inoculation: ↓ acyl-GPCs, and↑ kynurenine derivatives, bile acids, carnitine esters, tricarboxylic acid cycle intermediates; and pregnen-sulfated and androgenic steroids **(2) Genes associated with sepsis non-survivors versus survivors** Genes with strong association with sepsis non-survivoral: FA metabolism, BCAA catabolism, inflammation, transcription factors, mitochondria and peroxisomes **(3) Cross correlation analysis (metabolome and transcriptome) of high dose survivors and non-survivors: the two sepsis subgroups** Four very robust correlations were identified by this analysis between. Three positive correlationS: (1) kynureninase and kynurenine pathway metabolites, and peroxisomal genes; (2) tricarboxylic acid cycle intermediates and apoptosis and inflammatory response genes; (3) acyl-GPCs and carnitine esters, and genes of BCAA catabolism, beta-oxidation and peroxisomal lipid oxidation; and (4) negative correlations between acyl-GPCs and lysophosphatidylcholine acyltransferase 2 (LPCAT2; an enzyme that can metabolism acyl-GPCs to phosphatidylcholines or acetylate acyl-GPCs to form platelet activating 1-alkyl, 2-acyl-GPCs)	**Logistic regression model was built using four metabolites**: lysophosphatidylcholine 1-stearoyl-GPC, kynurenine, isovalerylcarnitine and taurolithocholate-3-sulfate (sulphated bile acid) The AUROC of the model 's ability to differentiation infection and non-infection in the primate cohort was 0.9675 for the model based on all four metabolites and 0.9519 for a model based on stearoyl-GPC alone The AUROC of the model 's ability to diagnosis sepsis in two human cohorts was 0.78 in the RoCI cohort and 0.6672 and 0.8213 at enrolment and 24-hours post enrolment in the CAPSOD cohort	PCA, using Pearson product-moment correlation coefficient, (to assess relationships among many quantitative variables by three-dimensional clustering. ANOVA (for all pairwise comparisons; 5% FDR)

Table 1.1 continued

2104	Steelman *et al*	Serum LC-MS/MS	Cohort (1) Pre and post induction of acute laminitis: an inflammatory condition that frequently ocurs secondarily to sepsis or SIRS as a result of gastro-intestinal diseases (the equine equivalent of MODS) (n=6) (1) Pre-induction of acute laminitis (2) Post-induction of acute laminitis	LC-MS data demonstrated greater differentiation of the pre and post induction samples than analyses based on the GS-MS data ↑ acyl carnitine and amino acids including alanine, kynurenine, taurine and aromatic amino acids and ↓ 3- hydroxybutyrate, citrulline, cysteine, a phosphatidylcholine: PC36:3) and the lyso-PC palmitoyl lysolectithin Citrulline and D-lactate were deemed the most discriminatory of the metabolites in the first cohort	Correlation analyses revealed the importance of two sets of differentiating metabolites: acyl carnitines post induction of acute laminitis and saturated FAs prior to induction; consistent with a dysregulation of fatty acids metabolism in the post induction group	PCA, PLS-DA and two-tailed, paired t-tests in pre and post-laminitis
			Cohort (2) Comparison of citrulline and D-lactate: the most discriminatory of the metabolites in the first cohort, in a second cohort of horses at risk of developing acute laminitis (1) Poor outcome: acute laminitis (n = 5) or non-survival (n= 1) (2) Good outcome: uncomplicated recovery and no acute laminitis (n = 13) (3) Healthy controls (n = 23)	**(1) Combined good and poor outcome groups versus healthy control** ↓ plasma concentrations of citrulline, expressed as a percentage of total free amino acids (p = 0.08) **(2) Citrulline as a predictive marker of the development of acute laminitis or non-survival:** using a cutoff of 2.1% of total free amino acids, citrulline had a sensitivity, specificity and negative predictive value of 83%, 62%, and 89%, respectively. **(3) Poor outcome and good outcome versus healthy controls:** Four amino acids also differed significantly (p= 0.05) among the 3 comparison groups of the second cohort despite not being identifed as capable of differentiating between the pre and post induction of acute laminitis in the first cohort studies. These were ↑ alanine, valine, and glycine; and ↓ serine in the combined good and poor outcome groups compared to the healthy controls. **(4) Poor outcome versus good outcome groups** Of these only glycine differed significantly between the two outcome groups and was shown to be able to predict the onset of laminitis with similar accuracy as citrulline (p=0.04), sensitivity of 83%, a specificity of 69%, and a negative predictive value of 89%.		ANOVA for comparisons between control and good and poor outcome groups

The other two studies were based on LCMS analyses of plasma in the first study (Liu, Zheng, Ji, *et al.*, 2010) and urine in the second (Laiakis, Hyduke & Fornance Jr, 2012). In the first study (Liu, Zheng, Ji, *et al.*, 2010) there were four groups of subjects that had each undergone a different combination of two procedures from a list of four possibilities consisting of CLP-induced sepsis, thermal injury (to induce severe burns) and shams of both procedures. (This resulted in the following groups: CLP-induced sepsis and sham burns, sham sepsis and burns, sepsis and burns, and shams of both procedures). In the second study there were five groups: three exposed to different levels of radiation, one with LPS induced endotoxaemia and a control group (Laiakis, Hyduke & Fornance Jr, 2012).

Despite the differences between these two studies, several similarities were demonstrated in the metabolic differences between the dual control group and the single pathology 'sepsis' (or LPS-induced endotoxaemia) group. This included increases in pyrimidines, a key component of nucleic acids, in the 'sepsis' group of both studies compared to the dual control group, supporting the importance of nucleic acids in sepsis. However, in the study by Liu *et al* (Liu, Zheng, Ji, *et al.*, 2010) increases in the pyrimidine uracil were demonstrated in both the single pathology sepsis group and the dual sepsis and burns group. Furthermore, in the same study, the presence of burns or sepsis alone was also associated with a reduction in uric acid, the breakdown product of purines: the complementary base pairing of pyrimidines in nucleic acids. This reduction in uric acid is consistent with reduction in the turnover of purines and therefore supports the increases nucleic acids in study suggested by the increases in pyrimidines. Overall, the findings of this study are limited by the overlap of the metabolites associated with the single and dual pathology groups. However, this study did demonstrate five metabolites that were exclusively associated with the dual pathology group (sepsis and burns) suggesting that the development of sepsis in a patient with burns (non-infected cause of SIRS) could be differentiated from patients with either burns or sepsis using metabolomics.

Overall, the most consistent finding demonstrated by these four metabonomic studies between subjects with experimentally induced sepsis and controls were metabolites of energy metabolism that are consistent the increases in the mobilisation of energy sources that are associated with sepsis such as FA and ketone bodies.

Since the start of this project, there have been four additional metabolic profiling studies published (Li, Hou, Wang, *et al.*, 2012; Li, Liu, Wu, *et al.*, 2013; Langley, Tipper, Bruse, *et al.*, 2014; Steelman, Johnson, Jackson, *et al.*, 2014) comparing the metabolic differences of animal model of sepsis to controls. Three of these studies contained a separate validation component to support the initial metabolic profiling component of the study.

In one of these studies (Li, Hou, Wang, *et al.*, 2012), LC-MS was used to examine the metabolic changes of lymphatic fluid from a CLP-induced rat model of sepsis and compare these to changes in the plasma and lymph levels of the pro-inflammatory cytokines TNF-α, interleukin 1β and interleukin 6. Increases in all three of these cytokines were demonstrated in both the plasma and lymph samples from the septic group compared to the control. Ten lymph metabolites were shown to be important to the differentiation of the sepsis and control groups. This consisted of increases in the sepsis group in creatinine, phenylalanine, isonicotinic acid (vitamin B_3), choline and 5-azacytidine (a DNA methyltransferase inhibitor); and decreases in 1-O-hexadecyl-2-lyso-glycero-3-phosphorylcholine (a lyso-PC), alanine, 4-amino-5-hydroxymethyl-2-methylpyrimidine and asymmetric dimethylarginine. These results are consistent with the mobilisation and utilisation of lipids, proteins and amino acids as alternative sources of energy that occurs in sepsis. It is also consistent with systemic metabolic changes demonstrated by the previous studies of animal models of sepsis.

In two of the four additional studies, the metabolic profiles of animal models of sepsis were examined using an exploratory cohort followed by the validation of these findings in a second cohort. In this first study (Steelman, Johnson, Jackson, *et al.*, 2014), both cohorts were of horses. The subject of this investigation was acute laminitis, an inflammatory disease of the foot that frequently occurs in horses with sepsis or systemic inflammation triggered by GI diseases, often regarded as an equine equivalent of an organ dysfunction as part of a multi-organ dysfunction syndrome (MODS) (Smith, 2015). In the first part of this study, both high performance liquid chromatography (HPLC)-quadrupole time-of-flight (Q-TOF)-MS/MS and gas chromatography (GS)-Q-TOF-MS analyses were performed on serum taken from a cohort of horses before and after the induction of laminitis secondary to the administration of an excess of carbohydrates. Multivariate analyses based on the LC-MS/MS data demonstrated greater differentiation of the pre-and post-induction samples than the analyses based on the GS-MS/MS data. Metabolites characterising the post induction samples identified using the LC-MS data included increases in acyl carnitine and amino acids including alanine, kynurenine, taurine, and aromatic amino acids and decreases in 3- hydroxybutyrate (ketone body), citrulline, cysteine, a phosphatidylcholine PC (36:3) and the lyso-phosphatidylcholine (lyso-PC) palmitoyl lysolectithin. Correlation analyses of all the metabolic differences between the pre-and post-induction samples were also performed. These analyses revealed the importance of acyl carnitines in the post- but not the pre- samples and saturated FAs in the pre- but not the post samples, consistent with a dysregulation of fatty acids metabolism in the post-induction group. Citrulline and D-lactate were deemed the most discriminatory of the metabolites and were therefore subjected to further evaluation, in a second cohort of horses at risk of developing acute laminitis. IgA a marker of the immune function of the intestines were also measured. This cohort was divided according to outcome and labelled as sick and advanced, if they had a good (uncomplicated recovery) or poor outcome (which included death or the development of acute laminitis), respectively; and compared to a group of healthy control horses. No significant differences were demonstrated between the three groups in the plasma and serum IgA concentrations. The plasma concentrations of citrulline were lower in the

good and poor outcome groups compared to the control group, and tended to be lower in the poor outcome group compared to the good outcome group (p=0.08)). As a marker of the development of acute laminitis or non-survivor, using a cut-off of 2.1% of the total free amino acids, citrulline had a sensitivity of 83%, a specificity of 62%, and a negative predictive value of 89%.

In the second study with two cohorts (Langley, Tipper, Bruse, *et al.*, 2014), the metabolic profiles associated with the onset and progression of bacteraemia in an animal model were examined, followed by the validation of the relevance of these finding to humans. This study started with an assessment of the metabonomic and transcriptomic changes associated with the inoculation of primates (*Macaca fascicularis*) with the bacteria *Escherichia coli*. Plasma samples were taken prior to the inoculation and day 1, 2 and 5 after inoculation, in addition to tissue from the liver, lung and spleen and blood, taken at necropsy. The primates were divided into two groups based on the receipt of a high or low dose inoculation. Comparison of temporal changes in the metabolome of the sepsis survivors and non-survivors and their metabolic profiles at baseline demonstrated dynamic changes in metabolites of six different pathways that could potentially be used in the early diagnosis and prediction of outcome in sepsis. These changes consisted of decreases in acyl glycerophosphocholines (lysophosphatidylcholines), and increases in kynurenine derivatives (kynurenate, kynurenine, quinolinate, serotonin, tryptophan, and xanthurenate); bile acids, carnitine esters, TCA cycle intermediates; and pregnen-sulfated and androgenic steroids.

The pathways identified by the transcriptome data (blood and organs), as particularly associated with survival from sepsis were those of FA metabolism, BCAA catabolism, inflammation, transcription factors, mitochondria, and peroxisomes. The overall conclusion of these data was that non-survival from sepsis is associated with a genomic response that may be responsible for metabolic and

mitochondrial dysfunction in energy production and that the lung contributes to these systemic metabolic responses.

A correlation analysis was used to integrate the lung transcriptome and the plasma metabolome. The greatest dynamic changes in the plasma metabolome were demonstrated by the non-survivors, the correlation of changes between the high dose survivors and non-survivors was therefore chosen as the focus of this correlation analysis. Four very strong mechanistic correlations were identified by this analysis. These consisted of positive correlations between kynureninase and kynurenine pathway metabolites, and peroxisomal genes; TCA cycle intermediates (succinate, malate, and fumarate) and the inflammatory response and cell death genes; and acyl-GPCs and carnitine esters, and genes involved in BCAA-degradation, beta-oxidation and peroxisomal lipid oxidation.

In addition there was also a negative correlations between acyl-GPCs and lysophosphatidylcholine acyltransferase 2 (LPCAT2), an enzyme that can metabolise acyl-GPCs to phosphatidylcholines or acetylate acyl-GPCs to form platelet activating factors (PAFs; 1-alkyl, 2-acylglycerophosphocholines) (Yamashita, Hayashi, Nemoto-Sasaki, *et al.*, 2014).

A logistic regression model was built using four metabolites that were chosen based on their association with the pathophysiology of the disease and their high sensitivity in identifying sepsis in the first cohort. These metabolites were the lysophosphatidylcholine 1-stearoyl-GPC, kynurenine, isovalerylcarnitine and taurolithocholate-3-sulfate (sulphated bile acid). The AUROC curve of the model's ability to differentiate infection from non-infection in this primate cohort based on all four metabolites and stearoyl-GPC alone were comparable at 0.9675 and 0.9519, respectively. The four-metabolite model was also shown to be capable of diagnosing sepsis in two human cohorts with

AUROC curves of 0.78 in a registry of critical illness (RoCI) cohort (Dolinay, Kim, Howrylak, *et al.*, 2012); and 0.6672 and 0.8213 at enrolment and 24-hours post enrolment in the Community Acquired Pneumonia & Sepsis Outcome Diagnostics (CAPSOD) cohort (Kamisoglu, Haimovich, Calvano, *et al.*, 2015), discussed in Section 1.3.4.2.

The overall conclusions of this study were that the metabolic pathways with the greatest importance to survival in sepsis involved FA oxidation, mitochondrial function, and peroxisome activation.

Both studies with two cohorts (exploratory and validation) demonstrated the importance of FA and amino acid metabolism to the outcome in sepsis, with a significant amount of overlap in the findings from the exploratory parts of these studies. Other comparisons were however, limited by the use of a non-septic model in the exploratory cohort in the first study and the validation component focusing predominantly on citrulline.

The fourth study (Li, Liu, Wu, *et al.*, 2013) did not include an additional validation component and its primary aim was to examine metabolic changes associated with the use of two different herbal remedies in an animal model of sepsis (mice). The two herbal remedies were called the LXHX and the QRJD formulae and consisted of Caulis Sargentodoxae, Radix, Paeoniae Rubra, Moutan Cortex; and Rhizoma Corydalis and Radix et Rhizoma Rhei, Radix Scutellariae, Anemone chinensis; and China Ixeris, respectively. This study involved a comparison of three groups of subjects with CLP-induced sepsis and a control group. Two of the three sepsis groups received one of the two above-mentioned herbal remedies, in addition to undergoing the CLP procedure. The third sepsis group underwent the CLP procedure alone and the control group underwent a sham CLP procedure, and neither of these two group receive a Chinese herbal remedy. Differences in the relative concentrations of 18 metabolites were demonstrated between the control group and the sepsis group that did not receive an herbal

remedy. The differences consisted predominantly of metabolites concerned with energy metabolism, lipid transport and mobilisation, and amino acids. These findings were therefore consistent with the earlier studies based on NMR analyses of plasma from rats with CLP-induced sepsis, (as discussed above) but failed to add any further insights into metabolic changes of sepsis not related to Chinese herbal medicines.

Collectively, the results of all of these metabonomic animal studies of sepsis are consistent with changes in FA and amino acid metabolism being potential biomarkers that could be used to diagnose sepsis and the pathways of the greatest importance to survival in sepsis are involved in FA oxidation, and the function of mitochondria and peroxisomes.

1.3.4.2 Clinical Studies

1.3.4.2.1 Critically ill patients with SIRS versus healthy controls

The first two metabolic profiling studies in critically ill patients was carried out in patients with trauma (Mao, Wang, Wang, *et al.*, 2009; Cohen, Serkova, Wiener-Kronish, *et al.*, 2010) (see Table 1.2). This consisted of two ^{1}H-NMR based studies of blood comparing metabolic changes associated with good and bad outcome in patients with trauma: one comparing uncomplicated SIRS to MODS and the other comparing survivors and non-survivors. In the first study involving whole blood (Mao, Wang, Wang, *et al.*, 2009), the SIRS group was associated with increases in amino acids (predominantly BCAAs) and glucose; whereas the MODS group were associated with increases in FFAs, glycerol, creatinine, and lactate. The most discriminating markers of non-survival in the second study were increases in serum levels of lipids such as TAG and mono-unsaturated fatty acids and glycerophospholipids, (identified by their glycerol heads), in addition to increases in glucose, glutamate, ketone bodies and lactate. Increases in both serum lipids and lactate were therefore associated with a poor outcome in both

studies; this consistency support both their role as biomarkers of outcome in trauma and the role of metabolic profiling in critically ill patients.

Table 1.2 Clinical metabolic profiling studies of critically ill patients with non-infected SIRS and sepsis. KEY: 11-HETE: 11-hydroxyeicosatetraenoic acid, ANOVA: analysis of variance, AA: arachidonic acid, BCAA: branched-chain amino acid, COX: cyclooxygenase, FDR: false discovery rate, FA: fatty acid, GPC: glycerophosphocholine, HC: healthy control, lysoPC: lysophosphatidylcholine, MODS: multi-organ dysfunction syndrome, O-PLS: orthogonal-PLS, PC: phosphatidylcholine; PLS: projection to latent structures, PLS-DA: PLS-discriminative analysis, PCA: principal component analysis, PGE_2: prostaglandin E_2, SIRS: systemic inflammatory response syndrome, TAG: triacylglyceride, TCA: tricarboxylic acid; TXB_2: thromboxane B_2.

Year	Author	Samples; platform	Subjects	Results: differentiating metabolites identified	Additional results	Statistical methods
			Critical ill patients with SIRS versus healthy controls			
2009	Mao *et al*	Serum ^{1}H-NMR	3 groups : (1) Severe trauma and SIRS (n = 26) (2) Severe trauma and MODS(n = 26) (3) Healthy controls (n= 26)	**MODS versus SIRS and both trauma groups versus healthy controls:** MODS: ↑ free fatty acids, glycerol, creatinine and lactate; SIRS:↑amino acids (predominantly BCAAs) and glucose		PCA; O-PLS-DA
2010	Cohen *et al*	Whole blood ^{1}H NMR	3 groups: (1) Severe trauma survivors (n= 23) (2) Severe trauma non-survivors (n= 9) (3) Healthy controls (n = 7)	**Non-survival versus survival and both trauma versus healthy controls:** ↑glucose, glutamate, ketone bodies, lactate and lipids: TAGs, mono-unsaturated fatty acids and glycerophospholipids		PLS-linear-discriminative analysis
2011	Park *et al*	Plasma ^{1}H-NMR	3 groups: (1) Acute lung injury treatment arm (n = 6) (2) Acute lung injury placebo arm (n = 6) (3) Healthy controls (n= 8)	**(1) Acute lung injury treatment versus acute lung injury placebo:** ↑lysyl moiety of albumin on day 2; alanine, LDL and VLDL on day 3; and valine and cholesterol on days 2 and 3; in addition to correlations between time and concentration of 1-methylhistidine, alanine, valine and HDL in the albumin treatment group. **(2) Treatment and placbeo acute lung injury versus healthy controls:** no details except a time-dependent trajectory of the treatment group towards healthy controls' metabolic profile		PCA, mixed model repeated measures ANOVA and two-sample t-tests
			Critically ill patients with sepsis versus healthy controls			
2011	Stringer et al	Plasma ^{1}H-NMR	2 groups: (1) Sepsis related acute lung injury (n = 13) (2) Healthy controls (n = 6)	**Sepsis related acute lung injury versus healthy controls:** ↑ adenosine, glutathione and phosphatidylserine; ↓sphingomyelin		An unpaired Student's t-test (FDR of 5%)
2012	Bruegel *et al*	Whole blood: LPS activated	2 groups: (1) Sepsis (n=25) (2) Healthy controls (n= 15)	**LPS activated whole blood samples sepsis versus healthy controls:** ↓ release of AA, five AA analogues; COX-dependent AA metabolites: PGE2, 11-HETE; TXB2; (2) statistically significant ↓ in AA, PGE2, 11-HETE; TXB2 that were associated with unfavourable outcome at 2 weeks and a increased disease severity	**Septic versus healthy controls:** ↓ inducibility of COX-2 mRNA	T -test and Mann-Whitney U test for normally and non-normally distributed data ($p<0.05$)
			Critically ill patients with sepsis versus non-infected SIRS			
2012	Schmerler *et al*	Plasma LC-MS/MS	3 groups: (1) Sepsis (n=30) (2) Non-infected SIRS (n= 33)	**Sepsis versus non-infected SIRS:** ↑acyl-carnitines and glycerophosphatidylcholines: particularly an acyl-carnitine with 10 carbons and one double bond (C10:1) and a diacyl-glycerophosphatidylcholine PC with total of 32 carbons and no double bonds (PCaa32:0)		Student's t -test and Mann-Whitney U test for normally and non-normally distributed data ($p<0.05$) with Bonferroni correction.

Table 1.2 continued

2013	Langley *et al*	Plasma LC-MS/MS	3 groups: (1) Sepsis non-survivors (n= 31) (2) Sepsis survivors (n= 90) (3) Non-infected SIRS (n= 29)	**(1) Sepsis non-survivors versus survivors:** significant ↑ 17 amino acid catabolites, 16 carnitine esters, 11 nucleic acid catabolites, five metabolites of glycolysis and the TCA cycle (citrate, dihydroxyacetone, malate, pyruvate, and phosphate), and four free fatty acids; in addtion to ↓ seven glycerophosphocholines (GPCs) and glycerophosphoethamolamine (GPE) esters; ↑ lactate, and acyl-carnitines were the most discriminatory **(2) Sepsis survivors versus non-infected SIRS:** ↓TCA cycle metabolites citrate and malate, glycerol, glycerol 3-phosphate, phosphate, 21 amino acids and their catabolites, 12 GPCs and GPE esters, and six carnitine esters	Trends: Anabolic steroids were decreased in the sepsis non-survivors, whereas the catabolic steroid cortisone was increased	PCA and Bayesian factor analysis and ANOVA with renal function and liver disease as fixed effects to control fof these confounding factors
2013	Blaise *et al*	Plasma ^{1}H-NMR	2 groups: (1) Trauma with the development of sepsis (n= 10) (2) Trauma without the development of sepsis (n= 12)	**Trauma with secondary sepsis versus trauma without sepsis:** ↑ aspartate and citrate (TCA cycle) , valine (BCAA), beta-hydroxybutyrate (ketone body); and allantoin (oxidation product of uric acid)		PCA; O-PLS-DA
2014	Seymour *et al*		2 groups: (1) Sepsis and pneumonia non-survivors (n= 15) (2) Sepsis and pneumonia survivors (n= 15)	**Sepsis non-survivors versus sepsis survivors:** ↑ in sulfated bile acids (taurochenolate sulfate and glycochenolate sulfate; p<0.01 for both) and primary bile acids (taurocholate; p<0.05); steroid metabolism (↑ cortisol (p<0.01), cortisone (p<0.05), and sulfated hormones (5-alpha-pregnan-3alpha, 20-beta-diol disulfate, 21 hydroxypregnenolone disulfate, pregnanediol-3-glucuronide, and pregnenolone sulfate; p<0.04 for all)); and oxidative stress, including five nucleic acids (allantoin, N1-methyladenosine,N2, N2-dimethylguanosine, N6-carbamoylthreonyladenosine and pseudouridine) were shown to have significantly ↑ in non-survivors compared to survivors.	**(1) In vitro human monocyte stimulation studies:** β-pseudouridine induced a significant release of TNFα and IL-1β, and allantoin significantly increased IL-1β. **(2) Mouse model of caecal ligation and puncture-induced** significant ↑ in both liver and kidney homogenate at 8hr of pseudouridine (p = 0.026 and 0.01, respectively) and N1-methyladenosine and allantoin in the liver (p = 0.031) and kidney (p=0.01) homogenates, respectively	Wilcoxon signed rank test (p=0.05); FDRs were estimated for each metabolite using q values and only metabolites with q< 0.1 were deemed significant. Differentiating metabolites were determined using random forests obtained using a supervised classification technique based on decision trees
2014	Su *et al*	Serum LC-MS/MS	4 groups: (1) Severe sepsis or septic shock (n= 25) (2) Uncomplicated sepsis: (n= 10) (3) Non-infected SIRS (n= 15) (4) Healthy controls (n= 15)	**(1) Sepsis cohort versus non-infected SIRS versus healthy controls**: clear separation on PCA score plots; differentiating metabolites of HCs not investigated **(2) Sepsis versus non-infected SIRS:** ↓ lactitol dehydrate (a hydrophilic carbohydrate) and S-phenyl-d-cysteine and ↑ in S-(3-methylbutanoyl)-dihydrolipoamide-E (intermediate in the synthesis of branched chain fatty acids and in the degradation of branched chain amino acids) and N-non-anoyl glycine **(3) Severe sepsis/septic shock versus uncomplicated sepsis:** ↓glyceryl-phosphoryl-ethanolamine (a membrane breakdown product of phosphatidylethanolamines), Ne, Ne-dimethyl-lysine, phenylacetamide (intermediate in phenylalanine metabolism) and d-cysteine (p<0.05); **(4) death within 48 hours :** ↓ S-(3-methylbutanoyl)-dihydrolipoamide-E, phosphatidylglycerol (22:2 (13Z, 16Z)/0:0), glycerophosphocholine and S-succinyl glutathione (p<0.05)		PCA, O-PLS and PLS-DA

Table 1.2 continued

2015	Kamisoglu *et al*	Plasma LC-MS/MS	4 groups: (1) Sepsis non-survivors (n= 31) (2) Sepsis survivors (n= 90) (3) LPS-induced endotoxaemia in healthy controls (4) Non-infected SIRS (n= 29)	**(1) Sepsis cohort and healthy controls with LPS-induced endotoxaemia versus non-infected SIRS:** ↑ 2-hydroxybutyrate (a by-product in the synthesis of glutathione), mannose (carbohydrate), bilirubin and lipids including acyl-carnitines, docosapentaenoate (C22:5 FA), palmoioleate (C16:1 FA) and the steroid pregen-diol disulphate; and ↓ 2-palmItoyl-GPC (16:0) (lyso-PC) and amino acids **(2) Sepsis survivors versus non-survivors** ↑ acyl-carnitines were the most discriminatory metabolites	Welch's t-test (unequal variances ; α = 0.05); Benjamini and Hochberg methods to calculate q values and metabolites with p- and q-value < 0.05 deemed significant

These two trauma metabolic profiling studies were followed by a ^{1}H NMR study (Park, Jones, Ziegler, *et al.*, 2011) based on serial plasma samples from a subset of patients from a randomised controlled trial (RCT) comparing the use of albumin to placebo in the treatment of acute lung injury (ALI) of multiple causes. In this RCT, an improvement in oxygenation (in addition to normalisation of the albumin levels) was associated with the treatment with albumin and furosemide compared to treatment with placebo and furosemide. The patient samples in this accompanying NMR study were therefore divided into two groups: treatment and placebo. The metabolic profiles of samples taken from these two groups at baseline (prior to randomisation to these treatment groups) and on days one, two, three and seven after randomisation, were compared with each other and a group of healthy controls. Multivariate statistical analyses of the metabolic differences between the three groups of the study failed to demonstrate any separation of the baselines samples but did demonstrate separation of the two patient groups from day two onwards. Univariate analyses of the metabolic differences demonstrated between the two treatment groups demonstrated statistically significant increases in the lysyl moiety of albumin on day two, alanine, LDL and VLDL on day three; and valine and cholesterol on both days two and three. It is noted that the lysyl moiety was the only component of albumin that contributed towards the separation of the two treatment groups on the *unsupervised* multivariate statistical analyses (principal component analysis) plots. The effect of time on the quantities of the differentiating metabolites was then evaluated using mixed models of repeated measures of variance. Significant correlations were demonstrated between time and the concentrations of HDL, 1-methylhistidine, alanine and valine in the albumin group samples. The fact that these metabolites are unrelated to albumin strengthened the authors' argument that the separation of the placebo and the albumin groups of the multivariate statistical analyses (MVA) was not solely as a consequence of albumin metabolites. Moreover, it provided further support of the role of these metabolites in the underlying pathophysiology of ALI; the correlations between the differentiating metabolites and time in this study, also support the use of serial metabolic profiling to track changes related to organ failures and outcome. Further support of the ability of metabolites to

predict outcome was also illustrated by the trajectory towards the healthy controls profiles, demonstrated by the albumin group's day seven samples. The clustering together of the patients from each of the two treatment arms in this study, involving patient with ALI secondary to a range of aetiologies, suggests that the patient's response to the ALI may have more influence on metabolic profile than aetiology.

1.3.4.2.2 Critically ill patients with sepsis versus healthy controls

In 2011, the first metabolic profiling study dedicated solely to metabolic changes associated with sepsis was published by Stringer *et al* (Stringer, Serkova, Karnovsky, *et al.*, 2011). This landmark study consisted of a comparison of a cohort of patients with sepsis-induced acute lung injury and healthy volunteers and included a univariate analysis of the metabolites detected in their plasma samples using ^{1}H NMRS. This demonstrated significant increases in the levels of the lipid metabolites phosphatidylserine, the ATP metabolite adenosine, and glutathione (a coenzyme of oxidation–reduction reactions in cells) and decreases in sphingomyelin, in the ALI group compared to the healthy controls. These changes were thought to represent changes in the metabolic pathways of endothelial barrier functions, energy mobilisation, oxidative stress and apoptosis in sepsis compared to the healthy state. These findings, particularly those related to changes in energy metabolism, were also consistent with the differences in levels of pyruvate, ketone body and fatty acid metabolism demonstrated by earlier studies comparing of animal model of sepsis and sham surgical controls.

A second metabolomic study comparing sepsis and healthy controls was performed by Bruegel *et al* using both lipopolysaccharide (LPS)-activated and non-activated (i.e. baseline) whole blood samples (Bruegel, Ludwig, Kleinhempel, *et al.*, 2012). In this study principal component analyses (PCA) of the LCMS-MS arrays of the samples from the baseline and LPS- activated samples from septic and control

groups were used to demonstrate nine arachidonic acid (AA; the polyunsaturated fatty acid omega-6 20:4) metabolites that could be used to differentiate between the groups.

This consisted of AA, five arachidonic acid analogues (identified using AA with eight deuterium atoms: AA-d_8 and differentiated according to their MS m/z and retention time), and the cyclooxygenase (COX)-dependent AA metabolites: prostaglandin-E_2 (PGE_2), 11-hydroxyeicosatetraenoic acid (11-HETE) and thromboxane-B_2 (TXB_2). The LPS-activated blood samples from the sepsis patients demonstrated significantly lower increases in AA, and PGE_2 and 11-HETE (two of the COX-dependent AA metabolites) from baseline compared to the healthy controls. Greater increases in these four metabolites between baseline and LPS-activated samples from second sepsis cohort was also demonstrated to be associated with a favourable outcome at day 14 and a reduced disease severity (severe sepsis as opposed to septic shock) on admission to the ICU. Genetic studies of COX-2 and microsomal prostaglandin E synthase-1 (mPGES-1; a biosynthetic enzyme of PGE_2) regulation were also performed to investigate the underlying mechanisms of the differential increases in the COX-2 dependent metabolites in the LPS-activated blood samples between the patients from the second sepsis cohort and healthy controls. These studies demonstrated a reduced inducibility of COX-2 mRNA in the second sepsis cohort compared to healthy controls but no significant differences in mPGES-1 induction between the two groups. These findings substantiated the inhibition of COX-2 in sepsis but failed to support the hypothesis of the direct inhibition of the downstream PGE_2 enzyme, PGES-1.

1.3.4.2.3 Critically ill patients with sepsis versus non-infected SIRS

The previous two 'proof of concept' studies of the use of metabolic profiling using ^{1}H-NMR and LCMS in patients with sepsis have been somewhat superseded by several studies comparing sepsis with more clinically relevant comparisons, such as patients with non-infected systemic inflammatory

response syndrome, as opposed to healthy controls. These have included four studies published in the last four years, each examining different aspects of the use of metabolic profiling in sepsis.

The first explored the use of LC-MS of plasma samples in the differentiation of patients with sepsis from those with non-infected SIRS (Schmerler, Neugebauer, Ludewig, *et al.*, 2012). This study identified acyl-carnitines and glycerophosphatidylcholines as the metabolites of the greatest importance to this differentiation, with sepsis being associated with significantly higher levels of these metabolites, especially an acyl-carnitine with 10 carbon atoms and one double bond (C10:1) and a diacyl-glycerophosphatidylcholine (with 32 carbon atoms and no double bonds; PCaa32:0).

The next study examined metabolic changes associated with the development of sepsis in trauma patients, using NMR analyses of plasma (Blaise, Gouel-Chéron, Floccard, *et al.*, 2013). In this study, the development of sepsis was associated with increases in metabolites of the tricarboxylic acid (TCA) cycle (aspartate and citrate), valine (BCAA), beta-hydroxybutyrate (ketone body); and allantoin, an oxidation product of uric acid. Under normal circumstances, uric acid is the end product of purine (nucleic acids) metabolism; and uric acid is only converted by oxidation to allantoin by reactive oxidative species in the context of oxidation stress. Allantoin is therefore considered as a biomarker of oxidation stress. Oxidative stress in sepsis, resulting in the oxidation of uric acid, could therefore, be responsible both the increases in allantoin associated with the development of sepsis in this study and decreases in uric acid levels demonstrated in the experimental model of sepsis in the metabonomic study by Liu *et al*, (Liu, Zheng, Ji, *et al.*, 2010) discussed in section 1.3.3.

In 2014, Su *et al* (Su, Huang, Zhu, *et al.*, 2014) performed a study of the metabolic differences between patients with sepsis, non-infected systemic inflammatory response syndrome and healthy controls using LCMS analyses of serum. This included two sepsis groups, one with uncomplicated sepsis and

the other with severe sepsis or septic shock. Comparisons of the group with non-infected systemic inflammatory response syndrome and the sepsis group as a whole, demonstrated statistically significant decreases in the levels of lactitol dehydrate and S-phenyl-d-cysteine and increases in S-(3-methylbutanoyl)-dihydrolipoamide-E and N-non-anoyl glycine in sepsis compared to the non-infected SIRS. Two subgroup analyses of the patients with sepsis were also performed to investigate metabolites associated with a greater severity of sepsis at presentation and death within 48 hours of the onset of sepsis. These analyses revealed that decreases in glyceryl-phosphoryl-ethanolamine (GPEs; phospholipid), Ne, Ne-dimethyl-lysine, phenylacetamide (an intermediate in phenylalanine metabolism) and d-cysteine ($p<0.05$) were associated with sepsis of a greater severity at presentation. Whereas decreases in S-(3-methylbutanoyl)-dihydrolipoamide-E, the phospholipids phosphatidylglycerol (22:2 (13Z, 16Z)/0:0) and glycerophosphocholine, and S-succinyl glutathione ($p<0.05$) were associated with death within 48 hours of their presentation. The significance of lipids in the differentiation these prognostic groups in this cohort of patients with sepsis is consistent with the findings of the two trauma studies discussed earlier which also demonstrated lipids, particularly glycerophospholipids and fatty acids, as important to the differentiation of patients with good and bad prognoses. Glutathione was also one of the metabolites characterising sepsis-induced acute lung injury compared to healthy controls in the metabonomic study by Stringer *et al* (Stringer, Serkova, Karnovsky, *et al.*, 2011).

More recently, Kamisoglu and colleagues have published the findings of a comprehensive study comparing LPS-induced endotoxaemia in healthy volunteers and patients with non-infected and infected SIRS (i.e. sepsis), taken from the Community Acquired Pneumonia & Sepsis Outcome Diagnostics (CAPSOD) study (Kamisoglu, Haimovich, Calvano, *et al.*, 2015). In this comparison, the metabolic responses shared by the LPS-induced endotoxaemia and sepsis groups consisted of 16 metabolites, 15 of which changed in the same direction. Whereas, of the 18 metabolites associated

with the non-infected SIRS and LPS-induced endotoxaemia groups, only eight changed in the same direction. Changes common to both the endotoxaemia and sepsis cohort included increases in 2-hydroxybutyrate (a by-product of glutathione synthesis), mannose (a monosaccharide involved in glucose metabolism and glycosylation), bilirubin, and lipids including acyl-carnitines, docosapentaenoate, palmoioleate and the steroid pregen-diol disulphate. There were also decreases in the lysophosphatidylcholine (lyso-PC) 2-palmItoyl-glycero-3-phosphocholine (16:0), the nucleotide uridine and four amino acids in these two groups compared to the non-infected SIRS. Moreover, the acyl-carnitines were the most discriminatory metabolites in the differentiation of sepsis survivors and non-survivors.

Comparison of the trends of the metabolic changes of the sepsis survivors, sepsis non-survivors and the endotoxaemia groups demonstrated a commonality in the changes of 19 metabolites between the LPS-induced endotoxaemia and sepsis survivors that were capable of differentiating between the sepsis survivors and non-survivors. These findings supported the study's hypothesis that LPS-induced endotoxaemia in humans is associated with an induction and a recovery phase that replicates a host response that is essential to the survival from sepsis that can be differentiated from the mal-adaptive response to sepsis that is associated with non-survival. Moreover, the metabolic differences demonstrated between LPS-induced endotoxaemia and non-infected SIRS also support the use of metabolic profiling in the differentiation of infected and non-infected SIRS.

The metabolic differences between the three groups of patients in the CAPSOD study (non-infected SIRS and the sepsis 28-day survivors and non-survivors) were originally reported in an earlier paper by Langley *et al* (Langley, Tsalik, van Velkinburgh, *et al.*, 2013). This paper reported significant differences between the sepsis survivors and non-survivors consisting of 17 amino acid catabolites, 11 nucleic acid catabolites, five metabolites of glycolysis and the TCA cycle, and four free fatty acids. In addition to

decreases in seven glycerophosphocholines (GPCs) and glycerophosphoethamolamine (GPE) esters, and an increased lactate, in the sepsis non-survivors compared to the sepsis survivors. Moreover, acyl-carnitines were shown to the most important metabolites in the differentiation of sepsis survivors and non-survivors. Several metabolic differences were also demonstrated between the sepsis survivors and the patients with non-infected SIRS. These included decreases in the TCA cycle metabolites citrate and malate, glycerol, glycerol 3-phosphate, phosphate, 21 amino acids and their catabolites, 12 GPC and GPE esters, and six carnitine esters in the sepsis survivors. This comparison of the sepsis survivors and the patients with non-infected causes of SIRS also demonstrated increased concentrations of six acetaminophen (paracetamol) catabolites and two androgenic steroids in the sepsis survivors.

In 2014, Seymour and colleagues published a study examining a similar cohort of patients to the sepsis cohort from the CAPSOD study (Seymour, Yende, Scott, *et al.*, 2013). In this later study, plasma samples from patients with sepsis secondary to CAP taken from the Genetic and Inflammatory Markers of Sepsis (GenIMS) study were analysed using LC-MS to determine the metabolic changes associated with 90-day survival. Univariate analyses based on this LC-MS data demonstrated differences between survivors and non-survivors, predominantly in metabolites of the stress response, bile acid (BA) metabolism and oxidative stress, of which five nucleic acids were shown to have significantly greater levels in non-survivors compared to survivors. Of these, pseudouridine was thought to be of the greatest importance and this metabolite was therefore chosen to be the subject of a series of further investigations in animal model of sepsis. These studies revealed increased levels of pseudouridine in both the liver and kidneys from mice with CLP-induced sepsis compared to control subjects (undergoing sham procedures). Pseudouridine was also shown to be capable of increasing the expression TNFα and interleukin-1β (IL-1β) in monocytes compared to controls in these animal models of sepsis, consistent with the study other findings suggesting pseudouridine may have a pro-inflammatory role in sepsis that is associated with a decreased 90-day survival rate.

Overall, these studies have demonstrated differential changes in six groups of metabolites between patients with sepsis and those with non-infected SIRS. These changes consisted of decreases in BCAAs and increases in acyl carnitines, GPCs, and metabolites of the TCA cycle, ketone bodies and non-BCAAs. In addition, the studies examining survival demonstrated non-survival in sepsis was characterised by decreases in glycerophospholipids and increases in acyl-carnitines, nucleic acids, and catabolites of non-carbohydrate energy sources.

Furthermore, these clinical metabolic profiling studies of sepsis have demonstrated the potential of metabonomics and metabolomics as clinical tools in the early diagnosis of sepsis, markers of severity at presentation and the prediction of the outcome in terms of survival. Other factors related to the outcomes in sepsis that have not been addressed by these studies include the development of organ failures. There are also gaps in our knowledge with regards to the feasibility of the metabolic profiling in patients with sepsis based on NMR analyses of urine. Study sought to address these gaps in our knowledge of the metabolic profiling of patients with sepsis; with a view to identifying metabolic signatures of sepsis that could aid the diagnosis of outcomes in sepsis.

1.4 Nuclear magnetic resonance spectroscopy

The information in this section on NMR was derived from multiple sources including three key reference textbooks (Hore, 1995; Friebolin, 1998; Günther, 1995).

Nuclear magnetic resonance spectroscopy exploits the characteristic spin that the nuclei of many isotopes of elements such as ^{1}H possess. Atomic nuclei contain positively charged protons, neutrons with a neutral charge, and are orbited by negatively charged electrons that shield the nucleus from

external forces such as an external magnetic force. All of these subatomic particles can be viewed as spinning on their axes. Atomic nuclei have an overall spin (*I*) if the sum of the number of neutrons and protons is an odd number, in which case they have half an integral spin (*I*=½; e.g.^{1}H) or an integral odd multiple of ½. If there is an odd number of both neutrons and protons, they have an integral spin (e.g. *I*=1). The spinning of a positively charged nucleus, such as ^{1}H, induces a nuclear magnetic moment (μ) or a force which is a combination of the degree of rotation enforced upon it by other external magnets (known as the torque) and the strength of its pull on other magnets. This magnetic moment (μ) is proportional to its the nuclear spin (*I*) by the following equation $\mu = \gamma I h/2\pi$; where γ is the gyromagnetic ratio (an intrinsic physical property of each nucleus) and h is Planck's constant.

In the presence of an external magnetic field (B_o), the nuclei rotate about the axis of the B_0. Atomic nuclei can exist in a number of possible spin states according to the equation: $2I + 1$; atomic nuclei that have a ½ spin (*I*) such as ^{1}H, therefore exist in two spin states: one with a higher energy state and one with the lower energy state. The magnetic moment (μ) of the lower energy state is aligned with the external magnet (B_o) known as the α, parallel or +½ state, whereas the μ of the higher energy state spins opposite to the direction of B_0, known as the β, anti-parallel or -½ state. There is an excess of nuclei in the parallel state (N_α) compared to the anti-parallel (N_β) in the presence of an external magnetic field, described by the Boltzmann distribution: $N_\alpha / N_\beta = e^{\Delta E/kT}$, where ΔE is the energy difference between the two energy states, *k* is the Boltzmann constant (k=1.3806 x 10^{-23} J/Kelvin) and T is the temperature in Kelvin ([K] = [°C] + 273.15). The alignment of the nuclei with the external magnetic field about the z –axis is not perfect: there is a small degree of rotation or torque, which causes the spinning nuclei to wobble or precess about the z axis like a spinning gyroscope. This precession has an angular frequency called the Larmor frequency (ω_0), an angular frequency, which is related to the gyromagnetic ratio (γ) of the nuclei according to the following equation: $\omega_0 = \gamma B_0$ or in frequency term $\nu_0 = \gamma B_0/2\pi$. The Larmor frequency is the frequency required to transit from lower to

higher energy states and is given by the following equation: $\Delta E = h\nu_0 = h\gamma B_0/2\pi$. This equation illustrates that the energy difference between these two states, which is very small, is proportional to the strength of the external magnetic field and can therefore be increased by increasing the strength of the external magnetic field.

An NMR machine includes two magnets: one to produce the external magnetic field that causes separation of the ^1H nuclei into two energy states and a second one to provide the energy for some of the nuclei to transit from lower energy state to the higher energy state. In the example of ^1H NMR this is within the radiofrequency (RF) range. The coil that is used to provide the second magnetic field is also used to detect the frequency and amplitude of the signal produced by the nuclei when they resonate. Ordinarily, the application of the RF pulse in the direction of the precessing nuclei would shift the overall alignment of the magnetisation of the proton nuclei into an antiparallel (negative) state of longitudinal magnetisation (M_z) associated with an increase in the number of nuclei in the higher energy state. Longitudinal magnetisation involves precession in a vertical direction which is difficult to visualise and is therefore not ideal. If, however, the RF pulse is applied at a 90° angle the direction of magnetisation is shifted from being in a vertical direction (around z axis) to being in x-y plane, described as transverse magnetisation (M_{xy}) (see Figure 1.1).

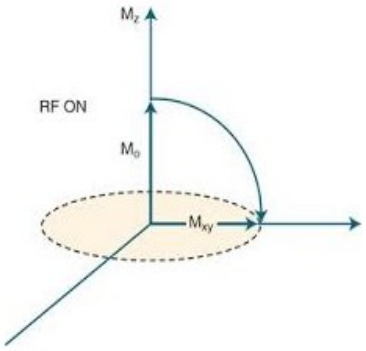


Figure 1.1 Illustration of the conversion of longitudinal magnetization (M_z) to transverse (M_{xy}) magnetization (signal) with the application of a 90° RF pulse. KEY: RF: radiofrequency.

When the RF pulse is stopped, the nuclei that moved from the lower energy state to the higher energy state, flip back to the lower energy state and emit the extra energy at the frequency of this energy transition. This relaxation phase involves the loss of kinetic energy through two different processes. The first process is called spin-lattice relaxation (T_1). Nuclei within a sample have both rotational and vibrational motion but are held together within a lattice. The movement of nuclei in the higher energy state within this lattice results in the loss of their excess energy and causes them to return to their lower energy state. The spin-lattice relaxation is dependent on the mobility of the lattice. The T_1 relaxation phase is associated with the resumption of their original orientation of precessing around the z axis and thus the return of the longitudinal magnetization of the nuclei. The second process results from loss of energy due to neighbouring nuclei causing each other to flip between the two energy states, which is called spin-spin relaxation, T_2 phase. These two phases of relaxation are detected and amplified by the NMR machine. The T_2 phase relaxation involves the visualisation of the loss of transverse magnetisation (NMR signal) which, in view of its exponential decrease with time, is called the free induction decay (FID). NMR machines can either deliver RF pulses that irradiate each set of nuclei in turn or excite all the proton nuclei in a molecule at the same time. In the case of the latter and more common technique, the resonance signals are collected together producing a summation plot of signals measured against time. This is then processed using a Fourier transformation: a mathematical analysis which converts this complex time domain signal into the frequency domain spectrum that constitutes the typical raw NMR spectrum, with frequency signals plotted against amplitude (as illustrated in Figure 1.2).

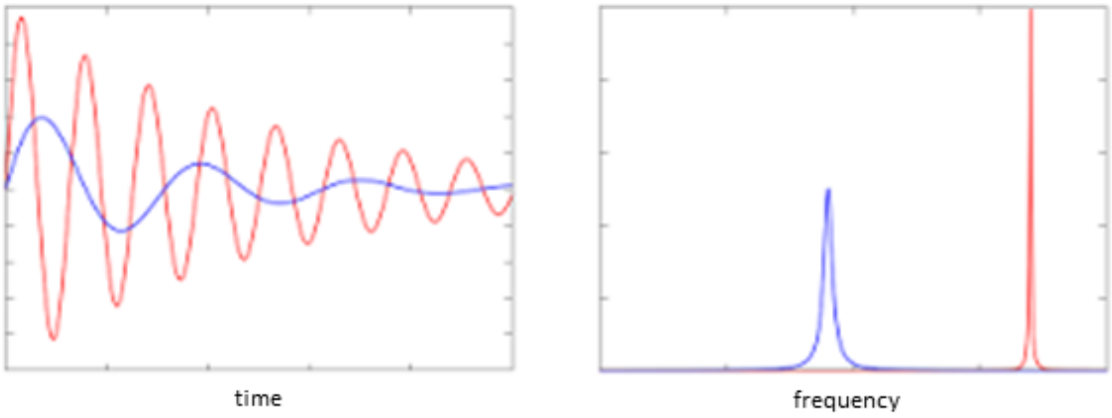


Figure 1. 2 Illustration of the process of Fourier transformation used to convert the NMR time domain signals into a frequency domain spectrum.

The ability to identify compounds in a sample using NMR spectroscopy relies on differences in the behaviour of proton nuclei in different chemical and molecular electronic environments that causes proton signals with a range of different resonance frequencies. These differences are caused by differences in the shielding of the nuclei of the protons by electrons. The main factors determining the shielding effect of electrons are the affinity for electrons (electronegativity) of the elements and the electron density: the greater the electron density, the greater the nuclei are shielded from the applied magnetic field. Resonance signals on the right side of the NMR spectrum (upfield) indicate proton nuclei that are more shielded than those on the left side of the spectrum (downfield). In other words, the nuclei that are more shielded (higher electron density) are exposed to a lower effective magnetic field.

On NMR spectrum, unlike other forms of spectroscopy, the location of resonance signals is dependent on the external magnetic field strength of the instrument being used. The specific location of NMR signals is therefore reported in relation to a reference signal of a standard compound that is added to the sample: most commonly 3-(trimethylsilyl)-propionate-2,2,3,3-d_4 (TMSP-d_4), which produces a single sharp peak. The frequency difference between the standard ($v_{standard}$) and the other compounds

($v_{compound}$) in the sample is called chemical shift and is dependent on the strength of the external magnetic field. To adjust for this field dependency, this frequency difference is divided by the operating frequency ($v_{operating}$) of the spectrometer, ($v_{compound}$-$v_{standard}$)/$v_{operating}$; and given the numerator is expressed in hertz and the dominator in megahertz producing a very small number, the chemical shift is expressed in parts per million (ppm). Using this system, the proton resonances of the majority of organic compounds lie within a 12 ppm range and resonances in ppm are directly comparable across NMR instrument with different magnetic field strength.

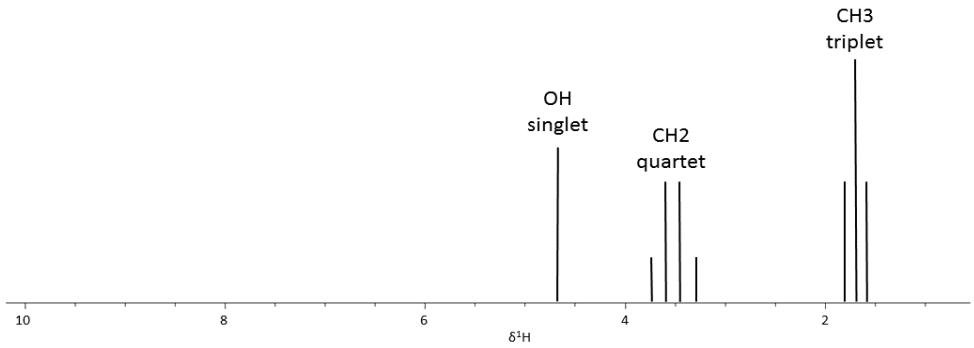


Figure 1.3 Illustration of ^{1}H NMR spectrum of ethanol demonstrating the singlet, quartet, and triplet of its hydroxy (OH), methylene (CH_2) and methyl (CH_3) groups, respectively.



Figure 1.4 Illustration of the possible spin orientations of methylene (CH_2) and methyl (CH_3) groups.

Compounds that contain different groups of protons such as methyl (CH_3) and methylene (CH_2), exhibit proton resonance signals in multiplets instead of a single NMR signals. This occurs as a result of the

multiple number of possible spin orientations of the protons in these groups. Using the ^{1}H NMR spectrum of ethanol, shown in Figure 1.3, as an example, the methyl group CH_3 peak is split into a triplet (three peaks), whereas the methylene group CH_2 is split into a quartet (four peaks). This occurs as consequence of interactions between these two groups of protons and is called coupling. It is noted that the space between each of the peaks in these multiplets is equal. This is called the coupling constant *J* and it can be used to illustrate that these signals are part of a multiplet attributed to a group of protons. The methylene group contains two protons, each of which can be aligned with the external magnetic field or opposing it. These give four possible spin states (see Figure 1.4): one where the two protons are aligned with external field, one where they are both opposing it, and two spins states where the two protons are in opposite directions. The spins paired in the opposite direction of the external magnetic field cause a reduction in the field experienced by the methyl protons. This shielding effect results in a marginally stronger field strength is required to cause them to resonate, i.e. an up-field shift. Conversely, spins paired in the same direction of the external field cause a slight increase in the field experienced by the methyl protons resulting in a downshift resulting from the protons resonating at a slight lower external magnetic strength. These two spin combinations are responsible for the smaller peaks either side of the central peak which represents the resonance of the two pairs of spins that are in opposite directions. The effect of the four possible spin orientations of the methylene protons on methyl proton can be viewed of as a 1:2:1 ratio: one causing an upshift, two causing no movement and one causing a down-shift. The methyl group, on the other hand, has three protons resulting in eight possible spin orientations, split into a 1:3:3:1 ratio (see Figure 1.4): one group (of three) causing an up-shift, one group causing a down-shift and two groups of three magnetically equivalent combinations one causing an upshift and the other a downshift with peaks of greater magnitude than the peaks representing the effect of just one group.

Spin-echo sequences can be used to correct for some of the magnetic field inhomogeneity (variations in the field at different parts of the sample) that causes some spins to slow down due to lower field

strength, while others speed up due to higher field strength and go on ahead of the slower ones. This problem causes the signal to decay. By applying a 180° pulse after the delay period of the first 90° pulse the transverse magnetisation is flipped by 180°. The slower spins are moved ahead of the faster spins by virtue of a 180° flip, as illustrated in Figure 1.5. The faster spins will catch up with the slower spins, that will drift back towards the net overall main moment; enabling a complete refocusing, resulting an accurate T_2 FID to be recorded. Large molecules such as lipids are particularly affected by such magnet field inhomogeneity, and this sequence is therefore frequently applied to blood samples that contain macromolecules such as lipids.

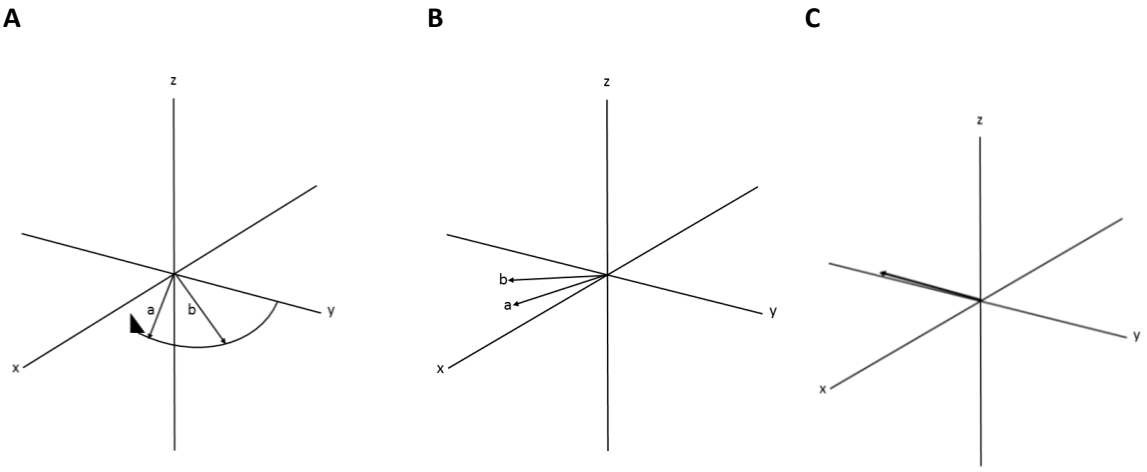


Figure 1.5 Illustration of the effect of magnet inhomogeneity using a vector model in which two vectors rotating in the transverse plane are used to represent two nuclei magnetisations rotating at different frequencies and the effect of a 180-degree RF pulse. KEY: RF: radiofrequency pulse.

A. Vector b is rotating at a lower frequency due to exposure to lower field strength; whereas vector a is rotating with a higher frequency due to exposure to a higher field strength.

B. Following the application of a 180-degree RF pulse the vectors are rotated around the x axis by 180 degrees resulting in vector b being ahead of vector a.

C. The frequencies of the two vectors remains unchanged with vector b rotating at a slower frequency than vector a. Eventually vector a catches up with vector b and they are then described as being re-focussed.

1.4.1 Two-dimensional Nuclear magnetic resonance spectroscopy

Two-dimensional (2-D) NMR experiments can provide information about the structures of complex compounds by instigating the transfer of energy between nuclei connected by certain types of bonds.

2-D NMR experiments can either be signals from the same isotope (described as homonuclear) or two different isotopes (termed heteronuclear; e.g. ^{1}H and ^{13}C). In both cases, there is an extra phase in addition to the three stages of 1-D experiment: preparation, evolution, and detection periods. In ^{1}H-^{1}H 2-D NMR experiments this extra phase is called the mixing period and follows the evolution period, after the RF pulse has been applied (preparation) and the nuclei have been left to precess. During this mixing period, a second RF pulse is applied and there is the transfer of magnetisation between nuclei. This transfer only occurs between nuclei connected by covalent bonds and the RF pulse sequence can be adjusted according to whether distant or close bonds are under investigation. The transfer of magnetisation results in a change in the resonance frequency of the nuclei involved in the exchange. This change in frequency can be visualised on Fourier transformed 2-D NMR data plots as cross peaks, as illustrated in Figure 1.6. Nuclei that do not undergo such exchange retain the same precession frequency coordinate on each axis and therefore lie along the diagonal of the 2-D spectrum plot and are called diagonal peaks on 2-D NMR plots. In summary, it is the cross signals on 2-D NMR spectra that indicate the interaction between two nuclei of interest. The principle is the same in heteronuclear 2-D NMR experiments, where nuclei of the two different isotopes are excited in turn using two sequential RF pulses of different frequency ranges. The interactions between nuclei of these isotopes can be determined and thus utilised to determine structural bonds between these isotopes.

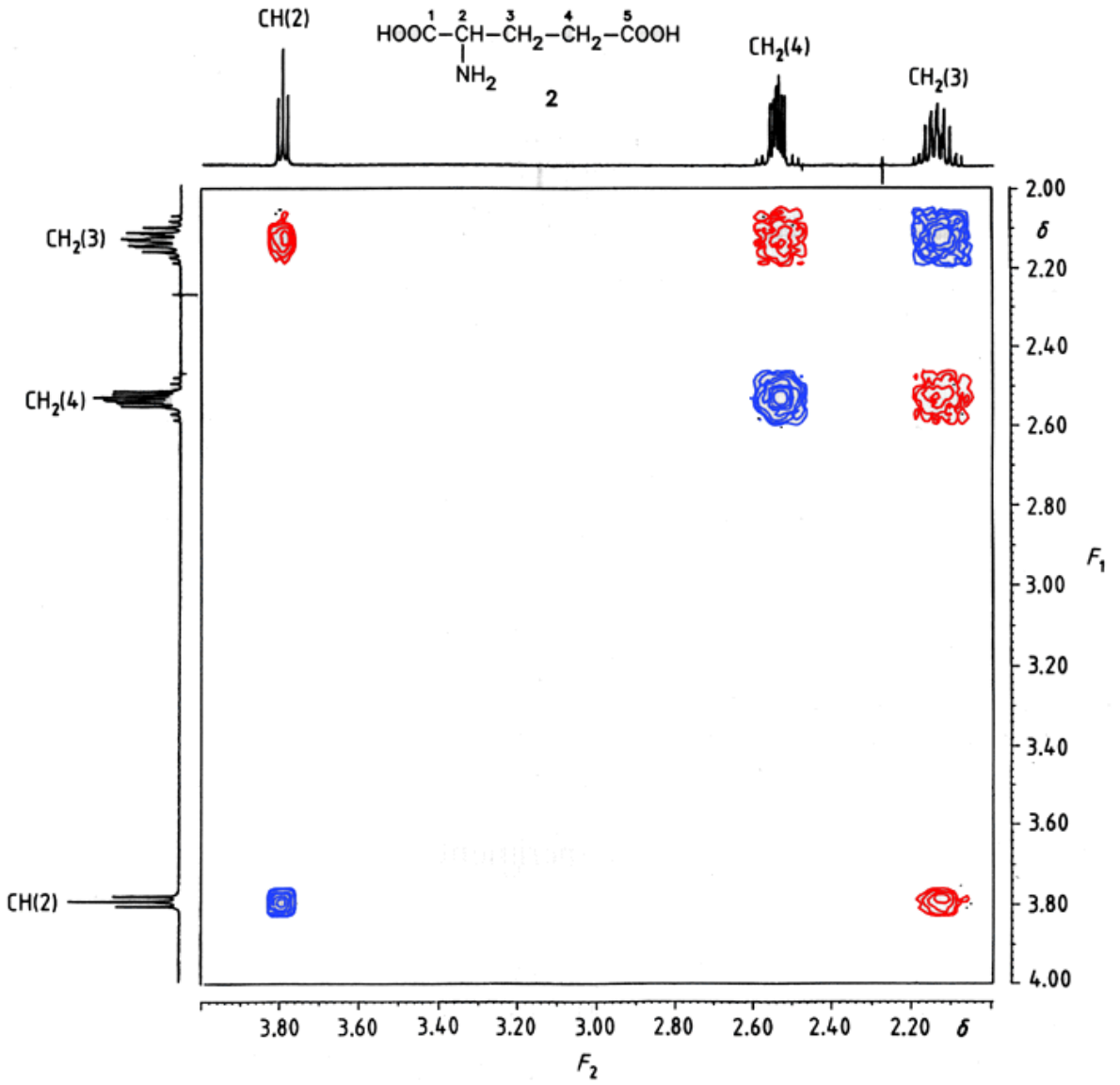


Figure 1.6. A schematic illustration of a topographical map representing a 2-D ^{1}H-^{1}H (homonuclear) NMR COSY spectrum of glutamic acid (From: Anthony Crasto 2-D COSY NMR spectroscopy lecture, online) are shown on left and top, and their corresponding frequency axes are on the right and bottom, respectively. This topographical map demonstrates connectivity of adjacent nuclei by the lack of the same precession frequency in the 2 NMR spectra (2 and 3 and 3 and 4) resulting in cross peaks (in red) that are off the diagonal. Conversely, a lack of connectivity between adjacent nuclei is demonstrated by retention of the same precession frequency in the 2 NMR spectra (2 and 4) resulting in diagonal peaks (in blue).

1.5 Mass Spectroscopy

Mass spectrometry is a method of chemical analysis in which the identity and proportions of compounds within a sample are determined based on their mass to charge ratio (m/z). Mass spectrometers can be viewed as high vacuum, low pressure tube systems that are divided into five parts. The first part is the injection point where the sample is introduced into the system after being vaporised, if they are not already in a gaseous state. The other four parts of the spectrometer form a series of compartments that are responsible for the sequential processes of ionisation, acceleration, combined deflection, and separation; and detection of the resulting signal. In the ionisation compartment the vaporised sample is bombarded with a beam of high speed electrons. This is most commonly performed using electrospray ionisation (ESI) and results in the formation of positively or negatively charged ions, depending on the mode selected. This predominantly results in ions with a positive or negative charge of one but particles with greater charges can also be formed. The newly formed ions are then accelerated along the spectrometer and through a strong magnetic field. The magnet is used to deflect the path of a selection of the ions of a particular m/z ratio towards an ion detector at the end of the spectrometer. The extent of deflection induced by the magnet is determined by the mass and the speed of the ions and the strength of the magnet. For a given set of parameters, heavier ions of a higher mass are deflected less than lighter ones of a lower mass. It is therefore possible to vary the strength of magnet to select every mass in turn. When the ions hit the ion detector at the end of the tube an electrical current is generated. These electrical signals are amplified and their amplitudes analysed by a computer that determines the mass and relative abundance of all the ions in the sample. The record of the signals produced by MS is called mass spectra, where the m/z ratio is plotted against their intensities (amplitudes). The intensities of the signals on MS spectra reflect their relative abundance in the sample being analysed. The tallest peak is called the base peak and is arbitrarily given a value of 100 and this is used as a reference to determine the relative proportion of all the other ions in the sample.

Advances in MS technology have led to several additions to the basic components of a mass spectrometer described here. These have included tandem MS-MS and time-of-flight (TOF) mass spectrometers. Tandem mass spectrometers have at least two analysers separated by a collision cell. Following the initial analysis in the first analyser, an inert gas in introduced into the next analyser together with a selection of sample's ions, described as parent ions. The gas collides with this collection of ions and causes their fragmentation. The fragments are then used to identify the parent ions. In a TOF mass spectrometer, the fundamental processes of ionisation, acceleration and detection are the same but the method of separation is different. Instead of using a magnet of varying strength to cause the separation of the ions according to their mass/charge ratio, the ions are separated based on their time of flight following their accelerating through a high voltage in a drift region (fight tube) which is determined by their m/z (with ions of greater mass having longer TOFs).

1.5.1 LCMS

1.5.1.1 Ultra-Performance LCMS

Liquid Chromatography-mass spectroscopy combines the physical separation technique of liquid chromatography and MS. In liquid chromatography (LC) the sample or mixture is dissolved in a fluid named the mobile phase which carries it through a column or plane that contains a solid adsorbent substance such as silica that acts as a stationary phase. If the stationary phase is more polar than the mobile phase, then the method is described as normal phase LC (NPLC) and the reverse is described as reverse phase LC (RPLC). Ultra-performance LCMS (UP-LCMS) refers to the sample being forced at a high pressure by the mobile phase through the column containing the stationary phase. The components of sample are separated according to their individual interactions with the adsorbent compound of the stationary phase, as they flow through the separation column.

The main reference textbook used throughout this section 1.5 was 'Mass Spectrometry – Principles and Applications (Hoffmann & Stroobant, 2007)

.

1.6 Multivariate statistical data analysis

1.6.1 Data reduction and pre-processing of the spectral data prior to statistical analysis

Prior to undergoing multivariate statistical data analysis, NMR and MS spectral data undergo a sequence of processes to control for different types of technical and systemic variation; regions of the spectra which could potentially introduce bias to the analysis, are removed. This ensures comparability of the spectra data set and is termed pre-processing. This process varies according to the analytical platforms and sample types. Having completed the pre-processing of the spectral arrays, a spreadsheet of each dataset is extracted and subjected to multivariate statistical analyses.

Metabonomics involves the generation of spectral data containing vast numbers of metabolite signals, with each metabolite usually being represented by more than one signal. Conventionally, a data set is defined as a data matrix or table containing N rows and K columns, with the rows and columns representing individual observations (e.g. samples) and variables (e.g. chemical shift intervals, m/z ratios), respectively. The data sets in metabonomics are therefore huge, with thousands of correlated variables, and the use of serial samples from the same patient exacerbating this problem further. For these reasons, the more conventional methods of multivariate statistical analyses (MVA) cannot be applied to these data sets and other forms of multivariate modelling must be used instead. These alternative methods of multivariate statistical analyses are based on the principle that more information can be gained from datasets containing thousands of variables by focusing on the variables that vary the most between the samples, instead of focusing on individual metabolites.

1.6.2 Principal Component analysis

The majority of the MVA used in metabonomics are based on the principles of principal component analysis (PCA): a process that allows an approximation of the data set to be made by examining the relation between the individual variables and focusing on non-correlated variables. Principal component analysis is based on the principal that co-related variables are providing the same information. This concept can be visualised if we consider a data set containing three variables, e.g. x, y, and z, and four samples that has been plotted on a 3-dimensional (3D) co-ordinate plot, in which, each axis is used to represent each of the three variables. If two of the variables are co-related, the co-ordinate plot will demonstrate that although three axes are used to describe the data set, it only really varies in two directions. The data could therefore, be summarised well using a 2-dimenisonal (2-D) plane (two axes) i.e. two variables instead of three. The first step of this process is the construction of a covariance matrix of the data set to demonstrate which variables are correlated. This information is first used to eliminate one of each pair of correlated variables. It is then used to produce linear combinations of the variables that can summarise the data set as a whole, using the least number of variables. In terms of the co-ordinate plot (geometrically), the linear combination of the variables which forms a line of best fit for all the data points, and thereby summarises the data using the least number of variables, is called the first principal component (PC). This line is determined in a least square sense: whereby the square of distance between the plane and all the data points is minimised, resulting in a line of best fit for all the data points. This is a well-defined method of characterising the line which spans the main variation in the data. In this way, PCA transforms the original set of correlated variables into a new set of uncorrelated variables. Principal components are therefore analogous to approximations of the linear equations of basic forms of multivariate analyses (e.g. x=3y+4z,) with each PC defining a new axis. For this reason, PCA is a form of modelling. Having defined the line of best fit for all the data points or main variation in the data set, the second greatest amount of variation in the data (not explained by the first PC) will be perpendicular or orthogonal to the first PC. Each PC is ranked in order of the percentage of the variation explained by that PC and is

orthogonal to the preceding PC. The orthogonal nature of PCs, means that they can be rotated to form the horizontal (x) and vertical (y) axes of a coordinate plot. This plot is called the scores plot and contains both the samples and the variables and is therefore described as a bi-plot. Each PC can be regarded as a weighted scoring system, with each variable (e.g. a metabolite signal) assuming a different level of importance described as their weight or loading value. The loadings values of the variables of each PC are displayed in loadings plots and the position of individual observations (e.g. samples) on the scores plot is determined by the composite scores for each of the PCs of scores plot. The majority of the variation of a data set will usually be captured by the first two or three PCs. A 2-D or 3D scores plot involving these components is therefore most commonly used when presenting the PCA data with the corresponding loadings plot.

Having summarised the data, the PCA scores plot is examined for trends, such as clusters of observations and outliers. There are two types of outliers: score and orthogonal outlier (see Figure 1.7). Score outliers are samples that have extreme values of the variables (e.g. extreme concentration of metabolite signals) of the greatest importance to the principal components of the PCA model, which causes them to have extreme score values. This means, that although these samples fit the model, their extreme score values result in them being separated from other clusters of samples, at a distance described as the score distance. Orthogonal outliers are samples that contain unusual variables that are not present in the majority of the samples and are not well represented by the PCA model. This causes them to lie far away from the other samples, at a perpendicular distance to the PCs of the scores plot described as the orthogonal distance. On a PCA scores plot, a Hotelling perimeter is often used to indicate a 95% confidence interval (i.e. cut-off values for orthogonal and score distances), beyond which samples are considered as outliers.

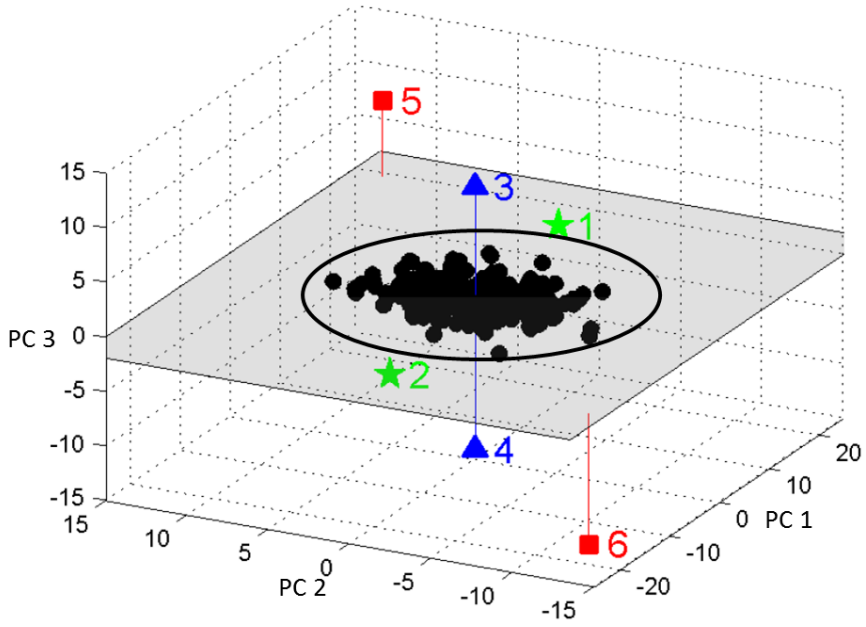


Figure 1.7 Illustration of different types of PCA outliers. The two-dimensional PCA plane is highlighted in grey. The unnumbered black observations fit the PCA model that is representative of the majority of the dataset and they therefore lie within the Hotelling's perimeter of the scores plot (black ellipse). The green observations are called score outliers. They follow the PCA model and therefore lie within the two-dimensional plane of the scores plot but have extreme score values causing them to lie outside of the Hotelling's perimeter. The blue and red observations are not well represented by the PCA model. They contain variables that are not shared by the majority of the dataset. This causes them to lie outside of two-dimensional plane of the scores plot at perpendicular distance called the orthogonal distance and are called orthogonal outliers. The blue observations have small values for the variables of importance to the two PCs of the PCA and so lie in close proximity to the black observations whereas the red observations have large scores for these variables are therefore both score and orthogonal outliers.

1.6.3 PLS, OPLS and OPLS-DA

To acquire an unbiased assessment of the data, PCA models are constructed without the knowledge of the ''groups'' of the observations and is therefore described as an *unsupervised* technique. In the context of metabonomics, samples that are clustered together on PCA scores plot have similar metabolic profiles. Following the construction of the PCA scores plot, the investigator will assess if there are any metabolic differences between groups. Furthermore, if different groups of samples cluster at different regions of the plots this suggests that the differentiating metabolites involved in the PCs of the model can be used to differentiate between the two groups, (which may or may not be the clinical classes under investigation). This differentiation is usually tested using a multivariate statistical analysis method that involve knowledge of these classes. These are called *supervised* analyses and are used to determine if the class of an observation can be predicted using the variables identified as differentiating by the model. Most of the supervised multivariate statistical analyses used in metabonomics are also based on PCA, (utilised as a mean of data reduction). The commonest example in metabonomics is projection to latent structure (PLS) regression analysis. However, unlike PCA, the PCs in *supervised* multivariate statistical analyses are derived from variables that vary the most between the classes of the model and are used to differentiate between them.

The aim of a multiple regression analysis is to use the historical relationship between the independent and dependent variables of a data set to predict the dependent variable (group or class) of an observation (e.g. sample) based on the composition of their independent variables (e.g. metabolites). Linear regression models assume the relationship between these two types of variables is a straight line. In PLS regression models this goal is achieved by combining the use of PCA and multiple linear regression. In PLS, PCs are used to transform the original set of independent variables into a new set of independent variables. However, unlike in PCA, where the first PC spans the main variation in the data, the first PC in *supervised* analyses such as PLS is a linear combination of the independent variables that vary the most between the dependent variables (classes).

Geometrically, the first PC in PLS is the line of best fit of the data points of a coordinate plot demonstrating how these differentiating independent variables vary according to the dependent variables (groups). This line of best fit for all the data points is determined using a least square method: whereby the square of distance between the plane and all the data points is minimised. In metabonomics, the dependent variables are the groups or classes (e.g. clinical characteristic). However, the variables being measured are metabolite signals that are not independent of one other and are therefore, usually referred to as predictors instead of independent variable; and the classes are called the response variables.

Orthogonal signal correction (OSC) is mathematical operation that can be used to reduce or remove the systemic variation from either the X (predictors) or Y (response) data that is not important to the covariance or linear correlation between the predictor and response variables. Orthogonal signal correction-PLS is an extension of PLS, in which an OSC is applied to the data before the PLS analysis is carried out. This divides the systemic variation in the X data into two components: one with a linear correlation to Y data and one without a linear correlation to Y data. The latter constitutes an orthogonal component that filters out the systemic variation unrelated to the linear correlation between the response and predictor variables.

Both PLS and O-PLS analyses can contain many response variables or classes. PLS and O-PLS discriminative analyses (DA) are extensions of PLS and O-PLS regressions, respectively, in which the regression models are used to discriminate or differentiate between a discrete number of dependent variables or classes.

The outputs of supervised multivariate statistical analyses based on PCA include scores plots demonstrating the ability of the model to differentiate between the groups and a variety of different loading plots demonstrating the predictor variables responsible for this differentiation. The ability of

the *supervised* analyses such as PLS to differentiate between the groups is usually assessed using three main evaluation parameters. The first is the number of components used to construct the model, which is related to over-fitting. The percentage of the variation explained by the X and Y matrices of the model is given by the R^2X and R^2Y values, respectively, and the predictability of the model is represented by the Q^2Y value. The Q^2Y is the cross-validated correlation value derived using a method of cross validation, in which, the samples of the model are partitioned into subsets, the analysis is performed one subset, labelled the training set, and then validated on the other subset called the validation set. This technique is an iterative process, in which different combinations of the training and validation subsets are used and the average results of these assessments are used to evaluate of the accuracy of the model to predict the dependent variable of an observation (e.g. a sample's group). The R^2Y and the Q^2Y values should ideally be similar indicating an equal contribute by each of the samples to the class separation of the model. The Q^2Y values is however, usually lower than the R^2Y but if the Q^2Y is considerably lower than the R^2Y then the model is not robust suggestive of overfitting, affecting its likely predictability in additional external cohorts.

A cross-validated analysis of variance (CV-ANOVA) p value can be used for supervised models as a measure of significance of the observed group separation. Analysis of variance involves calculations of the variance of means, also known as sum of squares. Firstly, the sum of the squares within the groups and the total sum of the squares of the samples of all the groups is calculated; these two calculations are used to calculate the sum of squares between the groups. The sum of squares within groups is then obtained using three calculations. Firstly, the means of the observations of each group is calculated. Next, the square of the difference between each observation and the mean of that group is calculated [(observation -mean) ^{2}] and then these values are summated [$\sum$ (observation -mean) ^{2}]. Lastly, the sum of the [$\sum$ (observation -mean) ^{2}] for each group is summated to produce the sum of the squares within groups. To calculate the total sum of squares of all the samples, all the samples are

considered as one group and the square of the difference of each observation and the mean of the whole group is summated. The sum of squares between groups is then calculated, using the following formula: sum of squares between groups = total sum of squares - sum of squares within groups. The sum of squares between groups is then divided by its degrees of freedom, which is the number of groups minus one, and the sum of squares within groups is then divided by its degrees of freedom, which is total number of observations minus the number of groups. The final calculation is the ratio of these two equations, i.e. the ratio of sum of squares between groups divided by its degrees of freedom (numerator) and the sum of squares within groups divided by its degrees of freedom (denominator). This is called the F ratio and is the found variation of the group average divided by the expected variation of the group averages. The results of the F ratio and the degrees of freedom of both the numerator and the denominator of this equation are then compared with tables of critical values to determine if the null hypothesis should be accepted or rejected. These tables of critical values are based on F ratio distribution curves with F ratio on x axis and relative frequency on y axis, in which the position of the F ratio is determined and everything to the left of the critical value is in the rejection area).

The information in this section was devised from multiple resources including the following key references:(Lindon, Nicholson & Homes, 2007; Eriksson, Johansson, Kettaneh-Wold, *et al.*, 2006; Wold, Esbensen & Geladi, 1987; Cseke, Kaufman, Podila, *et al.*, 2003; Wheelock & Wheelock, 2013).

1.6.4 Metabolite identification: STOCSY, databases; literatures

The methods used in the identification of metabolites can be divided into platform specific and generalised. The identification of metabolites using NMR spectroscopy is aided by distinctive signal patterns on NMR spectra. Methods applied to both NMR and MS includes comparisons with spectra from the literature, and local and public developed databases such as the human metabolome

database (HMBD; http://www.hmba.ca) for both NMR and MS; and MS databases such as ChemSpider (http://www.chemspider.com/), Kyoto Encyclopedia of Genes and Genomes database (KEGG; (http://www.genome.jp/kegg/), LIPID MAPS (http://www.lipidmaps.org/), METLIN (http://metlin.scripps.edu/) and PubChem (http://pubchem.ncbi.nlm.nih.gov/).

Statistical total correlation spectroscopy (STOCSY) is also used to aid the identification of both drug and non-drug metabolites. In this method, the correlation coefficient and covariance of correlated metabolite signals are identified and displayed on a plot resembles a spectra (Cloarec, Dumas, Craig, *et al.*, 2005). In the example of NMR, the correlated signals are colour-coded and displayed along the x axis. The colours are used to represent the correlation coefficient of the signals and the direction of the signal deflection represents a positive correlation (upwards) and a negative correlation (downwards).

1.7 Aims and objectives

The aim of the work described in this Thesis as a whole is to characterise the metabolic response of patients with severe sepsis and determine metabolic signatures associated with their clinical outcomes using methods of metabolic profiling based on both ^{1}H-Nuclear magnetic resonance and mass spectroscopy. This is divided into three parts. Firstly, the demonstration of the feasibility of ^{1}H-nuclear magnetic resonance spectroscopy as a method of global metabolic profiling in patients with a critical illness, of which severe sepsis is a leading cause. This includes the development of a ^{1}H-Nuclear magnetic resonance database of drug standards as a reference to aid the identification of drug metabolites and enable their differentiation from metabolic changes related to endogenous metabolites. The global metabolic consequences of severe sepsis were then examined in a cohort of patients using a method of metabolic profiling based on the ^{1}H-Nuclear magnetic resonance spectroscopy of both urine and serum samples. This was followed by the characterisation of the

changes in the lipid profiles of the patients from sepsis cohort as a consequence of sepsis related liver injury using a technique optimised for the detection of lipid subspecies based on UPLC-MS analyses of plasma samples. The results of these three sections of this study are reported separately in chapters three, four and five as illustrated in the outline of the structure of the thesis below:

Chapter 1: Introduction to sepsis, metabolic changes in sepsis, metabonomics and multivariate statistical analyses

Chapter 2: Methodology

Chapter 3: Validation of NMR analysis of urine as a method of global metabolic profiling in critically ill patients

Chapter 4: Global metabolic responses in patients with severe sepsis and sepsis-induced organ dysfunction

Chapter 5: Characterisation of the lipid subspecies associated with sepsis-induced liver dysfunction using a lipid profiling technique based on UP-LCMS

Chapter Six: Discussion and concluding remarks

Chapter 2: Methodology

Materials and methodology shared by the chapters are described here to avoid duplication. This includes the standardised procedures for the sample preparation and ^{1}H NMR analyses of biofluids and drug standards, the processing and multivariate statistical analyses of the spectral data and metabolite identification. Whereas materials and methodology specific to individual chapters are described within the methods section of their respective chapters. This includes the methodology of the UPLC-MS based lipid profiling of plasma samples from the sepsis cohort which is specific to chapter five and therefore described in the methods section of chapter five (Section 5.3).

2.1 Materials

2.1.1 NMR

2.1.1.1 Chemicals

HPLC grade water, hydrochloric acid (HCl) 37% w/w, potassium hydroxide (KOH, 45% w/w) solution and deuterium oxide (D_2O, 99.9 atom % D), disodium hydrogen phosphate (Na_2HPO_4, 99.999% ACS, anhydrous), sodium dihydrogen phosphate (NaH_2PO_4, 99%, anhydrous), sodium azide (NaN_3, 99.9%) and 3-(trimethylsilyl) propionic-2,2,2,3-d_4 acid (TMSP-d_4) sodium salt, (98 atom % D) were purchased from Sigma-Aldrich (UK).

2.1.1.2 Equipment

5mm diameter NMR tubes purchased from Sigma-Aldrich (UK).

Amicon Ultra 0.5ML 3K Centrifugal Filter devices were purchased from Merck Millipore

2.1.2 UPLC-MS

2.1.2.1 Chemicals

HPLC grade water, methanol (MEOH), methyl-tert-butyryl ether (MTBE), isopropanol (C_3H_8O), 1% formic acid, 10mM ammonium formate (CH_5NO_2) and leucine encephalin were purchased from Sigma-Aldrich (UK); HPLC-grade acetonitrile (C_2H_3N) was purchased from Romil Ltd.

2.1.2.2 Equipment

An Acquity UPLC CSH C18 2.1x100mm, 1.7 µm, column, pre-column filter: ACQUITY UPLC Col. In-Line Filter Kit, UPLC-MS vials with preloaded inserts and 96 well plates, polypropylene, 350 µL were purchased from Waters Corporation.

2.2 Validation cohort: unselected critically ill patients

2.2.1 Study patients

See Section 3.3.1.

2.2.2 Sample collection

See Section 3.3.2.

2.2.3 Clinical data collection

See Section 3.3.3.

2.2.4 Sample preparation for NMR analysis

Two aliquots of the urine sample collected at each time point were used in this study, one filtered and one unfiltered. The filtered samples were filtered using Amicon Ultra 0.5 mL 3K centrifugal filter

devices to remove the hydroxyethyl starch (HES), after the filters had been pre-rinsed five times to remove the preservative glycerol (see Sections 1.6.3-5 of Appendix I). Filtration reduced the volume of urine available for the filtered urine samples. To keep the overall volume of both sets of samples constant, different ratios of urine to sodium phosphate buffer were used for each set. One litre of the urine phosphate buffer (pH 7.4) was prepared by adding 5.25 g of the weak acid NaH_2PO_4 and 28.85 g of Na_2HPO_4, a salt of its conjugate base, 1 mM TMSP-d_4 (0.179g) and 3 mM NaN_3 (0.195g) to a 1L volumetric flask. In this phosphate buffer, TMSP-d_4 acts as the chemical shift reference compound (as described in Section 1.4) and 3 mM NaN_3 is added to prevent decomposition of the sample by bacteria.

These regents were then dissolved in 200 µl of D_2O using a sonicator at 40°C and the pH adjusted to 7.4 using HCl before adding HPLC grade water to make the solution up to 1L. Unfiltered samples consisted of 400 µl of urine and 250 µl of urine buffer; whereas, filtered samples consisted of 300 µl of urine and 350 µL of urine buffer. In both cases, the urine/buffer samples were centrifuged at 10,000 g for 10 minutes and 600 µL of the supernatant was placed into NMR tubes with an outer diameter of 5 mm.

2.2.5 ^{1}H NMR spectroscopic analysis of filtered and non-filtered urine

All ^{1}H NMR spectra were acquired on a Bruker DRX 600 MHz spectrometer (Rheinstetten, Germany) operating at 600.13 MHz using a 5-mm TXI (Triple Resonance Probes) probe. The ^{2}H resonance of the D_2O solvent was used to lock the field. A standard one-dimensional (1-D) NMR pulse [recycle delay (RD)-90º-t_1-90º-t_m-90º-acquire free induction decay (FID)] was employed for the acquisition of all spectra at 300 K. The water peak was suppressed by selective irradiation during RD of 2 s and mixing time (t_m) of 100 ms. t_1 was fixed to 3 µs. The 90º pulse length was adjusted to 10 µs. A total of 256 scans were recorded into 32 k data points with a spectral width of 20 ppm. An exponential function was applied to FID prior to Fourier transformation, which broadened the line by 0.3 Hz. Each spectrum was phased, baseline-corrected and referenced to the internal standard TMSP-d_4 set at 0 ppm.

2.2.6 Pre-processing of the spectral data

Prior to undergoing multivariate data analysis, NMR and MS spectral data are pre-processed to control for different types of (technical and systemic) variation and unwanted regions of the spectra are removed. This ensures the spectra of each data set are comparability. This process varies according to the analytical platform and sample type; the pre-processing of NMR and MS are therefore discussed separately in sections 2.5 and 5.3.5, respectively. Having completed the pre-processing of the spectral arrays, a spreadsheet of each dataset (with rows and columns representing individual spectra and the variables, e.g. ppm of the NMR signals) was extracted and uploaded in SIMCA-13 software (Umetrics AB) for multivariate statistical analysis.

2.3 ^{1}H NMR Drug standards database

2.3.1 List of drugs

The drugs and intravenous (IV) fluids in the ^{1}H NMR Drug standards database are listed in Appendix II.

2.3.2 Sample preparation

The drugs and fluids in the NMR drug standard database came in three formats: solutions, powders, and tablets. For powder, 20 mg of the powder was dissolved in 200 µL of water. The mixture was vortexed and centrifuged at 10,000 g for 10 mins, and 200 µL of supernatant was collected for subsequent NMR sample preparation. For tablets, a variable number of tablets were crushed into fine powder using a pestle and mortar and 20mg of the resulting power was dissolved in 300 µL of water and was prepared following the aforementioned steps. For drugs that were already in solution, 200 µL of solution was used for NMR preparation.

Once, the drugs were in solution, 200µL of this solution was mixed with 400µL of drug buffer, (pH 7.4 and each litre consisting of 28.85 g Na_2HPO_4, 5.25 g NaH_2PO_4, 1 mM TMSP-d_4 (0.179g) and 3 mM NaN_3(0.195g) in 1L D_2O) and centrifuged at 10,000 g for ten minutes and 600µl of the supernatant was then placed into a 5mm diameter micro-tube. Four of the drugs that came in solution (8.4% $NaHCO_3$, naloxone, glycopyrronium bromide, and hydroxocobalamin were very diluted and so repeat samples of these drugs were also prepared using 500 µL of the drug and 50 µL of the drug buffer.

2.3.3 NMR analysis of drug standards

^{1}H NMR spectra were acquired using the methodology described in Section 2.2.5, except for the number of scans that were acquired, which was 64 in the first sample run, and 512 in second sample run of a select number of samples with very low drug concentrations (the three colloid fluids: Gelosfusine, Voluven and Volulyte).

2.4 Sepsis cohort of critically ill patients

2.4.1 Study patients

see Section 4.3.1.

2.4.2 Sample collection

The collection of urine, serum and plasma samples from the sepsis cohort is described in section 4.3.2.

2.4.3 Clinical data collection

See Section 4.3.3.

2.4.4 Sample preparation for NMR analysis

2.4.4.1 Urine

Urine samples were prepared using the same methodology described for the unfiltered urine in section 2.2.4.

2.4.4.2 Serum

300µl of serum was mixed with 300 µl of serum buffer (pH 7.4 and consisting of 1.064g Na_2HPO_4, 0.08g TMSP-d_4, and 1mL 4% NaN_3 in each 100ml D_2O: H2O, v/v 1:4). The samples were centrifuged for 10 minutes at 10,000 g and 600 µl of the supernatant was placed into 5 mm diameter NMR tubes.

2.4.5 NMR analysis of urine and serum

Standard 1-D spectra of the urine samples were acquired using the parameters described in section 2.2.5 with 256 scans.

Standard 1-D spectra of the serum samples were acquired using the pulse sequence [RD-90º-t_1-90º-t_m-90º-acquire FID] was employed for the acquisition of all spectra at 310 K. The water peak was suppressed by selective irradiation during RD of 4 s and mixing time (t_m) of 10 ms. t_1 was fixed to 3 µs. The 90º pulse length was adjusted to 10 µs. A total of 64 scans were recorded into 64 k data points with a spectral width of 20 ppm.

An additional ^{1}H NMR spectra was acquired for serum samples using a Carr-Purcell-Meiboom-Gill (CPMG) pulse sequence to improve the visualisation of low molecular weight molecules and suppress signals from the macromolecules present in serum. The CPMG spectra were acquired using the same parameters as described in section 2.2.5, with exception of the pulse sequence which was a spin-echo pulse sequence RD-90°-(τ-180°-τ)$_n$-acquire FID] with a spin relaxation delay of (2ητ) of 160 ms.

2.5 Pre-processing, data reduction and multivariate statistical data analyses of each NMR dataset

Each set of spectra was processed together. Urinary and drug standard spectra were automatically phased, baseline-corrected and referenced to the internal standard 3-TMSP-d_4, set at 0 ppm, using a MATLAB script developed locally (Imperial Phenome Centre) by Tim Ebbels. Phasing, baseline correction and referencing of serum spectra was performed automatically immediately following acquisition using software associated with the spectrometer (Topspin, Bruker Rheinstetten, Germany) and spectra were referenced to the α-glucose signal at 5.22 ppm. Prior to any further processing an examination of the complete data set of ^{1}H NMR spectra of both urine and serum was made and compared with the ^{1}H NMR spectra from the healthy control samples of urine and serum. No further processing or analyses were made of the of ^{1}H NMR spectra of these control samples. A digital representation of each spectra was created using another MATLAB script developed locally (by Dr O Cloarec).

Distortion of the baseline usually surrounds the water signal despite attempts to suppress this signal. This may distort or obscure signals of interest. Urea signals in urine was also excluded due to the exchange between H and D resulting in an inaccurate concentration. These signals are therefore described as unwanted and are usually removed. In both urinary and serum spectra, the water region between 4.96 and 4.77ppm, and a region containing noise and the between -1.0 and 0.47 ppm were removed. The region containing the urea signal between 6.2 and 5.72 ppm was also removed from the urinary spectra.

Two forms of alignment were applied to urinary spectra to minimise variation caused by factors such as pH: a generalised form of alignment performed automatically, followed by a manual form of fine alignment. Both were achieved using departmental MATLAB scripts.

Each set of urinary and serum ^{1}H NMR spectral data underwent normalisation and scaling prior to multivariate statistical analysis. Probabilistic quotient normalisation was performed to control for systemic variation such as urine dilution (Dieterle, Ross, Schlotterbeck, *et al.*, 2006); in addition to the variation in metabolites present in samples, using locally developed MATLAB scripts. Probabilistic quotient normalization assumes that the concentrations of the variables of interest (importance) influence only sections of the metabonomic spectrum, whereas, dilution will affect all the spectrum's signals. It transforms each metabonomic spectra according to an estimate of the most probable dilution, derived from the ratio or quotient of the variables of interest and a reference spectrum. The first step of probabilistic quotient normalisation is the construction of a reference spectrum based on the median spectrum: a spectrum with the median value or quantity of each variable; so that there is an equal probability of the observed quantity lying above or below it on a frequency distribution of all the quantities. For each spectrum, the quotient or ratio of the quantity of each variable of interest and the reference spectrum is then calculated and the median of all the quotients is predicted. All the variables of each spectrum are then divided by the median quotient estimated for that spectrum.

Unit variance scaling, which scales the signals according to the standard deviation of the metabonomic data was performed to control for technical variation related to peak intensities, (in which higher peak intensities are associated with a disproportionally greater level of importance than smaller peak intensities) using SIMCA-13 (Umetrics). The same software was then used to perform the two forms of multivariate statistical analyses. Principal component analysis (PCA) was applied to each spectral data set to obtain an overview of the data set as a whole and identify outlying samples followed by

PCA of the spectral data from each of the sampling time points. This was followed by building orthogonal-partial least square-discriminative analysis (O-PLS-DA) models based on spectral data from each of the sampling points to investigate the metabolic differences between each of the clinical classes under investigate, at each of these time points.

The reliability of the O-PLS-DA models was analysed using the three main evaluation parameters: the number of components used to construct the models, the R^2 or percentage of the variation explained by the model and the cross-validated correlation or Q^2Y value. A cross-validated analysis of variance ANOVA (CV-ANOVA) p value of each model was also used a measure of significance of the model's observed group separation (see Section 1.6.3). Both sets of evaluation were performed using the aforementioned SIMCA-13 software (Umetrics).

2.6 Metabolite identification

2.6.1 STOCSY, databases and the literature

The identification of metabolite using NMR spectroscopy is aided by its reproducibility: metabolites have distinctive signal patterns on NMR spectra. The NMR drug standards database aided the identification of both parent drugs and their metabolites in the subsequent NMR experiments of bio-fluids (see section 3.4.3.1.1). Statistical total correlation spectroscopy (STOCSY) was also used to aid the identification of both drug and non-drug metabolites (3.4.3.1.2). In addition to the use of spectra in published literature such as 'The Human Urine Metabolome' by Bouatra *et al* (Bouatra, Aziat, Mandal, *et al.*, 2013) and 'The Human Serum Metabolome' by Psychogios *et al* (Psychogios, Hau, Peng, *et al.*, 2011a) and the pubic database the human metabolome database (HMBD; http://www.hmba.ca).

2.6.2 NMR data: 2D-NMR

Two-dimensional NMR scans were acquired to improve the resolution of signals of metabolites that were overlapping in the 1-D NMR spectra. This method was applied to a small number of samples to aid the identification of specific metabolites. In contrast, to 1D NMR experiments, 2-D experiments provide additional structural information, by recording and displaying, the behaviour of nuclei, at two frequencies, opposed to one (see section 1.4).

2.7 UPLC-MS analyses

The methodology of the UPLC-MS based lipid profiling is specific to chapter five and therefore described in the methods section of chapter five (Section 5.3).

Chapter 3: Validation of ^{1}H NMR spectroscopic analysis of urine as a global metabolic profiling method in critically ill patients

3.1 Introduction

3.1.1 Critical illness and sepsis

Critical illness is any condition that causes an acute deterioration in physiology associated with morbidity or mortality within minutes or hours (Adhikari, Fowler, Bhagwanjee, *et al.*, 2010). It is frequently associated with secondary organ failures and often results in the need for organ support, in addition to interventions targeting the underlying disease process. Many of these interventions are pharmacological agents such as drugs and intravenous fluids, including total parenteral nutrition (TPN). This can lead to the administration of many pharmacological agents with many patients receiving an excess of ten different agents.

Sepsis is one of the leading causes of critical illness (Blanco, Muriel-Bombin, Sagredo, *et al.*, 2008). The evaluation of the feasibility of metabonomics based on ^{1}H NMR analyses of urine from a cohort of critically ill patients was therefore performed prior applying this approach to the study of the sepsis cohort.

3.1.2 Complexity of the metabolome of patients with critical illness

The human metabolome includes both endogenous and exogenous metabolites (Nicholson & Lindon, 2008). Drug metabolites form an important part of exogenous metabolites and their metabolism usually involves the liver or kidneys, or both. Dysfunction of these organs can therefore affect the metabolism of many drugs and involve complex interactions between these organs (Smith, Yogaratnam, Levasseur-Franklin, *et al.*, 2012). Compared with most other hospital inpatient cohorts, critically ill patients have an increased incidence of acute liver and renal dysfunction (Blanco, Muriel-Bombin, Sagredo, *et al.*, 2008). The metabolism of one drug can be affected by the co-administration

and metabolism of other drugs (Smith, Yogaratnam, Levasseur-Franklin, *et al.*, 2012). The complexity of these drug interactions is reported to increase with an increasing number of administrated drugs. This is likely to compound the effect of changes in drug metabolism secondary to organ dysfunctions (Smith, Yogaratnam, Levasseur-Franklin, *et al.*, 2012). Both of these factors affecting drug metabolism co-exist in many critically ill patients. Drug metabolites are therefore likely to be of great importance to the metabolic changes of these patients.

Urine, as the end product of a major site of metabolism, is often thought to provide a good global metabolic profile (Nicholson & Lindon, 2008). It is also likely to provide greater insights into the metabolic changes that can occur in renal dysfunction. Blood, on the other hand, is more likely to reflect changes that occur secondary to liver dysfunction (Psychogios, Hau, Peng, *et al.*, 2011b). The metabolic disturbances in patients with sepsis only or sepsis-induced organ dysfunction are two of the key aims of this project. The global characterisation of the metabolic changes of sepsis in this study has therefore included the use of urine, serum, and plasma.

3.2 Aim

The first aim of this chapter was to demonstrate the validity of metabonomics based on ^{1}H NMR spectroscopic analyses of urine as a feasible approach to study critically ill patients, described here as the validation cohort. The second aim was to demonstrate a clinical utility of this method: by demonstrating its ability to predict 28-day survival and differentiate between patients with and without renal and liver dysfunction. The ability of this method to differentiate between patients with and without respiratory, cardiovascular, haematological, and central nervous system dysfunction was also investigated.

3.3 Materials and methods

3.3.1 Study patients

The validation cohort consisted of thirty adult patients with critical illness recruited from the Adult Intensive Care Unit (ICU) at the Hammersmith Hospital in London, over two periods: May 2010 and December 2012, and January 2013, as part of an observational study of biomarkers of renal failure in critical illness. Twenty-seven patients were recruited during the first period and three during the second. This observational study therefore determined the eligibility criteria, sample size and timing of sampling. All critically ill patients were eligible for study enrolment, except patients with pre-existing, dialysis dependent renal failure.

The small number of patients recruited to this study despite the wide eligibility criteria was due to limitations in terms of resources (research team collecting the samples) and other competing interests (other clinical trials and research projects). This was illustrated by the increased recruitment rate in second recruitment period following a change in some of these rate-limiting factors. Prior ethical approval had been acquired (research ethic committee approval number 07/H0710/81) and written informed consent or assent from next of kin was obtained as appropriate.

3.3.2 Sample collection

Urine samples were collected at two time points (TPs): a sample at enrolment to the study (TP0) and second sample, 24 hours later (TP1). At each time point, 10 ml of urine was aspirated from the sampling port of the urinary catheter, using a needle and syringe. Each sample was transferred to cryogenic tubes and centrifuged for 10 minutes at 10,000 g. Five 1ml aliquots of supernatant were then transferred into separate cryogenic tubes; two for use in this study. Each aliquot was labelled with a code incorporating the patient's study number, TP, and aliquot letter, and stored at -80°C until analysis.

3.3.3 Clinical data collection

Data was manually collected from the patients' medical records. Three sets of data were collected: patient demographics, drug administration and daily clinical variables. The first data set included ethnicity, age, the cause of their critical illness, and Acute Physiology and Chronic Health Evaluation II (APACHE II) scores (Knaus, Draper, Wagner, *et al.*, 1985) on admission to ICU. APACHE II is a severity of illness classification system calculated in patients within 24 hours of admission to ICU (see Table 3.1). It is a points-based scoring system in which the APACHE II score is the sum of an acute physiology score (Table 3.1 A), age points (Table 3.1 B) and chronic health points (Table 3.1 C). The minimum and maximum scores are zero and 71, respectively and the higher the APACHE II score, the greater the severity of the illness and risk of death. The timings of drugs administered from the time of admission to hospital until 48 hours after the second sample time point were recorded. This information was used to determine the drugs administered prior to each of the sample time point and therefore, demonstrate the potential parent drug and metabolites that could be found in individual's urinary samples, and the sample set as a whole. Daily clinical data was collected from 24 hours before study enrolment and seven days after. This included extremes of the patients' blood biochemistry, inotrope requirements and physiological parameters, and was used to calculate their daily sequential organ failure assessment (SOFA) scores (Table 3.2). Length of ICU stay and ICU and hospital survival were also recorded.

Table 3.1 Acute Physiology and Chronic Health Evaluation II scoring system. APACHE II score is the sum of the Acute Physiology Score (A), age points (B) and the chronic health status points (C). Key: A-a DO_2: alveolar to arterial oxygen gradient; FiO_2: fractional inspired O_2, K: potassium, Na: sodium.

A

Acute Physiology Score is the sum of the 12 individual variable points									
Acute Physiological variable	**High abnormal range**						**Low abnormal range**		
Acute Physiology Scores	**4**	**3**	**2**	**1**	**0**	**1**	**2**	**3**	**4**
1 Rectal Temp (°C)	≥41	39-40.9		38.5-38.9	36-38.4	34-35.9	32-33.9	30-31.9	≤29.9
2 Mean Arterial Pressure	≥160	130-159	110-129		70-109		50-69		≤49
3 Heart Rate	≥100	140-179	110-139		70-109		50-69	40-54	≤39
4 Respiratory Rate (per minute)	≥50	35-49		25-34	12-24	10-11	6-9		≤5
5 A-aDO_2 or PaO_2 (mmHg)									
a. FiO_2≥0.5 record A-aDO_2	≥500	350-499	200-349		<200				
b. FiO_2≤0.5 record PaO_2					PaO_2 >70	PaO_2 61-70		PaO_2 55-60	PaO_2 <55
6 Arterial pH	≥7.7	7.6-7.69		7.5-7.59	7.33-7.49		7.25-7.32	7.15-7.24	<7.15
7 Serum bicarbonate (mmol/L)	52	41-51.9		32-40.9	22-31.9		18-21.9	15-17.9	<15
8 Serum K (mmol/L)	≥7	6-6.9		5.5-5.9	3.5-5.4	3.3-4	2.5-2.9		<2.5
9 Serum Na (mmol/L)	≥180	160-179	155-159	150-154	130-149		120-129	111-119	110
10 Serum creatinine (mg/dL)	3.5	2-3.4	1.5-1.9		0.6-1.4		<0.6		
11 Haemocrit (%)	≥60		50-59.9	46-49.9	30-45.9		20-29.9		<20
12 White Blood cells (total) X 10^9/L	≥40		20-39.9	15-19.9	3-14.9		1-2.9		<1

B

Age Score	
<44	**0**
45-54	**2**
55-64	**3**
65-74	**5**
≥75	**6**

C

Chronic Health Status Points	
Elective postoperative patient with:	
immunocompromise	**2**
history of severe organ insufficiency	**2**
Nonoperative patient or emergency postoperative patient with:	
immunocompromise	**5**
history of severe organ insufficiency	**5**

In each patient, organ dysfunction scores at the two sample time points were calculated using the sequential organ failure assessment (SOFA) (Vincent, Moreno & Takala, 1996) and the acute kidney injury network (AKIN) (Mehta, Kellum, Shah, *et al.*, 2007) scoring systems for liver, respiratory, cardiovascular, and haematological dysfunction, and kidney dysfunction, respectively (as shown in Tables 3.2 and 3.3). In the AKIN classification system, kidney dysfunction is defined by a stage of greater than zero and ranges from one to three; in the SOFA system, organ dysfunction is defined by a score of greater than zero and ranges from one to four. Both the urine output and glomerular

filtration rate (GFR) criteria were used to determine the AKIN stage and the most severe degree of renal injury of these two criteria was recorded. For liver and kidney dysfunction, the scores were dichotomised: patients with dysfunction were given a score of one and those without dysfunction, a score of zero. However, for the other four organ dysfunctions (respiratory, cardiovascular, haematological, and central nervous system), dividing the samples into dichotomised groups resulted in very imbalanced sample numbers in the two groups. Therefore, for these four organ dysfunctions, the samples were also divided into five groups according to the five individual SOFA scores for each organ dysfunction (zero to four). This was done to enable two sets of MVAs to be performed, one with the samples divided into two dichotomised groups and the other with samples divided into five groups.

Table 3.2 Sequential Organ Failure Assessment (SOFA) scoring system. Key: *: with respiratory support; ~: adrenergic agents administered for at least 1 hour; doses in µg/kg per minute.

Variables		SOFA score 0	1	2	3	4
Respiratory	**PaO_2/FiO_2, mmHg**	>400	≤400	≤300	≤200*	≤100*
Coagulation	**Platelets x $10^3/\mu L$**	>150	≤150	≤100	≤50	≤20
Liver	**Bilirubin, mg/dL (µmol/L)**	1.2 (<20.5)	1.2-1.9 (>20.5)	2.0-5.9 (>32.5)	6.0-11.9 (>100.9)	>12.0 (>205)
Cardiovascular	**Hypotension**	MAP >70mmHg without vasopressors	MAP <70mmHg without vasopressors	Dopamine ≤5 or dobutamine (any dose)~	Dopamine>5, adrenaline ≤0.1 or noradrenaline ≤0.1~	Dopamine>15, adrenaline >0.1 or noradrenaline >0.1~
Central nervous system	**GCS**	15	13-14	10-12	6-9	<6
Renal	**Serum creatinine, mg/dL (µmol/L) or urine output, in mL/day**	<1.2 (<110)	1.2-1.9 (110-170)	2.0-3.4 (171-299)	3.5-4.9 (300-440) <500mL/day	>5.0 (>440) <200mL/day

Table 3.3 Acute Kidney Injury Network (AKIN) scoring system. Key SCr: serum creatinine.

Stage	Serum Creatinine criteria	Urine output criteria
1	Increase in SCr ≥ 0.3mg/dL (≥ 26.4 µmol/L) or increase ≥ 150-200% from baseline	> 0.5mL/kg/per hour for more than 6 hours
2	Increase in SCr ≥ 200-300% from baseline	> 0.5mL/kg/per hour for more than 12 hours
3	Increase in SCr >300% from baseline or SCr ≥ 4.0mg/dL (≥ 354 µmol/L) with an acute increase ≥ 0.5 mg/dL (≥ 44 µmol/L)	> 0.3mL/kg/per hour for 24 hours or anuria for 12 hours

3.3.4 Sample preparation for NMR analysis

For each patient, two aliquots of urine from each time point were used in this study: one unfiltered and one filtered. The NMR experiments of unfiltered urine were performed first when 27 patients had been recruited and the available urine sample was incomplete, with samples from one or both TPs being unavailable in some cases, resulting in a total of 47 samples instead of 54. Whereas a complete set of urine samples from both TPs from all the patients was available at the end of the study when all 30 patients had been recruited, giving a total of 60 samples for the NMR experiments involving filtered urine. The methodology of the preparation of the urine samples for NMR analysis has been described in Section 2.2.4.

3.3.5 ^{1}H NMR spectroscopic analyses of filtered and non-filtered urine and multivariate data analyses

The standardised procedures for the ^{1}H NMR spectroscopy analyses of the filtered and non-filtered urine and the multivariate statistical analyses of the spectral data have been described in Sections 2.2.5 and 2.5, respectively.

3.4 Results

3.4.1 Patient Meta data - demographics and clinical data of the validation cohort

Table 3.4 Characteristics of the validation cohort: demographics and baseline clinical variables (A) including the baseline Acute Kidney Injury Network (AKIN) and Sequential Organ Failure Assessment (SOFA) scores in more detail (B). Key: APACHE II: Acute Physiology and Chronic Health Evaluation II, COPD: Chronic Obstructive Pulmonary Disease, ICU: Intensive Care Unit, IHD: Ischaemic Heart Disease, IQR: interquartile range, NYHA: New York Heart Association functional classification, *: SOFA scores except for renal, which are AKIN scores.

A

Characteristic	**All patients - Urine** n= 30 n(%) or median [IQR]
Age (years)	63 [43-76]
Gender (male)	20 (66.7)
APACHE II	20 [14-27]
Organ dysfunction scores*	
Renal	0[0-2]
Liver	0 [0-1]
Respiratory	2 [1-3]
Cardiovascular	3 [0-4]
Haematological	1 [0-2]
Neurological	2 [0-4]
Baseline serum creatinine	87 [73-156]
Baseline serum total bilirubin	14 [9-31]
Co-morbidity	
IHD	8 (26.7)
NYHA IV	4 (13.3)
Severe COPD	3 (10)
Chronic renal failure	2 (6.7)
Cancer	3 (10)
Cirrhosis	6 (20)
Immunocompromised	4 (13.3)
Diabetes	4 (13.3)
Recent trauma	0
Admission type	
Medical (Non operative)	25 (83.3)
Surgery – Emergency(Operative)	5 (16.7)
Surgery – Elective(Operative)	0
Diagnostic group (reason for admission)	
Post cardiac arrest	6 (20)
Cardiovascular	5 (16.7)
Respiratory	1 (3.3)

Table 3.4 continued

Gastro-intestinal - medical	3 (10)
Gastro-intestinal - surgical/operative	3 (10)
Infection	8 (26.7)
Neurologic	1 (3.3)
Obstetric	2 (6.7)
Trauma	1 (3.3)
Clinical outcomes	
Length of ICU stay	5 [3-9]
ICU mortality	8 (26.7)
Hospital mortality	12 (40)

B

	Organ dysfunction scores*				
Organ dysfunction	**0**	**1**	**2**	**3**	**4**
Renal	17	5	3	5	NA
Liver	18	5	5	2	0
Respiratory	3	5	9	10	3
Cardiovascular	12	1	0	7	10
Haematological	15	4	5	5	1
Neurological	14	0	3	2	11

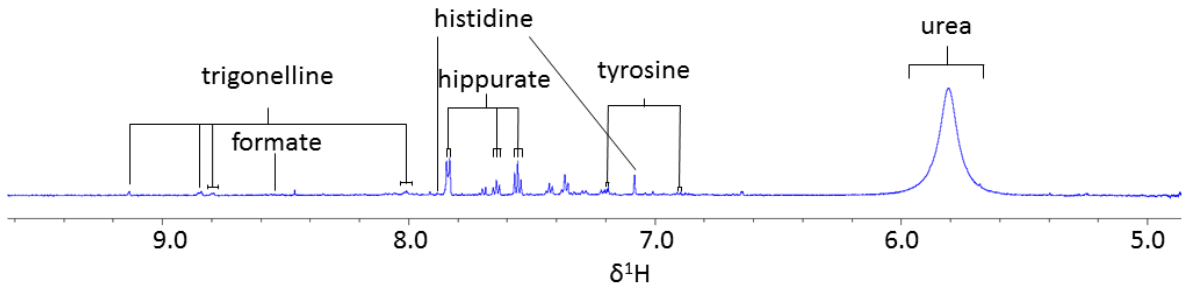
3.4.2 ^{1}H NMR spectroscopy of urine from critically ill patients

Typical ^{1}H NMR spectra of urine from a healthy control and an individual from the validation cohort are shown in Figures 3.1 and 3.2, respectively. Metabolites identified in urine from both the validation cohort and the healthy control included formate, hippurate, urea, creatinine, creatine, glycine, trimethylamine and dimethylamine. A list of the metabolites identified in the urine from both sources are shown in Tables 3.5. In addition to the metabolites common to both sets of urine, the urine samples from the validation cohort also demonstrated several resonances consistent with signals belonging to pharmaceutical drugs. In most cases, the parent drug appeared to be responsible for the majority of these signals, see Section 3.4.3.

The ^{1}H NMR spectra of the urine samples from the validation cohort demonstrated a considerable degree of variation. The administration of pharmaceutical agents appeared to be responsible for a significant proportion of this variation, particularly the use of antibiotics and the hydroxyethyl starch

(HES) based resuscitation fluid Volulyte. This can be illustrated by comparing the urine spectra shown in Figure 3.2, which was taken from a patient not given either Volulyte or any antibiotics prior to this sample being taken to the spectra from patients given these drugs. Examples of urinary spectra from patients from the validation cohort given Volulyte, Tazocin and Co-amoxiclav are shown in Figures 3.3, 3.5 and 3.6 respectively; and a composite of the spectra shown in Figures 3.2 and 3.3 is shown in Figure 3.4. In the case of Volulyte, comparison of the spectra from the recipient (Figure 3.3) and non-recipient of Volulyte (Figure 3.2) and the composite of these two spectra shown in Figure 3.4, demonstrated the addition of broad peaks and distortion of the baseline in the patient given Volulyte. Whereas, comparisons of the urinary spectra from the patient not given any antibiotics (shown in Figure 3.2) and the spectra from individuals given either Tazocin (Figure 3.5) or Co-amoxiclav (Figure 3.6), predominantly demonstrates the addition of several peaks in the spectra from the patients given of these antibiotics compared to patient not given any antibiotics. The differences between the ^{1}H NMR urinary spectra from the recipient and non-recipient of Volulyte, highlighted by the composite of these spectra, also appeared to be responsible for the most significant differences between the spectral arrays of the validation cohort as a whole, and between the spectral arrays of the validation cohort and healthy controls.

A



B

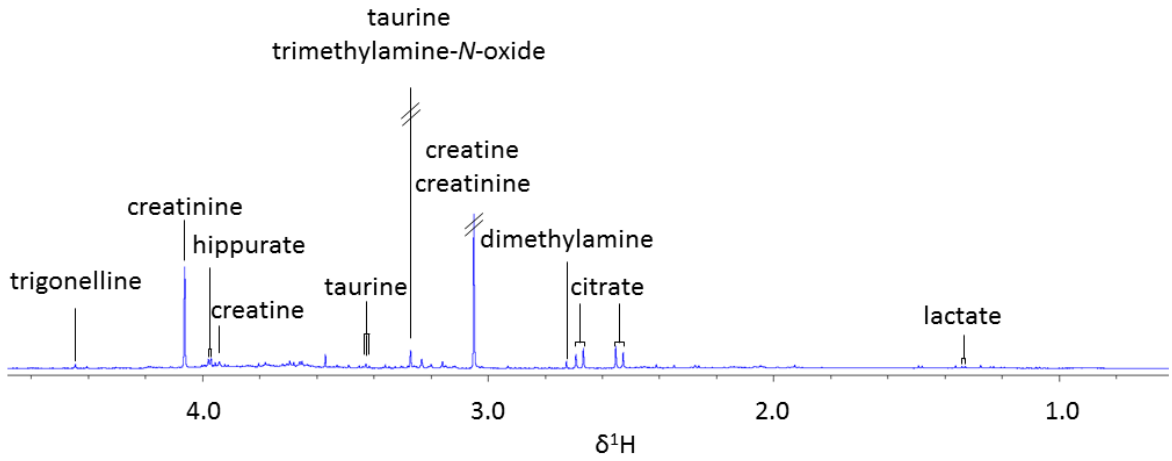
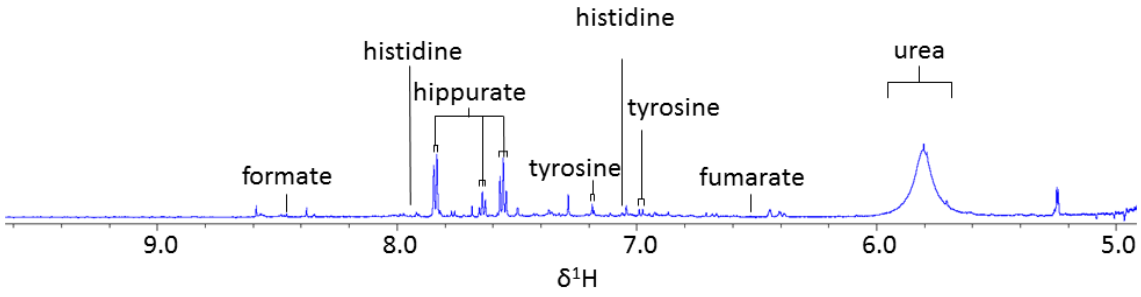


Figure 3.1 A typical 600MHz 1D ^{1}H NMR spectrum of regions 9.7-4.8 ppm (A) and 4.6-0.8 ppm (B) from a urine sample from a healthy control illustrating the urinary metabolites usually detected by this method of metabolic profiling.

A



B

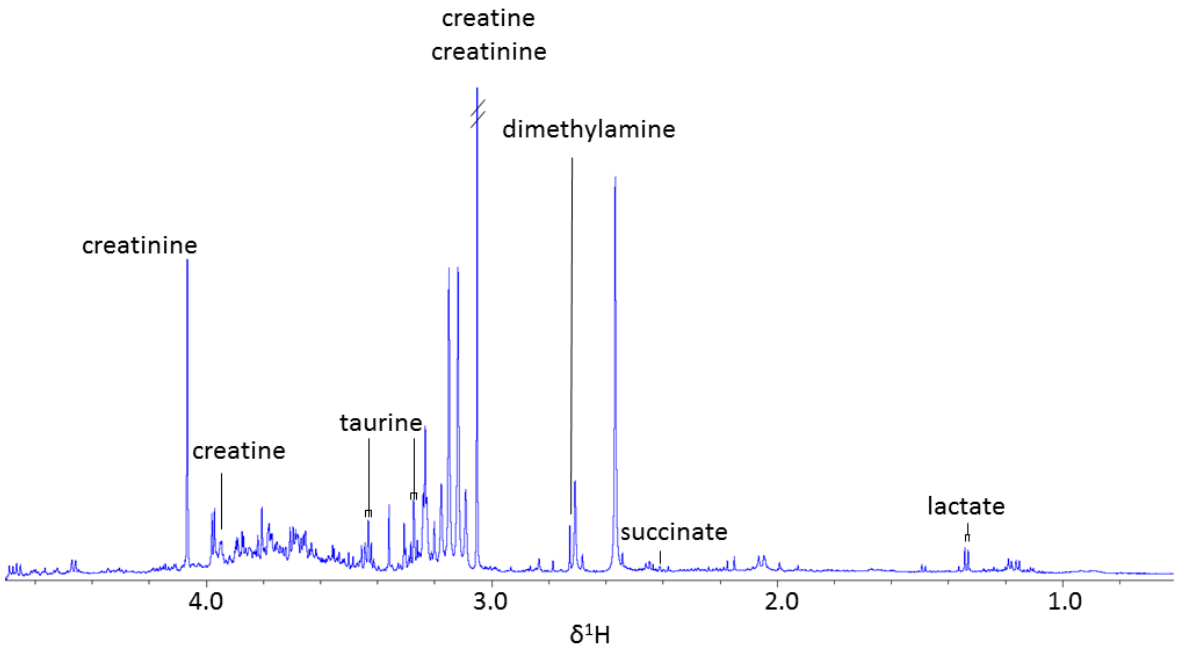
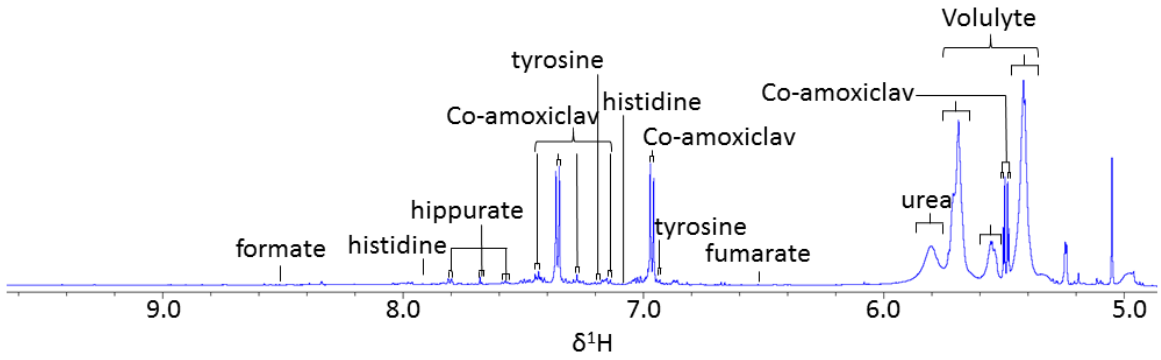


Figure 3.2 A 600MHz 1-D ^{1}H NMR spectrum of regions 9.7-4.8 ppm (A) and 4.6-0.8 ppm (B) of urine from an individual from the validation cohort not given the hydroxyethyl starch based fluid Volulyte or any antibiotics, illustrating the metabolites detected by this method in urine from this cohort.

A



B

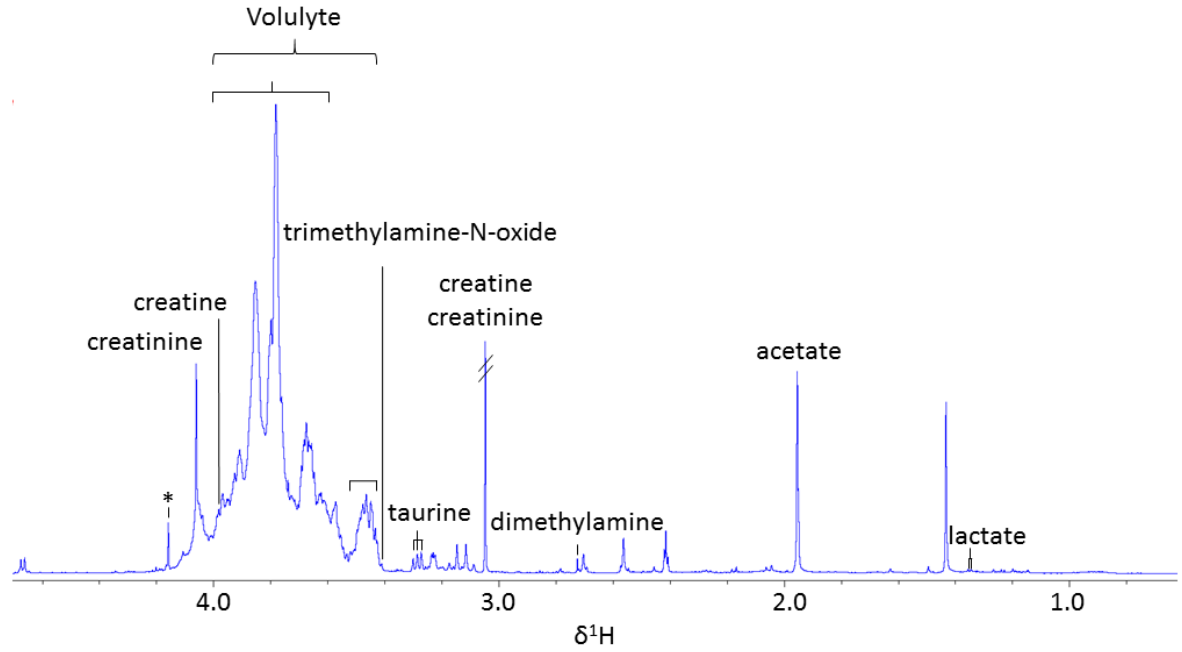
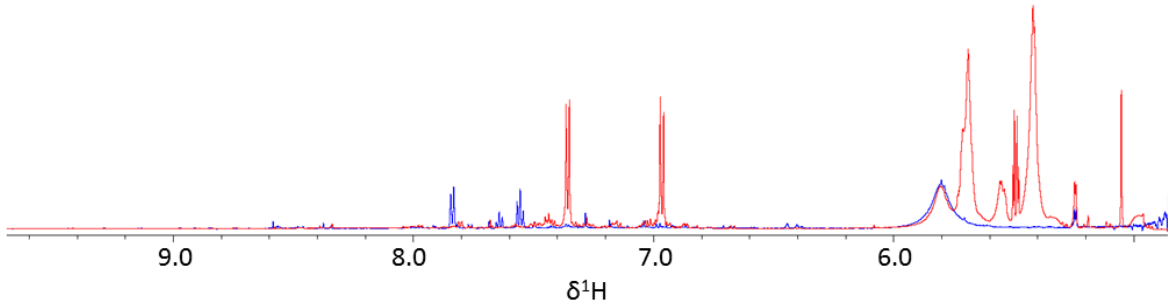


Figure 3.3 A 600MHz 1-D ^{1}H NMR spectrum of regions 9.7-4.8 ppm (A) and 4.6-0.8 ppm (B) of unfiltered urine from a hydroxyethyl starch (Volulyte) recipient from the validation cohort demonstrating a combination of urinary metabolites typical detected by this method in addition to signals of the hydroxyethyl starch. Key: All the signals marked Co-amoxiclav are signals of the parent drug of Co-amoxiclav unless otherwise indicated; KEY: *: signal present in both Tazocin and Co-amoxiclav drug standard.

A



B

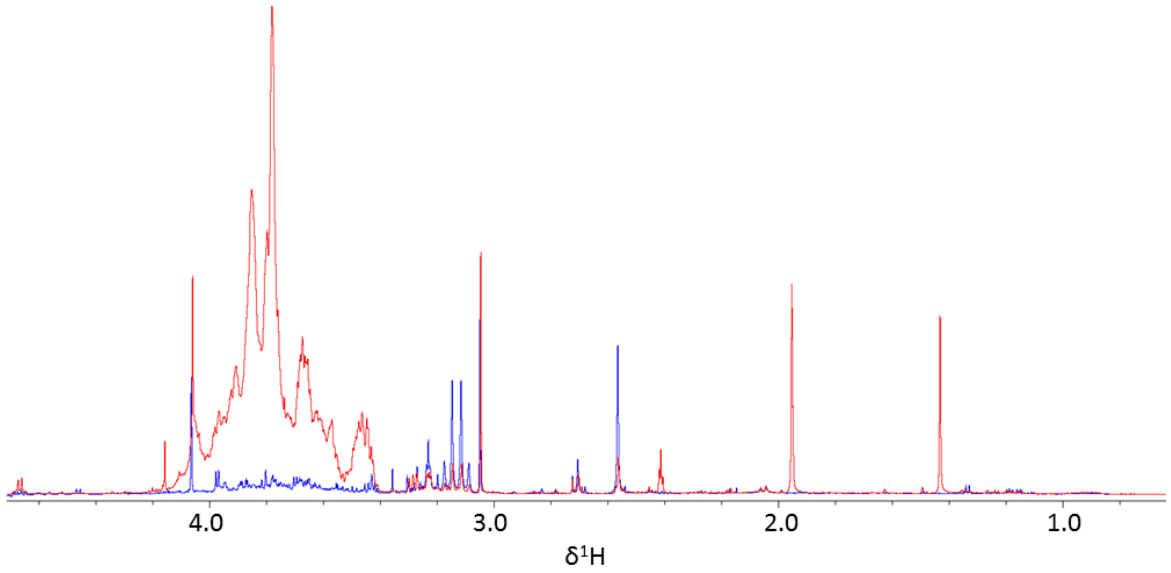
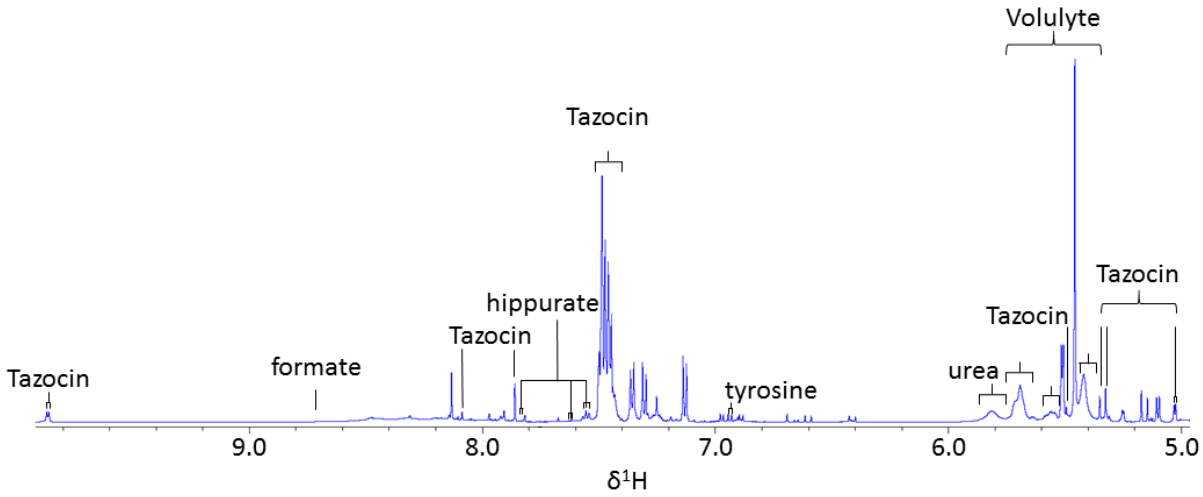


Figure 3.4 A composite of two 600MHz 1-D ^{1}H NMR spectra of regions 9.7-4.8 ppm (A) and 4.6-0.8 ppm (B) of unfiltered urine from individuals from validation cohort, illustrating the differences between spectra from a recipient (red) and non-recipient (blue) of hydroxyethyl starch.

Table 3.5 Non-drug metabolites identified in the 600MHz 1-D ^{1}H NMR spectra of urine from (i) the validation cohort and (ii) the healthy control shown in Figure 3.1 and their chemical shifts and signal multiplicities. Key: s: singlet; d: doublet; t: triplet; q: quartet; o: octet; m: multiplet; bs: broad signal; dd: doublet of doublets.

Metabolites	H group					δ ^{1}H (multiplicity)					cohort urine	control urine
1-methylnicotinamide	H2	H6	H4	H5	CH3	9.28	8.97 (d)	8.90 (d)	8.18 (t)	4.48 (s)	yes	no
acetate	CH_3					1.92 (s)					yes	yes
citrate	CH_2(i)	CH_2(ii)				2.66 (d)	2.54 (d)				no	yes
creatine	CH_2	CH3				3.94 (s)	3.04 (s)				yes	yes
creatinine	CH_2	CH3				4.06 (s)	3.04 (s)				yes	yes
dimethylamine	CH_3					2.72 (s)					yes	yes
formate	CH					8.46 s					yes	yes
fumarate	CH					6.53 (s)					yes	no
glycine	CH					3.57 (s)					yes	yes
hippurate	2,6-CH	4-CH	3,5-CH		CH2	7.84 (d)	7.63 (t)	7.55 (t)	3.97 (d)		yes	yes
histidine	H_3	H5	αCH	βCH2(i)	βCH2(ii)	7.83 (s)	7.08 (s)	4.00 (dd)	3.3 (dd)	3.1 (dd)	yes	yes
lactate	CH	CH_3				4.12 (q)	1.32 (d)				yes	yes
lipid signal	=CH-C***H*** $_2$-CH					2.73 (bs)					yes	no
lipid signal	C***H*** $_2$C=C					2.01 (bs)					yes	no
lysine	αCH	βCH_2	γCH_2	δCH_2	εCH_2	3.76 (t)	1.90 (m)	1.73 (q)	1.48 (m)	3.03 (t)	yes	no
succinate	2x CH_2					2.41 (s)					yes	no
taurine	CH_2NH_2	CH_2SO_3				3.43 (t)	3.27 (t)				yes	yes
trigonelline	H2	C6H	C4H	C5H	CH3	9.11 (s)	8.84 (m)	8.82 (m)	8.07 (m)	4.43 (s)	no	yes
trimethylamine	3x CH_3					2.89 (s)					yes	yes
trimethylamine-N-oxide	3 x CH3					3.27 (s)					yes	yes
tyrosine	2,6-CH	3,5-CH	CH	CH_2(i)	CH_2(ii)	7.20 (d)	6.90 (d)	3.90 (dd)	3.2 (dd)	3.1 (dd)	yes	yes
UNK	-					8.33 (d)					yes	no
UNK	-					3.13 (q)					yes	no
UNK	-					3.19 (bs)					yes	no
UNK	-					2.56 (s)					yes	no
UNK	-					2.49 (s)					yes	no
UNK	-					2.46 (bs)					yes	no
UNK	-					2.38 (bs)					yes	no
UNK	-					2.29 (bs)					yes	no
UNK	-					1.93 (bs)					yes	no
UNK	-					1.86 (s)					yes	no
UNK	-					1.41 (bs)					yes	no
UNK	-					1.30 (d)					yes	yes
UNK	-					0.90 (o)					yes	no
urea	exchanged					5.75 (bs)					yes	yes

A



B

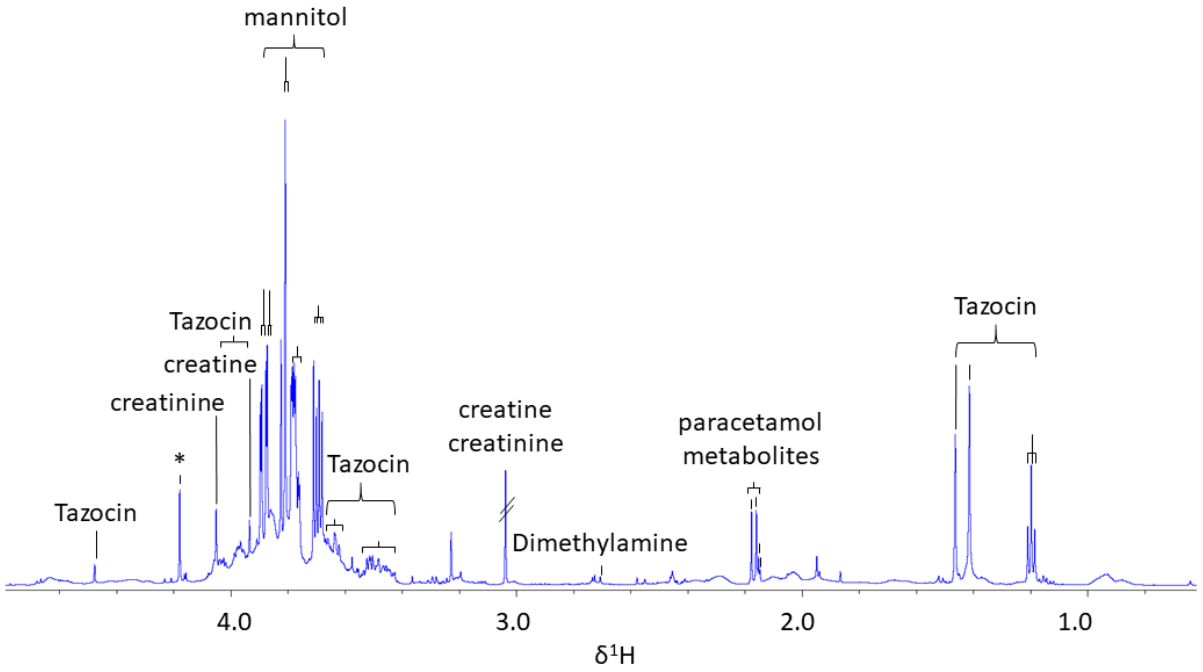
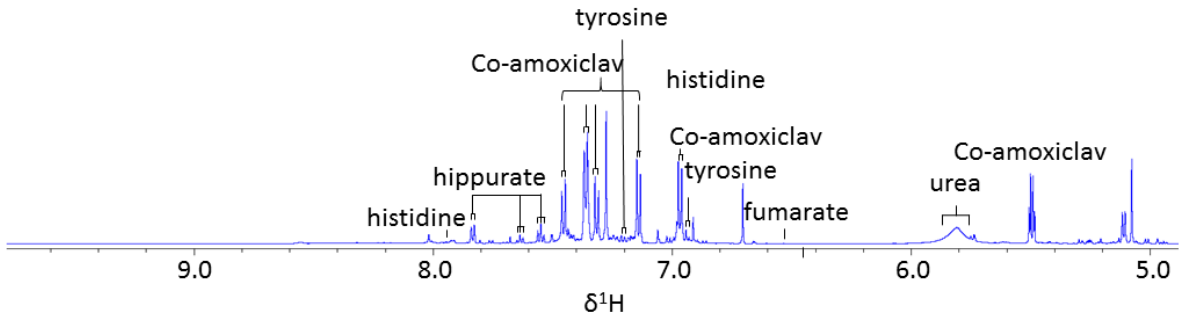


Figure 3.5. A 600MHz 1D ^{1}H NMR spectrum of urine from a recipient of the drug Tazocin as the only antibiotic, or structurally similar drug administered, regions 9.7-4.8 ppm (A) and 4.6-0.8 ppm (B) illustrating the detection of usual urinary metabolites in addition to signals of Tazocin. KEY: *: signal present in both the Tazocin and Co-amoxiclav drug standards.

A



B

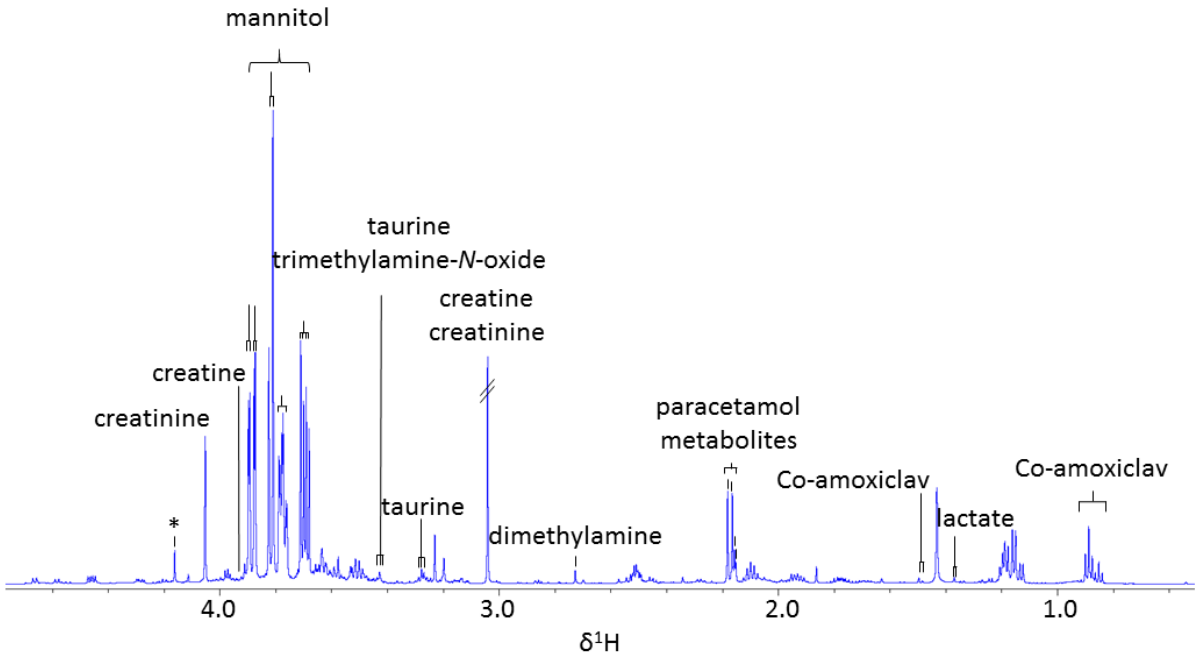


Figure 3.6. A 600MHz 1D ^{1}H NMR spectrum of urine from a recipient of the drug of Co-amoxiclav as the only antibiotic, or structurally similar drug administered, divided into 9.7-4.8 ppm (A) and 4.6-0.8 ppm (B) illustrating of the detection of usual urinary metabolites in addition to signals of Co-amoxiclav. KEY: *: signal present in both the Tazocin and Co-amoxiclav drug standards.

3.4.3 Methods used to identify metabolites in urinary spectra: non-drugs & drugs

3.4.3.1 ^{1}H NMR spectroscopy of drugs commonly used in ICU

The urinary spectra shown in the previous section illustrated the complexity of the metabolic profiles of critically ill patients including the addition of signals from pharmaceutical drugs. One of the difficulties is being able to identify them, due to lack of a NMR database of drugs that are commonly used in the ICU. To enrich the database, the top 100 drugs and intravenous fluids administered to critically ill patients were profiled using ^{1}H NMR spectroscopy (see Appendix II). This ^{1}H NMR parent drug database was used to identify metabolites not identified using local or public databases. Herein, the term parent drug refers to the un-metabolised drug standards, whereas drug metabolites are a set of compounds derived from the parent drug through biochemical modifications.

The metabolism of the drugs in the drug standards database is considerably variable. Of the different subgroups of drugs, the antibiotics tend to undergo the least extensive metabolism with the highest percentage of the drug excreted in urine unchanged (20 to 99 percent). Whereas, the vasoactive drugs such as adrenaline and dopamine (amines), steroids, opiates (such as morphine and alfentanil) and neuroactive drugs such as propofol and lorazepam, undergo the most extensive metabolism with as little as less than one percent in some cases and less than five to 10 percent, in the majority of cases, excreted unchanged. Approximately 75 percent of the drugs in the drug standards database undergo hepatic metabolism, with or without the addition of renal metabolism; and the majority of these drugs are excreted by the kidneys, in addition to being excreted by other routes such as via bile and faecal excretion.

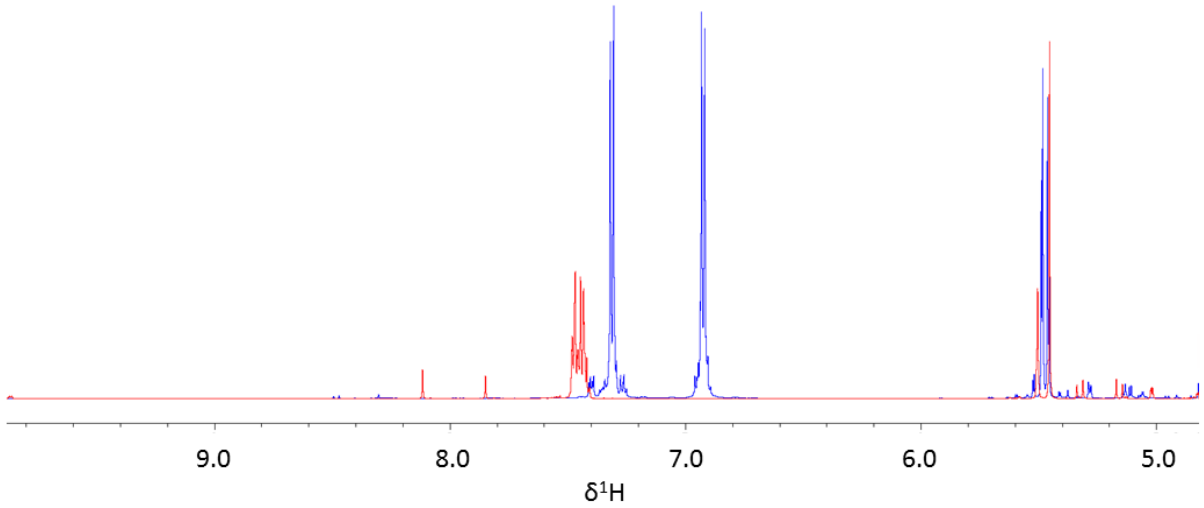
3.4.3.1.1 Identification of ^{1}H NMR signals of parent drugs using drug standards

In the validation cohort, the antibiotics Tazocin and Co-amoxiclav were two of the most commonly administered drugs and are therefore good examples of the use of the ^{1}H NMR drug standard database

in the identification of drugs and their metabolites. Their high prevalence in the sample set also increases their chances of being a confounding factor. The identification of these two drugs and their metabolites was therefore very important.

A composite of 1-D ^{1}H NMR spectra of the Tazocin and Co-amoxiclav drug standards is shown in Figure 3.7. This illustrates the signals of the parent drugs and highlights their differences. Comparisons of this composite and the individual 1-D ^{1}H NMR spectra of the drug standards of these two drugs (Figures 3.8 and 3.10) were made with the urinary spectra of recipients of these two antibiotics (see examples shown in Figure 3.5 and 3.6). This revealed that the majority of the signals of the parent drug of these two drugs were detectable in the urinary spectra of recipients of these drugs.

A



B

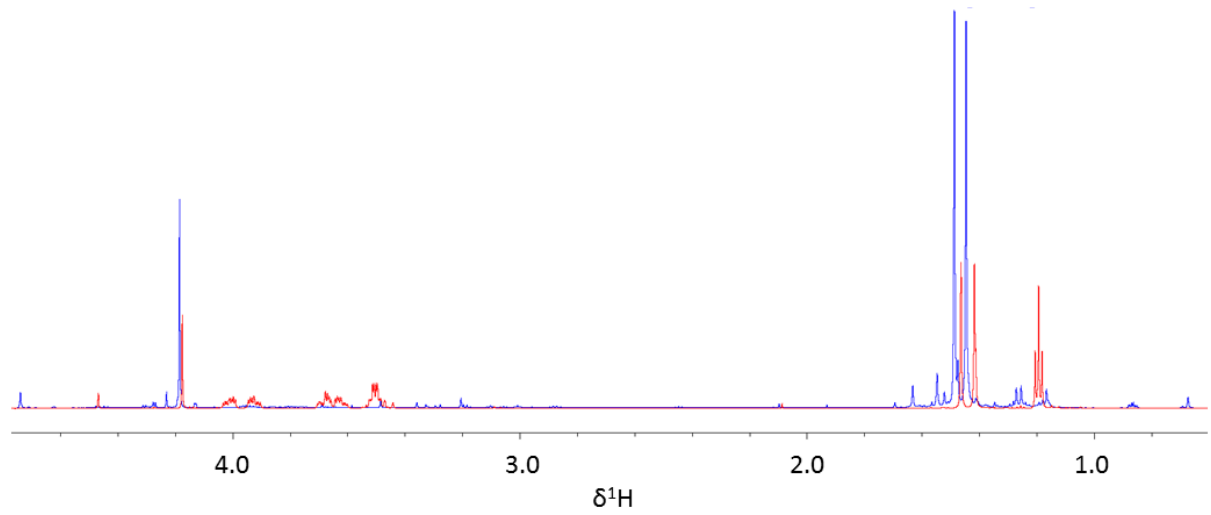


Figure 3.7 A composite of 600MHz 1-D ^{1}H NMR spectra regions 9.7-4.8 ppm (A) and 4.6-0.8 ppm (B) of the Tazocin (red) and Co-amoxiclav (blue) drug standards illustrating signals of these two antibiotics and highlighting their differences.

3.4.3.1.2 Identification of drug metabolites using statistical total correlation spectroscopy (STOCSY)

Statistical total correlation spectroscopy (STOCSY) involves the calculation of the correlation coefficient and covariance between the intensity of a given driver peak and all data points in a spectrum. The results are then displayed on a plot which resembles the original spectrum. In the case of NMR, the signals are displayed along the x axis according to their δ^1H locations. For each unknown peak with a relatively high intensity, a 1-D STOCSY was performed using this resonance as the driver peak, to identify correlated resonances. Comparisons of the NMR spectra of the drug standards such as the composite of Tazocin and Co-amoxiclav shown in Figure 3.7 were used to identify characteristic peaks of the drug standards. These driver peaks were then utilised in statistical total correlation spectroscopy analyses of the urinary spectra of the validation cohort to aid the identification of metabolites of the parent drugs in the urinary spectra; it can also be used to identify daughter (breakdown) compounds. The success of a STOCSY relies on the use of a driver peak that is free from overlapping peaks and unique or of high specificity to the compound of interest.

On a STOCSY plot the Pearson correlation coefficient is represented by a colour scale, red at the top of the scale representing a high statistical correlation (r = 1) with the chosen driver peak and blue at the bottom of the scale representing a low correlation (r = 0). Whereas a positive and negative covariance is represented by an upward and downwards deflection of the signal, respectively. Highly correlating resonances can be either from the parent drug or its metabolites. A list of the resonances present in the NMR spectrum of the parent drug was used to differentiate between resonances of the parent drug, from those of its metabolites.

In the example of Tazocin, a distinctive multiplet was demonstrated at δ^1H 7.49 and 7.48 in the NMR spectra of the Tazocin standard (Figure 3.8) and urinary spectra from recipients of Tazocin from the validation cohort, respectively. The slight difference in the chemical shift of this multiplet in the two spectra was thought to be related to slight differences in sample pH. This multiplet was chosen as the driver for STOCSY to identify signals of both the parent drug and its metabolites in the ^{1}H NMR spectra

of urine from this cohort as illustrated in Figure 3.9. Comparison of this STOCSY and the NMR spectra of the Tazocin drug standard illustrates two key features. Firstly, all the peaks in the STOCSY plot demonstrating a high correlation with the driver peak, resemble signals present in the NMR spectra of the Tazocin standard, consistent with them being signals of the parent drug as opposed to metabolites. Secondly, the majority of the signals of the Tazocin standard demonstrated in Figure 3.8 appear to be present in the STOCSY of the urinary spectra. Of these, the majority demonstrate a high correlation with the driver peak (as expected) however, some peaks in heavily congested regions of the spectra, (with several overlapping peaks), do not demonstrate any significant correlation with the driver peak.

A doublet located at δ^1H 7.32 ppm in the NMR spectra of the Co-amoxiclav standard (see Figure 3.10) and δ^1H 7.31 in the urinary spectra from recipients of Co-amoxiclav from the validation cohort ppm was chosen as the driver peak in the STOCSY used to identify signals of Co-amoxiclav and its metabolites. The dominance of the antibiotic Co-amoxiclav in the NMR spectra of this cohort cannot be over stated. Co-amoxiclav was administered to over a third of the patients in this cohort and the ^{1}H NMR spectra of the Co-amoxiclav standard revealed a total of 156 signals (see Figure 3.10 and Appendix II). The composite figure of the NMR spectra of the drug standards of Tazocin and Co-amoxiclav shown in Figure 3.7 illustrates the overlap demonstrated by the ^{1}H NMR signals of these two structurally related antibiotics. Given the presence of the majority of the signals of Tazocin shown in the STOCSY of the urinary spectra data set, considerable overlap in the signals of these two antibiotics in the urinary spectra was anticipated.

To avoid confusion between the signals of these two drugs, the doublet at δ^1H 7.31 in the urinary spectra was utilised, as the 'driver peak' in the STOCSY of the urinary ^{1}H NMR spectra to identify the metabolites of Co-amoxiclav since it is a unique peak for the drug illustrated by the NMR spectra of

Co-amoxiclav. The resonances demonstrating statistical correlation to the signal at δ^1H 7.31 of the urinary ^{1}H NMR spectra identified by the STOCSY are illustrated in Figure 3.11. This included a considerable number of signals demonstrating high and medium levels of correlation with the driver peak, assigned to the Co-amoxiclav. Comparison of the NMR spectra of the Co-amoxiclav standard shown in Figure 3.10 and the STOCSY used to investigate Co-amoxiclav signals in the urinary spectra (Figure 3.11), demonstrated that the majority of the signals with a greatest correlation to the STOCSYs driver peak were from the parent drug. There were however a few exceptions: such as the multiplet at δ^1H 2.17, shown in the STOCSY in Figure 3.11, that was not present in the drug standard of Co-amoxiclav but demonstrated a high correlation with the driver peak. Of the signals associated with a moderate correlation (coefficient of 0.7-0.6) to the driver peak, differentiating between signals from the parent drug and drug metabolites was made incredibly difficult by the vast number of signals associated with the parent drug (Figure 3.10) and their overlap with other signals.

In the example of hydroxyethyl starch a distinctive multiplet at δ^1H 3.79 identified using the ^{1}H NMR spectra drug standard (see Figure 3.12) was used as the driver peak of the STOCSY used to identify signals of this starch as shown in Figure 3.13. All the signals of the parent drug demonstrated by the ^{1}H NMR spectra of the drug standard were present in the urinary^{1}H NMR spectra of the validation cohort with the addition of the metabolite acetate (present in the isotonic solution of Volulyte).

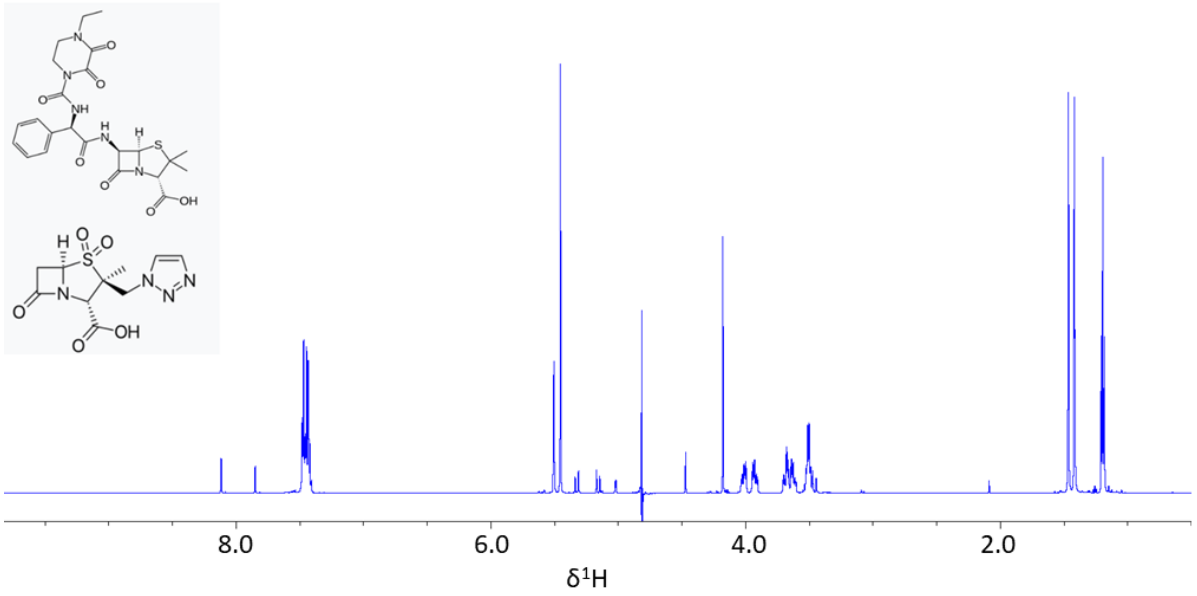


Figure 3.8 A 600MHz 1D ^{1}H NMR spectra of the drug standard of Tazocin: δ^{1}H 10-0.5 ppm and inserts of the structure of two components of Tazocin: Piperacillin (top) and Tazobactam (bottom).

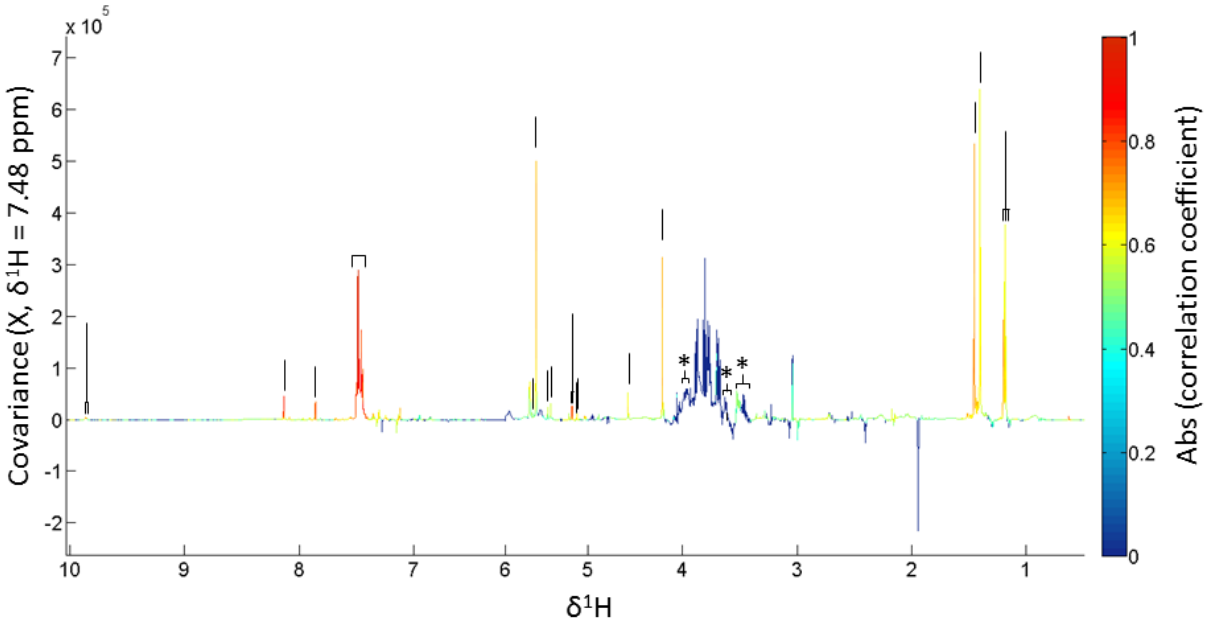


Figure 3.9 Illustration of the use of 1-D STOSCY of 600MHz 1-D ^{1}H NMR spectra of unfiltered urine from the validation cohort utilising the signal at δ^{1}H 7.48, as the 'driver' peak, to identify parent drug (labelled) and metabolites of the drug Tazocin. Signals from the parent drug are labelled and those with a low correlation with the driver peak are also starred (*).

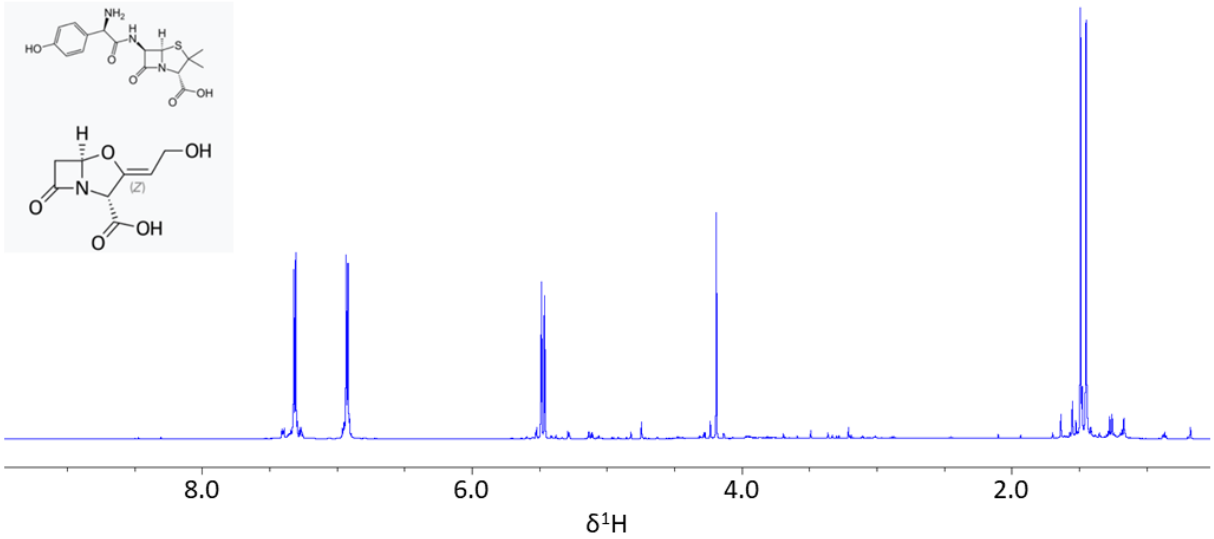


Figure 3.10 600MHz 1D ^{1}H NMR spectra of the drug standard of Co-amoxiclav: δ^{1}H 10 - 0.5 ppm and inserts of the structure of two components of Co-amoxiclav: Amoxicillin (top) and Clavulanic acid (bottom).

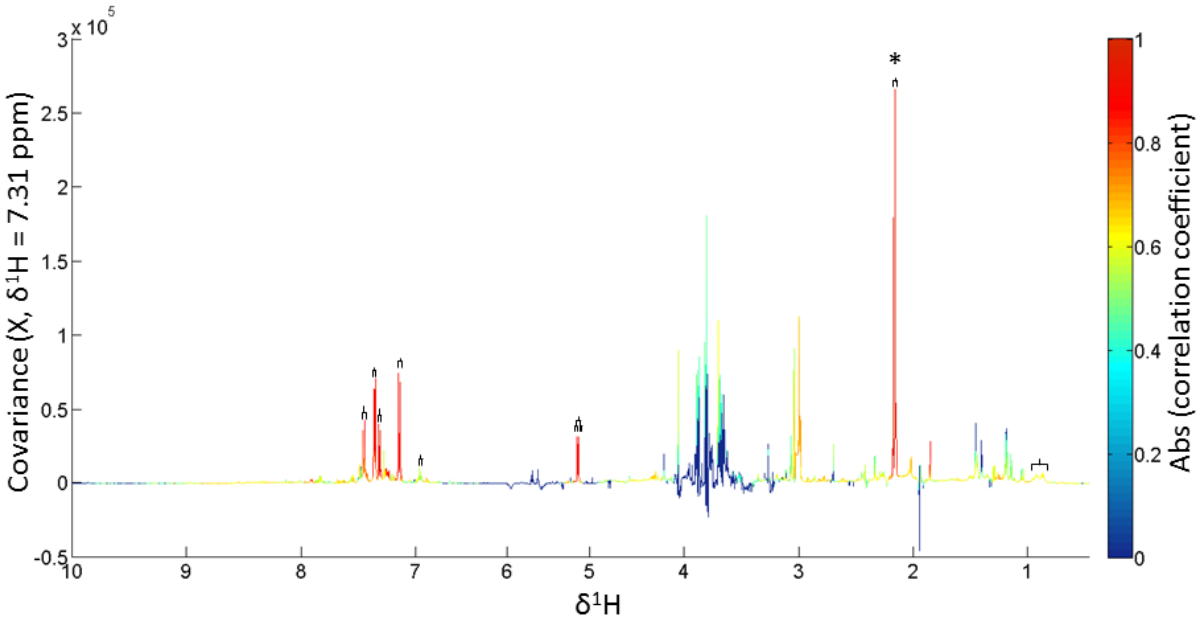


Figure 3.11 Illustration of the use of 1-D STOSCY of 600MHz 1D ^{1}H NMR spectra of unfiltered urine from the validation cohort utilising the signal at δ^{1}H 7.31ppm as the 'driver' peak, to identify signals of the parent drug (labelled) and metabolites of Co-amoxiclav δ^{1}H 10-0.5ppm. The signal that is both labelled and starred is an example of a signal with a high correlation with the driver peak that is not present in the drug standard of Co-amoxiclav; and may or may not a metabolite of Co-amoxiclav.

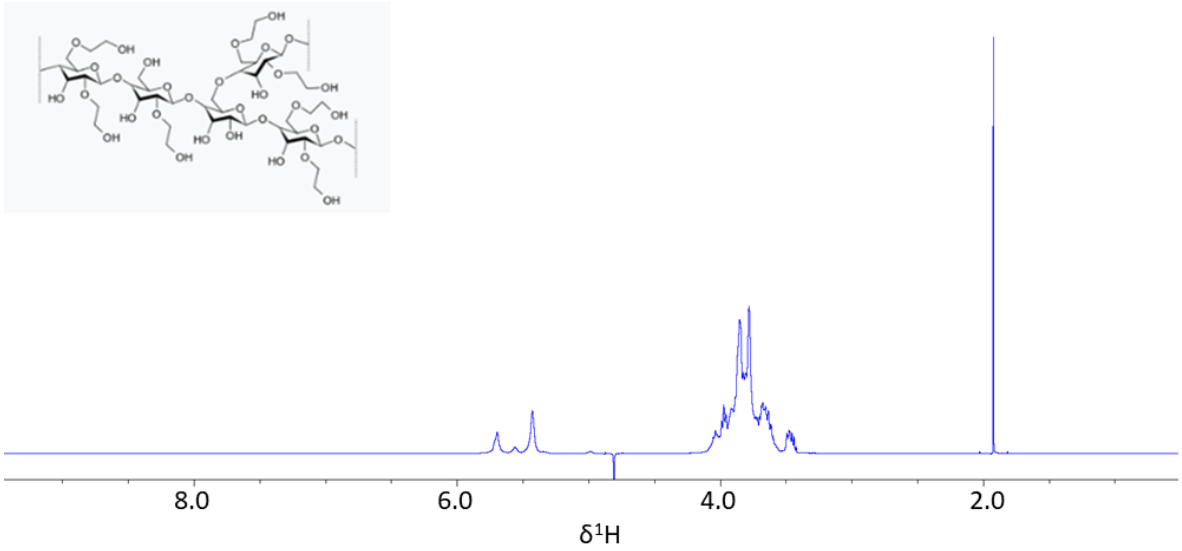


Figure 3.12 A δ^1H 9.8 - 0.8 ^{1}H NMR spectra of the hydroxyethyl starch Volulyte drug standard and an insert of the structure the hydroxyethyl starch.

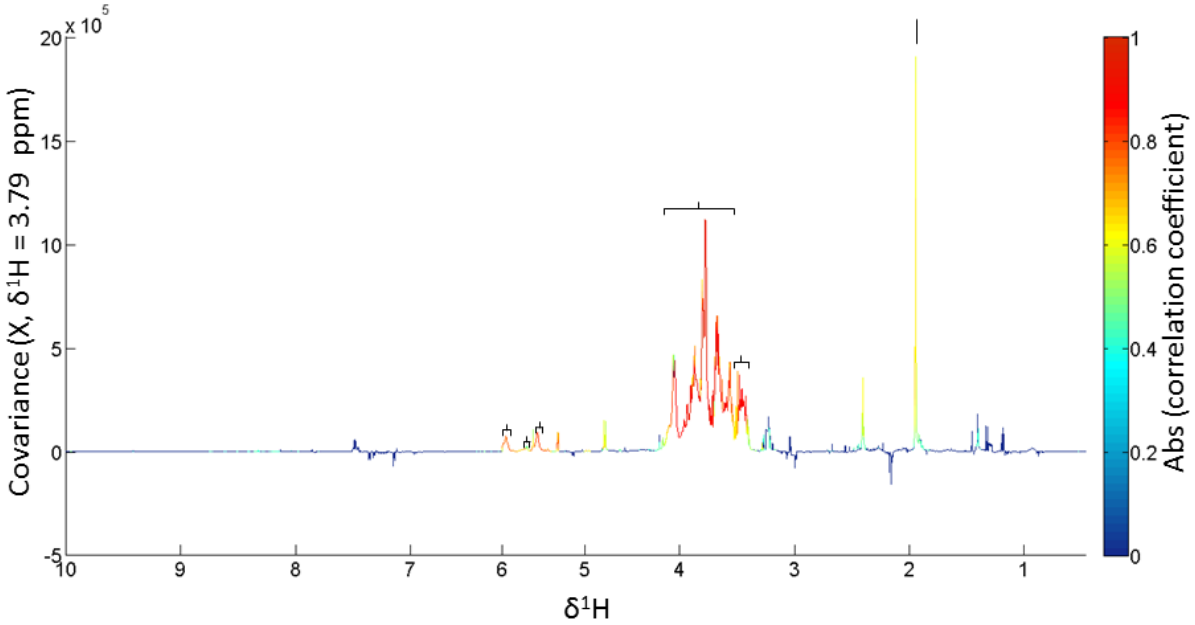


Figure 3.13 Illustration of the use of 1-D STOSCY of 600MHz 1D ^{1}H NMR spectra of unfiltered urine from the validation cohort utilising the signal at δ^1H 3.79ppm as the 'driver' peak, to identify signals of the parent drug (labelled) and metabolites of the hydroxyethyl starch Volulyte.

3.4.4 Multivariate statistical analyses of ^{1}H NMR spectra of unfiltered validation cohort urine – organ dysfunction and ICU Survival

Principal component analysis was performed on the probabilistic quotient normalised 1-D ^{1}H NMR spectral data of unfiltered urine from the VC from both time points, totalling 47 samples, (see Section 3.3.4 for details), using unit variance scaled data and SIMCA-13 software. This *unsupervised* method of multivariate statistical analysis was used to provide an overview of the metabolic variation of the data set as a whole. A total of two principal components were calculated to construct the models and 30.8% of the variance was explained by these two components. The PCA scores plot (Figure 3.14) demonstrated three samples lying outside of the perimeter of the Hotelling's T^2 95% confidence ellipse: two close to the perimeter referred as intermediate outliers and one at a greater distance or extreme outlier. This was shown to be both a scores and an orthogonal outlier, with relatively high values of the broad signals in the region of 4.1-3.2 ppm and it was therefore excluded from subsequent analyses (see Appendix III Figures 1 and 2). The same method of PCA was then applied to the normalised 1-D ^{1}H-NMR spectral data of the remaining 46 samples of unfiltered VC urine samples, following the exclusion of the extreme outlier (see Figure 3.15). All subsequent analyses of the unfiltered urine samples from the ICU validation cohort were with the exclusion of the extreme outlier (defined as lying outside of the >+/-200 boundary of the Hotelling's T2 95% confidence interval).

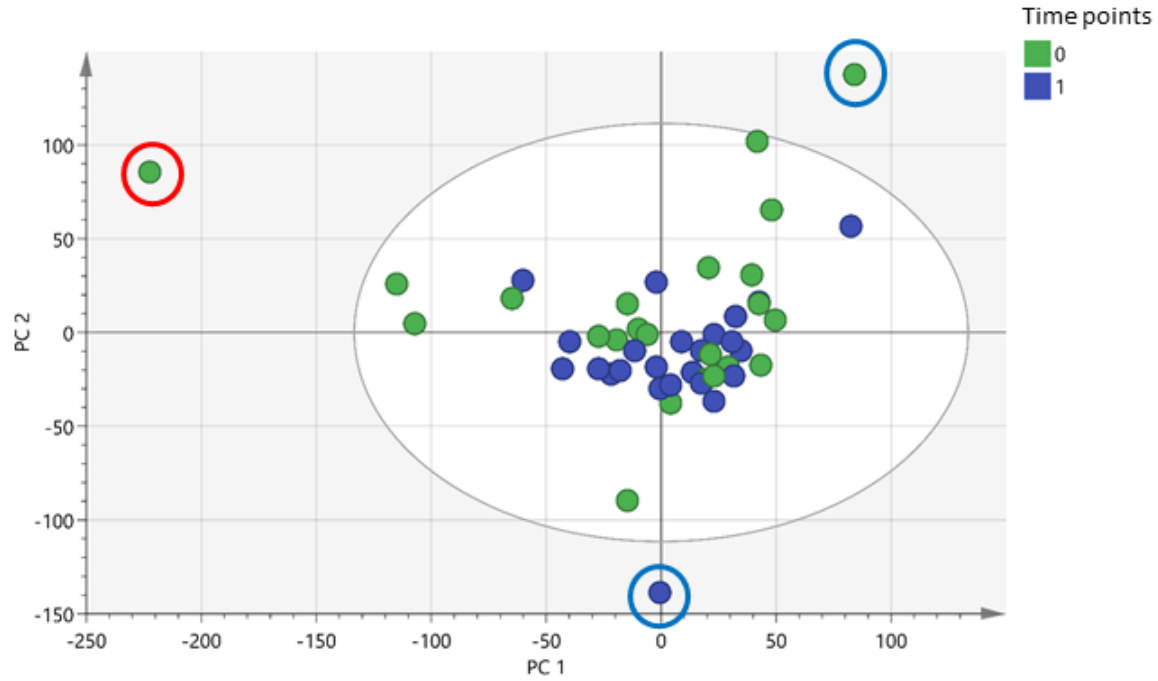


Figure 3.14 PCA scores plot derived from ^{1}H NMR spectra of unfiltered urine from the validation cohort (47 samples) illustrating the metabolic variation of the data set as a whole and three outliers: one extreme (circled in red) and two intermediate outliers (circled in blue) of the perimeter of the Hotelling's T^2 95% confidence ellipse.

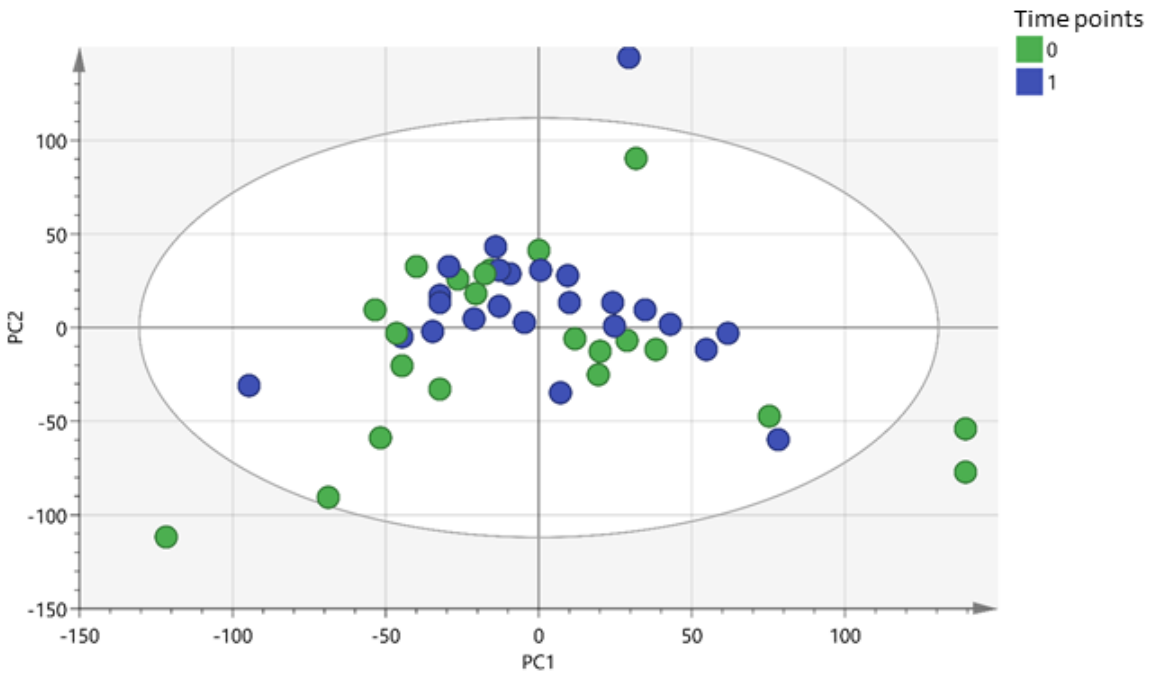


Figure 3.15 PCA scores plot derived from ^{1}H NMR spectra of unfiltered urine from the validation cohort (46 samples) following the exclusion of one extreme outlier illustrating the metabolic variation of this data set as a whole.

This was followed by constructing individual time point PCA models using all the spectral data from each time point, with separates models assessing the separation of the samples at that time point according to each of the seven clinical classes under investigation (see Section 3.3.3). One to three principal components were calculated for each model and the samples were colour coded according to the presence (group 1) or absence (group 0), of death or dysfunction (kidney or liver), in blue (1) and green (0), respectively. From here onwards, these are referred as the renal, liver and 28-day survival classes. The percentage of the variation explained (R^2X) and predicted (Q^2X) by the PCA models of the spectral data from time points zero and one are listed in Table 3.6. One example of each of the PCA models of the data from the individual time points are illustrated in Figures 3.16 (time point zero) and 3.17 (time point one): in both examples, the samples were labelled according to their renal dysfunction classes. No evidence of separation was demonstrated between the samples according to any of the seven clinical classes by any of the PCA scores plots of data from the two time points.

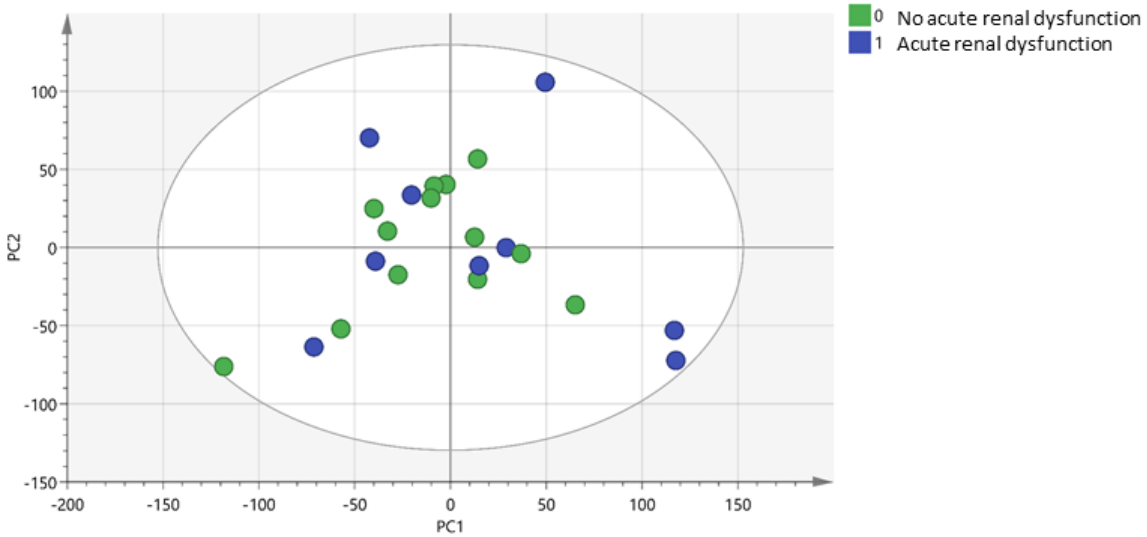


Figure 3.16 PCA scores plot based on ^{1}H NMR spectra of unfiltered urine from the validation cohort taken at time point zero (22 samples) illustrating no separation of samples according to presence (1) or absence (0) of renal dysfunction.

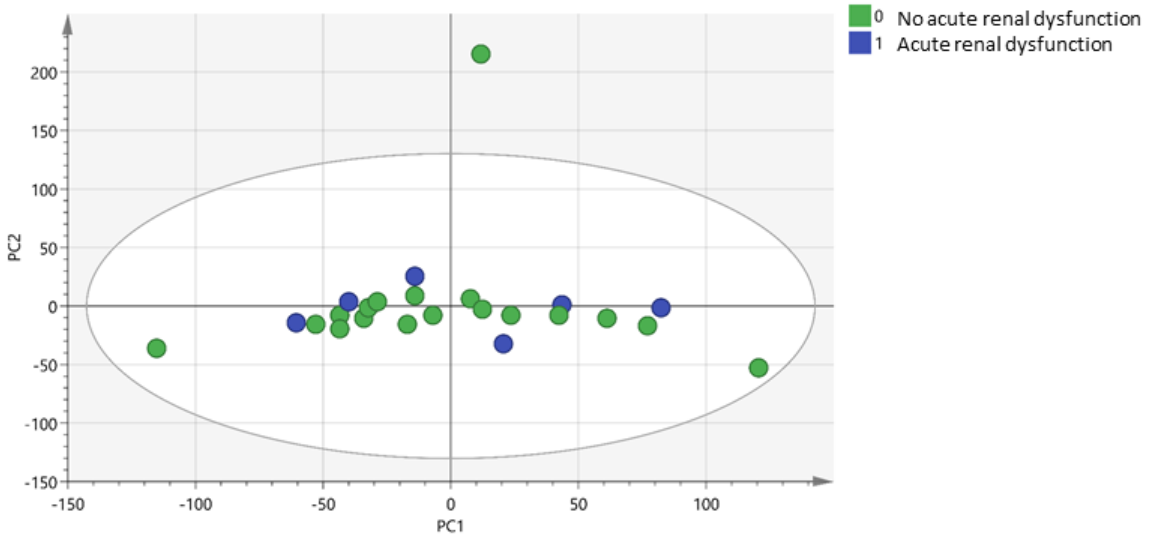


Figure 3.17 PCA scores plot based on ^{1}H NMR spectra of unfiltered urine from the validation cohort taken at time point one (24 samples) illustrating no separation of samples according to presence (1) or absence (0) of renal dysfunction.

Table 3.6. Results of the evaluation parameters of PCAs of 1-D ^{1}H NMR spectra of unfiltered urine from the validation cohort taken at time points zero and one: the percentage of the variation explained (R^2X) and predicted (Q^2X) by the model. KEY: PC: principal component.

Principal Component Analyses				
Sample set: time point (n=sample number)	All samples (n=47)	All samples minus one outlier (n=46)	Time point 0 (n=22)	Time point 1 (n=24)
Number of PCs	2	2	2	1
R^2X	0.308	0.3	0.365	0.188
Q^2	0.103	0.144	0.138	0.058

A supervised O-PLS-DA method was used to build models using NMR spectral data from individual time points as the X matrix and the dichotomised class data (e.g. presence or absence of renal dysfunction) as the dummy Y matrix for each of the seven clinical classes. All models were based on the unit variance-scaled spectral data using one PLS component and one or two orthogonal components. One orthogonal component was used, unless the use of two, resulted in a significantly

greater model, indicated by an increase in the Q^2Y of greater or equal to 0.05 and the p value of the cross validation performed using an analysis of variance. The main evaluation parameters of the best O-PLS-DA models based on the two sets of dichotomised clinical classes: (i) AKI, acute liver injury and ICU survival; and (ii) respiratory, cardiovascular, haematological, and central nervous system dysfunction are listed in Tables 3.7 and 3.8A, respectively. In the case of the latter four classes, O-PLS-DA models with the samples divided in five groups were also constructed; the evaluation parameters of the best of these models are shown in Table 3.8B. The percentage of the variation explained by the model (R^2X) ranged from 0.344 to 0.149 for models based on AKI, acute liver injury and ICU survival (Table 3.7); and 0.543 to 0.130 (Table 3.8A) and 0.219 to 0.077 (Table 3.8B) for the models based on the other four classes, with the samples divided into two and five groups, respectively. The predictability of all three sets of the models were low with one exception. This was demonstrated by Q^2Y values that ranged from 0.162 to -0.101 for the models of AKI, acute liver injury and ICU survival (Table 3.7); and 0.154 to -0.356 (Table 3.8A), and 0.040 to -0.170 (Table 3.8B) for the dichotomised models of the other four classes and the models with five groups based on these four classes, respectively. The one exception was the time point zero haematological model with the samples divided into two groups. However, the large difference of between the Q^2Y and the R^2Y values of 0.559 of this model is highly suggestive of over-fitting. Moreover, the cross-validated analysis of variance (CV-ANOVA) p value, a measure of significance of the observed group separation, of all the models of all three sets was non-significant. In summary, the O-PLS-DA models built using unfiltered urine data from individual time points, failed to demonstrate any significant separation (metabolic differences) between the dichotomised classes of AKI, acute liver injury, ICU survival, or respiratory, cardiovascular, haematological, and central nervous system dysfunction.

Table 3.7 Results of the evaluation parameters of O-PLS-DA models based on 1-D ^{1}H NMR spectra of unfiltered urine from the validation cohort taken at time points zero and one. Illustration of the percentage of the variation explained by the X (R^2X) and Y matrices (R^2Y) and predicted by the Y matrix* (Q^2Y) of the models evaluating samples based on their renal, liver and ICU survival classes. Key: CV-ANOVA: cross-validated analysis of variance, *: Y matrix contains the class information.

OPLS-DA		Acute Kidney injury		Acute Liver injury		Intensive Care Unit survival	
Sample set: time point (n=sample number)		Time point 0 (n=22)	Time point 1 (n=24)	Time point 0 (n=22)	Time point 1 (n=24)	Time point 0 (n=22)	Time point 1 (n=24)
Group 0: good outcome (no injury/survival)		13	18	13	19	17	20
Group 1: poor outcome (injury/non-survival)		9	6	9	5	5	4
Number of components	Predictive	1	1	1	1	1	1
	Orthogonal to X	0	1	0	1	2	2
Model statistics	R^2X	0.149	0.203	0.182	0.246	0.344	0.338
	R^2Y	0.510	0.789	0.520	0.785	0.901	0.922
	Q^2	0.042	-0.002	0.160	-0.101	0.162	0.101
	$R^2Y - Q^2$	0.468	0.791	0.360	0.886	0.739	0.821
CV-ANOVA	P VALUE	0.665	1.000	0.191	1.000	0.811	0.918

Table 3.8 Results of the evaluation parameters of O-PLS-DA models based on 1-D ^{1}H NMR spectra of unfiltered urine from the validation cohort at time points zero and one. Illustration of the percentage of the variation explained by the X (R^2X) and Y matrices (R^2Y) and predicted by the Y matrix* (Q^2Y) of the models evaluating samples based on their respiratory, cardiovascular, haematological, and central nervous system classes with the samples divided into two (A) and five groups (B). Key: CV-ANOVA: cross-validated analysis of variance; SOFA: Sequential Organ Failure Assessment, *: Y matrix contains the class information.

A

OPLS-DA		Respiratory		Cardiovascular		Haematological		Central Nervous System	
Sample set: time point (n=sample number)		Time point 0 (n=22)	Time point 1 (n=24)	Time point 0 (n=22)	Time point 1 (n=24)	Time point 0 (n=22)	Time point 1 (n=24)	Time point 0 (n=22)	Time point 1 (n=24)
Group 0: good outcome (no injury)		3	0	9	7	13	15	11	14
Group 1: poor outcome (injury)		19	24	13	17	9	9	11	10
Number of components	Predictive	1	N/A	1	1	1	1	1	1
	Orthogonal to X	1		0	1	5	1	2	1
Model statistics	R^2X	0.222		0.130	0.216	0.543	0.216	0.361	0.205
	R^2Y	0.887		0.585	0.753	0.998	0.755	0.924	0.828
	Q^2	-0.114		0.154	-0.200	0.439	-0.231	-0.356	-0.077
	$R^2Y - Q^2$	1.001		0.431	0.953	0.559	0.986	1.280	0.905
CV-ANOVA	P VALUE	1.000		0.204	1.000	0.590	1.000	1.000	1.000

B

OPLS-DA		Respiratory		Cardiovascular		Haematological		Central Nervous System	
Sample set: time point (n=sample number)		Time point 0 (n=22)	Time point 1 (n=24)	Time point 0 (n=22)	Time point 1 (n=24)	Time point 0 (n=22)	Time point 1 (n=24)	Time point 0 (n=22)	Time point 1 (n=24)
SOFA = 0		3	0	9	7	13	15	11	14
SOFA = 1		4	5	1	0	3	5	0	0
SOFA = 2		6	10	0	0	3	2	3	1
SOFA = 3		8	8	6	3	2	1	2	2
SOFA = 4		1	1	6	14	1	1	6	7
Number of components	Predictive	1	1	1	1	1	1	1	1
	Orthogonal to X	0	0	0	0	1	0	1	0
Model statistics	R^2X	0.190	0.130	0.219	0.077	0.188	0.081	0.173	0.147
	R^2Y	0.157	0.200	0.241	0.361	0.309	0.208	0.150	0.198
	Q^2	-0.004	-0.170	0.040	-0.157	0.000	-0.041	-0.106	-0.027
	$R^2Y - Q^2$	0.161	0.370	0.201	0.518	0.309	0.249	0.256	0.225
CV-ANOVA	P VALUE	1.000	1.000	0.741	1.000	1.000	1.000	1.000	1.000

3.4.5 Multivariate statistical analyses of ^{1}H NMR spectra of unfiltered validation cohort urine - Hydroxyethyl starch classes

The PCA and O-PLS-DA performed on ^{1}H NMR spectra of unfiltered ICU validation cohort urine failed to demonstrate any separation according to renal dysfunction, liver dysfunction or 28-day survival. The PCA scores plot of the model built using ^{1}H NMR spectral data from all the samples did however, reveal evidence of separation based on the receipt of the hydroxyethyl starch (HES) containing fluid Volulyte, as shown in Figure 3.18. Investigation of this class separation was prompted by the evidence from the raw ^{1}H NMR spectral data of the urine suggesting resonances of Volulyte (parent drug) were responsible for significant differences between the spectra as a whole, as discussed earlier (see Section 3.4.2). In the ^{1}H NMR spectra of the urine from the validation cohort, resonances identified as belonging to the hydroxyethyl starch Volulyte (using a combination of the drug standard and the STOCSY method) included broad signals at δ^1H 5.69, δ^1H 5.55 and δ^1H 5.42; a multiplet at δ^1H 3.78 and a singlet at δ^1H 1.92 (see Section 3.4.3.1.2 and Figures 3.12 and 3.13).

An O-PLS-DA method was applied to build a model using the NMR spectral data from all the samples as the X matrix and HES dichotomised classes based on the receipt of HES, as the dummy Y matrix. The model was based on the unit variance scaled data using one PLS component and one orthogonal component. The scores and the loadings plots are demonstrated in Figure 3.19. The separation of the

samples according to the starch classes demonstrated by this O-PLS-DA model was clearer than the PCA of this data set. The signals with the highest correlation coefficients ($r \geq 0.6$) on the S-line plot of the loadings (Figure 3.19C), and thus, greatest contribution to the separation of the two starch classes by this model were predominantly resonances of Volulyte.

This led to the hypothesis that Volulyte was acting as a confounding factor in the first part of the validation component of this project, i.e. the lack of separation according to the clinical classes of interest was due to important metabolites in the region affected by the starch.

This hypothesis was tested by repeating the multivariate statistical analyses on 1-D ^{1}H NMR analyses of urine from the validation cohort following the removal of the hydroxyethyl starch using a method of filtration (as described in Appendix I).

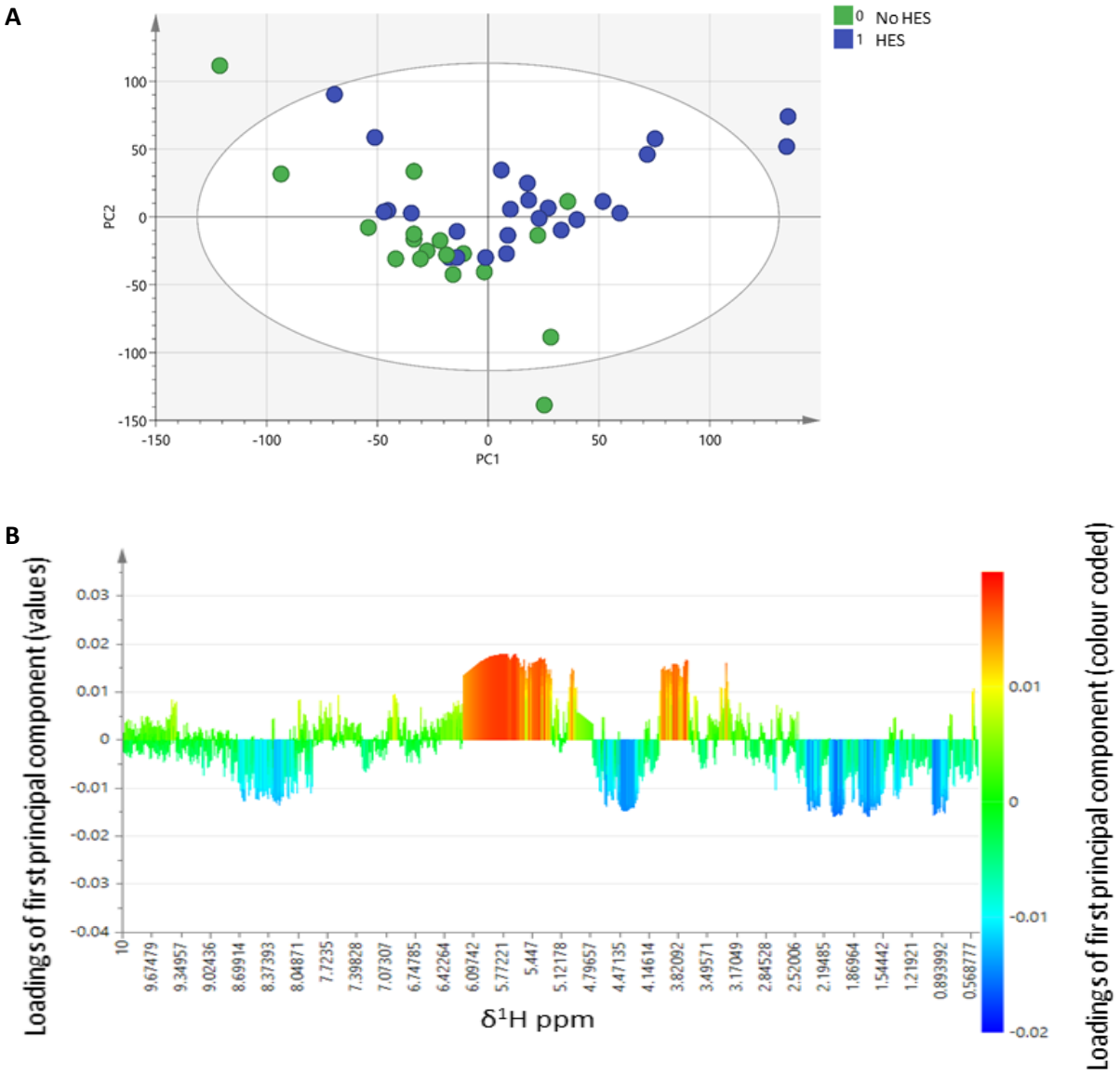


Figure 3.18 Scores (A) and loadings (B) plots of a PCA based on ^{1}H NMR spectral data of unfiltered urine from the validation cohort with samples colour coded according to receipt (1) and non-receipt (0) of the hydroxyethyl starch Volulyte. A. PCA scores plot illustrating evidence of separation of the samples based on the receipt of the hydroxyethyl starch. B. PCA Loading Column plot of the first PC demonstrating the contribution of the urinary metabolite signals detected by ^{1}H NMR responsible for the partial separation of the samples based on the receipt of the hydroxyethyl starch by the first PC. This illustrates metabolite signals with the highest positive loadings of the first PC (associated with receipt of HES) between δ^{1}H 6.21-5.53; δ^{1}H 5.49-5.30; δ^{1}H 5.01–4.99; δ^{1}H 4.01-3.71 and δ^{1}H 3.29-3.28ppm. KEY: Colour scale of the loadings ranges from the highest positive and negative loadings in red and blue, respectively. KEY: HES: hydroxyethyl starch.

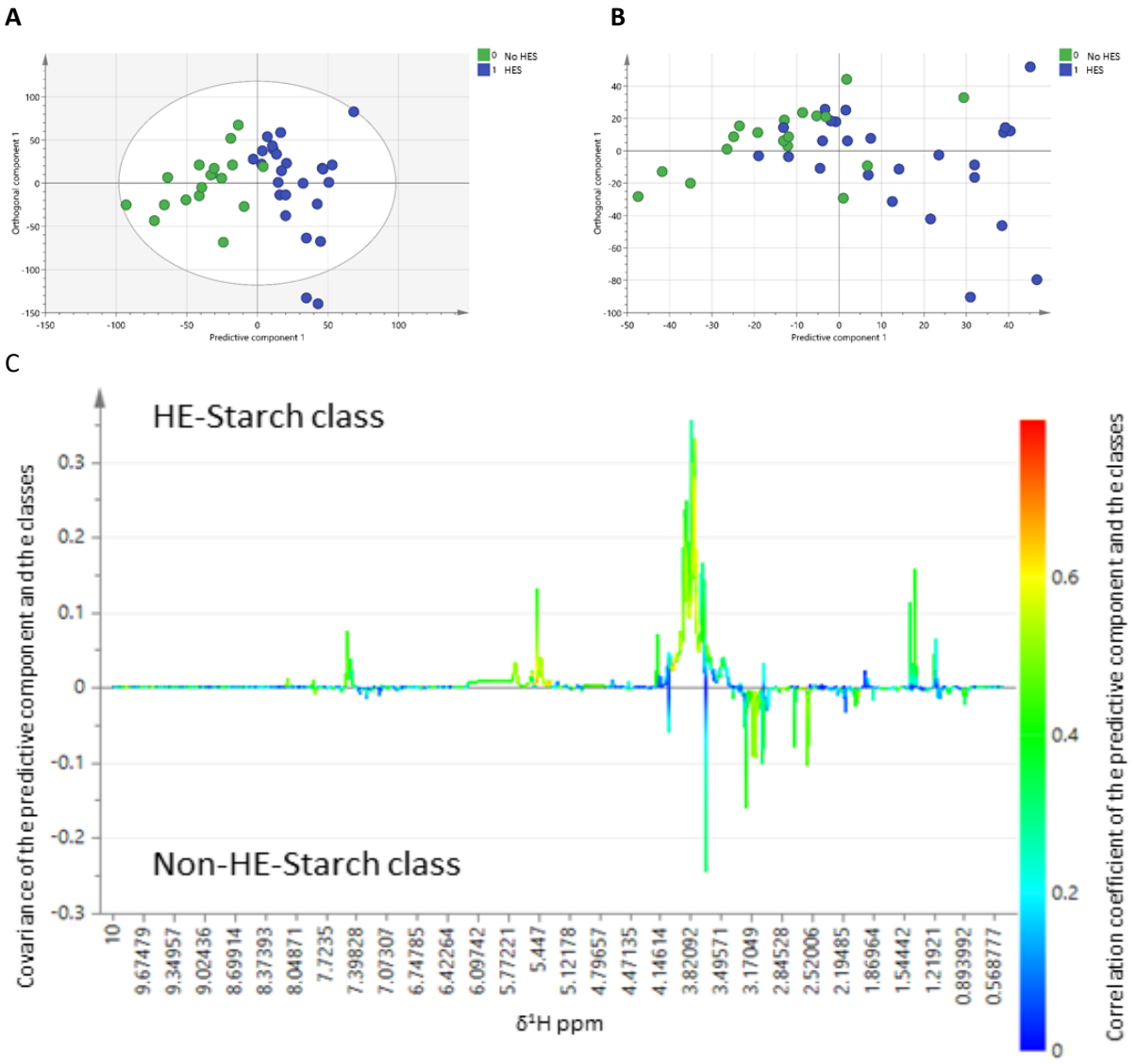


Figure 3.19 O-PLS-DA scores (A) and cross-validated scores (B) plots derived from ^{1}H NMR spectral data of unfiltered urine samples from the validation cohort illustrating separation of samples according to the non-receipt (0) and receipt (1) of the hydroxyethyl starch based fluid Volulyte (R^2X=0.237, R^2Y =0.695; Q^2Y=0.354). The cross-validated scores plot illustrates the significance of the observed group separation measured using a method of CV-ANOVA (p=0.002). The corresponding O-PLS-DA loadings plot (C) illustrating the covariance and correlation coefficients of the metabolite signals of the predictive component of the model responsible for the separation of the two hydroxyethyl starch groups. KEY: CV-ANOVA: cross-validated analysis of variance, HES: hydroxyethyl starch.

3.4.6 ^{1}H NMR spectroscopy of filtered urine from critically ill patients

A composite of two ^{1}H NMR spectra of urine from a patient who was given the hydroxyethyl starch (HES) based resuscitation fluid Volulyte is shown in Figure 3.20. Both spectral arrays are from NMR analyses of aliquots of urine taken from the same sample but processed differently: one was filtered to remove the HES present in the Volulyte administered to the patient (as detailed in Appendix I Section 1.5.4) and the other was processed unfiltered. This comparison is used to illustrate the broad signals of HES at δ^{1}H 5.69 (δ^{1}H 5.72-5.59), δ^{1}H 5.55 (δ^{1}H 5.60-5.50) and δ^{1}H 5.42 (δ^{1}H 5.46-5.36), a multiplet at δ^{1}H 3.78 (δ^{1}H 4.09-3.43); a singlet at δ^{1}H 1.92; and the greater resolution of the non-HES signals present in these regions following the removal of the starch. The region most affected by the starch was δ^{1}H 4.1-3.4, as highlighted in Figure 3.20C, where a distinctive multiplet of Volulyte is situated at δ^{1}H 3.78 (4.09-3.43). The removal of the starch resulted in an improvement in the resolution of the signals in this region, and thus, aided the identification of the signals in the region that were previously overlapping with the signals of the starch. This region was later shown to be a commonplace for signals of drug metabolites such as mannitol as shown in the ^{1}H NMR spectra of urine from recipient of mannitol but not Volulyte shown in Figure 3.5 (identified using the ^{1}H NMR spectra of the drug standard of mannitol and a method of STOCSY). Multiple comparisons of the ^{1}H NMR spectra analyses of the unfiltered and filtered urine from same samples were made. These analyses demonstrated no significant loss of other metabolites, (i.e. those not associated with the starch) as a consequence of the filtration process, (See Figures 3.20 and 3.21 for examples).

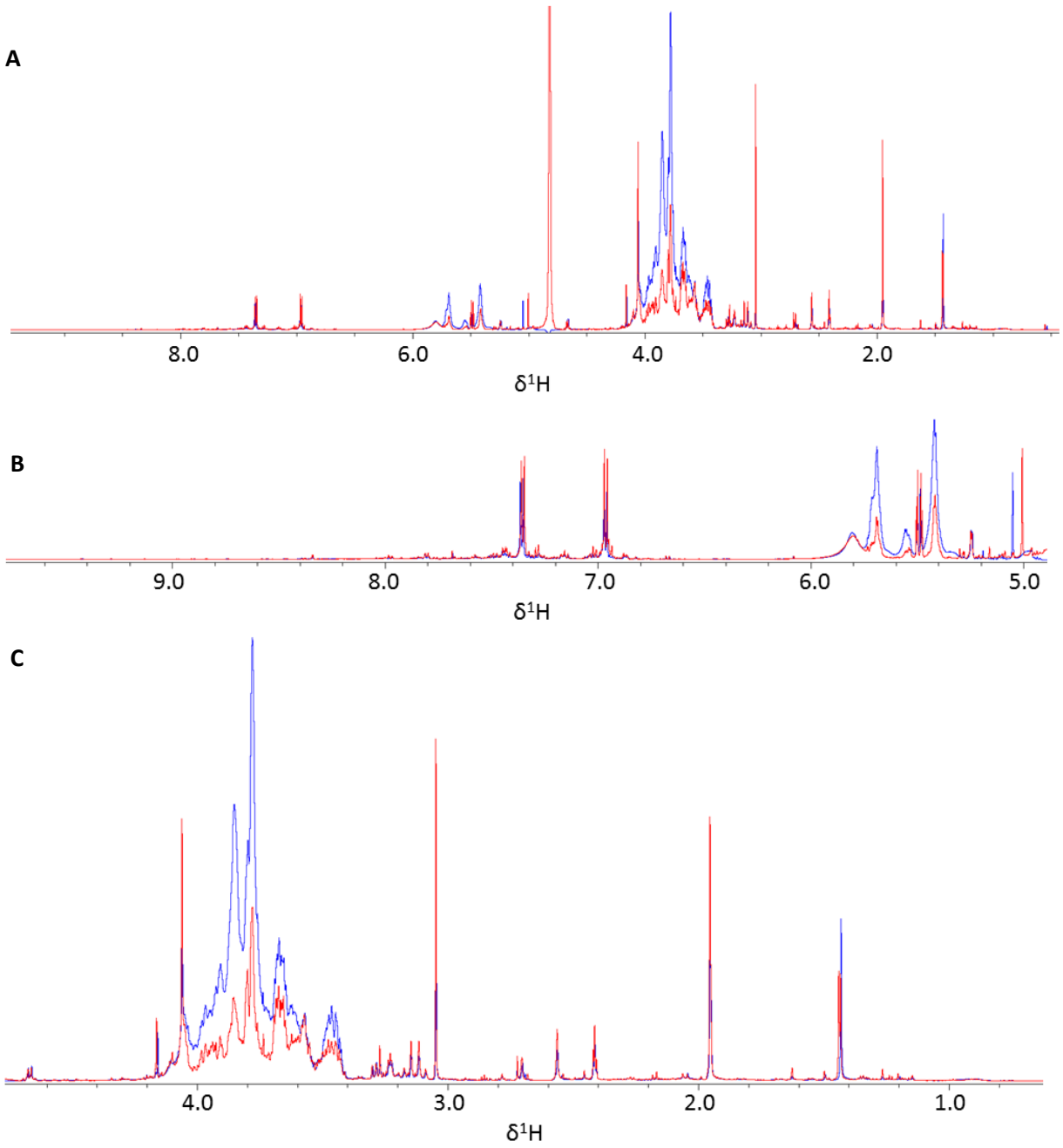


Figure 3.20 A composite of two 600MHz 1D ^{1}H NMR spectra of urine aliquots taken at the same time point from an individual from the validation cohort given hydroxyethyl starch, one unfiltered (blue) and one filtered (red), prior to NMR analysis. Regions δ^{1}H 9.7-0.5, 9.7-4.8 and 4.6-0.8 ppm of the ^{1}H NMR spectra are shown in Figures (A), (B) and (C), respectively. An illustration of broad signals of HES at δ^{1}H 5.69 (δ^{1}H 5.72-5.59), δ^{1}H 5.55 δ^{1}H (5.60-5.50) and δ^{1}H 5.42 (δ^{1}H 5.46-5.36), a multiplet at δ^{1}H 3.78 (4.09-3.43); a singlet at δ^{1}H 1.92 (acetate); and the greater resolution of the non-HES signals present in the same region following the removal of the starch *via* filtration.

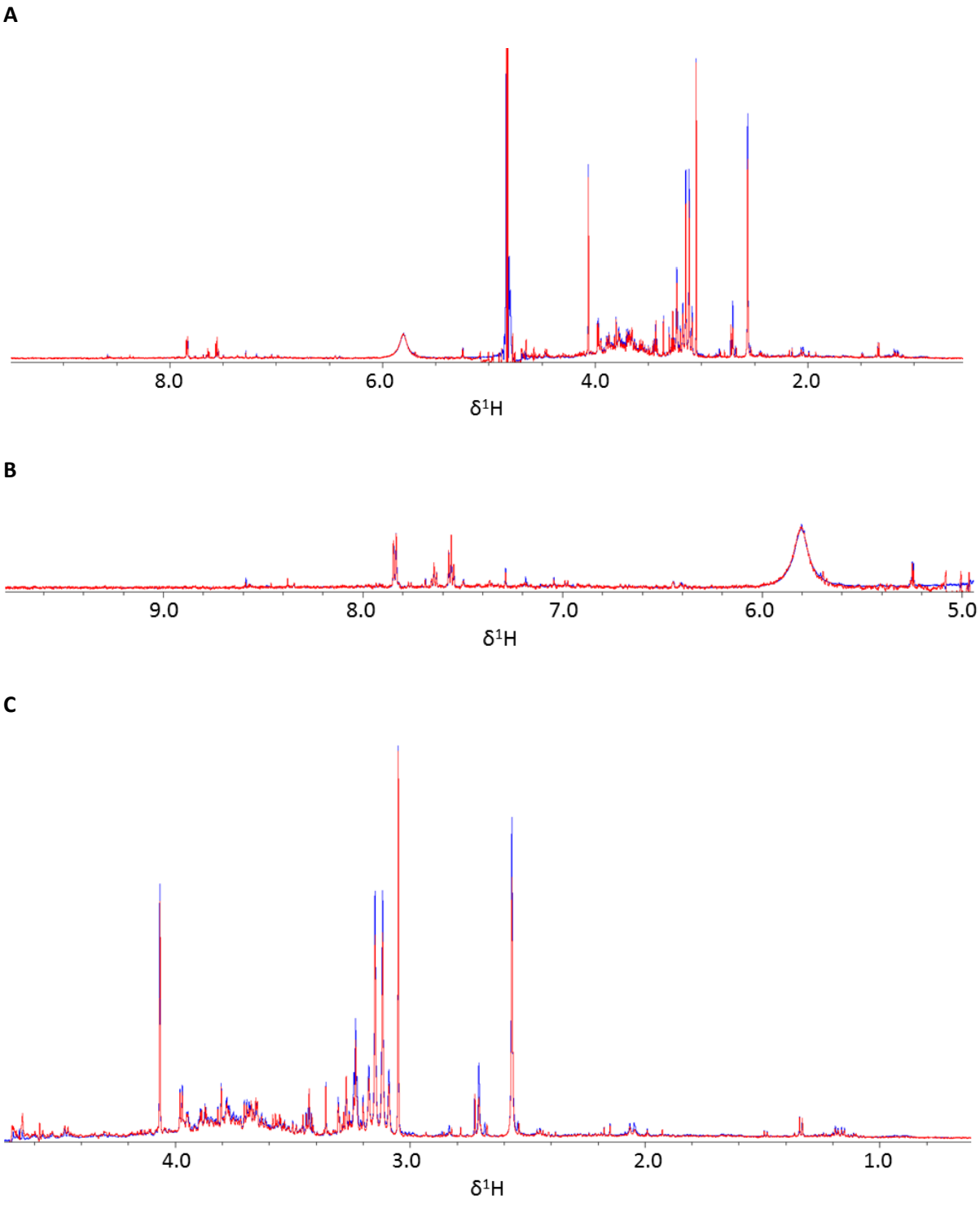


Figure 3.21. A composite of two 600MHz 1D ^{1}H NMR spectra of urine aliquots taken at the same time point from an individual from the validation cohort not given hydroxyethyl starch, one unfiltered (blue) and one filtered (red), prior to NMR analysis illustrating of no apparent loss of metabolites associated with use of filtration. Regions δ^{1}H 9.7-0.5, 9.7-4.8 and 4.6-0.8 ppm of the ^{1}H NMR spectra are shown in Figures (A), (B) and (C), respectively.

3.4.7 Multivariate statistical analyses of ^{1}H NMR spectra of filtered validation cohort urine – organ dysfunction and ICU survival

The same PCA and O-PLS-DA methods performed on the probabilistic quotient normalised 1-D ^{1}H NMR spectral data of the unfiltered urine from the validation cohort were applied to normalised 1-D ^{1}H NMR spectral data of the filtered urine from the same patients, using SIMCA software. (NB at the time of the performance of the NMR analyses of the filtered urine, the validation cohort sample set consisted of a complete set of samples from the both time points from 30 patients; as opposed to the incomplete set of 47 samples from 27 patients used in the NMR analyses of unfiltered urine (See Section 3.3.4). All of these models were performed using unit variance scaling and started with a PCA model based on the 1-D ^{1}H NMR spectral data from all the 60 filtered urine samples. This led to the identification of three extreme outliers (Figure 3.22). Examination of the raw spectral data revealed these to be scores outliers with two of the outliers having relatively (extremely) low values of the majority of the metabolites and one of the outliers to have relatively high values of many of the metabolites particularly in the region of 4.1-3.4 ppm (see Appendix III Figures 3 to 5). A PCA model of the 1-D ^{1}H NMR spectral data from the remaining 57 filtered urine samples was then performed, to obtain an overview of the dataset following the exclusion of the extreme outliers. This was constructed using the first two principal components and these components explained 24.37% of the total variance (Figure 3.23). Following this, a set of PCA models of spectral data from each of the two time points was constructed. This consisted of separate models assessing separation of the samples according to the same three classes applied to the unfiltered urine: renal and liver dysfunction and ICU survival. The percentages of the variation, explained (R^2X) and predicted (Q^2) by the PCA models from each time point are shown in Table 3.9. No evidence of separation, between the samples according to any of the seven clinical classes was demonstrated by any of the PCA scores plots from either of the time points. Examples of PCA scores plots from each of the time points are demonstrated in Figures 3.24 and 3.25, with samples labelled according to their renal classes.

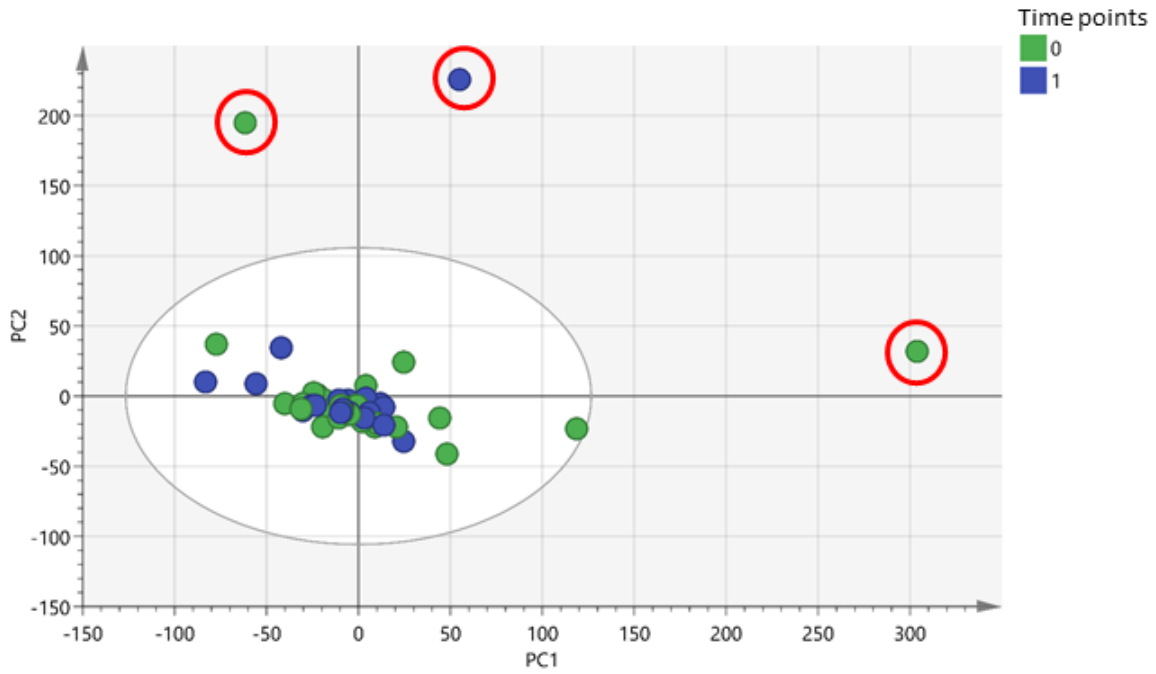


Figure 3.22 A PCA scores plot based on 1-D ^{1}H NMR spectral data of all the filtered urine samples from the validation cohort illustrating the metabolic variation of the data set as a whole (60 samples) and three extreme outliers (circled in red).

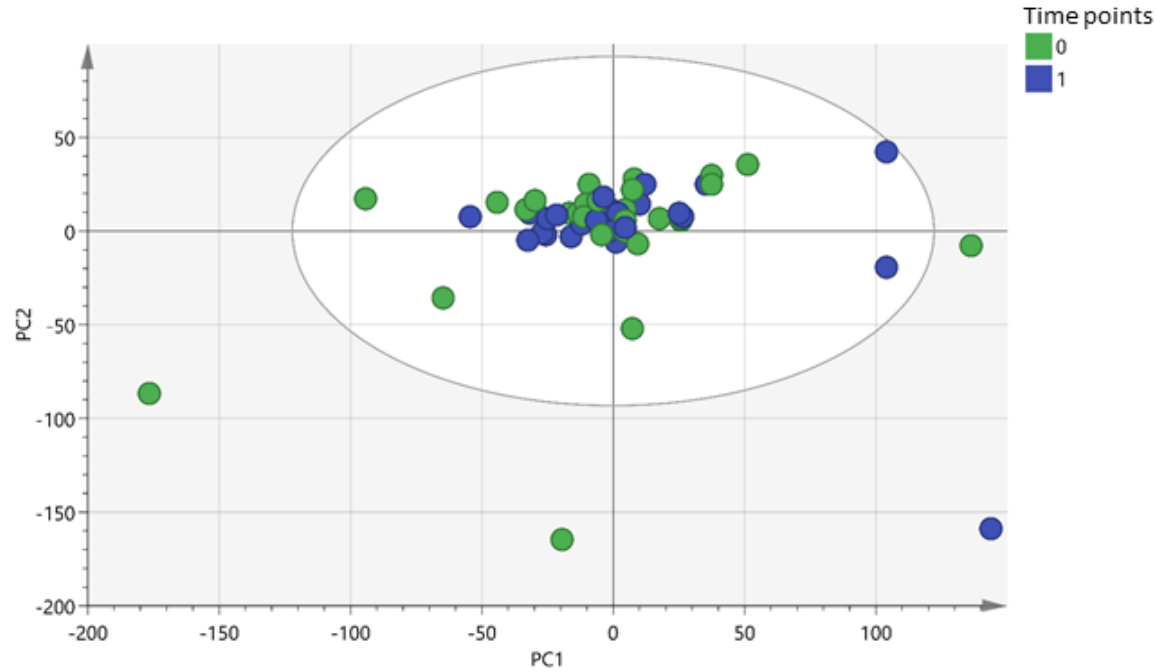


Figure 3.23 A PCA scores plot derived from 1D ^{1}H NMR spectral data of all the filtered urine samples from the validation cohort, following the exclusion of the three extreme outliers, illustrating the metabolic variation of the remaining 57 samples.

Table 3.9 Results of the evaluation parameters of PCAs of 1-D ^{1}H NMR spectra of filtered urine from the validation cohort taken at time points one and two: the percentage of the variation explained (R^2X) and predicted (Q^2X) by the model. KEY: PC: principal component.

Principal Component Analyses				
Sample set:time point (n=sample number)	All samples (n=60)	All samples minus 3 outliers (n=57)	Time point 0 (n=28)	Time point 1 (n=29)
Number of PCs	2	2	1	2
R^2X	0.282	0.244	0.182	0.337
Q^2	-0.0423	0.035	0.038	0.022

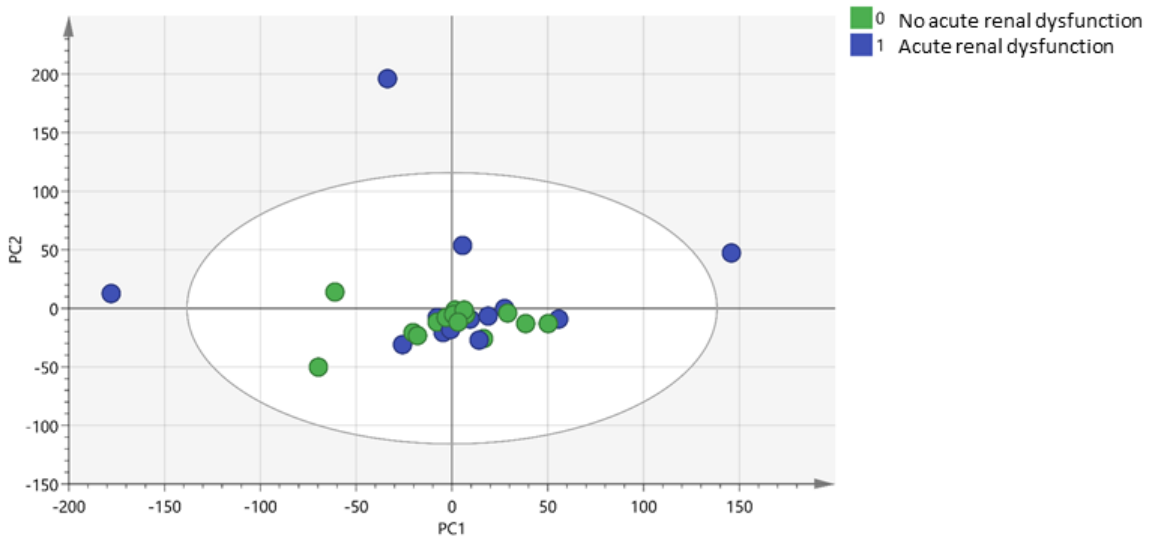


Figure 3.24 A PCA scores plot based on 1-D ^{1}H NMR spectra of filtered urine from the validation cohort taken at time point zero (28 samples) illustrating a lack of separation of samples according to presence (1) or absence (0) of renal dysfunction.

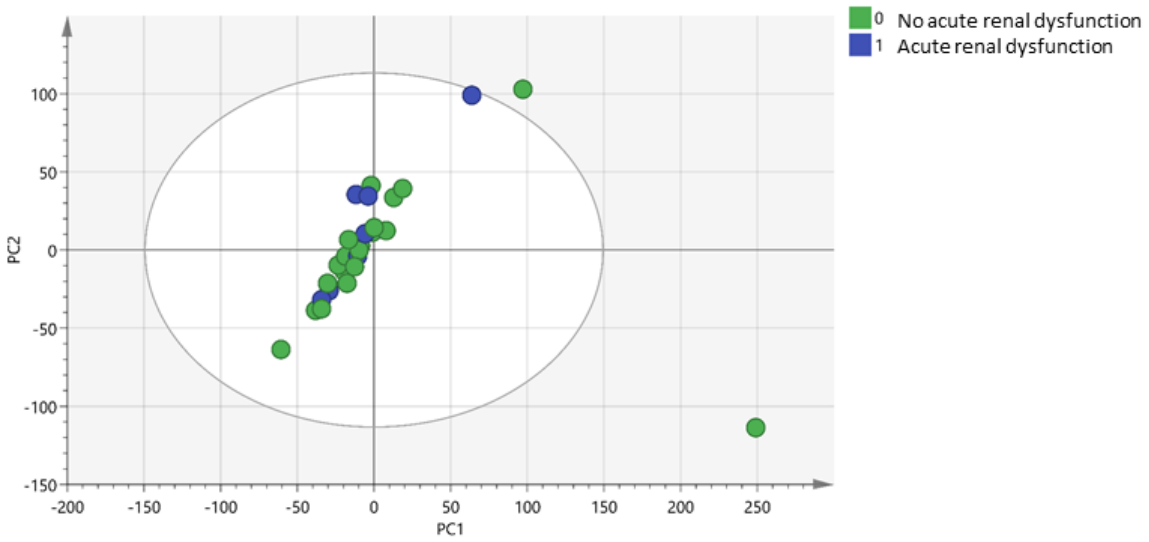


Figure 3.25 A PCA scores plot of 1-D ^{1}H NMR spectra of filtered urine from the validation cohort taken at time point one (29 samples) illustrating no clear separation of samples according to presence (1) or absence (0) of renal dysfunction.

Orthogonal-PLS-DA models were built using the 1-D ^{1}H NMR spectral data from individual time points as the X matrix and the dichotomised class information as the Y matrix were created for each of the seven clinical classes. Each model was based on one predictive PLS component, using the unit variance scaled data from one of the time points. Models constructed using one PLS component and one orthogonal component if there was significant improvement in terms of predictability compared with comparative models involving just the one PLS component (as described in Section 3.4.5). The main parameters used to evaluate these supervised models were the R^2X and the cumulative Q^2Y values. The results of all the evaluation parameters of these models are shown in Tables 3.10 and 3.11A. The percentage of the variation explained by the model (R^2X) ranged from 0.173 to 0.095 for models based on AKI, acute liver injury and ICU survival (Table 3.10); and 0.280 to 0.073 (Table 3.11A) and 0.235 to 0.130 (Table 3.11B), for the models based on the other four classes with the samples divided into two and five groups, respectively. The predictability of all the models were low. This was demonstrated by Q^2Y values that ranged from 0.150 to -0.324 for the models of AKI, acute liver injury and ICU survival, and 0.144 to -0.241 and 0.026 to -0.142 for the dichotomised models of the other four classes and the

models with five groups based on these four classes, respectively. The models of kidney function were shown to have the lowest predictability, with Q^2Y values of -0.118 and -0.324, for the models of time points zero and one, respectively.

Table 3.10 Results of the evaluation parameters of O-PLS-DA models based on 1-D ^{1}H NMR spectra of filtered urine from the validation cohort taken at TP0 and TP1. Illustration of the percentage of the variation explained by the X (R^2X) and Y matrices (R^2Y) and predicted by the Y matrix* (Q^2Y) of the models evaluating samples based on their renal, liver and ICU survival classes. Key: CV-ANOVA: cross-validated analysis of variance, *: Y matrix contains the class information.

OPLS-DA		Acute Kidney injury		Acute Liver injury		Intensive Care Unit survival	
Sample set: time point (n=sample number)		Time point 0 (n=28)	Time point 1 (n=29)	Time point 0 (n=28)	Time point 1 (n=29)	Time point 0 (n=28)	Time point 1 (n=29)
Group 0: good outcome (no injury/survival)		15	22	16	22	21	21
Group 1: poor outcome (injury/non-survival)		13	7	12	7	7	8
Number of components	Predictive	1	1	1	1	1	1
	Orthogonal to X	0	0	0	0	0	0
Model statistics	R^2X	0.099	0.095	0.138	0.104	0.141	0.173
	R^2Y	0.526	0.462	0.488	0.556	0.423	0.396
	Q^2	-0.118	-0.324	0.127	0.150	-0.204	0.059
	$R^2Y - Q^2$	0.644	0.786	0.361	0.406	0.627	0.337
CV-ANOVA	P VALUE	1.000	1.000	0.182	0.120	1.000	0.455

Table 3.11 Results of the evaluation parameters of O-PLS-DA models based on 1-D ^{1}H NMR spectra of filtered urine from the validation cohort taken at TP0 and TP.1 Illustration of the percentage of the variation explained by the X (R^2X) and Y matrices (R^2Y) and predicted by the Y matrix* (Q^2Y) of the models evaluating samples based on their respiratory, cardiovascular, haematological, and central nervous system classes with the samples divided into two (A) and five groups (B). Key: CV-ANOVA: cross-validated analysis of variance, SOFA: Sequential Organ Failure Assessment, *: Y matrix contains the class information.

A

OPLS-DA		Respiratory		Cardiovascular		Haematological		Central Nervous System	
Sample set: time point (n=sample number)		Time point 0 (n=28)	Time point 1 (n=29)	Time point 0 (n=28)	Time point 1 (n=29)	Time point 0 (n=28)	Time point 1 (n=29)	Time point 0 (n=28)	Time point 1 (n=29)
Group 0: good outcome (no injury)		3	0	11	7	14	15	13	16
Group 1: poor outcome (injury)		25	29	17	22	14	14	15	13
Number of components	Predictive	1	N/A	1	1	1	1	1	1
	Orthogonal to X	0		0	1	0	1	0	0
Model statistics	R^2X	0.073		0.160	0.280	0.108	0.231	0.074	0.129
	R^2Y	0.659		0.467	0.638	0.462	0.745	0.657	0.429
	Q^2	-0.078		0.144	-0.006	-0.124	0.095	-0.241	-0.077
	$R^2Y - Q^2$	0.737		0.323	0.644	0.586	0.650	0.898	0.506
CV-ANOVA	P VALUE	1.000		0.144	1.000	1.000	1.000	1.000	1.000

B

OPLS-DA		Respiratory		Cardiovascular		Haematological		Central Nervous System	
Sample set: time point (n=sample number)		Time point 0 (n=28)	Time point 1 (n=29)	Time point 0 (n=28)	Time point 1 (n=29)	Time point 0 (n=28)	Time point 1 (n=29)	Time point 0 (n=28)	Time point 1 (n=29)
SOFA = 0		3	0	11	7	14	15	13	16
SOFA = 1		5	6	1	0	3	5	0	0
SOFA = 2		9	9	0	0	5	3	3	1
SOFA = 3		9	11	6	5	5	5	2	2
SOFA = 4		2	2	10	16	1	1	10	9
Number of components	Predictive	1	1	1	1	1	1	1	1
	Orthogonal to X	0	0	1	0	0	0	0	0
Model statistics	R^2X	0.138	0.200	0.235	0.161	0.169	0.162	0.130	0.130
	R^2Y	0.141	0.150	0.318	0.202	0.104	0.129	0.174	0.178
	Q^2	0.026	0.003	0.047	-0.142	-0.049	-0.023	-0.092	-0.097
	$R^2Y - Q^2$	0.115	0.147	0.271	0.344	0.153	0.152	0.266	0.275
CV-ANOVA	P VALUE	0.902	0.992	0.961	1.000	1.000	1.000	1.000	1.000

3.5 Discussion

The first part of this study demonstrated the application of ^{1}H NMR spectroscopy as a feasible method of global metabolic profiling of urine from critically ill patients and that the development of a drug standard database was integral to this demonstration. However, the second part of this study failed to demonstrate the ability of a ^{1}H NMR spectroscopy-based method of metabolic profiling of urine to separate this cohort of critical ill patients into dichotomous or sub- groups of acute kidney, liver, respiratory, cardiovascular, or haematological dysfunction, or ICU survival. These two parts of this chapter's results will be discussed in turn.

3.5.1 ^{1}H NMR spectroscopy as a feasible method of global metabolic profiling of urine from critically ill patients

Demonstration of many of the common urinary metabolites in the ^{1}H NMR spectra of urine from the validation cohort was a fundamental component of the evidence supporting the feasibility of ^{1}H NMR spectroscopy as a (global) method of metabolic profiling of urine from critically ill patients. The metabolic differences demonstrated by the spectra from this cohort and one from a healthy control, also supported the validity of this method of metabolic profiling. These differences included fewer common urinary metabolites, signals identified as drug and drug metabolites; and the addition of a greater number of broad signals, in the spectra from the validation cohort. In the case of the latter, the additional broad signals demonstrated by the urinary spectra from the validation cohort but not the urinary spectra from the health control were only demonstrated by the spectra of the unfiltered urine. No other differences between the ^{1}H NMR spectra of the filtered and unfiltered urine from the validation cohort were detected; i.e. these broad signals including the intended targets, the HES signals, appeared to be the only metabolites removed by the filtration process. This is consistent with these broad signals belonging to lipids and other large macromolecules with a molecular weight of greater than 3kDa the molecular weight threshold of the filters used in the filtration process; (see Appendix I Section 1.5.4). The variability of the metabolites demonstrated across the ^{1}H NMR spectra

of urine from the validation cohort was considerable. Drug and drug metabolites were responsible for a significant amount of this variation.

The number of non-drug metabolites identified in ^{1}H NMR spectra of urine from the cohort was less than in previous studies that have described up to 70 metabolites being identified in human urine, utilising similar 1D ^{1}H NMR spectroscopy techniques (Yang, Wang, Zhou, *et al.*, 2008). The average number of resolved peaks in this study also appears to be lower than in the majority of these other studies. This includes a recent study of the human urine metabolome, in which an average of 167+/-19 compounds were identified per sample, and a total of 209 unique compounds were demonstrated in the samples as a whole (Bouatra, Aziat, Mandal, *et al.*, 2013). There are many possible explanations for the difference in the number of compounds identified by this and previous studies. The most likely cause is the greater number drugs metabolites, identified in the urine in this study. Many of the drugs, particularly the antibiotics used to treat patients in this cohort, have complex structures (Brunton, Parker, Blumenthal, *et al.*, 2008), resulting in large numbers of resonances including broad multiplets spanning spectral regions of up to 0.5ppm. The ^{1}H NMR spectra from this cohort also demonstrated the addition of several broad signals, not commonly found in human urine (Bouatra, Aziat, Mandal, *et al.*, 2013), most notably between δ^{1}H 2.8-0.8ppm. Lipids were responsible for some of these signals (Bouatra, Aziat, Manda*l, et al.*, 2013; Psychogios, Hau, Peng, *et al.*, 2011b); the others remain unidentified but could be due to proteins as a consequence of proteinuria secondary to acute renal dysfunction. Large molecules such as proteins can misalign the baseline of 1D ^{1}H NMR spectra (Beckonert, Keun, Ebbels, *et al.*, 2007). They can also overlap with other resonances in the spectra. All of these problems could have contributed to the inability of the NMR spectra to demonstrate all the non-drug metabolites present in urine from this cohort. The human microbiota, especially the gut microbiota plays an essential role in many metabolic processes. (Ursell, Metcalf, Parfrey, *et al.*, 2012). Modulations of the human microbiota by antibiotics can therefore have a profound effect on this role and result in changes in metabolites involved (Vernocchi, Del Chierico & Putignani, 2016). The

antibiotics administered to the validation cohort could therefore also be responsible for some of the metabolic differences between the urine from validation cohort and the healthy control

An important consideration is whether the presence of such a large number of drug related signals inhibits the usefulness or feasibility of this method of metabolic profiling; either by the need to identify all drug-related signals or by obscuring the metabolic changes of interest. One of the goals of metabolic profiling is to gain an understanding of the metabolic changes associated with different physiological conditions. NMR based profiling techniques are usually combined with multivariate statistical analyses to extract the metabolic features (signatures) associated with the physiological conditions being compared. The identification of all of the metabolites present on NMR spectra is therefore not essential to achieve this goal (Beckonert, Keun, Ebbels, *et al.*, 2007). It is however, important to be able to identify the metabolites that differ between the conditions of interest. The identification of all the signals of the parent drug and metabolites of all the drugs administered to this cohort was therefore not the aim of this study. It was however, important to demonstrate that it was possible to identify and thus differentiate, signals from drugs and drug metabolites signals from signals of non-drug metabolites, despite possible variations in the metabolism of the same drug and the interdependence of the metabolism of some drugs (Brunton, Parker, Blumenthal, *et al.*, 2008). In this study, the ^{1}H NMR drug standard database was used to determine the NMR signals of parent drugs and this information was used to select appropriate driver peaks for STOCSY analyses of the urinary spectra to identify and differentiate drug related signals from signals from non-drug metabolites. This method of identifying drug related signals also provided valuable information on the regions of NMR most affected by the drugs most commonly administered to this cohort: resuscitation fluids and antibiotics. This led to the detailed analysis of the NMR spectra of the antibiotics, Tazocin and Co-amoxiclav that demonstrated both antibiotics have signals located in the aromatic region, and the parent drug of the hydroxyethyl starch based fluid Volulyte, has several distinctive signals between δ^{1}H 5.72 and 5.36; and δ^{1}H 4.09 and 3.43. In this study, the initial identification of signals that

appeared characteristic of a single drug, such as Tazocin, involved a process of manual inspection of the drug standards database as a whole. This was efficiently aided by the knowledge of all the drugs administered to each patient before the two sampling time points.

One could argue, to be a valid method of metabolic profiling of urine in cohorts administered large numbers of drugs, the interpretation of apparent discriminatory metabolites will always require a standards database of all the drugs. In other words, although the identification of all drug related signals may not be necessary, without a drug standards database, the interpretation of discriminatory metabolites may not be possible. The development of a comprehensive drug standards database (that could be continuously updated with new drugs), i.e. the development of the equivalent of the widely available metabolites databases, could help resolve this problem. This is an ambitious but achievable aim.

One of the advantages of ^{1}H NMR spectroscopy is its reproducibility (Beckonert, Keun, Ebbels, *et al.*, 2007). Spectral data acquired on different spectroscopes of a similar configuration are usually comparable (Beckonert, Keun, Ebbels, *et al.*, 2007). One of the future directions of this project is the development of an automated system incorporating both the drug standards database and STOCSY to enable the rapid identification of drug metabolites. This information could then be used to provide the option of excluding resonances of drug metabolites from the multivariate statistical analyses of the spectral data. Two-dimensional ^{1}H NMR spectroscopy could also aid the identification of metabolites with overlapping resonances on 1-D ^{1}H NMR spectra and provide information about the structures of complex compounds by instigating the transfer of energy between nuclei connected by certain types of bonds (as described in Section 1.4.1)

Drug-related signals were responsible for a large part of the variation across the urinary spectra from the validation cohort. However, metabolites such as 1-methylnicotinamide and trigonelline, which

are usually demonstrated in human urine and some of unidentified broad signals also contributed to this variation with demonstrations of these metabolites in less than half of the unfiltered urinary spectra. Broad signals identified as lipids at δ^1H 2.73 and δ^1H 2.01, also contributed to the intra-cohort variability, although to a lesser extent, with both lipid signals being identified in many of the unfiltered urinary spectra.

3.5.2 The clinical utility of metabolic profiling based on ^{1}H NMR spectroscopy of urine in predicting outcomes of critically ill patients

At the start of this project, to the best of my knowledge, this was the first study of metabolic profiling of urine from critically ill patients based on^{1}H NMR spectroscopy. In this study, models based on a ^{1}H NMR spectroscopy-based method of metabolic profiling of urine, could not discriminate between patients based on dichotomised groups of their kidney dysfunction, liver dysfunction or ICU survival. This could be explained by the absence of differentiating metabolic signatures of these clinical conditions or a failure to detect them. The heterogeneity and size of this cohort of patients are the most likely explanations if the latter hypothesis is true. Factors affecting the outcome of patients with critical illness can be divided into three categories: their predisposition to an adverse outcome, the aetiology (and severity) of the insult itself and the response of the host to the insult. Predisposing factors includes innate factors such as genetics and demographics, and acquired factors such as comorbidities and social factors such as smoking and alcohol consumption; all of which affect the patient's physiological reserve to overcome such insults. Importantly, in the context of this study, all of these factors contribute to the variation of the metabolic profiles of this cohort. Although this cohort was united by the term critically ill, the causes of their critical illnesses were very varied, both in terms of the organ involved in the initial insult and mechanisms of the disease processes or pathogeneses involved, e.g. post-emergency bowel surgery for perforation versus decompensated valvular heart failure. Factors from both categories also affect the response, which can involve many different pathways or cascades of responses both at the site of the insult and within the circulation

and other organs. The extent of the impact each of these three factors have on individual outcomes also varies.

In critical illness, both organ dysfunction (Singer, De Santis, Vitale, *et al.*, 2004) and mortality are often divided into early and late; this division is often used to emphasise differences between the pathogenesis and other factors that are important determinants of these outcomes. Early acute kidney injury is usually used to describe AKI within 24-48 hours of admission (Bagshaw, George & Bellomo, 2008) i.e. the time period captured by this study (although there are no consensus definitions). Patients in this cohort were recruited at the onset of their critical illness. All the samples were taken within 48 hours of admission to the ICU (except for one time point two sample taken at 60 hours). The organ dysfunctions captured by this study would therefore be classed as early. The pathogenesis of early and late episodes are thought to differ, with increasing evidence to suggest that early episodes are related to the aetiology of the underlying illness; whereas the complex multisystem host response implicated in multi-organ dysfunction syndrome is believed to be responsible for AKI occurring during the later period (de Montmollin & Annane, 2011). This suggests that the pathogeneses of the organ dysfunctions examined in this cohort would vary according to the underlying cause of their illness. Such variation in the pathogeneses of the organ dysfunctions of this cohort might explain the absence of a metabolic signature of kidney or liver dysfunction in this cohort.

Much akin to organ dysfunctions occurring late in the course of critical illness, the initial insult is thought to have less impact on late mortality than factors related to the development of secondary organ dysfunction or MODS and the physiological reserve of the individual, such as co-morbidities (Suistomaa, Niskanen, Kari, *et al.*, 2002; Friedrich, Wilson & Chant, 2006; Hough, Caldwell, Cox, *et al.*, 2015). However, ICU or 28-day survival are a summation of both acute and late mortality and therefore very multifactorial. It is therefore, difficult to assess if the heterogeneity of the aetiologies

of the critical illnesses of this cohort was responsible for the inability of this method of metabolic profiling to differentiation between patients based on their ICU survival.

The failure to demonstrate metabolic signatures of ICU survival by the study, could also have been due to use of samples taken too soon after the onset of their critical illnesses. The aim of this part of the study was to demonstrate the use of this method of metabolic profiling to detect early markers of ICU survival. It is however, possible that metabolic signatures of this survival do exist but occur at a later stage. Alternatively, given that likelihood that the acute illness has more influence on the acute mortality of critical illness (Suistomaa, Niskanen, Kari, *et al.*, 2002), perhaps a metabolic signature of this early mortality would be detectable in a cohort with the same acute illness.

The failure to detect metabolic signatures of the clinical outcome measures in this study, may also, and were more likely, to have been due to the small size of the comparison groups. It could be argued, that despite the multiple levels of heterogeneity of the many factors implicated in determining these outcome measures, these outcomes groups were associated with subtle metabolic differences but the small sample sizes led to the study being too under-powered to detect them.

An alternative explanation for the failure to demonstrate metabolic signatures of these clinical conditions in this study is that there are not unique metabolic profiles associated with the specific organ dysfunctions studied. This seems unlikely based on the strong evidence to support such profiles in other acute illnesses (Coen, O'Sullivan, Bubb, *et al.*, 2005; Slupsky, Rankin, Fu, *et al.*, 2009; Rogers, McGeachie, Baron, *et al.*, 2014). However, as the severity of the illness in these patients is so severe it is possible that the "metabolic chaos" caused by the critical illness mean that more subtle differences between different organ dysfunctions are unable to be detected. This is also complicated by the multitude of drugs that are used to treat the patients and that these drug signatures hide other differentiating metabolic profiles.

3.6 Summary

Overall, this study demonstrates the feasibility of metabolic profiling of urine from critically ill patients based on ^{1}H NMR spectroscopy. Drug metabolites formed an important part of this cohort's metabonome and present a potential obstacle to the identification of metabolites, but this can be overcome with the combined use of a drug standards database and methods of STOCSY. Models based on this ^{1}H NMR spectroscopy method of metabolic profiling, however, failed to discriminate between patients based on dichotomised groups of their kidney dysfunction, liver dysfunction or 28-day survival. The relatively small numbers and the heterogeneity of their clinical characteristics, particularly the heterogeneity of the underlying cause of their critical illness are the most likely cause for these results. Therefore, larger numbers of more homogeneous patients are required to provide further evidence to support the use of metabolic profiling of urine in critically ill patients.

Chapter 4: Global metabolic responses in patients with severe sepsis and sepsis-induced organ dysfunction

4.1 Introduction

The feasibility of metabolic profiling of urine from critically ill patients based on ^{1}H NMR spectroscopy was demonstrated in Chapter three. Statistical models based on these ^{1}H NMR spectral data, however, failed to provide metabolite biomarkers that were correlated with kidney, liver, respiratory, cardiovascular, or haematological dysfunction or ICU survival. The small sample size and heterogeneity of the clinical characteristics of the validation cohort, especially the heterogeneity of the cause of their critical illness are likely to be responsible for these results. In the current chapter, a cohort of patients with septic shock who subsequently all received vasopressin was included and their urinary and blood serum samples were analysed using ^{1}H NMR spectroscopy-based metabolic profiling to investigate the global metabolic responses of the patients to severe sepsis. In contrast to the unselected critically ill cohort, the sepsis cohort has a greater sample size, strict eligibility criteria and they were recruited within six hours of admission to a critical care unit. It was hypothesised that these differences would result in greater success in demonstrating the clinical utility of metabolic profiling using ^{1}H NMR spectroscopic analyses of urine in this cohort compared to the unselected critically ill cohort.

4.2 Aim

The primary aim of the study was to characterise the global metabolic responses of patients to severe sepsis and determine metabolic signatures associated with sepsis-related acute renal and liver dysfunctions and 28-day survival. A secondary aim of the study was to determine the metabolic changes associated with the administration of hydrocortisone.

4.3 Materials and methods

4.3.1 Study patients

Fifty adult patients with septic shock were recruited between October 2010 and February 2012 from four London ICUs as part of the randomised controlled clinical trial entitled: Vasopressin and Corticosteroids in Septic Shock (VACS). The eligibility criteria, timing of the sampling and sample size was therefore determined by this trial and a priori sample size calculation was not undertaken for this reason. Sixty-one patients were recruited to the VACS trial but samples appropriate for NMR or LCMS analysis were only collected from fifty of those patients. This was a pilot trial used to test the hypothesis that there is an interaction between vasopressin and corticosteroids in septic shock and to assess the feasibility of using vasopressin as a first line vasopressor in this setting. The inclusion criteria was fulfilment of the 1992 American College of Chest Physicians/Society of Critical Care Medicine Consensus Conference definition of sepsis and hypotension requiring vasopressors (vasoconstrictors to maintain blood pressure) despite adequate fluid resuscitation (Bone, Balk, Cerra, *et al.*, 1992). The latter was defined as at least a one litre of intravenous (IV) fluid in the preceding four hours.

Patients were allocated to one of two treatment arms: vasopressin and hydrocortisone or vasopressin and placebo. The aim was that all patients received a vasopressin infusion as their initial vasopressor. This infusion was started at 0.013U/min and titrated up to a maximum of 0.06U/min to achieve a recommended target mean arterial pressure (MAP) of 65-75mmHg, unless a different target was felt to be clinically indicated. In emergency circumstances, in locations outside the ICU, (e.g. high dependency unit or emergency department) where the vasopressin study drug was not available, the use of conventional vasopressors was permitted as the initial vasopressor. In these circumstances, the patient had to be enrolled to the study within six hours of starting the conventional vasopressor infusion and once the vasopressin was titrated up the initial vasopressor was weaned off. Recruitment to the VACS trial was therefore not necessarily at the start of the septic episode but within six hours

of a diagnosis of septic shock. In all patients, if the target MAP was not achieved on the maximum dose of the vasopressin infusion, the patient received hydrocortisone or placebo according to their treatment allocation. The hydrocortisone or placebo was initiated at 50mg *qds* and weaned off with resolution of the septic shock as per the protocol used in the hydrocortisone therapy in septic shock study entitled CORTICUS (Sprung, Annane, Keh, *et al.*, 2008): 5 days at 50mg *qds*, 3 days at 50mg *bd* and then 3 days at once daily. In short, the cohort referred to as the sepsis cohort consisted of 50 adult patients with septic shock who all received vasopressin, in addition to either IV hydrocortisone or a placebo.

The VACS study had received ethical approval from the Oxford Research Ethics Committee and clinical trials authorisation from the Medicines and Healthcare Products Regulatory Agency, (EudraCT Reference: 2009-017636-41).

4.3.2 Sample collection

Urine, serum, and plasma samples were collected at four time points including prior to starting treatment with steroids or placebo and 6-12 hours, 24-36 hours and 7 days post the treatment. Five millilitres of urine were aspirated from the sampling port of the urinary catheter using a needle and syringe, transferred to cryogenic tubes, and centrifuged for 10 minutes at 10, 000 g (relative centrifugal force). Aliquots of 2 ml of the supernatant were transferred into cryogenic tubes: one for use in this study. Each aliquot was labelled with a code incorporating the patient's study number, site of collection, aliquot letter, and time point, and stored at -80°C until analysis. At each time point, 20 ml of blood was collected from an existing cannula, where possible. Approximately 10 ml of the blood was collected into ethylenediaminetetraacetic acid (EDTA) tubes on ice and centrifuged; the plasma was collected into cryogenic tubes and stored at -80°C until UPLC-MS analysis (see chapter five). The remaining 10 ml of the blood was collected into empty (plain) vacutainer tubes and allowed to clot by

keeping it undisturbed on ice for 30 minutes. The sample was then centrifuged at 2,000 g for 10 minutes at room temperature. Aliquots of the resulting supernatant, i.e. serum, was then pipetted into cryogenic tubes and stored at -80°C until NMR analysis.

All available samples were included in the study. However, due to lack of resources (research team availability) or anuria, (in the case of urine samples), this did not include a complete set of samples of all three biofluids for all the 50 patients at each of the four time points. Instead the sample collection consisted of 154 plasma samples, 100 serum samples and 125 urine samples from 50, 35 and 48 of the 50 patients of the sepsis cohort, respectively.

All the patients in the sepsis cohort had septic shock and received vasopressin following recruitment to the VACS trial. Urine and serum samples collected from two different healthy volunteers (a different biofluid from each volunteer), registered with the department of Surgery and Cancer, Faculty of Medicine Imperial College London, were used as healthy control samples.

4.3.3 Clinical data collection

Demographic and clinical data were collected from the patient's medical records and entered onto an online electronic case report form. Daily clinical data was collected from the time of study enrolment until discharge from the ICU. Patients were followed up until discharge from hospital and their outcomes including 28-day survival were determined.

To determine the metabolic signatures associated with sepsis-induced organ dysfunctions, 28-day survival and hydrocortisone administration each of these clinical classes were analysed separately with the samples divided into two groups: according to positive and negative outcome or the receipt

of hydrocortisone or placebo. At each time point, each patient was given a score for each the following organ dysfunction: kidney, liver, respiratory, cardiovascular, and haematological. The scores were dichotomised using the same methodology described in Section 3.3.3: with scores of one and zero representing dysfunction and no dysfunction, respectively. Acute liver, respiratory, cardiovascular and haematological dysfunction were defined as a score of 1-4 according to the sequential organ failure assessment (SOFA) scoring system (see Table 3.2) (Vincent, Moreno & Takala, 1996). Acute kidney dysfunction was defined as stages 1-3 of the acute kidney injury network (AKIN) classification according to both the serum creatinine and urine output criteria (see Table 3.3) (Mehta, Kellum, Shah, *et al.*, 2007). In addition to the dichotomised scores of acute respiratory, cardiovascular, and haematological dysfunctions assigned to the patients and their samples, the samples were also divided into five groups according to the five SOFA scores (zero to four) of each organ dysfunction. As described in Section 3.3.3 this was carried out to enable MVAs based on the samples in five groups and the dichotomised groups to be performed, in view of the imbalance in the sample numbers in the dichotomised groups.

In line with the scores for the organ dysfunction groups: the samples at each time point were divided into dichotomised groups of 28-day survival, in which the good (survival) and the poor outcomes (non-survival) were given a score of zero and one, respectively. At each time point, each patient was also given a treatment score according to their treatment allocation groups at each of the time points. Patients in the vasopressin and placebo group were given a score of zero and patients in the vasopressin and hydrocortisone group were given a score of one. The VACS study was an open label (receipt of the options of hydrocortisone and placebo was evident) pilot study in which cross over between the two treatment groups was permitted. In cases where cross over from the placebo to the hydrocortisone group had occurred, all the samples taken after such cross over were given a score of one to indicate they were now re-allocated to the treatment group. This was with the exception of

time point one and two samples which were taken at 6-12 hours, 24-36 hours post enrolment, respectively. These samples were excluded from the multivariate statistical analyses, in view of the inability to determine if they received steroids before or after these two sampling time points, as only daily steroid doses were record not the timings of the individual doses. Furthermore, each day was a calendar day, not 24-hour intervals after enrolment to the study. Conversely, some of the patients in the hydrocortisone group did not require the second study drug, i.e. hydrocortisone or placebo in addition to the vasopressin. The group receiving only of one of the two study drugs could be considered to be a different group to either of the two study arms and were therefore also excluded from the multivariate analyses of the samples according to their treatment groups. The significance of the differences between the metabolic profiles of the two groups of each of these four clinical classes was determined using multivariate statistical analyses of ^{1}H NMR spectroscopic analyses of urine and serum.

4.3.4 Sample preparation, ^{1}H NMR spectroscopy and pre-processing of the spectral data

The methodologies of the sample preparation,^{1}H NMR spectroscopy of the samples and the pre-processing of the spectral data are described in Sections 2.4.4, 2.4.5 and 2.5 respectively.

4.3.5 Multivariate statistical analyses and metabolite identification

Two forms of multivariate statistical analyses were applied to the pre-processed ^{1}H NMR spectral data of urinary samples from the sepsis cohort using SIMCA software. One without knowledge of samples classes, an unsupervised method of PCA and the other, O-PLS-DA, performed with knowledge of samples classes (e.g. AKI versus.no AKI). PCA analyses were used to obtain an overview of metabolic data as a whole and at the individual time points; whereas, O-PLS-DAs were only performed to identify classification-related metabolic differences between the groups at the individual time points.

The methodologies used in the multivariate statistical analyses of the ^{1}H NMR spectral data of the urine and serum samples and metabolites identification are described in Sections 2.5 and 3.4.3 respectively.

4.4 Results

4.4.1 Patient Meta data - demographics and clinical data of the sepsis cohort

Table 4.1 Characteristics of the sepsis cohort: demographics and baseline clinical variables (A) including the baseline Acute Kidney Injury Network (AKIN) and Sequential Organ Failure Assessment (SOFA) scores in more detail (B and C: for all patients with urine and serum samples available, respectively). Key: APACHE II: Acute Physiology and Chronic Health Evaluation II, COPD: Chronic Obstructive Pulmonary Disease, ICU: Intensive Care Unit, IHD: Ischaemic Heart Disease, IQR: interquartile range, NYHA: New York Heart Association functional classification, *: SOFA scores except for renal, which are AKIN scores.

A

Characteristic	**All patients - Urine** n= 48 n(%) or median [IQR]	**All patients - Serum** n=34 n(%) or median [IQR]
Age (years)	59 [50-71]	58 [51-71]
Gender (male)	27 (56)	19 (56)
APACHE II	21 [17-24]	21 [18-24]
Organ dysfunction scores*		
Renal	0 [0-2]	0 [0-2]
Liver	0 [0-1]	0 [0-2]
Respiratory	3 [2-3]	3 [2-3]
Cardiovascular	4 [1-4]	4 [1-4]
Haematological	0 [0-1]	1 [0-2]
Neurological	0 [0]	0 [0]
Baseline serum creatinine	87 [60-176]	90 [61-181]
Baseline serum total bilirubin	13 [8.0-32]	14 [8.0-33]
Co-morbidity		
IHD	1 (2.1)	1 (2.9)
NYHA IV	0	0
Severe COPD	2 (4.2)	2 (5.9)
Chronic renal failure	3 (6.3)	2 (5.9)
Cancer	4 (8.3)	4 (11.8)
Cirrhosis	8 (16.7)	8 (23.5)
Immunocompromised	2 (4.2)	2 (5.9)
Diabetes	4 (8.3)	4 (11.8)
Recent trauma	0	0
Admission type		
Medical (Non operative)	37 (77.1)	27 (79.4)
Surgery – Emergency (Operative)	10 (20.8)	7 (20.6)
Surgery – Elective (Operative)	1 (2.1)	0
Diagnostic group (reason for admission)		
Post cardiac arrest	2 (4.2)	2 (5.9)
Cardiovascular	1 (2.1)	0
Respiratory	15 (31.3)	11 (32.4)

Table 4.1 continued

Gastro-intestinal - medical	3 (6.3)	4 (11.8)
Gastro-intestinal - surgical/operative	8 (16.7)	4 (11.8)
Infection	16 (33.3)	10 (29.4)
Neurologic	1 (2.1)	1 (2.9)
Aspiration /Poisoning /Toxic	2 (4.2)	2 (5.9)
Clinical outcomes		
Length of ICU stay	12 [7-19]	11 [7-18]
Length of hospital stay	25 [16-49]	24 [13-47]
28 day mortality	12 (25)	10 (30)

B

	Organ dysfunction scores*				
Organ dysfunction	**0**	**1**	**2**	**3**	**4**
Renal	32	3	7	6	0
Liver	30	6	10	2	0
Respiratory	6	4	11	16	11
Cardiovascular	4	9	0	0	35
Haematological	28	9	7	3	1
Neurological	39	2	2	0	5

C

	Organ dysfunction scores*				
Organ dysfunction	**0**	**1**	**2**	**3**	**4**
Renal	21	3	6	4	0
Liver	20	4	9	1	0
Respiratory	5	2	7	14	6
Cardiovascular	2	8	0	0	24
Haematological	17	6	8	3	0
Neurological	27	2	2	0	3

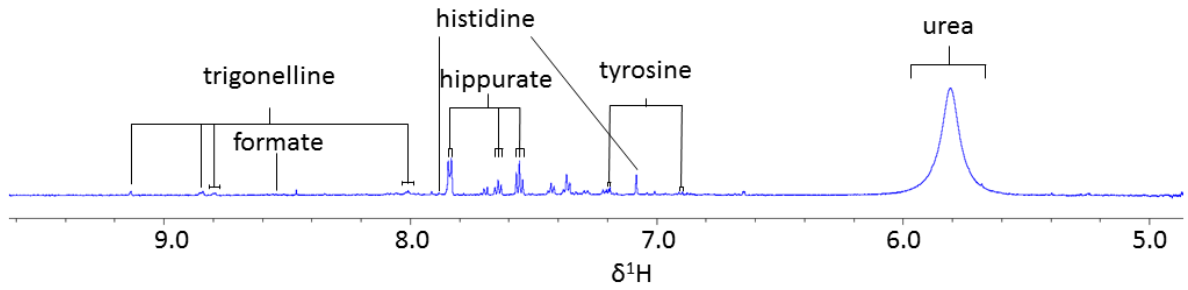
4.4.2 ^{1}H NMR spectroscopy-based metabolic profiling of urinary samples

4.4.2.1 ^{1}H NMR spectroscopy of urine in severe sepsis

Illustrations of typical ^{1}H NMR spectra of urine from a healthy control and two individuals from the sepsis cohort are shown in Figures 4.1-4.3 (aromatic and aliphatic regions in Figures A and B, respectively). Comparison of these spectra highlights the greater complexity of the spectra from the

sepsis cohort compared to ones from the healthy controls; with a greater number of signals many of which are overlapping in regions between at δ^1H 8.2 to 7.0 and 4.2 to 3.4 ppm. The spectra shown in Figures 4.2 and 4.3 are from two individuals from the sepsis cohort who received Co-amoxiclav and Tazocin, respectively. These are two of the commonest antibiotics used to treat community acquired pneumonia (CAP) and hospital acquired pneumonia (HAP), respectively. Spectra from recipients of these two antibiotics were therefore used as representative examples of the group as a whole. These two examples are typical of the ^{1}H NMR spectra of the sepsis cohort, with the presence of many signals from the common urinary metabolites, in addition to a large number of signals from drugs (parent and their metabolites). Signals from antibiotics, the main stay of treatment of sepsis were responsible for a significant number of the signals from drugs administered to this cohort. The methodology of the identification of signals from drugs, and both drug and non-drug metabolites have been described in Section 3.5.3. This included the use of ^{1}H NMR spectra of the parent drugs (drug standards) and STOCSY of urinary spectra of patients treated with the drugs. These analyses revealed that both Tazocin and Co-amoxiclav, like many of the antibiotics administered to this cohort, contributed a large number of signals to the urinary profiles. Moreover, there is a degree of overlap between the signals from the two drugs as illustrated in the composite figure of the ^{1}H NMR spectra of the parent drug of these two antibiotics shown in Figure 4.4. Non-drug metabolites identified in the urinary spectra from both the healthy control and the sepsis cohort were divided into metabolites only present in urine and metabolites found in the serum and urine spectra from both parties (see Table 4.5). Examples of the latter included formate, histidine, tyrosine, urea, lactate, creatinine, creatine, acetate, and glycine; whereas dimethylamine (DMA), hippurate, taurine and trimethylamine-*N*-oxide (TMAO) were only identified in the urinary spectra.

A



B

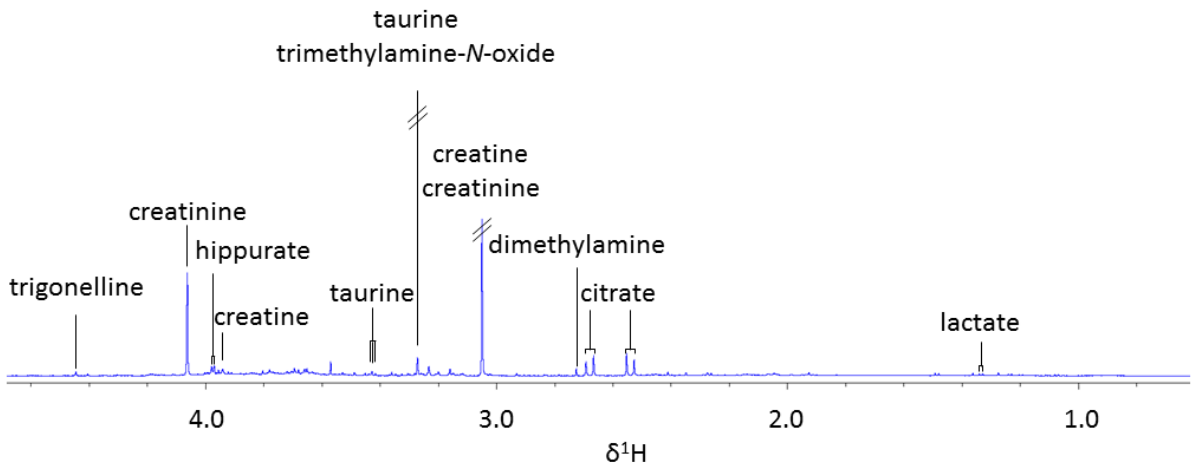
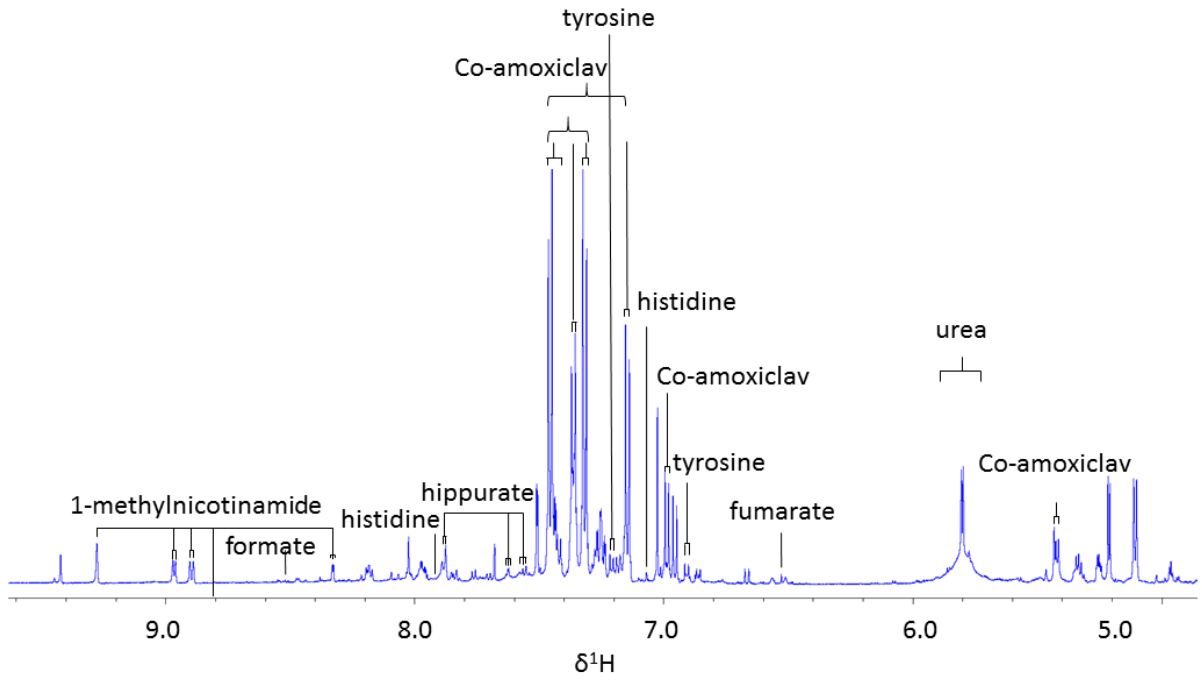


Figure 4.1. A typical 600MHz 1-D ^{1}H NMR spectrum of regions 9.7-4.8 ppm (A) and 4.6-0.8 ppm (B) from a urine sample from a healthy control illustrating the urinary metabolites usually detected by this method of metabolic profiling.

A



B

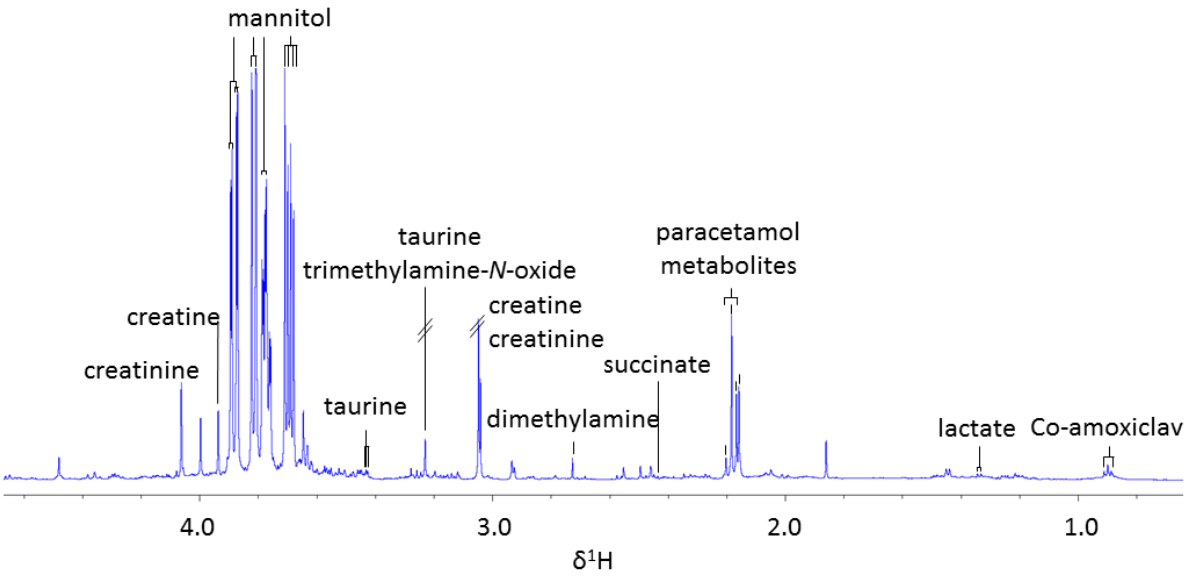


Figure 4.2. A 600MHz 1-D ^{1}H NMR spectrum of urine from a recipient of the drug of Co-amoxiclav as the only antibiotic, or structurally similar drug administered, divided into 9.7-4.8 ppm (A) and 4.6-0.8 ppm (B) illustrating of the detection of usual urinary metabolites in addition to signals of Co-amoxiclav.

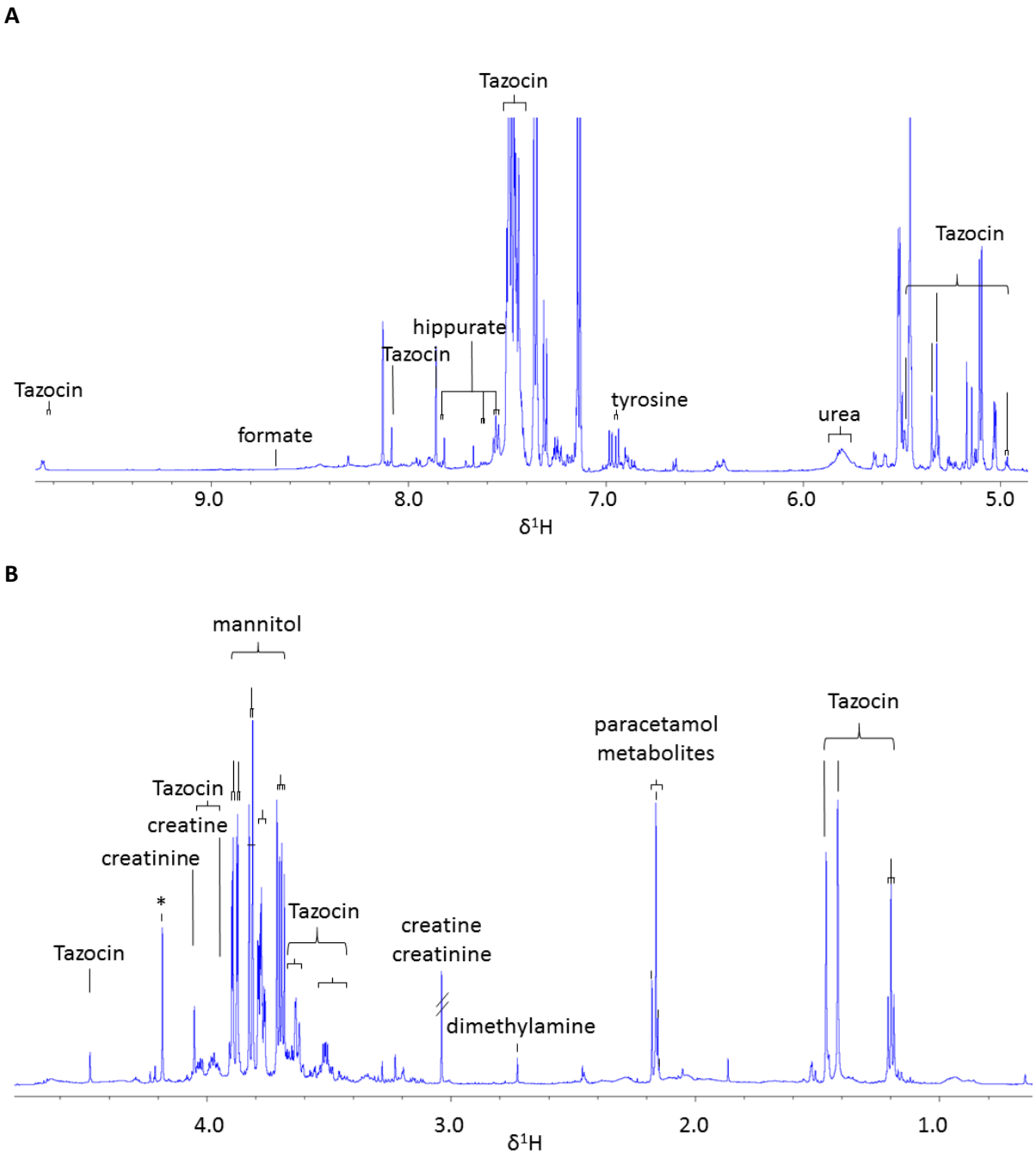
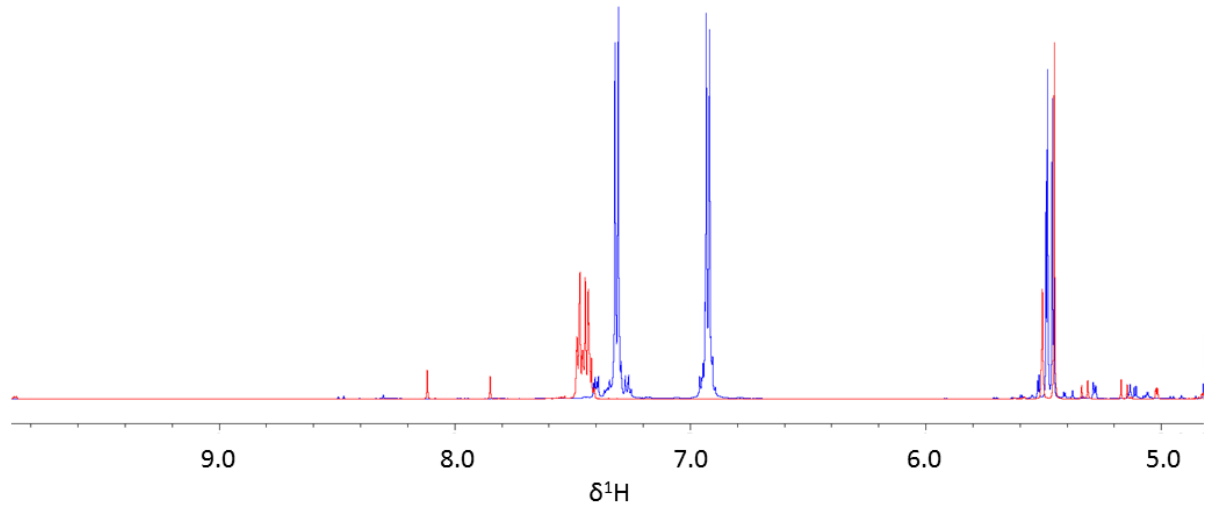


Figure 4.3. A 600MHz 1-D ^{1}H NMR spectrum of urine from a recipient of the drug Tazocin as the only antibiotic, or structurally similar drug administered, regions 9.7-4.8 ppm (A) and 4.6-0.8 ppm (B) illustrating the detection of usual urinary metabolites in addition to signals of tazocin. KEY: *: signal present in both the Tazocin and Co-amoxiclav drug standards.

A



B

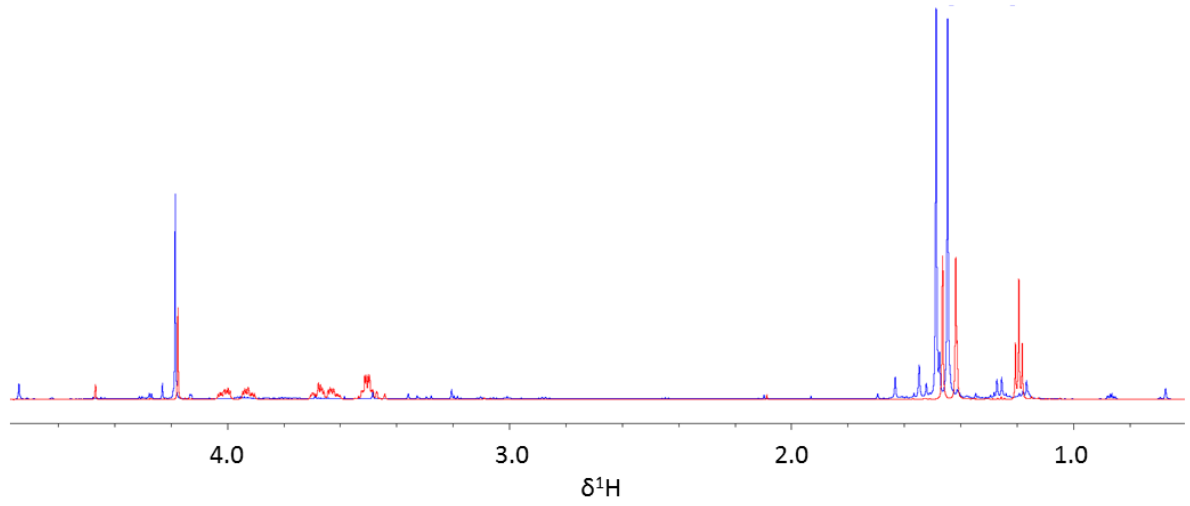


Figure 4.4 A composite of 600MHz 1-D ^{1}H NMR spectra of the Co-amoxiclav (blue) and Tazocin (red) drug standards regions 9.7-4.8 ppm (A) and 4.6-0.8 ppm (B) illustrating signals of these two antibiotics and highlighting their differences.

4.4.2.2 Multivariate analyses of ^{1}H NMR spectra of urine from patients with severe sepsis: identification of metabolites characterising the clinical classes

The urine sample set consisted of 125 samples from 48 patients divided into samples from four time points. This consisted of 21, 41, 37 and 26 samples from time points 0 (enrolment), 1 (day one), 2 (day two) and 3 (day seven) of the study, respectively (see Section 4.3.2). Of the samples from the first time point, 14 of the 21 samples were from patients with no evidence of AKI at this time point; this group was named time point 0 without AKI.

An unsupervised analysis of all the samples was performed first on the probabilistic quotient normalised and unit variance scaled 1-D ^{1}H NMR spectral data of urine from the sepsis cohort from all four time points using SIMCA software. This consisted of a PCA constructed with the first two principal components. The scatter scores plot of this PCA model (Figure 4.5) did not demonstrated any clear clustering of the samples. It did, however, reveal an extreme outlying sample lying very far away from the perimeter of the Hotelling's T^2 95% confidence ellipse. Examination of the raw spectral data revealed an experimental explanation for this extreme outlier and it was subsequently removed from the dataset (see Appendix III Figures 6 and 7).

The raw NMR data of the remaining 124 samples was pre-processed again and the same method of PCA was re-applied. The PCA scores plot of this second dataset (Figure 4.6) revealed three clusters of outlying samples just outside of the Hotelling's T^2 95% confidence ellipse and one outlier on its own in the right top-handed quadrant of the plot in close proximity to one of the clusters. All of these outliers were in close proximity to other samples and considered intermediate outliers, and therefore no further outliers were removed and the dataset of 124 samples was used for all subsequent analyses. No clear separation of the samples within the Hotelling's perimeters were demonstrated by this PCA model. The parameters of fit and predictability of the model were low with an R^2X and a $Q^2X\hat{w}$ of 0.312 and 0.236, respectively (Table 4.2). PCA models of the spectral data from each time point

were constructed. A PCA of the data from 14 samples from time point zero from patients without AKI was also produced. No clear evidence of separation of the samples were demonstrated by the PCA scores plots. The R^2X and a Q^2X of all five models were also low (Table 4.2).

To maximise the separation between the clinical classes (groups) and investigate classification-related metabolic differences, a series of supervised O-PLS-DA analyses of the samples from each time point was then carried out. This consisted of separate 'time point' models being constructed for each of the four time points with one set for each of the following seven classes: acute kidney injury, acute liver injury, 28-day survival, treatment group, and respiratory, cardiovascular, and haematological dysfunction. Samples from time point zero were taken prior to the administration of the two treatments, however, O-PLS-DA models involving the two treatment groups were constructed using all four time points, i.e. before and after the administration of the study drugs (placebo or corticosteroids, in addition, to vasopressin), to confirm that the baseline samples from two treatment groups were similar. To seek the predictive markers for AKI, 14 samples from time point zero from patients without AKI were divided into two groups based on the presence and absence of AKI at later time points and an O-PLS-DA model was constructed between the two groups. This was performed to investigate biomarkers capable of predicting the development of AKI before any clinical evidence of AKI is present that might aid to direct early aggressive treatment strategies for AKI. All the O-PLS-DA models were built using the NMR spectral data as the X matrix and the clinical class as the dummy Y matrix. Each model was based on one predictive projection to latent structures (PLS) component with one or two orthogonal components, if orthogonal component resulted in a significantly greater model. This was defined as an increase in the Q^2Y of greater or equal to 0.05 and a decrease in the p value of the cross-validated analysis of variance (CV-ANOVA) of the model (see Section 2.5).

The results of evaluation parameters of the best sixteen O-PLS-DA models of acute kidney injury, acute liver injury, 28-day survival, and treatment group are shown in Table 4.3: one model for each time

point for the AKI, acute liver injury and 28-day survival, and treatment classes; and one for model based on the development of AKI after time point zero (enrolment). This illustrates the predictability (Q^2Y) of all the models ranged from -0.302 to 0.336. However, the p value of the CV-ANOVA of the models, a measure of the significance of the class separation was shown to be non-significant ($p>0.05$ and ranged from 0.139 to 1) for all the models, consistent with there being no significant metabolic differences in the dichotomised groups of any models. The results of the evaluation parameters of the best O-PLS-DA models of respiratory, cardiovascular, and haematological dysfunction with the samples divided into two and five groups, are shown in Tables 4.4 A and B, respectively. The sample number in each of the dichotomised groups in the second group of organ dysfunctions, was very imbalanced. Respiratory and cardiovascular dysfunction were particularly affected, and in some cases, an O-PLS-DA model could not be performed because of lack of a second group. This led to the construction of a set of models with five sample groups. The Q^2Y values of the models with two groups ranged from -0.249 to 0.432 and ranged from -0.175 to 0.160 for the models with five groups; with the haematology model with two groups based on data from time point three (day 7) achieving the highest Q^2Y value. However, all of models, including the aforementioned haematology model were associated non-significant p values on CV-ANOVA (ranging from 0.193 to 1 and 0.396 to 1 for the models with two and five groups, respectively).

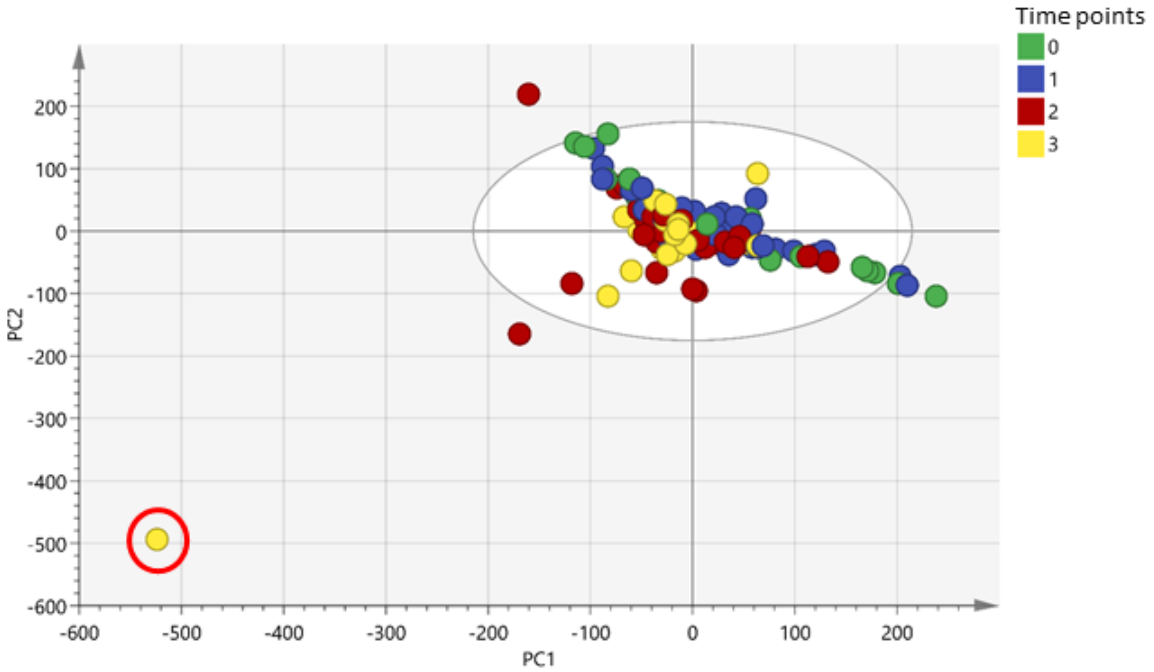


Figure 4.5. A PCA scores plot based on 1-D ^{1}H NMR spectra of all the 125 urinary samples from the sepsis cohort illustrating the metabolic variation of the data set as a whole and one extreme outlying sample (circled in red). Samples from time points 0, 1, 2 and 3 are colour coded in green, blue, red, and yellow, respectively.

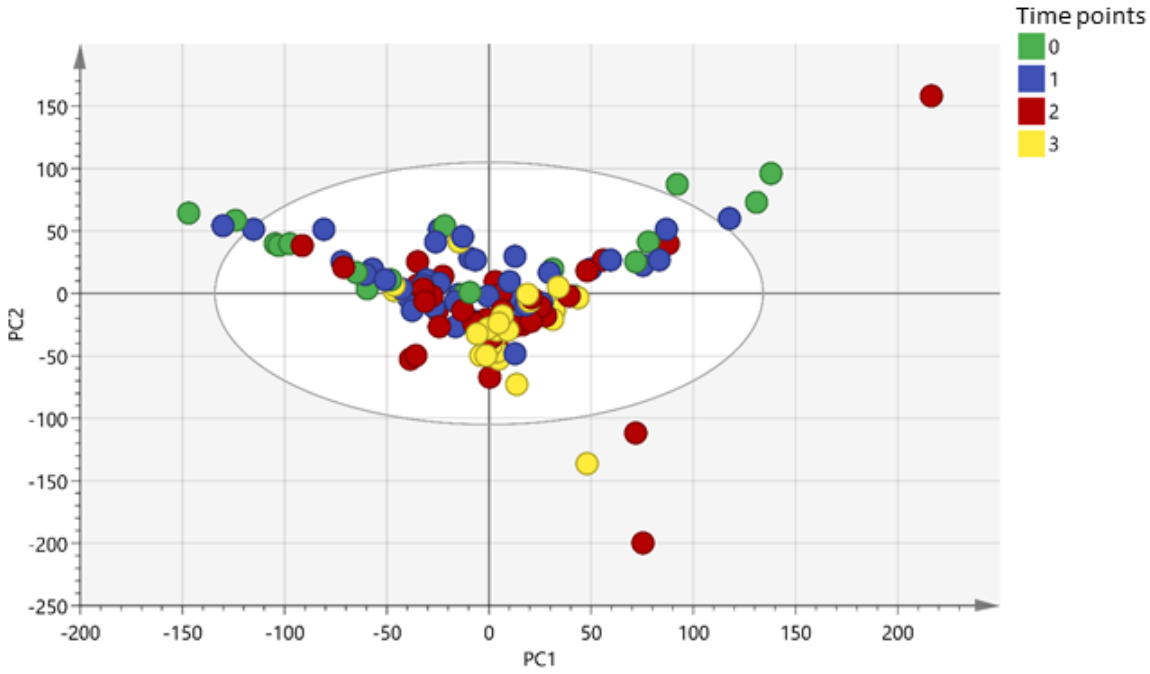


Figure 4.6 PCA scores plot derived from 1-D ^{1}H NMR spectra of 124 of the urinary samples from the sepsis cohort illustrating the metabolic variation of the data set as a whole following the exclusion of the extreme outlier shown in Figure 4.5. Samples from time points 0, 1, 2 and 3 are colour coded in green, blue, red, and yellow, respectively.

Table 4.2 Results of the evaluation parameters of PCAs based on 1-D ^{1}H NMR spectra of urine from the sepsis cohort. Key: PC: principal component; R^2X and Q^2X: variation explained and predicted by the model, respectively.

Principal Component Analyses							
Sample set: time point (n=sample number)	All samples (n=125)	All samples - one outlier (n=124)	Time point 0 without AKI (n=14)	Time point 0 (n=21)	Time point 1 (n=41)	Time point 2 (n=37)	Time point 3 (n=25)
Number of PCs	2	2	2	2	2	3	1
R^2X	0.342	0.312	0.522	0.476	0.373	0.443	0.221
Q^2X	0.183	0.236	0.259	0.272	0.254	0.138	-0.100

Table 4.3. Results of the evaluation parameters of O-PLS-DA models of 1-D ^{1}H NMR spectra of urine from the sepsis cohort. Illustration of the percentage of the variation explained by the X (R^2X) and Y matrices (R^2Y) and predicted by the Y matrix (Q^2Y) of the models evaluating samples based on five clinical classes: the development of AKI after TP0, acute kidney injury*, acute liver injury*, 28-day survival and treatment group. KEY: CV-ANOVA: cross-validated analysis of variance, Group 0: good outcome (no injury or survival) or placebo treatment group, Group 1: poor outcome (injury or non-survival) or hydrocortisone treatment group, TP: time point; *: at that time point.

OPLS-DA		**AKI after TP0**	**Acute Kidney injury**				**Acute Liver injury**				**28 day survival**				**Treatment group**			
Sample set: time point		TP0 without	TP0	TP1	TP2	TP3	TP0	TP1	TP2	TP3	TP0	TP1	TP2	TP3	TP0	TP1	TP2	TP3
(n=sample number)		AKI (n= 14)	(n=21)	(n=41)	(n=37)	(n=25)	(n=21)	(n=41)	(n=37)	(n=25)	(n=21)	(n=41)	(n=37)	(n=25)	(n=21)	(n=41)	(n=37)	(n=25)
Group 0: good outcome		5	15	17	20	13	14	21	24	14	15	28	31	20	13.000	16	24	11
Group 1: poor outcome		9	6	24	17	12	7	20	13	11	6	13	6	5	8.000	25	13	14
Number of components	**Predictive**	1	1	1	1	1	1	1	1	1	1	1	1	1	1	1	1	1
	Orthogonal to X	0	1	0	0	0	1	1	0	2	0	0	0	0	1	0	0	0
Model statistics	**R^2X**	0.307	0.175	0.222	0.166	0.180	0.175	0.160	0.146	0.366	0.257	0.233	0.182	0.123	0.480	0.175	0.154	0.143
	R^2Y	0.474	0.400	0.307	0.306	0.326	0.740	0.707	0.263	0.923	0.240	0.201	0.229	0.512	0.700	0.319	0.270	0.441
	Q^2Y	0.245	0.138	0.047	-0.052	0.010	0.138	-0.073	-0.302	0.149	-0.281	-0.145	-0.073	-0.046	0.336	-0.017	-0.029	0.025
	$R^2Y - Q^2$	0.229	0.262	0.260	0.358	0.316	0.602	0.780	0.565	0.774	0.521	0.346	0.302	0.558	0.364	0.336	0.299	0.417
CV-ANOVA	**P VALUE**	0.186	0.641	0.398	1.000	0.894	0.641	1.000	1.000	0.782	1.000	1.000	1.000	1.000	0.139	1.000	1.000	0.761

Table 4.4 Results of the evaluation parameters of O-PLS-DA models of 1-D ^{1}H NMR spectra of urine from the sepsis cohort. Illustration of the percentage of the variation explained by the X (R^2X) and Y matrices (R^2Y) and predicted by the Y matrix (Q^2Y) of the models evaluating samples based on their respiratory, cardiovascular, and haematological clinical classes with the samples divided into two (A) and five groups (B). KEY: CV-ANOVA: cross-validated analysis of variance, SOFA: Sequential Organ Failure Assessment, TP: time point.

A

OPLS-DA		Respiratory				Cardiovascular				Haematological			
Sample set: time point (n=sample number)		TP0 (n=21)	TP1 (n=41)	TP2 (n=37)	TP3 (n=25)	TP0 (n=21)	TP1 (n=41)	TP2 (n=37)	TP3 (n=25)	TP0 (n=21)	TP1 (n=41)	TP2 (n=37)	TP3 (n=25)
Group 0: good outcome (no injury)		3	1	1	0	2	0	0	6	14	21	17	13
Group 1: poor outcome (injury)		18	40	36	25	19	41	37	19	7	20	20	12
Number of components	Predictive	1	1	1	N/A	1	N/A	N/A	1	1	1	1	1
	Orthogonal to X	0	0	0		1			1	1	1	0	4
Model statistics	R^2X	0.336	0.189	0.100		0.400			0.268	0.414	0.309	0.156	0.534
	R^2Y	0.248	0.128	0.262		0.677			0.786	0.562	0.548	0.254	0.984
	Q^2Y	0.001	-0.109	-0.203		-0.249			0.252	-0.190	-0.105	-0.146	0.432
	R^2Y - Q^2Y	0.247	0.237	0.465		0.926			0.534	0.752	0.653	0.400	0.552
CV-ANOVA	P VALUE	0.990	1.000	1.000		1.000			0.193	1.000	1.000	1.000	0.330

B

OPLS-DA		Respiratory				Cardiovascular				Haematological			
Sample set: time point (n=sample number)		TP0 (n=21)	TP1 (n=41)	TP2 (n=37)	TP3 (n=25)	TP0 (n=21)	TP1 (n=41)	TP2 (n=37)	TP3 (n=25)	TP0 (n=21)	TP1 (n=41)	TP2 (n=37)	TP3 (n=25)
SOFA = 0		3	1	1	0	2	0	0	6	14	21	17	13
SOFA = 1		1	5	2	4	2	0	0	8	4	9	7	3
SOFA = 2		3	12	11	9	0	0	1	0	3	6	7	5
SOFA = 3		7	10	14	10	0	15	14	9	0	5	5	2
SOFA = 4		7	13	9	2	17	26	22	2	0	0	1	2
Number of components	Predictive	1	1	1	1	1	1	1	3	1	1	1	1
	Orthogonal to X	0	0	0	0	0	2	0	0	1	1	0	0
Model statistics	R^2X	0.335	0.102	0.164	0.170	0.076	0.373	0.179	0.371	0.431	0.305	0.151	0.214
	R^2Y	0.144	0.122	0.092	0.152	0.428	0.663	0.179	0.524	0.291	0.232	0.086	0.137
	Q^2Y	-0.063	-0.040	-0.143	-0.071	-0.156	0.160	0.004	0.086	-0.157	-0.060	-0.063	-0.035
	R^2Y - Q^2Y	0.207	0.162	0.235	0.223	0.584	0.503	0.175	0.439	0.448	0.292	0.149	0.172
CV-ANOVA	P VALUE	1.000	1.000	1.000	1.000	1.000	0.396	0.950	1.000	1.000	1.000	1.000	1.000

4.4.3 ^{1}H NMR spectroscopy-based metabolic profiling of serum

4.4.3.1 ^{1}H NMR spectroscopy of serum in severe sepsis

Representative examples of 1-D standard and CPMG ^{1}H NMR spectra of a serum sample, taken from a healthy control and an individual in the sepsis cohort are illustrated in Figures 4.7 and 4.8; and Figures 4.9 and 4.10, respectively.

The 1-D standard spectrum demonstrated a wide range of metabolites such as amino acids, simple carbohydrates, and lipids, in addition to signals from drugs. This resulted in overlap of the many of the signals, particularly in regions with broad signals from lipids. In other regions such as 4.1 to 3.2 ppm, broad signals appear to be responsible for considerable baseline distortion.

The spectra acquired using the CPMG pulse sequence benefitted from an attenuation of the effects of broad signals from macro-molecules evident in the 1-D standard spectra. This allows clearer visualisation of smaller metabolites particularly amino acids and considerably less baseline distortion in the region between 6-8ppm. Despite this, however, the broad signals of the lipids were still identifiable in the CPMG spectra. The non-drug metabolites identified in the spectra of the serum are listed in Table 4.5. This included amino acids such as alanine, valine, lysine, L-threoinine, tyrosine, histidine; the carboxylic acids formate and acetate; and intermediates of the tricarboxylic acid cycle fumarate and pyruvate, and anaerobic metabolism: lactate and alanine. The 1-D standard and CPMG spectra also demonstrated signals from the glyceryl back bone of lipids and signals of choline suggesting the presence of glycerophospholipids; phosphatidylcholine in particular.

Comparison of the representative 1-D standard and CPMG spectra of serum from an individual from the sepsis cohort shown in Figures 4.9 and 4.10 and the examples from a healthy control shown in Figures 4.7 and 4.8 demonstrates the spectra from the sepsis cohort exhibits the greater complexity. This included drug related metabolites and greater number of broad unidentified signals in the spectra from the patient with sepsis on review of the raw data as a whole. This comparison also shows that the majority of the endogenous metabolites are present in the spectra from the healthy control also present in patients with sepsis (see Table 4.5).

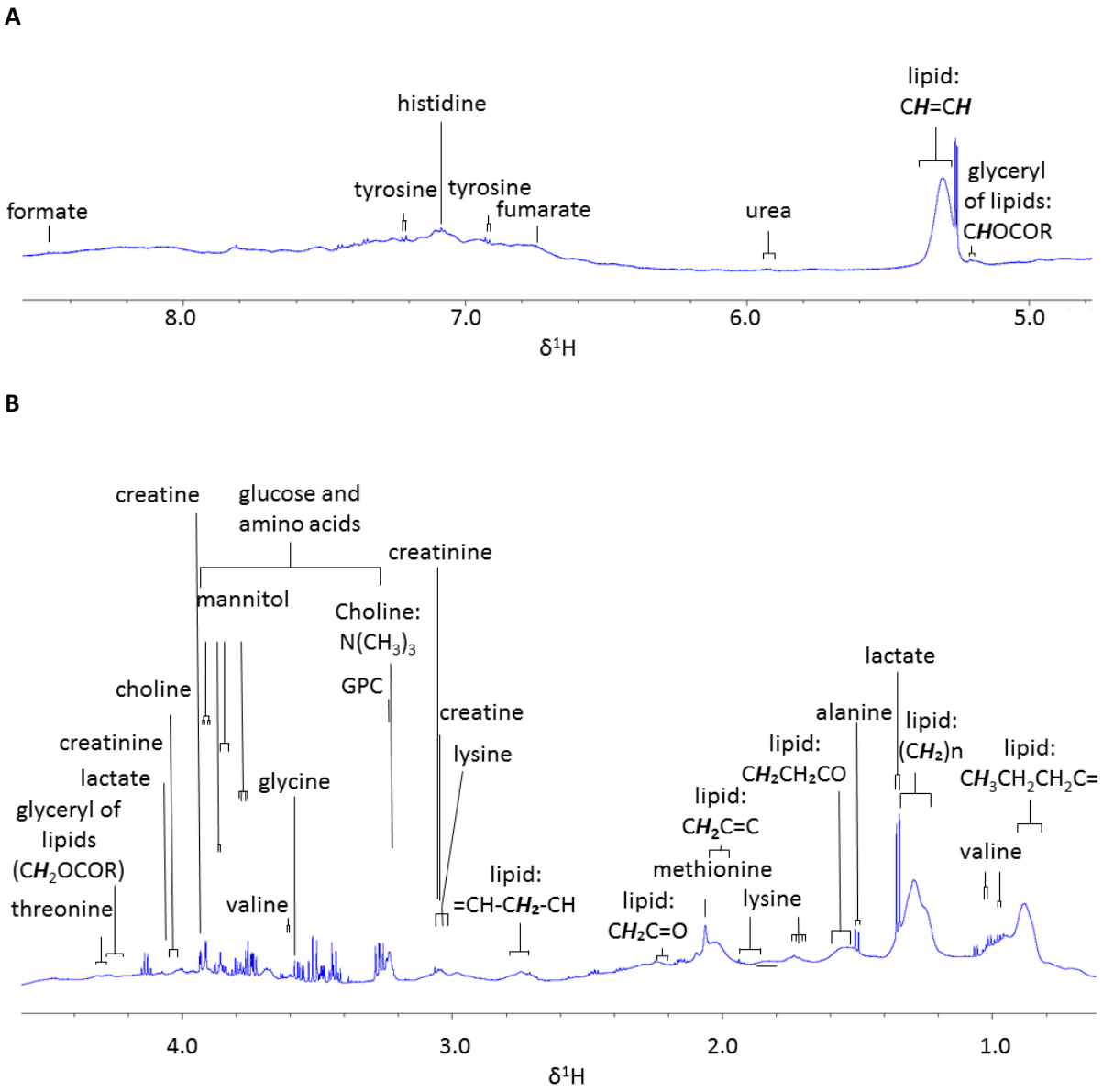
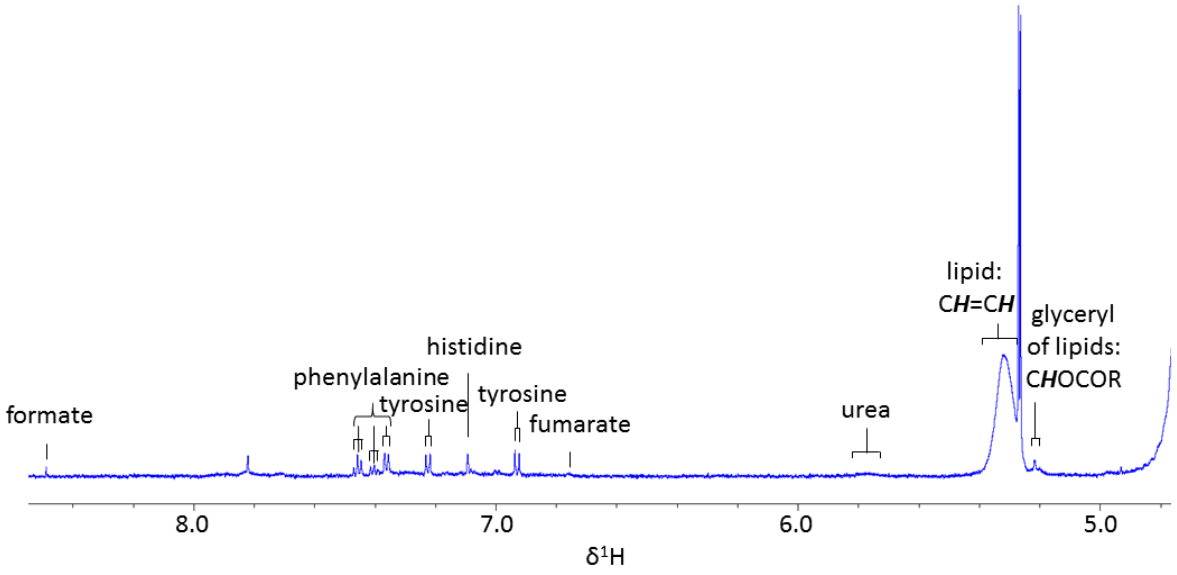


Figure 4.7. Typical 600MHz standard 1-D ^{1}H NMR spectrum of regions 9.7-4.8 ppm (A) and 4.6-0.8 ppm (B) from a serum sample from a healthy control illustrating the serum metabolites usually detected by this method of metabolic profiling. KEY: GPC: glycerophosphorylcholine.

A



B

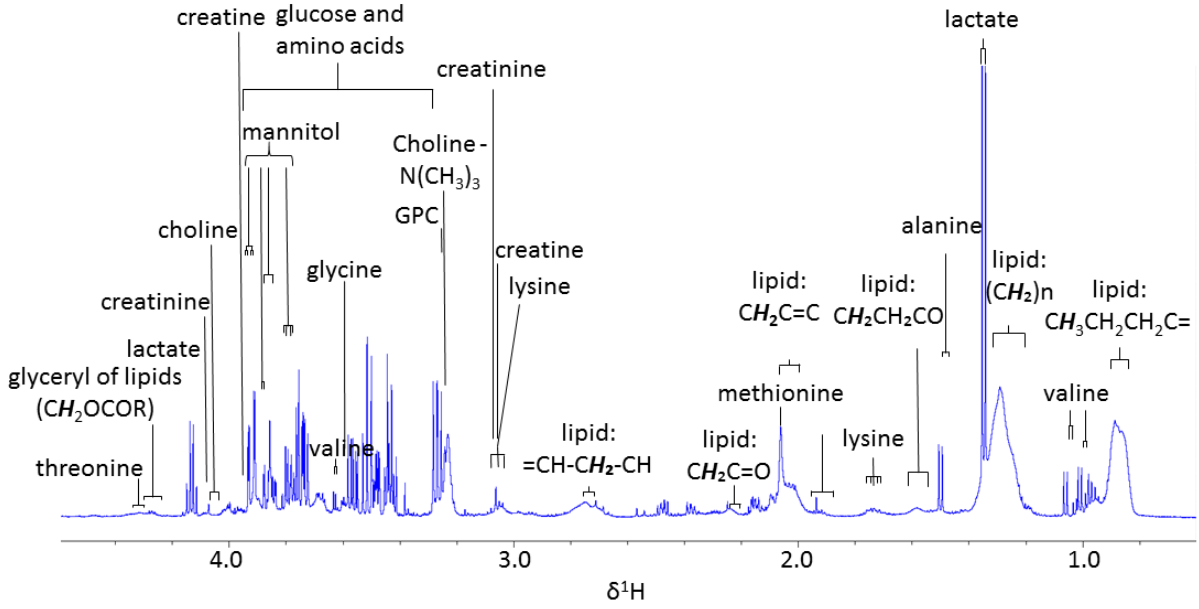
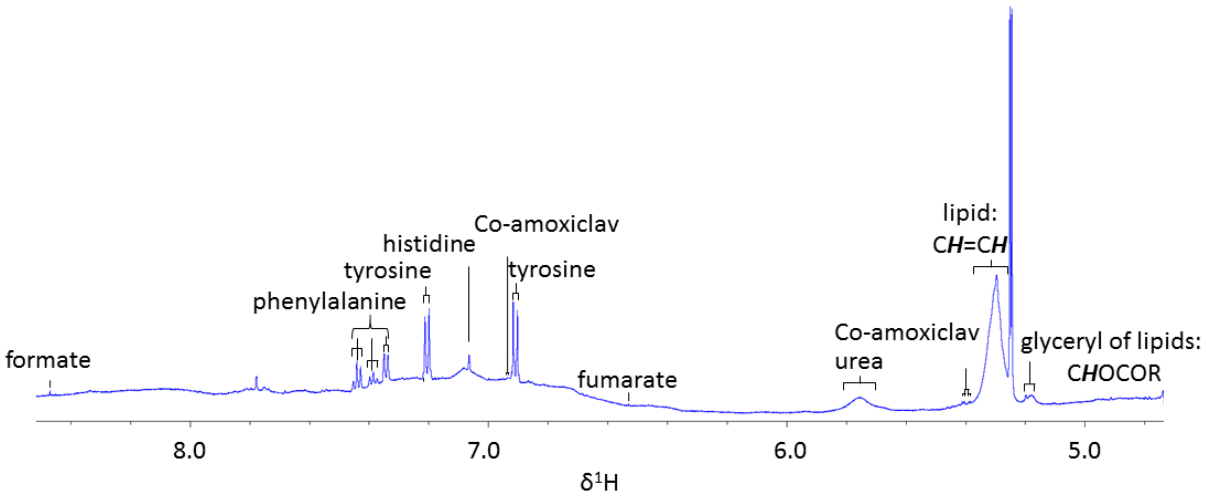


Figure 4.8. Typical 600MHz 1-D CPMG ^{1}H NMR spectrum of regions 9.7-4.8 ppm (A) and 4.6-0.8 ppm (B) from a serum sample from a healthy control illustrating the serum metabolites usually detected by this method of metabolic profiling. KEY: GPC: glycerophosphorylcholine.

A



B

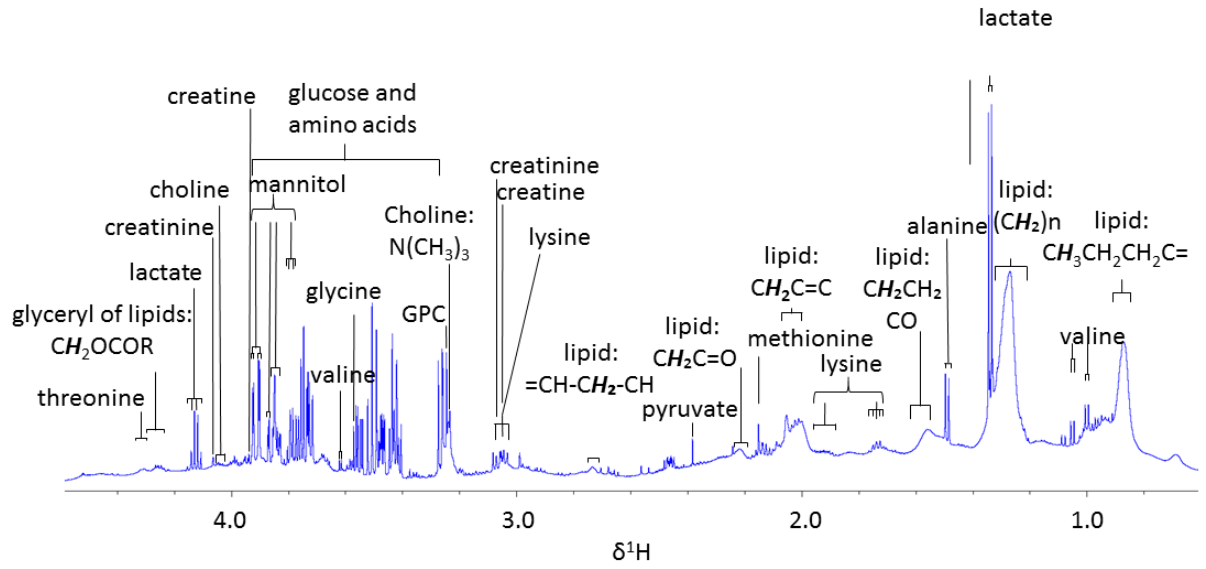
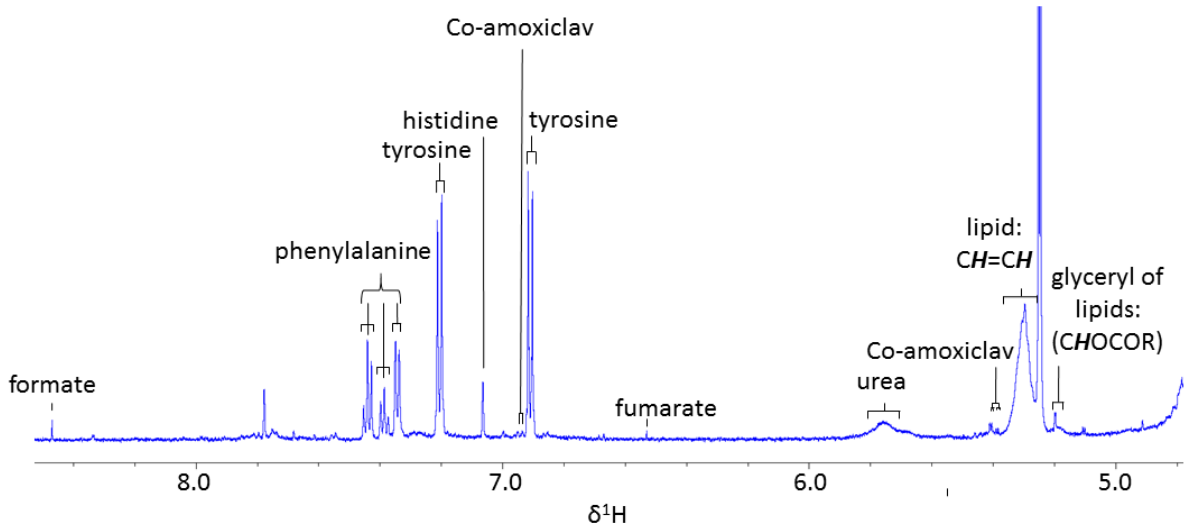


Figure 4.9 A 600MHz standard 1-D ^{1}H NMR spectra of serum from a recipient Co-amoxiclav as the only antibiotic, or structurally similar drug administered from the sepsis cohort, divided into 9.7-4.8 ppm (A) and 4.6-0.8 ppm (B) illustrating of the detection of serum metabolites in addition to signals of Co-amoxiclav. KEY: GPC: glycerophosphorylcholine.

A



B

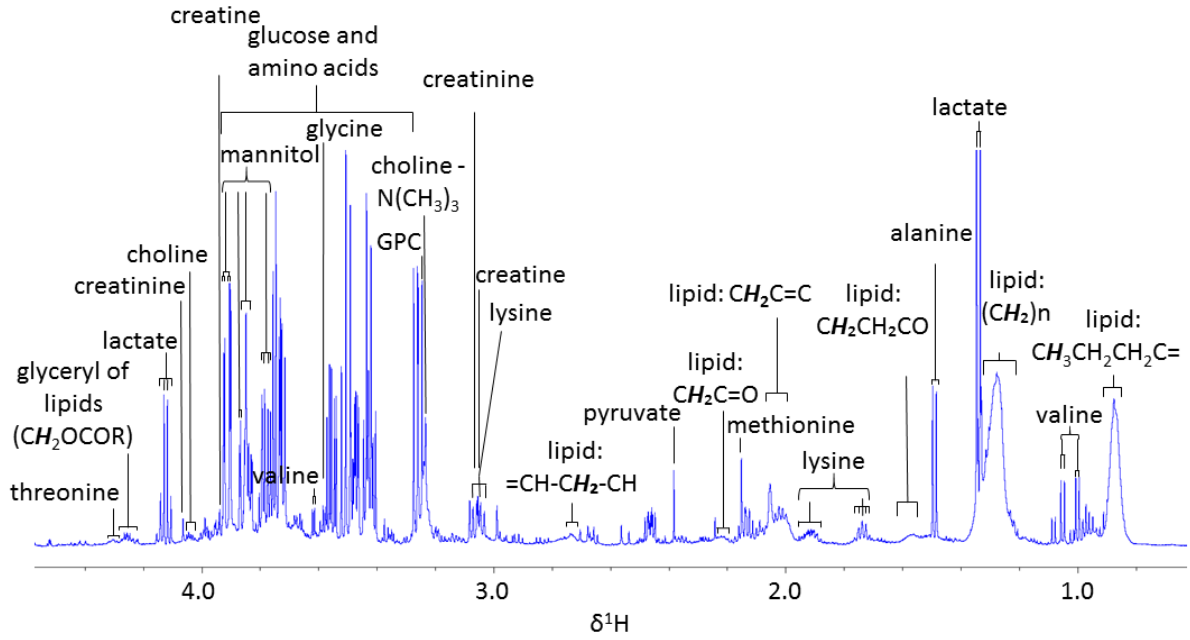


Figure 4.10 A 600MHz CPMG ^{1}H NMR spectra of serum from a recipient Co-amoxiclav as the only antibiotic, or structurally similar drug administered from the sepsis cohort, divided into 9.7-4.8 ppm (A) and 4.6-0.8 ppm (B) illustrating of the detection of serum metabolites in addition to signals of Co-amoxiclav. KEY: GPC: glycerophosphorylcholine.

Table 4.5 Non-drug metabolites identified in 600MHz standard 1-D ^{1}H NMR spectra of urine, and 1-D standard and CPMG ^{1}H NMR spectra of serum from: (i) the sepsis cohort and (ii) the healthy control (shown above) and their chemical shifts and signal multiplicities. Key: s: singlet; d: doublet; t: triplet; q: quartet; o: octet; m: multiplet; bs: broad signal; dd: doublet of doublets.

Metabolites	H group					δ ^{1}H (multiplicity)					Sepsis biofluids	Control biofluids
1-methylnicotinamide	H2	H6	H4	H5	CH_3	9.28 (s)	8.97 (d)	8.90 (d)	8.18 (t)	4.48 (s)	u	–
acetate	CH_3					1.92 (s)					s, u	s, u
alanine	CH	CH_3				3.79 (q)	1.48 (d)				s	s
choline	N-(CH_3)$_3$	α–CH_2	β–CH_2			3.21 (s)	4.07 (m)	3.52 (m)			s, u	s
citrate	CH_2(i)	CH_2(ii)				2.66 (d)	2.54 (d)				s.u	s, u
creatine	CH_2	CH_3				3.94 (s)	3.04 (s)				s, u	s, u
creatinine	CH_3	CH_3				4.06 (s)	3.04 (s)				s, u	s, u
dimethylamine	CH_3					2.72 (s)					u	u
formate	CH					8.46 s					s, u	s, u
fumarate	CH					6.53 (s)					s,u	s
glycerophosphoryl choline	N-(CH_3)$_3$					3.23 (s)					s	s
glyceryl of lipids	CHOCOR					5.18 (m)					s	s
glyceryl of lipids:	CH2OCOR					4.27 (m)					s, u	–
glycine	CH					3.57 (s)					s	s, u
hippurate	2,6-CH	4-CH	3,5-CH		CH_2	7.84 (d)	7.63 (t)	7.55 (t)	3.97 (d)		u	u
histidine	H_3	H5	αCH	β–CH_2(i)	β–CH_2(ii)	7.83 (s)	7.08 (s)	4.00 (dd)	3.30 (dd)	3.10 (dd)	s, u	s, u
lactate	CH	CH_3				4.12 (q)	1.32 (d)				s	s, u
lipid signal	C***H***=C***H***					5.30 (bs)					s	s
lipid signal	=CH-C***H***$_2$-CH					2.73 (bs)					s, u	s
lipid signal	C***H***$_2$C=O					2.22 (bs)					s	s
lipid signal	C***H***$_2$C=C					2.01 (bs)					s, u	s
lipid signal	C***H***$_2$$CH_2$CO					1.56 (bs)					s	s
lipid signal	(C***H***$_2$)$_n$					1.29 (bs)					s	s
lipid signal	C***H***$_3$$CH_2CH_2$C=					0.87 (bs)					s, u	s
lipid signal	C***H***$_3$(CH_2)$_n$					0.83 (bs)					s,u	–
lysine	αCH	βCH_2	γCH_2	δCH_2	εCH_2	3.76 (t)	1.90 (m)	1.73 (q)	1.48 (m)	3.03 (t)	s	s
methionine	αCH	βCH	γCH_2	*S*- CH_3		3.87 (t)	2.14 (m)	2.63 (t)	2.13 (s)		s	s
pyruvate	CH_3					2.38 (s)					s	–
succinate	2x CH_2					2.41 (s)					s, u	s, u
taurine	CH_2NH_2	CH_2SO_3				3.43 (t)	3.27 (t)				u	u
threonine	β-CH					4.27 (m)					s	s
trigonelline	H2	C6H	C4H	C5H	CH3	9.11 (s)	8.84 (m)	8.82 (m)	8.07 (m)	4.43 (s)	–	u
trimethylamine	CH_3					2.89 (s)					u	u
trimethylamine-N-oxide	CH3					3.27 (s)					u	u
tyrosine	2,6-CH	3,5-CH	CH	CH_2(i)	CH_2(ii)	7.20 (d)	6.90 (d)	3.90 (dd)	3.20 (dd)	3.10 (dd)	s, u	s, u
UNK	-					8.33 (d)					u	–
UNK	-					4.61 (bs)					s, u	–
UNK	-					4.40 (bs)					s, u	–
UNK	-					3.19 (bs)					s, u	–
UNK	-					2.56 (s)					s, u	–
UNK	-					2.49 (s)					u	–
UNK	-					2.46 (s)					s, u	s, u
UNK	-					2.45 (bs)					s, u	–
UNK	-					2.29 (bs)					s, u	–
UNK	-					2.11 (bs)					s, u	–
UNK	-					2.07 (bs)					s	
UNK	-					2.00 (q)					s	s
UNK	-					1.93 (bs)					s, u	–
UNK	-					1.86 (s)					u	–
UNK	-					1.80 (bs)					s, u	–
UNK	-					1.66 (bs)					s, u	–
UNK	-					1.41 (bs)					s, u	–
UNK	-					0.95 (bs)					s, u	–
UNK	-					0.90 (o)					u	–
urea	exchanged					5.75 (bs)					s, u	s, u
valine	αCH	βCH	γCH_3	γ′CH_3		3.62 (d)	2.28 (m)	0.99 (d)	1.04 (d)		s	s

4.4.3.2 Multivariate analyses of ^{1}H NMR spectroscopy of serum from patients with severe sepsis

The serum samples from the sepsis cohort consisted of 100 samples from the four time points with 15, 34, 31 and 20 samples from time points zero, one, two and three, respectively.

Multivariate analyses of the spectral data from the ^{1}H 1-D standard and CPMG NMR analyses of serum samples from the sepsis cohort were performed separately and followed the same pattern of PCAs and O-PLS-DAs performed on the spectral data of the urinary samples (section 4.4.2.2). Briefly, this consisted of PCAs of the dataset as a whole to provide an overview and identify outliers. This was followed by PCAs of samples from each time point, in addition to a separate PCA with samples from the first time point without evidence of AKI. In each case, one to three components were calculated for each model. O-PLS-DAs of samples from each time point were then performed, with separate models investigating each of the eight classes. Again, an additional model investigating the development of AKI after time point zero with the fore-mentioned subset of samples from TP0, was also performed.

4.4.3.2.1 Multivariate analyses of 1-D standard ^{1}H NMR spectroscopy of serum from patients with severe sepsis

The scores plot of a PCA of the 1-D standard NMR spectral data obtained from all the serum samples from the sepsis cohort is shown in Figure 4.11. The percentage of variance explained by this model was only 36.5% and although it failed to demonstrate any separation of the samples into groups, it did reveal seven outlying samples. Four intermediate outliers (near the boundaries of the Hotelling's perimeter); three in a cluster in right lower quadrant and near a fifth outlier and two extreme outliers in the right upper quadrants. Examination of the raw data revealed relatively high values of the metabolites in the spectra of these outliers, particularly in the region of 4.15-3.35 ppm and the two extreme outliers in the right upper quadrant were excluded from the data set (see Appendix III Figures 8 and 9). The raw data from the remaining 98 samples was then pre-processed again. A PCA model of the 1-D standard NMR data from this new data set was performed (shown in Figure 4.12). The variance

explained by this PCA model was 51.8%. It showed no clear separation of the samples into groups and no samples at the extremes of its axes; and no further samples were excluded from subsequent analyses. One to three components were calculated for each of PCA models based on samples from each time point. The results of evaluation parameters of these models are shown in Table 4.6. The variance explained by these models ranged from 0.527 to 0.686 and goodness of prediction (Q^2X) ranged from 0.19 to 0.407.

The results of the best O-PLS-DA models (based on 1-D standard ^{1}H NMR analyses of serum) used to investigate differences between samples from the dichotomised groups of the eight clinical classes are shown in Table 4.7 and Table 4.8A; and includes a separate model for each class for each of the available time points. The explained variation (R^2Y) and predictability (Q^2Y) of all the best models, ranged from 0.170 to 1 and -0.492 to 0.663, respectively. However, all the models were associated with p values above 0.05 that ranged from 0.072 to 1, consistent with no significant metabolic differences between any of groups of the eight clinical classes. The evaluation parameters of the O-PLS-DA models of respiratory, cardiovascular, and haematological dysfunction based on 1-D standard ^{1}H NMR analyses of serum samples divided into five groups is shown in Table 4.8B. The R^2Y and the Q^2Y values of these models, except the TP0 cardiovascular model were low and ranged from 0.066 – 0.4 and -0.284 – 0.035, respectively. The TP0 cardiovascular model, in contrast was associated with an R^2Y of 0.878 and a Q^2Y of 0.301; however, this resulted in a R^2Y - Q^2Y of 0.577 consistent with over-fitting. Moreover, the CV-ANOVA p values of all the models including this cardiovascular model were non-significant ($p > 0.05$) consistent no significant metabolic differences between the groups of these clinical classes.

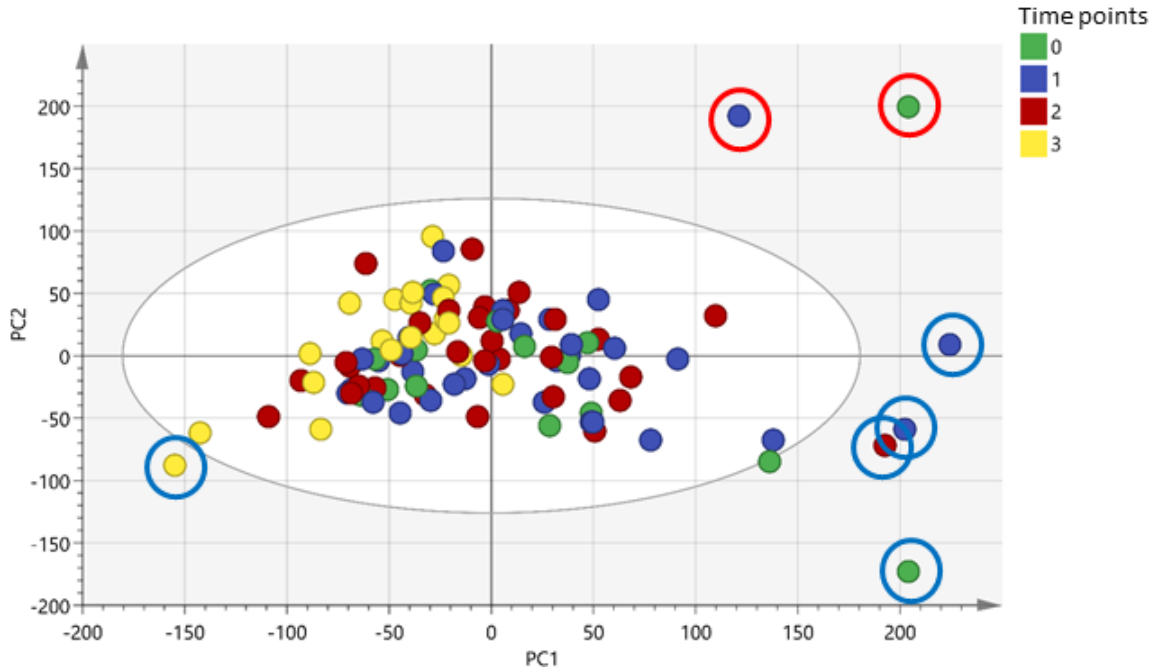


Figure 4.11 A PCA scores plot based on 1-D standard ^{1}H NMR spectra of all 100 serum samples from the sepsis cohort illustrating the metabolic variation of the data set as a whole and seven outlying samples: two extreme (circled in red) and five in close proximity to other samples (circled in blue). Samples from time points 0, 1, 2 and 3 are colour coded in green, blue, red, and yellow, respectively.

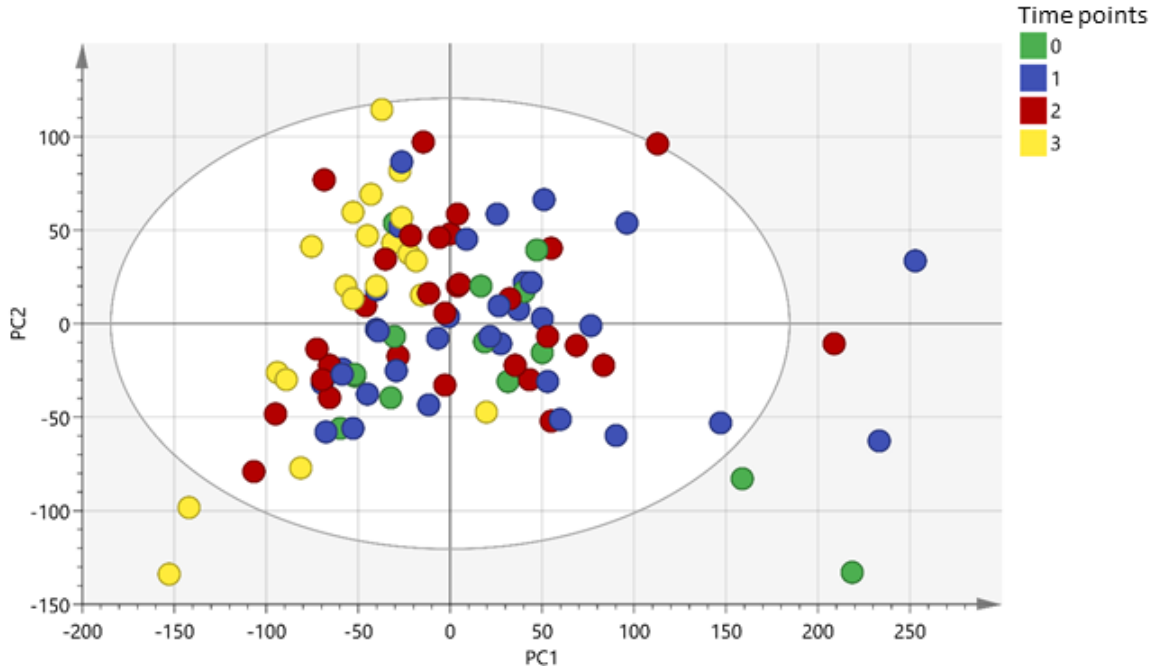


Figure 4.12. A PCA scores plot derived from 1-D standard ^{1}H NMR spectra of 98 serum samples from the sepsis cohort illustrating the metabolic variation of the data set as a whole following the exclusion of two extreme outlying samples shown in Figure 4.11. Samples from time points 0, 1, 2 and 3 are colour coded in green, blue, red, and yellow, respectively.

Table 4.6. Results of the evaluation parameters of PCAs based on 1-D standard ^{1}H NMR spectra of serum from the sepsis cohort. Key: PC: principal component; R^2X and Q^2X: variation explained and predicted by the model, respectively.

Principal Component Analyses							
Sample set: time point (n=sample number)	All samples (n=100)	All samples - two outliers (n=98)	Time point 0 without AKI (n=8)	Time point 0 (n=14)	Time point 1 (n=33)	Time point 2 (n=31)	Time point 3 (n=20)
Number of PCs	2	2	2	3	2	1	3
R^2X	0.517	0.518	0.644	0.686	0.531	0.527	0.686
Q^2X	0.371	0.469	0.190	0.310	0.407	0.403	0.311

Table 4.7 Results of the evaluation parameters of O-PLS-DA models of 1-D standard ^{1}H NMR spectra of serum from the cohort. Illustration of the percentage of the variation explained by the X (R^2X) and Y matrices (R^2Y) and predicted by the Y matrix (Q^2Y) of the models evaluating samples based on five clinical classes: the development of AKI after TP0, acute kidney injury*, acute liver injury*, 28-day survival and treatment group. KEY: CV-ANOVA: cross-validated analysis of variance, Group 0: good outcome (no injury or survival) or placebo treatment group, Group 1: poor outcome (injury or non-survival) or hydrocortisone treatment group, TP: time point; *: at that time point.

OPLS-DA		**AKI after TP0**	**Acute Kidney injury**				**Acute Liver injury**				**28 day survival**				**Treatment group**			
Sample set: time point		TP0 without	TP0	TP1	TP2	TP3	TP0	TP1	TP2	TP3	TP0	TP1	TP2	TP3	TP0	TP1	TP2	TP3
(n=sample number)		AKI (n= 8)	(n=14)	(n=33)	(n=31)	(n=20)	(n=14)	(n=33)	(n=31)	(n=20)	(n=14)	(n=33)	(n=31)	(n=20)	(n=14)	(n=33)	(n=31)	(n=20)
Group 0: good outcome		4	8	17	14	8	8	19	15	11	10	24	21	15	9.000	16	16	12
Group 1: poor outcome		4	6	16	17	12	6	14	16	9	4	9	10	5	5.000	17	15	8
Number of components	**Predictive**	1	1	1	1	1	1	1	1	1	1	1	1	1	1	1	1	1
	Orthogonal to X	0	2	0	0	1	2	1	1	1	0	0	2	0	2	2	0	1
Model statistics	**R^2X**	0.369	0.502	0.397	0.366	0.447	0.598	0.454	0.257	0.481	0.348	0.395	0.554	0.292	0.600	0.509	0.305	0.464
	R^2Y	0.464	0.940	0.234	0.244	0.571	0.927	0.534	0.689	0.652	0.365	0.287	0.661	0.308	0.843	0.750	0.244	0.571
	Q^2Y	-0.013	0.302	0.133	0.072	0.057	0.633	0.148	0.159	0.186	-0.083	0.161	0.122	-0.048	0.445	0.289	0.072	0.166
	$R^2Y - Q^2$	0.477	0.638	0.101	0.172	0.514	0.294	0.386	0.530	0.466	0.448	0.126	0.539	0.356	0.398	0.461	0.172	0.405
CV-ANOVA	**P VALUE**	1.000	0.643	0.118	0.351	0.920	0.098	0.326	0.323	0.512	1.000	0.072	0.761	1.000	0.359	0.147	0.816	0.575

Table 4.8 Results of the evaluation parameters of O-PLS-DA models of 1-D standard ^{1}H NMR spectra of serum from the cohort. Illustration of the percentage of the variation explained by the X (R^2X) and Y matrices (R^2Y) and predicted by the Y matrix (Q^2Y) of the models evaluating samples based on their respiratory, cardiovascular, and haematological clinical classes with the samples divided into two (A) and five groups (B). KEY: CV-ANOVA: cross-validated analysis of variance, SOFA: Sequential Organ Failure Assessment, TP: time point.

A

OPLS-DA		Respiratory				Cardiovascular				Haematological			
Sample set: time point (n=sample number)		TP0 (n=14)	TP1 (n=33)	TP2 (n=31)	TP3 (n=20)	TP0 (n=14)	TP1 (n=33)	TP2 (n=31)	TP3 (n=20)	TP0 (n=14)	TP1 (n=33)	TP2 (n=31)	TP3 (n=20)
Group 0: good outcome (no injury)		2	1	1	0	1	0	0	5	8	15	14	10
Group 1: poor outcome (injury)		12	32	30	20	13	33	31	15	6	18	17	10
Number of components	Predictive	1	1	1	N/A	1	N/A	N/A	1	1	1	1	1
	Orthogonal to X	0	0	0		0			0	1	0	1	0
Model statistics	R^2X	0.157	0.169	0.150		0.944			0.240	0.344	0.397	0.481	0.299
	R^2Y	0.440	0.345	0.328		1.000			0.228	0.632	0.170	0.395	0.354
	Q^2Y	-0.492	-0.305	-0.295		0.435			-0.178	-0.411	0.071	0.012	0.151
	$R^2Y - Q^2Y$	0.932	0.650	0.623		0.565			0.406	1.043	0.099	0.383	0.203
CV-ANOVA	P VALUE	1.000	1.000	1.000		0.990			1.000	1.000	0.331	0.988	0.249

B

OPLS-DA		Respiratory				Cardiovascular				Haematological			
Sample set: time point (n=sample number)		TP0 (n=14)	TP1 (n=33)	TP2 (n=31)	TP3 (n=20)	TP0 (n=14)	TP1 (n=33)	TP2 (n=31)	TP3 (n=20)	TP0 (n=14)	TP1 (n=33)	TP2 (n=31)	TP3 (n=20)
SOFA = 0		2	1	1	0	1	0	0	5	8	15	14	10
SOFA = 1		0	2	1	3	2	0	0	5	3	8	4	3
SOFA = 2		4	9	8	9	0	0	1	0	3	5	7	3
SOFA = 3		4	10	14	6	0	11	11	6	0	5	5	2
SOFA = 4		4	11	7	2	11	22	19	4	0	0	1	2
Number of components	Predictive	1	1	1	1	2	1	2	2	1	1	1	1
	Orthogonal to X	0	0	0	0	2	1	0	1	0	0	0	0
Model statistics	R^2X	0.269	0.349	0.198	0.312	0.671	0.479	0.445	0.664	0.350	0.399	0.363	0.222
	R^2Y	0.197	0.066	0.083	0.082	0.878	0.373	0.400	0.395	0.187	0.075	0.101	0.159
	Q^2Y	-0.016	0.032	-0.091	-0.163	0.301	-0.284	-0.035	0.026	-0.129	-0.023	-0.107	-0.014
	$R^2Y - Q^2Y$	0.213	0.034	0.174	0.245	0.577	0.657	0.435	0.369	0.316	0.099	0.208	0.173
CV-ANOVA	P VALUE	1.000	1.000	1.000	1.000	0.634	1.000	0.634	1.000	1.000	1.000	1.000	1.000

4.4.3.2.2 Multivariate analyses of ^{1}H CPMG NMR spectroscopy of serum from patients with severe sepsis

An overview of the ^{1}H CPMG NMR spectral data set as a whole was obtained using a PCA model of the data of all 100 serum samples from sepsis cohort. This was constructed using the first two PCs and the scatter scores plot of this model is shown in Figure 4.13. The percentage of variation explained by this model was 30.1% and it demonstrated some evidence of clustering of samples. This plot also demonstrated five outlying samples, three intermediate outliers and two extreme outliers, which were from the same samples as the extreme outliers excluded from the 1-D standard ^{1}H NMR dataset (see Section 4.4.3.2.1 and Appendix III Figures 10 and 11). These two samples were excluded from this data set and the remaining 98 spectra was pre-processed again, and the same method of PCA repeated. The scatter scores plot of this model demonstrated similar findings to the PCA of all 100 samples, with explained variation (R^2X) of 28.6%, in addition to a degree of clustering of some of the samples but no extreme outliers, as shown in Figure 4.14. No further samples were excluded from the data set and all subsequent analyses were performed using this data set of 98 samples.

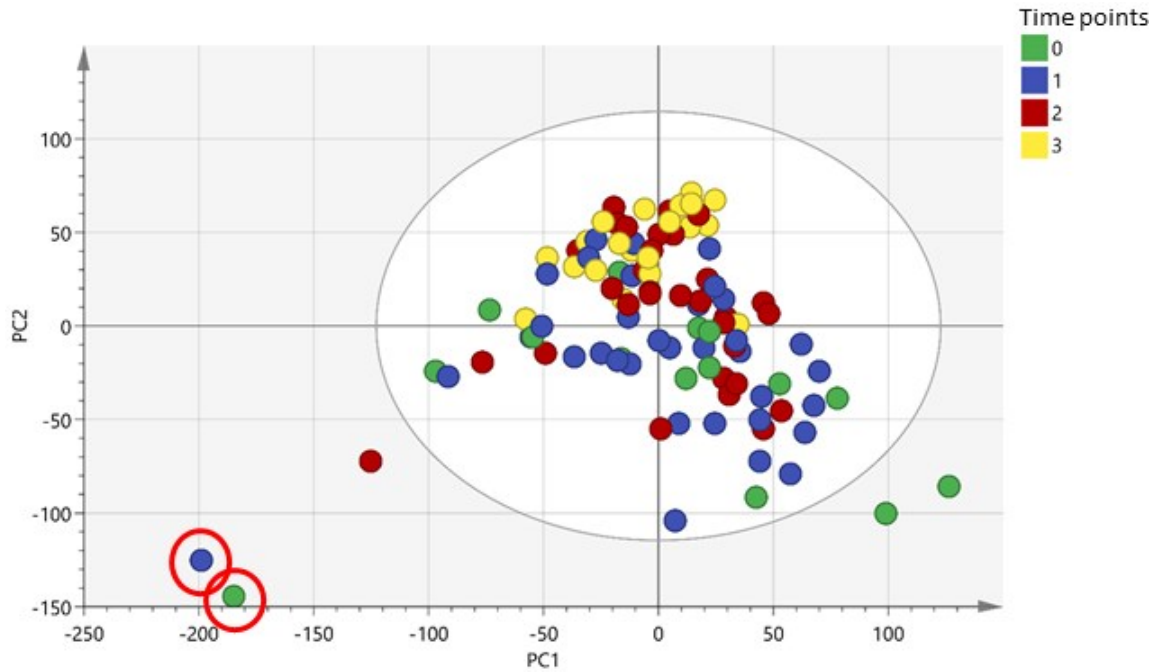


Figure 4.13. A PCA scores plot based on 1-D CPMG ^{1}H NMR spectra of all the 100 serum samples from the sepsis cohort illustrating the metabolic variation of the data set as a whole and two extreme outliers (circled in red). Samples from time points 0, 1, 2 and 3 are colour coded in green, blue, red, and yellow, respectively.

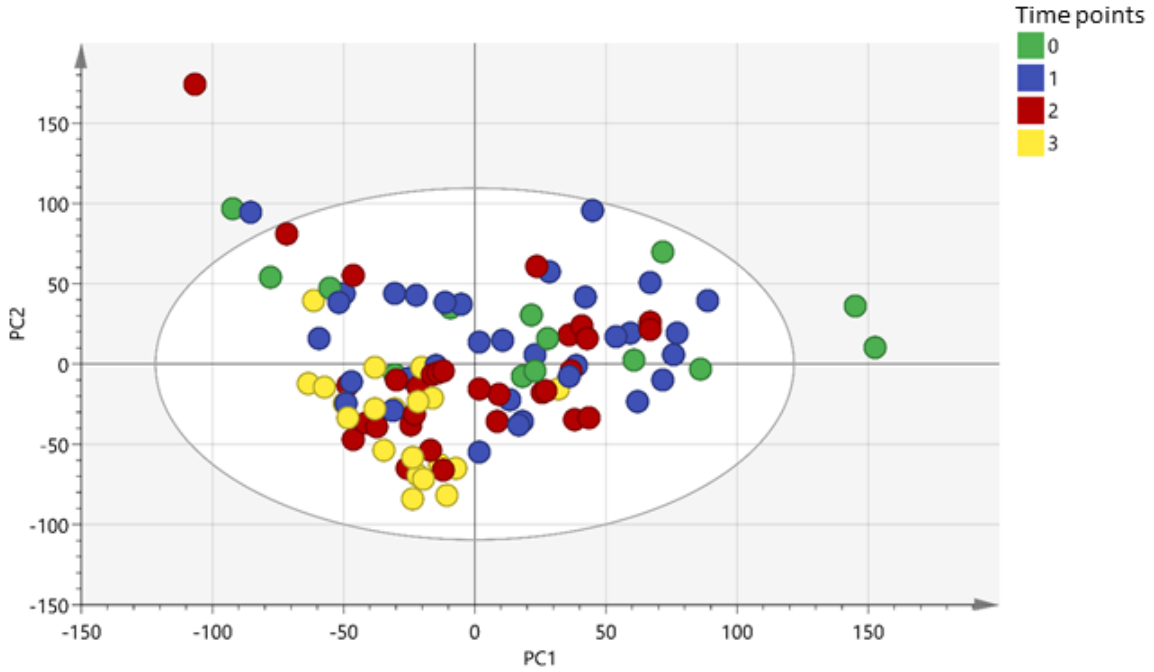


Figure 4.14. A PCA scores plot of 1-D CPMG ^{1}H NMR spectra of 98 serum samples from the sepsis cohort illustrating the metabolic variation of the data set as a whole following the exclusion of two extreme outlying samples shown in Figure 4.13. Samples from time points 0, 1, 2 and 3 are colour coded in green, blue, red, and yellow, respectively.

The results of the individual time point PCA models based on the 1-D ^{1}H NMR CPMG spectral data of the serum samples from each time point is shown in Table 4.9. All of these models were constructed using two principal components, except one model constructed using one. The variation explained by these models ranged from 0.308 to 0.557, whereas the goodness of prediction (Q^2X) ranged from 0.031 to 0.173. A PCA scores plot based on ^{1}H NMR CPMG spectra of serum samples from the sepsis cohort from time point three demonstrating a degree of separation according to their acute liver dysfunction classes is illustrated in Figure 4.15.

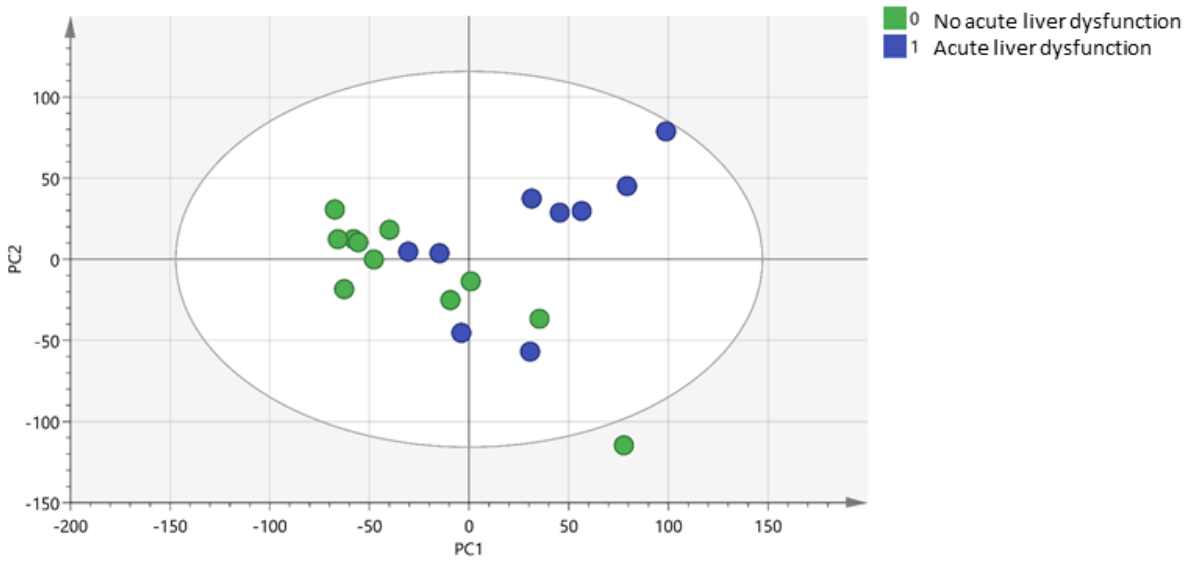


Figure 4.15. A PCA scores plot derived from 1-D CPMG ^{1}H NMR spectra of serum samples from the sepsis cohort from time point three (day seven) illustrating a degree of separation according to their acute liver dysfunction classes. KEY: Group 0: no acute liver dysfunction (green); Group 1: acute liver dysfunction (blue).

Orthogonal-PLS-DAs of the ^{1}H CPMG NMR spectral data of the serum samples from each time point were performed to investigate the metabolic differences between the dichotomised groups of each of the eight clinical classes and between the five individual SOFA groups of respiratory, cardiovascular, and haematological clinical classes. The results of the evaluation parameters of the best model in each

case, (i.e. the best one for each clinical class at each of the four time points) are shown in Tables 4.10, 4.11A and B. The predictability (Q^2Y) of eleven of these O-PLS-DA models was 0.247 or above.

This consisted of ten of the models with samples divided into two groups consisting of eight of the models of AKI, liver dysfunction, treatment, and 28-survival classes (shown in Table 4.10) and the time point zero cardiovascular and time point three haematological models (Table 4.11A); in addition to the cardiovascular time point zero model with the samples divided into five groups (shown in Table 4.11B). However, only two of these models (highlighted in blue in Table 4.10) have a CV-ANOVA associated with a significant p value of 0.05 or less; with one model having a CV-ANOVA associated with a p value just above this threshold at 0.064 and therefore not significant (highlighted in yellow in Table 4.10). The two models that have a CV-ANOVA associated with a significant p values were of acute liver injury and a treatment group model based on samples from time point one. In the case of the latter model, the large difference between the R^2Y and the Q^2Y of the model of greater 0.3 (0.578) indicated that this model was heavily over-fitted and was therefore deemed a poor model.

The acute liver injury model was constructed based on serum samples collected at the time point three (injury group n= 9; non-liver injury group n = 11) using one predictive PLS component. The uncross-validated scores plot of this O-PLS-DA model demonstrated three samples that were incorrectly identified as illustrated in Figure 4.16A. The percentage of explained variance and predictability of this model was 0.639 and 0.340, respectively. A method of CV-ANOVA was then applied to the O-PLS-DA model (as described in Section 1.6.3 and 2.5). The cross-validated scores plot of this model demonstrated a total of five incorrectly identified samples (as shown in Figure 4.16B) and the p value associated with this CV-ANOVA was 0.029.

Table 4.9 Results of the evaluation parameters of PCAs based on 1-D CPMG ^{1}H NMR spectra of serum from the sepsis cohort. Key: R^2X and Q^2X: variation explained and predicted by the model, respectively.

Principal Component Analyses							
Sample set: time point (n=sample number)	All samples (n=100)	All samples - two outliers (n=98)	Time point 0 without AKI (n=8)	Time point 0 (n=14)	Time point 1 (n=33)	Time point 2 (n=31)	Time point 3 (n=20)
Number of PCs	2	2	2	2	2	2	2
R^2X	0.301	0.286	0.557	0.431	0.308	0.330	0.311
Q^2X	0.197	0.247	0.031	0.143	0.173	0.162	0.068

Table 4.10. Composition and evaluation parameters of O-PLS-DA models of 1-D CPMG ^{1}H NMR spectra of serum from the sepsis cohort. Illustration of the percentage of the variation explained by the X (R^2X) and Y matrices (R^2Y) and predicted by the Y matrix (Q^2Y) of the models evaluating samples based on five clinical classes: the development of AKI after TP0, acute kidney injury*, acute liver injury*, 28-day survival and treatment group. KEY: CV-ANOVA: cross-validated analysis of variance, Group 0: good outcome (no injury or survival) or placebo treatment group, Group 1: poor outcome (injury or non-survival) or hydrocortisone treatment group, TP: time point; *: at that time point.

OPLS-DA		AKI after TP0	Acute Kidney injury				Acute Liver injury				28 day survival				Treatment group			
Sample set: time point		TP0 without	TP0	TP1	TP2	TP3	TP0	TP1	TP2	**TP3**	TP0	TP1	TP2	**TP3**	TP0	**TP1**	TP2	TP3
(n=sample number)		AKI (n= 8)	(n=14)	(n=33)	(n=31)	(n=20)	(n=14)	(n=33)	(n=31)	**(n=20)**	(n=14)	(n=33)	(n=31)	**(n=20)**	(n=14)	**(n=33)**	(n=31)	(n=20)
Group 0: good outcome		4	8	17	14	8	8	19	15	**11**	10	24	21	**15**	9.000	**16**	16	12
Group 1: poor outcome		4	6	16	17	12	6	14	16	**9**	4	9	10	**5**	5.000	**17**	15	8
Number of components	**Predictive**	1	1	1	1	1	1	1	1	**1**	1	1	1	**1**	1	**1**	1	1
	Orthogonal to X	1	1	1	2	2	1	2	1	**0**	2	0	1	**0**	2	**2**	1	1
Model statistics	**R^2X**	0.453	0.371	0.199	0.575	0.323	0.341	0.267	0.222	**0.175**	0.445	0.127	0.214	**0.178**	0.456	**0.290**	0.208	0.150
	R^2Y	0.945	0.887	0.792	0.953	0.983	0.903	0.921	0.780	**0.639**	0.989	0.451	0.781	**0.617**	0.989	**0.955**	0.806	0.948
	Q^2Y	0.261	0.427	0.247	0.308	0.159	0.114	0.208	0.079	**0.340**	-0.165	-0.035	0.197	**0.276**	0.466	**0.377**	0.229	0.154
	$R^2Y - Q^2$	0.684	0.460	0.545	0.645	0.824	0.789	0.713	0.701	**0.299**	1.154	0.486	0.584	**0.341**	0.523	**0.578**	0.577	0.794
CV-ANOVA	**P VALUE**	0.719	0.239	0.084	0.146	0.324	0.877	0.370	0.694	**0.029**	1.000	1.000	0.206	**0.064**	0.321	**0.040**	0.136	0.614

Table 4.11 Results of the evaluation parameters of O-PLS-DA models of 1-D CPMG ^{1}H NMR spectra of serum from the cohort. Illustration of the percentage of the variation explained by the X (R^2X) and Y matrices (R^2Y) and predicted by the Y matrix (Q^2Y) of the models evaluating samples based on their respiratory, cardiovascular, and haematological clinical classes with the samples divided into two (A) and five groups (B). KEY: CV-ANOVA: cross-validated analysis of variance, SOFA: Sequential Organ Failure Assessment, TP: time point.

A

OPLS-DA		Respiratory				Cardiovascular				Haematological			
Sample set: time point (n=sample number)		TP0 (n=14)	TP1 (n=33)	TP2 (n=31)	TP3 (n=20)	TP0 (n=14)	TP1 (n=33)	TP2 (n=31)	TP3 (n=20)	TP0 (n=14)	TP1 (n=33)	TP2 (n=31)	TP3 (n=20)
Group 0: good outcome (no injury)		2	1	1	0	1	0	0	5	8	15	14	10
Group 1: poor outcome (injury)		12	32	30	20	13	33	31	15	6	18	17	10
Number of components	Predictive	1	1	1	N/A	1	N/A	N/A	1	1	1	1	1
	Orthogonal to X	0	3	2		2			2	0	0	2	3
Model statistics	R^2X	0.292	0.356	0.245		0.482			0.292	0.200	0.140	0.262	0.401
	R^2Y	0.347	0.984	0.981		0.993			0.984	0.928	0.458	0.959	0.998
	Q^2Y	-0.246	0.006	0.044		0.327			0.149	-0.315	0.045	0.119	0.556
	$R^2Y - Q^2Y$	0.593	0.978	0.937		0.666			0.835	1.243	0.413	0.840	0.442
CV-ANOVA	P VALUE	1.000	1.000	0.951		0.593			0.880	1.000	0.503	0.772	0.116

B

OPLS-DA		Respiratory				Cardiovascular				Haematological			
Sample set: time point (n=sample number)		TP0 (n=14)	TP1 (n=33)	TP2 (n=31)	TP3 (n=20)	TP0 (n=14)	TP1 (n=33)	TP2 (n=31)	TP3 (n=20)	TP0 (n=14)	TP1 (n=33)	TP2 (n=31)	TP3 (n=20)
SOFA = 0		2	1	1	0	1	0	0	5	8	15	14	10
SOFA = 1		0	2	1	3	2	0	0	5	3	8	4	3
SOFA = 2		4	9	8	9	0	0	1	0	3	5	7	3
SOFA = 3		4	10	14	6	0	11	11	6	0	5	5	2
SOFA = 4		4	11	7	2	11	22	19	4	0	0	1	2
Number of components	Predictive	2	1	1	1	2	1	2	2	1	1	1	1
	Orthogonal to X	2	1	0	0	1	0	1	0	0	0	0	0
Model statistics	R^2X	0.535	0.223	0.149	0.085	0.492	0.141	0.317	0.240	0.172	0.155	0.110	0.187
	R^2Y	0.647	0.205	0.115	0.282	0.897	0.405	0.627	0.514	0.312	0.161	0.168	0.221
	Q^2Y	0.043	-0.054	-0.080	-0.236	0.361	-0.131	-0.091	-0.014	-0.246	-0.005	-0.081	0.036
	$R^2Y - Q^2Y$	0.605	0.259	0.195	0.518	0.536	0.536	0.718	0.528	0.558	0.166	0.249	0.185
CV-ANOVA	P VALUE	1.000	1.000	1.000	1.000	0.466	1.000	0.959	1.000	1.000	0.996	1.000	0.996

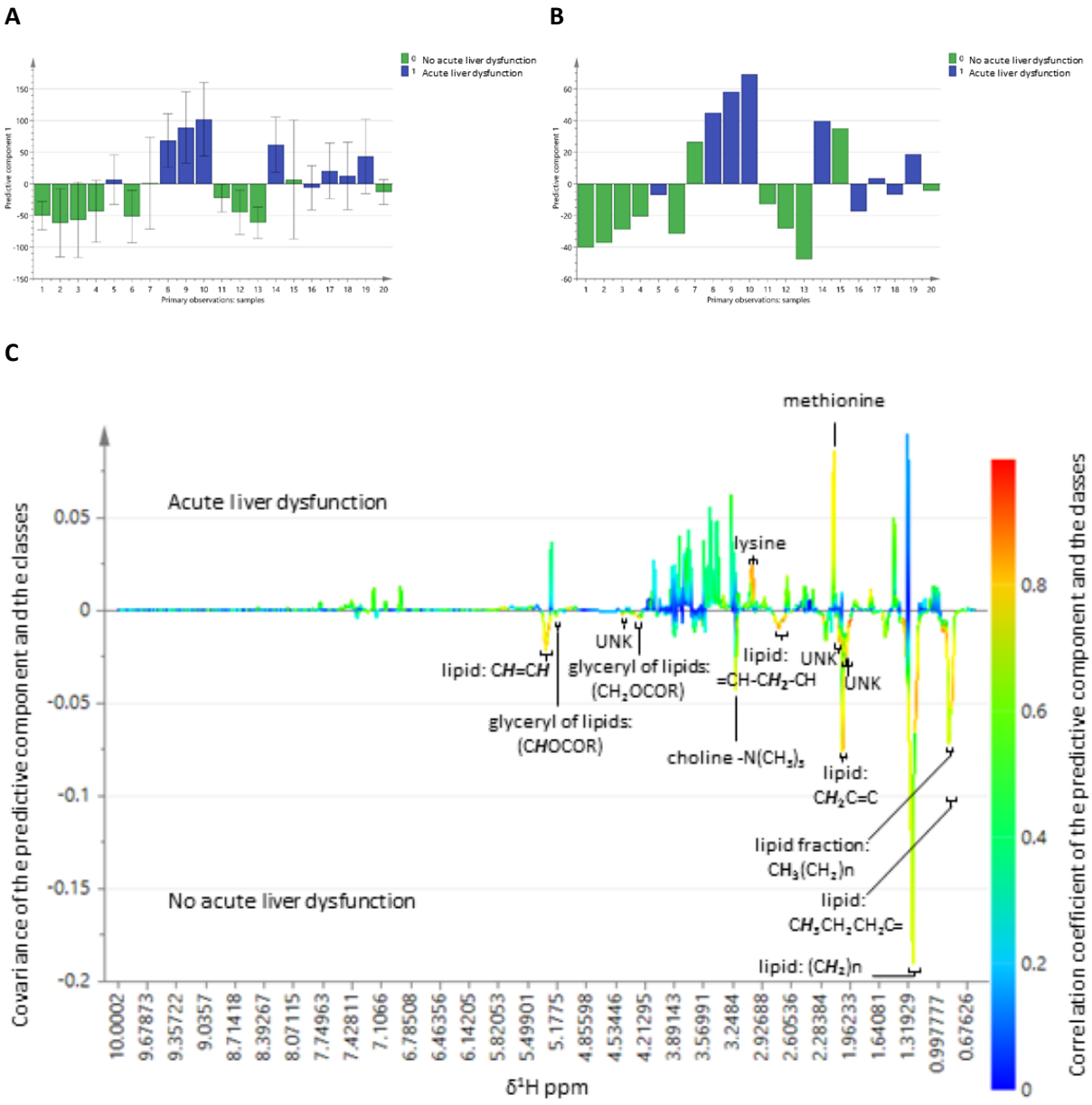


Figure 4.16. O-PLS-DA scores (A) and cross validated scores (B) plots derived from 1-D CPMG ^{1}H NMR spectra of serum from the sepsis cohort taken at time point three (day seven) illustrating separation of samples according to the presence or absence of acute liver dysfunction (R^2X=0.175, R^2Y=0.639; Q^2Y=0.340). The cross-validated scores plot illustrates the significance of the observed group separation measured using a method of CV-ANOVA (p=0.029). The corresponding O-PLS-DA loadings plot (C) illustrating the covariance and correlation coefficients of the metabolite signals of the predictive component of the model responsible for the separation of the acute liver injury groups. KEY: CV-ANOVA: cross-validated analysis of variance, UNK: unknown.

An S-line loadings plot of this O-PLS-DA model was used to identify the metabolite signals with the greatest contribution to the separation of these two groups of samples to determine the key metabolic differences between the two acute liver injury groups, as shown in Figure 4.16C. The loadings plot demonstrates both the covariance and the correlation coefficient between the metabolites and classification information. On an S-line loadings plot of an O-PLS-DA, the metabolite signals are displayed in a form that resembles the raw data, in this case, NMR spectra, and are coloured according to their degree of correlation (coefficient) with the two acute liver injury groups of the model. The correlation coefficient is represented by a colour scale that is illustrated in the colour bar on the right-hand side of the plot. The colours at the top of scale (red in Figure 4.16C) are used to represent the signals with the greatest influence on the separation of the two groups by the model's predictive component. The direction of change of the signals in relation to the two groups (covariance) is shown by the y-axis. An upwards and downwards deflection of the signals, represents a positive and negative covariance with the group with positive loadings values on the model's corresponding scores plot, respectively. In the O-PLS-DA scores plots shown in Figures 4.16A and 4.16B, the group associated with positive scores along the PLS predictive component is group one: the patients with acute liver injury (labelled in blue). Upwards deflections on this model's S-line loadings plot (Figure 4.16C) therefore represents metabolites that were higher in group one compared with the non-liver injury group, i.e. a positive covariance. It is noted that the samples incorrectly identified as a belonging to group one, i.e. from patients group zero (labelled in green) will also have positive scores on these O-PLS-DA scores plots. Conversely, downward deflections on this S-line plot reflects metabolites that are lower in the liver injury group than the non-liver injury. In both cases, the importance of this difference to the separation of the two groups is reflected by the correlation co-efficient, with a higher value indicating a greater importance to the separation (y axis on the right-hand side). The metabolites with signals in this O-PLS-DA model with a correlation coefficient of greater than 0.6 are listed in Table 4.12. This illustrates that the metabolites with the greatest influence on the separation of the two groups of acute liver injury were predominantly lipids, with a decrease in the acute liver injury group

compared with group without acute liver injury. Of these, the lipid signals at 0.83 and 0.87 ppm were consistent with the lipid signals of LDL and VLDL, respectively (Nicholson, Foxall, Spraul, *et al.*, 1995). Other metabolite changes of great importance to this separation were a decrease in choline and increases in the amino acids lysine and methionine, in the group with acute liver injury compared to the one without.

Table 4.12. Metabolic differences identified by O-PLS-DA models of acute liver injury based on ^{1}H NMR CPMG spectra of serum taken at time point three (day seven) from the sepsis cohort, constructed with one predictive and no orthogonal components. The percentage of the variation explained by the X (R^2X) and Y matrices (R^2Y), and predicted by the Y matrix (Q^2Y) of this model was 0.175, 0.639 and 0.340, respectively, and the p value of the CV-ANOVA was 0.029. Key: CV-ANOVA: cross-validated analysis of variance, s: singlet; d: doublet; t: triplet; q: quartet; m: multiplet; bs: broad signal; ↑ and ↓: increased and decreased levels of metabolites in acute liver injury compared with patients without liver injury, respectively.

Metabolite Identity	H groups	δ ^{1}H (multiplicity)	^{1}H δ ppm	Change	Correlation coefficient
choline	N-(CH_3)$_3$	s	3.21	↓	0.719
glyceryl of lipids	CHOCOR	bs	5.18	↓	0.733
glyceryl of lipids	C***H*** $_2$OCOR	m	4.27	↓	0.792
lipid signal	C***H*** =C***H***	bs	5.30	↓	0.791
lysine	εCH_2	t	3.03	↑	0.836
lipid signal	CH-C**H$_2$**-CH	bs	2.71	↓	0.802
lipid signal	C***H*** $_2$C=C	bs	2.01	↓	0.771
lipid signal	(CH_2)n	bs	1.27	↓	0.722
lipid signal	C***H*** $_3$$CH_2$$CH_2$C=	bs	0.87	↓	0.708
lipid signal	C***H*** $_3$(CH_2)$_n$	bs	0.83	↓	0.764
methionine	*S*- CH_3	s	2.13	↑	0.764
UNK	-	q	2.00	↓	0.803
UNK	-	bs	2.07	↓	0.816
UNK	-	bs	4.40	↓	0.840

4.5 Discussion

A method of metabolic profiling utilising 1-D standard and CPMG ^{1}H NMR spectroscopy was used in this study to characterise the metabolic response of the cohort of patients with sepsis as a consequence of acute organ dysfunctions, 28-day survival and steroid treatment. The metabolic profiling based on 1-D standard ^{1}H NMR of urine samples failed to demonstrate any metabolic differences between the dichotomised groups of each of these eight classes and five groups of three of these classes under investigation. This could be explained by the absence of differentiating metabolic signatures of these clinical conditions or a failure to detect them. Metabolic differences were, however, demonstrated between the patients with liver injury using a profiling technique based on the ^{1}H NMR CPMG analyses of their serum. The results demonstrated by these serum analyses argue against the absence of differentiating metabolic signatures of all of these clinical classes. Whereas the theory of failure of the urinary NMR analyses to detect the metabolic signatures of the liver injury is supported by the absence of the signals of the key metabolites identified by the serum analyses. These metabolic differences fell into three main categories: amino acids, lipoproteins, and lipids, each of which will be discussed in turn.

4.5.1 Amino acids in sepsis related liver injury

4.5.1.1 Increases in serum levels of lysine and methionine

Plasma levels of amino acids are a balance of their utilisation by organs, tissues, and catabolism on the one hand and their supply sources on the other. Increases in the serum levels of lysine and methionine were demonstrated on day seven of this study in the patients from the sepsis cohort with liver injury compared to those without. Theorising on the causes of these differences requires an understanding of the amino acid changes that occur in sepsis, the metabolism of lysine and methionine and how both may be affected by liver injury.

In sepsis, a small number of amino acids increase, which are the aromatic amino acids; phenylalanine, tyrosine, and tryptophan, the sulphur containing amino acids; methionine, cysteine and taurine and a dibasic amino acid, lysine. Whereas, a larger group that includes the aliphatic, acidic, and neutral amino acids and the dibasic amino acid arginine, decrease in sepsis. Examples of the aliphatic group includes; alanine, glycine and the three branched-chain amino acids (BCAAs), leucine, valine, and isoleucine. Glutamic and aspartic acid are the two acidic amino acids and asparagine, serine, threonine, and glutamine are the main neutral amino acids.

Sepsis is characterised by widespread proteolysis resulting in the release of amino acids from structural protein stores, especially from skeletal muscle (Hasselgren, Pedersen, Sax, *et al.*, 1988). At the same time, there is an increase in protein synthesis by the liver associated with enhanced hepatic extraction of amino acids (Druml, Heinzel & Kleinberger, 2001). There is also greater utilisation of amino acids as a fuel source, especially the BCAAs by peripheral tissues (Druml, Heinzel & Kleinberger, 2001). Despite increases in protein synthesis in the liver In sepsis, there is an overall net protein loss (Hasselgren, Pedersen, Sax, *et al.*, 1988).

Proteins contain 20 different amino acids. The fate of the amino acids released from proteins can be divided into their roles and their catabolism. The main role of these 20 amino acids is protein synthesis (Druml, Heinzel & Kleinberger, 2001). In sepsis, there is an increase in protein synthesis in the liver (Druml, Heinzel & Kleinberger, 2001). Any impairment in the synthetic function of the liver such as the hepatocellular injury associated with sepsis, could inhibit this process (Nesseler, Launey, Aninat, *et al.*, 2012). The inhibition of protein synthesis, however, should result in an increase in all the proteinogenic amino acids. This on its own therefore, is unlikely to be responsible for the increase in just two of the twenty proteinogenic amino acids (methionine and lysine), seen in the liver injury group in this study. However, in sepsis, the BCAAs are mainly extracted by peripheral tissues and used as a

fuel source. Furthermore, the main difference between the BCAAs and the other amino acids that demonstrate decreases in sepsis and the group containing the lysine and the aromatic and sulphur-containing amino acids that are associated with increases in sepsis, is the latter are more dependent on the liver for their catabolism (Brosnan & Brosnan, 2006; Tomé & Bos, 2007; Baile, Buckman, Lenzi, *et al.*, 2000; Dejong, van de Poll, Soeters, *et al.*, 2007).

Inhibition of the catabolism of lysine and methionine by the liver in the liver injury group of sepsis cohort is therefore, one possible explanation for the increases in these two amino acids in this group, compared to the group without liver injury. This alone, however, would be not explain the isolated increases in lysine and methionine given that the aromatic and sulphur-containing amino acids are also dependent on the liver for their metabolism. Possible explanations of how these findings and how they may co-exist will now be discussed.

Methionine is a sulphur containing amino acid (Brosnan & Brosnan, 2006); whereas lysine is a di-basic mono-carboxylic amino acid (Tomé & Bos, 2007). Despite their structural differences, they have two important metabolic features in common that are both dependent on the liver. The first is their role as the two precursors of the di-peptide carnitine and the second is their catabolism.

In humans, the biosynthesis of carnitine primarily occurs in the liver and kidneys from methionine and lysine (following three successive methylations of lysine to form trimethyllysine) (Bach, 1982). Carnitine is an essential factor in the β-oxidation of medium and long chain fatty acids and it has also been implicated in the oxidation of BCAAs (Bach, 1982). In β-oxidation of fatty acids, carnitine is responsible for transporting activated fatty acids across the inner mitochondrial membrane to enable their oxidation within the mitochondrial matrix. Although the formation of butyrobetaine from these

two amino acids can occur in any tissue, only the liver, kidneys and brain are capable of converting butyrobetaine to carnitine (Bach, 1982). Impairment in carnitine biosynthesis secondary to hepatic dysfunction could therefore be responsible or at least a contributing factor, in the increases in methionine and lysine demonstrated in the patients from the sepsis cohort with impaired liver compared to those without.

Methionine is also an important methyl donor (Brosnan & Brosnan, 2006). Following activation to *S*-adenosylmethionine (SAM), methionine donates a methyl group to an acceptor *via* a methyltransferase. There are over 60 methyltransferases in humans but there are two major ones. These are phosphatidylethanolamine *N*-methyltransferase (PEMT) which converts phosphatidylethanolamines (PEs) to phosphatidylcholines (PCs) and guanidoacetate *N*-methyltransferase (GNMT) which is responsible for creatine synthesis. This transmethylation reaction converts *S*-adenosylmethionine into *S*-adenosylhomocysteine (SAH) which is then hydrolysed to homocysteine and adenosine. Homocysteine then has two possible fates: catabolism *via* transsulfuration or remethylation to methionine.

Transsulfuration is the main route of methionine catabolism and takes place in the liver (Brosnan & Brosnan, 2006). Glycine *N*-methyltransferase is also capable of methionine catabolism but this only appears to occur when plasma methionine levels are high and also occurs in the liver (Brosnan & Brosnan, 2006). Methionine transsulfuration involves the conversion of homocysteine to cystathionine by cystathionine beta synthase followed by the conversion of cystathionine to cysteine by cystathionase. Cysteine can then be transformed into the tripeptide glutathione or used in proteins (Brosnan & Brosnan, 2006).

Glutathione is a host defence mediator that plays an important role in sepsis and many studies have demonstrated increases in its plasma levels in sepsis. These have included studies of the kinetics of methionine in sepsis that have demonstrated increases in the transsulfuration of methionine to cysteine are associated with an increase in the synthesis of glutathione in sepsis (Malmezat, Breuille, Pouyet, *et al.*, 2000). The catabolism of methionine *via* this transsulfuration pathway appears to be controlled by the demand for transmethylation. *S*-adenosylhomocysteine promotes its own production *via* positive feedback of the transmethylation of *S*-adenosylmethionine into *S*-adenosylhomocysteine, in addition to promoting the enzymes of transsulfuration and inhibiting the remethylation of homocysteine to methionine. When methionine levels exceed transmethylation demand, methionine cannot undergo transsulfuration (catabolism) which occurs in sequence after its transmethylation (Brosnan & Brosnan, 2006).

Both the transsulfuration and remethylation of homocysteine are dependent on the liver (Mato, Martínez-Chantar & Lu, 2008; Russmann, Junker & Lauterburg, 2002). Acute liver injury could therefore, result in no overall net change in serum levels of methionine, owing to both a reduction in the catabolism (transsulfuration of SAH) and regeneration of methionine (remethylation of SAH). However, the increases in glutathione synthesis *via* the trans-sulfuration pathway of the liver demonstrated in sepsis, could contribute to differences between patients with and without liver injury. Overall therefore, impairment of the trans-sulfuration pathway of the methionine cycle in the liver of the patients in liver injury group could explain the increased level of methionine in this group compared with the non-liver injury group. The lack of an associated decrease in glutathione in the liver injury group compared to the group without liver injury is however, unexplained.

In humans, the catabolism of lysine principally occurs in the liver through the saccharopine pathway (Tomé & Bos, 2007). This results in the formation of glutamate and α-aminoadipate and is an

irreversible process that is followed by deamination and obligatory oxidation (Tomé & Bos, 2007). This catabolism usually occurs at a constant rate, unless there is drop in lysine plasma levels to less than sixty percent. Hepatocellular injury would therefore be expected to impair this process and cause a rise in lysine plasma levels.

Individually, both sepsis and liver diseases have been shown to be associated with increases in sulphur- containing and aromatic amino acids and decreases in BCAAs (Mato, Martínez-Chantar & Lu, 2008; Russmann, Junker & Lauterburg, 2002; Basler, Meier-Hellmann, Bredle, *et al.*, 2002; Honda, Fukuda, Nakano, *et al.*, 2004; Ishikawa, 2012; Azuma, Maekawa, Kuwabara, *et al.*, 1989; Dejong, van de Poll, Soeters, *et al.*, 2007; Su, Li, Xie, *et al.*, 2015). This study extends the results of previous studies by comparing patients with sepsis and liver dysfunction to those with sepsis alone. In this sepsis cohort, no differences were demonstrated in the serum levels of either aromatic or branched-chain amino acids between those with or without liver injury.

The aromatic amino acids (AAAs) tyrosine and phenylalanine are dependent on the liver for their catabolism (Dejong, van de Poll, Soeters, *et al.*, 2007). Both tyrosine and phenylalanine were detected in the serum of the sepsis patients but no significant differences were demonstrated between those with or without liver injury. In the case of phenylalanine this may be explained by confounding factors such as exogenous sources of phenylalanine such as antibiotics (e.g. Co-amoxiclav). There is also some evidence that phenylalanine catabolism can also occur in the renal cortex of patients with the liver injury (Dejong, van de Poll, Soeters, *et al.*, 2007). The lack of a significant difference in the levels of tyrosine between the two groups is an unexpected finding. The aromatic region of the NMR spectral arrays where tyrosine resonances are located does contain several drug resonances resulting in a moderate degree of overlap of some of the resonances but this does not appear to affect the tyrosine ones. An alternative explanation for the lack of observed differences in the levels of tyrosine between

the liver injury and non-injury group is that the severity of the dysfunction in the liver injury group was insufficient to cause a significant rise in tyrosine. This theory is supported by the correlation between liver failure severity and plasma tyrosine: BCAA ratios (Yang, He, Cao, *et al.*, 2012).

The branched chain amino acids are unique in that they can be metabolised independently of the liver (De Bandt & Cynober, 2006). This could explain the lack of a significant difference between the patients with and without acute liver dysfunction.

The dichotomy in the levels of plasma amino acids that has been demonstrated in sepsis, in which the majority of amino acids decrease; whereas the levels of lysine, aromatic and sulphur-containing amino acids increase (Druml, Heinzel & Kleinberger, 2001) is presumed to be due to sepsis-related liver injury. This hypothesis is based on the essential role of the liver in the catabolism of the amino acids in the latter group, but this has not been confirmed. Increased levels of only two of amino acids from the latter group were demonstrated in the patients from the sepsis cohort with liver injury on day seven of the study compared to those without: lysine and methionine. This difference can in part be explained by the roles of these amino acids in the synthesis of carnitine and glutathione. Thus, although all the other amino acids in this group are dependent on the liver for their catabolism, these are the only two amino acids have been shown to have important synthetic roles in sepsis that will be affected by liver injury.

4.5.5 Lipoproteins and lipids in sepsis related liver injury

4.5.5.1 Decreases in serum levels of VLDL and LDL

In this study, decreases in signals consistent with those of very low-density lipoproteins (VLDL; at 0.87ppm) and its remnant low density lipoproteins (LDL; at 0.83 ppm) were demonstrated in the

serum samples of patients from a sepsis cohort with liver injury compared to those with normal liver function. Lipoproteins are essential to the transport of lipids in blood and are dependent on the liver for their synthesis (Murch, Collin, Hinds, *et al.*, 2007).

In sepsis, there are several changes that promote increases in the production of triacylglycerols (TAG) that are exported by the liver in VLDLs and result in increases in plasma levels of VLDLs and LDLs (Wendel, Paul & Heller, 2007). These include increases in lipolysis, resulting in increases in free fatty acids (FFA) that are taken up by the liver, in addition to the inhibition of fatty acid oxidation within the liver. These result in an increase in the conversion of fatty acids into TAGs, instead of their catabolism. The liver is solely responsible for the synthesis of components of VLDLs and their formation (Murray & Davis, 2003). The levels of circulating VLDL and LDL are therefore dependent on the synthetic function of the liver.

Sepsis-related liver injury has been shown to involve a combination of both hepatocellular injury and cholestasis (Nesseler, Launey, Aninat, *et al.*, 2012). Both of these processes can affect the synthetic function of the liver and could be responsible for the reductions in VLDL and LDL seen in the liver injury group. This may be as a consequence of impairments of the synthesis of the components of VLDLs, their assembly or both.

Reductions in VLDL and LDL have been demonstrated by other NMR profiling studies of liver dysfunction. Jiménez et al demonstrated reductions in LDL, as well as unsaturated lipids, in a cohort of patients with liver cirrhosis compared to a group of healthy controls, (Jiménez, Montoliu, Macintyre, *et al.*, 2010). Moreover, the sub-group of patients with acutely decompensated cirrhosis with evidence of hepatic encephalopathy demonstrated significantly lowered levels of both VLDL and LDL.

High density lipoproteins (HDL), form the other major group of lipoproteins. The main role of HDLs is the transport of circulating cholesterol to the liver. The mature HDL_2 evolves from an immature preβ-HDL (Murch, Collin, Hinds, *et al.*, 2007) within the circulation from apoprotein A-1 (apo-A1) from the liver, lipids from circulating chylomicrons, and free cholesterol and phospholipids from peripheral tissues to form HDL_3. Followed by the acquisition of further lipids and apoproteins by the HDL_3, through exchanges with other lipoproteins, including VLDLs, to produce the mature HDL_2 (Murch, Collin, Hinds, *et al.*, 2007).

In this study, no significant differences were demonstrated in the serum levels of HDL between those with and without liver injury. However, HDL was not identified by the NMR spectroscopic analyses of the serum samples in this study. There are several possible explanations that could explain this finding. These can be divided into factors related to the detection of HDL using 1-D ^{1}H NMR spectroscopy (Nicholson, Foxall, Spraul, *et al.*, 1995) and changes in the morphology of HDLs that occur in sepsis (Murch, Collin, Hinds, *et al.*, 2007). The detection of lipoproteins using NMR spectroscopy is based on signals produced as a result of the individual composition of lipids of associated with each subtype, as opposed to the protein present (Nicholson, Foxall, Spraul, *et al.*, 1995). Nuclear magnetic resonance signals of the individual lipids such as the TAGs within the lipoproteins are also detectable.

NMR spectroscopy is capable of identifying HDL in serum samples but these signals are difficult to detect in 1-D ^{1}H NMR spectra and often require the use non-standard pulse sequences or 2D spectroscopy (Nicholson, Foxall, Spraul, *et al.*, 1995). Signals of HDL molecules are usually located at 0.66 ppm on 1-D ^{1}H NMR spectra (Nicholson, Foxall, Spraul, *et al.*, 1995). These signals are produced by the cholesterol contained within the HDL molecule. Many of the pathways implicated in the immunomodulatory role of HDL in sepsis involve the lipids within the HDL molecule. These include esterified cholesterol (CE) and phospholipids, especially lysophosphatidylcholines and sphingolipids.

Given the evidence of the numerous interactions between HDL and the key mediators of sepsis, and the integral role of the liver and VLDL in the construction and function of HDL, it seems more likely that the levels of HDL, like those of VLDL and LDL were lower in the liver injury group but this difference was not detected by the NMR spectroscopy. This may be due to incredibly low levels in both groups and or as a result of modifications of the HDLs in sepsis resulting in NMR signals that are not recognised as belonging to HDL. However, the most likely explanation is that the NMR pulse sequences used in this study were not capable of detecting HDLs.

4.5.5.2 Decreases in serum levels of lipids

Decreases in the serum levels of several lipid signals were demonstrated in patients from the sepsis cohort with liver dysfunction, compared to those without on day seven of the study using a method of metabolic profiling based on CPMG analyses of serum coupled with multivariate statistical analyses. This consisted of decreases in eight lipid signals including two signals of the glycerol of lipids. Lipids with a glycerol backbone are called glycerides and are formed by the esterification of fatty acids to the glycerol molecule. Glycerides are divided into two groups. The first group are nonpolar, neutral glycerides. These can have fatty acids attached to one, two or all three of the carbon groups of the glycerol molecule and are called mono-, di- and tri-acylglycerols (more commonly known as tri-glycerides), respectively; triacylglycerols being the predominant form of lipids obtained from the diet. The other group, the phosphoglycerides have fatty acids attached to two of the carbon atoms and a phosphoryl group attached to the third. Serum levels of choline were also shown to be reduced in the liver injury group compared to non-liver injury group, in addition to lipids. Taken together this may indicate a reduction in choline containing lipids such as the phosphoglycerides, phosphatidylcholine, or two of its derivatives lysophosphatidylcholine and sphingomyelin. NMR is not a good analytical platform for identifying lipids and determining lipid species; therefore, further speculation of these species cannot be made of the basis of the NMR data of this study. As described in Section 2.4.5, ^{1}H

NMR CPMG spectra were acquired in addition to the 1-D standard ^{1}H NMR spectra of the serum samples to attenuate the signals from macromolecules such as albumin and some lipids to improve the resolution of lower molecular weight molecules. The 1-D standard NMR of serum should have been the better for lipid analysis than the CPMG spectra. It is however, possible that the attenuation of very large lipids and other non-lipid macromolecules in CPMG spectra was responsible for improvements in the visualisation of the differentiating lipids of this study.

The methods of ^{1}H CPMG NMR spectroscopy-based metabolic profiling utilised in this study failed to demonstrate metabolic changes associated with acute liver injury at any other time point except time point three (day seven). This could reflect the absence of early markers of acute liver injury; although this seems unlikely given the increasing body of evidence to the contrary (Tziolos, Kotanidou & Orfanos, 2015). The inability of the models of liver injury to detect metabolic differences at the earlier time points is however, inconsistent with previous reports of markers of liver injury as early as 15 hours after the onset of sepsis, demonstrated by LCMS analyses of plasma. One possible explanation that would take both findings into account is that early metabolic markers of liver injury were present in this study, but they are not detectable by the NMR analyses employed in this study. This hypothesis is supported by the differentiating metabolites demonstrated at time point three including lipids, the results of which were inconclusive owing to the inability of NMR to resolve subspecies of lipids.

4.5.6 Placebo versus steroid treatment groups

The O-PLS-DA model of the treatment groups based on the ^{1}H NMR CPMG data from serum samples from time point one (Table 4.10) was associated with a moderate Q^2Y value of 0.377 and a cross-validated ANOVA associated with a significant p value of 0.040. These model evaluation parameters are good and suggests that it has identified metabolites capable of differentiating between the two

treatment groups. However, the large difference between the R^2Y and the Q^2Y of 0.578 indicated that this model is heavily over-fitted and therefore unreliable.

The VACS trial set out to investigate the hypothesis that corticosteroids increases the responsiveness to vasopressin and vasopressin can increase ACTH to increase corticosteroid levels in septic shock and the effect these interactions on clinical outcomes such as organ dysfunctions and survival. The main finding of the VACS trial comparing these two treatment groups was the co-administration of vasopressin and hydrocortisone resulted in a shorter duration of vasopressin therapy and the use of a lower dose of vasopressin compared to administration of vasopressin and placebo (Gordon, Mason, Perkin*s, et al*., 2014a). However, despite these differences in vasopressin requirements no differences in 28-day mortality or daily SOFA assessments were demonstrated between the two treatment arms and no significant differences in the plasma vasopressin levels were demonstrated between the two treatments groups at any of the time points.

The expectation of the differences in the metabolic profiles of patients from the two treatment groups were derived from evidence of the impact of steroids on signalling and lipid metabolism; involving PCs and LysoPCs in particular (Lehmann, Sharawy, Zhou, *et al.*, 2012). The negative results obtained with the models of the two treatment arms were unexplained but not unsurprising, given the evidence suggesting subspecies of lipids are involved in the changes mediated by steroids in sepsis and these are not well resolved using NMR techniques (see above) (Lehmann, Sharawy, Zhou, *et al.*, 2012). More favourable results may be achieved using methods of lipid profiling using MS. Two patients crossed over from the placebo group to the treatment group; six samples across the four time points were affected by this cross-over. To avoid these cross-overs giving spurious results due to incorrect allocation, samples collected after the cross over period were assigned to the treatment group (see

Section 4.33). Crossover between the two treatment groups could not be responsible for failure to demonstrate metabolic differences between the hydrocortisone and placebo groups.

4.5.7 Acute Kidney Injury

Orthogonal-PLS-DA models were used to investigate AKI and the development of AKI in patients without AKI at baseline. All of these models failed to demonstrate metabolic signatures associated with AKI and the development of AKI. The failure to detect a metabolic signature capable predicting the development of AKI could be explained by the small number of available samples from time point zero, from patients without AKI. This consisted of a total of only eight serum samples (four from each group) and 14 urine samples (five from patients without AKI during the study period and nine from patients who did go on to develop AKI). The failure to detect metabolic differences between patients with and without AKI at the time of the samples, at all four time points is not clear. In the previous chapter, the failure of metabolic profiling of urine based on ^{1}H NMR analyses to demonstrate a clinical utility in a cohort of critically ill patients was predominantly attributed to the multiple levels of heterogeneity of this cohort and its small size. It was hypothesised that the greater sample size of the sepsis cohort would lead to better results with the use of this method of metabolic profiling in this cohort. This was not the case however, and it would seem that the heterogeneity of the sepsis cohort was still too great to detect a difference between these kidney injury groups. Again, the number of drugs administered to this cohort resulted in a large number of drug metabolites, which accounted for a significant degree of the metabolic variation unrelated, or not necessarily related to the clinical characteristics under investigation. It is therefore possible that the metabolic signatures of AKI were present but could not be detected owing to overlapping drug signals. Alternatively, the metabolic signatures of AKI may be very subtle and undetectable in the presence of the large amount of metabolic variation unrelated to AKI caused by both endogenous and exogenous metabolites including all of the drugs. The orthogonal signal correction of O-PLS-DA, was however used to filter

out metabolic variation un-related to the separation of the two AKI groups. It therefore seems more likely that overlapping drug signals was responsible for the failure to detect metabolic signatures of AKI.

Overall greater success was demonstrated by the metabolic profiling based on CPMG NMR analyses of serum compared to 1-D standard NMR analyses of both serum and urine. This included demonstration of metabolic differences of the dichotomised groups of acute liver injury using CPMG that were not demonstrated by either of the other two methods of profiling. The most likely explanation for the differences between the profiling based on 1-D standard and CPMG NMR analyses of serum was the greater resolution of lower molecular-weight metabolites of CPMG analyses. However, the majority of the metabolic differences demonstrated between both the groups of both of these classes were lipids which are large molecular-weight metabolites.

It was also envisaged that greater success would be achieved with the metabolic profiling of urine to demonstrate metabolic differences between the two renal classes under investigation than serum analyses, but again this was not the case with equally poor results with both. This was in in spite of the urine sample set being larger than the serum set.

The ^{1}H NMR spectroscopy-based metabolic profiling employed in this study also failed to detect metabolic changes associated with 28-day survival, acute respiratory, cardiovascular, and haematological dysfunction. This included metabolic profiling of both urine and both 1-D standard and CPMG analyses of serum. The cause of this failure is unclear, but much akin to the differentiation of patients with and without kidney dysfunction the most likely explanation is a combination of

heterogeneity of this cohort and overlapping drug signals obscuring potential metabolic signatures of these classes, especially ones in the urine samples.

4.6 Summary

This section of the study has demonstrated changes in amino acids, lipoproteins and lipids associated with liver injury that were detected seven days after the onset of sepsis. It has also demonstrated the use of a ^{1}H CPMG NMR spectroscopy-based metabolic profiling approach coupled with multivariate data analysis as a global screening tool that has then directed more targeted profiling methods such as lipidomics using LCMS.

Chapter Five: Lipid responses to severe sepsis and sepsis-induced organ dysfunction

5.1 Introduction

The NMR analyses of the serum samples from the sepsis cohort demonstrated that the lipids were particularly important to the differentiation of the patients with and without liver injury. Owing to the constraints of NMR, however, the exact lipid species involved could not be identified. Lipids can be divided into classes according to their function or their structural features. The Lipid Metabolites and Pathway Strategy (LIPID MAPS) lipid classification system is based on two fundamental structural components: keto-acyl and isoprene groups (Fahy, Subramaniam, Brown, *et al.*, 2005). In this system lipids are divided into the following eight categories: fatty acids, glycerolipids, glycerophospholipids, sphingolipids, saccharolipids, and polyketides (resulting from the condensation of keto-acyl groups); and sterol lipids and prenol lipids (resulting from condensation of isoprene groups). Each class is then divided into subspecies according to their individual structural features such as the specific fatty acids that they contain. The abbreviations for glycerophospholipids in the LIPID MAPS classification system were updated in 2009. Since then two-letter abbreviations are used for the molecular species of each class and denotes the head group of their class. This is followed by a description of the radyl side chains at positions sn-1 and sn-2, if applicable using the format: (*sn-1* C:db/ *sn-2* C:db), where C and db are used to represent the number of the carbon atoms and double bonds. The parentheses may also contain prefixes such as ''O'-'' and ''P'-'' which are used to represent the alkyl ether and 1Z-alkenyl ether (plasmalogen) species.

Methods of lipid profiling using ultra-performance liquid chromatography-mass spectroscopy (UPLC-MS) have recently been developed, that are capable of determining the individual lipid species present in biofluids and tissues. One such, method of UPLC-MS lipid profiling was applied to plasma samples

from the sepsis cohort to investigate the preliminary (NMR) findings of lipid differences between the sepsis patients with and without liver injury, in more detail. (NB. Serum run using NMR; whereas plasma run using MS in view of the plasma samples set being greater than the serum sample set and the MS techniques was validated for the use of both types of samples).

5.2 Aim

Determine lipid subspecies capable of differentiating between sepsis patients with and without liver injury.

5.3 Materials and methods

5.3.1 Study patients

See Section 4.3.1.

5.3.2 Sample collection

All available samples were included in study. This consisted of 154 plasma samples from 50 patients as detailed in Section 4.3.2.

5.3.3 Clinical data collection

See section 4.3.3 for details.

5.3.4 Sample preparation and lipid profiling using ultra-performance liquid chromatography coupled with mass spectroscopy analyses of plasma

5.3.4.1 Plasma sample preparation

A solvent mixture of methanol (MEOH) and methyl-tert-butyl ether (MTBE) (MEOH/MTBE 1:3, v:v) was used to precipitate proteins and extract lipids from plasma and quality control samples prepared by pooling 2 µl of each plasma sample. This was achieved by mixing 100 µl of the solvent mixture with 100 µl of each sample using a vortex for one minute, followed by five minutes rest and centrifugation at 13,000 g at 4°C for 20 minutes. Samples were then stored on dry ice and the supernatant was removed. The lower organic lipid-containing phase was then collected and the solvent evaporated under vacuum. Just prior to injection into the UPLC-MS system, the organic extracts were reconstituted using 150 µl of a solvent mixture of water/acetonitrile (ACN)/isopropanol (ISP) (1:1:2, v:v:v). Samples were then vortexed for one minute before being centrifuged at 13,000 g at 4°C for 10 minutes and transferred into LC-MS vials with preloaded inserts (Waters Corp, USA).

5.3.4.2 UPLC-MS lipid profiling

Metabolites were separated by ultra-performance liquid chromatography (UPLC) using an Acquity UPLC System (Waters Corp, USA) and an Acquity UPLC CSH C18 2.1x100 mm, 1.7 µm, column (Waters Corp, USA). The column was fixed at a temperature of 55°C and a flow rate of 0.4 mL per minute (min). Solvent mixtures of 10 mM ammonium formate and 0.1% formic acid in ACN/water (60:40, v:v) and ISP/ACN (90:10, v:v), were used as mobile phases A and B, respectively. Metabolites were eluted over 20 minutes using varying percentages of the two solvents. The elution solvent composition and gradient with time, at each stage was as follows, with a non-linear gradient unless otherwise stated: 60-57% A (0.0-2.0 min), 57-50% A (2.0-2.1 min); linear gradient 50-46% A (2.1-12.0 min), 46-30% A (12.0-12.1 min; linear gradient), 30-1% A (12.1-18 min), 1-60% A (18.0-18.1 min), 60% A (18.1-20.0 min). The injection volumes of the positive and negative ionisation modes were 5 µL and 15 µL,

respectively. Quality control samples were used to assess the reproducibility and performance of the system. The quality control samples were injected after every 10 injections of the test samples. Mass spectrometry spectra were acquired using a Premier quadruple time-of-flight (Q-TOF) (Waters MS Technologies Ltd., UK) operating with an electrospray ionization (ESI) source, a scan time of 0.20 s and inter-scan delay of 0.02 s. Mass spectroscopy, tandem MS-MS and MS^E scans were obtained. Mass accuracy was achieved using a mass lock solution of 0.25 ng/µL of leucine encephalin in 50% ACN and 0.1% formic acid. Lock mass scans were acquired with a scan time of 0.20 s and a frequency of 30 s. The mass to charge ratios (m/z) of the positive and negative mode scan range from 50 to 1200. The cone voltage, source temperature and desolvation gas of both modes was set at 30 v, 120°C and 800 L/h, respectively. A capillary voltage of 3KV and desolvation temperature of 400°C was used in the positive mode and a capillary voltage of 2.5KV and desolvation temperature of 350°C was used in the negative mode.

Electrospray ionization lipid profiling using UPLC-MS is divided into positive and negative modes. The range of (lipid) metabolites detected by each mode is different but with a significant degree of overlap. The spectral data from the two modes can therefore increase recovery of the number of metabolites detected in the samples.

5.3.5 Processing of MS data, multivariate statistical analyses, and metabolite identification

Chromatographic data from each mode underwent peak-picking, retention time alignment and peak-grouping to ensure comparability (XCMS package, Metlin Scripps Research Institute, USA). Spectra were normalised to median-fold peak intensity using Excel (Microsoft corporation), and Pareto scaling, which involves mean-centred data that is divided by the square root of the standard deviation was applied prior to multivariate statistical analyses (SIMCA-13 software, Umetrics).

The UPLC-MS data from positive and negative modes were analysed separately using the same methods of multivariate analyses applied to the spectral data from the NMR experiments: principal component analysis (PCA) and orthogonal partial least square-discriminative analysis (OPLS-DA). Principal component analysis was first applied to the data set as a whole to provide an overview of the metabolic variation of the samples from all four TPs and identify extreme outliers. Separate PCA models were then constructed using the spectral data from each of the four time points. An additional model was also constructed using the data from a subset of samples from TP0, from patients without any evidence of AKI at that TP. Each PCA model was constructed using one to three PCs, which is usually sufficient to capture the majority of the metabolic variation, and the model with the best fit and predictability was selected. Four sets of five OPLS-DA models were constructed with each set containing five models utilising the spectral data from one time point with the samples divided according one of each of the five classes. An additional model was also constructed using the data from the sub-set of samples from patients without AKI at TP0 in order to predict the development of AKI.

5.3.5.1 Selection of statistically significant features (metabolite signals)

For OPLS-DA models capable of differentiating between samples from two clinical groups, an S-line loadings plot of the model was used to identify the metabolite signals with the greatest contribution to the separation of these groups. This type of loadings plot demonstrates both the covariance and the correlation between the metabolite signals and the clinical classes. These two factors both describe the direction and degree of metabolite signal (variables) changes in relation to clinical classes. On an S-line loadings plot, the covariance is displayed on the x-axis and the correlation coefficient is displayed on the y-axis. Significant features can be extracted from this S-plot (or a tabulated form of this data), using an initial screening process, which filters out metabolite signals with a low correlation or a low covariance and a poor chromatographic peak shape (Figure 5.1). A good peak shape was

defined as a symmetrical or meeting the criteria Gaussian peak (narrow peak width at 50% of the peak height and a tailing factor of 1.0, measured at 5% of the peak height). Features of poor peak shape included asymmetry at 10% of the peak height resulting in peak fronting or tailing, using the following criteria: a tailing factor of 1.0 at 5% of the peak height. Although there are no strict criteria for the cut off values for the correlation values used in S-line loading plots, the most commonly used values are in keeping with those by proposed by Evans (Evans, 1996) in relation to Pears coefficient (Wiklund, Johansson, Sjöström, *et al.*, 2008). In this study, moderate and high correlation coefficient were defined as of greater than +0.75 or less than -0.75 is generally viewed as a high level and between 0.4 to 0.75 or -0.4 to -0.75, a moderate one. The statistical significance of the signals passing the initial screening process is then assessed further using a series of univariate tests in which each signal must meet a strict set of criteria to be considered significant and worth pursuing further (identifying). These criteria included a p value of <0.05 on univariate t-testing, based on the assumption of unequal variance, and demonstrating the reproducibility of the metabolite signal by having a correlation of variance (CV) of the signal intensity in the quality control samples of 30 percent or less.

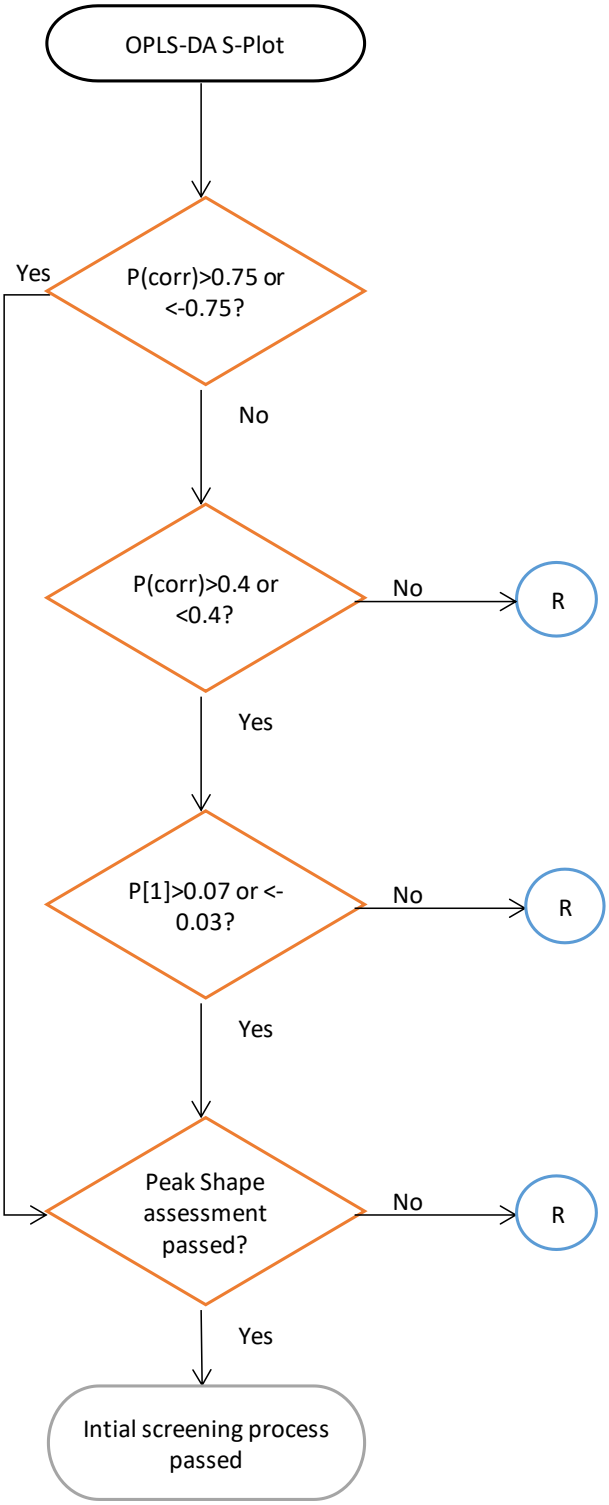


Figure 5.1 Metabolite feature selection initial screening process. KEY: P(corr): correlation coefficient, P [1]: covariance; R **reject.**

5.3.5.2 Metabolite identification: MS-MS; MS ^{E}

To meet the gold standard of metabolite identification in MS, the spectral features of the metabolites in question, need match those of authentic compounds, analysed under the same experimental conditions (Sumner, Amberg, Barrett, *et al.*, 2007). Metabolite identified by matching their MS-MS spectrum to standard compounds in this way have been described (Vorkas, Shalhoub, Isaac, *et al.*, 2015) as having level five assignment and the matching of the retention time of metabolite to a standard compound are described as a level four assignment. In the absence of reference compounds, putative assignments can be made. These assignments are aided by additional structural information derived from metabolite fragments from the acquisition of tandem positive and negative mode scans, and the use of MS^{E}: an iterative process of generating non-selective fragments from detectable metabolites. Tandem MS-MS and MS^{E} needs to be incorporated in the MS experiments and therefore requires forward planning at the experiment set-up stage. Level three assignments are made by matching the tandem MS spectra to MS identification databases such as METLIN (http://metlin.scripps.edu/), ChemSpider (http://www.chemspider.com/), PubChem (http://pubchem.ncbi.nlm.nih.gov/), Kyoto Encyclopedia of Genes and Genomes database (KEGG; http://www.genome.jp/kegg/) and LIPID MAPS (http://www.lipidmaps.org/). This includes use of tandem MS/MS with or without the use of MS^{E}.

Metabolites identified by matching of an accurate mass obtained through the use of technologies capable of achieving high mass accuracy (such Q-TOF) to a MS identification database as well as tandem MS spectrum matching to *in-silico* fragmentation patterns are described as a level two. Whereas, level one or a tentative assignment is used to describe metabolites assigned solely by the matching an accurate mass to an MS identification database. Finally, where only the compound class can be derived from the MS data the metabolite is regarded unidentified and is labelled as unknown.

5.4 Results

5.4.1 Demographics and clinical data of the sepsis cohort

Table 5.1 Characteristics of the sepsis cohort: demographics and baseline clinical variables (A) including the baseline Acute Kidney Injury Network (AKIN) and Sequential Organ Failure Assessment (SOFA) scores in more detail (B) for all patients with plasma samples available. Key: APACHE II: Acute Physiology and Chronic Health Evaluation II, COPD: Chronic Obstructive Pulmonary Disease, ICU: Intensive Care Unit, IHD: Ischaemic Heart Disease, IQR: interquartile range, NYHA: New York Heart Association functional classification, *: SOFA scores except for renal, which are AKIN scores.

A

Characteristic	**All patients - Plasma** n = 50 n(%) or median [IQR]
Age (years)	60 [51-71]
Gender (male)	27 (54)
APACHE II	21[17-24]
Organ dysfunction scores*	
Renal	0 [0-2]
Liver	0 [0-2]
Respiratory	3 [2-3]
Cardiovascular	4 [2-4]
Haematological	0 [0-1]
Neurological	0 [0]
Baseline serum creatinine	90 [61-181]
Baseline serum total bilirubin	13.5 [8-33]
Co-morbidity	
IHD	1 (2)
NYHA IV	0
Severe COPD	2 (4)
Chronic renal failure	3 (6)
Cancer	8 (16)
Cirrhosis	5 (10)
Immunocompromised	2 (4)
Diabetes	5 (10)
Recent trauma	0
Admission type	
Medical (Non operative)	38 (78)
Surgery – Emergency (Operative)	11 (22)
Surgery – Elective (Operative)	1 (2)

Table 5.1 continued

Diagnostic group (reason for admission)	
Post cardiac arrest	2 (4)
Cardiovascular	1 (2)
Respiratory	16 (32)
Gastro-intestinal - medical	4 (8)
Gastro-intestinal - surgical/operative	8 (16)
Infection	16 (32)
Neurologic	1 (2)
Aspiration /Poisoning /Toxic	2 (4)
Clinical outcomes	
Length of ICU stay	11 [6.0-19]
Length of hospital stay	25 [13-49]
28 day mortality	14 (28)

B

	Organ dysfunction scores*				
Organ dysfunction	**0**	**1**	**2**	**3**	**4**
Renal	32	3	9	6	0
Liver	30	6	12	2	0
Respiratory	6	4	11	18	11
Cardiovascular	4	9	0	0	37
Haematological	28	10	8	3	1
Neurological	41	2	2	0	5

5.4.2 Ultra-Performance Liquid Chromatography-Mass Spectroscopy-based lipid profiling of plasma

5.4.2.1 Multivariate analyses of lipid profiling using UPLC-mass spectroscopy: investigation of the lipid metabolites characterising the clinical classes

The total number of plasma samples from the 50 patients from the sepsis cohort was 154. This consisted of 25 samples collected at enrolment, 17 samples of which were from patients without AKI at TP0, and 50, 48 and 31 samples collected on days one, two and seven of the study, respectively.

The UPLC-MS data from the positive and negative modes were analysed separately. The PCA scores plots of the positive and negative modes of the UPLC-MS lipidomic profiles of all 154 samples are shown in Figures 5.2 and 5.3, respectively. PCAs are performed without prior knowledge of the clinical classes of the samples. The samples on the PCA scores plots can then be labelled according these classes, to better visualise the samples clustering and distribution. The PCA scores plots derived from the positive mode UPLC-MS data of all samples demonstrated partial separation of the samples along the second PC according to their liver injury classes. The PCA scores plots of the negative mode data of all the samples demonstrated a degree of separation according to their liver injury classes along the first PC.

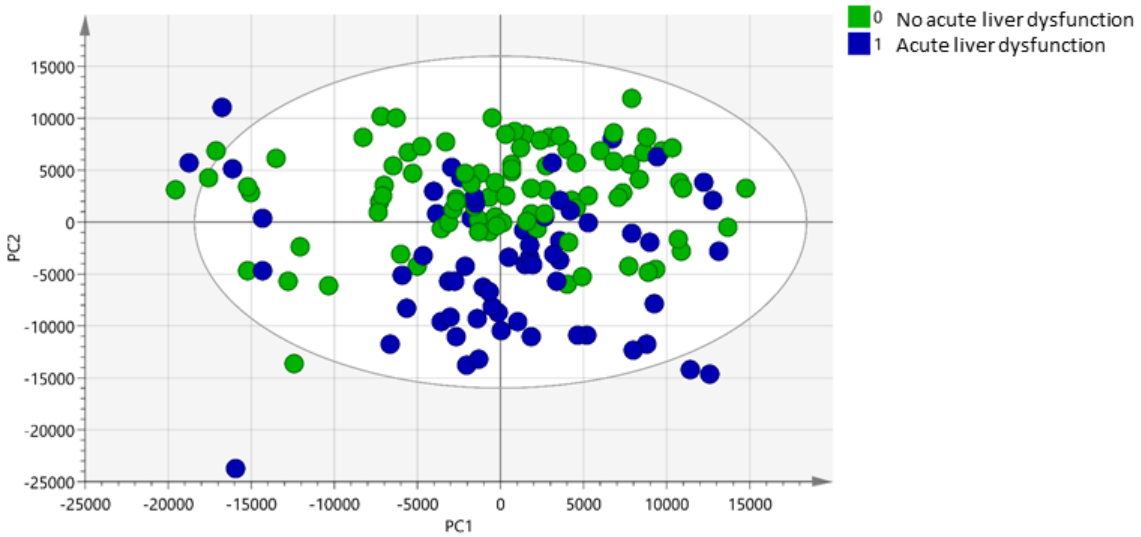


Figure 5.2. PCA scores plots of lipid profiles based on positive mode UPLC-MS of the plasma samples from the sepsis cohort from all four time points (n=154) labelled according to their liver injury groups: no injury in green (group 0) and liver injury in blue (group 1). This demonstrates a degree of separation of the samples according to their liver injury classes along the second principal component. KEY: PC: principal component.

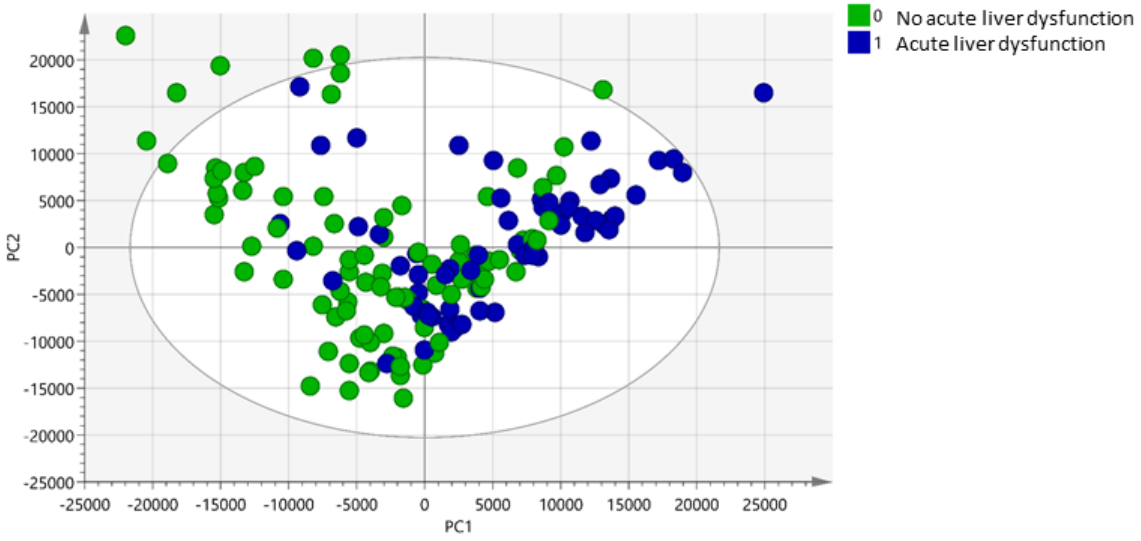


Figure 5.3. PCA scores plots of lipid profiles based on negative mode UPLC-MS of the plasma samples from the sepsis cohort from all four time points (n=154) labelled according to their liver injury groups: no injury in green (group 0) and liver injury in blue (group 1). This illustrates partial separation along the first PC that appears in part to be related to metabolic changes of liver injury. KEY: PC: principal component.

The evaluation parameters of the PCAs of based on the positive and negative mode data of the plasma samples from all four time points as shown in Figures 5.2 (positive) and 5.3 (negative), and individual time points are illustrated in Tables 5.2A (positive) and 5.2B (negative). These tables illustrate that R^2X (fit) and the Q^2X (predictability) of the both of these PCAs were low at 0.313 and 0.215, and 0.196 and 0.11, for the positive and negative modes, respectively. Overall, the models from the individual TPs had low R^2X and Q^2 values, with time points one and three achieving the best results in terms of both fit and predictability.

Table 5.2 Summary of the principal component analysis models of lipid profiling based on positive (A) and negative (B) mode UPLC-MS analyses of the plasma samples from the sepsis cohort. Key: PC: principal component; R^2X and Q^2X: variation explained and predicted by the model, respectively.

A

Principal Component Analyses						
Sample set: time point (n=sample number)	All samples (n=154)	TP0 without AKI (n= 17)	TP0 (n=25)	TP1 (n=50)	TP2 (n=48)	TP3 (n=31)
Number of PCs	3	1	2	3	2	2
R^2X	0.313	0.176	0.304	0.346	0.226	0.316
Q^2	0.215	-0.049	0.035	0.157	0.484	0.131

B

Principal Component Analyses						
Sample set: time point (n=sample number)	All samples (n=154)	TP0 without AKI (n= 17)	TP0 (n=25)	TP1 (n=50)	TP2 (n=48)	TP3 (n=31)
Number of PCs	2	2	3	2	2	2
R^2X	0.196	0.341	0.386	0.219	0.221	0.302
Q^2	0.11	0.0127	0.047	0.050	0.098	0.122

O-PLS-DA models were constructed to investigate metabolic differences associated with the main five clinical classes; in addition to the other three clinical classes, (reflecting respiratory, cardiovascular, and haematological dysfunction) at each of the four time points Each model was constructed using

one predictive component, with the addition of one or two orthogonal components, if their addition led to a significant improvement in their evaluation parameters. This resulted in seven of the positive mode models and three of the negative mode models of the first set of clinical classes having orthogonal components; whereas, all of the other positive and negative mode models were constructed using one predictive component only. To investigate the predictive biomarkers for AKI, a subset of samples from patients without AKI at time point zero was used to construct an O-PLS-DA model with the clinical diagnosis after this time point (e.g. develop AKI versus no AKI after time point one) as classification information. Each model was constructed using the UPLC-MS spectral data from one of the time points as the X matrix and data from one of the five clinical classes to form the dummy Y matrix.

The evaluation parameters of the first set OPLS-DA models are shown in Table 5.3. The O-PLS-DA models based on UPLC-MS positive mode data were associated with a poor predictability for the discrimination of the acute kidney injury, 28-day survival and treatment classes. The poor predictability was indicated by either low or negative Q^2Y values, ranging from -0.419 to 0.082; with one exception, which was associated with a large difference between the R^2Y and the Q^2Y values (i.e. greater 0.5), suggestive of over fitting of the model, and in all cases the CV-ANOVA of the models were associated with p values greater than 0.05.

However, the O-PLS-DA models constructed to investigate differences between samples from patients with and without acute liver injury at each of the four time points were associated with a good predictability. The Q^2Y of the liver injury models ranged between 0.208 to 0.5 for the positive mode, and 0.281 to 0.438 for the negative mode models, with a difference of less 0.463 between the R^2Y and the Q^2Y, in all cases. The p values associated with the CV-ANOVAs of the liver injury models were less than 0.05 in all cases and lower than 0.005 in half of the models. The OPLS-DA scores plots of all the

liver injury models before and after an iterative process of cross validation are shown in Figures 5.4 – 5.11. With the exception of time point one, the predictability of the positive mode OPLS-DA models (Figures 5.4-5.7) increased with time. A similar pattern was also seen with the negative mode models (Figures 5.8-5.11); however, in this case, the increase in predictability was only seen in the first three time points.

Table 5.3. Results of the evaluation parameters of OPLS-DA models derived from a lipid profiling method based on positive (A) and negative mode (B) UPLC-MS analyses of the plasma samples from the sepsis cohort. Illustration of the percentage of the variation explained by the X (R^2X) and Y matrices (R^2Y) and predicted by the Y matrix (Q^2Y) of the models evaluating samples based on five clinical classes: the development of AKI after TP0, acute kidney injury*, acute liver injury*, 28-day survival and treatment group. KEY: CV-ANOVA: cross-validated analysis of variance, Group 0: good outcome (no injury or survival) or placebo treatment group, Group 1: poor outcome (injury or non-survival) or hydrocortisone treatment group, TP: time point; *: at that time point.

A

OPLS-DA		AKI after TP0	Acute Kidney injury				Acute Liver injury				28 day survival				Treatment group			
Sample set: time point (n=sample number)		TP0 without AKI (n=17)	TP0 (n=25)	TP1 (n=50)	TP2 (n=48)	TP3 (n=31)	**TP0 (n=25)**	**TP1 (n=50)**	**TP2 (n=48)**	**TP3 (n=31)**	TP0 (n=25)	TP1 (n=50)	TP2 (n=48)	TP3 (n=31)	TP0 (n=25)	TP1 (n=50)	TP2 (n=48)	TP3 (n=31)
Group 0: good outcome		7	17	23	20	14	**16**	**30**	**28**	**18**	18	36	34	25	9	29	28	16
Group 1: poor outcome		10	8	27	28	17	**9**	**20**	**20**	**13**	7	14	14	6	16	21	20	15
Number of components	Predictive	1	1	1	1	1	**1**	**1**	**1**	**1**	1	1	1	1	1	1	1	1
	Orthogonal to X	0	0	1	0	2	**0**	**0**	**1**	**2**	1	0	0	0	1	0	0	1
Model statistics	R^2X	0.149	0.114	0.108	0.072	0.291	**0.118**	**0.105**	**0.140**	**0.352**	0.184	0.102	0.091	0.170	0.178	0.083	0.073	0.239
	R^2Y	0.701	0.455	0.751	0.413	0.929	**0.618**	**0.490**	**0.864**	**0.938**	0.859	0.346	0.399	0.427	0.828	0.410	0.454	0.674
	Q^2	0.190	-0.419	-0.116	-0.188	0.357	**0.243**	**0.208**	**0.401**	**0.500**	-0.177	-0.080	-0.024	0.082	-0.361	-0.102	-0.300	-0.123
	$R^2Y - Q^2$	0.511	0.874	0.867	0.601	0.572	**0.375**	**0.282**	**0.463**	**0.438**	1.036	0.426	0.423	0.345	1.189	0.190	0.190	0.190
CV-ANOVA	P VALUE	0.228	1.000	1.000	1.000	0.076	**0.047**	**0.004**	**1.60E-04**	**0.006**	1.000	1.000	1.000	0.303	1.000	1.000	1.000	1.000

B

OPLS-DA		AKI after TP0	Acute Kidney injury				Acute Liver injury				28 day survival				Treatment group			
Sample set: time point (n=sample number)		TP0 without AKI (n=17)	TP0 (n=25)	TP1 (n=50)	TP2 (n=48)	TP3 (n=31)	**TP0 (n=25)**	**TP1 (n=50)**	**TP2 (n=48)**	**TP3 (n=31)**	TP0 (n=25)	TP1 (n=50)	TP2 (n=48)	TP3 (n=31)	TP0 (n=25)	TP1 (n=50)	TP2 (n=48)	TP3 (n=31)
Group 0: good outcome		7	17	23	20	14	**16**	**30**	**28**	**18**	18	36	34	25	9	29	28	16
Group 1: poor outcome		10	8	27	28	17	**9**	**20**	**20**	**13**	7	14	14	6	16	21	20	15
Number of components	**Predictive**	1	1	1	1	1	**1**	**1**	**1**	**1**	1	1	1	1	1	1	1	1
	Orthogonal to X	0	1	0	0	0	**0**	**0**	**0**	**0**	0	0	0	1	0	1	0	0
Model statistics	**R^2X**	0.155	0.196	0.086	0.079	0.162	**0.095**	**0.105**	**0.103**	**0.182**	0.109	0.083	0.091	0.246	0.113	0.128	0.072	0.070
	R^2Y	0.644	0.807	0.458	0.453	0.467	**0.722**	**0.591**	**0.643**	**0.525**	0.550	0.418	0.412	0.827	0.458	0.727	0.475	0.518
	Q^2	0.071	0.088	0.156	-0.099	0.190	**0.281**	**0.383**	**0.438**	**0.315**	-0.100	-0.148	0.075	0.207	-0.213	0.088	0.041	-0.403
	$R^2Y - Q^2$	0.573	0.719	0.302	0.552	0.277	**0.441**	**0.208**	**0.205**	**0.210**	0.650	0.566	0.337	0.620	0.671	0.639	0.435	0.921
CV-ANOVA	**P VALUE**	0.597	0.748	0.019	1.000	0.052	**0.026**	**1.19E-05**	**2.36E-06**	**0.005**	1.000	1.000	0.173	0.180	1.000	0.378	0.394	1.000

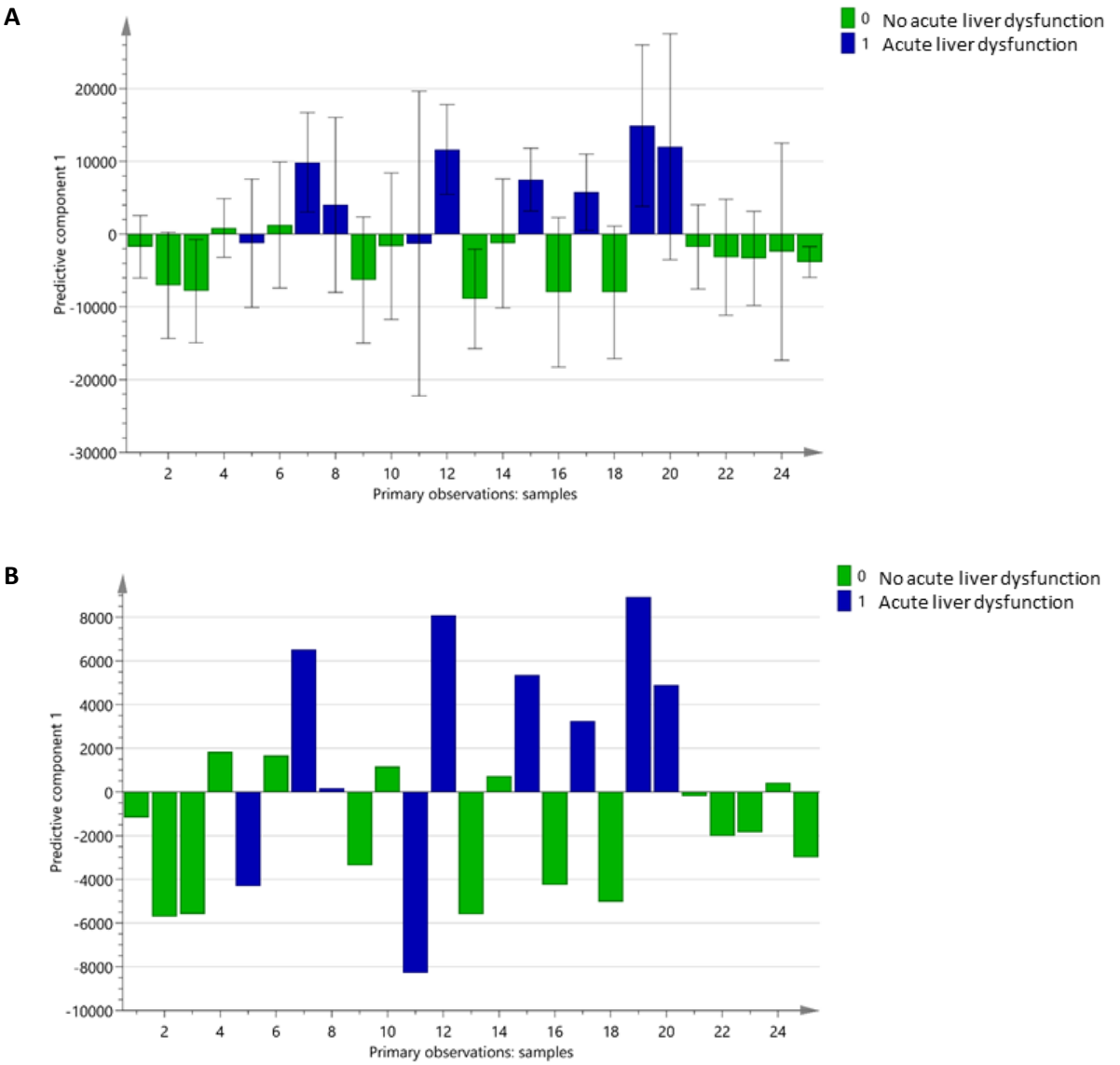


Figure 5.4. OPLS-DA scores plot (A) and cross-validated scores plot (B) based on positive mode (ESI) lipid profiling using UPLC-MS of plasma samples from the sepsis cohort taken at time point zero. This demonstrates evidence of separation between acute liver dysfunction (blue) and no liver dysfunction (R^2X=0.118, R^2Y=0.618; Q^2Y=0.243). Both models misclassified two samples from each group (four and six from the group without dysfunction and five and 11 from group with dysfunction). The cross-validated model (p=0.047) misclassified three additional samples from the group without dysfunction (10, 14 and 24). KEY: ESI: electron spray ionisation.

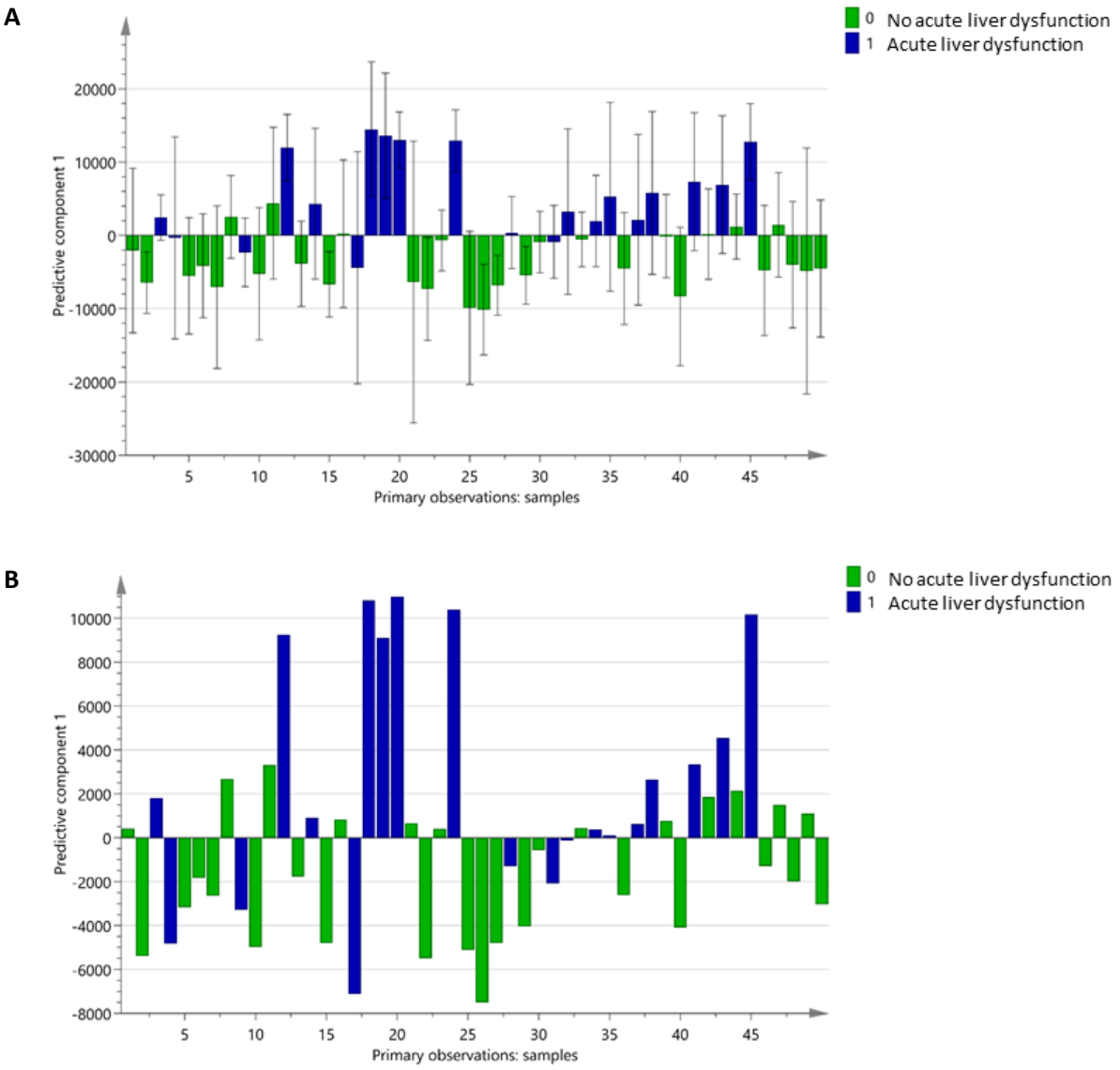
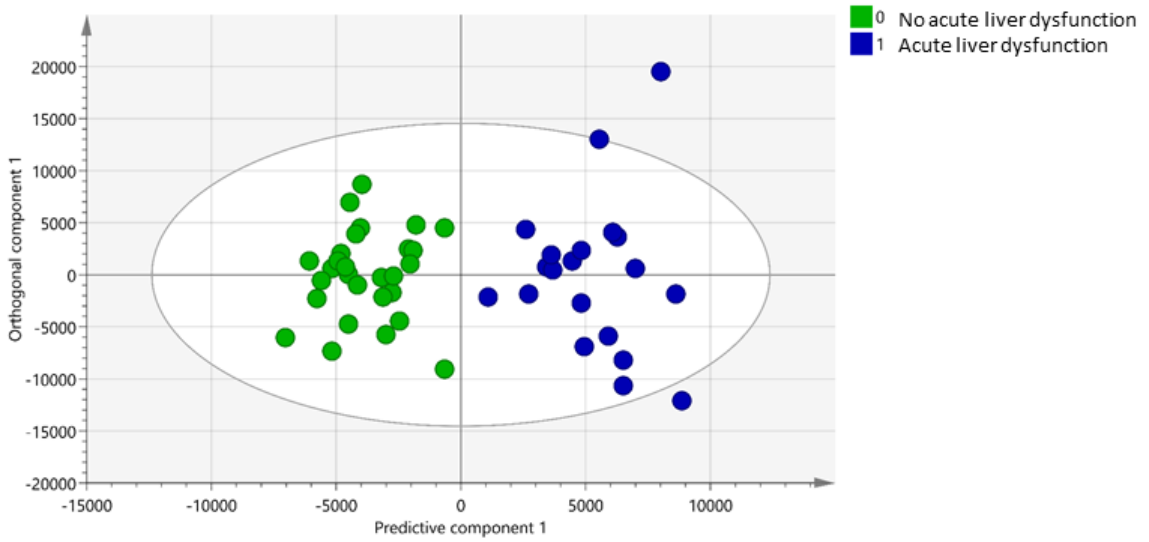


Figure 5.5. OPLS-DA scores plot (A) and cross-validated scores plot (B) derived from positive mode (ESI) lipid profiling using UPLC-MS spectroscopy spectra of plasma samples from the sepsis cohort taken at time point one. This demonstrates evidence of separation of the samples according to metabolic changes associated with acute liver dysfunction (blue) from those without acute liver dysfunction (green) (R^2X=0.105, R^2Y=0.490; Q^2Y=0.208). Six of the 30 no dysfunction samples (eight, 11, 16, 39, 42 and 44) and four of the 20 dysfunction samples (four, nine 17 and 31) were misclassified by both models. The cross-validated model (p=0.004) misclassified five additional samples: three from the no dysfunction group (one, 47 and 49) and two from the dysfunction group (28 and 32).

A



B

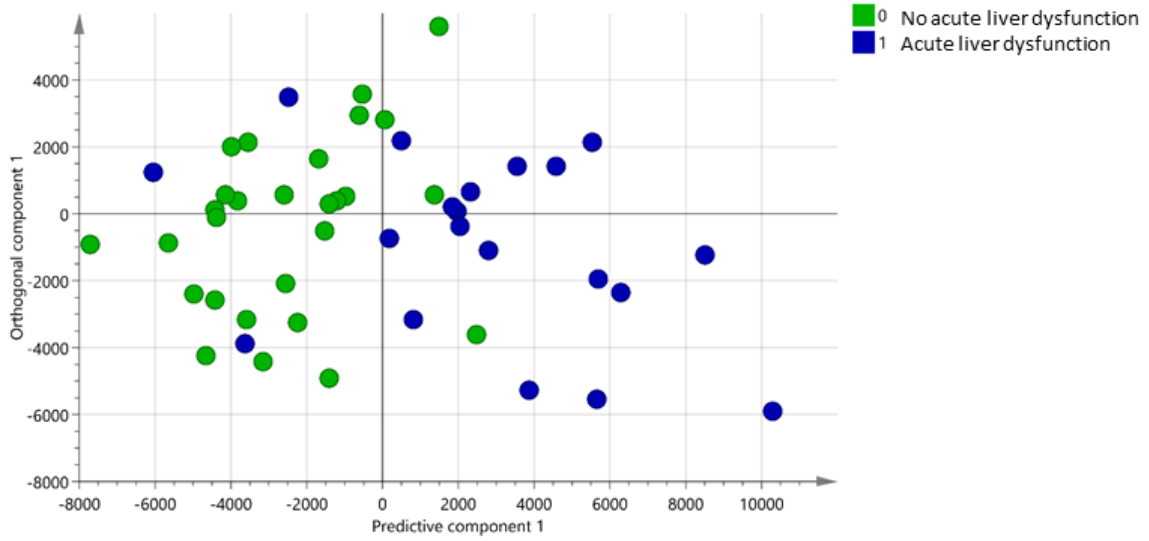


Figure 5.6. OPLS-DA scores plot (A) and cross-validated scores plot (B) derived from positive mode (ESI) lipid profiling using UPLC-MS spectroscopy spectra of plasma samples from the sepsis cohort taken at time point two. This demonstrates evidence of separation of the samples according to metabolic changes associated with acute liver dysfunction (blue) from those without acute liver dysfunction (green) (R^2X=0.140, R^2Y=0.864; Q^2Y=0.401). The un-cross validated model demonstrated no misclassified samples. The cross-validated model (p=1.60E-04) demonstrated seven misclassified samples: four samples from the group without dysfunction and three from the group with dysfunction.

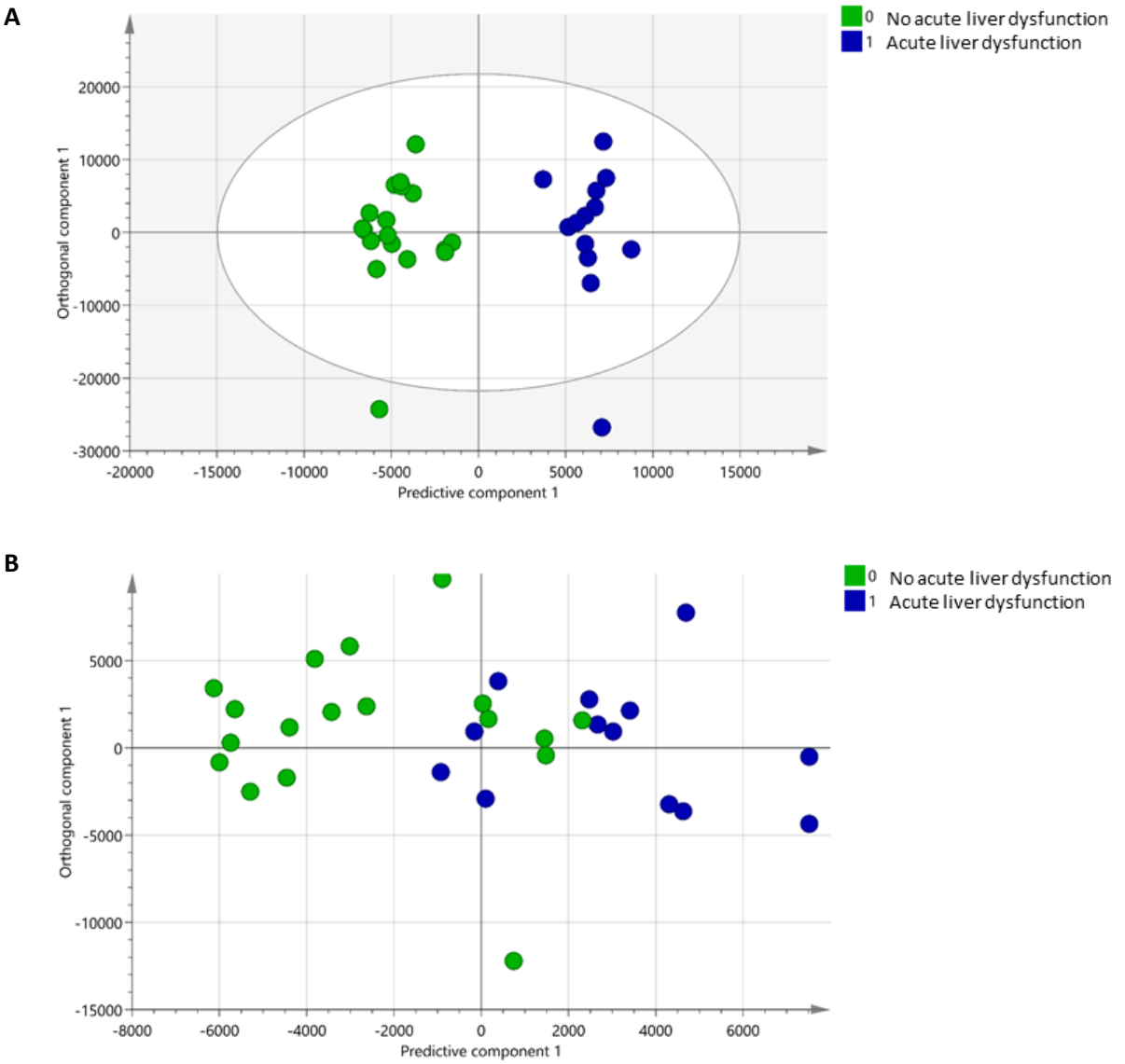


Figure 5.7. OPLS-DA scores plot (A) and cross-validated scores plot (B) derived from positive mode (ESI) lipid profiling using UPLC-MS spectroscopy spectra of plasma samples from the sepsis cohort taken at time point three. This demonstrates evidence of separation of the samples according to metabolic changes associated with acute liver dysfunction (blue) from those without acute liver dysfunction (green) (R^2X=0.352, R^2Y=0.938; Q^2Y=0.5). The un-cross validated model demonstrated no misclassified samples. The cross-validated model (p=0.006) demonstrated seven misclassified samples: five samples from the group without dysfunction and two from the group with dysfunction.

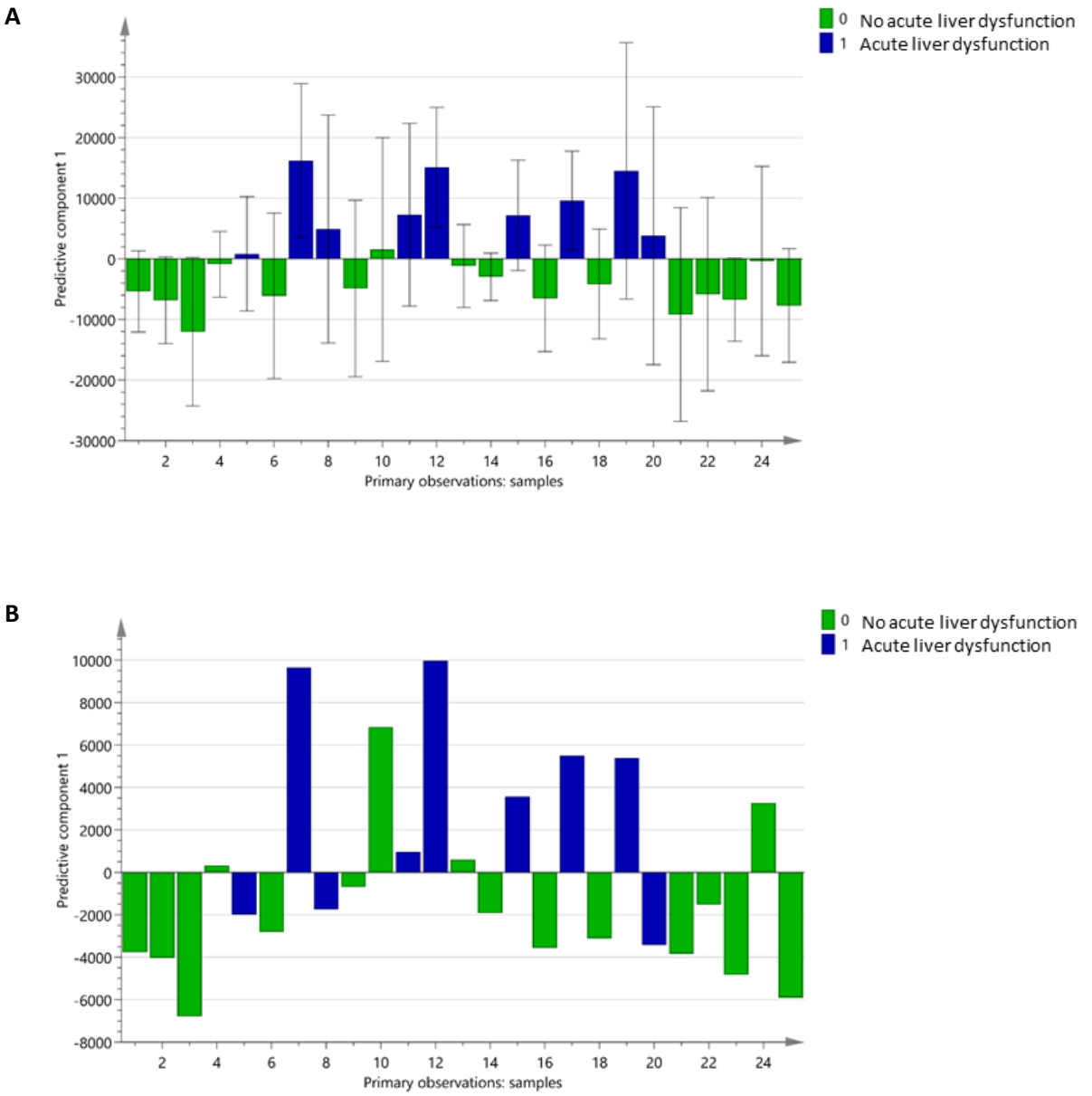


Figure 5.8. OPLS-DA scores plot (A) and cross-validated scores plot (B) derived from negative mode (ESI) lipid profiling using UPLC-MS spectroscopy spectra of plasma samples from the sepsis cohort taken at time point zero. This demonstrates evidence of separation of the samples according to metabolic changes associated with acute liver dysfunction (blue) from those without acute liver dysfunction (green) (R^2X=0.095, R^2Y=0.722; Q^2Y=0.281). Both models demonstrated the misclassification of one no dysfunction group sample (10). The cross-validated model (p=0.026) misclassified six additional samples: three from group without dysfunction (four, 11 and 24) and three from group with dysfunction (five, eight and 20).

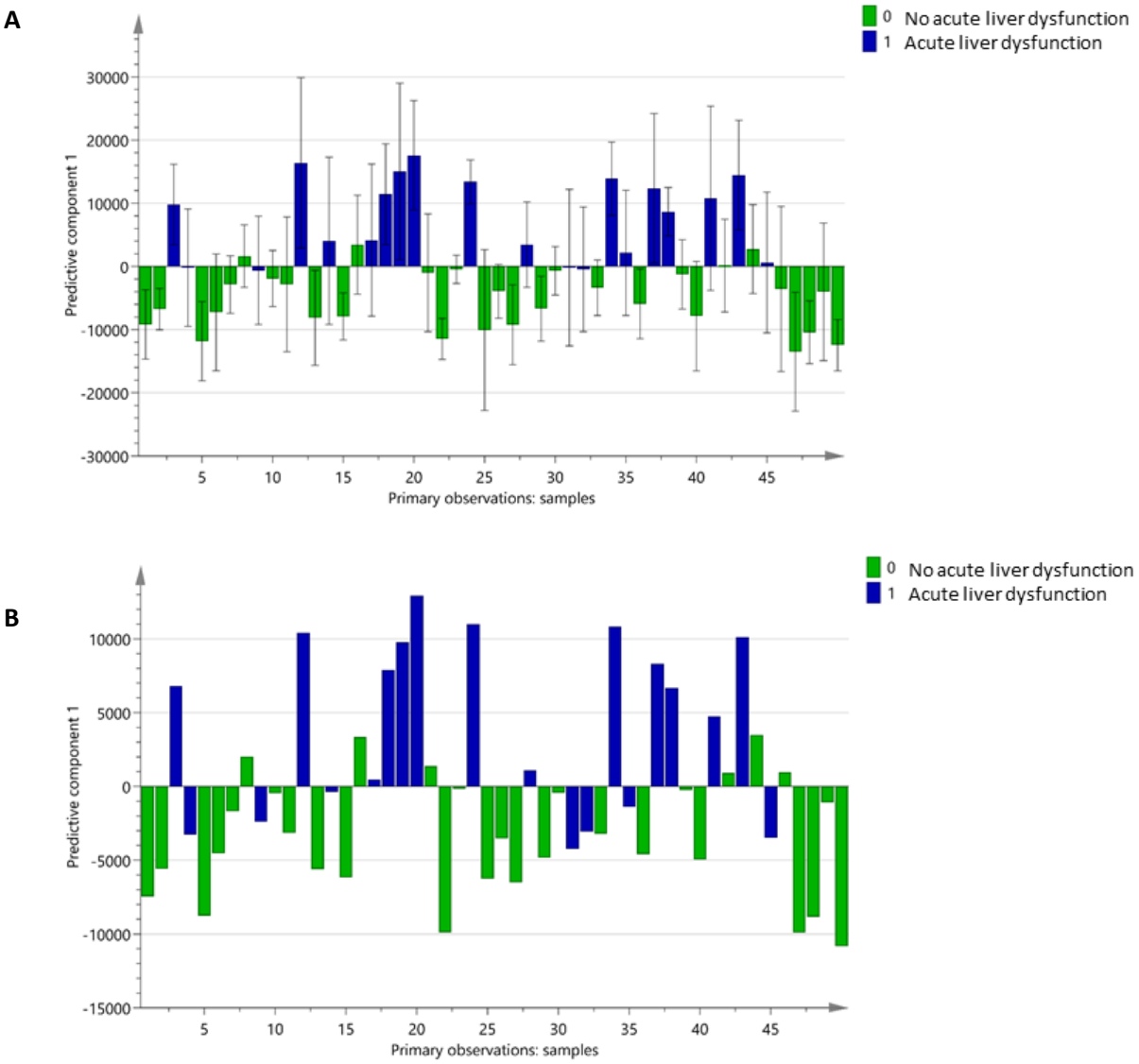


Figure 5.9. OPLS-DA scores plot (A) and cross-validated scores plot (B) derived from negative mode (ESI) lipid profiling using UPLC-MS spectroscopy spectra of plasma samples from the sepsis cohort taken at time point one. This demonstrates evidence of separation of the samples according to metabolic changes associated with acute liver dysfunction (blue) from those without acute liver dysfunction (green) (R^2X=0.105, R^2Y=0.591; Q^2Y=0.383). Both models demonstrated the misclassification of eight samples: four from the group without dysfunction (eight, 16, 42 and 44) and four from the group with dysfunction (four, nine, 31 and 32). The cross-validated model (p=1.19E-05) misclassified additional samples: two from the group without dysfunction (14, 16, 21and 46) and three from the group with dysfunction (14, 34 and 45).

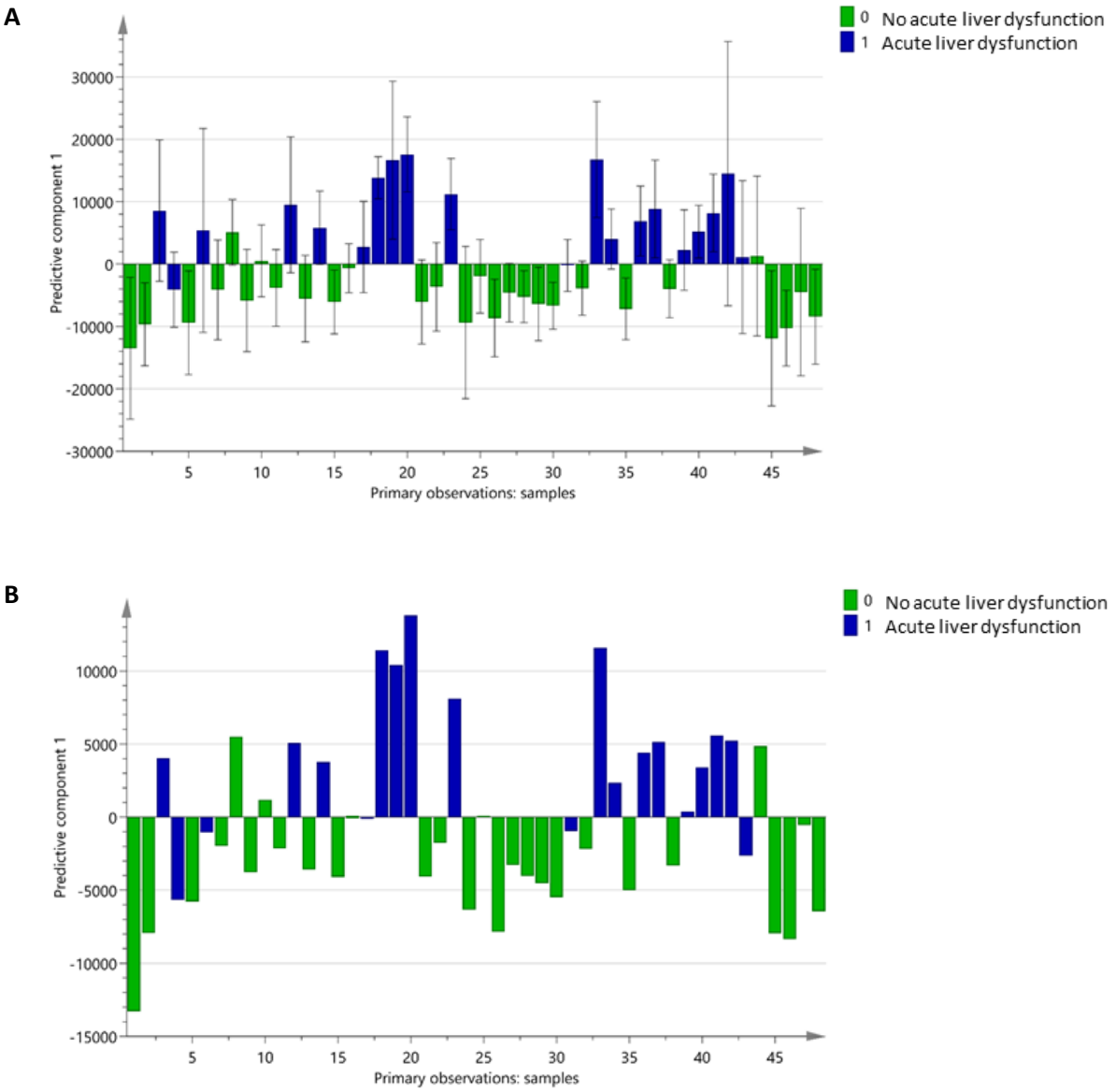
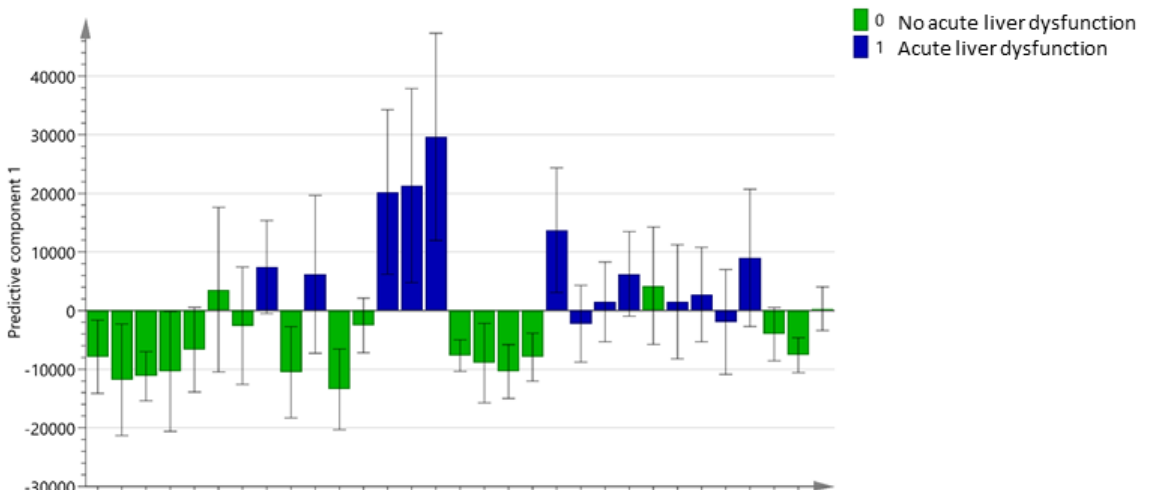


Figure 5.10. OPLS-DA scores plot (A) and cross-validated scores plot (B) derived from negative mode (ESI) lipid profiling using UPLC-MS spectroscopy spectra of plasma samples from the sepsis cohort taken at time point two. This demonstrates evidence of separation of the samples according to metabolic changes associated with acute liver dysfunction (blue) from those without acute liver dysfunction (green) (R^2X=0.103, R^2Y=0.643; Q^2Y=0.438). Both models demonstrated the misclassification of six samples: three from group without the dysfunction (eight, 10 and 44) and three from the group with dysfunction (four, 31 and 43). The cross-validated plot (p=2.36E-06) misclassified three additional samples: one by the group without dysfunction (25) and two by the group with dysfunction (six and 17).

A



B

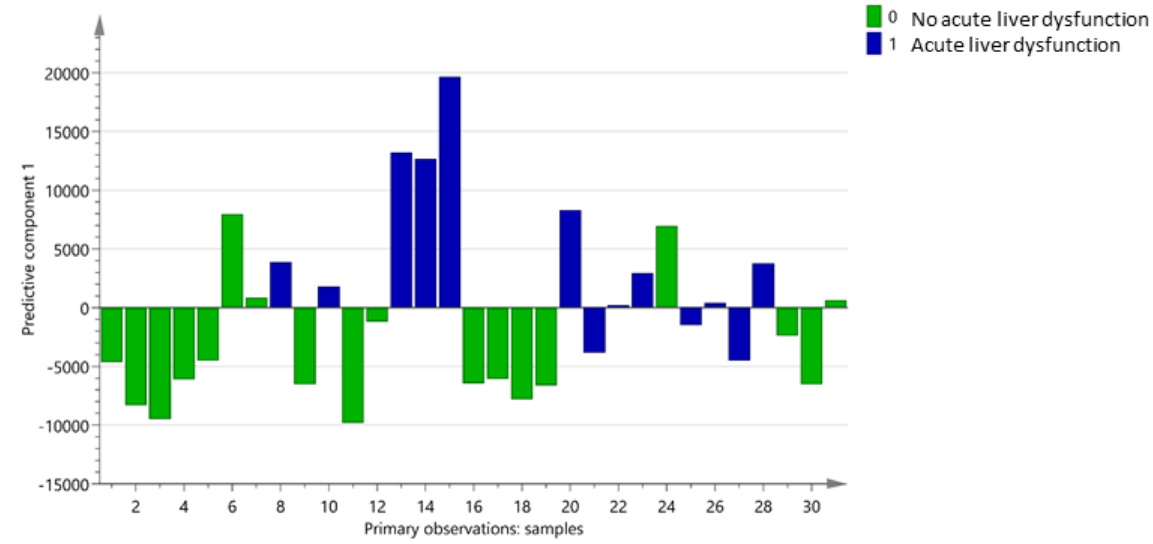


Figure 5.11. OPLS-DA scores plot (A) and cross-validated scores plot (B) derived from negative mode (ESI) lipid profiling using UPLC-MS spectroscopy spectra of plasma samples from the sepsis cohort taken at time point three. This demonstrates evidence of separation of the samples according to metabolic changes associated with acute liver dysfunction (blue) from those without acute liver dysfunction (green) (R^2X=0.182, R^2Y=0.525; Q^2Y=0.315). Both models demonstrated the misclassification of five samples: three from group without the dysfunction (six, 24 and 31) and two from the group with dysfunction (21 and 27). The cross-validated plot (p=0.005) misclassified one additional sample from each group, (seven and 25, for group without and with dysfunction, respectively).

The OPLS-DA models of the respiratory, cardiovascular, and haematological dysfunction based on LCMS data were divided into two sets: one constructed with dichotomised groups and the other with data divided according to the samples five SOFA scores. The evaluation parameters of the OPLS-DA models based on the positive and negative modes of data divided into two groups are shown in Table 5.4A (positive) and B (negative) and the models with five groups are shown Table 5.5A (positive) and B (negative). Table 5.4 demonstrates a great imbalance in the number of samples in the models of respiratory and cardiovascular dysfunction with two groups. This includes two time points with no samples in the group without cardiovascular dysfunction and thus no models could be constructed with data based on these time points. The samples in the haematological models with two groups, in contrast, were more evenly divided between the two groups and yielded the best results with the highest Q^2Y and CV-ANOVA associated with significant p values ($p<0.05$). This included three models based on positive mode data from time points one to three and the model based on negative mode data from time point three. However, the difference between R^2Y and Q^2Y of the model based on positive mode data from time point one is greater than 0.5 consistent with overfitting and was therefore not investigated further. The O-PLS-DA models based on positive mode data from time points two and three and negative mode data from time point three are shown in Figures 5.12-5.14. In the cases of both modes, the best preforming model was the haematological model based on data from time point three (day seven).

Table 5.4 Results of the evaluation parameters of OPLS-DA models derived from a lipid profiling method based on positive (A) and negative mode (B) UPLC-MS analyses of the plasma samples from the sepsis cohort. Illustration of the percentage of the variation explained by the X (R^2X) and Y matrices (R^2Y) and predicted by the Y matrix (Q^2Y) of the models evaluating samples based on their respiratory, cardiovascular, and haematological clinical classes with the samples divided into two groups. KEY: CV-ANOVA: cross-validated analysis of variance, TP: time point.

A

OPLS-DA		Respiratory				Cardiovascular				Haematological			
Sample set: time point (n=sample number)		TP0 (n=25)	TP1 (n=50)	TP2 (n=48)	TP3 (n=31)	TP0 (n=25)	TP1 (n=50)	TP2 (n=48)	TP3 (n=31)	TP0 (n=25)	TP1 (n=50)	TP2 (n=48)	TP3 (n=31)
Group 0: good outcome (no injury)		3	1	1	1	2	0	0	8	16	24	22	15
Group 1: poor outcome (injury)		22	49	47	30	23	50	48	23	9	26	26	16
Number of components	Predictive	1	1	1	1	1	N/A	N/A	1	1	1	1	1
	Orthogonal to X	2	0	0	0	1			1	0	2	1	0
Model statistics	R^2X	0.283	0.050	0.037	0.097	0.179			0.198	0.101	0.275	0.165	0.167
	R^2Y	0.955	0.460	0.682	0.519	0.810			0.748	0.533	0.836	0.778	0.538
	Q^2	0.469	-0.279	-0.202	-0.200	-0.176			-0.036	-0.435	0.323	0.299	0.322
	$R^2Y - Q^2$	0.486	0.739	0.884	0.719	0.986			0.784	0.968	0.513	0.479	0.216
CV-ANOVA	P VALUE	0.051	1.000	1.000	1.000	1.000			1.000	1.000	0.008	0.004	0.004

B

OPLS-DA		Respiratory				Cardiovascular				Haematological			
Sample set: time point (n=sample number)		TP0 (n=25)	TP1 (n=50)	TP2 (n=48)	TP3 (n=31)	TP0 (n=25)	TP1 (n=50)	TP2 (n=48)	TP3 (n=31)	TP0 (n=25)	TP1 (n=50)	TP2 (n=48)	TP3 (n=31)
Group 0: good outcome (no injury)		3	1	1	1	2	0	0	8	16	24	22	15
Group 1: poor outcome (injury)		22	49	47	30	23	50	48	23	9	26	26	16
Number of components	Predictive	1	1	1	1	1	N/A	N/A	1	1	1	1	1
	Orthogonal to X	0	0	0	2	1			2	0	0	1	0
Model statistics	R^2X	0.122	0.078	0.066	0.323	0.169			0.313	0.089	0.081	0.135	0.187
	R^2Y	0.522	0.234	0.439	0.944	0.843			0.894	0.250	0.462	0.726	0.505
	Q^2	0.014	-0.214	-0.266	0.142	-0.318			0.332	-0.109	0.074	0.151	0.281
	$R^2Y - Q^2$	0.508	0.448	0.705	0.802	1.161			0.562	0.359	0.388	0.575	0.224
CV-ANOVA	P VALUE	0.854	1.000	1.000	0.682	1.000			0.107	1.000	0.163	0.126	0.010

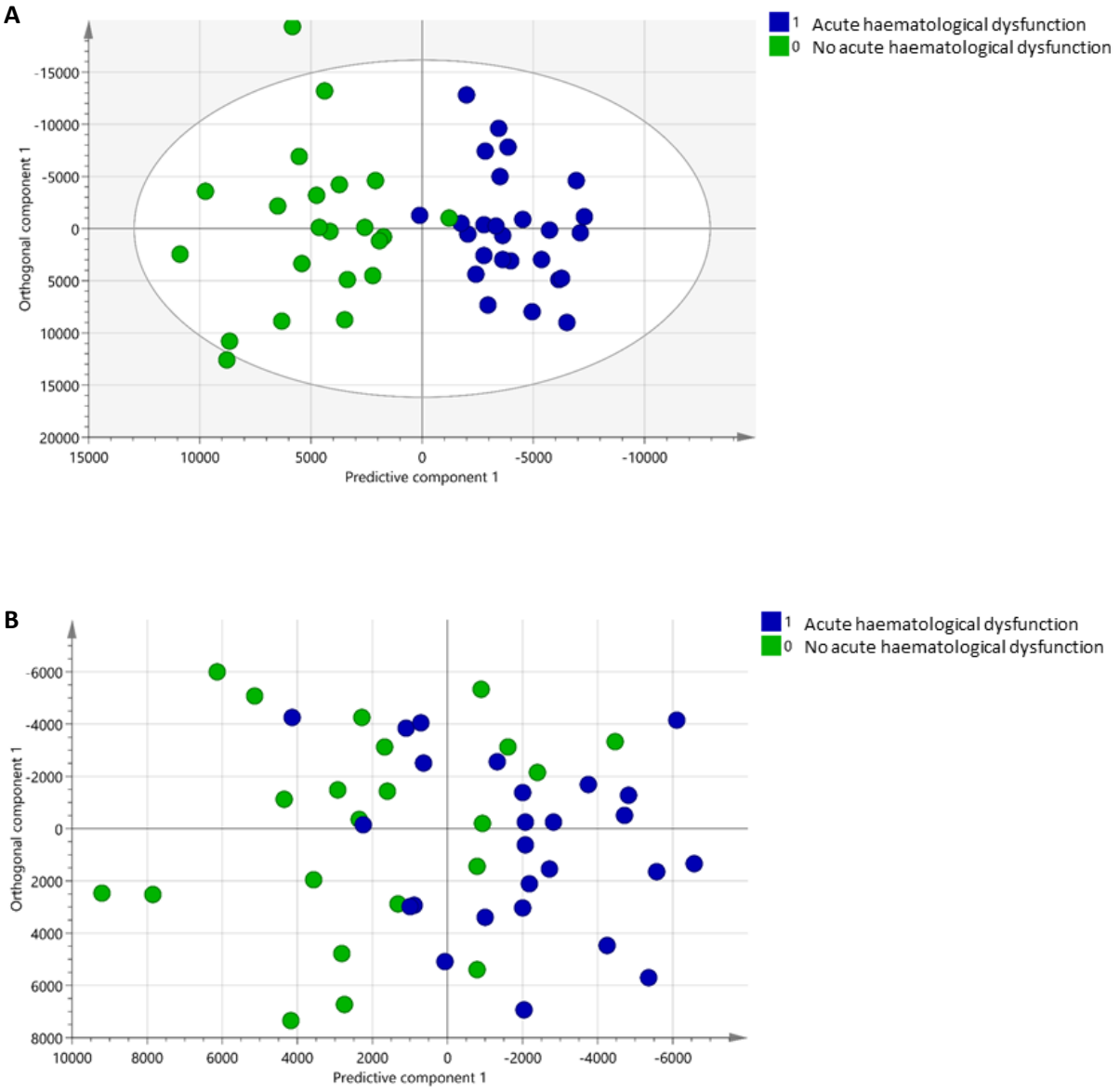


Figure 5.12. OPLS-DA scores plot (A) and cross-validated scores plot (B) derived from positive mode (ESI) lipid profiling using UPLC-MS spectroscopy spectra of plasma samples from the sepsis cohort taken at time point two. This demonstrates evidence of separation of the samples according to metabolic changes associated with acute haematological dysfunction (blue) from those without acute haematological dysfunction (green) (R^2X=0.165, R^2Y=0.778; Q^2Y=0.299). One samples from each group was misclassified by the un-crossed validated model (A). The cross-validated model (p=0.004) demonstrated 14 samples that were misclassified: seven from each group.

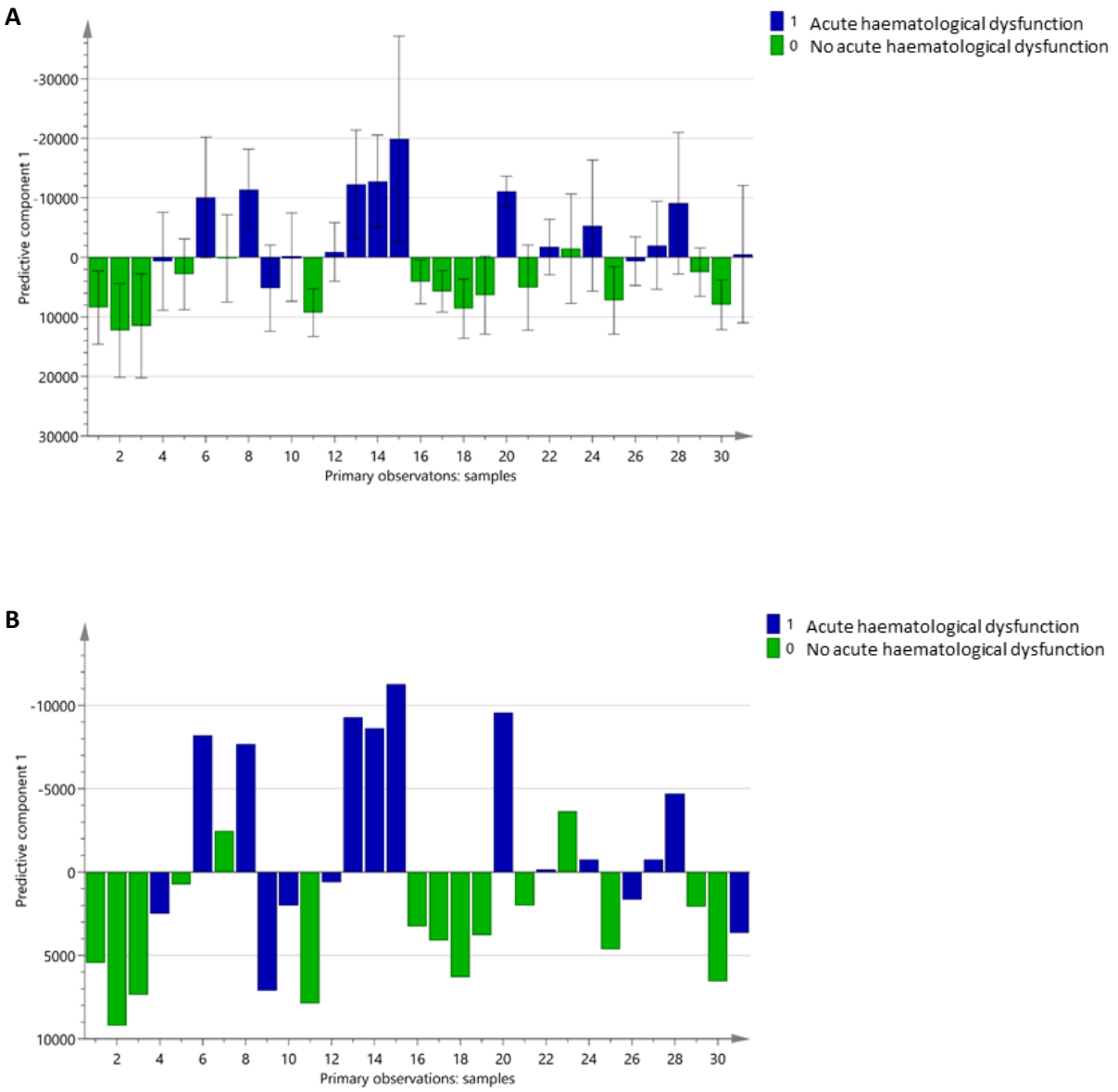


Figure 5.13. OPLS-DA scores plot (A) and cross-validated scores plot (B) derived from positive mode (ESI) lipid profiling using UPLC-MS spectroscopy spectra of plasma samples from the sepsis cohort taken at time point three. This demonstrates evidence of separation of the samples according to metabolic changes associated with acute haematological dysfunction (blue) from those without acute haematological dysfunction (green) (R^2X=0.167, R^2Y=0.538; Q^2Y=0.322). One sample from the group without dysfunction (23) and three from the group with dysfunction (four, nine and 26) were misclassified by both model. The cross-validated model (p=0.004) misclassified four additional samples: one from group without dysfunction (seven) and three from the group with dysfunction (10, 12 and 31).

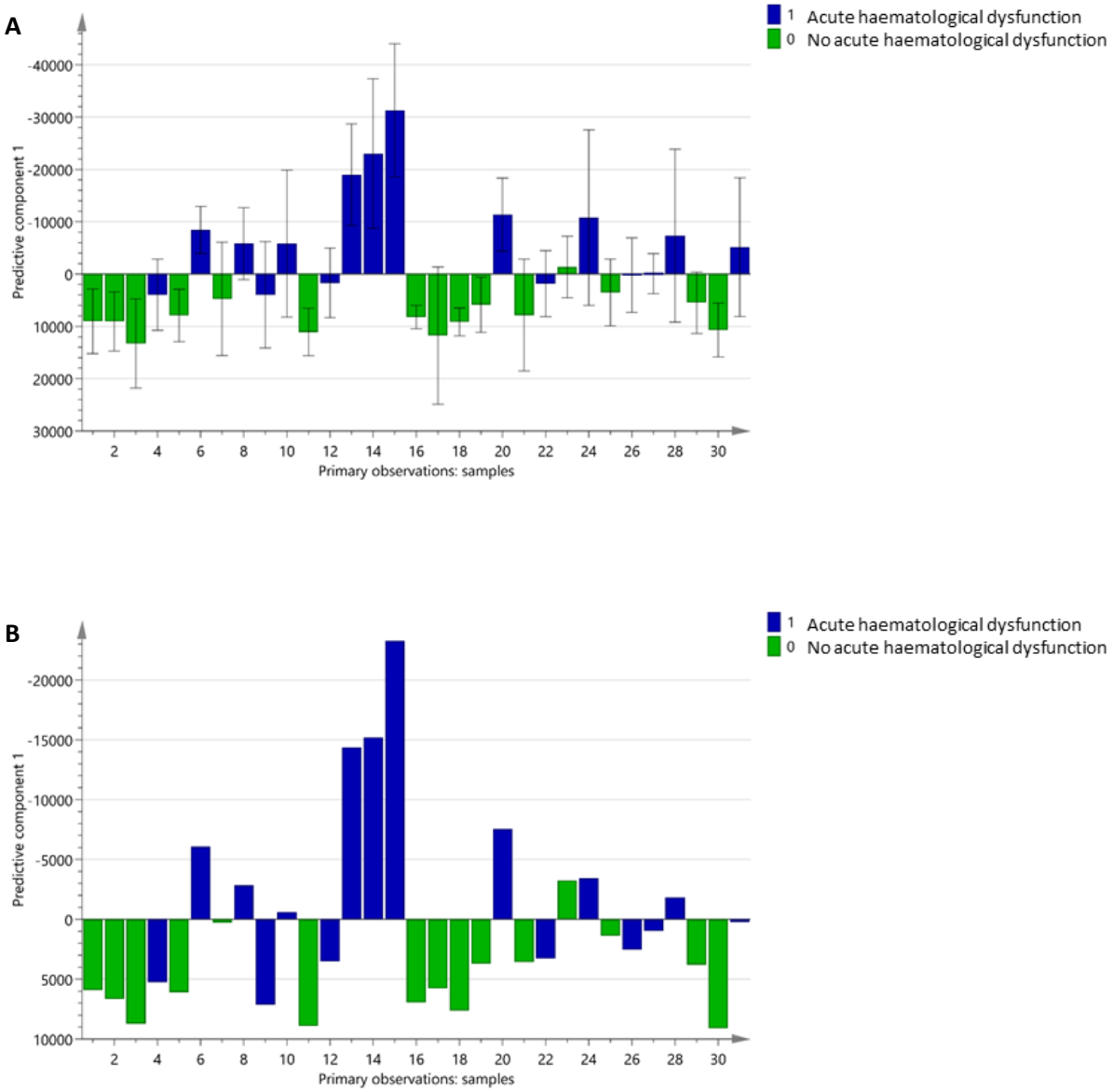


Figure 5.14. OPLS-DA scores plot (A) and cross-validated scores plot (B) derived from negative mode (ESI) lipid profiling using UPLC-MS spectroscopy spectra of plasma samples from the sepsis cohort taken at time point three. This demonstrates evidence of separation of the samples according to metabolic changes associated with acute haematological dysfunction (blue) from those without acute haematological dysfunction (green) (R^2X=0.187, R^2Y=0.505; Q^2Y=0.281). Both models misclassified six samples: one from the group without dysfunction (23) and five from the group with dysfunction (four, nine, 12, 22 and 26). The cross-validated model (p=0.01) misclassified two additional samples from the group with dysfunction (27 and 31).

The results of the sets of O-PLS-DA models of respiratory, cardiovascular, and haematological dysfunction based on positive and negative mode LCMS data of samples from individual time points divided according to their five SOFA scores are shown in Table 5.5A (positive) and B (negative). These tables demonstrate a more even distribution of the samples between some of the five groups in the models of respiratory and cardiovascular dysfunction compared with the dichotomised models of these organ dysfunctions. Whereas, the distribution of the samples between the groups the haematological models with five groups (shown in Table 5.5), is poorer than the distribution of the samples in the haematological models with two groups (shown in Table 5.4). The evaluation parameters of all the models of all three clinical classes and both modes of LCMS data were universally poor. This is except for the cardiovascular time point zero (enrolment) model, based on positive mode data. However, a prerequisite of inclusion in the VACS trial and therefore this study was a MAP of less than 65mmHg requiring vasopressors, i.e. a cardiovascular SOFA score of at least three but the SOFA scoring system does not take the use of vasopressin as a vasopressor, into account, resulting in SOFA scores of zero in two patients and a score of one in three patients at time point zero.

Table 5.5 Results of the evaluation parameters of OPLS-DA models derived from a lipid profiling method based on positive (A) and negative mode (B) UPLC-MS analyses of the plasma samples from the sepsis cohort. Illustration of the percentage of the variation explained by the X (R2X) and Y matrices (R2Y) and predicted by the Y matrix (Q2Y) of the models evaluating samples based on their respiratory, cardiovascular, and haematological clinical classes with the samples divided into five groups. KEY: CV-ANOVA: cross-validated analysis of variance, SOFA: Sequential organ failure assessment, TP: time point.

A

OPLS-DA		Respiratory SOFA				Cardiovascular				Haematological			
Sample set: time point (n=sample number)		TP0 (n=25)	TP1 (n=50)	TP2 (n=48)	TP3 (n=31)	TP0 (n=25)	TP1 (n=50)	TP2 (n=48)	TP3 (n=31)	TP0 (n=25)	TP1 (n=50)	22	TP3 (n=31)
SOFA = 0		3	1	1	1	2	0	0	8	16	24	9	15
SOFA = 1		1	5	2	4	3	0	0	9	5	11	9	4
SOFA = 2		4	12	14	12	0	0	1	0	3	8	6	7
SOFA = 3		9	13	20	12	0	28	19	9	0	22	2	3
SOFA = 4		8	19	11	2	20	35	28	5	1	0	26	2
Number of components	Predictive	1	1	1	2	1	1	1	1	1	3	2	1
	Orthogonal to X	1	0	0	0	1	0	0	0	0	1	0	0
Model statistics	R^2X	0.205	0.124	0.095	0.255	0.200	0.084	0.116	0.188	0.127	0.317	0.194	0.179
	R^2Y	0.220	0.225	0.130	0.278	0.535	0.296	0.283	0.187	0.216	0.615	0.279	0.181
	Q^2	-0.064	-0.064	-0.028	0.00	0.199	-0.463	0.142	0.071	-0.129	0.111	0.060	0.068
	$R^2Y - Q^2$	0.284	0.289	0.158	0.278	0.336	0.759	0.141	0.116	0.345	0.504	0.219	0.113
CV-ANOVA	P VALUE	1.000	1.000	1.000	1.000	0.011	1.000	0.000	0.112	1.000	0.998	0.501	0.139

B

OPLS-DA		Respiratory				Cardiovascular				Haematological			
Sample set: time point (n=sample number)		TP0 (n=25)	TP1 (n=50)	TP2 (n=48)	TP3 (n=31)	TP0 (n=25)	TP1 (n=50)	TP2 (n=48)	TP3 (n=31)	TP0 (n=25)	TP1 (n=50)	TP2 (n=48)	TP3 (n=31)
SOFA = 0		3	1	1	1	2	0	0	8	16	24	9	15
SOFA = 1		1	5	2	4	3	0	0	9	5	11	9	4
SOFA = 2		4	12	14	12	0	0	1	0	3	8	6	7
SOFA = 3		9	13	20	12	0	28	19	9	0	22	2	3
SOFA = 4		8	19	11	2	20	35	28	5	1	0	26	2
Number of components	Predictive	1	1	1	1	1	1	1	3	1	2	4	1
	Orthogonal to X	0	0	0	0	2	0	0	0	0	0	1	0
Model statistics	R^2X	0.121	0.090	0.107	0.149	0.273	0.788	0.091	0.323	0.089	0.166	0.360	0.190
	R^2Y	0.174	0.120	0.107	0.124	0.060	0.322	0.299	0.629	0.250	0.343	0.620	0.185
	Q^2	-0.053	-0.095	-0.026	-0.084	0.083	-0.324	0.036	0.178	-0.109	0.023	0.072	0.061
	$R^2Y - Q^2$	0.227	0.215	0.133	0.208	-0.023	0.646	0.263	0.451	0.359	0.320	0.548	0.124
CV-ANOVA	P VALUE	1.000	1.000	1.000	1.000	0.680	1.000	0.246	0.796	1.000	0.997	0.987	0.211

5.4.2.2 Structural assignment of the lipid metabolites characterising the liver dysfunction classes

S-loadings plots of the OPLS-DA models of liver INJURY were used to identify the metabolite signals with the greatest contribution to the separation of the liver dysfunction and non-dysfunction samples from each time point. The metabolites signals identified as important at each of the four time points by the OPLS-DA models of liver dysfunction, from both modes, demonstrated a significant degree of overlap. In other words, most of the signals capable of differentiating between the two groups were the same at each of the four time points. Confirmation of the importance of the metabolite signals with the greatest contribution to the separation of the dichotomised liver groups was performed using the criteria of an initial screening process illustrated in Figure 5.1 and described in Section 5.3.5.1. Briefly, this consisted of the signals on the S-loadings plot having a correlation coefficient of either >0.75 or <-0.75 or >0.4 or <-0.4 and a covariance value of >0.07 or <-0.03, in addition to a good peak shape (see Section 5.3.5.1). Signals passing this initial screening process then underwent a series of univariate tests and were deemed significant if they achieved a p value of <0.05 on univariate t-testing of the liver dysfunction and non-liver dysfunction groups and a correlation of variance of the signal intensity in the quality control samples of 30 percent or less. Both assessments were performed on all the metabolite signals of importance, with the data from each time point being analysed separately.

The results of these analyses are reported in Tables 5.6A (positive) and B (negative). All the metabolites listed in these tables satisfied the criteria of both the OPLS-DA and univariate t-testing at one of the four time points. The criteria of both sets of assessments were satisfied at all four time points by eight of the 16 differentiating metabolites identified by the positive mode and by seven of the metabolites at three time points; which consisted of time points one to three, in six of these seven metabolites. In most cases, where both sets of criteria were not met all four time points, it was the univariate criteria that had not been met: these are values are in red in Tables 5.6A and B and signals associated with a correlation coefficient of <0.4 or >-0.4 are in blue.

Twenty-three of the metabolite signals detected by the negative mode analyses, satisfied the criteria of both the OPLS-DA and univariate t-testing at one of the four time points and ten of these 23 signals satisfied both sets of criteria at all four time points. Much akin to the positive mode data, the inability of signals to satisfy the criteria of both sets of assessments was due to the p value of two-tailed, t-test comparisons of the two groups not achieving statistical significance in the majority of cases; with time point zero being affected the most. Moreover, the majority of these metabolites detected by the negative mode analyses that did not meet the t-test criteria were predominantly unidentified unknowns and two tentatively assigned to the drug vecuronium and its metabolite 3-desacetyl vecuronium.

Metabolites signals satisfying both sets of criteria at one of the four time points were subjected to metabolite identification. Metabolites considered to be statistically significant in the differentiation of the two liver dysfunction groups are also listed in Tables 5.6A and B (under level of assignment). This included the use of putative assignments using online MS identification databases, tandem MS-MS and MS^E, (see Section 5.3.5.2).

Table 5.6 List of the statistically significant features of the OPLS-DA models of liver dysfunction derived from positive (A) and negative (B) ESI modes of lipid profiling using UPLC-MS of plasma samples from the sepsis cohort taken at enrolment to the study (TP0) and days one (TP1), two (TP2), and seven (TP3), after enrolment.

KEY: ESI: electrospray ionization; m/z: mass-to-charge ratio; ΔDa (found - theoretical m/z): difference between the identified metabolite and the theoretical m/z in Daltons; p(1) and p(corr): covariance and correlation coefficient of the metabolite to the clinical class of the OPLS-DA model, where a positive correlation means higher concentrations of the metabolites in the liver dysfunction group compared to the non-dysfunction group; QC CV: cross variance of the metabolite concentration in the quality control samples; MS/MS: tandem MS; MS^E: an iterative process of MS leading to the generation of non-selective metabolite fragments; TP: time point; values highlighted in red: a p value of >0.05 (non-statistically significant) on univariate t-testing comparing the liver dysfunction and non-liver dysfunction groups; values highlighted in blue: low p (corr) i.e. between > -0.4 and < 0.4; values highlighted in bold: QC CV >30%.

For all the phospholipids, the abbreviations refer to the head group (fatty acid at sn-1: sn-2 positions) PC: phosphatidylcholine; PC (0-): phosphatidylcholine ether; lysoPC: lysophosphatidylcholine; PI: phosphatidylinositol; SM: sphingomyelin; UKN: unknown i.e. unidentified.

A

Metabolite name	Level of metabolite assignment	Molecular formula [complex adduct] as detected	Retention time (min)	m/z (found)	m/z (theoretical)	ΔDa (found - theoretical m/z)	TP0				TP1				TP2				TP3				QC CV %
							OPLS-DA model		uni-variate analyses		OPLS-DA model		uni-variate analyses		OPLS-DA model		uni-variate analyses		OPLS-DA model		uni-variate analyses		
							p(1)	p(corr)	t-test p value	Fold change	p(1)	p(corr)	t-test p value	Fold change	p(1)	p(corr)	t-test p value	Fold change	p(1)	p(corr)	t-test p value	Fold change	
PC(14:0/16:0)	MS/MS	$C_{38}H_{77}NO_8P$+ [M+H]+	5.58	706.54	706.5387	0.0052	0.11	0.75	1.29E-02	1.98	0.13	0.78	5.24E-03	1.65	0.08	0.41	1.05E-02	1.41	0.08	0.51	4.87E-03	1.57	7
PC(16:0/16:0)	MS/MS	$C_{40}H_{81}NO_8P$+ [M+H+]+1	7.37	734.57	734.5694	0.0040	0.33	0.87	7.78E-03	1.82	0.31	0.84	3.02E-04	1.60	0.27	0.59	2.55E-04	1.53	0.25	0.65	1.36E-03	1.62	8
PC(O-18:0/16:1)	level 1: tentative	$C_{42}H_{85}NO_7P$+ [M+H]+	8.88	746.61	746.6058	0.0039	0.18	0.79	1.48E-02	1.80	0.18	0.77	2.59E-03	1.80	0.16	0.54	4.87E-03	1.81	0.08	0.32	7.99E-02	1.54	54
PC(O-30:0)	MS[E]	$C_{38}H_{79}NO_7P$+ [M+H]+	6.56	692.56	692.5520	0.0094	0.02	0.52	1.29E-01	1.78	0.02	0.63	3.13E-02	1.64	0.03	0.58	4.59E-03	1.80	0.02	0.51	1.59E-02	2.28	10
PC(O-32:0) or PC(O-16:0/16:0)	MS/MS	$C_{40}H_{83}NO_7P$+ [M+H]+	8.72	720.59	720.5907	0.0029	0.10	0.76	2.52E-02	1.76	0.09	0.67	9.89E-03	1.25	0.12	0.66	2.42E-04	1.74	0.10	0.54	6.71E-03	1.85	10
PC(O-34:2)	MS/MS	$C_{42}H_{85}NO_7P$+ [M+H]+	7.22	744.59	744.5907	0.0027	0.04	0.38	2.82E-01	1.14	0.06	0.48	3.72E-02	1.15	0.09	0.65	2.27E-04	1.99	0.05	0.41	3.43E-02	1.50	7
lysoPC(16:0)	MS alone	$C_{24}H_{51}NO_7P$+ [M+H+]+1	1.17	497.34	497.3437	-0.0002	-0.07	-0.49	5.78E-02	-1.19	-0.11	-0.69	5.91E-05	-1.45	-0.14	-0.67	4.34E-05	-1.39	-0.12	-0.61	7.57E-04	-1.59	10
lysoPC(18:0)	MS[E]	$C_{26}H_{55}NO_7P$+ [M+H+]+2	1.63	526.38	526.3783	0.0000	-0.02	-0.43	5.07E-02	-1.39	-0.14	-0.62	1.07E-03	-1.47	-0.04	-0.50	2.15E-03	-1.29	-0.04	-0.49	6.49E-03	-1.33	11
lysoPC(20:4)	MS/MS	$C_{28}H_{51}NO_7P$+ [M+H+]+1	0.97	545.35	545.3403	0.0053	-0.04	-0.42	7.91E-02	-1.38	-0.06	-0.63	3.72E-06	-1.71	-0.05	-0.42	3.39E-02	-1.43	-0.05	-0.43	4.61E-02	-1.56	10
lysoPC(22:6)	MS/MS	$C_{30}H_{51}NO_7P$+ [M+H]+	0.93	568.34	568.3400	0.0007	-0.07	-0.58	2.54E-02	-1.77	-0.07	-0.63	3.18E-05	-1.80	-0.07	-0.47	5.12E-03	-1.80	-0.07	-0.56	1.38E-03	-1.81	9
SM(d18:2/18:0)	MS/MS and MS[E]	$C_{41}H_{82}N_2O_6P$+ [M+H]+	5.72	729.59	729.5910	0.0019	-0.11	-0.67	4.79E-02	-1.43	-0.12	-0.64	2.60E-04	-1.58	-0.11	-0.46	4.90E-03	-1.30	-0.11	-0.54	2.94E-03	-1.83	9
SM(d36:1)	MS/MS	$C_{41}H_{84}N_2O_6P$+ [M+H]+	7.28	731.61	731.6067	0.0025	-0.06	-0.30	7.80E-01	-1.08	-0.03	-0.47	1.40E-03	-1.27	-0.16	-0.55	1.27E-03	-1.36	-0.15	-0.56	7.29E-04	-2.06	9
UKN	NA		3.37	619.49			0.02	0.55	9.03E-02	1.87	0.01	0.31	2.22E-01	1.22	0.03	0.48	7.97E-03	1.98	0.02	0.42	3.27E-02	2.38	8
UKN (query peptide)	NA		0.81	611.29			0.02	0.66	8.49E-03	11.13	0.01	0.49	3.27E-04	6.79	0.03	0.68	5.60E-05	6.55	0.02	0.59	8.80E-03	7.86	9
UKN (query peptide)	NA		0.66	583.26			0.02	0.49	4.69E-02	3.60	0.02	0.65	4.70E-04	4.59	0.03	0.68	6.55E-05	4.79	0.03	0.52	1.75E-02	6.03	10
UKN (query peptide)	NA		0.72	597.27			0.02	0.63	1.81E-02	8.83	0.02	0.66	1.06E-04	8.06	0.03	0.71	4.24E-05	11.77	0.03	0.50	3.89E-02	13.66	7
UKN (query lyso-lipid dimer)	NA		1.22	1017.7			-0.01	-0.35	7.49E-02	-3.23	-0.02	-0.45	1.49E-03	-3.11	-0.03	-0.57	1.26E-04	-2.94	-0.03	-0.56	1.43E-03	-1.74	16

B

Metabolite name	Level of assignment	Molecular formula [complex adduct] as detected	Retention time (min)	m/z (found)	m/z (theoretical)	ΔDa (found - theoretical m/z)	TP0				TP1				TP2				TP3				QC CV %
							OPLS-DA model		uni-variate analyses		OPLS-DA model		uni-variate analyses		OPLS-DA model		uni-variate analyses		OPLS-DA model		uni-variate analyses		
							p(1)	p(corr)	t-test p value	Fold change	p(1)	p(corr)	t-test p value	Fold change	p(1)	p(corr)	t-test p value	Fold change	p(1)	p(corr)	t-test p value	Fold change	
a cholesterol glucuronide	MS/MS	$C_{33}H_{53}O_7^-$ [M-H]-	2.65	561.3818	561.3797	0.0023	0.03	0.36	6.74E-02	2.09	0.03	0.40	8.01E-03	1.80	0.03	0.371	7.88E-03	1.65	0.03	0.37	3.14E-03	1.84	4
a steroid glucuronide	(in source fragsments)	$C_{33}H_{38}O_{10}^-$ [M-H]-	0.66	611.38	611.3801	-0.0001	0.03	0.64	1.72E-02	3.32	0.02	0.56	3.50E-04	3.03	0.03	0.572	6.43E-05	3.28	0.03	0.57	5.09E-03	5.07	10
glycocholic acid	MS/MS	$C_{26}H_{42}NO_6^-$ [M-H]-	0.62	464.304	464.3018	0.0022	0.07	0.54	4.03E-02	8.33	0.07	0.41	1.32E-03	13.12	0.08	0.525	4.92E-03	6.74	0.08	0.53	1.88E-01	2.00	3
hydroxy-eicosanoic acid	level 1: tentative	$C_{20}H_{39}O_3^-$ [M-H]-	2.63	327.2915	327.2905	0.0005	0.02	0.43	1.24E-01	1.32	0.03	0.47	2.13E-02	2.08	0.03	0.518	2.08E-02	2.94	0.03	0.52	9.74E-02	4.10	16
PC(16:0/16:0)	same as positive	$C_{41}H_{81}NO_{10}P^-$ [M+FA-H]-	7.34	778.5626	778.5603	0.0027	0.15	0.69	2.12E-03	2.06341	0.14	0.70	4.14E-05	1.59892	0.11	0.564	6.56E-04	1.55139	0.11	0.56	1.67E-04	1.63302	3
PC(O-18:0/16:1)	same as positive	$C_{23}H_{85}NO_{10}P^-$ [M+FA-H]-	8.86	790.5999	790.6040	-0.0040	0.06	0.46	1.22E-02	1.6143	0.05	0.48	9.23E-03	1.43838	0.07	0.596	8.32E-03	1.46039	0.07	0.60	1.19E-02	1.35427	23
PC(O-32:0) or PC(O-16:0/16:0)	same as positive	$C_{41}H_{83}NO_9P^-$ [M+FA-H]-	8.67	764.581	764.5811	-0.0001	0.03	0.45	1.39E-02	1.7091	0.04	0.52	4.18E-03	1.74518	0.04	0.556	1.02E-02	1.5667	0.04	0.56	3.58E-03	2.00218	5
PI(16:0/18:1)	MS/MS	$C_{43}H_{80}O_{13}P^-$ [M-H]-	5.70	835.5393	835.5342	0.0048	0.05	0.65	1.85E-03	1.81816	0.04	0.46	8.49E-03	1.83299	0.03	0.422	3.23E-03	1.7726	0.03	0.42	1.58E-03	1.85084	25
lysoPC(16:0)	same as positive	$C_{25}H_{51}NO_9P^-$ [M+FA-H]-	1.18	540.3316	540.3307	0.0013	-0.20	-0.55	3.85E-02	-1.42557	-0.25	-0.68	2.44E-03	-1.61016	-0.25	-0.704	1.77E-05	-1.543	-0.25	-0.70	4.14E-03	-1.32478	3
lysoPC(22:6)	same as positive	$C_{31}H_{51}NO_9P^-$ [M+FA-H]-	0.94	612.3323	612.3307	0.0013	-0.07	-0.57	2.21E-02	-2.2213	-0.07	-0.65	7.80E-05	-1.85853	-0.06	-0.597	3.37E-03	-1.89404	-0.06	-0.60	2.65E-03	-1.44262	3
PC(16:0/22:6)	MS/MS	$C_{47}H_{83}NO_{10}P^-$ [M+FA-H]-	5.42	850.5627	850.5603	0.0027	-0.11	-0.52	3.00E-02	-1.86855	-0.10	-0.54	1.94E-02	-1.65815	-0.08	-0.44	3.06E-02	-1.54963	-0.08	-0.44	2.48E-04	-2.36809	26
SM(d18:2/18:0)	same as positive	$C_{42}H_{82}O_8P^-$ [M+FA-H]-	5.70	773.5832	773.5892	-0.0062	-0.06	-0.41	8.75E-02	-1.47345	-0.07	-0.48	1.38E-04	-1.72344	-0.05	-0.357	1.75E-03	-1.40862	-0.05	-0.36	1.63E-03	-1.75459	21
SM(d36:1)	same as positive	$C_{42}H_{84}O_8P^-$ [M+FA-H]-	7.25	775.5991	775.6049	-0.0059	-0.04	-0.24	5.80E-01	-1.05587	-0.08	-0.49	1.22E-02	-1.25295	-0.07	-0.432	1.06E-03	-1.26584	-0.07	-0.43	8.59E-04	-1.63311	2
UKN	NA		0.61	313.123			0.13	0.77	1.65E-02	4.77	0.13	0.76	1.33E-04	5.33	0.13	0.705	5.16E-04	5.67	0.13	0.70	4.37E-02	4.31	4
UKN	NA		0.67	426.262			0.03	0.60	5.34E-02	2.12	0.03	0.56	4.80E-03	2.36	0.03	0.557	4.39E-03	4.77	0.03	0.56	7.28E-02	4.79	10
UKN	NA		0.91	429.299			0.04	0.61	6.68E-02	1.68	0.03	0.49	2.89E-02	1.28	0.04	0.538	1.59E-02	1.84	0.04	0.54	2.79E-02	4.35	5
UKN	NA		2.54	539.432			0.05	0.54	7.16E-02	2.47	0.04	0.43	6.47E-02	1.85	0.04	0.469	5.59E-03	2.45	0.04	0.47	1.40E-02	2.86	4
UKN	NA		2.55	540.435			0.03	0.44	8.05E-02	2.34	0.02	0.42	6.82E-02	1.50	0.02	0.448	6.46E-03	2.58	0.02	0.45	1.51E-02	3.62	22
UKN (query oligopeptide)	NA		0.67	516.293			0.03	0.60	5.46E-02	3.71	0.03	0.48	8.77E-03	6.84	0.03	0.485	2.27E-02	4.45	0.03	0.48	1.47E-01	1.17	4
UKN (query oligopeptide)	NA		1.74	583.255			0.04	0.60	7.41E-02	3.13	0.04	0.68	6.13E-05	8.67	0.04	0.597	7.35E-04	8.10	0.04	0.60	1.52E-02	14.88	30
UKN (query PI)	NA		7.45	863.563			0.03	0.58	3.97E-02	2.07326	0.03	0.51	8.72E-03	1.73551	0.04	0.681	1.60E-03	1.91984	0.04	0.68	1.23E-02	1.46827	7
desacetyl vecuronium)	NA		3.36	495.406			0.03	0.48	8.86E-02	2.69	0.03	0.45	6.45E-02	1.73	0.03	0.427	1.09E-02	2.06	0.03	0.43	8.57E-03	2.61	6
UNK (query vecuronium)	NA		2.25	537.416			0.03	0.40	1.39E-01	2.22	0.03	0.36	6.20E-02	1.40	0.03	0.386	9.50E-03	1.86	0.03	0.39	1.12E-02	2.70	9

The most significant metabolic changes responsible for the differentiation of patients with and without liver dysfunction demonstrated by O-PLS-DAs based on the UPLC-MS positive and negative mode data consisted of 18 identified metabolites and 15 unknowns. Six of the identified metabolites were demonstrated by both modes: a phosphatidylcholine (PC), a PC ether, two lysophosphatidylcholines (lysoPCs) and two sphingomyelins (SMs). A further ten metabolic differences were demonstrated by the positive mode model: one PC, two PC ethers, two lysoPCs and five unknowns (Table 5.6A). One of the unknown features with an m/z of 1017.7 and a retention time of 1.22 minutes is possibly a lyso-lipid dimer and three of the unknown features had low retention times (less than two minutes) consistent with them being peptides. In addition to the six detected by both modes, a further seventeen metabolite signals were shown to be important to the differentiation of the liver dysfunction groups by the OPLS-DA based on the negative mode data. This included one phosphatidylcholine, one phosphatidylcholine ether, one phosphatidylinositol (PI), hydroxy-eicosanoic acid, glycocholic acid and two glucuronides: one steroid and one cholesterol. There were also ten metabolite signals of importance to the negative O-PLS-DA models that remained unidentified. Many of the unknowns had low retention times and molecular weight consistent with them belonging peptides or oligopeptides and two of the signals were tentatively assigned as vecuronium and one of its metabolites, 3-desacetyl vecuronium.

Most of the metabolites responsible for the differentiation of the liver dysfunction groups demonstrated by O-PLS-DA models from both modes of this UPLC-MS data demonstrated increased plasma levels in the dysfunction group compared to the non-dysfunction group. This included hydroxy-eicosanoic acid, the bile acid glycocholic acid, a cholesterol glucuronide, a steroid glucuronide, all of the phosphatidylcholine ethers [PC(O-30:0), PC(O-32:0) or PC(O-16:0/16:0), PC(O-18:0/16:1), PC (O-34:2)], the one phosphatidylinositol [PI(16:0/18:1)], and three of the four phosphatidylcholines [PC(14:0/16:0), PC(16:0/16:0), PC(O-18:0/16:1)]. This compares with decreased

plasma levels in the liver dysfunction group compared to the non-dysfunction group in six of identified metabolites: two sphingomyelins [SM (d18:2/18:0) and (d36:1)], three lysophosphatidylcholines [lysoPC (16:0), (18:0), (20:4) and (22:6)] and the phosphatidylcholine PC (16:0/22:6); in addition to a possible lyso-lipid dimer.

5.4.2.3 Structural assignment of the lipid metabolites characterising haematological dysfunction classes

The same method of using S-loadings plots of the OPLS-DA models followed by a series of univariate analyses as illustrated in Figure 5.1 and described in the previous section, was applied to the three models capable of differentiating between patients with and without haematological dysfunction. The results of these analyses are reported in Tables 5.7 and 5.8; and 5.9 and 5.10, for the models based on the positive and negative modes, respectively.

The criteria of both sets of assessments were fulfilled by a total of 49 metabolite features identified by the positive mode and therefore, deemed differentiating metabolites. This is with the exception of two metabolites: one metabolite that did not meet the t-test criteria at one of the two time points (highlighted in red in Table 5.7) and one metabolite with a cross variance (coefficient of variation; CV%) in the quality control samples that was greater than 30 percent (highlighted in bold in Table 5.7). Eleven of these metabolites were identified as differentiating metabolites both on days two and seven (time points 2 and 3); and two and 36 of these metabolites were identified as differentiating on day two and seven (alone), respectively. Of these, eleven were identified as differentiating metabolites of the liver injury models that have been structural assigned and listed in Table 5.6A, (including the aforementioned two metabolites that failed to fulfil all of the criteria required to be deemed statistically significant), and these are listed in Table 5.7 The remaining 38 differentiating metabolites remain unidentified (see Table 5.8). This include four metabolites that are differentiating metabolites

at both time points; one from the time point two model and the remaining 33 that are from the time point three model alone.

The haematological O-PLS-DA model based on negative mode data from time point three identified 47 metabolites that fulfilled both sets of assessments required to be deemed differentiating. Of these, seven were identified as differentiating metabolites of the liver injury models that have been structural assigned and listed in Table 5.6B and 40 remain unidentified; the structural assigned and unidentified differentiating metabolites of this haematological model are shown in Tables 5.9 and 5.10, respectively.

Twelve of the most significant metabolites responsible for the differentiation of patients with and without haematological dysfunction demonstrated by the OPLS-DAs based on UPLC-MS positive and negative mode data had been structurally assigned and identified as differentiating metabolites of liver dysfunction. This consisted of four lyso-PCs, two sphingomyelins, three PCs and three PC-ethers. Seven of these lipids were identified by both modes; four was identified by the positive mode and one was identified by negative mode.

Table 5.7 List of the structurally assigned statistically significant features of the OPLS-DA models of haematological dysfunction derived from positive ESI modes of lipid profiling using UPLC-MS of plasma samples from the sepsis cohort taken on days two (TP2), and seven (TP3), after enrolment.

KEY: ESI: electrospray ionization; m/z: mass-to-charge ratio; ΔDa (found - theoretical m/z): difference between the identified metabolite and the theoretical m/z in Daltons; p(1) and p(corr): covariance and correlation coefficient of the metabolite to the clinical class of the OPLS-DA model, where a negative correlation means higher concentrations of the metabolites in the haematological dysfunction group compared to the non-dysfunction group; QC CV: cross variance of the metabolite concentration in the quality control samples; MS/MS: tandem MS, MS^E: an iterative process of MS leading to the generation of non-selective metabolite fragments; TP: time point; values highlighted in red: a p value of >0.05 (non-statistically significant) on univariate t-testing comparing the liver dysfunction and non-liver dysfunction groups; values highlighted in bold: QC CV >30%.

For all the phospholipids, the abbreviations refer to the head group (FA at sn-1: sn-2 positions) PC: phosphatidylcholine; PC (0-): phosphatidylcholine ether; lysoPC: lysophosphatidylcholine; SM: sphingomyelin.

Time points	Metabolite name	Level of metabolite assignment	Molecular formula [complex adduct] as detected	Retention time (min)	m/z (found)	m/z (theoretical)	ΔDa (found - theoretical m/z)	TP2				TP3				QC CV%
								OPLS-DA model		uni-variate analyses		OPLS-DA model		uni-variate analyses		
								p(1)	p(corr)	t-test p value	Fold change	p(1)	p(corr)	t-test p value	Fold change	
TPs 2 and 3	PC(16:0/16:0)	MS/MS	$C_{40}H_{81}NO_8P$+ [M+H+]+1	7.37	734.57	734.5694	0.0040	-0.25	-0.57	3.91E-03	1.44	-0.2	-0.736	2.57E-02	1.27	8
	SM(d36:1)	MS/MS	$C_{38}H_{77}NO_8P$+ [M+H]+	5.58	706.54	706.5387	0.0052	-0.10	-0.51	1.55E-03	1.38	-0.1	-0.83	3.53E-03	1.60	7
	lysoPC(16:0)	MS/MS	$C_{40}H_{83}NO_7P$+ [M+H]+	8.72	720.59	720.5907	0.0029	-0.09	-0.55	9.85E-04	1.32	-0.1	-0.515	4.86E-02	1.64	10
	SM(d18:2/18:0)	MS/MS	$C_{42}H_{85}NO_7P$+ [M+H]+	7.22	744.59	744.5907	0.0027	-0.06	-0.42	3.50E-03	1.57	-0	-0.447	4.37E-03	1.69	7
	PC(14:0/16:0)	MS/MS	$C_{41}H_{84}N_2O_6P$+ [M+H]+	7.28	731.61	731.6067	0.0025	0.17	0.60	4.66E-03	-1.32	0.14	0.669	7.82E-03	-1.93	9
	PC(O-32:0) or PC(O-16:0/16:0)	MS alone	$C_{24}H_{51}NO_7P$+ [M+H+]+1	1.17	497.34	497.3437	-0.0002	0.10	0.50	4.15E-02	-1.04	0.09	0.648	4.06E-03	-1.34	10
	PC(O-34:2)	MS/MS and MS^E	$C_{41}H_{82}N_2O_6P$+ [M+H]+	5.72	729.59	729.5910	0.0019	0.13	0.56	1.51E-02	-1.20	0.08	0.56	**1.21E-01**	-1.44	9
TP2 only	PC(O-18:0/16:1)	level 1: tentative	$C_{42}H_{85}NO_7P$+ [M+H]+	8.88	746.61	746.6058	0.0039	-0.12	-0.41	1.45E-02	1.26					**54**
TP3 only	lysoPC(22:6)	MS/MS	$C_{30}H_{51}NO_7P$+ [M+H]+	0.93	568.34	568.3400	0.0007					0.07	0.729	8.09E-04	-2.25	9
	lysoPC(20:4)	MS/MS	$C_{28}H_{51}NO_7P$+ [M+H+]+1	0.97	545.35	545.3403	0.0053					0.06	0.692	4.87E-03	-1.74	10
	lysoPC(18:0)	MS^E	$C_{26}H_{55}NO_7P$+ [M+H+]+2	1.63	526.38	526.3783	0.0000					0.05	0.832	4.27E-04	-1.52	11

Table 5.8 List of the unidentified statistically significant features of the OPLS-DA models of haematological dysfunction derived from positive ESI modes of lipid profiling using UPLC-MS of plasma samples from the sepsis cohort taken on days one (TP1), two (TP2), and seven (TP3), after enrolment; only features that were present in two or more of the models are shown here.

KEY: ESI: electrospray ionization; m/z: mass-to-charge ratio; p(1) and p(corr): covariance and correlation coefficient of the metabolite to the clinical class of the OPLS-DA model, where a negative correlation means higher concentrations of the metabolites in the haematological dysfunction group compared to the non-dysfunction group; QC CV: cross variance of the metabolite concentration in the quality control samples; TP: time point.

Time points	Retention time (min)	m/z (found)	TP2				TP3				QC CV%
			OPLS-DA model		uni-variate analyses		OPLS-DA model		uni-variate analyses		
			p(1)	p(corr)	t-test p value	Fold change	p(1)	p(corr)	t-test p value	Fold change	
TPs 2 and 3	7.37	735.58	-0.17	-0.58	2.76E-03	1.50	-0.14	-0.732	2.64E-02	1.23	6
	7.37	736.58	-0.08	-0.56	7.53E-03	1.45	-0.07	-0.723	4.57E-02	1.23	8
	5.59	707.58	-0.07	-0.49	3.10E-03	1.37	-0.07	-0.834	9.72E-04	1.61	25
	8.9	747.61	-0.09	-0.45	4.10E-03	1.40	-0.08	-0.586	9.36E-03	1.36	29
TP2 only	5.73	730.6	0.09	0.56	1.78E-02	1.04					10
TP3 only	5.8	754.55					-0.06	-0.825	2.07E-02	1.31	5
	7.38	756.56					-0.06	-0.8	2.58E-02	1.17	6
	5.8	732.56					-0.24	-0.683	3.92E-02	1.23	7
	5.8	734.56					-0.09	-0.69	3.20E-02	1.27	7
	7.99	745.6					-0.05	-0.609	1.01E-02	3.42	8
	5.43	704.58					-0.11	-0.571	1.06E-02	1.12	22

Table 5.8 continued

	8.71	813.62		0.22	0.864	3.31E-04	-2.06	7
	0.93	569.35		0.04	0.739	7.06E-04	-2.29	8
	5.45	808.58		0.08	0.642	2.30E-03	-1.62	8
	1.51	524.37		0.08	0.777	5.82E-03	-1.37	8
	1.09	546.36		0.09	0.673	3.39E-03	-1.84	9
	7.29	732.61		0.09	0.673	7.59E-03	-1.79	9
	7.85	836.62		0.10	0.728	8.41E-05	-2.36	9
	5.6	832.59		0.09	0.555	8.61E-03	-2.48	9
	7.2	834.61		0.22	0.75	5.34E-04	-2.17	10
	1.17	991.68		0.08	0.794	8.56E-04	-1.58	10
	7.2	835.61		0.15	0.737	5.27E-04	-1.81	10
	9.49	838.64		0.05	0.636	2.29E-02	-1.37	10
	1.17	498.35		0.05	0.663	3.78E-03	-1.36	10
	7.86	837.63		0.07	0.743	3.45E-05	-2.34	10
	13.58	816.71		0.09	0.656	3.13E-02	-1.42	11
	1.51	525.38		0.05	0.796	2.44E-03	-1.39	11
	6.58	785.59		0.21	0.782	1.47E-03	-1.59	11
	13.59	817.71		0.05	0.654	2.62E-02	-1.37	12
	1.17	992.68		0.06	0.791	8.01E-04	-1.70	12
	1.11	547.36		0.05	0.648	1.29E-02	-1.26	15
	5.56	834.6		0.04	0.614	3.97E-03	-2.46	16
	12.79	809.66		0.05	0.695	4.30E-03	-1.23	16
	4.91	802.54		0.04	0.632	7.91E-03	-1.59	19
	6.76	810.6		0.12	0.626	1.77E-02	-2.09	19
	9.71	760.64		0.07	0.675	2.69E-03	-2.15	19
	8.73	814.63		0.10	0.785	1.55E-03	-1.56	20
	9.7	759.64		0.12	0.76	1.55E-03	-1.64	23

Table 5.9 List of the structurally assigned statistically significant features of the OPLS-DA models of haematological dysfunction derived from negative ESI modes of lipid profiling using UPLC-MS of plasma samples from the sepsis cohort taken on day seven (TP3), after enrolment.

KEY: ESI: electrospray ionization; m/z: mass-to-charge ratio; ΔDa (found - theoretical m/z): difference between the identified metabolite and the theoretical m/z in Daltons; TP: time point; p(1) and p(corr): covariance and correlation coefficient of the metabolite to the clinical class of the OPLS-DA model, where a negative correlation means higher concentrations of the metabolites in the haematological dysfunction group compared to the non-dysfunction group; QC CV: cross variance of the metabolite concentration in the quality control samples; MS/MS: tandem MS, MS^E: an iterative process of MS leading to the generation of non-selective metabolite fragments.

For all the phospholipids, the abbreviations refer to the head group (fatty acid at sn-1: sn-2 positions) PC: phosphatidylcholine; PC (0-): phosphatidylcholine ether; lysoPCs: lysophosphatidylcholine; SM: sphingomyelin.

Metabolite name	Level of assignment	Molecular formula [complex adduct] as detected	Retention time (min)	m/z (found)	m/z (theoretical)	ΔDa (found - theoretical m/z)	TP3				QC CV%
							OPLS-DA model		uni-variate analyses		
							p(1)	p(corr)	t-test p value	Fold change	
PC(16:0/16:0)	same as positive	$C_{41}H_{81}NO_{10}P$-[M+FA-H]-	7.34	778.5626	778.5603	0.0027	-0.11	-0.69	2.25E-02	1.23	3
PC(O-18:0/16:1)	same as positive	$C_{23}H_{85}NO_{10}P$-[M+FA-H]-	8.86	790.5999	790.6040	-0.0040	-0.05	-0.49	1.82E-02	1.13	23
SM(d36:1)	same as positive	$C_{42}H_{84}O_8P$-[M+FA-H]-	7.25	775.5991	775.6049	-0.0059	0.09	0.65	1.37E-02	-1.63	2
SM(d18:2/18:0)	same as positive	$C_{42}H_{82}O_8P$-[M+FA-H]-	5.70	773.5832	773.5892	-0.0062	0.06	0.65	2.74E-02	-1.47	21
PC(16:0/22:6)	MS/MS	$C_{47}H_{83}NO_{10}P$-[M+FA-H]-	5.42	850.5627	850.5603	0.0027	0.08	0.69	1.59E-04	-2.33	26
lysoPC(22:6)	same as positive	$C_{31}H_{51}NO_9P$-[M+FA-H]-	0.94	612.3323	612.3307	0.0013	0.07	0.77	1.67E-04	-2.06	3
lysoPC(16:0)	same as positive	C25H51NO9P-[M+FA-H]-	1.18	540.3316	540.3307	0.0013	0.28	0.83	1.56E-03	-1.36	3

Table 5.10 List of the unidentified statistically significant features of the OPLS-DA models of haematological dysfunction derived from negative ESI modes of lipid profiling using UPLC-MS of plasma samples from the sepsis cohort taken on day seven (TP3), after enrolment.

KEY: ESI: electrospray ionization; m/z: mass-to-charge ratio; p(1) and p(corr): covariance and correlation coefficient of the metabolite to the clinical class of the OPLS-DA model, where a negative correlation means higher concentrations of the metabolites in the haematological dysfunction group compared to the non-dysfunction group; QC CV: cross variance of the metabolite concentration in the quality control samples; TP: time point.

Retention time (min)	m/z (found)	TP 3				QC CV%
		OPLS-DA model		uni-variate analyses		
		p(1)	p(corr)	t-test p value	Fold change	
7.33	778.591	-0.10	-0.63	2.11E-02	1.16	2
7.34	779.567	-0.07	-0.67	3.73E-02	1.19	2
0.58	117.055	-0.08	-0.57	1.55E-02	1.87	3
0.62	314.140	-0.09	-0.84	2.29E-02	5.10	3
0.61	313.1230	-0.19	-0.82	0.03	3.90	4
0.49	552.179	-0.11	-0.56	2.80E-02	22.52	6
0.5	313.059	-0.07	-0.55	2.64E-02	1.91	6
0.95	311.223	-0.10	-0.70	2.58E-02	2.49	6
0.49	508.190	-0.08	-0.60	3.12E-02	14.65	6
0.49	553.183	-0.06	-0.56	2.75E-02	18.01	6
0.83	359.204	-0.07	-0.69	4.37E-03	78.14	8
0.61	314.121	-0.09	-0.81	2.18E-02	5.19	8
0.69	255.160	-0.05	-0.54	1.98E-02	3.54	8
0.51	566.195	-0.08	-0.67	4.87E-02	5.54	9

Table 5.10 continued

8.68	858.620	0.04	0.71	5.28E-04	-1.95	3
13.74	667.653	0.04	0.61	3.52E-03	-1.69	3
1.63	569.366	0.11	0.76	6.50E-04	-1.72	3
6.43	828.614	0.12	0.78	5.86E-04	-1.50	3
0.98	589.337	0.06	0.69	1.33E-02	-1.77	4
12.56	858.658	0.07	0.56	4.30E-02	-1.17	4
0.98	588.332	0.11	0.70	1.17E-02	-1.76	4
1.18	1035.670	0.06	0.86	6.49E-04	-1.58	4
1.18	541.335	0.14	0.79	4.91E-03	-1.30	4
7.25	776.604	0.06	0.64	1.61E-02	-1.53	4
4.9	825.551	0.06	0.63	1.21E-03	-1.85	5
1.1	590.344	0.08	0.70	1.33E-02	-1.51	5
8.68	856.608	0.10	0.74	1.02E-04	-1.95	5
7.16	879.640	0.05	0.66	8.73E-05	-1.74	9
7.17	878.621	0.07	0.65	1.30E-04	-1.71	11
1.18	1035.710	0.06	0.76	5.97E-03	-1.63	12
7.17	878.595	0.07	0.62	2.41E-04	-1.57	15
7.17	879.600	0.05	0.65	9.20E-05	-1.75	18
8.68	857.616	0.08	0.74	1.10E-04	-2.16	19
5.42	851.568	0.06	0.70	1.16E-04	-2.25	22
1.18	542.337	0.06	0.75	3.90E-03	-1.35	24
5.71	773.638	0.06	0.65	1.50E-02	-1.44	25
4.9	824.547	0.08	0.62	2.97E-03	-1.70	26
5.42	851.635	0.06	0.69	1.92E-04	-2.12	26
1.1	541.315	0.06	0.83	1.82E-03	-1.50	27
9.65	803.632	0.08	0.74	1.53E-03	-1.51	30

5.5 Discussion

5.5.1 Liver dysfunction

A UPLC-MS based lipid profiling technique was used to expand on the evidence supporting a decrease in glyceride and choline containing lipids in the serum from patients from the sepsis cohort with liver dysfunction compared to those without liver dysfunction using a method of metabolic profiling based on NMR.

As described earlier in Section 5.1, lipids can be divided into eight categories based on their structural features (Fahy, Subramaniam, Brown, *et al.*, 2005). This includes fatty acids, glycerophospholipids (also known as phosphoglycerides) and sphingolipids. In this study, differences in 18 plasma lipids were demonstrated between the patients with and without liver dysfunction. This consisted of thirteen phospholipids; the free (unbound) fatty acid hydroxy-eicosanoic acid and three conjugated lipids: a steroid, a cholesterol, and the bile acid glycocholic acid, each of which will be discussed in order. Several unidentified features were also shown to be important to the differentiation of the two liver dysfunction groups. These included two features with characteristics consistent with the paralysing agent vecuronium and its metabolite 3-desacetyl-vecuronium and five features with characteristics of oligopeptides. However, no further structural information could be determined beyond their compound class for these oligopeptides and so they have been labelled 'unknowns' and will not be discussed further.

Taken together, the UPLC-MS data from both modes demonstrated differences between the patients of the sepsis cohort, with and without liver dysfunction in thirteen phospholipids: four lyso-phosphatidylcholines, two sphingomyelins, three phosphatidylcholine ethers, one phosphatidylinositol and three phosphatidylcholines. Collectively, these phospholipids can divided into glycerophospholipids and the sphingolipid, sphingomyelin (Fahy, Subramaniam, Brown, *et al.*, 2005). Structurally, both of these types of lipids have a three carbon backbone with fatty acids attached to one or two of the three carbon molecules and a phosphate containing head group

attached to the third (Murray & Davis, 2003). Fatty acids are made up of an aliphatic hydrocarbon chain with a carboxylic acid on the end (Fahy, Subramaniam, Brown, *et al.*, 2005). Sphingomyelins have a sphingosine backbone and a phosphorylcholine head. Whereas, phosphoglycerides form one half of a group of lipids that have a glycerol backbone (glycerides), and have a phosphoryl head group. Phosphoglycerides can then be further divided into four groups: phosphatidylethanolamines, phosphatidylserines, phosphatidylinositols and phosphatidylcholines, according to whether they contain an ethanolamine, serine, inositol or choline head groups, respectively (Murray & Davis, 2003).

Lysophosphatidylcholines, sphingomyelin and the free fatty acid hydroxyl-eicosanoic acid are all direct derivatives of phosphatidylcholines, whereas, phosphatidylcholine ethers and phosphatidylinositols share many structural features with phosphatidylcholines but are not direct derivatives of them (Murray & Davis, 2003). In summary, these lipids are either structurally related or derivatives of phosphatidylcholines.

The fatty acids attached to the three-carbon back bone of the phosphatidylcholines, lysophosphatidylcholines and sphingomyelins do not all correspond. For example, the fatty acids of the lyso-phosphatidylcholines were 16:0, 18:0, 20:4, 22:6 and the fatty acids of the phosphatidylcholines were 14:0, 16:0 and 22:6. The changes in the thirteen phospholipids demonstrated in the two liver dysfunction groups are therefore likely to be related, but not all directly related, i.e. not the result of a direct catabolic reaction such as the hydrolysis of a phosphatidylcholine into a lyso-phosphatidylcholine, with the removal of one of the fatty acids (Murray & Davis, 2003). The direction of the change of all the lyso-phosphatidylcholines and the sphingomyelins, and one of the phosphatidylcholines was the opposite of all the other phosphatidylcholines, in the two liver dysfunction groups. Decreases in the hydrolysis of PC (16:0/16:0) to lyso-PC (16:0) in the liver dysfunction group could explain the opposite direction of change of these two phospholipids. However, the changes in the other lyso-phosphatidylcholines and sphingomyelins, cannot, therefore,

be explained by such direct reactions such as a reduction in their corresponding precursor phosphatidylcholine.

Compared to the non-liver dysfunction group, the liver dysfunction group was associated with increased levels of the phosphatidylcholines: PC (14:0/16:0) and PC (16:0/16:0) and decreases in the phosphatidylcholine PC (16:0/22:6). This discordance in the direction of change of these phosphatidylcholines and the differences in the fatty acids of many of the phospholipids that differed between the two liver dysfunction groups is consistent with sepsis-induced liver dysfunction being associated with phospholipid changes resulting from three separate changes.

The first proposed change is the increased availability of 16- and 18-carbon fatty acids in sepsis based on increases in C16:0, C16:1 and C18:1 that has been shown to occur in patients with sepsis shock (Rival, Cinq-Frais, Silva-Sifontes, *et al.*, 2013). It is hypothesised that this results from the combination of increased lipolysis of adipose tissue (Martinez, Chiolero, Bollman, *et al.*, 2003), which is rich in C16:0, C16:1 and C18:1 fatty acids (Hodson, Skeaff & Fielding, 2008), coupled with inhibition of fatty acid oxidation (catabolism) relative to circulating triacylglycerol levels in sepsis (Giovannini, Boldrini, Castagneto, *et al.*, 1983), resulting in an increased release of these fatty acids. These changes would be expected to cause an increase in phosphatidylcholines with 16- and 18-carbons and a reduction in the usual complement of phosphatidylcholines, in both liver dysfunction groups. In the healthy state, the most abundant phosphatidylcholines in plasma are ones with 18 or 16-carbon fatty acids at position *sn*-1, with one or no double bonds (e.g. 16:1;, 16:0), and unsaturated fatty acids at position *sn*-2 with between 16 and 22 carbons and up to six double bonds (e.g. 22:6) (Pynn, Henderson, Clark, *et al.*, 2011).

Both hepatocellular dysfunction and cholestasis can occur in sepsis-related liver dysfunction (Graham, 1940; Bauer, Press & Trauner, 2013). In the liver dysfunction group, hepatocellular dysfunction is thought to be responsible for a second change: a reduction in the synthesis of the so-called 'septic' group of phosphatidylcholines e.g. PCs with 16- and 18-carbon fatty acids. On their own, these two

changes would have resulted in the equal levels of the usual complement of phosphatidylcholines (i.e. PCs with fatty acids with between 16 and 18 carbons PCs at *sn*-1 and unsaturated FAs at position *sn*-2 with between 16-22 carbons) and a lower level of the 'septic' phosphatidylcholines in the liver dysfunction group, compared to the non-liver dysfunction group. However, the addition of cholestasis in sepsis related liver dysfunction (Graham, 1940; Bauer, Press & Trauner, 2013) provides a mechanism for the increased levels of phosphatidylcholines with 14 and 16-carbon fatty acids: [PC(16:0/16:0) and PC(14:0/16:0)] in the liver dysfunction group, compared to the non-dysfunction group, due to the inhibition of their secretion in bile secondary to cholestasis (Nesseler, Launey, Aninat, *et al.*, 2012). Evidence to support this theory includes, demonstrations of the preferential secretion of phosphatidylcholines with 16 or less carbon saturated fatty acids at the sn-1 position in bile in the healthy state (Farms, 1998). The secretion of PCs into bile canaliculi requires the translocation of PCs from the inner to the outer leaflet of the canalicular membrane. This process is performed by the canalicular transport glycoprotein multidrug resistance 3 (MDR-3) and protects the membranes of the intrahepatic bile duct from bile acid-induced hepatotoxicity (Elferink, Tytgat & Groen, 1997). Inhibition of the MDR-3 protein inhibits the secretion of PCs and results in bile acid-induced hepatotoxicity (de Vree, Jacquemin, Sturm, *et al.*, 1998). This has been demonstrated in patients with mutations of the gene encoding for the MDR-3 glycoprotein (de Vree, Jacquemin, Sturm, *et al.*, 1998) and in mice deficient in the MDR-2 glycoprotein: the murine equivalent of the human MDR-3 protein (Smit, Schinkel, Elferink, *et al.*, 1993).

PCs with 18-carbon fatty acids should not be affected by cholestasis in this way and as such the non-liver dysfunction group would be expected to have higher levels of PCs with 18-carbon fatty acids, resulting from their increased availability of 18-carbon fatty acids in sepsis. The absence of this finding is unexplained; it is possible that there was a difference in the levels of PCs with 18-carbon fatty acids between the two liver groups but it was not significant enough to be detected by the OPLS-DA models. This theory is supported by a study showing that the most significant differences in the levels of fatty

acids of plasma phospholipids between patients with septic shock and healthy controls was in the levels of C16:1 fatty acid palmitoleic acid (Rival, Cinq-Frais, Silva-Sifontes, *et al.*, 2013).

Phosphatidylcholine (16:0/22:6) was the only phosphatidylcholine sub-species, which showed lower plasma levels in the liver dysfunction group than the non-liver dysfunction group. This can be explained by the differential production of phosphatidylcholines with polyunsaturated fatty acids (PUFAs) such as 22:6 by the hepatic enzyme phosphatidylethanolamine *N*-methyltransferase (PEMT) and the synthesis of phosphatidylcholines with medium length fatty acids with only a few or no double bond that are usually produced by the cytidine diphosphate choline (CDP-choline) pathway (Pynn, Henderson, Clark, *et al.*, 2011). Phosphatidylcholine (16:0/22:6) is one of the usual complement of phosphatidylcholines in health that is not usually secreted in bile but instead fulfils an important role in providing a source of polyunsaturated fatty acids (Farms, 1998). A reduction in phosphatidylethanolamine *N*-methyltransferase activity secondary to hepatocellular dysfunction in the liver dysfunction group, could therefore be, a plausible explanation for the reduction of PC (22:6) in the liver dysfunction group, compared to the non-dysfunction group.

The plasma levels of four lysophosphatidylcholines (and two sphingomyelins) were lower in the liver dysfunction group than the non-liver dysfunction group. The fatty acids of these lysophosphatidylcholines ([16:0], [18:0], [20:4]; [22:6]) are the same as those found in the usual complement of PCs produced by the liver (Pynn, Henderson, Clark, *et al.*, 2011). The proposed reductions in the usual complement of phosphatidylcholines in sepsis, coupled with further reductions secondary to hepatocellular dysfunction in the liver dysfunction group, could therefore, be responsible for the lower levels of these lyso-phosphatidylcholines in the liver dysfunction group, compared to the non-dysfunction group. Lecithin-cholesterol acyltransferase (LCAT) is a hepatic enzyme that catalyses the conversion of phosphatidylcholines to lysophosphatidylcholines; usually as a result of the removal of the fatty acids from the *sn*-2 position (Murch, Collin, Hinds, *et al.*, 2007).

Reductions in the activity of LCAT secondary to hepatocellular dysfunction, could therefore also be responsible for the lower levels of lysophosphatidylcholines in the liver dysfunction group.

Lecithin-cholesterol acyltransferase has been described as the most sensitive marker of hepatocellular dysfunction (McIntyre, 2004). It is also one of the enzymes contained within HDLs, where it has an essential role in the conversion of phosphatidylcholines into lysophosphatidylcholines and the liberation of a fatty acids used to esterify free cholesterol (Murch, Collin, Hinds, *et al.*, 2007). Phospholipids such as phosphatidylcholines and lysophosphatidylcholines are responsible for the majority of the lipid content of the major lipoproteins: VLDL, LDL and HDL (Murray & Davis, 2003). Lysophosphatidylcholines are mainly associated with LDL but HDL is also a source of phosphatidylcholines that can be converted to lysophosphatidylcholines by LCAT (Murch, Collin, Hinds, *et al.*, 2007). The lipid component of lipoproteins are extracted from protein component during lipid extract phase of the plasma sample preparation and the proteins are precipitated out.

The hydrolysis of phosphatidylcholines into lysophosphatidylcholines and esterified cholesterol (CE), forms an important part of the maturation of pre-β-HDL into HDL_3, which goes on to form the fully matured HDL_2 molecule (Murch, Collin, Hinds, *et al.*, 2007). Reductions in HDL-associated enzymes such as LCAT have been demonstrated in sepsis (Murch, Collin, Hinds, *et al.*, 2007), but associations between these reductions and liver function were not been specifically addressed by these or any other studies.

Phospholipase A_2 (PLA_2) is another enzyme that can catalyse the conversion of phosphatidylcholines into lysophosphatidylcholines. However, studies have shown an increase in phospholipase A_2, in sepsis, which would promote the conversion of phosphatidylcholines into lyso-phosphatidylcholines (Murch, Collin, Hinds, *et al.*, 2007). Moreover, the production of PLA_2 is not restricted to the liver, and therefore, it is unlikely to be responsible for the differences in the lyso-phosphatidylcholines demonstrated by the two liver dysfunction groups.

There is increasing evidence of the beneficial role of lysophosphatidylcholines within HDL molecules in sepsis, with the greatest amount of evidence for lyso-phosphatidylcholines with saturated 18-carbon fatty acid chains being the most protective, as shown in animal models of both sepsis and endotoxaemia (Murch, Collin, Hinds, *et al.*, 2007). A reduction in these beneficial effects secondary to the reduction in the lyso-phosphatidylcholines demonstrated by the patients with sepsis related liver dysfunction in this study, could be related to the poorer outcome associated with the development of liver dysfunction in sepsis (Brun-buisson & Mondor, 2004; Angus, Linde-Zwirble, Lidicker, *et al.*, 2001; Cheng, Xie, Yao, *et al.*, 2007).

Sphingomyelins are also derivatives of phosphatidylcholines (Murray & Davis, 2003). The combination of a reduction in the usual complement of phosphatidylcholines secondary to sepsis coupled with hepatic dysfunction could be responsible for the lower levels of two sphingomyelin subspecies demonstrated in the patients with liver dysfunction group compared to those without. There is however, increasing evidence to suggest that sepsis-related liver dysfunction is associated with an increase in sphingomyelinase activity that results in an increase in the catabolism of sphingomyelins into ceramides and phosphocholine which induces the production of reactive oxygen species resulting in hepatic apoptosis (Claus, Bunck, Bockmeyer, *et al.*, 2005; García-Ruiz, Colell, Mari, *et al.*, 2003). More recent clinical evidence supporting this theory has included a study demonstrating a higher ceramide to sphingomyelin ratio, in addition to a lower lysophosphatidylcholine to phosphatidylcholine ratio was associated with a poorer outcome in the group of patients with sepsis, and this was related to liver dysfunction in some but not all cases (Drobnik, 2003). Collectively these studies support the role of a sphingomyelinase in the pathogenesis of liver dysfunction in sepsis and the decreases in the plasma levels of lysophosphatidylcholines demonstrated in the liver dysfunction group in this study.

The plasma levels of the phosphatidylinositol (16:0/18:1) was higher in the liver dysfunction group than the non-liver dysfunction group. The biosynthesis of phosphatidylinositols is unrelated and very different to the main biosynthetic pathways of phosphatidylcholines and phosphatidylethanolamines (Payrastre, Missy, Giuriato, *et al.*, 2001). Instead of the sequential addition of phosphate, cytidine diphosphate (CDP) and diacylglycerol (DAG), the biosynthesis of phosphatidylinositols involves a direct reaction between cytidine diphosphate diacylglycerol (CDP-DAG) and inositol, catalysed by CDP-DAG inositol phosphatidyltransferase. The main association of phosphatidylinositols and sepsis is evidence of the role of the lipid kinase phosphoinositide 3 kinase (PI3K) in the activation signalling pathways in sepsis through the phosphorylation of phosphatidylinositols (Recknagel, Gonnert, Westermann, *et al.*, 2012).

Phosphatidylinositols are an integral component of plasma membranes and play a crucial role in many important metabolic pathways (Payrastre, Missy, Giuriato, *et al.*, 2001). These roles include providing an anchor for proteins within membranes and signal transmission across membranes. Phosphatidylinositol signalling pathways, are initiated by an extracellular signalling molecule binding with a G-protein on the exterior cell surface membrane and activating a membrane-bound enzyme such as phospholipase C. The enzyme then catalyses the phosphorylation of the PI, and results in the release of DAG. The phosphorylated PI activates the opening of calcium channels on the membrane of smooth endoplasmic reticulum and mitochondria resulting in calcium entry into the cytosol, which together with the DAG helps activate protein kinase C. This leads to the phosphorylation of other intracellular proteins, resulting in changes in their catalytic abilities, which brings about the intended cellular responses.

Phosphoinositide 3 kinase (PI3K) has been implicated in several roles in both sepsis and sepsis-related hepatotoxicity involving the activation of signalling pathways (Recknagel, Gonnert, Westermann, *et*

al., 2012). This has included evidence from Recknagel *et al* (Recknagel, Gonnert, Westermann, *et al.*, 2012) demonstrating phosphoinositide 3-kinase gamma (PI3Kγ) acting as lipid kinase in leukocytes capable of generating phosphatidylinositol 3,4,5-triphosphate that led to the recruitment and activation of downstream signalling mediators. Unlike other members of the PI3K family, PI3Kγ is activated by G-protein coupled-receptors that respond to chemotactic ligands and in the aforementioned study, this was shown to be essential to its role in the migration of both myeloid and lymphoid cells. Phosphoinositide 3-kinase gamma (PI3Kγ) has also been shown by other studies, to be important to other leukocyte functions such as neutrophil oxidative burst, T cell proliferation and mast cell degranulation (Venable, Ameriks, Blevitt, *et al.*, 2010). This evidence supports a role of PI3Kγ in signal transmission in sepsis and the increases in the plasma levels of the phosphatidylinositol (16:0/18:1) in the liver dysfunction group, may related to the role of a phosphatidylinositol 3,4,5-triphosphate in this PI3-K mediated pathway.

The plasma levels of the conjugated bile acid glycocholic acid (GCA) were higher in the patients with liver dysfunction compared to those without. There is evidence from multiple non-sepsis studies implicating conjugated bile acids in the initiation of hepatocyte apoptosis, by directly increasing the cell surface density of the death receptor, Fas (Faubion, Guicciardi, Miyoshi, *et al.*, 1999; Miyoshi, Rust, Roberts, *et al.*, 1999; Sodeman, Bronk, Roberts, *et al.*, 2000). In these studies, bile acids such as glycochenodeoxycholate (GCDC) resulted in the apoptosis of hepatocytes that targeted cells expressing functional canalicular bile-salt export pumps (BSEP): the transporter responsible for the secretion of monovalent taurine- and glycine-conjugated bile acids. The overall conclusion from these studies was that canalicular bile-salt export pumps were crucial to the mechanism of bile acid induced apoptosis of hepatocytes. The increased levels of the conjugated bile acid glycocholic, may therefore be related to the pathogenesis of SRLI.

The investigators of the aforementioned study by Recknagel *et al* (Recknagel, Gonnert, Westermann, *et al.*, 2012), subsequently hypothesised that PI3Kγ may be involved in the targeting of the canalicular BSEP and hepatic metabolism of bile acids in sepsis-related liver dysfunction. In a series of investigations utilising several different '–omics' studies, they demonstrated impairments of both phase I and II metabolisms and hepatobiliary transport of bile acids that were associated with the induction of PI3Kγ signalling, as early as six hours after the induction of sepsis, in their animal model of peritonitis. This was followed, 15 hours after the induction of the sepsis, by the disruption of the conjugation of bile acids, followed by the accumulation of both unconjugated and conjugated bile acids, bilirubin, and xenobiotics within hepatocytes.

Primary bile acids are synthesised from cholesterol within hepatocytes; and are divided in monovalent or divalent. Monovalent BAs are conjugated with taurine or glycine; whereas divalent are conjugated with either sulphur or glucuronic acid, in addition to taurine or glycine. Bile acids are secreted in bile by being transported across the canalicular membrane of the hepatocyte by the BSEP if they are monovalent and multi-drug resistant protein-2 (MRP2; murine) or multi-drug resistance protein-3 MDRP3; human) if they divalent. MRP2 (murine or MDRP3 is also responsible for the canalicular transport of phosphatidylcholines, organic anions, bilirubin, and reduced glutathione. Bile acids that are present in the blood in the portal vein and its branches are transported into hepatocytes by sodium-taurocholate co-transporting polypeptides (NTCPs) if they are conjugated with taurine or glycine and organic anion-transporting polypeptides (OATPs) if they not. Organic anion-transporting polypeptides are also responsible for the transport of organic anions. Importantly, in the above study, the features of cholestasis in the liver were preceded by disturbances of two of the bile acid canalicular transporters: MRP2 and BSEP. These hepatic findings were associated with increases in the plasma levels of both unconjugated and conjugated bile acids and lipids in the sepsis group compared to sham (surgical) control group; however, the increases in unconjugated BAs outweighed those of the

conjugated BAs resulting in an increased ratio of the unconjugated to conjugated BAs (Recknagel, Gonnert, Westermann, *et al.*, 2012). This data included, evidence linking the induction of PI3Kγ and the disruption of MRP2, the murine equivalent of the human transport glycoprotein MDR3 that is responsible for the translocation of phosphatidylcholine required for their secretion in bile canaliculi. The secretion of PCs in bile protects the canalicular membrane from the hepatotoxicity of bile acids, (as discussed above). This study by Recknagel *et al*, therefore supported the hypothesis that PI3Kγ induction is associated with bile acid-induced toxicity in sepsis-related liver dysfunction secondary to the inhibition of the secretion of PCs that protects the canalicular membrane from the toxic effects of bile acids. These investigations also demonstrated a reduction in bile acid-coenzyme A: amino acid *N*-acyltransferase, an enzyme responsible for facilitating bile acid conjugation, in addition to the neutrophilic recruitment in the liver consistent with previous demonstrations in the sepsis-related liver dysfunction.

In the current study, the plasma levels of the conjugated bile acid glycocholic acid and both a steroid and a cholesterol conjugated with glucuronide were shown to be higher in the patients from the sepsis cohort with liver dysfunction compared to the group without. The study by Recknagel *et al*, (Recknagel, Gonnert, Westermann, *et al.*, 2012) also included a metabolomic component involving a cohort of patients with sepsis. In contrast to the findings of the animal component, increases in the plasma levels of both conjugated and unconjugated bile acids were demonstrated in this cohort of patients with sepsis. The results of the clinical component of their study are therefore consistent with the increases in the conjugated bile acids and lipids demonstrated by this project. It is also worth noting that the current study involved comparisons of patients with sepsis, with and without liver dysfunction, whereas, in the study by Recknagel *et al,* all of the patients had sepsis-related liver dysfunction and the bile acids levels were compared to that of normal levels.

The other lipids that were greater in the liver dysfunction group compared to the non-dysfunction group were four phosphatidylcholine ethers and the fatty acid hydroxy-eicosanoic acid (20:0). Phosphatidylcholines ethers are like phosphatidylcholines but contain one fatty acid and one fatty alcohol instead of two fatty acids. They are divided into two groups: plasm*e*nyl-phosphocholines (plasm*e*nyl-PCs; also, known as phosphatidylcholine plasmalogens) that contain a vinyl ether double bond near the oxygen atom and plasm*a*nyl-phosphocholines (plasmanyl-PCs) that contain an ether bond without a double bond. Plasm*e*nyl- and plasm*a*nyl-phosphocholines are also known as alkenyl- and alkyl-ethers, respectively and are described using the systematic names of 1-alkenyl-2-acyl- or 1-alkyl-2-acyl-glycero-3-phosphocholine, as recommended by the IUPAC-IUBMB guidelines (Fahy, Subramaniam, Murphy, *et al.*, 2009). The phosphatidylcholine ethers that differed between the two liver dysfunction groups were both plasmanyl-phosphocholines i.e. 1-alkyl-2-acyl-glycero-3-phosphocholines.

Plasmanyl-phosphatidylcholines are found in significant amounts in circulating cells such as neutrophils and macrophages compared to relatively low amounts in other tissues (Choy, Skrzypczak, Lee, *et al.*, 1997). However, with the exception of platelet activating factor (PAF; which is technically a plasmanyl-PCs although it contains acetate instead of a fatty acid with a hydrocarbon chain), there is no other substantial evidence to suggest that plasm*a*nyl-phosphocholines they may have a role in sepsis (Yost, Weyrich & Zimmerman, 2010). Likewise, other than hydroxy-eicosanoic acid being a derivative of the inflammatory mediator eicosanoic acid, there is no evidence to suggest that this particular derivative has specific role in sepsis or sepsis related liver dysfunction (Murch, Collin, Hinds, *et al.*, 2007). There is however, substantial amount of evidence supporting the role of platelet activating factor in sepsis (Yost, Weyrich & Zimmerman, 2010).

Under normal conditions, PAF is produced by the de novo pathway but under pathological conditions such as inflammation and sepsis, it is produced by remodelling (Yost, Weyrich & Zimmerman, 2010).

In this case, lysophosphatidylcholine acetyltransferase is responsible for the addition of acetate instead of a long chain acyl group in the remodelling process of the lyso-phosphatidylcholine-ether (Venable, Zimmerman, Mcintyre, *et al.*, 1993). Evidence for the role of PAF in sepsis initially arose from early reports from human cell models implicating PAF in the basic cellular responses of sepsis such as activation of neutrophils (Yost, Weyrich & Zimmerman, 2010). These were later followed by evidence of a more specific role of PAF in neutrophils and its involvement in the extrusion of neutrophil extracellular traps used in the entrapment and killing of bacteria (Yost, Cody, Harris, *et al.*, 2012). Since then, animal models of sepsis have also provided evidence of associations between pro-inflammatory cytokines such as TNF-α and PAF (Jeong, Jung, Lee, *et al.*, 2009), in addition to evidence supporting the role of PAF in the increased vascular permeability and vaso-reactivity seen in sepsis (Göggel, Winoto-Morbach, Vielhaber, *et al.*, 2004; Camerer, Regard, Cornelissen, *et al.*, 2009). The roles of PAF in sepsis suggested by these in vitro human and in vivo animal studies have been investigated by more recent clinical observational studies (Vincent, Spapen, Bakker, *et al.*, 2000; Schuster, Metzler, Opal, *et al.*, 2003; Li, Stuart, Zhang, *et al.*, 2009). These have included a study of plasma from a cohort of patients with sepsis in which PAF was shown on the surface of their platelets, which supports the theory that the activation of cells such as platelets occurs via interactions between cell surface receptors and circulating PAF (Vincent, Spapen, Bakker, *et al.*, 2000). Some clinical studies have also suggested an imbalance between the synthesis of PAF and its catabolism by platelet activating factor-acetylhydrolase (PAF-AH) is a crucial determinant of outcome in sepsis (Schuster, Metzler, Opal, *et al.*, 2003). These have included a study demonstrating a relationship between inter-individual variations in both PAF-AH levels and PAF-AH genotype and outcome in sepsis (Li, Stuart, Zhang, *et al.*, 2009). So far, strategies used to inhibit PAF mediate pathways have had variable results (Vincent, Spapen, Bakker, *et al.*, 2000; Schuster, Metzler, Opal, *et al.*, 2003). Although, the inconsistence of these results is thought to be related to the dynamic variation in the levels of endogenous PAF, suggesting its inhibition needs to be directed at individuals during periods of demonstrated increased PAF activity.

The increases in the plasmanyl-PC ethers in this study could represent an increase in precursors that are remodelled into PAF through the substitution of the fatty acid on the sn-2 of the glycerol backbone, with acetate. Platelet activating factor molecules can have a variety of different long chain alcohols at the *sn*-1 position of their glycerol molecule but ones with 16 or 18 carbons are the most common (Yost, Weyrich & Zimmerman, 2010). The increases in hydroxy-eicosanoic acid may therefore, also be related to this remodelling process: with the production of hydroxy-eicosanoic acid from the fatty acid of eicosanoic acid, following its removal from a phosphatidylcholine-ether.

5.5.2 Haematological dysfunction

The lipidomic analyses performed in this study were aimed at expanding on the findings of the metabolic signatures of liver dysfunction demonstrated by the earlier CPMG ^{1}H NMR analyses of serum. Metabolic signatures of the other seven clinical classes investigated in this study were also performed. These revealed metabolites capable of differentiating between patients with and without haematological dysfunction but no other metabolic signature demonstrated by these analyses.

Metabolites capable of differentiating between patients with and without haematological dysfunction were demonstrated on days two and seven. Of these, eleven have been structurally assigned, eight of these metabolites were demonstrated on days two and seven; and three were only differentiating metabolites on day seven. Collectively, these metabolites were eleven of the 18 metabolites associated with the differentiation of liver dysfunction demonstrated at all four time points. In this study, a platelet count of less than 150 x 10^{9}/l defined haematological dysfunction (a haematological SOFA score of greater than zero). Both sepsis and liver dysfunction are associated with low platelets. In sepsis, low platelets can be caused by a variety of both immune and non-immune mechanisms

including sequestration and destruction of activated platelets in the liver. There is a close relationship between low platelets and liver failure, although the exact mechanisms of this relationship have not been elucidated and may be different in the context of different aetiologies. It has been postulated that low platelets in the context of liver dysfunction is due to low thrombopoietin produced by the liver. However, in at least, paracetamol-induced liver failure, this does not seem to be the case as demonstrated by the complex, non-linear relationship demonstrated by a recent study of thrombopoietin levels in patients with paracetamol-induced liver failure.

The possible explanations for why there is an overlap in the differentiating metabolites of low platelets and liver dysfunction in the sepsis cohort of this study, need to take into account three factors: 1. Low platelets are associated with liver dysfunction; 2. Sepsis, in itself, outside of the context of liver dysfunction is associated with low platelets and therefore some of the patients with low platelets may not had liver dysfunction; 3. Most the patients with low platelets also had liver dysfunction, (77 percent of the patients on day two and 81 percent of the patients on day seven); and so the overlap could be due to the overlap in the patients in each of the dysfunction groups rather than a true association (null hypothesis).

Taking all three of these factors into account, although, the overlap in the differentiating metabolites of low platelets and liver dysfunction could have been due to chance, (i.e. to accept the null hypothesis), it seems more plausible that this overlap is due to differences in the metabolic signatures of low platelets in sepsis with and without liver dysfunction. Moreover, patients with sepsis-induced liver dysfunction and low platelets, may have a different metabolic signature to the patients with SRLI and a normal platelet count, related to the additional mechanisms involved in the reduction in platelets in liver dysfunction.

5.5.3 Placebo versus steroids treatment groups

The sepsis cohort was recruited as part of the VACS trial comparing vasopressin co-administered with either placebo or hydrocortisone in septic shock. The aim of this trial was to investigate the hypothesis that in septic shock corticosteroids can reduce or reverse the hypo-responsiveness to vasopressin and vasopressin can enhance ACTH levels resulting in increases in corticosteroid levels.

The VACS trial demonstrated reductions in the overall duration in vasopressin requirements in the hydrocortisone group compared to the placebo one but no significant differences were demonstrated in the doses or levels of vasopressin when measured between days two and seven of the trial (time points two and three, respectively). Furthermore, despite the shorter duration of vasopressin treatment in the hydrocortisone group, no significant differences in daily SOFA scores or 28-day survival were demonstrated.

Metabolic differences between these two treatment groups were investigated to determine whether the addition of hydrocortisone had led to any detectable changes in metabolic processes that had not been translated into significant differences in the clinical outcomes or vasopressin levels of these groups. No metabolic differences between the two treatment groups were demonstrated by either the NMR profiling of urine and serum or the LCMS lipidomic analyses of plasma. Evidence suggests the effects of steroids in sepsis are mediated by sub-species of lipids and involve signalling pathways and lipid metabolism. The inability of the NMR analyses to demonstrate any metabolic differences between the treatment groups are therefore not surprising; given the inability of NMR analyses to determine lipid sub-species. However, greater success was anticipated with the lipidomic LCMS analyses; particularly since PCs and lyso-PCs have been implicated in this process and these subspecies of lipids were detected by this method of lipid profiling. The shorter duration in vasopressin treatment in the hydrocortisone group compared to the placebo group, suggested that steroids can reduce the hypo-responsiveness to vasopressin in septic shock, even if the vasopressin levels remain unchanged. The inability to detect any differences in lipid between the two treatment groups could simply reflect

the absence of any significant impact on the metabolic processes and a failure to detect any subtle differences. Alternatively, the metabolic differences may simply have been unidentified by both the NMR and the lipidomic analyses and the cause of this remains unexplained.

5.6 Summary

In summary, the main metabolites responsible for the differentiation of the patients from the sepsis cohort with and without liver dysfunction, demonstrated using an UPLC-MS technique of lipid profiling of plasma in this study, were glycerophosphocholines, sphingomyelins, a free fatty acid, two lipid glucuronides and a conjugated bile acid. The glycerophosphocholines were divided into phosphatidylcholines, phosphatidylcholine ethers and lysophosphatidylcholines. This included discordance in the direction of change of the phosphatidylcholines that differed between the two groups, in addition to increases in phosphatidylcholines ethers and decreases in both lysophosphatidylcholines and sphingomyelins in the dysfunction group compared to the non-dysfunction group. The most likely explanation for the discordance of the phosphatidylcholines is differences in the synthesis and biliary excretion of sub-species of phosphatidylcholines according to the length of their fatty acid chains. In contrast, decreases in the usual complement of phosphatidylcholines is the most plausible explanation for the decreases in lysophosphatidylcholines and sphingomyelins. Reductions in LCAT, the enzyme responsible for catalysing the conversion of phosphatidylcholines to lysophosphatidylcholines secondary to hepatocellular dysfunction is also likely to be a contributing factor to the reductions in the lysophosphatidylcholines in the liver dysfunction group compared to the non-dysfunction group. Phosphoinositide 3 kinase has been implicated in the inhibition of the transport protein responsible for the biliary excretion of conjugated lipids and bile acids. The increases in a phosphatidylinositol, the conjugated bile acid glycocholic acid and the two conjugated lipids demonstrated by the subgroup of the sepsis cohort with liver dysfunction could therefore, all be related to the inhibition of these transport proteins. Overall, the metabolite differences between sepsis patients with and without liver dysfunction demonstrated by this method of lipid profiling are consistent with evidence of the combination of cholestasis and

hepatocellular dysfunction that occurs in sepsis-related liver dysfunction and could be useful in its early diagnosis.

Most of the glycerophosphocholines and sphingomyelins responsible for the differentiation of patients from the sepsis cohort with and without liver dysfunction demonstrated by the UPLC-MS lipidomic profiling were also capable of differentiating between patients with a normal and a low platelet count. This incomplete overlap is most likely due to the combination of the both sepsis and liver dysfunction being independently associated with a low platelet; and the variety of mechanisms capable of effecting the platelet count in sepsis.

Chapter 6: Conclusion

Sepsis is associated with a wide range of complications including multiple organ failures and is the leading cause of critical illness and death in intensive care units (ICUs) (Blanco, Muriel-Bombin, Sagredo, *et al.*, 2008). Organ dysfunctions in sepsis is associated with an increased early mortality and there are currently no accurate diagnostic tools capable of detecting their onset (Blanco, Muriel-Bombin, Sagredo, *et al.*, 2008). There are also no tests capable of reliably predicting the risk of death in sepsis. This study set out to determine metabolic signatures associated with sepsis-related organ dysfunctions and death using metabolic profiling based on NMR and MS analyses of biofluids that could be used to predict the onset of organ dysfunction and death, respectively. This started with the validation of the feasibility of a method of metabolic profiling based on NMR analyses of urine, in a validation cohort of critically ill patients which led to the development of an NMR drug standards database to aid the identification of drug related signals on NMR spectra.

6.1 Integration of the hypotheses and the empirical findings of the study

6.1.1 Validation of metabonomics based on ^{1}H NMR spectroscopic analysis of urine as a global metabolic profiling method in critically ill patients

The feasibility of ^{1}H NMR analyses of urine as a method of profiling in critically ill patients was demonstrated by the characterisation of the metabolic profiles of urine from both the validation and the sepsis cohorts, in addition to comparisons to ^{1}H NMR spectra of urine from healthy controls. This included the detection of metabolites that are commonly found in health and a large number of signals from parent drugs and their metabolites. This was coupled with the use of multivariate statistical analyses to determine the metabolic signatures of the clinical groups under investigation that focus on the differences between these groups, as opposed to identifying all of the detected signals, which is impractical. Differentiating between drug and non-drug signals is important to the identification of

differentiating metabolites, particularly in critically ill patients who can receive more than ten pharmaceutical drugs. The identification of drug metabolites in this cohort was aided by the development of a drugs standards database of NMR spectra of the parent drug of 120 drugs and fluids. This was then coupled with a method of statistical correlation analyses (STOCSY), to identify metabolites of the parent drug.

6.1.2 The clinical utility of metabonomics based on 1-D ^{1}H standard NMR analyses of urine and serum in the sepsis cohort

The clinical utility of profiling based on NMR analyses of urine was not demonstrated in either the validation or the sepsis cohort. In both cohorts, this method of metabolic profiling failed to differentiate between the presence and absence of up to six acute organ dysfunctions, predict the risk of death (ICU or 28-day mortality), or predict the onset of AKI in the sepsis cohort. Initially, the presence of a starch based resuscitation fluid was hypothesised as a confounding factor that could be responsible for this failure in the validation cohort. This hypothesis was disproven by repeating the NMR analyses using a duplicate set of the urine samples following the removal of this starch component of Volulyte *via* a process of ultra-filtration of the urine. After these repeat experiments also failed to detect metabolic signature of the clinical classes under investigation in the validation cohort, the heterogeneity of this cohort was hypothesised as the main cause of the failure to demonstrate this clinical utility. Other explanations included the small sample size and the large number of drug signals inhibiting the detection of metabolic signatures of these clinical classes. The above hypothesis that the heterogeneity of the validation cohort was the main cause of the failure to demonstrate the clinical utility of this method of urinary metabolic profiling was then tested in the sepsis cohort. This was the main focus of this study. The sepsis cohort was greater in number and were united by the cause of their critical illness. Greater success was therefore anticipated with the use of the same method of metabolic profiling based on NMR analyses of urine tested in the validation

cohort. This was not the case. This method of profiling based on NMR analyses of urine also failed to demonstrate any metabolites that were capable of differentiating between any of the acute organ dysfunction or outcome groups evaluated in the sepsis cohort. The 1-D standard ^{1}H NMR analyses of serum samples from sepsis cohort also failed to demonstrate any differentiating metabolites associated with any of these clinical classes.

6.1.3 Metabolic signatures of acute liver dysfunction in the sepsis cohort demonstrated by ^{1}H CPMG NMR analyses of serum and UPLC-MS analyses of plasma

In contrast, to the 1-D standard ^{1}H NMR analyses of serum, the 1-D CPMG ^{1}H NMR analyses of serum samples from the sepsis cohort demonstrated a metabolic signature capable of differentiating between the samples from day seven of the study based on their liver dysfunction groups. This demonstration of metabolic signatures of acute liver dysfunction supported the use of NMR as a metabolic profiling technique with clinical utility in sepsis. However, the inability to replicate such findings with the use of both urine from the same time point and 1-D standard NMR analyses of the same samples implies that CPMG NMR analyses of serum is superior at detecting metabolic signatures of pathophysiological changes in complex patients with multiple levels of heterogeneity such as those with sepsis or critical illness due to other causes. This superiority is likely to have arisen from the greater resolution of the compounds and the reduction in the number of drug signals, compared to the standard 1-D serum and urine NMR analyses, respectively. The diversity of metabolites NMR is capable of detecting, makes it a great global metabolic profiling technique that is often used to direct more targeted analyses (Beckonert, Keun, Ebbels, *et al.*, 2007). This use of NMR was exemplified in this study. The CPMG NMR analyses of serum provided evidence of metabolic signatures of liver dysfunction containing 14 key differentiating metabolites that fell into three groups: amino acids, lipoproteins, and lipids. The amino acids were lysine and methionine and their increased serum concentration in the liver dysfunction group compared to the non-liver dysfunction group is consisted

with dependency on the liver for their catabolism and role in the synthesis in carnitine, a mediator in lipid oxidation that has been shown to increase in sepsis.

The metabolic signatures of liver dysfunction demonstrated by the CPMG NMR analyses of serum included signals of choline, glycerol of lipids and lipid signals consistent with LDL and VLDL. Taken together these suggested that lipoproteins and glycerides such as phosphoglycerides with choline head-groups and their metabolites constituted part of the differentiating metabolites of liver dysfunction. Although, the NMR analyses were unable to confirm the presence of lipoproteins or determine the exact lipid species or subspecies, they provided enough information to guide further investigation using UPLC-MS based lipidomic analyses.

These predictions were confirmed with the majority of the lipids of the metabolic signatures of liver dysfunction demonstrated by the lipidomic analyses being phosphoglycerides: phosphatidylcholines (PCs), phosphatidylcholine ethers, a phosphatidylinositol, in addition, to two phosphatidylcholines derivatives, sphingomyelin (SM) and lysophosphatidylcholines (lyso-PCs). This supported the validity of the results of the NMR analyses of the serum samples from the sepsis and the use of this technique as a global method of metabolic profiling. The other lipids demonstrated by the lipidomic analyses as differentiating metabolites of liver dysfunction, that were not foreseen by the finding of the NMR analyses included three conjugated lipids: a conjugated bile acid, a cholesterol, and a steroid. The strength of the results of the metabolic signatures of liver dysfunction demonstrated by the lipidomic analyses was also substantiated by the consistency (uniformity) in the differentiating lipids demonstrated at all four sampling time points.

The changes in the PCs is likely to be the consequence of at least three different mechanisms. A reduction in the synthesis of the usual complement of PCs (a wide range of PCs as opposed to PCs with

fatty acids with 16 to 18 carbons) secondary to hepatocellular damage, a reduction in PCs with long chain polyunsaturated fatty acids (PUFAs) and cholestasis resulting in the accumulation of PCs with 16 to 18 carbon fatty acids. Reductions in synthesis of the usual complement of PCs was the most likely cause of the reductions in lysoPCs and SMs. However, the activation of sphingomyelinases in sepsis may also be responsible for the reductions in the SMs. The increases in the PCs with 16 carbon FAs, the conjugated bile acid, glycolic acid and a phosphatidylinositol are all in keeping with a hypothesis of sepsis-induced cholestasis, proposed and investigated by Recknagel and colleagues (Recknagel, Gonnert, Westermann, *et al.*, 2012). They hypothesised that in sepsis related liver dysfunction, phosphoinositide 3 kinase (PI3K) mediates the inhibition of PCs and bile acid transporters that results in failure of the secretion of PCs and bile acids in bile and exposes hepatocytes to the toxic effects of bile acids that are prevented by the secretion of PCs in bile under normal circumstances. Through a series of investigations involving different '–omics' studies they provided overwhelming evidence supporting this hypothesis (Recknagel, Gonnert, Westermann, *et al.*, 2012). The increases in PCs and bile acids in this study are consistent with inhibition of the PC and bile acid transporters by PI3K in sepsis resulting in cholestasis, followed by bile acid mediated hepatotoxicity as a consequence. The decreases in the PI demonstrated in the liver dysfunction group compared to the non-dysfunction group, could reflect the use of this PI as a substrate for PI3K, acting as a key mediator of the inhibition of the PC and bile acid transporters, in addition to its other suggested roles in sepsis-induced cholestasis. Possible inducers of PI3K include endotoxins or cytokines released in sepsis.

6.2 Unanswered questions

The main unanswered questions raised by the NMR component of this study centred on the cause of the inability of the CPMG NMR analyses of serum to detect metabolic profiles associated with the presence of AKI, predict the onset of AKI or capable of differentiating between the treatment classes (placebo or steroid, in addition to vasopressin). There was also the question of whether an automated

system of detecting and eliminating drug signals coupled with STOCSY would improve the clinical utility of NMR analyses of NMR in critically ill patients.

The most likely explanation for the inability to detect metabolic profiles of the AKI classes in both cohorts using the NMR methods used in this study was probably the combination of subtle metabolic differences and the metabolic disarray of these very heterogeneous patients. With the addition of a small sample size in the comparison used to investigate a signature predictive of the development of AKI. Evidence supporting this hypothesis includes the striking nature of the lipid signals that comprised the majority of the differentiating metabolites associated with liver dysfunction on day seven of the study demonstrated by the CPMG NMR spectra of serum. These lipid signals were also visible but not well resolved on the 1-D standard NMR spectra of serum, which is likely to be responsible for the inability of this method of serum profiling to produce the same results as the CPMG NMR analyses of the same samples. Proteins are more likely to be a key feature of renal dysfunction as opposed to lipids, and this is also likely to have had some bearing on the different results obtained with both the NMR and the lipid analyses of these two organ dysfunctions. Although proteins are not present in urine under normal circumstances, proteinuria can be a feature of renal dysfunction. Proteins are large molecular weight molecules and as such produce broad signals on NMR spectra (Bouatra, Aziat, Mandal, *et al.*, 2013); these may have been present as signals that were either indistinct or obscured by overlapping signals. 1-D ^{1}H NMR is therefore not an ideal platform for the detection of metabolic changes involving proteins (Beckonert, Keun, Ebbels, *et al.*, 2007).

The VACS trial investigated the hypotheses that corticosteroids can improve arterial responsiveness to vasopressin and vasopressin can increase corticosteroid levels by increasing ACTH secretion in severe sepsis, by comparing the co-administration of vasopressin with either placebo or hydrocortisone in the sepsis cohort. The duration of vasopressin treatment was shorter in the hydrocortisone group compared to the placebo arm but no significant differences were demonstrated in the doses or levels of vasopressin on days two and seven of the trial, the daily sequential organ

failure assessment (SOFA) scores or 28-day mortality (Gordon, Mason, Perkins, *et al.*, 2014b). These findings were in keeping with the hypothesis that corticosteroids can increase the vascular response to vasopressin but does not support the implication that this will result in an improvements in clinical outcomes (Ertmer, Bone, Morelli, *et al.*, 2007).

Metabolic profiling was performed in this study using NMR and UPLC-MS lipidomic analyses to investigate metabolic changes that may have occurred as a result of the addition of hydrocortisone to vasopressin, despite the inability to demonstrate a significant impact on the clinical outcomes of the steroid treatment group. No metabolic signatures of the addition of hydrocortisone to vasopressin were demonstrated by either the NMR profiling of urine and serum or the LCMS lipidomic analyses of plasma. Evidence suggests that treatment with corticosteroids is associated with lipid signalling involving PCs and lyso-PCs (Lehmann, Sharawy, Zhou, *et al.*, 2012). The lipid profiling was therefore expected to be more successful than the NMR analyses in terms of revealing potential mediators of such lipid signalling in response to corticosteroids in sepsis.

It was also anticipated that one of these methods of metabolic profiling might be able to detect metabolic changes associated with physiological changes such changes in organ perfusion and vascular responsiveness. This was with a view to investigating the interactions between vasopressin and corticosteroids in severe sepsis that were not translated into statistically significant differences in the clinical outcomes of steroid treatment arm of the VACS trial. The inability to demonstrate metabolic differences between the placebo and treatment groups remains unexplained. Possible explanations would include changes that were predominantly confined to proteins unresolved by NMR analyses and not targeted by lipidomic LCMS analyses.

The number of samples collected at each of the time points ranged from 21-41 in the urinary NMR analyses, 14-33 in the NMR serum analyses and 25-50 in the LCMS analyses. (This is with the exception of the assessment of metabolic changes that could be used to predict the development of AKI, which consisted of 14 and eight patients in the urine and serum NMR analyses, respectively and 17 patients in the LCMS plasma analyses). This is comparable to the samples sizes of the other metabolic profiling studies in patients with sepsis (see Section 1.3.4), although the greater the sample size, the greater the anticipated success of demonstrating metabolic differences between clinical groups especially heterogeneous cohorts such as sepsis ones.

6.3 Theoretical and practical implications of the study's findings

The importance of the lipid signatures of liver dysfunction demonstrated by the lipidomic analyses of plasma is that it is in keeping with the hypothesis that phosphoinositide 3 kinase (PI3K) is a key mediator in sepsis-induced cholestasis resulting in bile acid-mediated hepatocellular toxicity (Recknagel, Gonnert, Westermann, *et al.*, 2012) and PI3K could therefore be a potential target in its prevention. The increases in the PCs and conjugated lipids including the bile acid glycolic acid on the other hand, could be potential biomarkers of the early diagnosis of sepsis-induced cholestasis. Moreover, there is increasing evidence to suggest that cholestasis plays a greater role in sepsis-related liver dysfunction than hepatocellular dysfunction and may precede, or in fact, may be the main cause of hepatocellular damage mediated by the accumulation of bile acids within the hepatocytes. These findings are in keeping with this hypothesis and support further investigations of these potential biomarkers of the early detection of sepsis-induced cholestasis and measures of the enzymatic activity of PI3Kγ (Ciraolo, Gulluni & Hirsch, 2014) that could potentially enable the prevention of irreversible sepsis-induced hepatocellular dysfunction. It is envisaged that a panel of potential biomarkers of the development of sepsis-induced liver dysfunction, could be determined using the metabonomic methods employed in this study (LCMS lipid profiling coupled with O-PLS-DAs and univariate analyses).

O-PLS-DA models of this panel could then be subjected to ROC curve analyses to determine its clinical utility as a predictive test for individuals with sepsis with normal liver function according to currently available methods.

In contrast, the decreases in lyso-PCs, SM, PC ethers and the PC with a long chain PUFA demonstrated by the liver dysfunction group compared to the non-dysfunction group are consistent with decreases in the synthetic function of the liver as a consequence of hepatocellular dysfunction. These changes could therefore be potential biomarkers of the onset of the hepatocellular damage in sepsis-induced liver dysfunction. The CPMG NMR analyses of serum demonstrated increases in the amino acids lysine and methionine in the liver dysfunction group compared to the non-dysfunction Both of these amino acids are dependent on the liver for their removal from plasma (either through their utilisation in the biosynthesis of other compounds or their catabolism) (Brosnan & Brosnan, 2006). Increases in lysine and methionine in the group with liver dysfunction compared to those without is therefore, in keeping with the development of hepatocellular dysfunction and could also be potential biomarkers of hepatocellular damage in sepsis.

6.4 Limitations of the study

The majority of patients in this study who had sepsis-related liver dysfunction during the study period, had already developed some degree of liver dysfunction at the time of enrolment. This led to an insufficient number of patients who developed sepsis-related liver dysfunction during the study period, to be able to assess metabolic predictors of its onset. The metabolic signatures of sepsis related liver dysfunction demonstrated by this study, may however, also be predictive of the development of liver dysfunction in sepsis.

The full range of liver SOFA scores were used to determine the presence or absence of liver dysfunction in the patient cohorts of this study. This is in line with the general consensus that recommends the use of scoring systems that quantifies the degree of liver dysfunction based on solely

on serum total bilirubin levels. It also has the advantage of including all patients with liver dysfunction, which is in keeping with the hypothesis that even a low-level liver dysfunction impacts upon the outcome of patients with septic shock, which is supported by recent study by Nessler *et al* (Nesseler, Launey, Aninat, *et al.*, 2016). Using data from the PROWESS-SHOCK trial they demonstrated a significant relationship between the new onset of liver dysfunction defined as an increase in liver SOFA score from 0 or worsening liver dysfunction after baseline (defined as any increase in liver SOFA score from baseline greater than 0), and 28-, 90- and 180-day mortality. In this study, enrolment to the PROWESS-SHOCK trial was taken as the baseline and the inclusion criteria included sepsis with shock (defined by the Bone criteria) and clinical evidence of hypoperfusion despite vasopressors and fluids for at least four hours above a defined threshold. Previous studies supporting a link between mortality and both liver dysfunction and liver failure have included the French EPISEPSIS study (Brun-Buisson, Meshaka, Pinton, *et al.*, 2004) and a Chinese study by Cheng *et al* (Cheng, Xie, Yao, *et al.*, 2007). In all three of these studies, liver failure was defined as a liver SOFA score of 3-4 and liver dysfunction included patients with SOFA score of 1 and 2.

Liver SOFA score is determined by total bilirubin level alone. The lack of specificity of this single parameter of liver dysfunction is acknowleged. Causes of hyperbilirubinaemia in sepsis can be due to a variety of reasons other than sepsis-induced liver dysfunction including cold agglutinin-associated haemolytic anaemia, drug-induced haemolysis, and transfusion reactions for example. Moreover, hyprerbilirubinaemia secondary to non-liver aetiologies is not only common in patients with sepsis but increases with time, and thus metabolic profiling as a predictor of liver dysfunction, defined on the basis of bilirubin alone, particularly at day seven, has limitations. Studies from the USA often use ultrasound findings of acute and subacute necrosis of the liver or hepatic infarction as evidence of acute liver failure. However, it could be argued that these are features of liver dysfunction at the failure end of the spectrum and the intention of this study was to differentiate between patients with any degree of liver dysfunction from those without, with a view to determining early and predictive

markers of sepsis related liver dysfunction. In this study, patients were scored using the full range of liver SOFA scores but the supervised multivariate analyses of the lipidomic analyses were performed using binary scores of the presence or absence of liver dysfunction, owing to the small numbers of samples of each of the five liver subgroups divided according to the five liver SOFA scores.

Limitations with the use of SOFA scores to define organ failures in general are acknowledged. Cardiovascular and respiratory SOFA scores are based on physiological parameters in addition to being treatment-related, which can vary between healthcare institutions, patients and within the same patient. Respiratory could be viewed as the *'cleanest'* in terms of having the least confounding factors. Confounders of the CVS score includes high vasopressor requirements to counteract sedation tolerance and the use of additional vasopressors or inotropes not included in this scoring system such as Levosimendan, milrinone and vasopressin, which is particularly relevant to this study. This is highlighted by the patients with cardiovascular SOFA score of zero at enrolment to the VACS trial, a cohort who were required to have septic shock requiring vasopressors to meet the inclusion criteria of the trial and therefore should have a cardiovascular SOFA score of at least three.

In contrast, the renal SOFA score, is based on the serum creatinine or urine output alone unlike other renal scoring system such as AKIN and RIFLE, which also include the RRT as a treatment-related variable. The omission of RRT in the renal SOFA score will score patients would do not meet the creatinine or urine output criteria of the scores of one to four because of the early initiation of RRT as zero; whereas the other AKI scoring or classification systems regard RRT as the surrogate for the highest stage.

The liver and haematological (coagulation) SOFA scores are based on one single blood parameter (bilirubin and platelet count, respectively) which are associated with a lack specificity for their respective organ dysfunctions in most examples of critical illnesses involving multiple organs including

sepsis. Hyperbilirubinaemia in sepsis for example, can be due to a variety of reasons other than sepsis induced liver dysfunction, as discussed above and non-haematological causes of low platelets includes drug-induced such as heparin-induced thrombocytopenia.

The GCS is often poorly assessed and influenced by the level of sedation; it is therefore unreliable (Arts, de Keizer, Vroom, *et al.*, 2005) and did not form part of the SOFA of the sepsis cohort in this study.

Ostensibly, in the absence of specific pharmacological treatment modalities for sepsis-related liver dysfunction, it would seem unlikely that any pharmaceutical drugs or fluids could be responsible for the metabolic differences demonstrated by the two liver dysfunction groups. Especially, the differences demonstrated by the NMR component of the study, in view of an extensive database of drugs that would have aided the identification of any drug confounders, even in the absence of knowledge of the drug history before and during the study period. However, it is acknowledged that without knowledge of the drugs administered before each of the sampling time points, it is impossible to exclude the possibility that drugs and fluids may be responsible for the differences in this study; especially the lipids demonstrated by the LCMS lipidomic profiling. Furthermore, it is also possible that differences in the metabolism of the same drugs in the two groups could be responsible for the metabolic differences demonstrated by the two liver dysfunction groups. However, although these differences in drug metabolism may not help elucidate the underlying pathogenesis of sepsis-related liver dysfunction, they may still be useful biomarkers of sepsis-related liver dysfunction.

Drug-induced liver dysfunction could also be wholly or partially responsible for the metabolic differences demonstrated between the two liver dysfunction groups, as opposed to being due to SILI. Although, drug-induced liver dysfunction (DILI) is relatively uncommon, ICU patients are more likely to develop DILI because of the increased number of drugs administered which increases the risk of

potential interactions resulting in changes in their pharmacokinetics which increases the risk of DILI. Complex interactions between the liver and kidney affecting the pharmacokinetics of drugs also occur in the context of dysfunction of one or both organs, and is prevalent in patients with sepsis. All of the sepsis cohort had septic shock and would have therefore received intravenous antibiotics, one of the commonest causes of IV drug-induced liver dysfunction. All of these factors would have increased the risk of DILI in the sepsis cohort. Furthermore, in a study of DILI secondary to IV medications by Ghabril and colleagues (Ghabril, Fontana, Rockey, *et al.*, 2013), 33 percent of all the DILI occurred within a week of the drug being administered; which corresponds with the time period of this study (within six hours of treatment for septic shock and therefore likely to be within 48 hours of the administration of a course of IV antibiotics).

The validation cohort of chapter three were recruited as part of a clinical study to investigate biomarkers of organ dysfunctions in critical illness particularly acute kidney dysfunction. At the time of recruitment its use in a metabolic profiling study was not known and the entry criteria was relatively unrestricted, including the onset of the critical illness; although all patients were recruited within 48 hours of admission to the ICU. Consequently, this cohort exhibited a wide degree of variation in many of factors that can contribute to the metabolic variation of the patients' biofluids, unrelated to the clinical classes under investigation, that could and ideally would have been, otherwise been controlled for. Despite its shortcomings however, this cohort was a readily available resource that provided invaluable information on the use of metabolic profiling in critically ill patients including the impact the number of drugs administered to most ICU patients has on NMR analyses of urine. Information that was of great use in later NMR experiments on the samples from the sepsis cohort described in chapter four.

6.5 Future directions

The metabolic signatures of sepsis-related liver dysfunction demonstrated by this study are also likely to be predictors of the onset of cholestasis and hepatocellular dysfunction of sepsis. This hypothesis could not be tested in the current study because of the small number of patients who went on to develop liver dysfunction after enrolment. The reason for this small number was that the majority of patients who had SRLI during the study period already had evidence of SRLI at enrolment. One future direction of further research would be to test this theory in patients at risk of developing sepsis with the intention of collecting baseline plasma samples before the development of SRLI in the patients who go on to develop sepsis.

Another area of further research highlighted by this study is the development of an automated computer software system capable of differentiating between drug and non-drug metabolites. This would incorporate both a comprehensive drug database of spectra from the chosen metabonomic platform and a method of STOCSY to enable the removal of selected drug signals from the spectral data prior to the performance of supervised analyses used to determine metabolic signatures of the classes being investigated.

In summary, the metabolic signatures demonstrated by this study warrants further investigation in patients at risk of developing sepsis, to investigate their potential as both biomarkers of the early onset of sepsis induced liver dysfunction and expand on the pathophysiology of this common and important cause of mortality.

References

Adhikari, N.K.J., Fowler, R.A., Bhagwanjee, S. & Rubenfeld, G.D. (2010) Critical care and the global burden of critical illness in adults. *The Lancet*. [Online] 376 (9749), 1339–1346. Available from: doi:10.1016/S0140-6736(10)60446-1.

Angus, D.C., Linde-Zwirble, W.T., Lidicker, J., Clermont, G., et al. (2001) Epidemiology of severe sepsis in the United States: analysis of incidence, outcome, and associated costs of care. *Critical care medicine*. [Online] 29 (7), 1303–1310. Available from: doi:10.1097/00003246-200107000-00002.

Arts, D.G.T., de Keizer, N.F., Vroom, M.B. & de Jonge, E. (2005) Reliability and accuracy of Sequential Organ Failure Assessment (SOFA) scoring. *Critical Care Medicine*. [Online] 33 (9), 1988–1993. Available from: doi:10.1097/01.CCM.0000178178.02574.AB.

Azuma, Y., Maekawa, M., Kuwabara, Y., Nakajima, T., et al. (1989) Determination of branched-chain amino acids and tyrosine in serum of patients with various hepatic diseases, and its clinical usefulness. *Clinical Chemistry*. [Online] 35 (7), 1399–1403. Available from: http://www.clinchem.org/content/35/7/1399.abstract.

Bach, a (1982) Carnitine biosynthesis in mammals. *Reproduction, nutrition, development*. [Online] 22 (4), 583–596. Available from: doi:10.1042/0264-6021:3610417.

Bagshaw, S.M., Bennett, M., Haase, M., Haase-Fielitz, A., et al. (2010) Plasma and urine neutrophil gelatinase-associated lipocalin in septic versus non-septic acute kidney injury in critical illness. *Intensive Care Medicine*. [Online] 36 (3), 452–461. Available from: doi:10.1007/s00134-009-1724-9.

Bagshaw, S.M., George, C. & Bellomo, R. (2008) Early acute kidney injury and sepsis: a multicentre evaluation. *Critical care (London, England)*. [Online] 12 (2), R47. Available from: doi:10.1186/cc6863.

Baile, W.F., Buckman, R., Lenzi, R., Glober, G., et al. (2000) SPIKES-A six-step protocol for delivering bad news: application to the patient with cancer. *The oncologist*. [Online] 5 (4), 302–311. Available from: doi:10.1634/theoncologist.5-4-302.

De Bandt, J.-P. & Cynober, L. (2006) Therapeutic Use of Branched-Chain Amino Acids in Burn, Trauma, and Sepsis. *J.Nutr.* 136308S–313S.

Basler, T., Meier-Hellmann, A., Bredle, D. & Reinhart, K. (2002) Amino acid imbalance early in septic encephalopathy. *Intensive Care Medicine*. [Online] 28 (3), 293–298. Available from: doi:10.1007/s00134-002-1217-6.

Bauer, M., Press, A.T. & Trauner, M. (2013) The liver in sepsis: patterns of response and injury. *Current opinion in critical care*. [Online] 19 (2), 123–127. Available from: doi:10.1097/MCC.0b013e32835eba6d.

Beckonert, O., Keun, H.C., Ebbels, T.M., Bundy, J., et al. (2007) Metabolic profiling, metabolomic and metabonomic procedures for NMR spectroscopy of urine, plasma, serum and tissue extracts. *Nat Protoc*. [Online] 2 (11), 2692–2703. Available from: doi:10.1038/nprot.2007.376.

Blaise, B.J., Gouel-Chéron, A., Floccard, B., Monneret, G., et al. (2013) Metabolic phenotyping of

traumatized patients reveals a susceptibility to sepsis. *Analytical chemistry*. [Online] 85 (22), 10850–10855. Available from: doi:10.1021/ac402235q.

Blanco, J., Muriel-Bombin, A., Sagredo, V., Taboada, F., et al. (2008) Incidence, organ dysfunction and mortality in severe sepsis: a Spanish multicentre study. *Critical care (London, England)*. [Online] 12 (6), R158. Available from: doi:\url{10.1186/cc7157}.

Bone, R., Balk, R., Cerra, F., Dellinger, R., et al. (1992) accplsccm consensus conference for Sepsis and Organ Failure and. *Chest*. 1011644–1655.

Bouatra, S., Aziat, F., Mandal, R., Guo, A.C., et al. (2013) The Human Urine Metabolome. *PLoS ONE*. [Online] 8 (9). Available from: doi:10.1371/journal.pone.0073076.

Brosnan, J. & Brosnan, M. (2006) 5th Amino Acid Assessment Workshop. *The Journal of nutrition*. [Online] 136 (6), 16365–16405. Available from: https://www.pkdiet.com/pdf/eaa/aminoacidwrksp.pdf.

Bruegel, M., Ludwig, U., Kleinhempel, A., Petros, S., et al. (2012) Sepsis-associated changes of the arachidonic acid metabolism and their diagnostic potential in septic patients*. *Critical Care Medicine*. [Online] 40 (5), 1478–1486. Available from: doi:10.1097/CCM.0b013e3182416f05.

Brun-Buisson, C., Meshaka, P., Pinton, P. & Vallet, B. (2004) EPISEPSIS: A reappraisal of the epidemiology and outcome of severe sepsis in French intensive care units. *Intensive Care Medicine*. [Online] 30 (4), 580–588. Available from: doi:10.1007/s00134-003-2121-4.

Brun-buisson, C. & Mondor, C.H.U.H. (2004) EPISEPSIS: a reappraisal of the epidemiology and outcome of severe sepsis in French intensive care units. *Intensive Care Medicine*. [Online] 30 (4), 580–588. Available from: doi:10.1007/s00134-003-2121-4.

Brunton, L., Parker, K., Blumenthal, D. & Buxton, I. (2008) *Goodman & Gilman's: Manual of Pharmacology and Therapeutics*. [Online]. Available from: doi:10.1016/S0163-7258(02)00291-7.

Camerer, E., Regard, J.B., Cornelissen, I., Srinivasan, Y., et al. (2009) Sphingosine-1-phosphate in the plasma compartment regulates basal and inflammation-induced vascular leak in mice. *Journal of Clinical Investigation*. [Online] 119 (7), 1871–1879. Available from: doi:10.1172/JCI38575DS1.

Carré, J.E. & Singer, M. (2008) Cellular energetic metabolism in sepsis: The need for a systems approach. *Biochimica et Biophysica Acta - Bioenergetics*. [Online] 1777 (7–8), 763–771. Available from: doi:10.1016/j.bbabio.2008.04.024.

Chawla, L.S., Seneff, M.G., Nelson, D.R., Williams, M., et al. (2007) Elevated plasma concentrations of IL-6 and elevated APACHE II score predict acute kidney injury in patients with severe sepsis. *Clinical journal of the American Society of Nephrology : CJASN*. [Online] 222–30. Available from: doi:10.2215/CJN.02510706.

Cheng, B., Xie, G., Yao, S., Wu, X., et al. (2007) Epidemiology of severe sepsis in critically ill surgical patients in ten university hospitals in China. *Crit Care Med*. [Online] 35 (0090–3493 (Print)), 2538–2546. Available from: doi:10.1097/01.CCM.0000284492.30800.00.

Choy, P.C., Skrzypczak, M., Lee, D. & Jay, F.T. (1997) Acyl-GPC and alkenyl/alkyl-GPC:Acyl-CoA acyltransferases. *Biochimica et Biophysica Acta - Lipids and Lipid Metabolism*. [Online] 1348 (1–2), 124–133. Available from: doi:10.1016/S0005-2760(97)00114-8.

Ciraolo, E., Gulluni, F. & Hirsch, E. (2014) *Methods to measure the enzymatic activity of PI3Ks*. 1st edition. [Online]. Elsevier Inc. Available from: doi:10.1016/B978-0-12-801329-8.00006-4.

Claus, R.A., Bunck, A.C., Bockmeyer, C.L., Brunkhorst, F.M., et al. (2005) Role of increased sphingomyelinase activity in apoptosis and organ failure of patients with severe sepsis. *Faseb J*. [Online] 19 (12), 1719–1721. Available from: doi:04-2842fje [pii]\r10.1096/fj.04-2842fje.

Cloarec, O., Dumas, M., Craig, A., Barton, R.H., et al. (2005) Statistical Total Correlation Spectroscopy : An Exploratory Approach for Latent Biomarker Identification from Metabolic H NMR Data Sets Statistical Total Correlation Spectroscopy : An Exploratory Approach for Latent Biomarker Identification from Metabolic. *Analytical Chemistry*. [Online] 77 (5), 1282–1289. Available from: doi:10.1021/ac048630x.

Coen, M., O'Sullivan, M., Bubb, W. a, Kuchel, P.W., et al. (2005) Proton nuclear magnetic resonance-based metabonomics for rapid diagnosis of meningitis and ventriculitis. *Clinical infectious diseases : an official publication of the Infectious Diseases Society of America*. [Online] 41 (11), 1582–1590. Available from: doi:10.1086/497836.

Cohen, M.J., Serkova, N.J., Wiener-Kronish, J., Pittet, J.-F., et al. (2010) 1H-NMR-Based Metabolic Signatures of Clinical Outcomes in Trauma Patients—Beyond Lactate and Base Deficit. *The Journal of Trauma: Injury, Infection, and Critical Care*. [Online] 69 (1), 31–40. Available from: doi:10.1097/TA.0b013e3181e043fe.

Cseke, L.J., Kaufman, P.B., Podila, G.K. & Tsai, C.-J. (2003) *Handbook of Molecular and Cellular Methods in Biology and Medicine, Second Edition*. [Online]. CRC Press. Available from: https://books.google.com/books?id=6N-l3XNVQscC&pgis=1.

Dejong, C., van de Poll, M., Soeters, P., Jalan, R., et al. (2007) *Aromatic amino acid metabolism during liver failure*. [Online] Available from: http://discovery.ucl.ac.uk/113976/.

Dellinger, R.P., Carlet, J.M., Masur, H., Gerlach, H., et al. (2004) Surviving Sepsis Campaign guidelines for management of severe sepsis and septic shock. *Critical care medicine*. 32 (3), 858–873.

Dieterle, F., Ross, A., Schlotterbeck, G. & Senn, H. (2006) Probabilistic quotient normalization as robust method to account for dilution of complex biological mixtures. Application in1H NMR metabonomics. *Analytical Chemistry*. [Online] 78 (13), 4281–4290. Available from: doi:10.1021/ac051632c.

Dolinay, T., Kim, Y.S., Howrylak, J., Hunninghake, G.M., et al. (2012) Inflammasome-regulated cytokines are critical mediators of acute lung injury. *American Journal of Respiratory and Critical Care Medicine*. [Online] 185 (11), 1225–1234. Available from: doi:10.1164/rccm.201201-0003OC.

Drobnik, W. (2003) Plasma ceramide and lysophosphatidylcholine inversely correlate with mortality in sepsis patients. *The Journal of Lipid Research*. [Online] 44 (4), 754–761. Available from: doi:10.1194/jlr.M200401-JLR200.

Druml, W., Heinzel, G. & Kleinberger, G. (2001) Amino acid kinetics in patients with sepsis. *Am J Clin Nutr*. [Online] 73 (5), 908–913. Available from: http://www.ncbi.nlm.nih.gov/entrez/query.fcgi?cmd=Retrieve&db=PubMed&dopt=Citation&list_uids=11333844.

Elferink, R.P., Tytgat, G.N. & Groen, A.K. (1997) Hepatic canalicular membrane 1: The role of mdr2 P-glycoprotein in hepatobiliary lipid transport. *Faseb J*. [Online] 11 (1), 19–28. Available from: http://www.ncbi.nlm.nih.gov/pubmed/9034162.

Eriksson, L., Johansson, E., Kettaneh-Wold, N., Trygg, C., et al. (2006) Pca. *Multi- and Megavariate Data Analysis Part 1, Basic Principles and Applications*. 39–62.

Ertmer, C., Bone, H.-G., Morelli, A., Van Aken, H., et al. (2007) Methylprednisolone Reverses

Vasopressin Hyporesponsiveness in Ovine Endotoxemia. *Shock*. [Online] 27 (3), 281–288. Available from: doi:10.1097/01.shk.0000235140.97903.90.

Evans, J.D. (1996) *Straightforward Statistics for the Behavioral Sciences*. 122.

Fahy, E., Subramaniam, S., Brown, H.A., Glass, C.K., et al. (2005) A comprehensive classification system for lipids. *Journal of lipid research*. [Online] 46839–861. Available from: doi:10.1194/jlr.E400004-JLR200.

Fahy, E., Subramaniam, S., Murphy, R.C., Nishijima, M., et al. (2009) Update of the LIPID MAPS comprehensive classification system for lipids. *Journal of lipid research*. [Online] 50 SupplS9–S14. Available from: doi:10.1194/jlr.R800095-JLR200.

Farms, T. (1998) *Determinants of the Selection of Phosphatidylcholine Molecular Species for Secretion into Bile in the Rat*. (617), 631–637.

Faubion, W.A., Guicciardi, M.E., Miyoshi, H., Bronk, S.F., et al. (1999) Toxic bile salts induce rodent hepatocyte apoptosis via direct activation of Fas. *Journal of Clinical Investigation*. [Online] 103 (1), 137–145. Available from: doi:10.1172/JCI4765.

Friebolin, H. (1998) *Basic One- and Two-Dimensional NMR Spectroscopy*. Wiley-VCH, Weinheim.

Friedrich, J.O., Wilson, G. & Chant, C. (2006) Long-term outcomes and clinical predictors of hospital mortality in very long stay intensive care unit patients: a cohort study. *Critical care (London, England)*. [Online] 10 (2), R59. Available from: doi:10.1186/cc4888.

García-Ruiz, C., Colell, A., Mari, M., Morales, A., et al. (2003) Defective TNF-α-mediated hepatocellular apoptosis and liver damage in acidic sphingomyelinase knockout mice. *Journal of Clinical Investigation*. [Online] 111 (2), 197–208. Available from: doi:10.1172/JCI200316010.

Ghabril, M., Fontana, R., Rockey, D., Jiezhun, G., et al. (2013) Drug-induced Liver Injury Caused by Intravenously Administered Medications. *Journal of Clinical Gastroenterology*. [Online] 47 (6), 553–558. Available from: doi:10.1097/MCG.0b013e318276bf00.

Giovannini, I., Boldrini, G., Castagneto, M., Sganga, G., et al. (1983) Respiratory quotient and patterns of substrate utilization in human sepsis and trauma. *JPEN. Journal of parenteral and enteral nutrition*. [Online] 7 (3), 226–230. Available from: doi:10.1177/0148607183007003226.

Göggel, R., Winoto-Morbach, S., Vielhaber, G., Imai, Y., et al. (2004) PAF-mediated pulmonary edema: a new role for acid sphingomyelinase and ceramide. *Nature medicine*. [Online] 10 (2), 155–160. Available from: doi:10.1038/nm977.

Gordon, A.C., Mason, A.J., Perkins, G.D., Stotz, M., et al. (2014a) The Interaction of Vasopressin and Corticosteroids in Septic Shock. *Critical Care Medicine*. [Online] 42 (6), 1325–1333. Available from: doi:10.1097/CCM.0000000000000212.

Gordon, A.C., Mason, A.J., Perkins, G.D., Stotz, M., et al. (2014b) The interaction of vasopressin and corticosteroids in septic shock: a pilot randomized controlled trial. *Critical care medicine*. [Online] 42 (6), 1325–1333. Available from: doi:10.1097/CCM.0000000000000212.

Graham, G. (1940) The Role of the Liver in Diabetes Mellitus. *British medical journal*. [Online] 2 (4163), 513–516. Available from: doi:10.3109/08830185.2014.889129.

Günther, H. (1995) *NMR Spectroscopy. Basic Principles, Concepts and Applications in Chemistry.* Second edi. Wiley.

Günther, S. & Redl, H. (2012) *Pathophysiology of Shock, Sepsis, and Organ Failure*.

Harrison, D.A., Welch, C.A. & Eddleston, J.M. (2006) The epidemiology of severe sepsis in England, Wales and Northern Ireland, 1996 to 2004: secondary analysis of a high quality clinical database, the ICNARC Case Mix Programme Database. *Critical care (London, England)*. [Online] 10 (2), R42. Available from: doi:10.1186/cc4854.

Hasselgren, P.O., Pedersen, P., Sax, H.C., Warner, B.W., et al. (1988) Current concepts of protein turnover and amino acid transport in liver and skeletal muscle during sepsis. *Arch Surg*. [Online] 123 (8), 992–999. Available from: http://www.ncbi.nlm.nih.gov/entrez/query.fcgi?cmd=Retrieve&db=PubMed&dopt=Citation&list_uids=3293552.

Hodson, L., Skeaff, C.M. & Fielding, B.A. (2008) *Progress in Lipid Research Fatty acid composition of adipose tissue and blood in humans and its use as a biomarker of dietary intake*. [Online] 47348–380. Available from: doi:10.1016/j.plipres.2008.03.003.

Hoffmann, E. De & Stroobant, V. (2007) *Mass Spectrometry - Priniples and Applications.* [Online]. Available from: doi:10.1002/mas.20296.

Honda, T., Fukuda, Y., Nakano, I., Katano, Y., et al. (2004) Effects of liver failure on branched-chain α-keto acid dehydrogenase complex in rat liver and muscle: comparison between acute and chronic liver failure. *Journal of Hepatology*. [Online] 40 (3), 439–445. Available from: doi:10.1016/j.jhep.2003.11.003.

Hore, P. (1995) *Nuclear Magnetic Resonance*. 1st edition. Oxford University Press.

Hough, C.L., Caldwell, E.S., Cox, C.E., Douglas, I.S., et al. (2015) Development and Validation of a Mortality Prediction Model for Patients Receiving 14 Days of Mechanical Ventilation. *Critical Care Medicine*. [Online] 43 (11), 2339–2345. Available from: doi:10.1097/CCM.0000000000001205.

Iglesias, J., Marik, P.E. & Levine, J.S. (2003) Elevated serum levels of the type I and type II receptors for tumor necrosis factor-alpha as predictive factors for ARF in patients with septic shock. *American journal of kidney diseases : the official journal of the National Kidney Foundation*. [Online] 41 (1), 62–75. Available from: doi:10.1053/ajkd.2003.50024.

Ishikawa, T. (2012) Branched-chain amino acids to tyrosine ratio value as a potential prognostic factor for hepatocellular carcinoma. *World Journal of Gastroenterology*. [Online] 18 (17), 2005–2008. Available from: doi:10.3748/wjg.v18.i17.2005.

Izquierdo-Garcia, J.L., Nin, N., Ruiz-Cabello, J., Rojas, Y., et al. (2011) A metabolomic approach for diagnosis of experimental sepsis. *Intensive Care Medicine*. [Online] 37 (12), 2023–2032. Available from: doi:10.1007/s00134-011-2359-1.

Jeong, Y. Il, Jung, I.D., Lee, C.M., Chang, J.H., et al. (2009) The novel role of platelet-activating factor in protecting mice against lipopolysaccharide-induced endotoxic shock. *PLoS ONE*. [Online] 4 (8). Available from: doi:10.1371/journal.pone.0006503.

Jiménez, B., Montoliu, C., Macintyre, D. a, Serra, M. a, et al. (2010) Serum Metabolic Signature of Minimal Hepatic Encephalopathy by H-Nuclear Magnetic Resonance research articles. *Journal of Proteome Research*. 5180–5187.

Kaffarnik, M.F., Lock, J.F., Vetter, H., Ahmadi, N., et al. (2013) Early diagnosis of sepsis-related hepatic dysfunction and its prognostic impact on survival: a prospective study with the LiMAx test. *Critical care (London, England)*. [Online] 17 (5), R259. Available from: doi:10.1186/cc13089.

Kamisoglu, K., Haimovich, B., Calvano, S.E., Coyle, S.M., et al. (2015) Human metabolic response to

systemic inflammation: assessment of the concordance between experimental endotoxemia and clinical cases of sepsis/SIRS. *Critical care (London, England)*. [Online] 1971. Available from: doi:10.1186/s13054-015-0783-2.

Khovidhunkit, W. (2004) Effects of infection and inflammation on lipid and lipoprotein metabolism: mechanisms and consequences to the host. *The Journal of Lipid Research*. [Online] 45 (7), 1169–1196. Available from: doi:10.1194/jlr.R300019-JLR200.

Knaus, W. a, Draper, E. a, Wagner, D.P. & Zimmerman, J.E. (1985) APACHE II: a severity of disease classification system. *Critical care medicine*. [Online]. 13 (10) pp.818–829. Available from: doi:10.1097/00003465-198603000-00013.

Kumar, A., Roberts, D., Wood, K.E., Light, B., et al. (2006) Duration of hypotension before initiation of effective antimicrobial therapy is the critical determinant of survival in human septic shock. *Crit Care Med.* [Online] 34 (0090–3493 (Print)), 1589–1596. Available from: doi:10.1097/01.CCM.0000217961.75225.E9.

Laiakis, E.C., Hyduke, D.R. & Fornance Jr, A.G. (2012) Comparison of Mouse Urinary Metabolic Profiles after Exposure to the Inflammatory Stressors γ Radiation and Lipopolysaccharide. *Radiation Research*. [Online] 177187–199. Available from: doi:10.1038/nature13314.A.

Langley, R.J., Tipper, J.L., Bruse, S., Baron, R.M., et al. (2014) Integrative 'Omic' Analysis of Experimental Bacteremia Identifies a Metabolic Signature That Distinguishes Human Sepsis from Systemic Inflammatory Response Syndromes. *American Journal of Respiratory and Critical Care Medicine*. [Online] 190 (4), 445–455. Available from: doi:10.1164/rccm.201404-0624OC.

Langley, R.J., Tsalik, E.L., van Velkinburgh, J.C., Glickman, S.W., et al. (2013) An integrated clinico-metabolomic model improves prediction of death in sepsis. *Science translational medicine*. [Online] 5 (195), 195ra95. Available from: doi:10.1126/scitranslmed.3005893.

Lehmann, C., Sharawy, N., Zhou, J. & Pavlovic, D. (2012) Metabolomic analysis as biomarker to study steroid hormone administration in sepsis. *Medical Hypotheses*. [Online] 79 (3), 329–330. Available from: doi:10.1016/j.mehy.2012.05.025.

Li, S., Stuart, L., Zhang, Y., Meduri, G.U., et al. (2009) Inter-individual variability of plasma PAF-acetylhydrolase activity in ARDS patients and PAFAH genotype. *Journal of Clinical Pharmacy and Therapeutics*. [Online] 34447–455. Available from: doi:10.1111/j.1365-2710.2008.01014.x.

Li, Y., Hou, M., Wang, J.-G., Wang, T., et al. (2012) Changes of lymph metabolites in a rat model of sepsis induced by cecal ligation and puncture. *The journal of trauma and acute care surgery*. [Online] 73 (6), 1545–1552. Available from: doi:10.1097/TA.0b013e31826fc9e7.

Li, Y., Liu, H., Wu, X., Li, D., et al. (2013) An NMR metabolomics investigation of perturbations after treatment with Chinese herbal medicine formula in an experimental model of sepsis. *Omics : a journal of integrative biology*. [Online] 17 (5), 252–258. Available from: doi:10.1089/omi.2012.0096.

Lin, Z.Y., Xu, P.B., Yan, S.K., Meng, H.B., et al. (2009) A metabonomic approach to early prognostic evaluation of experimental sepsis by 1H NMR and pattern recognition. *NMR in Biomedicine*. [Online] 22 (6), 601–608. Available from: doi:10.1002/nbm.1373.

Lindon, J.C., Nicholson, J.K. & Homes, E. (2007) *Handbook of Metabonomics and Metabolics*. Elsevier BV (ed.).

Liu, X.R., Zheng, X.F., Ji, S.Z., Lv, Y.H., et al. (2010) Metabolomic analysis of thermally injured and/or septic rats. *Burns*. [Online] 36 (7), 992–998. Available from: doi:10.1016/j.burns.2010.03.015.

Malmezat, T., Breuille, D., Pouyet, C., Buffiere, C., et al. (2000) Methionine transsulfuration is increased during sepsis in rats. *American Journal of Physiology: Endocrinology and Metabolism*. [Online] 279 (0193–1849), E1391–E1397. Available from: d:%5C1Refman12%5CPDF%5CRef_ID-3564.PDF.

Mao, H., Wang, H., Wang, B., Liu, X., et al. (2009) Systemic metabolic changes of traumatic critically ill patients revealed by an NMR-based metabonomic approach. *Journal of Proteome Research*. [Online] 8 (12), 5423–5430. Available from: doi:10.1021/pr900576y.

Martensson, J., Bell, M., Oldner, A., Xu, S., et al. (2010) Neutrophil gelatinase-associated lipocalin in adult septic patients with and without acute kidney injury. *Intensive Care Medicine*. [Online] 36 (8), 1333–1340. Available from: doi:10.1007/s00134-010-1887-4.

Martinez, A., Chiolero, R., Bollman, M., Revelly, J.-P., et al. (2003) Assessment of adipose tissue metabolism by means of subcutaneous microdialysis in patients with sepsis or circulatory failure. *Clinical physiology and functional imaging*. [Online] 23 (5), 286–292. Available from: doi:10.1046/j.1475-097X.2003.00512.x.

Mato, J.M., Martínez-Chantar, M.L. & Lu, S.C. (2008) Methionine Metabolism and Liver Disease. *Annual Review of Nutrition*. [Online] 28 (1), 273–293. Available from: doi:10.1146/annurev.nutr.28.061807.155438.

Mazul-Sunko, B., Zarkovic, N., Vrkic, N., Antoljak, N., et al. (2004) Proatrial natriuretic peptide (1-98), but not cystatin C, is predictive for occurrence of acute renal insufficiency in critically ill septic patients. *Nephron - Clinical Practice*. [Online] 97 (3), 103–107. Available from: doi:10.1159/000078638.

McIntyre, N. (2004) *The Liver in Biology and Disease*. Principles of Medical Biology. [Online]. Elsevier. Available from: doi:10.1016/S1569-2582(04)15011-3 [Accessed: 18 December 2015].

Mehta, R.L., Kellum, J. a, Shah, S. V & et al. (2007) Acute Kidney Injury Network: report of an initiative to improve outcomes in acute kidney injury. *Crit Care*. [Online] 11 (2), R31. Available from: doi:10.1186/cc5713.

Michie, H.R. (1996) Metabolism of sepsis and multiple organ failure. *World Journal of Surgery*. [Online]. 20 (4) pp.460–464. Available from: doi:10.1007/s002689900072.

Miyoshi, H., Rust, C., Roberts, P.J., Burgart, L.J., et al. (1999) Hepatocyte apoptosis after bile duct ligation in the mouse involves Fas. *Gastroenterology*. [Online] 117 (3), 669–677. Available from: doi:10.1016/S0016-5085(99)70461-0.

de Montmollin, E. & Annane, D. (2011) Year in review 2010: Critical Care--Multiple organ dysfunction and sepsis. *Critical care (London, England)*. [Online] 15236. Available from: doi:10.1186/cc10359.

Murch, O., Collin, M., Hinds, C.J. & Thiemermann, C. (2007) Lipoproteins in inflammation and sepsis. I. Basic science. *Intensive care medicine*. [Online] 33 (1), 13–24. Available from: doi:10.1007/s00134-006-0432-y.

Murray, R.K. & Davis, J.C. (2003) *Harper ' s Illustrated Biochemistry*. [Online]. Available from: doi:10.1016/0307-4412(88)90029-5.

Nejat, M., Pickering, J.W., Walker, R.J., Westhuyzen, J., et al. (2010) Urinary cystatin C is diagnostic of acute kidney injury and sepsis, and predicts mortality in the intensive care unit. *Critical care (London, England)*. [Online] 14 (3), R85. Available from: doi:10.1186/cc9014.

Nesseler, N., Launey, Y., Aninat, C., Morel, F., et al. (2012) Clinical review: The liver in sepsis. *Critical*

care (London, England). [Online] 16 (5), 235. Available from: doi:10.1186/cc11381.

Nesseler, N., Launey, Y., Aninat, C., White, J., et al. (2016) Liver Dysfunction Is Associated with Long-Term Mortality in Septic Shock. *American Journal of Respiratory and Critical Care Medicine*. [Online] 193 (3), 335–337. Available from: doi:10.1164/rccm.201508-1660LE.

Nicholson, J.K., Foxall, P.J., Spraul, M., Farrant, R.D., et al. (1995) 750 MHz 1H and 1H-13C NMR spectroscopy of human blood plasma. *Analytical chemistry*. [Online] 67 (5), 793–811. Available from: doi:10.1021/ac00101a004.

Nicholson, J.K. & Lindon, J.C. (2008) Systems biology: Metabonomics. *Nature*. [Online] 455 (7216), 1054–1056. Available from: doi:10.1038/4551054a.

De Paepe, P., Belpaire, F.M. & Buylaert, W. a (2002) Pharmacokinetic and pharmacodynamic considerations when treating patients with sepsis and septic shock. *Clinical pharmacokinetics*. [Online] 41 (14), 1135–1151. Available from: doi:10.2165/00003088-200241140-00002.

Park, Y., Jones, D.P., Ziegler, T.R., Lee, K., et al. (2011) Metabolic effects of albumin therapy in acute lung injury measured by proton nuclear magnetic resonance spectroscopy of plasma: A pilot study. *Crit Care Med*. [Online] 39 (10), 2308–2313. Available from: doi:10.1097/CCM.0b013e31822571ce.

Payrastre, B., Missy, K., Giuriato, S., Bodin, S., et al. (2001) Phosphoinositides : key players in cell signalling, in time and space. *Cellular Signalling*. [Online] 13 (6), 377–387. Available from: doi:10.1016/S0898-6568(01)00158-9.

Psychogios, N., Hau, D.D., Peng, J., Guo, A.C., et al. (2011a) The human serum metabolome. *PLoS ONE*. [Online] 6 (2). Available from: doi:10.1371/journal.pone.0016957.

Psychogios, N., Hau, D.D., Peng, J., Guo, A.C., et al. (2011b) The human serum metabolome. *PloS one*. [Online] 6 (2), e16957. Available from: doi:10.1371/journal.pone.0016957.

Pynn, C.J., Henderson, N.G., Clark, H., Koster, G., et al. (2011) Specificity and rate of human and mouse liver and plasma phosphatidylcholine synthesis analyzed in vivo. *Journal of lipid research*. [Online] 52 (2), 399–407. Available from: doi:10.1194/jlr.D011916.

Recknagel, P., Gonnert, F. a., Westermann, M., Lambeck, S., et al. (2012) Liver Dysfunction and Phosphatidylinositol-3-Kinase Signalling in Early Sepsis: Experimental Studies in Rodent Models of Peritonitis. *PLoS Medicine*. [Online] 9 (11), 9–10. Available from: doi:10.1371/journal.pmed.1001338.

Rival, T., Cinq-Frais, C., Silva-Sifontes, S., Garcia, J., et al. (2013) Alteration of plasma phospholipid fatty acid profile in patients with septic shock. *Biochimie*. [Online] 95 (11), 2177–2181. Available from: doi:10.1016/j.biochi.2013.08.006.

Rivers, E., Nguyen, B., Havstad, S., Ressler, J., et al. (2001) Early goal-directed therapy in the treatment of severe sepsis and septic shock. *The New England journal of medicine*. [Online] 345 (19), 1368–1377. Available from: doi:10.1056/NEJMoa010307.

Rogers, A.J., McGeachie, M., Baron, R.M., Gazourian, L., et al. (2014) Metabolomic derangements are associated with mortality in critically ill adult patients. *PLoS ONE*. [Online] 9 (1), 1–7. Available from: doi:10.1371/journal.pone.0087538.

Russmann, S., Junker, E. & Lauterburg, B.H. (2002) Remethylation and transsulfuration of methionine in cirrhosis: studies with L-[H3-methyl-1-C]methionine. *Hepatology (Baltimore, Md.)*. [Online] 36 (5), 1190–1196. Available from: doi:10.1053/jhep.2002.36499.

Schmerler, D., Neugebauer, S., Ludewig, K., Bremer-Streck, S., et al. (2012) Targeted metabolomics

for discrimination of systemic inflammatory disorders in critically ill patients. *The Journal of Lipid Research*. [Online] 53 (7), 1369–1375. Available from: doi:10.1194/jlr.P023309.

Schuster, D.P., Metzler, M., Opal, S., Lowry, S., et al. (2003) Recombinant platelet-activating factor acetylhydrolase to prevent acute respiratory distress syndrome and mortality in severe sepsis: Phase IIb, multicenter, randomized, placebo-controlled, clinical trial. *Critical care medicine*. [Online] 31 (6), 1612–1619. Available from: doi:10.1097/01.CCM.0000063267.79824.DB.

Seymour, C.W., Yende, S., Scott, M.J., Pribis, J., et al. (2013) Metabolomics in pneumonia and sepsis: An analysis of the GenIMS cohort study. *Intensive Care Medicine*. [Online] 39 (8), 1423–1434. Available from: doi:10.1007/s00134-013-2935-7.

Shapiro, N.I., Trzeciak, S., Hollander, J.E., Birkhahn, R., et al. (2010) The Diagnostic Accuracy of Plasma Neutrophil Gelatinase-Associated Lipocalin in the Prediction of Acute Kidney Injury in Emergency Department Patients With Suspected Sepsis. *Annals of Emergency Medicine*. [Online] 56 (1), 52–59.e1. Available from: doi:10.1016/j.annemergmed.2010.02.010.

Singer, P.M., De Santis, V., Vitale, D. & Jeffcoate, W. (2004) Multiorgan failure is an adaptive, endocrine-mediated, metabolic response to overwhelming systemic inaflammation. *Lancet*. [Online] 364 (9433), 545–548. Available from: doi:10.1016/S0140-6736(04)16815-3.

Slupsky, C.M., Rankin, K.N., Fu, H., Chang, D., et al. (2009) Pneumococcal pneumonia: Potential for diagnosis through a urinary metabolic profile. *Journal of Proteome Research*. [Online] 8 (12), 5550–5558. Available from: doi:10.1021/pr9006427.

Smit, J.J.M., Schinkel, A.H., Elferink, R.P.J.O., Groen, A.K., et al. (1993) Homozygous disruption of the murine MDR2 P-glycoprotein gene leads to a complete absence of phospholipid from bile and to liver disease. *Cell*. [Online] 75 (3), 451–462. Available from: doi:10.1016/0092-8674(93)90380-9.

Smith, B. (2015) *Large Animal Internal Medicine*. 5th edition. Elsevier.

Smith, B.S., Yogaratnam, D., Levasseur-Franklin, K.E., Forni, A., et al. (2012) Introduction to drug pharmacokinetics in the critically ill patient. *Chest*. [Online] 141 (5), 1327–1336. Available from: doi:10.1378/chest.11-1396.

Sodeman, T., Bronk, S.F., Roberts, P.J., Miyoshi, H., et al. (2000) Bile salts mediate hepatocyte apoptosis by increasing cell surface trafficking of Fas. *Am.J Physiol Gastrointest.Liver Physiol*. 278 (6), G992–G999.

Sprung, C.L., Annane, D., Keh, D., Moreno, R., et al. (2008) Hydrocortisone therapy for patients with septic shock. *The New England journal of medicine*. [Online] 358 (2), 111–124. Available from: doi:10.1056/NEJMoa071366.

Steelman, S.M., Johnson, P., Jackson, A., Schulze, J., et al. (2014) Serum metabolomics identifies citrulline as a predictor of adverse outcomes in an equine model of gut-derived sepsis. *Physiological genomics*. [Online] 46 (10), 339–347. Available from: doi:10.1152/physiolgenomics.00180.2013.

Stringer, K. a, Serkova, N.J., Karnovsky, A., Guire, K., et al. (2011) Metabolic consequences of sepsis-induced acute lung injury revealed by plasma ^{1}H-nuclear magnetic resonance quantitative metabolomics and computational analysis. *American journal of physiology. Lung cellular and molecular physiology*. [Online] 300 (1), L4–L11. Available from: doi:10.1152/ajplung.00231.2010.

Su, L., Huang, Y., Zhu, Y., Xia, L., et al. (2014) Discrimination of sepsis stage metabolic profiles with an LC/MS-MS-based metabolomics approach. *BMJ Open Respiratory Research*. [Online] 1 (1),

e000056–e000056. Available from: doi:10.1136/bmjresp-2014-000056.

Su, L., Li, H., Xie, A., Liu, D., et al. (2015) Dynamic Changes in Amino Acid Concentration Profiles in Patients with Sepsis. *Plos One*. [Online] 10 (4), e0121933. Available from: doi:10.1371/journal.pone.0121933.

Suistomaa, M., Niskanen, M., Kari, A., Hynynen, M., et al. (2002) Customised prediction models based on APACHE II and SAPS II scores in patients with prolonged length of stay in the ICU. *Intensive Care Medicine*. [Online] 28 (4), 479–485. Available from: doi:10.1007/s00134-002-1214-9.

Sumner, L.W., Amberg, A., Barrett, D., Beale, M.H., et al. (2007) Proposed minimum reporting standards for chemical analysis: Chemical Analysis Working Group (CAWG) Metabolomics Standards Initiative (MSI). *Metabolomics*. [Online] 3 (3), 211–221. Available from: doi:10.1007/s11306-007-0082-2.

Tomé, D. & Bos, C. (2007) Lysine requirement through the human life cycle. *The Journal of nutrition*. [Online] 137 (6 Suppl 2), 1642S–1645S. Available from: doi:137/6/1642S [pii].

Tziolos, N., Kotanidou, A. & Orfanos, S.E. (2015) Biomarkers in infection and sepsis: Can they really indicate final outcome? *International Journal of Antimicrobial Agents*. [Online] 46S29–S32. Available from: doi:10.1016/j.ijantimicag.2015.10.010.

Ursell, L.K., Metcalf, J.L., Parfrey, L.W. & Knight, R. (2012) Definig the Human Microbiome. *Nutrition Reviews*. [Online] 70 (Suppl 1), S38–S44. Available from: doi:10.1111/j.1753-4887.2012.00493.x.Defining.

Venable, J., Ameriks, M., Blevitt, J., Thurmond, R., et al. (2010) Phosphoinositide 3-Kinase Gamma (PI3Kγ) Inhibitors for the Treatment of Inflammation and Autoimmune Disease. *Recent Patents on Inflammation & Allergy Drug Discovery*. [Online] 4 (1), 1–15. Available from: doi:10.2174/187221310789895603.

Venable, M.E., Zimmerman, G. a, Mcintyre, T.M. & Prescott, S.M. (1993) Platelet-activating factor: as phospholipid autacoid with diverse actions. *Journal Of Lipid Research*. 34691–702.

Vernocchi, P., Del Chierico, F. & Putignani, L. (2016) Gut microbiota profiling: Metabolomics based approach to unravel compounds affecting human health. *Frontiers in Microbiology*. [Online] 7 (JUL). Available from: doi:10.3389/fmicb.2016.01144.

Vincent, J., Moreno, R. & Takala, J. (1996) The SOFA (Sepsis related Organ Failure Assessment) score to describe organ dysfunction / failure. *Intensive care …*. [Online] 707–710. Available from: doi:10.1007/BF01709751.

Vincent, J.L., Spapen, H., Bakker, J., Webster, N.R., et al. (2000) Phase II multicenter clinical study of the platelet-activating factor receptor antagonist BB-882 in the treatment of sepsis. *Critical Care Medicine*. 28 (3), 638–642.

Vorkas, P.A., Shalhoub, J., Isaac, G., Want, E.J., et al. (2015) Metabolic Phenotyping of Atherosclerotic Plaques Reveals Latent Associations between Free Cholesterol and Ceramide Metabolism in Atherogenesis. *Journal of Proteome Research*. [Online] 14 (3), 1389–1399. Available from: doi:10.1021/pr5009898.

de Vree, J.M., Jacquemin, E., Sturm, E., Cresteil, D., et al. (1998) Mutations in the MDR3 gene cause progressive familial intrahepatic cholestasis. *Proceedings of the National Academy of Sciences of the United States of America*. [Online] 95 (January), 282–287. Available from: doi:10.1073/pnas.95.1.282.

Walshe, C.M., Odejayi, F., Ng, S. & Marsh, B. (2009) Urinary glutathione S-transferase as an early marker for renal dysfunction in patients admitted to intensive care with sepsis. *Critical care and resuscitation : journal of the Australasian Academy of Critical Care Medicine*. [Online] 11 (3), 204–209. Available from: http://www.ncbi.nlm.nih.gov/sites/entrez?Db=pubmed&Cmd=Retrieve&list_uids=19737123&dopt=abstractplus%5Cnpapers://347a0d64-8b48-4dcf-b0a7-00f094a7599b/Paper/p748.

Wendel, M., Paul, R. & Heller, A.R. (2007) Lipoproteins in inflammation and sepsis. II. Clinical aspects. *Intensive care medicine*. [Online] 33 (1), 25–35. Available from: doi:10.1007/s00134-006-0433-x.

Wheeler, D.S., Devarajan, P., Ma, Q., Harmon, K., et al. (2008) Serum neutrophil gelatinase-associated lipocalin (NGAL) as a marker of acute kidney injury in critically ill children with septic shock. *Critical care medicine*. [Online] 36 (4), 1297–1303. Available from: doi:10.1097/CCM.0b013e318169245a.

Wheelock, Å.M. & Wheelock, C.E. (2013) Trials and tribulations of 'omics data analysis: assessing quality of SIMCA-based multivariate models using examples from pulmonary medicine. *Molecular BioSystems*. [Online] 9 (11), 2589–2596. Available from: doi:10.1039/c3mb70194h.

Wiklund, S., Johansson, E., Sjöström, L., Mellerowicz, E.J., et al. (2008) Visualization ofGC/TOF-MS-Based Metabolomics Data for Identification of Biochemically Interesting Compounds Using OPLS Class Models. *Analytical Chemistry*. [Online] 80 (1), 115–122. Available from: doi:10.1021/ac0713510 CCC.

Wold, S., Esbensen, K. & Geladi, P. (1987) Principal component analysis. *Chemometrics and Intelligent Laboratory Systems*. [Online] 2 (1–3), 37–52. Available from: doi:10.1016/0169-7439(87)80084-9.

Wolfe, R.R. & Martini, W.Z. (2000) Changes in Intermediary Metabolism in Severe Surgical Illness. *World Journal of Surgery*. [Online] 24 (6), 639–647. Available from: doi:10.1007/s002689910105.

Yamashita, A., Hayashi, Y., Nemoto-Sasaki, Y., Ito, M., et al. (2014) Acyltransferases and transacylases that determine the fatty acid composition of glycerolipids and the metabolism of bioactive lipid mediators in mammalian cells and model organisms. *Progress in Lipid Research*. [Online] 53 (1), 18–81. Available from: doi:10.1016/j.plipres.2013.10.001.

Yang, J., He, J., Cao, H., Zhao, X., et al. (2012) Correlation between plasma amino acid profiles and the various stages of hepatitis B infection. *European journal of clinical microbiology & infectious diseases : official publication of the European Society of Clinical Microbiology*. [Online] 31 (8), 2045–2052. Available from: doi:10.1007/s10096-011-1538-x.

Yang, W., Wang, Y., Zhou, Q. & Tang, H. (2008) Analysis of human urine metabolites using SPE and NMR spectroscopy. *Sci. China Ser. B-Chem.* [Online] 51 (3), 218–225. Available from: doi:10.1007/s11426-008-0031-6.

Yost, C.C., Cody, M.J., Harris, E.S., Thornton, N.L., et al. (2012) *Impaired neutrophil extracellular trap (NET) formation : a novel innate immune deficiency of human neonates Impaired neutrophil extracellular trap (NET) formation : a novel innate immune deficiency of human neonates*. [Online] 113 (25), 6419–6427. Available from: doi:10.1182/blood-2008-07-171629.

Yost, C.C., Weyrich, A.S. & Zimmerman, G. a. (2010) The platelet activating factor (PAF) signaling cascade in systemic inflammatory responses. *Biochimie*. [Online]. 92 (6) pp.692–697. Available from: doi:10.1016/j.biochi.2010.02.011.

Appendix I

1 Hydroxyethyl Starch Removal Experiments

1.1 Introduction: Hydroxyethyl Starch

Starch is composed of two polysaccharides – amylose and amylopectin. Plant starch is usually 20-30% amylose and 70-80% amylopectin. In humans, amylopectin undergoes rapid hydrolysis by amylase, but this can be modified by glucose substitutions. Hydroxyethyl starch, is a derivative of amylopectin, with hydroxyethyl groups, substituted for some of the glucose molecules. The ratio of hydroxyethyl groups to glucose units is called the molar substitution and influences its degradation. In the validation cohort, the hydroxyethyl starch (HES) solution Volulyte was administered intravenously to hypotensive patients. Volulyte and Voluven are both intravascular volume expanders that contain 60g/L of a hydroxyethyl starch, with a molar substitution of 0.4 and an average molecular weight of 130 KDa, in an isotonic solution of sodium chloride. Their only difference is the composition of their isotonic solution, in that Volulyte contains acetate, potassium, and magnesium in addition to sodium chloride.

1.2 The removal of Hydroxyethyl Starch

Chemical precipitation and ultrafiltration are two methods that can used to extract solids such as starch, from solutions. Both methods were tested in this study.

Chemical precipitation occurs when the solubility of a substance in a solvent is changed, either by changing the solvent or by transforming the substance into an insoluble one. In 1919, Mellanby *et al* (Mellanby, 1919) demonstrated the precipitation of the soluble components of starch, using two methods: one using iodine and other using colloidal iron. Both methods resulted in the formation insoluble starch complexes. In the iron experiments, the soluble component of potato starch, (labelled granulose) was divided into three parts. The bulk, which was precipitated by iron alone, a second

component precipitated by the combination of iron and electrolytes and a third component not precipitated by either approach. In contrast, the use of iodine and electrolytes resulted in the complete precipitation of all of the soluble components of the starch and the precipitation of the final fraction yielded a blue colour. These findings supported their conclusions: that potato starch solutions contain a variety of polymers, the main constituent, amylopectin is soluble and up to 100% of the soluble components can be precipitated, depending on the method employed. The hydroxyethyl starch in Voluven is readily soluble in water at room temperature. It was hypothesised that the methods capable of precipitating amylopectin, demonstrated by these experiments, would be capable of precipitating hydroxyethyl starch out of the urine samples. This theory was tested on samples of both Voluven and urine.

Chemical reactions, such as precipitation, can be associated with unwanted side effects. Using precipitation, to remove the HES from the urine samples, could therefore be associated with changes to the chemical characteristics of the urine or its metabolites. In view of this possibility, an alternative method of HES removal was also investigated.

Ultrafiltration is a type of membrane filtration that can be used to separate the components of a colloid such as HES solution based on their molecular weight (MW). This technique utilises a semipermeable membrane with pores relating to a specified MW. The suspended solids and solutes of a greater MW are retained by the membrane and form the retainate; the solutes of a lower MW and the water, pass through the membrane and become the filtrate. With the use of ultrafiltration to remove HES from the urine samples, the HES would be collected as the retainate.

1.3 Hypotheses

1. Starch can be precipitated out of solution using the following methods:
    i. Iodine and electrolytes

ii. Colloidal iron and potassium sulphate (K_2SO_4)

2. Starch can be removed using ultrafiltration

1.4 Aims and objectives

1. Investigation of the precipitation of HES from HES solution (Voluven), using the two methods:
    i. Potassium iodide and magnesium ($MgSO_4$)
    ii. Colloidal iron and potassium sulphate (K_2SO_4)
2. Assessment of the removal of HES from the HES solution Voluven using ultrafiltration
3. Apply successful methods of HES removal to human urine samples from a patient given HES and a healthy control not given HES to determine if the removal of HES was associated with any unwanted side effects, such as, the addition, loss, or alteration of the metabolites, in these samples.

1.5 Methodology

1.5.1 Materials

Chemicals for the precipitation experiments

HPLC grade water and methanol (MEOH) and iron (III) chloride ($FeCl_3$ anhydrous, powder, ≥99.99%), potassium sulphate (K_2SO_4) anhydrous, ASC reagent grade, ≥99.5%, magnesium sulphate ($MgSO_4$), anhydrous, ASC reagent grade, ≥99.5%, and potassium iodide (KI) anhydrous, ASC reagent grade, ≥99% were purchased from Sigma-Aldrich (UK),

NMR experiments

See section 2.1

Filters

Centriprep 2ml centrifugal filter devices and Amicon Ultra 0.5mL 3K centrifugal filter devices were purchased from Millipore S.A.S.

Nasosep Centrifugal Filter device were purchased from Pall Corporation.

1.5.2 Precipitation method 1: Iodine and electrolytes

Different quantities of 5% potassium iodide and water were added to a series of three tubes each containing 500μL of 6% HES solution (Voluven containing 60g/L HES and 18g/L NaCl), followed by the addition of 30μL of magnesium sulphate ($MgSO_4$ 1M) (as shown in the Table 1). A fourth tube containing 100μL of water and 500μL of 6% HES solution was also prepared as a control sample. After five minutes, the tubes were examined for the presence of precipitants and a colour change.

Table 1 Starch precipitation experiments using potassium iodide and magnesium sulphate (A) and composition of the solutions (B).

A

Composition (volume in mL)	Experiment 1	Experiment 2	Experiment 3	Experiment 4
Voluven 130/0.04 (6%)	500	500	500	500
Potassium iodide (5%)	30	40	50	0
Magnesium Sulphate (1M)	30	30	30	0
Water	40	30	20	100
Total volume in mL	600	600	600	600

B

	Voluven 130/0.04: 6% HES (60g/L) in 0.9% NaCl solution (9g/L)	5% Potassium iodide	1M Magnesium Sulphate
Formula Weight	130.00g/mol HES; 58.44g/mol NaCl	166.00g/mol KI	120.37g/mol $MgSO_4$
Volume	1000mL	100mL	100mL
Mass	60g HES; 9g NaCl	5g	12.037g

1.5.3 Precipitation method 2: Colloidal Iron and electrolytes

Differing quantities of 0.2M K_2SO_4, colloidal iron and water were added to a three of a series of four tubes, containing 500μL of 6% HES solution (Voluven) and 1000μL of water was added to the fourth

tube, as a control sample (see Table 2). Then after five minutes, either 125μL or 250μL of 0.2M K_2SO_4 was added to the three non-control samples and the samples were left to stand for five minutes.

Table 2 Starch precipitation experiments using colloidal iron and potassium sulphate (A) and composition of the solutions (B).

A

Composition (volume in mL)	Experiment 1	Experiment 2	Experiment 3	Experiment 4
Voluven 130/0.04 (6%)	500	500	500	500
Colloidal Iron (5% Iron (III) chloride)	500	500	750	0
Potassium sulphate (0.2M)	125	250	250	0
Water	375	250	0	1000
Total volume in mL	1500	1500	1500	1500

B

	Voluven 130/0.04: 6% HES (60g/L) in 0.9% NaCl solution (9g/L)	5% Iron (III) chloride ($FeCl_3$)	0.2M Potassium sulphate (K_2SO_4)
Formula Weight	130.00g/mol HES; 58.44g/mol NaCl	162.2g/mol	174.221g/mol
Volume	1000mL	1000mL x 2	1000mL
Mass	60g HES; 9g NaCl	50g/L	34.84g

1.5.3.1 Preparation for NMR analysis

All four samples were then transferred to separate Eppendorf tubes and centrifuged for 10 min at 10,000 g (13, 000 rpm). Two hundred and fifty μL of the supernatant of each sample was then mixed with 400mμL of phosphate buffer, (pH 7.4 and consisting of 28.85 g Na_2HPO_4, 5.25 g NaH_2PO_4, 1 mM TMSP-d_4 (0.179g) and 3 mM NaN_3(0.195g) in 1L D_2O). The samples were then centrifuged for 10 minutes at 10,000 g (13, 000 rpm) and 600μL of the resulting supernatant was placed into 5mm NMR tubes.

1.5.3.2 NMR analysis of the colloidal iron and electrolyte precipitation experiment samples

^{1}H NMR spectra were acquired using the methodology described in Section 2.2.5.

1.5.4 Ultrafiltration method

In the absence of guidance on the molecular weight cut off of filters for polysaccharides, the filter choice was based on the guidance for proteins. These recommended the use of a filter with a MW cut off of three to six times smaller than the MW of the solutes that will form the retainate. The maximum MW of the intended retainate HES is 150 KDa; a filter with a MW cut off of 3kDa was therefore chosen.

Three types of centrifugal tube filter devices were tested: Centriprep, Nasosep and Amicon Ultra-0.5. Each device consists of a sample collector containing the filter membrane and a filtrate collector. In all three sets of experiments four types of samples were tested: urine containing HES (either urine spiked with HES or from a patient given HES), urine without HES, filter rinse fluid (deionised water) and HES solution (Voluven).

The Centriprep device was tested first. This device requires a minimum sample volume of 750µl; whereas the other two are micro-centrifuge devices designed for 500µl samples. To conserve sample volume, urine from a healthy control spiked with HES was used instead of urine from a patient given HES and prior to be filtered by the Centriprep device, 500µl of each sample were brought up to volume of 750 µl using water. Samples were filtered by inserting the collector of the filter device inside the filtrate collector (i.e. centrifuge tube) and adding 500µl (Nasosep; Amicon) or 750µl (Centriprep) of the sample and centrifuging the device. The retainate was recovered by placing the collector upside down in a second centrifuge tube and spinning it again for two minutes. The filtrates and retainates from the samples and rinse cycles were then labelled accordingly. The filters were pre-rinsed using a rinsing solvent in place of the sample. In the Centriprep device experiments, the use of aqueous MEOH to pre-rinse the filters compared with deionised water alone; whereas, in the other two sets of experiments, a series of ten rinse cycles were performed using 500 µl per cycle of deionised water alone. In view of the unwanted modifications in the Centriprep device experiments, only a small number of experiments were performed using this device: as a proof of principle. This was followed

by a comprehensive set of experiments with each of the other two devices using undiluted samples and urine taken from a patient given HES (as opposed to urine spiked with HES solution used in the Centriprep device experiments). Moreover, triplicates of all samples were analysed and the optimal number of rinsing cycles to remove contaminants was also determined.

1.5.4.1 Preparation for NMR analysis

In each case, both filtered and unfiltered and all sample types, 400µl of each sample was mixed with 250µl of 0.2M urine phosphate buffer (pH =7.4 and consisting of 28.85 g Na_2HPO_4, 5.25 g NaH_2PO_4, 1 mM TMSP-d_4 (0.179g) and 3 mM NaN_3(0.195g) in 1L D2O: H2O, v/v 1:4), and centrifuged for 10 min at 10,000 g (13, 000 rpm). A total of 600 µl of the resulting supernatant was then placed into 5mm NMR tubes.

1.5.4.2 NMR analysis of the filtration experiment samples

^{1}H NMR spectra were acquired and processed using the methodology described in Sections 2.2.5 and 2.5, respectively.

1.5.4.3 Comparison of filtered and unfiltered samples

The removal of HES from samples of the HES solution and urine containing HES (urine spiked with HES or from a patient given HES), were assessed by comparing the ^{1}H NMR spectra of filtered and unfiltered samples. The ^{1}H NMR spectra of filtered and unfiltered samples were also compared to investigate the effect of filtration on metabolites not related to HES. This included both samples with and without HES present.

1.6 Results

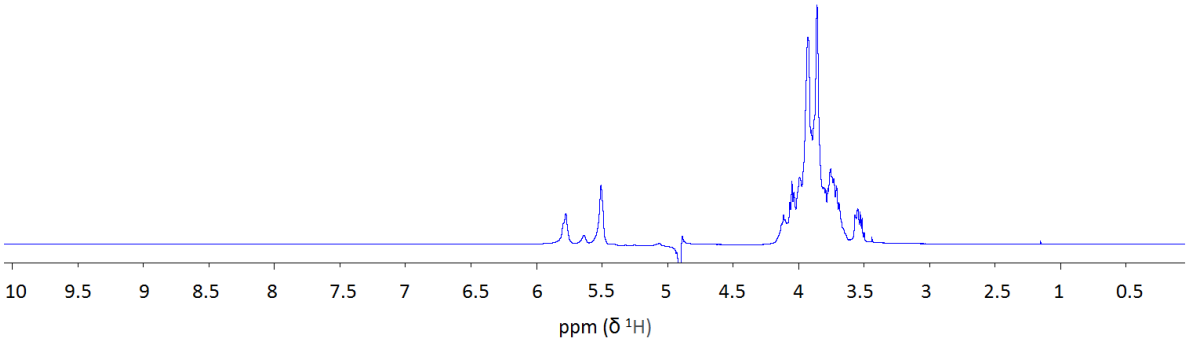
1.6.1 Precipitation method 1: Iodine and electrolytes

Despite, varying the quantities of the iodine, potassium iodine and magnesium sulphate, their addition to HES solution did not result in visible precipitant or blue colour that occurs with the formation of starch-iodine complexes.

1.6.2 Precipitation method 2: Colloidal iron and electrolytes

The supernatants of samples from the iron precipitation experiments were analysed using ^{1}H-NMR spectroscopy. Resonances of HES were identified in the ^{1}H-NMR spectra of the supernatants of samples of HES solution and urine spiked with HES, treated with colloidal iron and magnesium sulphate, (see Figure 1).

A



B

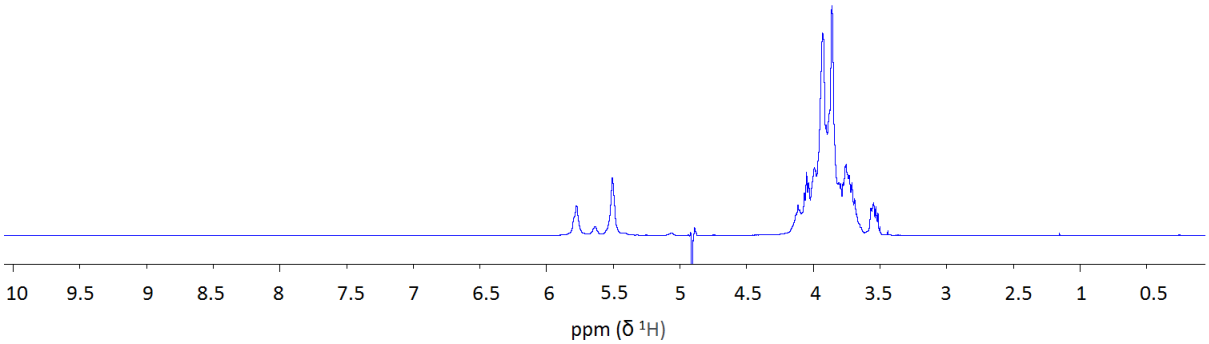


Figure 1 Illustration of HES signals in the ^{1}H NMR spectra of a sample of HES solution treated with colloidal iron and potassium sulphate (A), and an untreated control sample of HES solution (B).

1.6.3 Ultrafiltration experiments

A summary of the NMR analyses of samples from the filtration experiments are shown in Table 3. This demonstrates the effect of filtration on the metabolites identified and the main differences between the three different filter devices. Examples of NMR arrays of filtered and unfiltered samples from the experiments testing the Centriprep, Nasosep and Amicon devices are shown are Figures 2 and 3; 4; and 5 and 6, respectively.

Table 3 Characteristics of the filter device and the running order and results of the filtration experiments.

Filter device name	Filter membrane composition	Size	Removal of HES and its metabolites	Optimal rinsing protocol (glycerol removal)	Loss of non-HES metabolites as a consequence of filtration	Conclusion
1.Centriprep	regenerated cellulose	2ml	Successful	Not tested	Nil identified	Impractical size
2. Nasosep	polyethersulfone polymer	0.5ml	Unsuccessful	4 x 5 minutes and 1 x 10 minutes	No assessed	Unsuccessful at HES removal
3.Amicon Ultra-0.5	regenerated cellulose	0.5ml	Successful	4 x 5 minutes and 1 x 10 minutes	Nil identified	Successful but increased sample preparation time by 30 minutes.

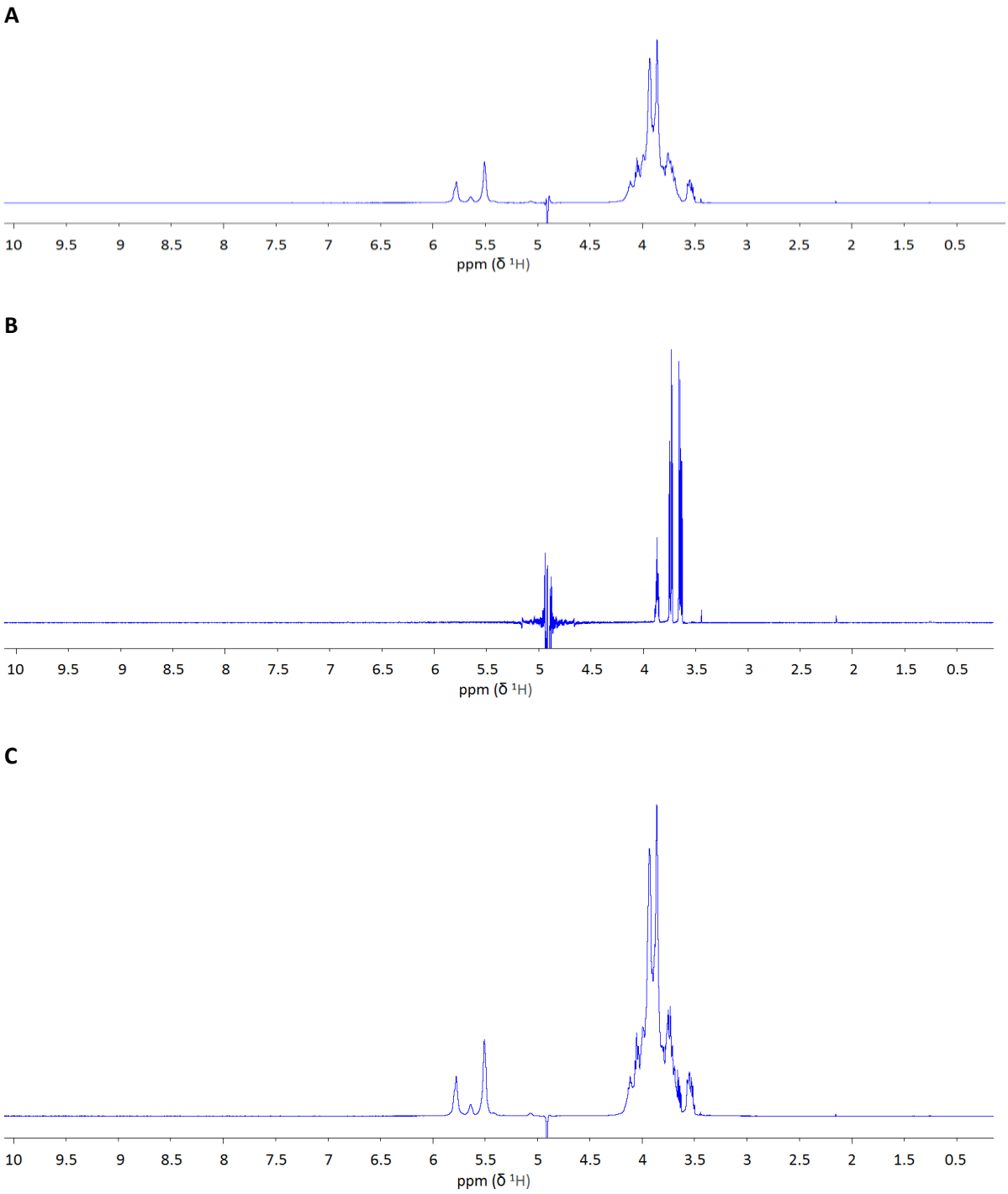


Figure 2 ^{1}H NMR spectra of a sample of unfiltered HES solution (A) and the filtrate (B) and retainate (C) of a sample of HES solution filtered with the Centriprep filter device. Resonances of HES demonstrated in the spectra of the sample of unfiltered HES solution (A) and the retainate of the filtered HES solution(C) but they are not seen in spectra of the filtrate of the filtered sample (B).

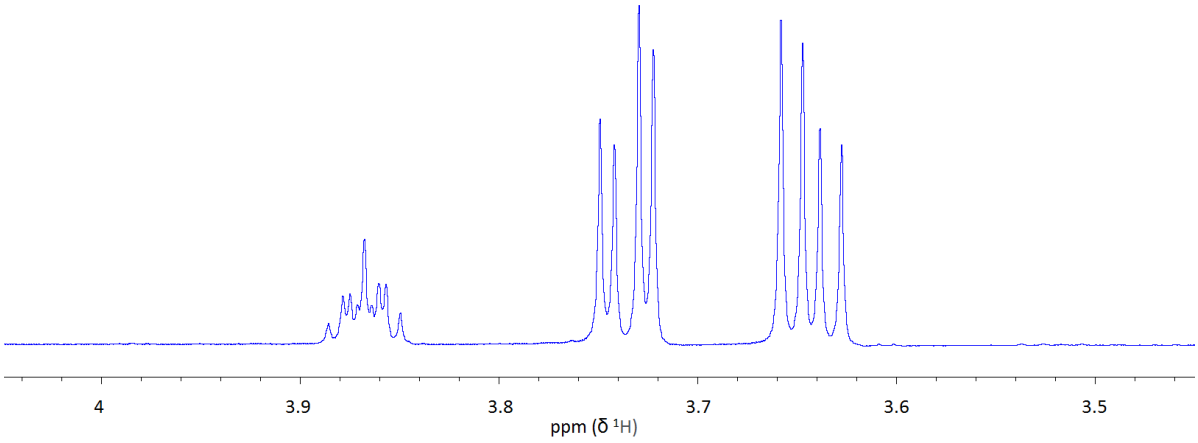
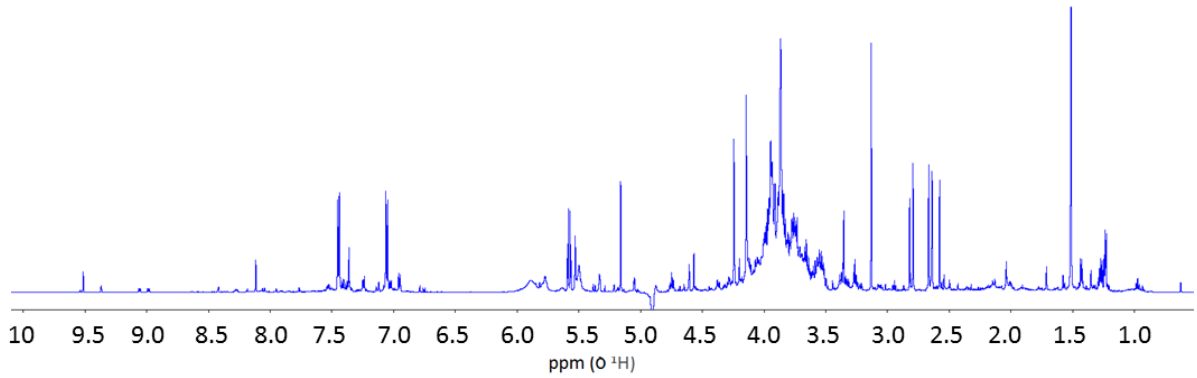


Figure 3 ^{1}H-NMR spectra of the filtrate of the filtered sample of HES solution (same sample as shown in Figure 2B): region between 4-3.5 ppm, illustrating the addition of resonances of glycerol after filtration with the Centriprep device

A



B

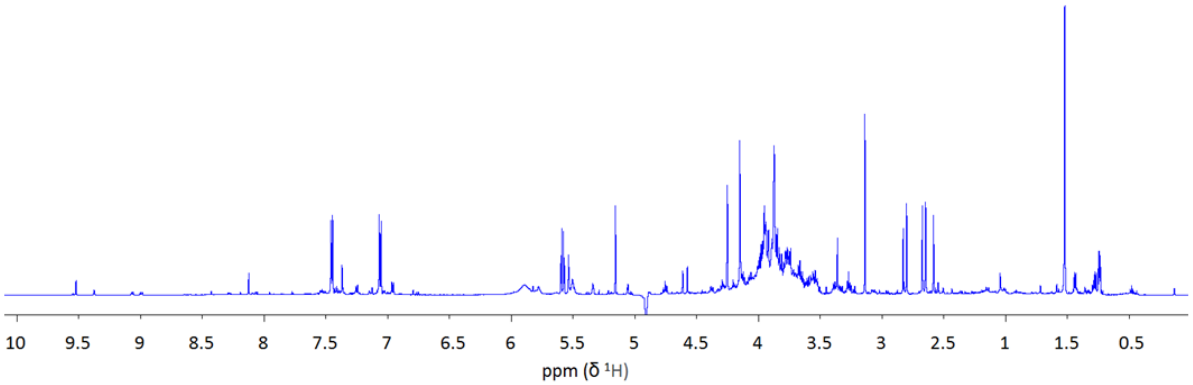
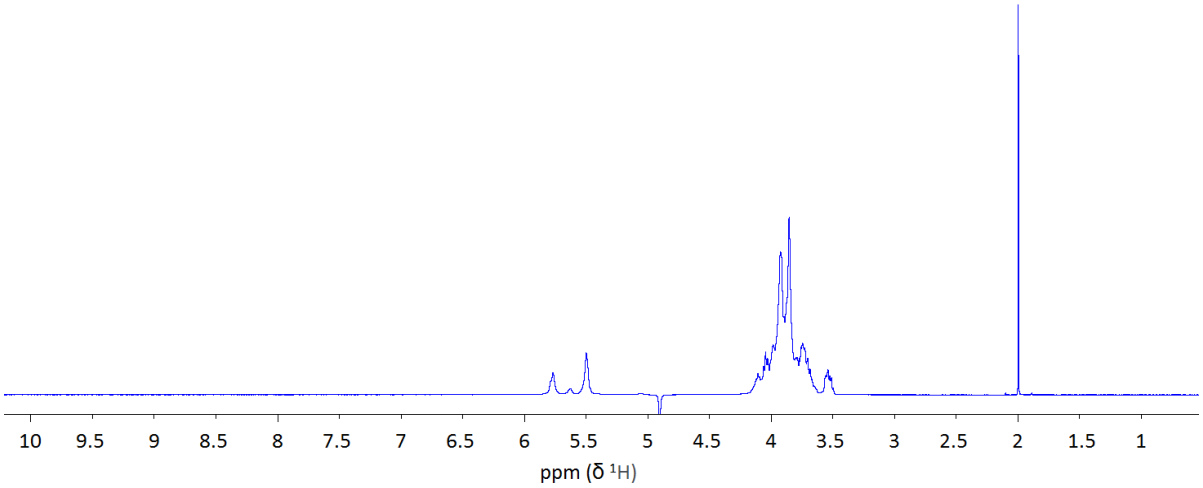


Figure 4 ^{1}H NMR spectra of samples of urine taken from a patient given HES solution before (A) and after (B) filtration with the Nasosep filter device. Resonances of the HES are illustrated in both samples.

A



B

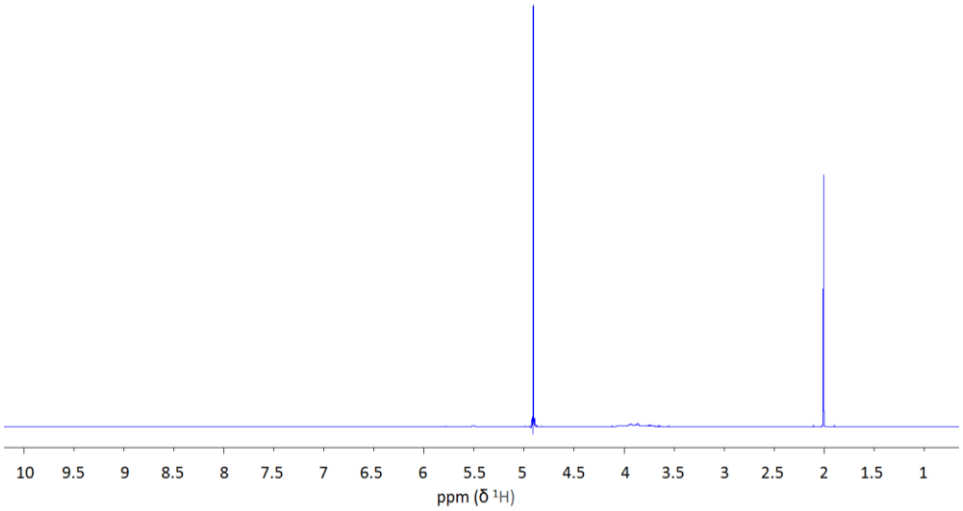


Figure 5 ^{1}H NMR spectra of samples of HES solution before (A) and after (B) filtration with the Amicon filter device. Resonances of the HES are illustrated in the spectra of the unfiltered sample but not in the spectra of the filtered sample.

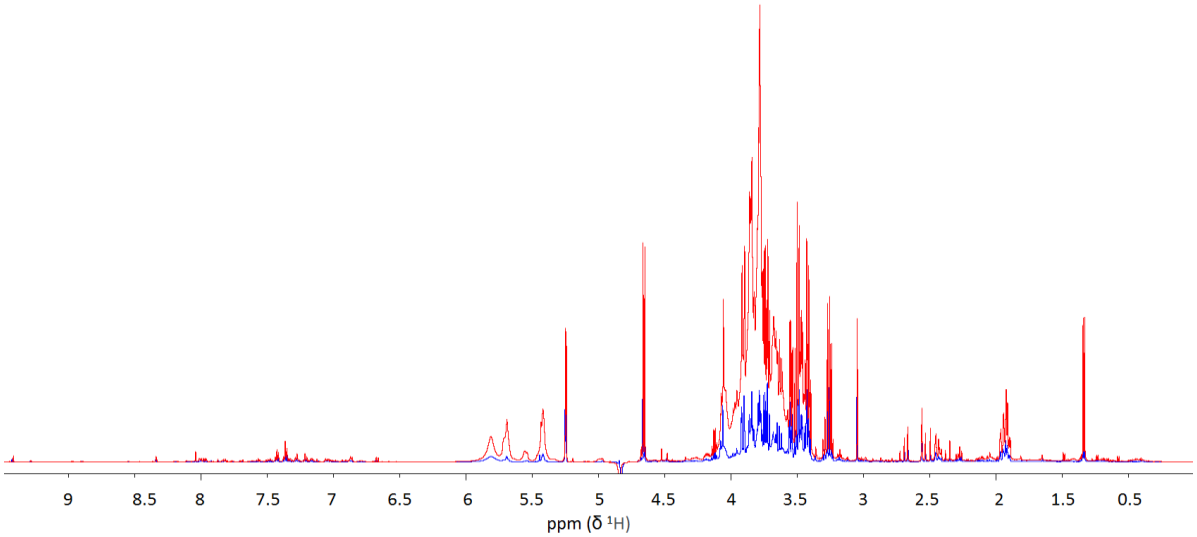


Figure 6 ^{1}H NMR spectra of samples of urine taken from a patient given HES solution before (A) and after (B) filtration with pre-rinsed Amicon filter device illustrating improved resolution of the resonances of urinary metabolites of the filtered sample in region between 4.2-3.4 ppm and the absence of glycerol.

1.6.4 Hydroxyethyl starch removal

1.6.4.1 Centriprep device

Comparisons of filtered and unfiltered samples of both HES solution (see Figure 2) and urine spiked with HES from the first set of experiments were consisted with the successful removal of HES by the Centriprep device. A comprehensive review of the ^{1}H NMR spectra of filtered samples and their unfiltered controls did not identify the loss of any metabolites, as a consequence of the filtration. It did however; demonstrate the addition of glycerol as illustrated in Figure 3.

1.6.4.2 Nasosep device

Resonances of HES and its metabolites were demonstrated in the NMR spectra of HES-containing samples filtered with the Nasosep device. This included a sample of the HES solution and urine from a patient given HES solution (see Figure 4) and confirmed the failure of the Nasosep device to remove HES and its metabolites from these samples.

1.6.4.3 Amicon

Resonances of HES and its metabolites were not identified in the NMR spectra of HES containing samples filtered with the Amicon device confirming their successful removal (see Figure 5). No loss of metabolites was demonstrated with the use of the Amicon device but the addition of glycerine was noted.

1.6.5 Pre-rinsing of the filters

The use of solvents to pre-rinse the filters was also compared. In the Centriprep experiments, two rinsing steps with a MEOH/water (1:1) mixture resulted in similar quantities of glycerol in the filtered samples as two rinses with deionised water alone.

The repeat experiments with the Nasosep and Amicon filters included a series of ten rinsing cycles of the filters with deionised water, to investigate the removal of the filter preservative glycerol. After five pre-rinses, (four lasting five minutes and one lasting 10 minutes), the use of the filters was no longer associated with the addition of glycerol, as illustrated in Figure 6.

In summary, neither of the precipitation methods led to precipitation of HES, whereas, two of the filter devices removed both HES, and its metabolites, from the samples. Use of filters did not appear to cause the loss of any other metabolites but they needed to be pre-rinsed five times, to prevent the addition of glycerol.

The most obvious explanation for the failure of the precipitation of HES demonstrate

The starch precipitation methods used in this study have been successfully applied to non-modified starches. The structural modifications of HES is therefore the most likely explanation for the failure of these methods to precipitate the HES, demonstrated in this study.

The most likely explanation for the failure seen with Nasosep device, despite the success of the first device (Centriprep), is the composition of its filter membrane. In the Centriprep device, it is composed of regenerated cellulose, whereas, in the Nasosep device, it is made from a modified polyethersulfone

polymer. The membrane of the Amicon filters is also composed of regenerated cellulose; the success seen with both of these filters, therefore supports this theory.

Damage caused by pre-rinsing could also have been responsible for the failure of the Nasosep device. This theory was investigated by repeating the experiments with the use un-rinsed filters; however, despite omitting the rinsing, the Nasosept device still failed to filter out the HES.

Overall, the Amicon filters are most suited to this application. Their size is compatible with the micro-centrifuges used in the preparation of NMR samples, (unlike the Centriprep device) and their glycerol preservative is removable. The main disadvantage is the extra preparation time pre-rinsing requires.

1.7 References

Mellanby, J. (1919) The Composition of Starch. Part I. Precipitation by Colloidal Iron. Part II. Precipitation by Iodine and Electrolytes. *Biochem J*. 13 (1), 28–36.

Appendix II

Table 1 List of the drugs in the 1-D ^{1}H NMR drug standards database, their preparation, and their signal multiplicities. Key: s: singlet; d: doublet; t: triplet; q: quartet; quint: quintet; sext: sextet; sept: septet; o: octet; n: nonet; undec: undectet; duodec: duodectet; m: multiplet; ; bs: broad signal; dd: doublet of doublets; dt: doublet of triplets; dq: doublet of quartets; dquint: doublet of quintets; td: triplet of doublets; ; qt: quartet of doublets; ddd: doublet of doublet of doublets; dddd: doublet of doublet of doublet of doublets; drug: pharmaceutical agents including intravenous fluids.

Drug	Preparation	δ ^{1}H (multiplicity)											
Actrapid Human Insulin	solution	7.22 t	6.84 dt	6.79 s	6.74 dd	3.91 m	3.79 m	3.66 dd	3.57 q	3.53 dd	3.44 q	2.30 s	
Adenosine	solution	8.35 s	8.25 s	6.08 d	4.44 m	4.30 q	3.92 dd	3.85 dd	2.24 s	1.93 s	1.49 s	1.37 s	1.33 s
		1.31 s	1.30 s	1.19 d	1.10 s	1.05 s	1.01 s	0.89 s	0.17 s				
Adrenaline	solution	7.01 d	6.96 m	6.91 dd	6.88 dd	4.34 s	3.79 q	3.64 dd	3.28 m	3.26 s	2.77 s	2.75 s	
Alfacalcidol (vitamin D_{3})	solution	7.92 d	6.93 dt	5.23 t	5.20 m	5.17 m	5.13 m	5.10 bs	5.03 bs	4.95 d	4.65 d	4.50 d	4.34 t
		4.28 d	4.23 s	4.20 bs	3.99 s	3.95 m	3.73 m	2.60 dd	1.29 t	1.19 t	1.08 t	0.90 bs	0.90 bs
Alpha-tocopherol (vitamin E)	solution	7.88 d	7.56 t	7.49 t	6.99 dd	6.27 m	6.15 sext	5.82 d	5.56 d	5.31 m	5.27 d	5.09 d	4.84 s
		4.65 d	4.23 d	4.12 d	4.06 t	4.01 d	3.94 m	3.89 m	3.81 m	3.69 m	3.61 s	3.59 s	3.56 q
		3.53 d	3.51 s	3.48 m	3.41 m	3.25 t	1.99 bs	1.92 s	1.82 d	1.59 s	2.00 s	1.85 s	1.82 s
		1.44 s	1.23 bs	1.15 d	1.07 s	0.80 s							
Ambisone	powder	5.42 d	4.23 d	4.06 t	3.90 m	3.83 m	3.77 t	3.69 s	3.57 dd	3.48 t	2.41 s		
Aminophylline	solution	8.00 s	7.83 s	7.65 s	3.70 m	3.67 d	3.66 bs	3.57 s	3.46 s	3.41 s	3.36 s	0.34 t	3.29 s
		3.17 s	3.11 t	3.05 t	2.99 d	2.86 d	2.76 s	2.69 m	2.62 s	1.94	1.20 t		
Amiodarone	tablet	5.45 s	5.24 d	4.68 d	4.47 d	3.96 m	3.91 d	3.89 d	3.87 dt	3.86 s	3.84 s	3.82 dd	3.78 m
		3.74 m	3.64 s	3.61 m	3.59 d	3.56 m	3.75 t						
Amlodipine	tablet	7.82 d	7.59 dt	7.50 d	7.38 d	7.29 t	7.21 d	5.36 s	4.10 m	3.95 d			
Aspirin	tablet	7.83 d	7.69 d	7.64 d	7.51 t	7.47 t	7.37 t	7.28 dd	7.23 t	7.15 d	7.01 d	6.97 q	7.02 d
		4.68 d	4.46 d	3.76 m	3.30 t	2.68 d	2.55 d	2.34 s	1.14 d				
Atorvastatin	tablet	8.46 s	7.34 bs	7.17 m	5.24 d	4.68 d	4.46 d	3.96 m	3.91 d	3.89 d	3.87 d	3.85 d	3.82 d
		3.80 d	3.78 m	3.74 m	3.71 s	3.68 m	3.65 s	3.61 m	3.59 d	3.56 m	3.42 bs	3.30 t	2.28 m
		1.92 s	1.44 d	1.17 s									
Atracurium	solution	7.82 d	7.59 dt	6.96 m	6.80 dd	6.73 m	6.65 dd	6.57 d	6.44 d	6.40 dd	6.37 m	6.31 m	6.22 m
		6.16 m	6.12 s	5.95 m	5.88 s	5.70 m	5.60 m	4.54 q	4.24 m	4.15 m	3.98 m	3.83 m	3.68 s
		3.58 m	3.47 dd	3.43 s	3.41 s	3.40 bs	3.38 bs	3.34 m	3.22 m	3.09 d	2.95 m	1.76 m	1.54 m
		1.25 m	1.00 t										
Benzyl penicillin	powder	7.42 t	7.35 dd	5.52 d	5.44 d	5.07 d	4.60 d	4.56 s	4.36 s	4.24 s	3.80 m	3.75 s	3.68 q
		3.61 d	3.58 s	3.56 s	3.53 s	3.50 s	3.43 m	3.40 m	3.31 s	2.08 s	1.93 s	1.67 s	1.53 ss
		1.39 s	1.23 d	1.18 m	1.04 s	1.02 s	1.01 s	0.91 t	0.87 dt				
Bisoprolol	tablet	7.40 d	7.05 d	6.52 s	4.55 s	4.35 sext	4.15 dddd	3.95 s	3.73 quint	3.67 s	3.73 quint	3.33 dd	3.27 s
		3.25 d	3.23 s	3.20 s	1.37 dd	1.20 s	1.19 s	1.17 d					
Bupivacaine	solution	7.27 t	7.23 d	4.13 dd	3.85 s	3.71 d	3.15 n	3.08 dd	2.42 d	2.21 s	1.99 m	1.76 m	1.40 sext
		0.93 t											
Calcium Gluconate (10%)	solution	4.09 d	3.74 m										
Carbocisteine	tablet	7.95 d	6.96 d	5.41 d	4.22 dd	4.05 t	3.84 m	3.67 m	3.56 dd	3.48 t	3.35 s	3.32 d	3.29 s
		3.16 dd	3.05 q	1.18									

Table 1 continued

Carbocisteine	solution	7.95 d	6.96 d	5.41 d	5.24 d	4.65 d	4.34 d	4.22 d	4.05 t	3.93 d	3.90 m	3.83 m	3.79 s
		3.77 t	3.70 s	3.68 s	3.66 d	3.64 s	3.56 dd	3.48 t	3.35 s	3.32 d	3.29 s	3.27 s	3.26 s
		3.25 d	3.22 s	3.20 d	3.16 dd	3.05 q	2.95 dq	2.60 dd	2.15 t	2.09 s	1.92 s	1.49 dq	1.25 t
		1.19 t	0.89 td										
Cefotaxime	powder	7.02 s	5.83 d	5.23 d	4.90 d	4.74 d	4.12 m	4.02 d	3.96 s	3.88 s	3.69 d	3.42 d	3.36 s
		2.23 d	2.11 s	2.00 s	1.93 s	1.82 s	1.51 s	1.37 s	1.30 m	1.18 m	1.10 t		
Ceftazidime	powder	8.97 d	8.58 t	8.09 t	6.94 s	5.87 d	5.60 d	5.35 d	5.30 d	3.65 d	3.22 d	1.48 d	
Ceftriaxone	solution	7.02 s	5.80 d	5.21 d	4.37 d	4.07 d	4.00 s	3.87 s	3.75 d	3.72 s	3.63 s	3.49 d	3.14 d
		2.92 dd	2.57 s	1.29 d	1.27 s								
Chlorpheniramine	solution	8.47 d	7.84 td	7.46 d	7.40 d	7.35 m	6.02 s	4.25 t	3.06 tt	2.85 s	2.63 m	2.53 m	1.18 d
Ciprofloxacin	solution	6.93 s	6.75 m	5.28 m	4.83 s	4.28 s	4.08 bs	3.79 m	3.66 dd	3.56 q	3.25 bs	2.75 bs	2.23 bs
		2.02 bs	1.56 bs	1.25 m	0.87 bs								
Clonidine	solution	7.56 d	7.40 t	3.78 s									
Clopidogrel	tablet	8.81 s	8.55 s	8.46 s	7.77 dd	7.68 d	7.53 m	7.39 d	7.35 d	7.33 s	7.25	6.75 t	6.61 s
		3.71 s	3.65 t	3.38 m	1.92 s	1.33 d	1.17 bs	1.15 d					
Co-amoxiclav (amoxicillin/clavulanic acid)	powder	8.49 s	8.47 s	8.40 s	8.30 s	8.22 s	7.96 dd	7.81 d	7.82 m	7.55 m	7.44 d	7.40 m	7.35 m
		7.31 d	7.29 s	7.27 d	7.25 s	7.18 d	7.06 d	6.95 m	6.93 s	6.92 d	6.91 s	6.90 s	6.89 s
		6.79 m	6.72 t	5.91 d	5.70 d	5.63 d	5.59 m	5.55 m	5.52 d	5.47 dd	5.41 d	5.38 s	5.36 s
		5.33 t	5.28 m	5.12 dd	5.06 m	4.95 d	4.91 m	4.84 s	4.82 s	4.74 s	4.71 s	4.69 s	4.62 s
		4.60 s	4.56 m	4.53 t	4.47 td	4.39 m	4.35 t	4.29 m	4.23 s	4.19 s	4.13 dd	4.06 s	4.01 d
		3.95 m	3.94 q	3.86 m	3.84 d	3.81 t	3.79 s	3.78 d	3.76 m	3.74 m	3.73 m	3.71 m	3.69 s
		3.68 s	3.67 d	3.66 s	3.64 s	3.62 dt	3.59 s	3.57 s	3.57 s	3.54 d	3.50 s	3.49 s	3.47 s
		3.46 s	3.41 t	3.36 s	3.33 s	3.30 s	3.28 s	3.21 s	3.18 t	3.08 s	3.06 tt	2.96 q	2.88 q
		2.83 t	2.80 s	2.62 d	2.56 m	2.45 t	2.42 s	2.35 d	2.31 s	2.35 s	2.21 s	2.15 s	2.12 m
		2.08 s	2.07 s	2.01 s	1.93 s	1.90 s	1.88 m	1.85 s	1.80 s	1.74 s	1.69 s	1.67 s	1.63 s
		1.61 d	1.59 s	1.57 s	1.55 s	1.52 s	1.51 s	1.48 s	1.47 d	1.41 s	1.40 s	1.38 s	1.34 d
		1.29 s	1.26 q	1.23 s	1.18 m	1.12 d	1.11 s	1.08 s	1.07 s	1.00 s	0.95 s	0.94 s	0.93 s
		0.90 s	0.87 sext	0.77 s	0.76 s	0.68 d	0.63 s	0.60 s	0.45 s	0.41 s	0.17 s	0.10 s	0.08 s
Codeine Phosphate	solution	6.94 d	6.80 d	5.76 d	5.42 d	5.24 d	5.10 d	4.83 s	4.68 d	4.47 d	4.41 sext	4.18 q	3.96 m
		3.91 d	3.89 d	3.87 d	3.86 d	3.85 s	3.83 d	3.81 d	3.78 m	3.74 m	3.68 m	3.65 s	3.64 s
		3.62 dd	3.61 d	3.56 dq	3.39 t	3.47 dt	3.31 m	3.10 bs	2.99 s	2.42 t	2.12 d		
Colomycin	powder	8.46 m	7.54 m	6.89 m	6.05 d	5.42 m	5.21 m	5.01 d	4.34 m	3.87 m	3.16 m	2.76 m	2.51 m
		2.10 m	1.63 m	1.27 m	0.90 m								
Co-trimoxazole (trimethoprim and sulfamethoxazole)	solution	7.61 d	7.57 s	6.80 d	6.54 s	5.72 s	3.88 quintd	3.78 s	3.66 q	3.54 dd	3.45 q	2.17 s	1.19 t
		1.15 d											
Cyclizine	solution	7.51 d	7.39 t	7.31 t	5.89 s	4.46 s	4.25 q	4.13 q	4.00 q	3.34 t	3.22 bs	3.03 bs	2.85 s
		2.58 s	1.94 s	1.46 m	1.34 d	1.24 d							
Cyclizine	tablet	7.55 d	7.41 t	7.32 t	5.24 d	4.68 d	4.47 d	4.52 s	4.46 d	3.96 m	3.91 d	3.89 d	3.87 d
		3.86 d	3.85 s	3.83 d	3.81 d	3.78 m	3.74 m	3.68 m	3.65 s	3.64 s	3.62 dd	3.61 d	3.56 dq
		3.30 t	2.84 s	1.27 s									

Table 1 continued

DaliVit: Palmitate, ascorbic acid, ergocalciferol,	solution	8.94 d	8.71 dd	8.47 s	8.25 m	8.20 s	8.04 m	7.89 d	7.81 s	7.73 m	7.67 s	7.60 m	7.46 m
nicotinamide, pyridoxine, riboflavin and thiamine		6.92 d	6.60 quint	6.39 s	6.08 m	5.57 dd	5.42 d	5.32 s	5.28 d	5.25 m	5.20 s	5.02 d	4.74 s
(vitamins A, C, D_2, B_3, B_6, B_2, and B_1, respectively)		4.71 s	4.65 m	4.60 s	4.57 m	4.55 s	4.53 d	4.48 m	4.37 m	4.31 s	4.29 s	4.23 d	4.18 s
		4.04 m	3.96 s	3.91 td	3.75 m	3.58 dd	3.49 t	3.42 m	3.35 m	3.27 dd	3.18 t	3.02 t	2.56 s
		2.45 m	2.36 s	2.30 bs	2.20 bs	2.02 s	1.87 m	1.57 m	1.29 m	1.02 s	0.89 s		
Dexamethasone	solution	7.56 d	6.39 d	6.23 s	4.82 s	4.80 d	4.56 d	4.42 d	3.79 m	3.66 dd	3.56 q	3.53 d	3.44 q
		3.23 s	3.15 s	3.12 s	3.06 m	2.74 td	2.54 m	2.21 d	2.12 dt	1.98 m	1.92 s	1.83 q	1.68 d
		1.56 s	1.48 qd	1.22 sept	1.19 t	1.00 s	0.89 d						
Diazepam	solution	5.32 bs	5.21 s	4.17 d	3.79 tt	3.66 dd	3.56 q	2.76 s	2.25 s	2.05 s	1.97 s	1.92 s	1.59 s
		0.88 s											
Digoxin	solution	3.87 m	3.65 q	3.53 dd	3.44 q	1.18 t	1.14 d						
Dipeptivan: *N* (2)-*L* -alanyl-*L* -glutamine	solution	7.62 s	6.89 s	4.18 dd	4.10 q	2.35 t	2.14 sext	1.98 sext	1.66 d	1.51 d	1.49 d	1.45 m	1.48 s
		1.42 s	1.39 d	1.36 d	1.04 m								
Dobutamine	solution	7.15 d	6.88 t	6.83 d	6.68 dd	3.95 bs	3.89 m	3.83 m	3.81 s	3.78 bs	3.76 bs	3.77 s	3.71 bs
		3.68 m	3.56 dd	3.45 q	3.21 m	2.83 td	2.70 sept	2.53 quint	1.99 n	1.80 n	1.33 d	1.15 d	
Dopamine	solution	7.41 s	7.13 s	7.05 d	7.00 s	6.92 d	6.87 d	6.82 s	6.81 s	6.76 dd	6.61 q	6.54 m	6.46 s
		6.09 s	5.44 q	3.35 t	3.20 t	3.11 t	2.99 t	2.88 t	2.77 t	2.71 s	2.50 q	1.93 s	1.33 t
		1.19 t	0.18 s										
Dopexamine	solution	7.40 dt	6.91 d	6.87 d	6.76 dd	4.09 t	3.66 q	3.63 s	3.44 t	3.29 dt	3.03 sext	2.91 t	1.66 d
		1.35 t	1.19 t										
Doxazocin	tablet	5.24 d	4.68 d	4.46 d	3.96 m	3.91 d	3.89 d	3.87 d	3.86 d	3.85 s	3.83 d	3.81 d	3.78 m
		3.74 m	3.68 m	3.65 s	3.64 s	3.62 dd	3.61 d	3.56 dq	3.30 t	2.82 s			
Enoxaparin	solution	7.51 m	7.41 m	7.34 m	5.99 d	5.59 bs	5.51 s	5.46 dd	5.41 s	5.31 bs	5.23 s	5.02 s	4.67 t
		4.61 m	4.54 d	4.51 d	4.48 d	4.04 m	3.61 s	3.55 sext	3.42 bs	3.28 d	2.05 s	1.92 s	1.82 s
		1.19 t	1.15 d										
Ephedrine	solution	7.49 m	7.44 m	5.17 d	3.56 sept	2.79 s	1.15 d						
Erythromycin	solution	5.09 dd	4.94 d	4.81 s	4.62 d	4.57 m	4.18 dd	4.12 m	3.98 m	3.78 m	3.78 m	3.52 m	3.32 m
		3.24 d	3.07 quint	2.87 m	2.76 bs	2.50 m	2.27 t	2.14 m	2.04 quint	1.95 m	1.84 m	1.70 m	1.58 s
		1.42 d	1.26 m	1.11 m	1.06 s	1.02 d	0.87 m	0.81 t					
Etomidate	powder	3.88 tdd	3.54 dd	3.44 q	1.14 d								
Ezetimibe	tablet	8.46 s	7.39 s	7.28 d	7.05 s	6.96 d	5.24 d	4.68 d	4.60 d	4.54 d	4.46 d	4.32 d	4.08 d
		4.02 t	3.96 m	3.91 d	3.89 d	3.87 d	3.86 d	3.85 s	3.83 d	3.81 d	3.78 m	3.74 m	3.68 m
		3.65 s	3.64 s	3.62 dd	3.61 d	3.56 dq	3.39 t	2.47 bs	2.30 bs	2.05 bs	1.71 bs	1.31 s	0.92 t
Flucloxacillin	powder	7.59 dt	7.47 d	7.31 t	5.60 d	5.51 d	4.16 s	3.69 s	2.80 m	2.75 s	2.74 s	2.70 s	2.59 s
		2.23 s	2.10 s	1.59 m	1.54 s	1.42 d	1.43 s	1.37 d	1.23 d	1.13 s	1.00 t		
Fluconazole	solution	8.07 s	4.52 t	3.93 t	2.68 s	2.65 s	2.62 s	2.55 s	2.52 s	2.41 s			
Folic Acid	solution	9.92 s	9.04 s	8.83 s	8.62 s	8.16 d	8.06 d	7.67 d	7.58 d	6.85 d	6.56 d	6.14 s	4.37 s
		4.33 s	4.31 q	3.54 dd	3.45 q	2.54 s	2.33 m	2.17 m	2.04 sext	1.19 t	1.11 d		
Frusemide	solution	8.37 s	7.48 s	7.01 s	6.43 m	6.37 s	4.50 s						

Table 1 continued

Gelofusine	solution	8.46 s	8.17 bs	7.31 m	7.09 m	6.98 s	6.83 d	4.39 bs	3.94 bs	3.65 s	3.57 s	3.22 s	3.00 s
		2.82 bs	2.78 s	2.68 bs	2.55 bs	2.48 d	2.45 s	2.41 s	1.86 bs	1.23 d	1.20 bs	1.18 d	0.90 bs
Gentamicin	solution	7.58 s	7.96 d	6.97 d	6.01 dd	6.02 d	6.01 s	5.98 d	5.95 dt	5.91 s	5.73 d	5.62 s	5.17 s
		4.34 s	4.28 t	4.24 dd	4.20 m	4.17 m	4.14 m	4.09 d	4.05 d	3.99 q	3.93 t	3.90 s	3.87
		3.86 s	3.82 q	3.79 s	3.78 s	3.78 s	3.76 s	3.74 s	3.72 s	3.70 s	3.66 q	3.62 s	3.60 dd
		3.58 s	3.57 s	3.56 s	3.55 s	3.54 bs	3.53 s	3.51 d	3.45 d	3.41 m	3.38 s	3.35 t	3.24 dd
		3.15 s	3.11 d	3.07 dd	2.93 s	2.87 s	2.85 s	2.80 d	2.75 s	2.74 m	2.63 s	2.61 s	2.58 s
		2.57 s	2.49 m	2.00 m	1.79 sext	1.60 m	1.50 s	1.49 d	1.47 s	1.37 s	1.34 d	1.31 m	1.19 t
		1.08 t	1.01 t										
Gliclazide	tablet	7.82 d	7.71 d	7.47 d	7.38 d	5.42 bs	5.24 d	4.68 d	4.46 d	3.96 m	3.91 d	3.89 d	3.87 d
		3.86 d	3.85 s	3.83 d	3.81 d	3.78 m	3.74 m	3.68 m	3.65 s	3.64 s	3.62 dd	3.61 d	3.56 dq
		3.30 t	3.14 bs	2.56 bs	2.44 s	2.41 s	2.23 t	1.92 s	1.57 m	1.42 bs	1.33 d		
Glyceryl trinitrate	solution	5.83 sept	5.68 bs	5.51 d	5.38 d	5.24 d	5.03 d	5.02 dd	4.89 s	4.86 d		4.65 d	4.52 d
		4.33 m	4.26 d	4.13 bs	4.11 d	4.03 m	4.01 m	3.95 m	3.90 dd	3.84 m	3.75 m	3.54 dd	3.51 d
		3.47 m	3.41 m	3.25 t									
Glycopyrrolate	solution	7.65 d	7.48 t	7.42 t	5.53 bs	3.82 dd	3.77 d	3.58 sext	3.21 s	3.17 quint	3.13 s	2.72 sept	2.15 quint
		1.63 m	1.25 m										
Haloperidol	solution	4.12 q	1.33 d										
Heparin	solution	7.97 s	7.94 d	7.81 d	7.56 m	7.42 m	7.29 m	6.95 d	5.41 bs	5.23 bs	4.81 m	4.66 s	4.56 s
		4.53 s	4.49 m	4.41 bs	4.35 bs	4.28 t	4.22 bs	4.16 bs	4.11 bs	4.04 m	3.89 s	3.71 m	3.41 m
		3.36 bs	2.79 s	2.76 s	2.60 dd	2.44 s	2.42 s	2.07 s	2.05 s	1.93 s	1.78 sext	1.19 t	1.00 t
Human albumin solution (20%)	solution	7.64 bs	2.59 bs	3.67 s	3.60 s	3.27 s	3.24 s	2.78 d	2.77 s	2.08 bs	1.96 s	1.90 m	1.53 d
		1.37 d	1.22 t	1.08 d	1.03 d	1.00 d							
Hydrocortisone	solution	5.73 s	5.08 dd	4.48 s	2.73 m	2.57 m	2.37 m	2.29 m	2.20 m	2.01 m	1.79 m	1.57 quint	1.41 s
		1.12 d	1.04 d	0.84 s									
Hydroxocobalamin (vitamin B_{12})	solution	8.21 t	7.75 bs	7.64 bs	7.29 d	7.19 d	7.17 s	7.04 m	6.95 s	6.89 m	6.83 s	6.57 s	6.46 d
		6.39 d	6.30 d	6.28 dd	6.24 d	6.19 s	4.29 m	4.22 m	4.16 m	4.02 m	3.74 m	3.62 m	3.56 dd
		3.52 d	3.46 td	3.37 s	3.34 d	3.26 m	2.91 m	2.79 m	2.74 d	2.71 m	2.67 m	2.63 d	2.61 d
		2.59 s	2.56 d	2.53 d	2.42 m	2.38 s	2.36 d	2.25 t	2.15 m	2.00 m	1.92 s	1.89 s	1.86 s
		1.57 dd	1.41 m	1.29 s	1.26 d	1.24 s	1.19 s	1.18 s	1.18 s	1.15 d	0.98 m	0.46 m	
Imipenem	solution	8.89 s	7.83 dd	6.58 t	6.46 t	4.82 s	4.31 m	4.22 m	3.91 q	3.59 m	3.42 m	3.36 s	3.14 m
		2.89 m	2.78 undec	2.62 m	2.50 t	2.41 m	2.31 s	2.17 m	2.00 m	1.61 m	1.42 m	1.29 d	1.19 s
		1.14 s	1.09 s	1.01 t	0.87 dd								
Labetalol	solution	7.79 q	7.43 sext	7.39 t	7.30 m	6.98 d	3.36 s	3.43 m	3.14 m	2.83 o	2.66 sext	2.11 duodec	1.91 duodec
		1.40 t											
Lactulose	solution	5.29 d	5.27 d	5.23 d	5.22 d	5.19 s	4.84 s	4.67 d	4.56 m	4.45 m	4.40 d	4.35 s	4.32 d
		4.29 d	4.25 m	4.20 s	4.12 dd	4.15 m	4.02 m	3.93 m	3.76 m	3.30 t	2.98 dd	2.68 s	2.67 s
		2.62 m	2.55 s	2.52 s	2.30 m	2.13 m	2.03 m	1.94 m	1.18 t	1.14 d			

Table 1 continued

Lansoprazole	tablet	7.42 sext	7.35 t	7.30 d	7.22 d	6.95 d	5.24 d	4.68 d	4.47 m	4.29 q	4.26 d	4.24 d	4.23 s
		4.22 s	4.21 s	4.17 q	4.13 q	4.11 q	4.06 dd	4.00 d	3.98 bs	3.95 dd	3.93 s	3.91 s	3.87 dd
		3.81 d	3.77 td	3.71 s	3.69 q	3.65 s	3.64 s	3.64 s	3.61 m	3.59 s	3.59 s	3.58 d	3.57 s
		3.57 s	3.56 sext	3.54 s	3.50 s	3.48 s	3.46 s	3.43 bs	3.39 bs	3.36 s	3.28 m	3.09 m	3.04 d
		3.02 s	2.84 s	2.80 s	2.79 s	2.77 s	2.76 s	2.74 d	2.72 d	2.69 d	2.66 s	2.60 d	2.58 s
		2.56 d	2.53 s	2.17 dd	1.99 s	1.92 s							
Laxido	solution	3.83 m	3.74 t	3.71 s	3.65 t	3.59 m							
Levofloxacin	solution	8.43 s	7.58 d	4.68 bs	4.50 dd	3.41 bs	2.95 s	1.53 d					
Levo-thyroxine	tablet	5.24 d	4.68 d	4.47 d	3.96 m	3.91 d	3.89 d	3.87 d	3.86 d	3.85 s	3.83 d	3.81 d	3.78 m
		3.74 m	3.68 m	3.65 s	3.64 s	3.62 dd	3.61 d	3.56 dq	3.39 t				
Linezolid	solution	7.45 d	7.42 s	7.23 m	5.51 d	5.38 d	5.24 s	5.10 d	4.93 sext	4.83 s	4.65 d	4.52 d	4.33 m
		4.24 t	4.13 m	4.11 d	4.03 q	3.93 t	3.90 dd	3.84 t	3.78 d	3.77 s	3.76 d	3.74 d	3.72 t
		3.71 s	3.62 q	3.54 dd	3.51 s	3.50 s	3.47 m	3.41 sext	3.26 t	3.13 t	2.66 d	2.54 d	2.01 s
Meropenem	solution	5.06 m	4.76 t	4.71 td	4.59 t	4.48 t	4.35 m	4.25 m	4.14 t	4.04 dd	3.95 m	3.62 m	3.45 m
		3.33 m	3.27 dd	3.23 d	3.19 m	3.14 s	3.13 s	3.11 s	3.08 s	2.99 s	2.93 s	2.87 s	2.81 quint
		2.72 s	2.68 m	2.62 q	2.55 m	2.24 s	2.22 t	1.94 m	1.88 t	1.84 m	1.77 quint	1.77 dt	1.61 s
		1.64 m	1.63 s	1.58 s	1.54 d	1.49 d	1.45 m	1.41 d	1.35 d	1.30 d	1.26 d	1.04 d	0.95 d
		0.95 m	0.88 t	0.17 t									
Metaraminol	solution	7.36 t	6.98 d	6.92 m	4.94 d	4.34 s	3.89 ddd	3.80 dd	3.68 ddd	3.55 dd	3.45 q	3.36 s	2.29 d
		1.59 d	1.30 d	1.20 d	1.15 d	1.09 d							
Methylprednisolone	powder	7.53 d	6.32 d	6.00 s	5.06 dd	4.47 s	2.66 bs	2.51 t	2.42 s	2.05 m	1.65 m	1.40 s	1.10 d
		0.96 d	0.85 s	0.74 m									
Metoclopramide	tablet	7.81 s	6.61 s	5.24 d	4.81 s	4.68 d	4.47 d	3.96 m	3.91 d	3.89 d	3.87 d	3.86 d	3.85 s
		3.83 d	3.81 d	3.78 m	3.74 m	3.68 m	3.65 s	3.64 s	3.62 dd	3.61 d	3.56 dq	3.39 t	3.30 q
		1.32 t											
Metoclopramide	solution	7.81 s	6.61 s	3.92 s	3.77 t	3.39 t	3.30 q	1.32 t					
Metoprolol	solution	7.27 d	7.00 d	4.34 s	4.13 ddd	3.72 t	3.51 sept	3.34 s	3.32 d	3.24 dd	2.86 t	1.37 dd	
Metoprolol	tablet	7.27 d	7.00 d	5.24 d	4.68 d	4.47 d	4.34 s	4.13 m	3.96 m	3.91 d	3.89 d	3.87 d	3.86 d
		3.85 s	3.83 d	3.81 d	3.78 m	3.74 m	3.72 t	3.68 m	3.65 s	3.64 s	3.62 dd	3.61 d	3.51 sept
		3.56 dq	3.34 s	3.32 d	3.30 t	3.24 dd	2.86 t	1.37 dd					
Metronidazole	solution	8.55 s	7.94 d	7.67 bs	5.07 s	4.57 s	4.12 q	3.69 bs	3.60 bs	3.50 bs	3.36 s	1.37 d	1.34 d
		1.16 bs											
Midazolam	solution	7.76 dd	7.66 dd	7.58 q	7.53 t	7.45 d	7.32 t	7.18 m	7.03 s	6.99 s	5.04 d	4.19 d	2.56 s
		2.10 s											
Milrinone	solution	8.62 d	8.19 s	7.46 d	5.24 dd	4.83 s	4.65 dd	4.12 q	3.90 dd	3.52 s	3.50 s	3.47 m	3.42 m
		3.25 t	2.44 s	1.33 t									
N -acetylcysteine	solution	8.15 d	8.03 d	7.37 d	7.25 d	5.00 s	4.79 s	4.61 q	4.49 m	4.41 s	4.39 t	4.32 m	4.29 s
		4.27 t	4.23 s	4.21 m	4.09 dd	3.98 dd	3.95 s	3.89 tdd	3.82 s	3.71 dd	3.66 s	3.63 s	3.55 dd
		3.49 dd	3.45 dd	3.39 dd	3.37 d	3.35 m	3.33 s	3.30 t	3.26 dd	3.17 dd	3.14 s	3.12 d	3.09 d
		3.07 d	3.04 m	3.07 s	3.01 bs	2.99 s	2.97 s	2.96 d	2.95 bs	2.92 m	2.90 d	2.39 s	2.18 s
		2.17 s	2.07 d	2.01 s	1.97 s	1.95 s	1.93 s	1.15 d					

Table 1 continued

Naloxone	solution	6.85 q	6.80 s	6.78 s	5.94 m	5.66 s	5.63 d	5.07 s	3.86 m	3.76 d	3.67 d	3.56 dd	3.45 s
		3.42 s	3.38 s	3.37 s	3.27 dd	3.11 d	3.07 t	3.04 d	3.01 d	2.80 td	2.71 td	2.36 dt	2.06 dt
		1.78 dd	1.77 td	1.20 s	1.18 dd	1.15 d	0.96 d	0.65 d					
Noradrenaline	solution	7.02 d	6.97 m	6.91 dd	6.88 dd	5.07 s	4.95 t	4.34 s	3.86 bs	3.83 d	3.79 q	3.68 s	3.66 s
		3.65 d	3.63 s	3.36 s	3.31 s	3.26 m	3.26 s	3.18 s	2.99 s	2.89 s	2.77 m	2.65 s	
Nystatin	solution	5.41 d	4.22 d	4.05 t	3.89 td	3.80 m	3.70 s	3.66 m	3.56 dd	3.47 t	1.19 t		
Omeprazole		9.03 s	8.46 s	8.07 s	7.57 d	7.18 d	7.07 dd	5.06 s	4.56 s	4.42 s	4.29 q	4.17 q	4.13 m
		3.99 dd	3.92 dd	3.87 dd	3.81 d	3.77 td	3.71 s	3.69 q	3.61 bs	3.57 q	3.46 s	3.43 bs	3.36 s
		3.34 bs	3.24 dd	3.18 s	3.17 d	3.15 s	3.09 d	2.95 s	2.84 dd	2.77 s	2.48 bs	2.35 bs	2.18 s
		2.15 q	2.05 bs	1.82 s	1.75 bs	1.61 bs	1.36 s	1.28 dt	1.17 m	1.13 bs	0.97 bs	0.88 bs	
Ondansetron	tablet	8.06 d	7.59 d	7.55 d	7.41 sext	7.33 d	7.25 d	5.24 d	4.68 d	4.47 d	3.96 m	3.91 d	3.89 d
		3.87 d	3.86 d	3.85 s	3.83 d	3.81 d	3.78 m	3.74 m	3.68 m	3.65 s	3.64 s	3.62 dd	3.61 d
		3.56 dq	3.39 t	3.08 s	2.68 s	2.65 s	2.54 t	2.36 quint	2.12 sept	2.79 bs	1.92 s	1.17 bs	
Pabrinex pair part 1 thiamine, riboflavin; pyridoxine (vitamins B_1, B_2 and B_6, respectively)	solution	9.45 s	8.06 s	7.70 s	5.47 s	3.90 t	3.20 t	2.58 s	2.50 d				
Pabrinex pair part 2 ascorbic acid and nicotinamide (vitamins C and B_3, respectively); and glucose	solution	8.92 d	8.70 dd	8.24 dt	7.59 ddd	5.26 d	4.68 d	4.53 d	4.05 m	3.92 dd	3.86 m	3.77 m	3.56 dd
		3.54 s	3.52 s	3.49 m	3.44 sext	3.28 t							
Pantoprazole	solution	8.09 d	7.63 d7	7.45 d	7.04 dd	6.99 d	6.92 s	6.80 s	6.67 s	4.63 d	3.88 s	3.68 d	3.38 s
		2.89 s	1.18 s										
Paracetamol	solution	7.39 d	7.25 d	7.16 d	7.12 d	7.04 d	6.94 dd	6.91 d	3.88 dd	3.81 d	3.77 td	3.69 q	2.26 s
		2.15 s	2.04 s	1.96 s									
Paracetamol	tablet	7.90 t	7.83 m	7.53 d	6.91	3.86 m	3.84 s	3.83 d	3.79 m	3.80 d	3.74 dd	3.66 m	3.55 dd
		3.45 dd	2.98 m	2.82 m	2.60 dd	2.15 s	1.15 d						
Perinopril	tablet	5.24 d	4.68 d	4.47 d	4.32 t	4.26 m	4.21 bs	4.18 m	3.96 m	3.91 d	3.89 d	3.87 d	3.86 d
		3.85 s	3.83 d	3.81 d	3.78 m	3.74 m	3.68 m	3.65 s	3.64 s	3.62 dd	3.61 d	3.56 dq	3.39 t
		3.15 t	2.29 m	2.09 t	2.06 s	2.04 s	1.97 q	1.79 d	1.63 m	1.48 s	1.47 bs	1.37 s	1.32 t
		1.30 s	1.28 s	1.27 d	1.20 d	0.90 quint							
Phytonadione (vitamin K)	solution	8.46 s	8.13 s	7.94 sext	7.48 q	7.41 q	6.83 s	6.80 s	6.74 s	6.73 s	6.70 s	6.45 s	6.10 s
		5.97 s	5.31 s	4.45 s	4.27 d	4.02 s	3.85 s	3.72 m	3.56 s	3.45 s	3.37 s	3.24 s	3.12 s
		2.74 s	1.50 m										
Propofol	solution	8.36 s	7.88 s	7.06 m	6.82 m	5.00 s	4.98 s	4.76 s	4.74 s				
Prostacyclin (epoprostenol)	solution	5.60 m	5.47 m	3.87 dd	3.81 dd	3.77 td	3.69 q	3.49 s	2.76 m	2.57 m	2.41 m	2.36 s	2.20 m
		2.04 m	1.58 m	1.30 s	0.87 m	0.17 s							
Protamine	solution	8.09 d	4.61 bs	4.48 d	4.44 t	4.33 bs	4.16 m	4.12 s	4.11 s	4.06 d	4.03 s	4.00 d	3.88 m
		3.77 d	3.66 q	3.40 t	3.21 s	2.48 d	2.31 sept	2.05 m	1.74 bs	1.42 d	1.19 t	1.15 d	0.97 dd
		0.89 m	1.68 m	1.62 dd	1.58 d	1.50 qt							
Ramipril	tablet	7.40 t	7.34 d	7.29 q	5.42 s	4.31 dd	4.27 dd	4.24 s	4.22 q	4.20 d	4.17 m	4.12 dd	3.98 t
		3.85 dd	3.78 dd	3.67 m	3.45 m	3.66 td	2.70 m	2.56 s	2.54 s	2.47 m	2.32 m	2.05 m	1.94 sept
		1.76 m	1.51 m	1.42 m	1.33 m	1.27 m	1.19 d						
Ranitidine	solution	6.87 s	6.67 d	6.40 s	4.30 s	3.86 s	2.93 s	2.84 s	2.83 s	2.71 s	2.61 s		
Ranitidine	tablet	6.87 s	6.67 d	6.40 s	4.30 s	3.86 s	3.47 t	2.93 bs	2.84 s	2.82 s	2.77 t	2.72 s	2.70 s
		2.61 s											

Table 1 continued

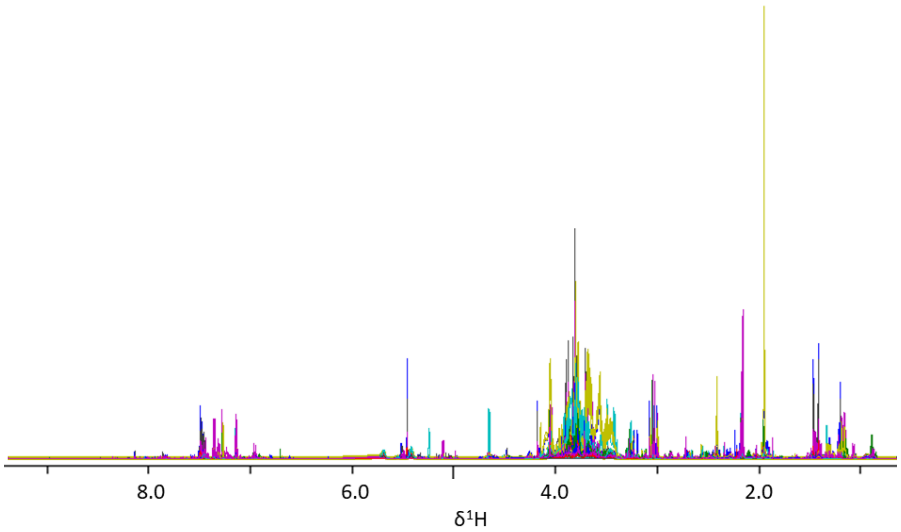
Risperidone	tablet	7.92 dd	7.45 dd	7.26 t	6.92 d		5.24 d	4.68 d	4.60 d	4.54 d	4.46 d	4.32 d	4.10 bs
		4.07 d	3.96 m	3.91 d	3.89 d	3.87 d	3.86 d	3.85 s	3.83 d	3.81 d	3.78 m	3.74 m	3.68 m
		3.65 s	3.64 s	3.62 dd	3.61 d	3.56 dq	3.48 bs	3.39 t	3.18 t	3.10 bs	2.97 dt	2.68 s	2.60 dd
		2.48 d	2.36 s	2.25 q	2.15 s	2.05 d	1.93 dquint	1.29 bs	1.18 bs	1.15 d			
Sando-Cal	solution	7.41 t	7.35 d	7.33 s	7.30 d	7.22 d	7.18 d	7.14 s	6.98 dd	5.41 bs	5.24 bs	4.12 m	4.04 s
		4.01 d	3.97 t	3.87 s	3.83 d	3.79 s	3.77 s	3.75 s	3.68 t	3.66 d	3.44 t	3.36 s	3.30 s
		3.26 dd	3.09 dd	2.80 s	2.76 dd	2.61 dd	2.45 s	2.42 s	2.38 s	1.82 s	1.33 dt	1.14 d	0.97 d
		0.92 q	0.84 d										
Senna	solution	7.93 d	7.02 s	6.99 d	6.97 s	6.94 d	6.26 t	6.15 sext	5.82 d	5.56 d	5.37 m	5.27 m	5.24 d
		5.13 m	5.06 m	4.98 m	4.83 s	4.65 d	4.26 t	4.20 m	4.12 m	4.00 m	3.75 m	3.44 m	1.82 s
		1.19 t											
Sodium Bicarbonate (8.4%)	solution	2.72 s	2.24 s	1.93 s	1.18 d	0.17 s							
Sodium Docusate	powder	7.94 d	7.92 s	6.97 d	5.49 s	5.46 s	5.37 m	5.14 m	4.96 t	4.85 s	4.64 m	4.51 d	4.46 d
		4.42 s	4.09 m	4.00 m	3.88 m	3.79 m	3.65 m	3.60 d	3.56 q	3.52 d	3.44 m	3.32 bs	1.89 bs
		1.14 d	1.02 t	0.90 bs									
Spironolactone	solution	7.95 d	6.95 d	5.42 d	5.12 d	4.01 m	3.75 m	3.55 dd	3.44 m	3.33 m5	3.23 s	2.60 dd	2.36 s
		2.25 bs	1.95 bs	1.92 s	1.84 dq	1.76 quint	1.64 m	1.53 m	1.43 m	1.28 d	1.16 d	0.99 t	0.87 t
Suxamethonium	solution	5.40 s	4.61 m	4.07 m	3.91 m	3.88 m	3.81 s	3.76 m	3.74 s	3.72 s	3.71 s	3.68 s	3.67 s
		3.65 s	3.64 m	3.53 t	3.47 t	3.41 bs	3.34 s	3.33 s	3.29 m	3.23 m	3.10 s	2.94 s	2.93 s
		2.91 bs	2.90 s	2.80 s	2.70 s	2.69 s	2.68 s	2.65 t	2.50 t	2.41 s	1.92 s	1.19 t	
Tazocin (pipercillin/tazobactam)	powder	9.86 d	8.28 s	8.11 d	8.09 d	8.01 s	7.95 s	7.85 d	7.81 s	7.60 m	7.56 quint	7.45 m	7.31 m
		5.62 s	5.60 d	5.58 bs	5.50 s	5.43 s	5.38 s	5.25 dd	5.31 s	5.13 d	5.02 dd	4.47 s	4.29 s
		4.27 d	4.22 s	4.21 d	4.18 s	4.14 s	4.15 d	4.13 s	4.05 s	3.97 dddd	3.55 s	3.54 s	3.93 qd
		3.47 d	3.46 s	3.44 d	3.08 d	2.53 d	2.50 d	2.09 s	1.93 s	1.72 s	1.63 s	1.61 s	1.60 bs
		1.55 bs	1.52 d	1.51 bs	1.50 s	1.44 d	1.36 s	1.30 d	1.29 s	1.26 t	1.19 t	1.15 s	1.12 bs
		1.09 t	1.05 s	0.65									
Teicloplanin	powder	7.22 bs	6.23 s	5.50 bs	3.56 bs	3.70 s	3.37 s	3.25 m	3.03 m	2.77 s	2.25 d	2.21 s	2.09 m
		1.92 s	1.50 d	1.41 s	1.30 s	1.09 bs							
Terlipressin	solution	1.92 s											
Tigecycline	solution	8.45 s	8.00 s	7.96 d	7.92 s	7.88 s	7.83 sext	7.72 s	7.69 s	7.61 s	7.33 s	7.28 s	6.45
		5.39 d	5.25 d	5.11 d	4.69 d	4.60 d	4.50 d	4.53 d	4.47 dd	4.34 d	4.23 s	4.12 s	3.97 m
		3.92 d	3.90 d	3.87 q	3.86 s	3.84 d	3.80 m	3.77 d	3.74 m	3.70 t	3.69 m	3.66 s	3.65 s
		3.62 m	3.60 t	3.57 m	2.99 dd	2.93 s	2.81 m	2.76 m	2.73 s	2.55 s	2.15 q	1.97 m	1.67 q
		1.55 s	1.45 s	1.38 s	1.34 s	1.32 s							
Tinzaparin	solution	5.99 d	5.59 bs	5.51 s	5.46 dd	5.41 s	5.31 bs	5.23 s	5.02 s	4.67 t	4.61 m	4.54 d	4.51 d
		4.48 d	4.04 m	3.61 s	3.55 sext	3.42 bs	3.28 d	2.05 s	1.92 s	1.19 t	0.17 s		
Tobramycin	powder	5.87 d	5.18 d	3.97 m	3.85 m	3.68 m	3.48 m	3.18 dd	2.49 dt	2.32 dt	2.03 dq	1.75 sept	1.15 d
		0.89 d											
Tramadol	solution	7.43 t	7.18 d	7.14 s	6.98 dd	3.88 s	2.94 dd	2.78 s	2.67 s	2.63 d	2.56 s	2.55 s	2.49 t
		2.33 tt	2.24 s	1.98 td	1.93 s	1.89 m	1.68 m	1.62 dd	1.58 d	1.50 qt			

Table 1 continued

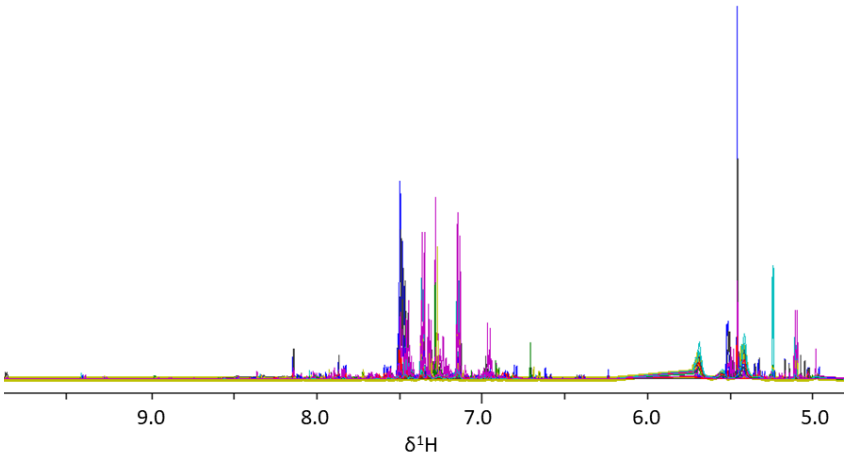
Tramadol	tablet	7.96 d	7.91 q	7.84 m	7.69 d	7.57 t	7.44 t	7.35 d	7.30 t	7.18 d	7.14 s	6.98 dd	5.41 d
		5.32 tt	5.24 d	4.67 d	4.45 d	4.37 dd	4.31 q	3.97 m	3.93 bs	3.91 bs	3.87 s	3.84 s	3.78 m
		3.73 m	3.70 s	3.63 m	3.44 t	3.29 t	2.94 dd	2.66 s	2.64 d	2.32 tt	2.26 s	2.24 t	2.13 d
		1.99 td	1.92 s	1.86 m	1.75 d	1.68 m	1.61 dd	1.58 d	1.50 qt	1.20 d	1.00 d	0.91 dd	0.78 d
Tranexamic acid	tablet	2.87 d	2.12 tt	1.89 dd	1.65 m	1.37 ddd	1.06 ddd						
Vecuronium	powder	5.26 d	5.16 m	4.82 d	3.87 dd	3.81 d	3.77 m	3.68 q	3.21 s	2.67 d	2.55 d	2.24 s	2.16 s
		0.96 s	0.87 s										
Volulyte	solution	5.69 bs	5.55 bs	5.42 bs	3.78 m	1.92 s							
Voluven	solution	5.69 bs	5.55 bs	5.42 bs	3.78 m								
Zopiclone	tablet	8.98 dd	8.62 d	8.60 d	8.54 d	8.24 d	8.07 dd	7.89 s	5.24 d	4.68 d	4.47 d	5.24 d	4.68 d
		4.47 d	3.96 m	3.91 d	3.89 d	3.87 d	3.86 d	3.85 s	3.83 d	3.81 d	3.78 m	3.74 m	3.68 m
		3.65 s	3.64 s	3.62 dd	3.61 d	3.56 dq	3.47 bs	3.39 t	3.24 t	3.18 t	3.11 bs	2.80 bs	2.50 s
		2.45 s	1.92 s	1.17 s									

Appendix III

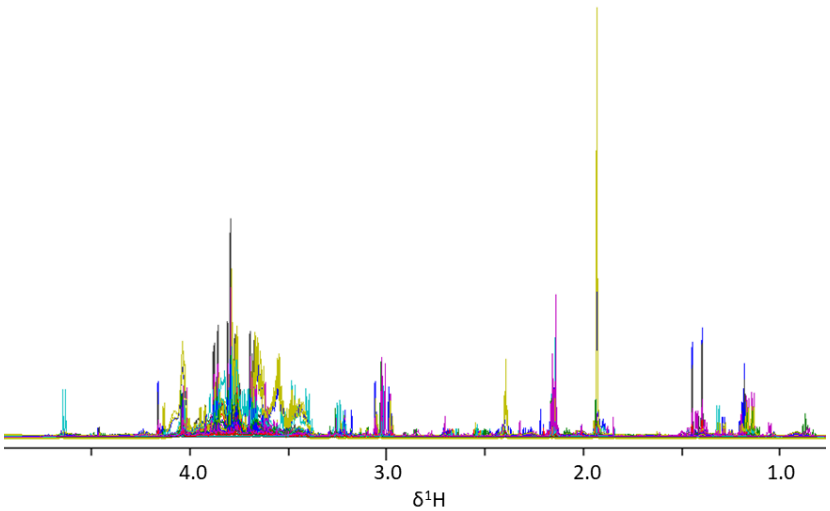
A



B



C



D

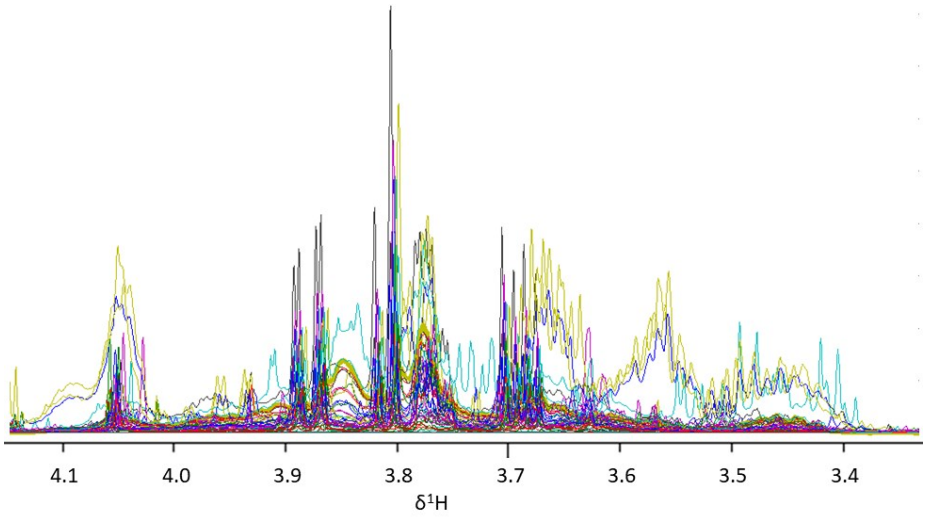


Figure 1 A composite of 600MHz 1-D ^{1}H NMR spectra of regions 9.7-0.8 ppm (A), 9.7-4.8 ppm (B), 4.6-0.8 ppm (C) and 4.15–3.35 ppm (D) of all the samples of unfiltered urine (47 in total) from the individuals from validation cohort with the extreme outlier identified by a PCA scores plot of this data set highlighted (in bold yellow) illustrating differences in the signals in the spectra of this outlier, in the region of 4.15-3.35 ppm, particularly in terms of the broad signals demonstrated by this outlier.

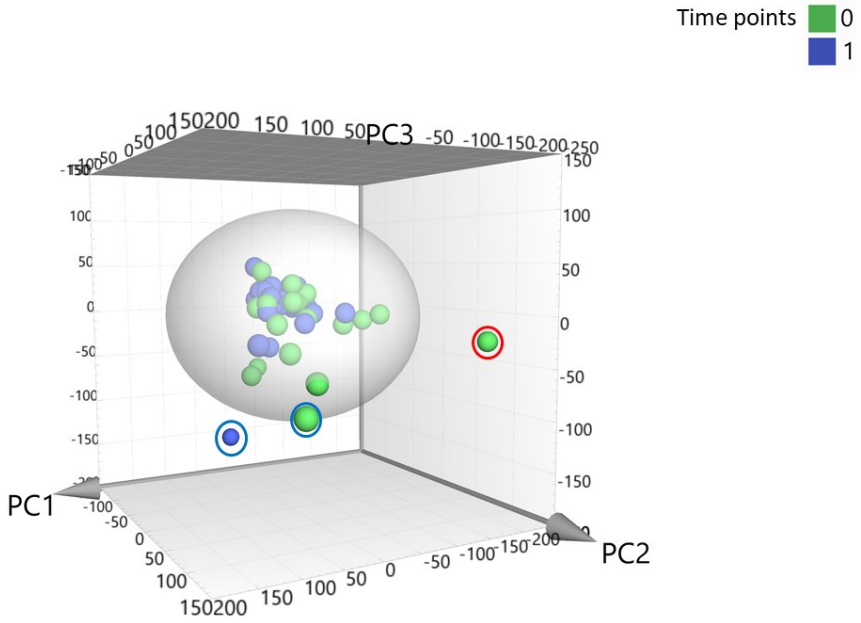
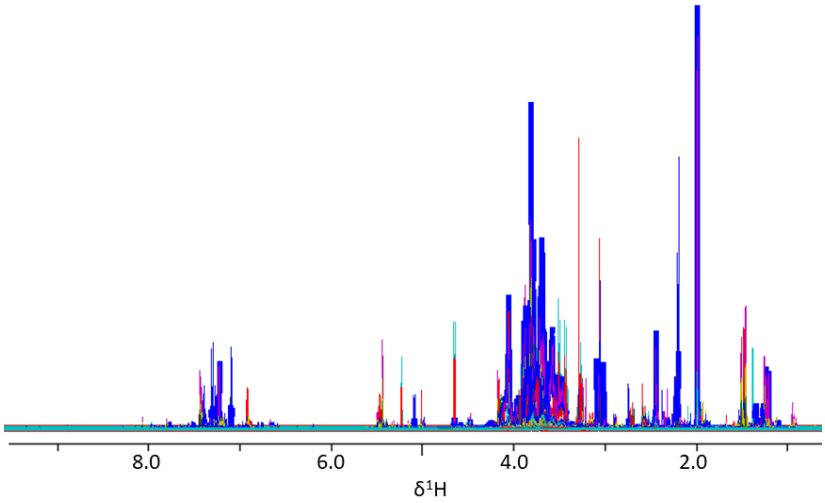
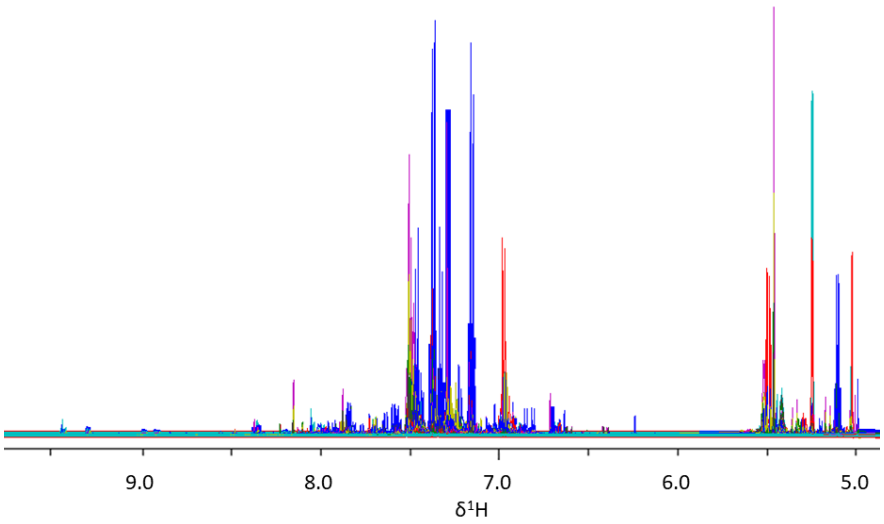


Figure 2 A 3-D PCA scores plot derived from ^{1}H NMR spectra of unfiltered urine from the validation cohort (47 samples) illustrating the metabolic variation of the data set as a whole and three outliers: one extreme (circled in red) that is both a scores and an orthogonal outlier and two intermediate outliers (circled in blue) of the perimeter of the Hotelling's T^2 95% confidence ellipse.

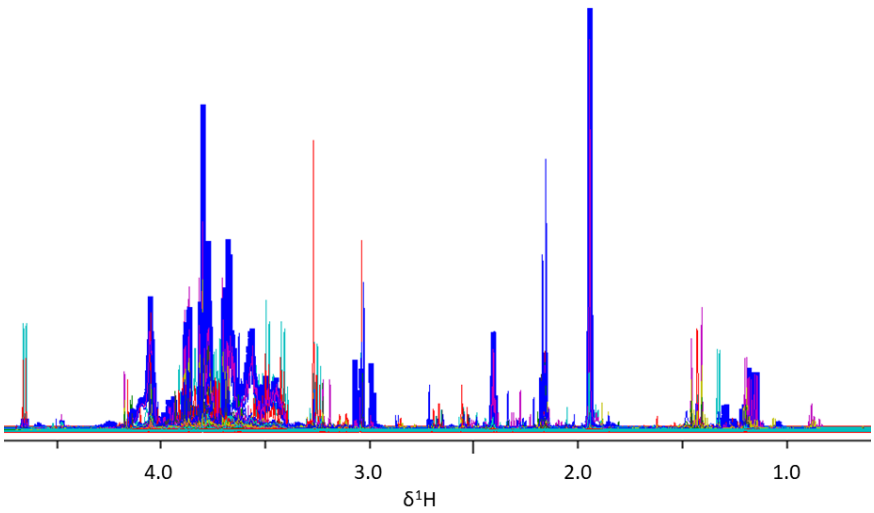
A



B



C



D

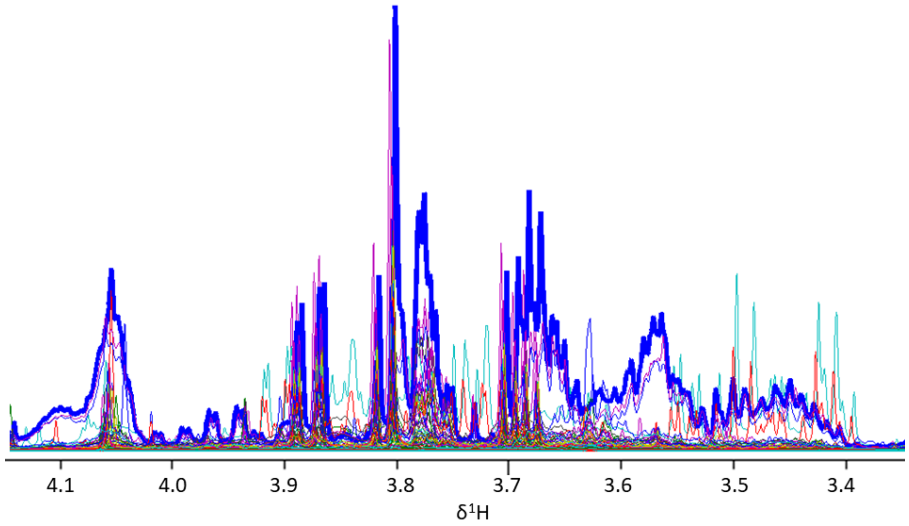


Figure 3 A composite of 600MHz 1-D ^{1}H NMR spectra of regions 9.7-0.8 ppm (A), 9.7-4.8 ppm (B), 4.6-0.8 ppm (C) and 4.15–3.35 (D) of all the samples of filtered urine (60 in total) from the individuals from validation cohort with the three extreme outlier identified by a PCA scores plot of this data set highlighted (in bold red, cyan and blue) illustrating differences in signals throughout the spectra in these outliers compared to the majority of the other samples. The outlier highlighted in blue has relatively high values of the many of the signals particularly in the region of 4.15-3.35 ppm; whereas the other two outliers have relatively low values of signals throughout the spectra but most clearly visualised in the aromatic region (B).

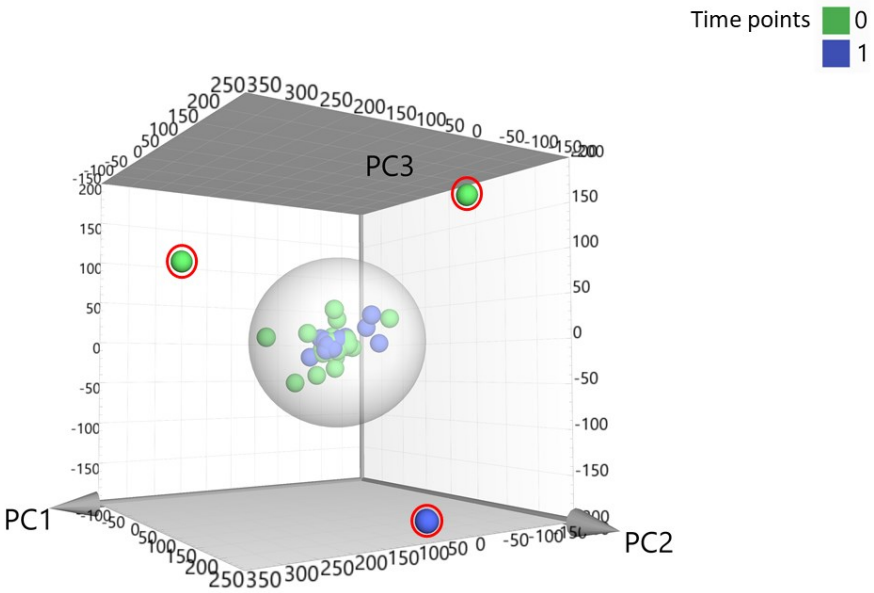


Figure 4 A PCA scores plot based on 1-D ^{1}H NMR spectral data of all the filtered urine samples from the validation cohort illustrating the metabolic variation of the data set as a whole (60 samples) and three extreme outliers (circled in red) that are both scores and an orthogonal outlier of the perimeter of the Hotelling's T^2 95% confidence ellipse.

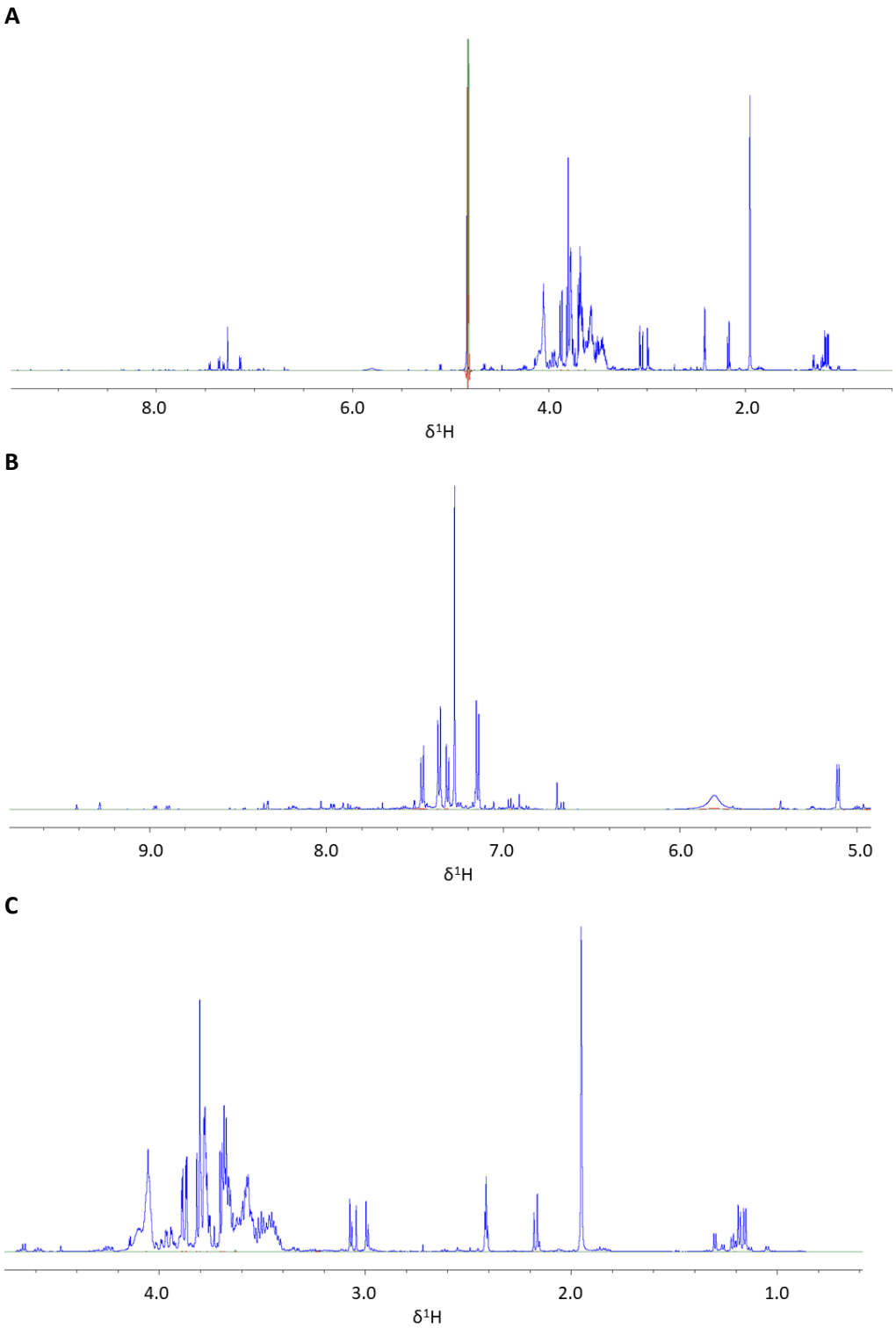
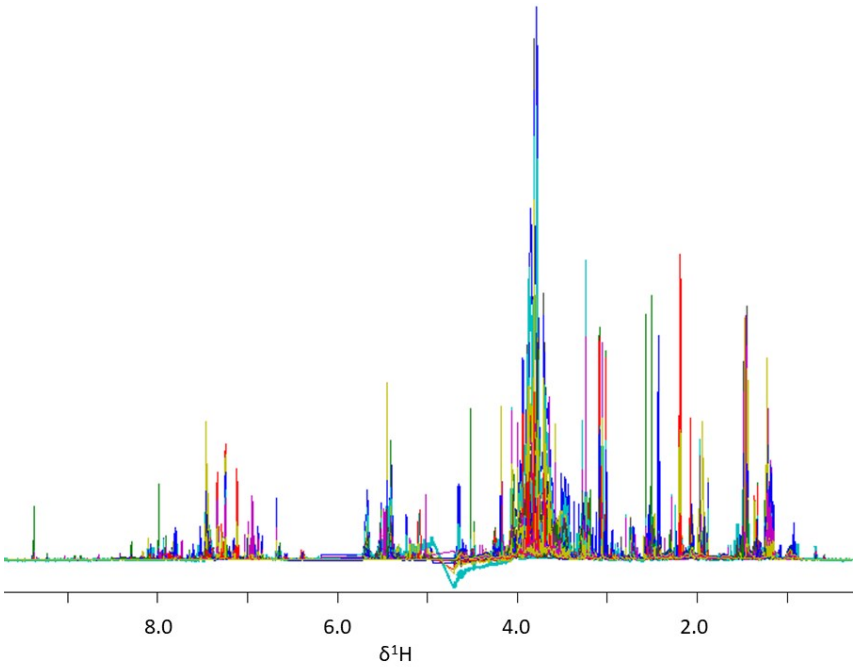


Figure 5 Composite of 1-D ^{1}H NMR spectra of regions 9.7-0.8 ppm (A), 9.7-4.8 ppm (B) and 4.6-0.8 (C) ppm of samples of filtered urine from the three extreme outliers identified by a PCA scores plot of the based on the NMR spectra of all 60 samples of filtered urine from the validation cohort. This illustrates the relatively low values of the metabolites in the red and green samples compared to the blue sample.

A



B

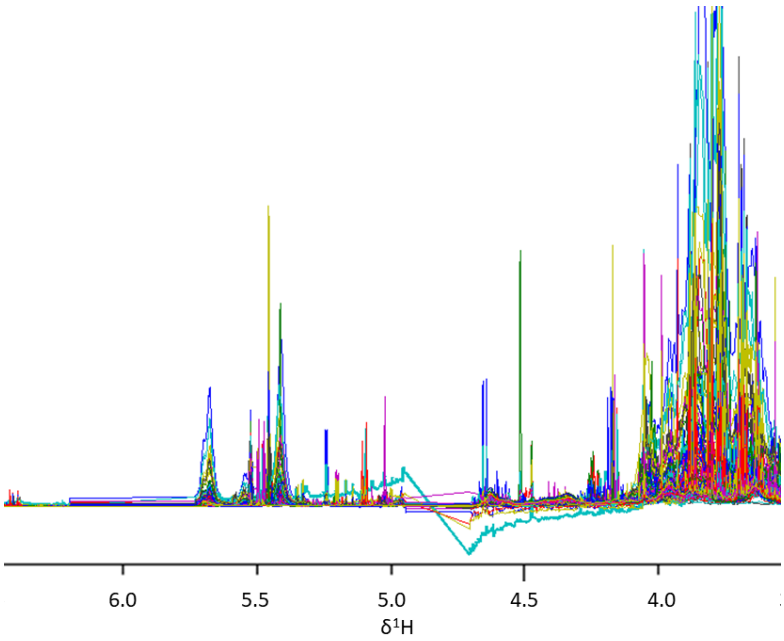


Figure 6 A composite of 600MHz 1-D standard ^{1}H NMR spectra of regions 9.7-0.8 ppm and 6.5-3.5 ppm (B) of all the samples of (unfiltered) urine (125 in total) from the individuals from sepsis cohort with one extreme outlier identified by a PCA scores plot of this data set highlighted (in bold cyan) illustrating errors in this spectrum in the region of 5.3-4.1 ppm.

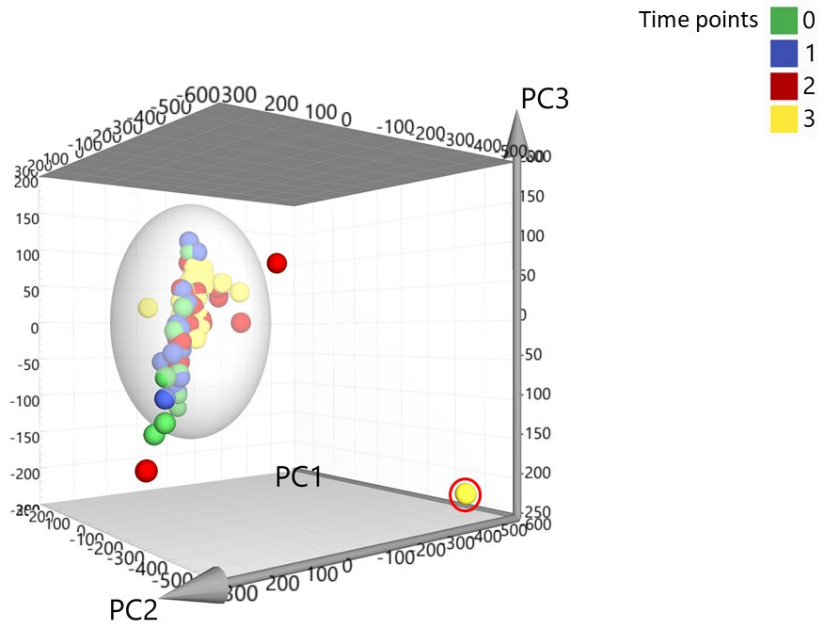
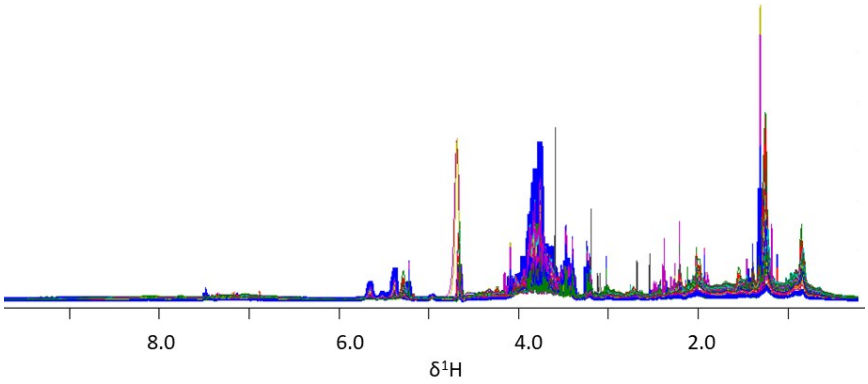
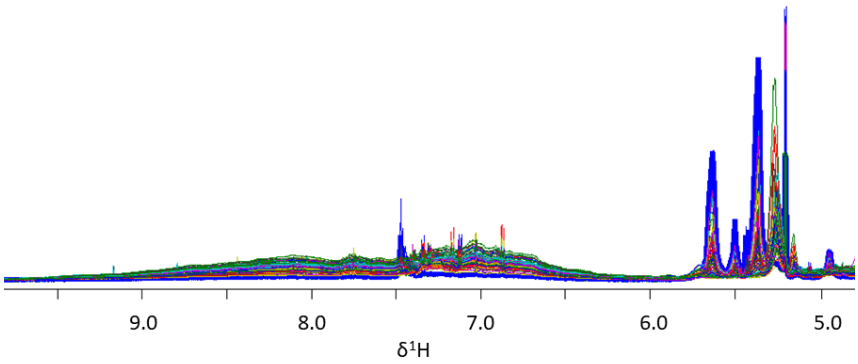


Figure 7 A 3-D PCA scores plot derived from 1-D standard ^{1}H NMR spectra of (unfiltered) urine from the sepsis cohort illustrating the metabolic variation of the data set as a whole and one extreme outlier (circled in red) that is both a scores and an orthogonal outlier of the perimeter of the Hotelling's T^2 95% confidence ellipse.

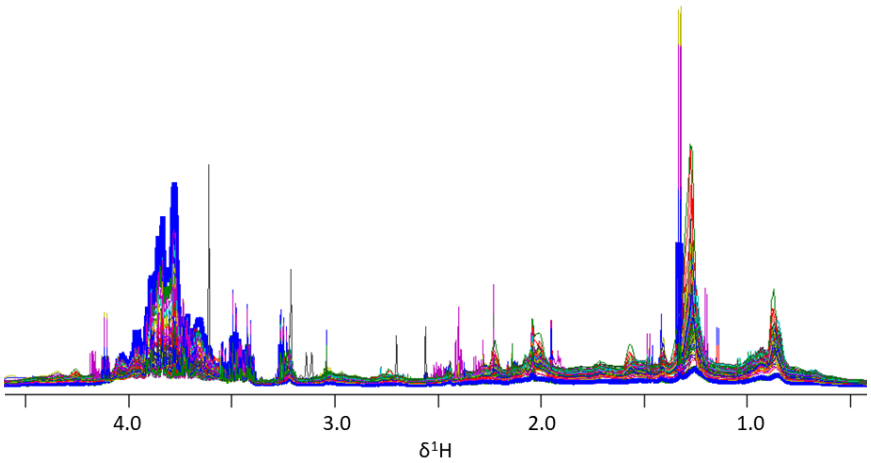
A



B



C



D

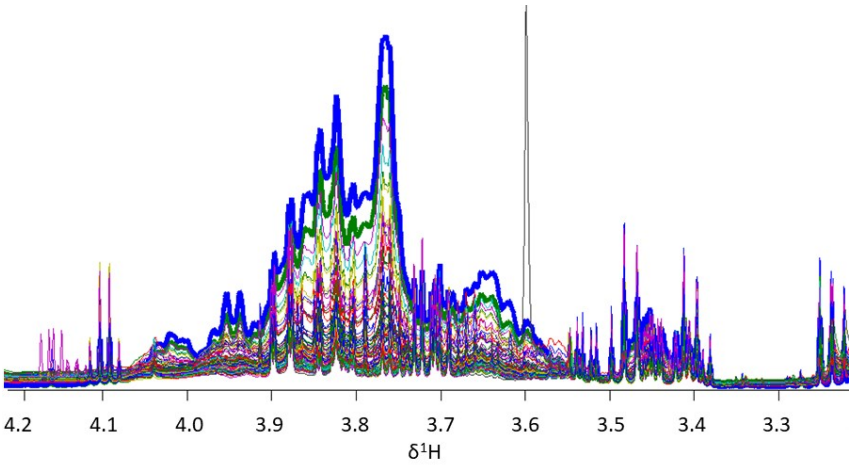


Figure 8 A composite of 600MHz 1-D standard ^{1}H NMR spectra of regions 9.7-0.8 ppm (A), 9.7-4.8 ppm (B), 4.6-0.8 ppm (C) and 4.15–3.35 (D) of all the samples of serum (100 in total) from the individuals from sepsis cohort with the two extreme outlier identified by a PCA scores plot of this data set highlighted (blue and green) illustrating relatively high values of the signals in the spectra of these outliers, particularly in the region of 4.15-3.35 ppm.

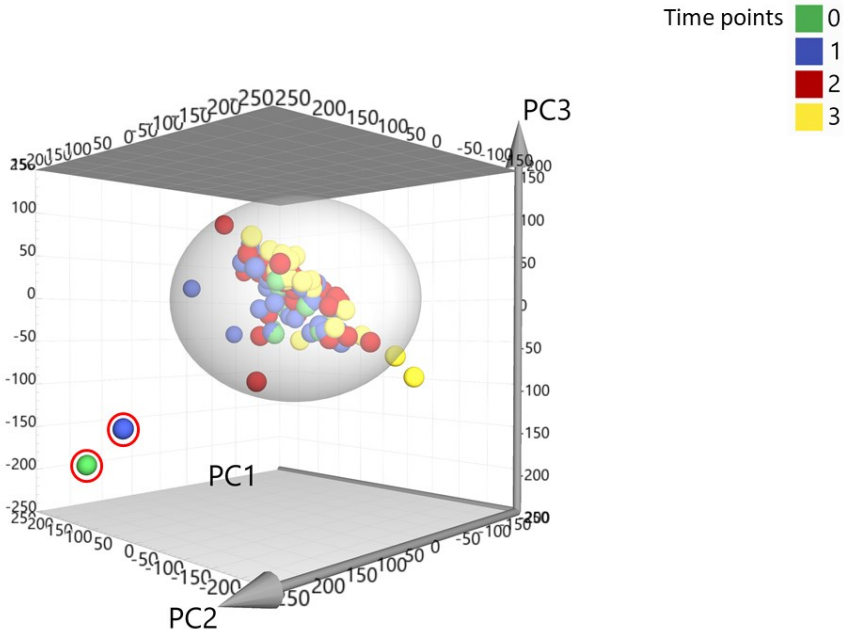
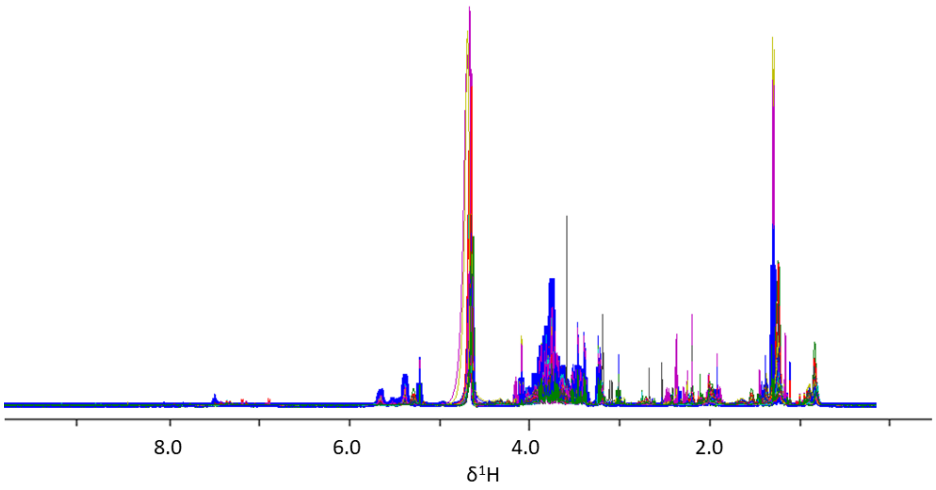
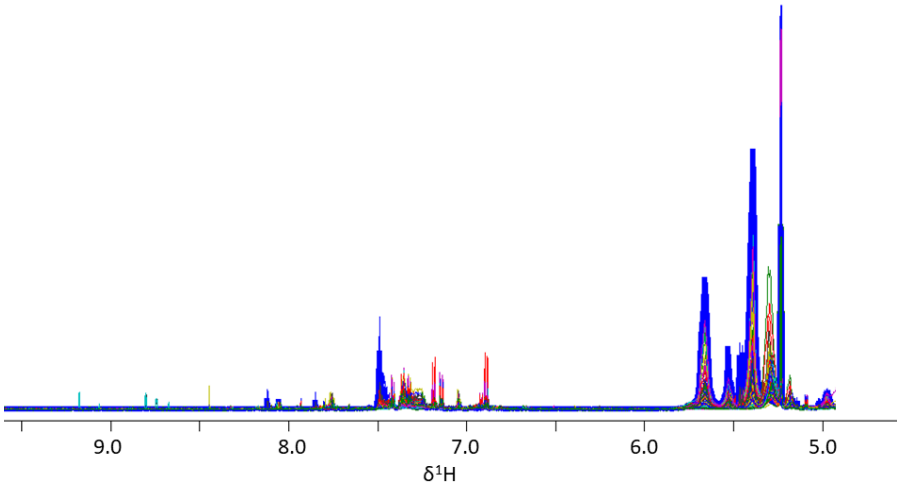


Figure 9 A 3-D PCA scores plot derived from 1-D standard ^{1}H NMR spectra of serum from the sepsis cohort (100 samples) illustrating the metabolic variation of the data set as a whole and two extreme outliers (circled in red) that are both a scores and orthogonal outliers of the perimeter of the Hotelling's T^2 95% confidence ellipse.

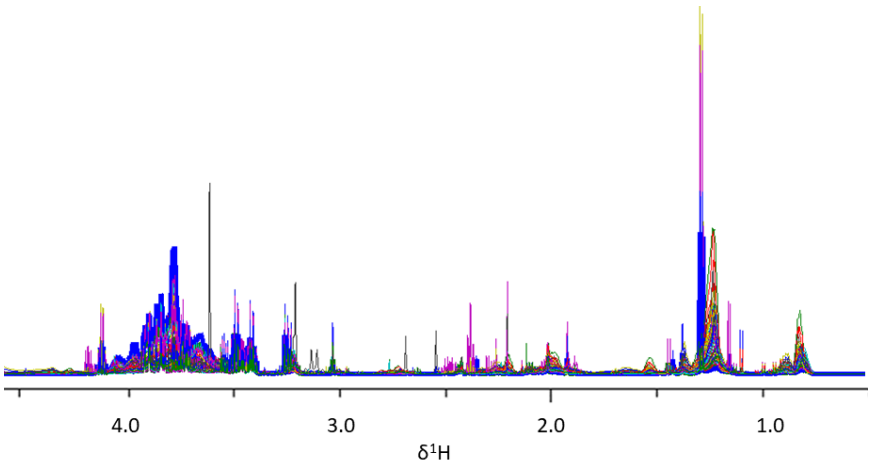
A



B



C



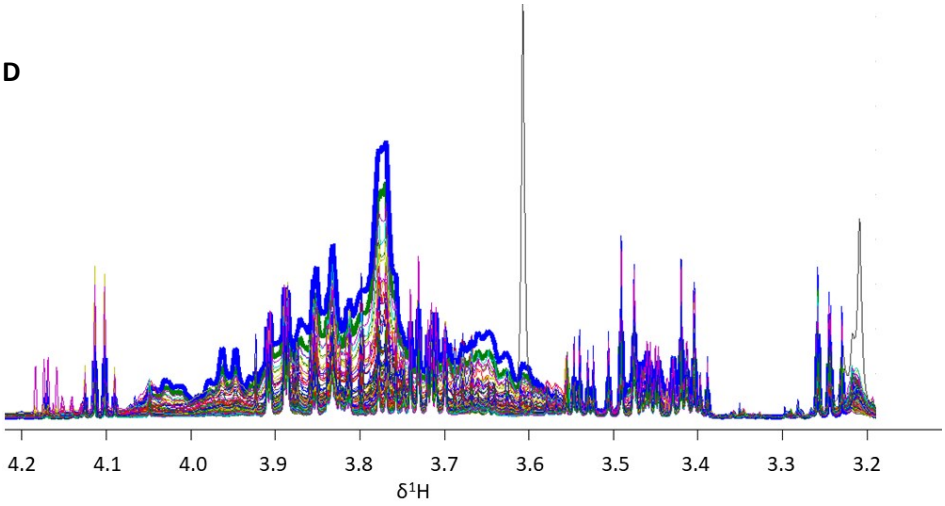


Figure 10 A composite of 600MHz 1-D CPMG ^{1}H NMR spectra of regions 9.7-0.8 ppm (A), 9.7-4.8 ppm (B), 4.6-0.8 ppm (C) and 4.15–3.35 ppm (D) of all the samples of serum (100 in total) from the individuals from sepsis cohort with the two extreme outlier identified by a PCA scores plot of this data set highlighted (blue and green) illustrating relatively high values of the signals in the spectra of these outliers, particularly in the region of 4.15-3.35 ppm.

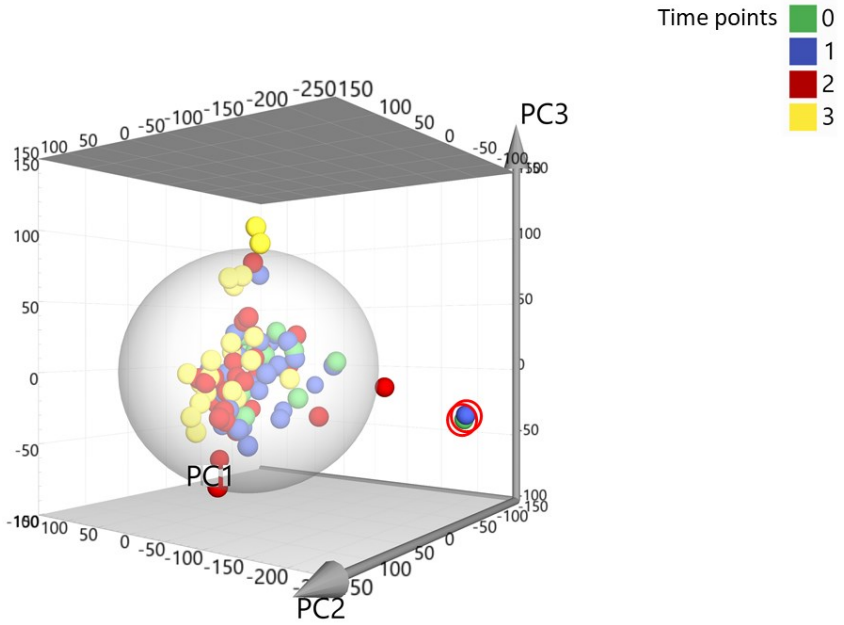


Figure 11 A 3-D PCA scores plot derived from 1-D CPMG ^{1}H NMR spectra of serum from the sepsis cohort (100 samples) illustrating the metabolic variation of the data set as a whole and two extreme outliers (circled in red) that is both a scores and orthogonal outliers of the perimeter of the Hotelling's T^2 95% confidence ellipse.